DOCTOR OF PHILOSOPHY

Synthesis and Testing of New Dyes for Dye-sensitized Solar Cells

Mohsen, Moneer

Award date:
2013

Awarding institution:
Bangor University

Synthesis and Testing of New Dyes for Dye-sensitized Solar Cells

By

Moneer Kadhm Mohsen

A thesis submitted in fulfilment of the requirements for the degree of Doctor of Philosophy in Bangor University

PhD supervisor - Dr Peter Holliman

PRIFYSGOL
BANGOR
UNIVERSITY

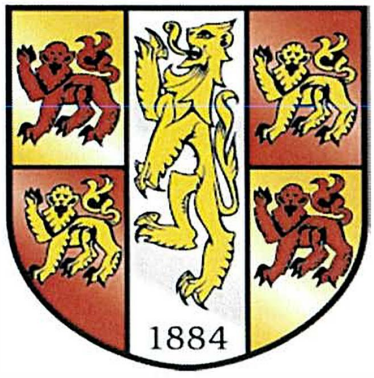

2013

Acknowledgements

I would like to express my deepest gratitude and sincere appreciation to my supervisor Dr Peter J. Holliman for his infinite support and constant encouragement throughout my research work. I would like also to thank him for his wide knowledge and creativity in science which was a great value to me.

I am grateful to Dr Arthur Connell for supporting and help me in my synthesis work and Dr Matthew Davies for help me in measure some devices and for good collaborations and scientific discussions.

I would also like to thank all the technician in school of chemistry, namely Mr Gwynfor Davies, Mr Denis Williams, Mr Mike Lewis, Mr Nicholas Welsby, Mr Glynne Evans and Mr Sam Page.

I would also like to thank all my friends and colleagues with whom I have had the pleasure to meet and work at the laboratory.

I would also like to thank the staff of the UK National Crystallography Service based at Southampton University and particulary Dr Mateusz Pitak for collecting and solving the crystallography data in this thesis, National Mass Spectrometry Service Centre based at Swansea University for running MS analyses, Tata Steel and Dyesol for help with device lifetime measurements and Prof Worsley's group at Swansea University for help with EQE measurements.

I would like to thank my wife for all her constant encouragement and support throughout research period.

Finally, I would like to thank Iraqi government especially Ministry of Higher Education and Scientific Research for supporting me financially to this scholarship.

List of abbreviation

DSCs	Dye-sensitized solar cells
D-π-A	Donor-π-conjugation-acceptor concept
PV	Photovoltaic
AM 1.5G	Air Mass 1.5 Global
TCO	Transparent Conductive Glass
FTO	Fluorine-doped Tin Oxide (F: SnO_2)
CB	Conduction Band
DSL-18NRT	Titania paste from Dyesol containing ~ 20 nm particles
HOMO	Highest Occupied Molecular Orbital
LUMO	Lowest Unoccupied Molecular Orbital
I-V	Current-Voltage Characteristics
η	Conversion Efficiency power
FF	Fill Factor
J_{sc}	Short-Circuit Current
V_{oc}	Open-Circuit Voltage
IPCE	Incident photon to current efficiency
NIR	Near-infrared
TPA	Triphenylamine
CDCA	Chenodeoxycholic acid
NBS	N-bromosuccinimide
BPO	Benzoyl peroxide

Publications

Work in this thesis has been included in the following journal paper and conference proceedings:-

"Ultra-fast Co-Sensitization and Tri-Sensitization of Dye-Sensitized Solar Cells with N719, SQ1 and Triarylamine Dyes", P.J. Holliman, M. Mohsen, A. Connell, M.L. Davies, K. Al-Salihi, M.B. Pitak, G.J. Tizzard, S.J. Coles, R.W. Harrington, W. Clegg, C. Serpa, O.H. Fontes, C. Charbonneau, M.J. Carnie, *J. Mat. Chem.*, 2012, **22**(26), 13318-13327.

"Increasing light harvesting in dye sensitized solar cells", P.J. Holliman, M.L. Davies, A. Connell, M. Mohsen, K. Al-Salihi, D. Al-Husenawi, E. Jones, Paper in *Conf. Proceedings - 8th Photovoltaic Science, Applications and Technology Conference – PVSAT-8*, 2-4th April 2012, Northumbria University, Newcastle.

"Low Cost Photovoltaics with "Go Faster" Stripes", P.J. Holliman, E.W. Jones, A. Connell, M. Mohsen, K. Al-Salihi, M.L. Davies, Paper in *Conf. Proceeding - 9th Photovoltaic Science, Applications and Technology Conference – PVSAT-9*, 10-12th April 2013, Swansea University.

Work from this thesis has also been awarded the following academic prizes:

2nd place in for the presentation entitled "Synthesis and Testing of New Dyes for Dye Sensitized Solar Cells" in the annual Royal Society of Chemistry North Wales Young Scientist Symposium held in the School of Chemistry, Bangor University Septemper 2012.

2nd place in the School of Chemistry's final year PhD presentations with talk entitled "Synthesis and Testing of New Dyes for Dye Sensitized Solar Cells" which took place 31st May 2012.

Abstract

This thesis concentrates on the development and synthesis of new metal-containing phthalocyanine and metal-free organic dyes for dye-sensitized solar cells (DSC). In this thesis attempts have been made to cover a broad region of visible light through the synthesis of three different dye families. The **N719** is the common dye was used as a sensitizer in DSC devices, which absorbs at 450-600 nm, while in this thesis were synthesized and developed three new types of dyes to work either side of **N719** absorb light at (400-450) nm for yellow and red single or di-linker dyes, cyanine and phthalocyanine dyes which absorb higher than 600 nm.

This thesis consists of six chapters. Chapter one includes a short history and introduction to dye-sensitized solar cells with a description of triarylamine, phthalocyanine and cyanine dyes, which are related to this thesis work.

The second chapter describes the experimental techniques which have been used to synthesize the target compounds and then tested them in DSC devices.

Chapter three describes the synthesis new triphenylamine dyes based on the donor-π- acceptor (D-π-A) concept. In this chapter three new dyes were synthesized; single-linker yellow dye 4-[2-(4-diphenylamino-phenyl)-vinyl]-benzoic acid (**5**), di-linker yellow dye 5-[2-(4-diphenylamino-phenyl)-vinyl]-isophthalic acid (**14**) and di-linker red dye (2Z, 2′Z)-3, 3′-(5-((E)-4-(diphenylamino) styryl)-1, 3-phenylene) *bis* (2-cyanoacrylic acid) (**12**). In addition, the single-linker red dye 2-cyano-3-{4-[2-(4-diphenylamino-phenyl) vinyl]-phenyl}-acrylic acid (**3**) was re-synthesized. These dyes included a triphenylamine donor moiety, a π-bridge (linker) and one or two carboxylic or cyanoacrylic acids as the acceptor moiety. During the synthesis of these triphenylamine dyes diphenyl-(4-vinyl-phenyl)-amine (**1**) was the main starting material which was used to synthesize all the triphenylamine dyes. This was synthesized by a Wittig reaction of 4-(N, N-diphenylamino)-benzaldehyde with potassium *tert*-butoxide and methyl triphenyl phosphonium iodide in distilled THF. The purpose was to compare single-linker and di-linker dyes to try to improve their DSC photovoltaic performance. In addition, these dyes were co-sensitized with other dyes to capture more light and to try to enhance the DSC performance. Single-linker red dye shows the highest overall conversion efficiency of 3.4%, while the other dyes ranged from 1.2-2.7%. Dye (**5**) shows the best results after co-sensitizing with **N719**

dye (7.5%). The stability of new single-linker yellow dye 4-[2-(4-diphenylamino-phenyl)-vinyl]-benzoic acid (**5**) was investigated, showed excellent stability during thermal and light soaking.

Chapter four describes the synthesis of cyanine dyes, which are the second type of dyes synthesized. The cyanine dyes 3-(2-((E)-2-((E)-3-((E)-2-(1-(2-carboxyethyl)-3,3-dimethylindolin-2-ylidene) ethylidene)-2-chlorocyclohex-1-en-1-yl) vinyl)-3, 3-dimethyl-3 H-indol-1-ium-1-yl)propanoate (**34**), 3-(2-((E)-2-((E)-3-((E)-2-(3-(2-carboxyethyl)-1,1-dimethyl-1H-benzo[e]indol-2(3H)-ylidene) ethylidene)-2-chlorocyclohex-1-en-1-yl)vinyl)-1, 1-dimethyl-1H-benzo[e]indol-3-ium-3-yl)propanoate (**35**) and cyanine derivatives 3-(2-((E)-2-((E)-2-chloro-3-((E)-2-(1-ethyl-3,3-dimethyl-1H-benzo[g]indol-2(3H)-ylidene)ethylidene) cyclohex-1-en-1-yl)vinyl)-1,1-dimethyl-1H-benzo[e]indol-3(2H)-yl)propanoic acid compound (**37**) and 3-(2-carboxyethyl)-2-(4-(diphenylamino)styryl)-1,1-dimethyl-1H-benzo[e]indol-3-ium (**38**) were synthesized by condensation reaction of heterocyclic groups 1-carboxyethyl-2, 3, 3-trimethylindolenium iodide (**29**), 1-carboxyethyl-2, 3, 3-trimethyl-1H-benzo [*0*]-indolium iodide (**30**), (E)-2-chloro-3-(hydroxymethylene)cyclohex-1-enecarbaldehyde (**33**), 1-ethyl-2, 3, 3-trimethylindolenium iodide and 4-(N, N-diphenylamino)-benzaldehyde as discussed earlier. The cyanine dyes (**34**), (**35**) and (**37**) absorb near the infrared light (NIR) at around 800 nm, while (**38**) absorbs at around 550 nm. These compounds show over all conversion efficiency from 0.05-0.25%. In addition the influence of co-adsorbents as additives to improve the photovoltaic parameters and the film thickness of semiconductor, are reported in this chapter.

Chapter five describes the synthesis of phthalocyanine dyes. The new unsymmetrical phthalocyanine 2, 3-di (4-benzoic acid)-7^2,12^2,17^2-hexa (2, 6-diphenylphenoxy)-tribenzo-5, 10, 15, 20-tetrazaprophyrin zinc (**24**) and the symmetrical phthalocyanine 2^2, 7^2, 12^2, 17^2 octa (2, 6-diphenylphenoxy)-tetrabenzo-5, 10, 15, 20-tetrazaprophyrin zinc (**26**) were successfully prepared. Many attempts were also made to synthesize 2, 3-di (4-benzoic acid)-7^2,12^2,17^2-hexa (2, 6-diphenylphenoxy)-tetrabenzo-5, 10, 15, 20-tetrazaprophyrin zinc (**28**) but without success. Purity is the main problem for phthalocyanine dyes, and this chapter successfully developed a new method to resolve the purity problem was developed. The phthalocyanine dye (**24**) absorbs light

in the near the infrared region (NIR) around 708 nm, and shows over all conversion efficiency of up to 0.7%.

Finally, chapter six includes conclusions of the thesis work, and suggestions for future work.

Contents

Chapter 1

Introduction

1.1 Introduction

Industrial development all over the world, has led to a dramatic increase in global energy consumption, which has reached more than $4x10^{20}$ Joules per year and is expected to increase rapidly in the future. [1] Currently, six main sources of energy are used globally as follows; 44% is petroleum, 20% is from natural gas, 25% is coal, 2.5% is hydroelectric power, 2.4% is nuclear power and 0.2% is non-hydro renewable energy; giving an overall split of 95% fossil fuel and 5% renewable energy. [2] However, the use of fuels has caused increasing environmental pollution and depletion of natural resources, such that global emissions of carbon dioxide from the combustion of fossil fuels has increased between 1980 and 2001 from 5 billion per year to 6.6 billion metric tons carbon equivalent per year. [2] Importantly rising energy demands could be met by using renewable energy sources to reduce the negative impacts resulting from the use of fossil fuels. [3] Hence, low carbon energy generation has become one of the crucial scientific and technological challenges of the 21st century. There are different types of renewable energy resource such as geothermal energy, tidal energy, biomass energy, hydropower energy, wind energy and solar energy including solar thermal and photovoltaic energy production.[4, 5]

In this context, the Sun supplies the Earth with about $3x10^{24}$ J of annually in the form of solar radiation, which is estimated to be approximately 10,000 times the current energy consumption of the world's population. [6] This means that a covering of 0.1% of the Earth's surface by solar cells panels with 10% efficiency would be enough to meet current needs. [1] In other words, the sun's energy provides about 600 TW per year, so 10% efficient solar cells could produce 60 TW per year of power. [7] In practice, solar energy can be divided into two different types; solar thermal and solar photovoltaic. [8] Solar thermal uses the heat of the sun to produce hot water and/or air, for heating, etc. while solar photovoltaics use sunlight to produce electricity. [8]

Solar cells are normally classified into three types. First generation solar cells consist of crystalline silicon and are expensive to produce because they use high purity silicon. [7] These devices make up more than 85% of current solar cell market, either as single crystal or multi-crystalline of silicon with laboratory scale cell conversion efficiencies of up to 25%. [9] Second generation solar cells have been known since the early 1990s and are also known as thin film technology. These use thin film deposits

of semiconductor materials such as amorphous silicon (a-Si), cadmium telluride (CdTe), copper-indium-gallium selenide (CIGS) or copper-indium sulphide (CIS). Thin film PV is predicted to have a lower cost than c-Si but have lower efficiency. [7] Third generation PV technologies include dye-sensitized solar cells, (DSC) polymer solar cells and nanocrystalline solar cells. [10] These are less well developed technologies with much research focussed on increasing device efficiency and reducing processing costs. [11]

In this thesis, the main area of study has been the development and testing of sensitizers for dye-sensitized solar cells (DSC). In recent years, DSC technology has become a subject of intensive research due to the relatively low cost of raw materials and the ease of device fabrication compared to other solar cells technologies. [12] There are two types of dye for dye sensitized solar cells (DSC); namely metal-organic complexes and metal free-organic dyes. [13] For instance Grätzel *et al.* have developed metal-organic dyes based on ruthenium polypyridyl complexes [14] (e.g. ruthenium dyes such as N3 [15] or black dye [16]) producing conversion efficiencies of more than 10 % whilst metal-free organic dyes have shown efficiencies of more than 9 % for **C219** dyes [17] and 11 % for porphyrin dyes. [18]

1.2 History of Solar Cells

The term "Photovoltaic" comes from the Greek *photo* meaning light and *voltaic*, from the name of Italian physicist Volta after whom the unit volt is named. The photovoltaic effect was first discovered by the French physicist Becquerel in 1839 who studied photoelectric experiments with liquid state devices. [6] He observed that an electric current was produced when using two platinum electrodes coated with AgCl or AgBr placed in (an electrically conducting) solution was exposed to light. Forty years later, workers studied the first solid state PV device using selenium. When in 1876, William Adams and Richard Day reported that selenium could be used to produce photoconductivity. [19] Following this the first solar cell was built in 1883 by Charles Fritts, who covered selenium with thin layers of gold to form junctions. [19] He reported that the selenium produced a current, "that is continuous, constant and of considerable force with exposure to sunlight". [20] It is estimated that the device had approximately 1% efficiency. In the following years, Moser

introduced the concept of dye sensitization by using erythrosine dye on silver halide electrodes. [16] Albert Einstein then explained the photoelectric effect in 1905, [20] for which he received the Noble prize in physics in 1921. In 1940, Russel Ohi first discovered a n-junction solar cell which was made in a silicon crystal. [21]

In the 1950s photovoltaic devices were developed using crystalline silicon. In 1954, the first silicon solar cell reported by Chapin achieved an efficiency of 6%. [22] Furthermore, in 1954 cadmium sulphide was used in a p-n junction photovoltaic device. Several years after followed studies of indium phosphide, cadmium telluride and gallium arsenide. [20] The first use of TiO_2 as a semiconductor in a dye-sensitized for solar cell was in USA and this was reported in a patent in 1978. This cell was based on dye sensitization of anatase TiO_2 particles with an N-methylphenazinium dye. [23] However, dye-sensitized solar cells remained unsuccessful until 1990s. Then in 1991, O'Regan and Grätzel reported a high efficiency dye-sensitized solar cell using nanoparticulate titanium oxide as the semiconductor electrode sensitized with a ruthenium (bipyridyl) complex dye and using an iodine iodide electrolyte. [14]

1.3 Dye-sensitized solar cells

The history of dye-sensitized solar cells goes back to the 19th century. In 1873, Vogel[12] first reported and worked on semiconductor sensitization. He sensitized silver halide emulsions with dyes and shifted the photosensitivity to the infrared. In 1887, Moser changed the concept of dye enhancement from photography to photoelectrochemical cells and applied that on silver halide electrode by using erythrosine dye. [12] The theoretical concept of dye-sensitization remained in dispute until the 1960's. The reason it was not clear was due to competing concepts like electron transfer or energy coupling. Tributsch and Gerischer [24] proved the mechanism of electron injection. This work was done using ZnO in 1968. Many attempts to develop DSCs were not successful because they used a smooth semiconductor surface. Matsumura and Alonso [25] tried to increase efficiency by using ZnO electrodes, but this was unsuccessful and the efficiency was still lower than 1%, and the dye was unstable. In, 1991 Grätzel and co-workers [7] developed DSC devices, with efficiency 7%, using mesoporous TiO_2 with high internal surface area. Then Nazeeruddin *et al.*[15] reported dye-sensitized solar cells with efficiency

more than 10% in 1993. The chemisorption concept of the dye on the semiconductor surface was developed in the following years, [26, 27] along with the use of particles to increase the surfaceinterface. [28] TiO_2 became the best electrode material, [12] with the advantages that TiO_2 is non-toxic, inexpensive, and plentiful. [29]

The best DSC reported so far has achieved a conversion efficiency of 12.3% by co-sensitizing zinc porphyrin dye (**YD2-o-C8**) with (**Y123**) dye using a $Co^{(II/III)}$ tris(bipyridyl) based redox electrolyte, which will discussed later. [30] In addition, advantages of DSCs are that they show efficiency increases with temperature from 20°C-60°C and are less affected by low light levels compared with silicon cells. [29]

In addition, natural dyes have been investigated (e.g. chlorophyll dye and monascus yellow dye) which produced efficiency of 4% and 2%, respectively. [31] Synthetic dyes have been studied for many years with the aim of producing longer dye excitation lifetimes, strong light absorption in the visible spectrum and efficient metal to ligand charge transfer for ruthenium dyes. [32] Metal-free organic dyes have been tested as sensitizers for DSCs [13] which include merocyanine, [33, 34, 35, 36] hemicyanine, [37, 38, 39, 40] cyanine, [41, 42, 43] coumarin, [44, 45] perylene, [46, 47] indoline, [48, 49] oligothiophene, [50, 51] dialkylamine dyes, [52, 53] and triphenylamine dyes. [54, 55, 56]

1.4 Solar radiation

The solar spectrum is the light emitted from the sun which can be divided into three different wavelength regions; the ultraviolet, visible and infrared regions. Atmospheric absorption and the sun's position affect the light passing through the atmosphere. Ultraviolet light is filtered by ozone, and water whilst CO_2 absorbs in the infrared region showing features at 900, 1100, 1400, H_2O at 1800 and CO_2 at 2600 nm. [7]

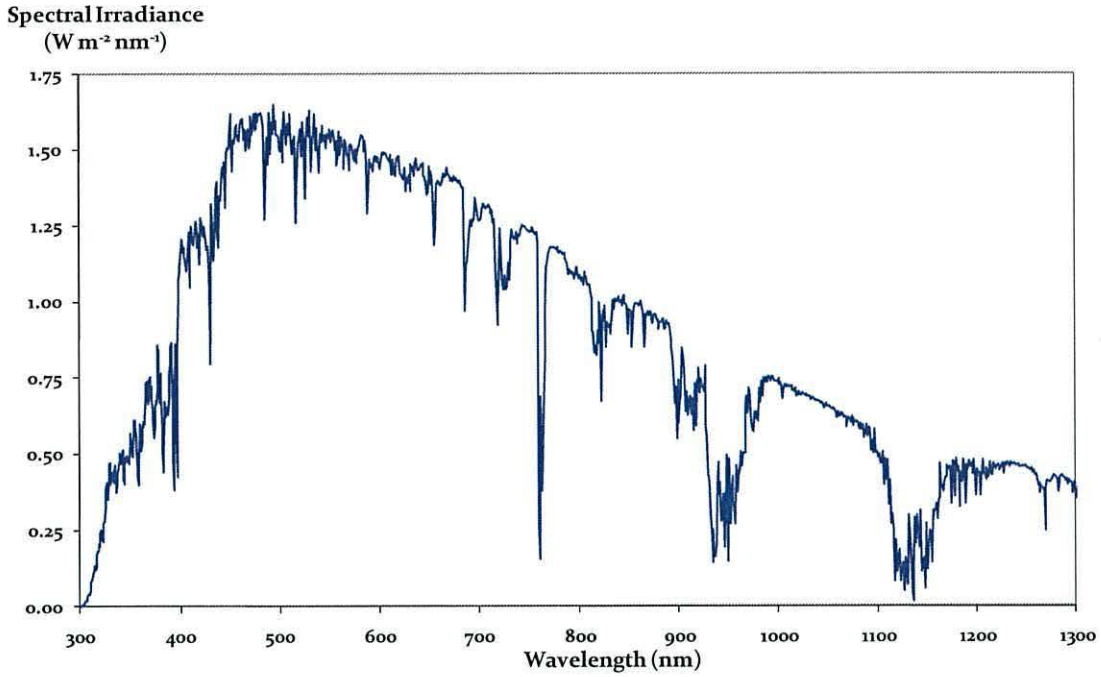

Figure 1.1. The AM1.5 solar spectrum (www.nrel.com).

The maximum solar spectrum radiation reaches Earth when the sun is directly overhead (i.e. at the equator) giving shortest path length. The path length of light through the atmosphere is called the air mass (AM), which can be determined by $AM=1/\cos\Phi$.

Where Φ= angle of elevation of the sun.

The standard efficiency measurement of solar cells is AM 1.5 G (global), $\Phi= 42^{o}$. [7]

1.5 Structure and operating principle of the dye-sensitized solar cells

DSC devices consist of four main components; (a) dye molecules adsorbed on the TiO_2 or ZnO semiconductor surface, (b) semiconductor particles coated on transparent conducting glass (TCO), (c) an electrolyte containing a redox couple such as I_3^-/I^- and (d) a counter electrode (typically transparent conducting glass coated by platinum). These work together to convert the solar energy to electricity energy as shown in Figure 1.2. [57, 58]

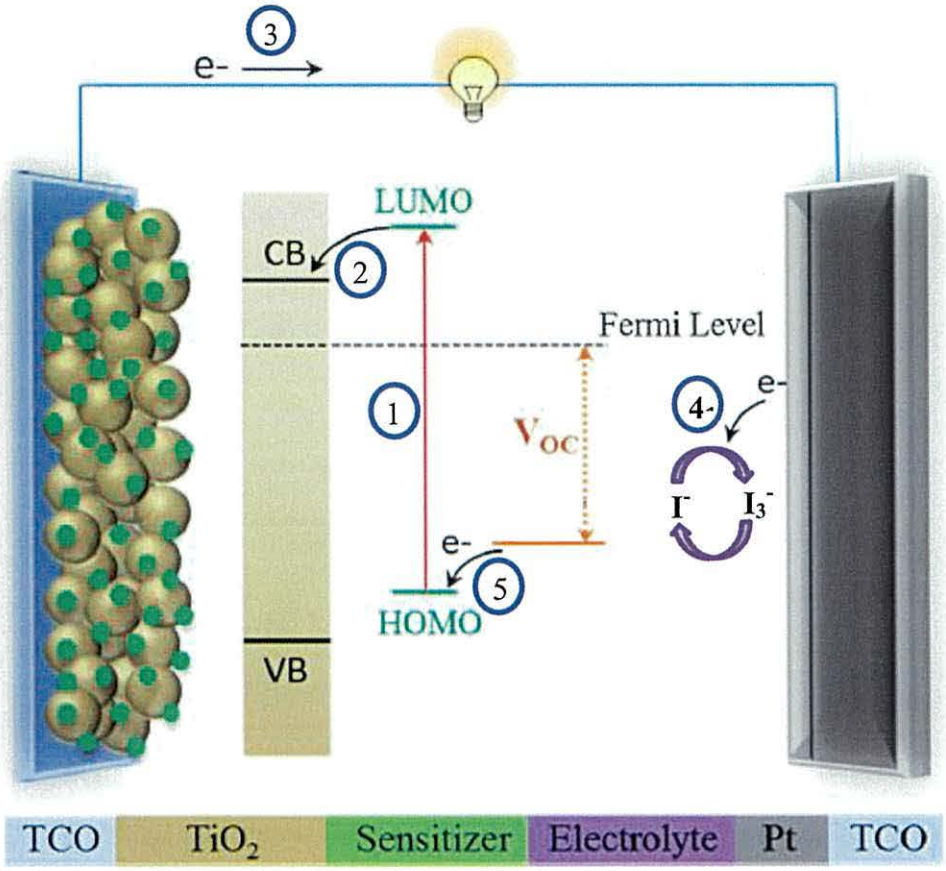

Figure 1.2. Schematic representation of the composition and the operating princible of a DSC. [57]

In this system, dye-sensitization is important in that these semiconductors have wide band-gaps, [59] and otherwise only UV or near-UV light could excite electrons into the TiO_2 conducting band. In addition to TiO_2, other wide band-gap semiconductors such as ZnO, Nb_2O_2 and SnO_2 can also be used. [60] A carboxylic acid is generally used to make a link between the dye and semiconductor to increase the electronic coupling between them which is important for efficient charge injection.

During DSC operation, an incoming photon from sunlight is absorbed by the dye which is on the surface of TiO_2. The dye is excited by the incident photon from its ground state (S^o) to an excited state (S^*) (step 1, Eq.1.1).

$$S + h\upsilon \rightarrow S^* \qquad \text{Absorption} \qquad \text{Eq. 1.1}$$

The electron is then injected into the conduction band (C.B.) of the semiconductor leaving the dye molecule in an oxidized state (S^+), (step 2, Eq.1.2).

$$S \rightarrow S^{+} + e^{-}(TiO_2)$$ Electron injection Eq. 1.2

The injected electron moves through the TiO_2 nanocrystalline film to arrive at the transparent conductive glass (TCO) on the working electrode and then travels around the external circuit to the other transparent conducting counter electrode (typically Pt-coated TCO glass) (step 3). At the counter electrode, the electron reduces triiodide in the electrolyte to iodide (step 4, Eq.1.3),

$$I_3^{-} + 2e^{-}(Pt) \rightarrow 3I^{-}$$ Reduction Eq. 1.3

which then diffuses into the pores of the TiO_2 film to reduce the oxidized dye back to its original state (step 5, Eq.1.4). [61, 58, 62]

$$2S^{+} + 3I^{-} \rightarrow 2S + I_3^{-}$$ Regeneration Eq. 1.4

Some of the most important advantages of DSC devices compared to silicon based solar cells are their reduced sensitivity to impurities, their operation across a wide range of temperatures and different angles of incident light, low production costs, and high device flexibility where different materials may be used in the manufacture such as ceramic, glass, plastic, fabric and metal substrates. DSC disadvantages include lower conversion efficiency and shorter life of the device. [60]

1.5.1 The Counter electrode

The counter electrode is one of the most important components in the DSC, and platinum is the most commonly used counter electrode catalyst. [63] Usually, the counter electrode substrate is a transparent conductive -glass (TCO) such as fluorine-doped tin oxide (FTO) glass, which is then coated with the platinum layer which acts as a catalyst to regenerate I^{-}. [32] There are different methods used for coating a Pt catalyst onto the TCO surface and the performance depends on which method is used, e.g. electrochemically [64, 23] sputtering, [15] or spin deposition. [65] In 1997, Papageorgiou *et al.* [66] developed a new coating called the platinum cluster catalyst method. This catalyst produced excellent kinetic performance, chemical and electrochemical stability, reduced cost by using less platinum, and also had good optical transparency. The disadvantages of using platinum as counter electrodes are that it is expensive and potential Pt dissolution in the electrolyte which can reduce devices stability over time. So this has led chemists to think about alternative

catalysts, such as those containing carbon black and graphite. [67, 68] Reports have included efficiency of 9% under AM 1.5 simulated sun light using carbon as a catalyst-based DSC device. [32] In 1996, Kay and Grätzel [67] reported a new porous carbon counter electrode catalyst, made from a mixture of carbon black and graphite powder with titanium oxide used as a binder for the structure. This type of counter electrode appears to have high conductivity due to the connection between the carbon black particles.

1.5.2 Electrolyte

Iodine/triiodide (I^-/I^-_3) is the traditional and most commonly used liquid electrolyte redox couple in DSCs. There is the possibility of the electrolyte containing other additives to enhance performance in DSCs operation. So far, acetonitrile is the best solvent used in electrolyte DSCs. [32] However, the high volatility of acetonitrile makes it easier to be lost through the device's sealing. [67] It cannot be used in commercial DSCs because it is toxic and is classed as a carcinogen. [69] Other solvents have emerged as alternatives to acetonitrile (e.g. methoxyacetonitrile (MAN) and 3-methoxypropionitrile (MPN)). These are seen as good candidates due to their higher boiling points and lower-toxicity compared with acetonitrile. In 1991 Grätzel and O'Regan [14] used a mixed solvent of ethylene carbonate: acetonitrile (80:20, v/v) with other additives such as lithium or potassium iodide to improve the performance of the electrolyte. [7] Other solvents used in the electrolyte include e.g. ethylene carbonate, [14] propylene carbonate, [70] butyronitrile, glutaronitrile, [71] or methoxyacetonitrile. [72]

In 2001 Wolfbauer *et al.* [73] reported important points about the redox couple in the electrolyte with the performance of DSCs. They also reported the effect of iodide salt additives to the electrolyte e.g. LiK, [14] LiI, [64] alkyl methylimidazolium iodide, [23] They concluded that the ionic size affected the performance of the electrolyte with smaller cations (e.g Li^+) giving the best performance. Organic compounds have also been used to improve the device performance. Kong *et al.* reported the adding carboxylic acids such as acetic acid to the electrolyte increased J_{sc}. In contrast, the V_{oc} reduced. Frank and co-workers have studied adding pyridine derivatives e.g. 4-*t*-

butylpyridine and they have been concluded that these additives increase V_{oc} and η. They reported the reason was due to nitrogen's lone pair donating properties. [74]

1.5.3 The Semiconductor

TiO_2 is the most common nanocrystalline semiconductor, which has been used extensively in DSCs due to its low cost, [75] high stability under solar irradiation and in solvents, its non-toxicity and high photosensitivity. [14] TiO_2 can also be prepared with high surface area, [76] which provides maximum adsorption sites for dyes on the semiconductor surface. In addition, another important property of TiO_2 is the energy levels which should be slightly lower than the energy level of the excited state (LUMO) of the dye molecules, which leads to effective electron injection from the dye to the semiconductor. [77, 78] There are three crystalline structures of TiO_2; anatase, rutile and brookite, with anatase being the most commonly used in DSCs because it has a wider band gap structure of 3.2 eV compared to rutile's 3.0 eV. [7] ZnO is the best alternative semiconductor material to TiO_2 in DSC due to it having a wide band gap, which is similar to the energy levels of TiO_2. [78] However, ZnO tends to have lower electron injection than TiO_2 and greater instability to acidic dyes.

1.6 Incident Photon to Current Efficiency (IPCE)

IPCE can measure the conversion of incident light into electrons at different λ, which can be represented by Equation (1). [79] IPCE is the product of the light harvesting efficiency (LHE), yield of charge injection (Φ_{inj}), charge collection efficiency at the back contact (η_{coll}) and quantum yield of regeneration (Φ_{reg}). [79]

$$IPCE = LHE.\Phi_{inj}.\eta_{coll}.\Phi_{reg} \quad (1)$$

The surface area of the semiconductor and the light absorption of the sensitizer play important roles in determining the LHE value. [80] Practically IPCE measurements are performed with monochromatic light and calculated by using (Equation 2). [81] IPCE can also be defined by the number of electron produced from the incident light at different λ.

$$\text{IPCE\%} = \frac{1240\ I_{sc}\ (\mu A/cm^2)}{\lambda(nm) P_{in}\ (W/m^2)} \qquad (2)$$

Where I_{sc} is the short-circuit photocurrent density for monochromatic irradiation and λ and P_{in} are wavelength and the light intensity, respectively.

The solar energy to the electricity energy conversion efficiency is determined by (Equation 3). [81]

$$\eta = \frac{I_{sc}\ V_{oc}\ FF}{P_{in}} \qquad (3)$$

Where I_{sc}= short circuit photocurrent density.

V_{oc}= open circuit voltage

FF = cell fill factor and P_{in} the intensity of the incident light.

Fill factor is another important parameter in photovoltaic cell devices which measures the squareness of the I-V curve and is represented by the ratio of the voltage and current at the maximum power point to the short circuit current and open circuit voltage or the degree to which the voltage and the current match at the maximum power point (Equation 4), [20] as shown in Figure 1.3.

$$FF = \frac{I_{max}\ V_{max}}{I_{sc}\ V_{oc}} \qquad (4)$$

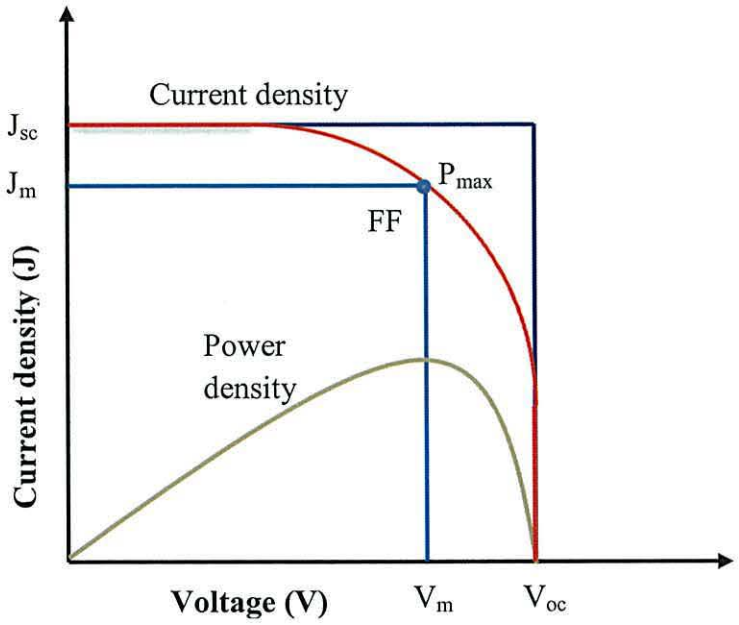

Figure 1.3. The current-voltage (black) and power-voltage (grey) characteristics of an ideal cell. Power density reaches a maximum at a bias Vm, close to V_{oc}. [20]

1.7 Dyes for dye-sensitized solar cells (DSC)

This thesis studies dyes for DSC. This section reviews previous reports of DSC dyes.

1.7.1 Metal organic dyes

1.7.1.1 Ruthenium complex dyes

Ruthenium dyes have played an important role in the progress of DSC devices as sensitizers, due to their photochemical properties and high stability in the oxidized state. [82] As mentioned earlier O'Regan and Grätzel used a ruthenium dye in their Nature paper in 1991 and they gained a conversion efficiency of 7.1%. [14] After 1991 DSC research started to flourish and evolve. Nazeeruddin *et al.* [15] in 1993 achieved a conversion efficiency of 10% with the same ruthenium dye which have been used in 1991, is a *cis*-di(thiocyanato)-*bis*(2,2'-bipyridyl-4,4-dicarboxylate)ruthenium(II) complex so-called (**N3**) Figure 1.4, which included one ruthenium metal localized in the centre of the complex.

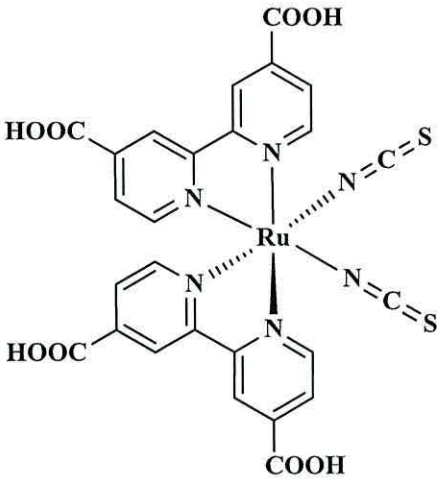

Figure 1.4. The molecular structure of **N3** dye. [15]

In 1997, Nazeeruddin *et al.* reported ruthenium Black Dye which covers the whole visible range into the near-infrared region with conversion efficiency of 10.4%. [83] In 2005, Nazeeruddin *et al.* [84] reported a high conversion efficiency (11.2%) with a dye called **N719** which was related to **N3**, but this dye contained two tetrabutylammonium ions in the structure compared with $4H^+$ counter ions in N3, (Figure 1.5).

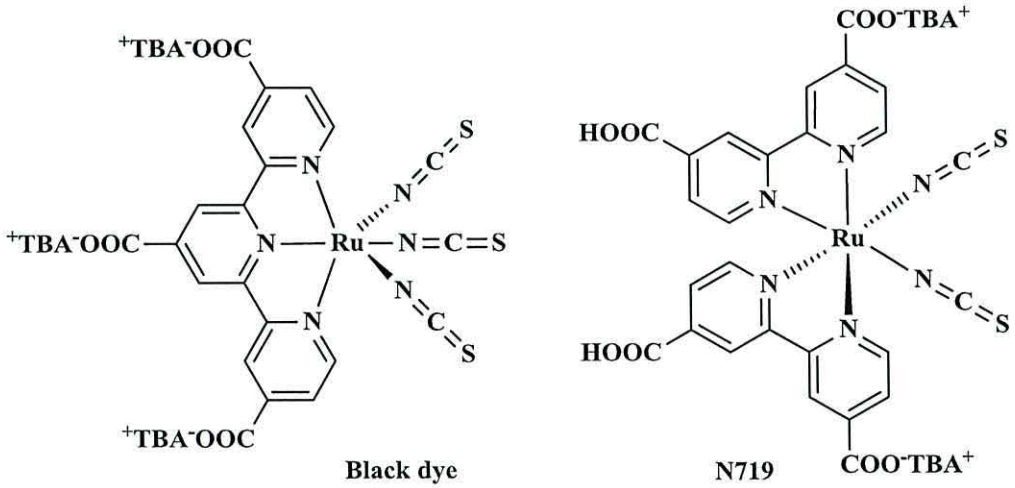

Figure 1.5. Molecular structures of **Black Dye** [85] and **N719** dye. [84]

All these complexes contain carboxylic acid groups as anchoring groups, which is the most commonly used DSC anchoring group. There is one disadvantage in using this type of dyes, which can be summarised by the long-term stability which can be affected by the presence of water, leading to slow desorption of the photosensitizers

from the semiconductor surface. For this reason phosphonate anchoring groups have been tested, Ru [(Me_2bipy) (HP-terpy) (NCS)], Me_2bipy= 4, 4'-dimethyl-2, 2'-bipyridine, H_2P-terpy= 2, 2': 6', 2''-terpyridine-4'-phosphonate. These dyes can be desorbed from the semiconductor surface using alkaline solvent. [86]

In 2000, Grätzel *et al.* [87] prepared and investigated ruthenium (II)-poly-pyridine complexes shown in Figure 1.6. These contained the catechol functional group (1, 2-dihydroxyphenyl), to attach on the TiO_2 surface. These complexes showed strong linking on TiO_2 surfaces which was faster than for carboxylic acid groups. However, the I-V data was lower than Ru complexes containing carboxylic acids. Complex (**1.1**) showed overall converting efficiency 1.9%, while complex (**1.2**) showed 1.5%. This may have been due to the aggregation of dye on TiO_2 surface so they used different types of additives to improve and prevent the aggregation of the dye on TiO_2 surface such as chenodeoxycholic acid (CDCA).

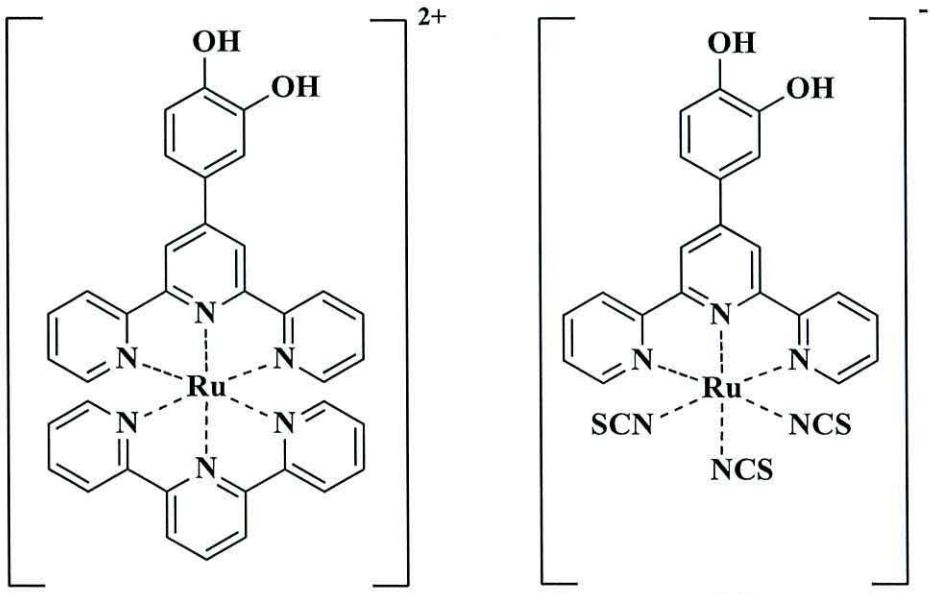

Figure 1.6. Molecular structure of ruthenium complexes (**1.1**) $[Ru(terpy)(H_2L)][PF_6]_2$ and complex (**1.2**) $[Bu_4N][Ru(H_2L)(NCS)_3]$; H_2L= [4'-(3,4-dihydroxyphenyl)-2,2':6',2''-terpyridine]. [87]

The high cost of ruthenium and limited device performances because these dyes cannot harvest photons above 650 nm, has led researchers to think of alternative dyes like metal- free organic dyes such as coumarin, triphenyl based, indoline and oligothiophene dyes or metal-complexes porphyrin dyes to fabricate DCS. [88] In this

thesis phthalocyanine-zinc dyes have been studied, which are type of metal porphyrin dyes, which absorbs near infrared region (NIR) of the solar spectrum.

1.7.1.2 Metal porphyrin dyes

Braun and Tcherniac were the first group who synthesised pthalocyanine (Pc) **(1.3),** Figure 1.7. They discovered a dark blue insoluble material, as a minor product in the preparation of *0*-cyanobenzamide, from phthalimide and acetic acid in 1907 at the South Metropolitan Gas Company in London. [89] Diesbach and Vonder Weid discovered metal derivatives of Pc in 1927, by refluxing *0*-dibromobenzene with copper cyanide in pyridine. They obtained a 23% yield. [90] The term phthalocyanine is derived from the Greek naphtha, meaning "rock oil" and cyanine, meaning "blue". [89] Linstead [91] used this term in the 1930's to describe this new class of materials. He suggested that Pc is a symmetrical macrocycle consisting of 4-iminoisoindoline units with a central cavity to accommodate different metal ions. Robertson confirmed this structure a short time later using X-ray diffraction. [90] It was observed that the structure of Pc is very close to the naturally occurring porphyrin system and also contains an 18 π electron inner core.

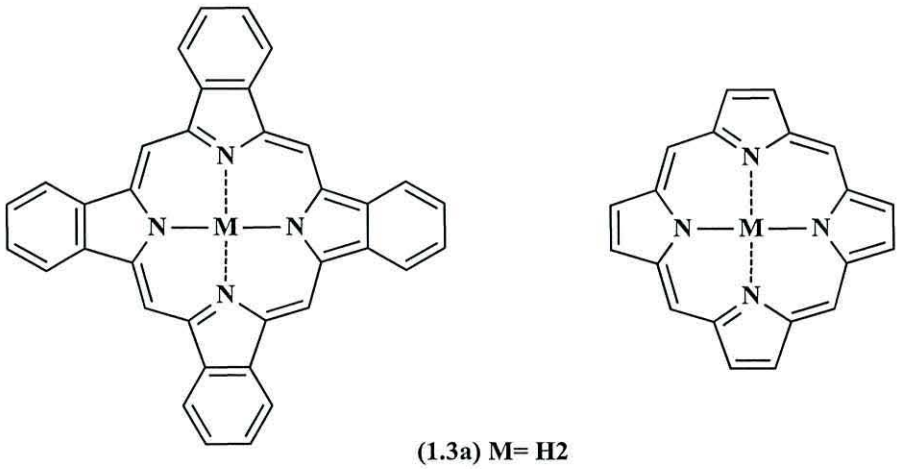

(1.3) **(1.3a) M= H2** **(1.3b) M= metal** **(1.4)**

Figure 1.7. General structures of phtalocyanine **(1.3)** and porphyrin **(1.4)**. [90]

Scientists have used porphyrin as a sensitizer in DSCs. The first example was reported in 1993 with overall efficiency 2.6%. [92] In addition porphyrin has many reaction sites, eight β position and four meso position, (Figure 1.8). [92]

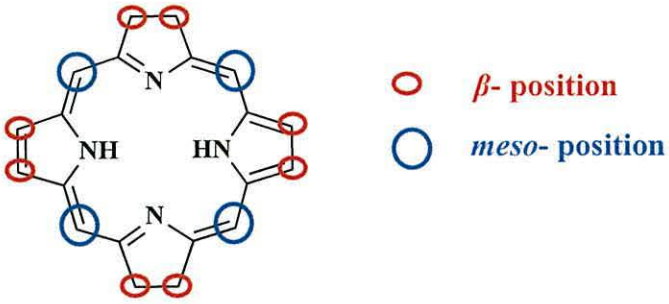

Figure 1.8. Typical structure of a porphyrin showing the four *meso*- and the eight β-position which can be functionalized for porphyrin-sensitized solar cells. [92]

The electronic spectrum of phthalocyanine with four peripheral benzyl groups is red shifted, compared with porphyrins due to the additional delocalization of the π electrons. However, aggregation is a common problem in most phthalocyanines. [93, 94] The main reason for synthesis phthalocyanines for use as sensitizers in DSC is their strong absorption in the near infrared region. In contrast, the main drawbacks encountered when using phthalocyanines as sensitizers in DSC is their aggregation and lack of directionality in the excited state. [95, 96] One important requirement to improve light-harvesting is to improve the directionality of electron transfer from the excited state of the dye to the conduction band of the semiconductor. To do this Reddy *et al.* [97] developed a novel unsymmetrical zinc phthalocyanine **PCH001** (**1.9**) as shown in Scheme 1.1. They synthesized **PCH001** (**1.9**) by three steps; the first one was by reacting (**1.6**) with *tert*-butylphthalonitrile (**1.5**) and DBU in pentanol as the solvent. The reaction mixture was refluxed for 20h and the crude product was purified by column chromatography to produce (**1.7**). The second step was to synthesize (**1.8**) by Zinc metalation of the (**1.7**) with zinc acetate in DMF. Finally, the desired compound of **PCH001** (**1.9**) was synthesized byhydrolysis of (**1.8**) with Na/ethanol; the reaction mixture was stirred at room temperature for 7d. Then the solid resulting was redissolved in ethanol and the pH was adjusted to 3 by adding of dilute HCl.

The UV-Vis of **PCH001** (**1.9**) shows a maximum absorption at 692 nm (ε= 191000 $M^{-1}cm^{-1}$). This dye is composed of three *tert*-butyl and two carboxylic acid groups as push and pull effects, respectively. The main purpose of the two carboxylic acid groups is to anchor the sensitizer on the semiconductor surface and enhance electronic coupling between the excited state of the dye and the conduction band of

the semiconductor. The three alkyl (*tert*-butyl) group increase the dye solubility, decrease aggregation and tune the LUMO level to provide directionality. This increased the efficiency of **PCH001 (1.9)** up to 3.05%.

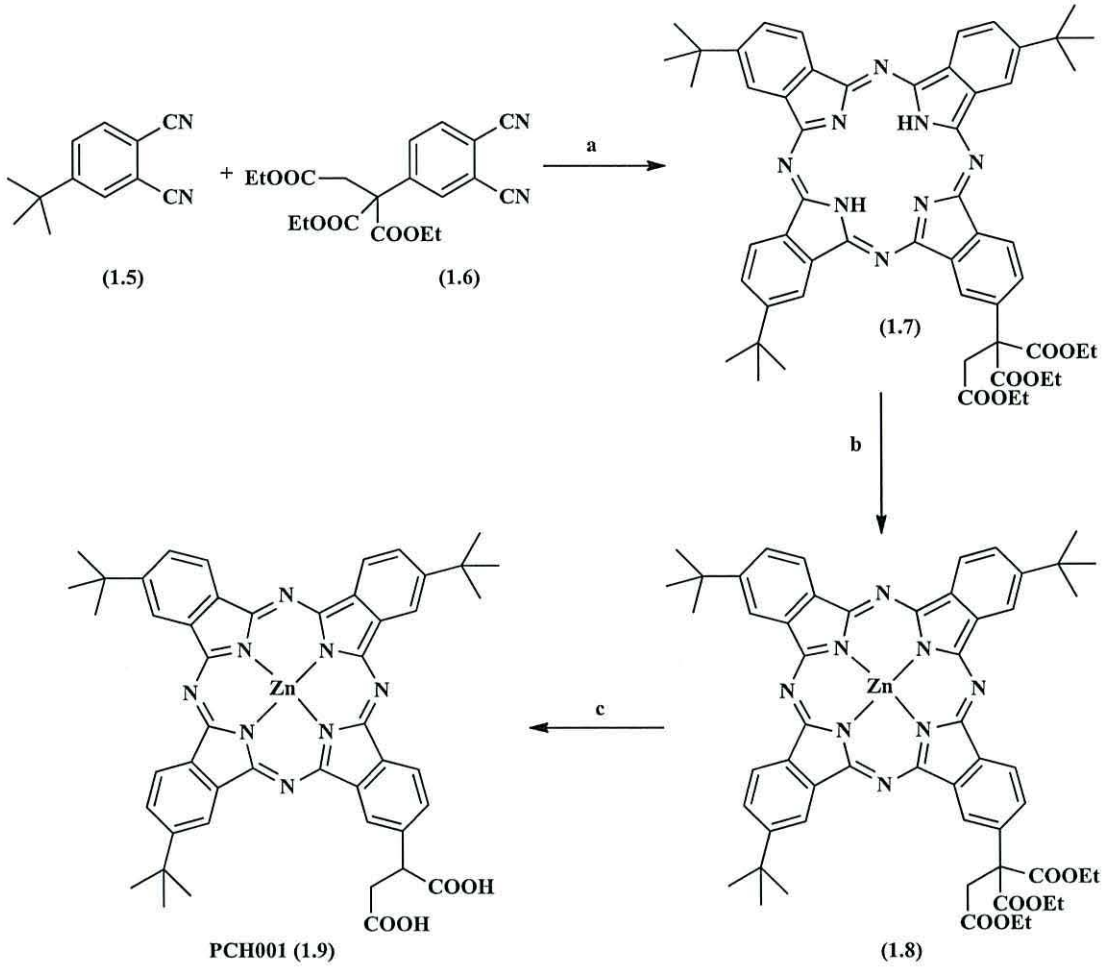

Scheme 1.1. Synthetic pathway of synthesis of **PCH001 (1.9)**, (a) DBU, pentanol, reflux 20h; (b) $Zn(OAc)_2$/DMF; (c) Na/ethanol 7 d. [97]

Girribabu *et al.* [95] reported a related unsymmetrical zinc phthalocyanine containing six alkoxy and two carboxylic groups **PCH003 (1.10)** Figure 1.9. These sensitizers gave (η) 3.5% for **PCH001 (1.9)** and 1.13% for **PCH003 (1.10)**.

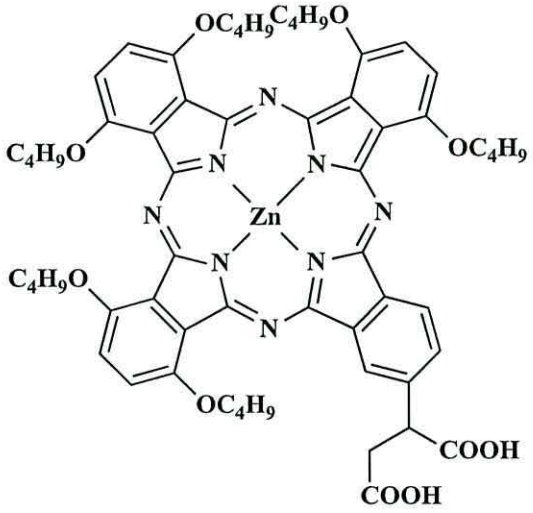

PCH003 (1.10)

Figure 1.9. Molecular structure of the unsymmetrical zinc phthalocyanine **PCH003 (1.10)**. [95]

Cid *et al.* [98] reported a new zinc-carboxyphthalocyanine **TT1 (1.12)**, which was synthesized by oxidation of the corresponding aldehyde compound (**1.11**) with sulfamic acid, as shown in Scheme 1.2.

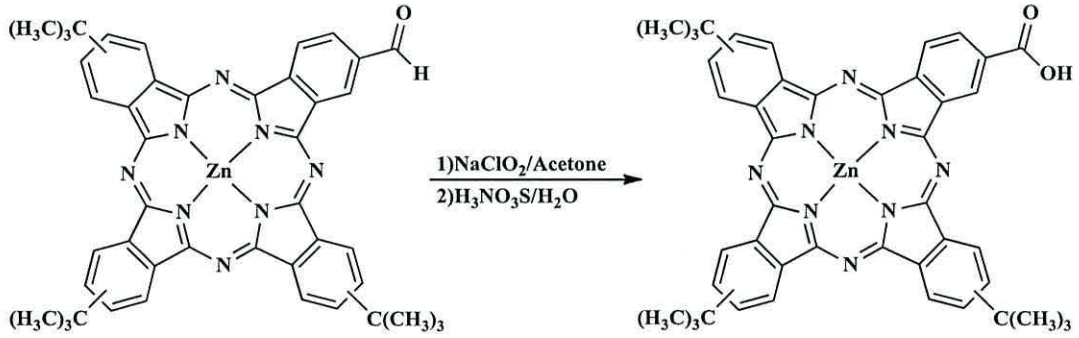

(1.11) **TT1 (1.12)**

Scheme 1.2. The synthetic pathway of zinc-carpoxyphthalocyanine **TT1 (1.12)**. [98]

TT1 (1.12) is composed of a carboxylic acid group which is linked directly to the Pc ring, and three *tert*-butyl groups that not only increase the solubility of **TT1 (1.12)** but also to minimize aggregation. This compound shows absorption at 680 nm in ethanol.

The long term stability of dye sensitized solar cells is another important factor that led Garcia-Iglesias *et al.* [99] to study the effect of anchoring groups on the stability of

the unsymmetrical zinc phthalocyanines **TT9 (1.13)** and **TT1 (1.12)** in DSC devices, (Figure 1.10).

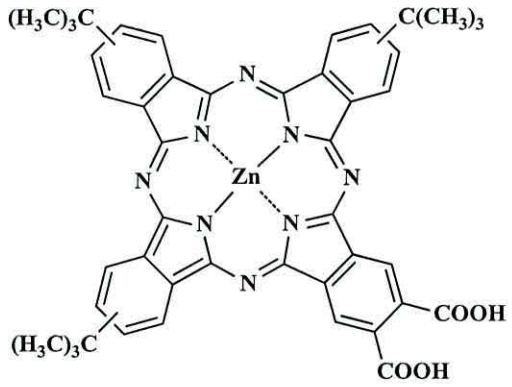

TT9 (1.13)

Figure 1.10. Molecular structure of zinc carboxyphthalocyanine **TT9 (1.13)**. [99]

After light soaking at 60°C for 1000 h, the **TT1 (1.12)** devices showed half the J_{sc}, while the **TT9 (1.13)** solar cell had not changed. This test shows the effect of number of anchoring groups on the stability of phthalocyanine dyes.

Several groups have also studied the influence of spacers between the anchoring group and the Pc sensitizer. Torres, Nizeeruddin and Palomore [96, 100] reported a series of Pc derivatives which contained mono-carboxylic acids as anchoring groups, as shown in Figure 1.11. These spacers were compared with **TT1 (1.12)** where the carboxylic acid (anchoring group) was directly connected to the Pc macrocycle.

The IPCE data for the Pc with insulating alkoxy or aryloxy spacers **(5** and **6)** showed lower η (1%). In contrast, dyes **(7, 10** and **11)** produced average power conversion efficiencies (2%), whilst **(8)** and **(9)** produced the best efficiency due to the rigid π-conjugated bridges which helped electronic coupling between the Pc dye and the semiconductor surface, (Table 1.1). These workers suggested that the anchoring group should remain as close as possible to the chromophore to get better coupling between dye and semiconductor of the TiO_2.

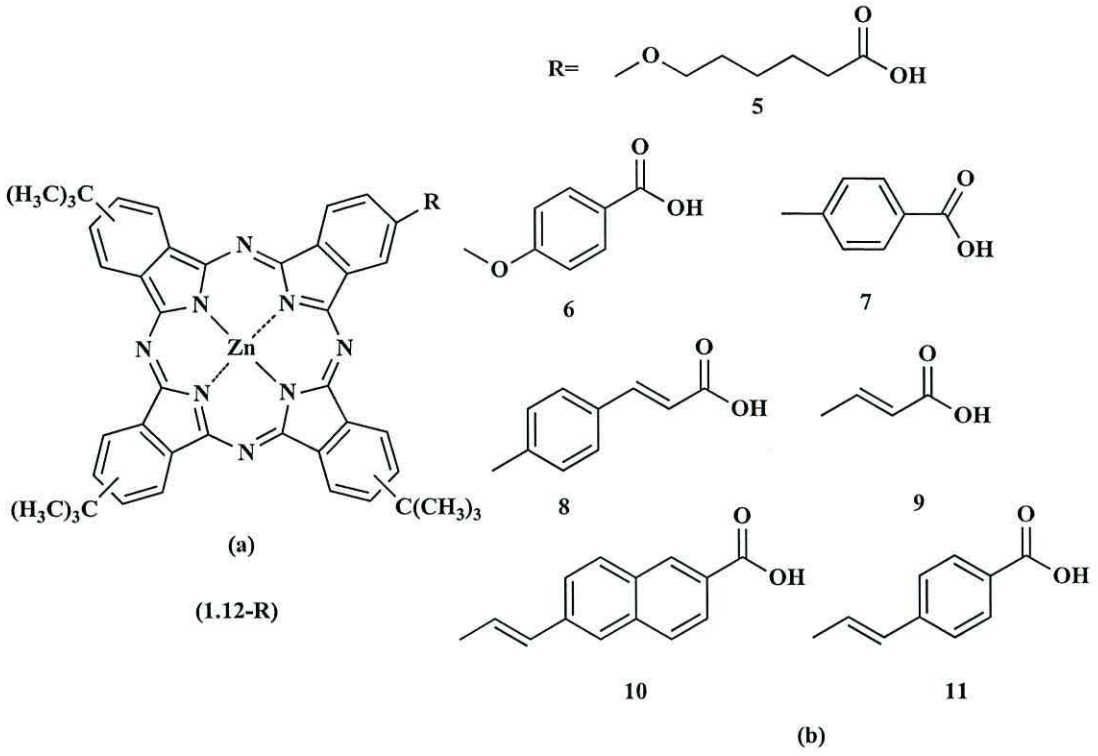

Figure 1.11. Molecular structure of (a) tri-*tert*-butyl carboxy-Zn (II) phthalocyanine (**1.12-R**), (b) bearing different spacers between the macrocycle and the carboxylic acid group.[96]

Table 1.1. Comparative photovoltaic data of tri-*tert*-butyl carboxy-Zn (II) Pc dyes bearing different spacers between the Pc and the carboxylic acid linker group.

Sensitizer	**TT-1 (1.12)**	**5**	**6**	**7**	**8**	**9**	**10**	**11**
η%	3.52	0.40	0.67	2.20	3.10	3.28	2.20	1.87

Eu *et al.* [101] synthesized and reported photovoltaic properties of a new zinc phthalocyanine carboxylic acid **ZnPc (1.17)** and metal-free **H_2Pc (1.16)** (Figure 1.12) using six bulky *tert*-butylphenyl groups to increase dye solubility and reduce aggregation. The precursor **1.14** was prepared by Suzuki-coupling reaction between 4, 5-dichlorophthalonitrile and 4-t-butylphenylboronic acid. The precursor **1.15** also was prepared using same reaction but between 4, 5-dichlorophthalonitrile and 4-(methoxycarbonylphenyl) boronic acid, as shown in Scheme 1.3.

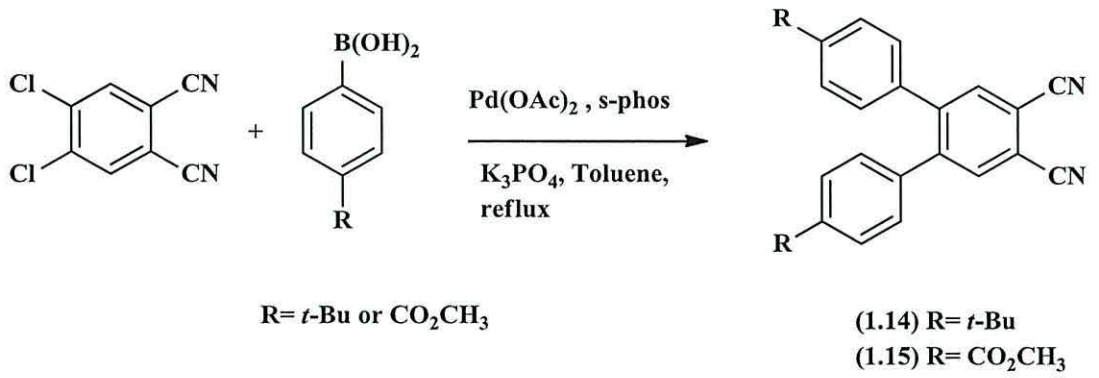

Scheme 1.3. The synthetic pathway of precursors **1.14** and **1.15**.

The H_2Pc was prepared by condensation of (**1.14** and **1.15**) in 1-pentanol in the presence of DBU (1,8-diaza-bicyclo[5.4.0]undec-7ene) to produce an ester that was then hydrolyzed in THF/methanol containing 40% KOH to produce H_2Pc. ZnPc was prepared by inserting zinc acetate to the core of the phthalocyanine esters. The resulting compound was hydrolyzed in THF/methanol containing 40% KOH to produce the desire compound ZnPc. H_2PC and ZnPc show maximum absorption at 681 and 691 nm in THF solution,

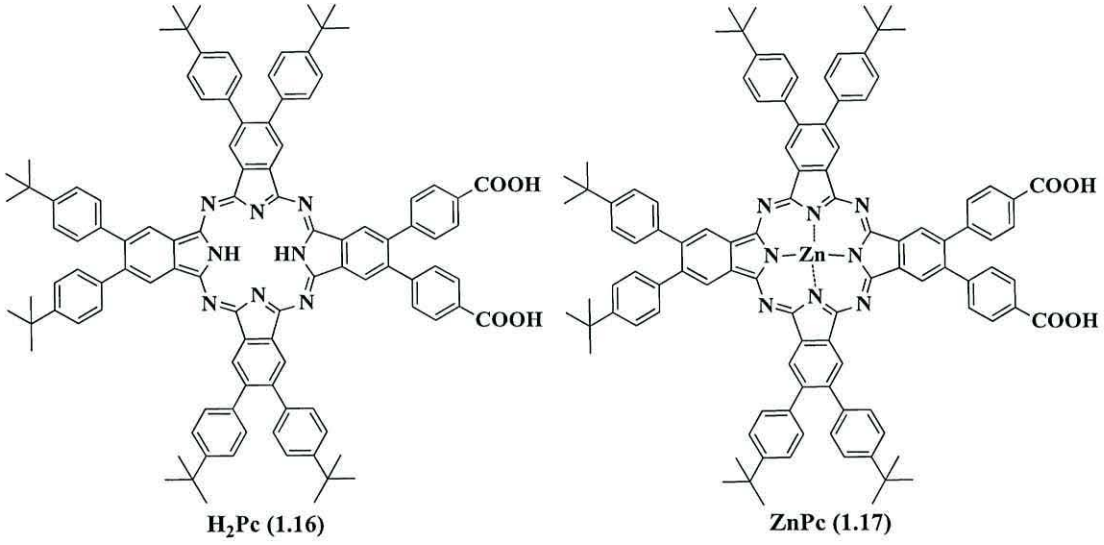

Figure 1.12. Molecular structure of phthalocyanine zinc carboxylic acid **ZnPc (1.17)** and metal-free **H_2Pc (1.16)**. [101]

The ZnPc showed a low conversion efficiency 0.57% so chenodeoxycholic acid (CDCA) was introduced as a coadsorbent to minimize the aggregation of ZnPc, but the result obtained remained poor which may have been due to poor electrical

linkage between the Pc sensitizer and the TiO_2 conduction band of the semiconductor through the inefficient phenylene spacer.

Yum *et al.* [102] studied the effect of adding chenodeoxycholic acid (CDCA, figure 1.13) to the **TT1 (1.12)** sensitizer, showing an increase in open-circuit voltage (V_{oc}), due to the band edge of TiO_2 being shifted to more negative potentials. [102] The coadsorbent led to a decrease of photocurrent (Table 1.2) due to less sensitizer being absorbed, because the CDCA occupies sites on the TiO_2 surface. Furthermore the J_{sc} was slightly increased by increasing the film thickness up to 9 μm showing (η) = 2.91% without CDCA, and 3.56% with CDCA.

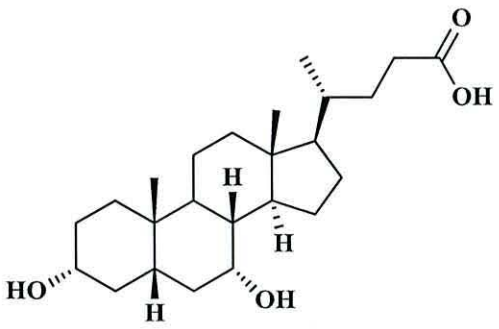

Figure 1.13. Molecular structure of the chenodeoxycholic acid **(CDCA)** coadsorbent. [96]

Table 1.2. Photovoltaic parameters of DSSCs with different **TT1/CDCA** ratios. [102]

CDCA (mM)	Thickness (μm)	J_{sc} (mA cm^{-2})	V_{oc} (mV)	η (%)
0	6	7.03	580	2.91
1	6	6.55	603	2.93
10	6	5.93	614	2.71
60	6	2.28	632	1.08
1	9	6.71	616	3.10
10	10 + 4	7.78	611	3.56

Recently, other reports have focussed on reducing aggregation of unsymmetrical zinc phthalocyanines. S. Mori *et al.* [103] reported a bulky unsymmetrical zinc phthalocyanine contain diphenylphenoxy groups to prevent aggregation and produced (η) = 4.6%, as shown in Figure 1.14. This higher efficiency result was

obtained without using CDCA as coadsorbent, due to the bulky groups reducing dye aggregation.

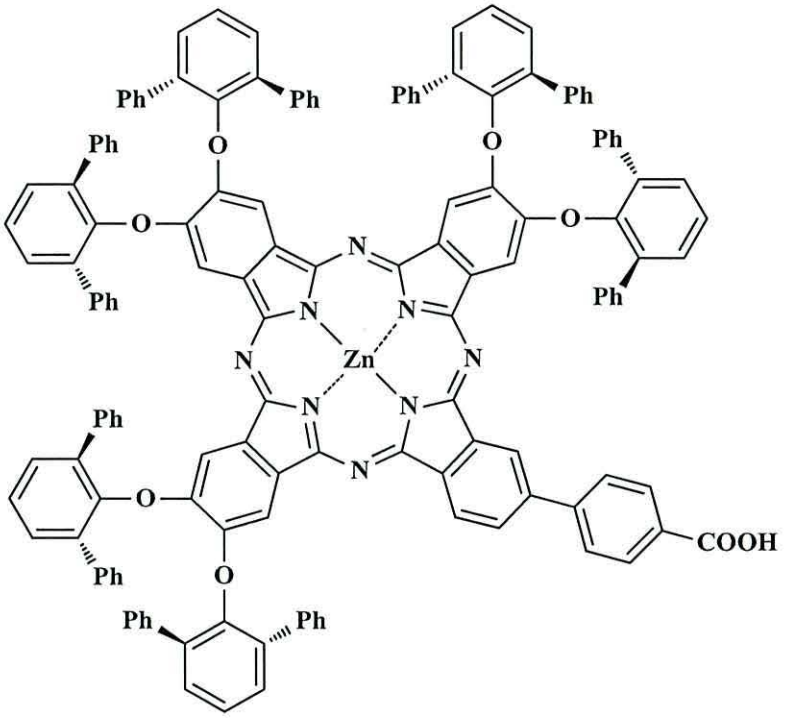

(1.18)

Figure 1.14. Molecular structure of phthalocyanine (**1.18**). [103]

Recently, Yella *et al.* [30] reported the highest DSC efficiency (12.3%) by using the zinc porphyrin dye (**YD2-*o*-C8**, **1.19**), Figure 1.15a, with two octyloxy groups in the *ortho* position of each *meso*-phenyl ring. The best devices were co-sensitized with the triphenylamine dye (**Y123**, **1.20**), (Figure 1.15b). Co $^{(II/III)}$ tris (bipyridyl) (**1.21**) was used as a redox electrolyte (Figure 1.15c) instead of traditional iodide/triiodide redox couple, due to the higher reduction potentials than that of I^-/I_3^-. [30]

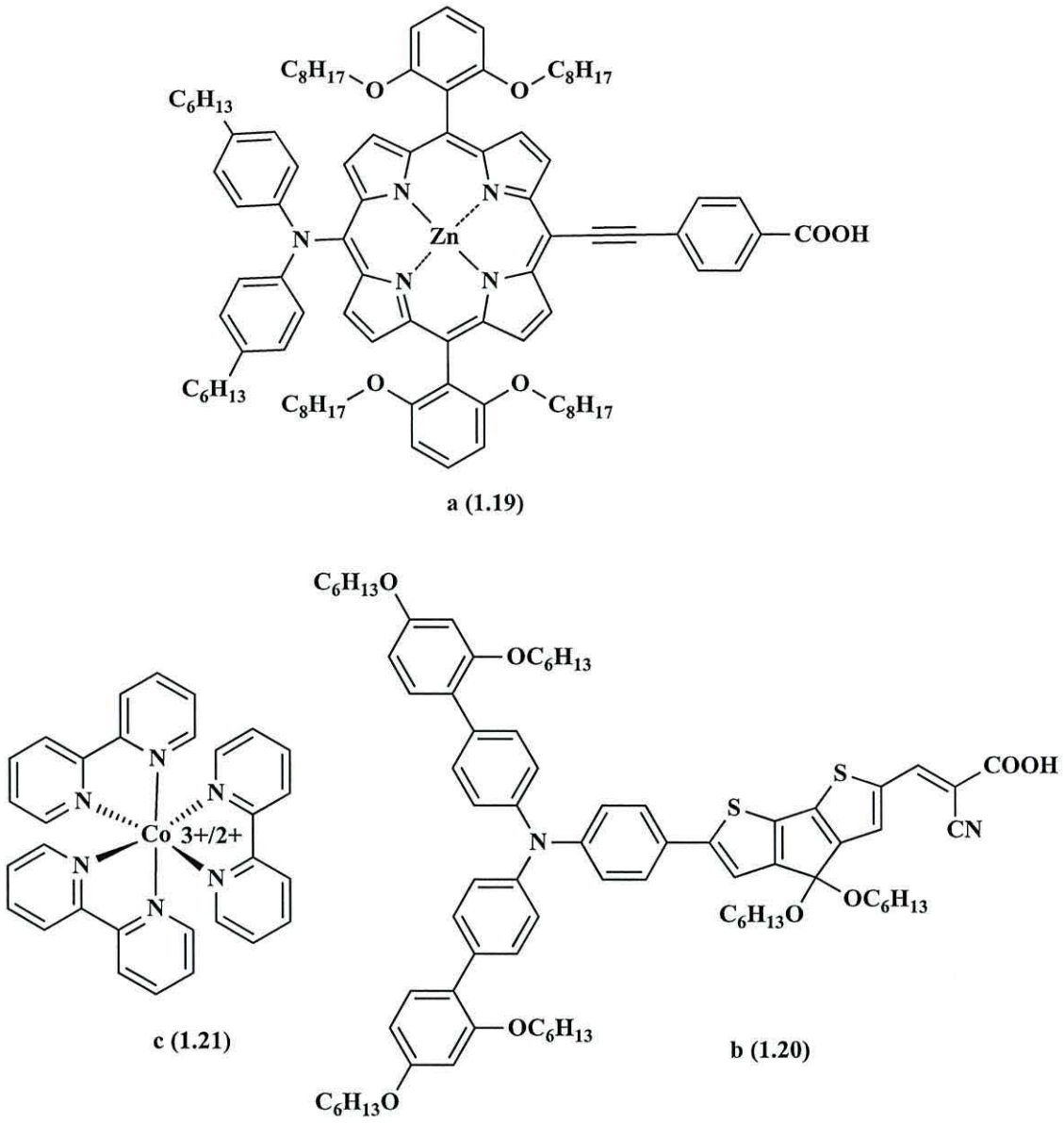

Figure 1.15. The molecular structure of the (a) porphyrin dye **YD2-*o*-C8 (1.19),** [30] (b) of the **Y123 (1.20)** dye [104] and (c) tris bipyridine cobalt complex (**1.21**). [104]

1.7.2 Metal-free organic dyes

1.7.2.1 Triphenylamine dyes

Metal-free organic dyes with D-π-A system consisting of a donor moiety, π-conjugated linker and acceptor group (Figure 1.16) are an alternative to ruthenium complex dyes. Recently, these have received more attention because they a) can be easier to design these types of dyes in variety molecular structures, b) can be cheaper

than ruthenium complexes and c) have higher molar extinction coefficients. There are many different types of metal-free organic dyes. In this thesis, the triphenylamine (TPA) moiety has been studied. This is the most commonly used electron-donor moiety in metal-free organic dyes, [105] and is expected to restrict the cationic charge on the semiconductor surface. In addition the steric hindrance of TPA helps reduce dye aggregation on the semiconductor surface. [106]

The donor groups play an important role in tuning the energy levels of sensitizers to affect the absorption spectra. [58] Hence the choice of a suitable donor groups in the D-π-A system is critical to the balance between photovoltage and spectral response. [107, 108, 109] The thickness of TiO_2 layers plays an important role in enhancing light absorption, but this can increase losses due to the longer transport distances in thicker films. [110, 111] Finally, the sensitizers can avoid π-stacked aggregation by using coadsorbents. [112, 96]

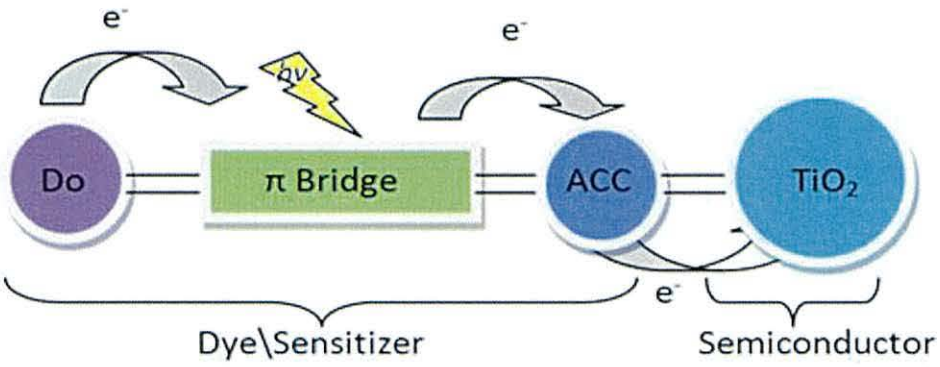

Figure 1.16. Design principle of an organic dye (D-π-A) system linking with TiO_2 photoanodes in DSC. [113]

1.7.2.1.1 Cyanoacrylic Acid as Acceptor and Anchoring Group

The carboxylic acid group is one of the most widely used anchoring groups. [114] In addition their derivatives e.g. carboxylate salts, esters, acetic anhydrides, acid chlorides and amides have also been tested as anchoring groups. [7] There are a variety linking types between the carboxylic acid and semiconductor surface [114] depending on the dye structure, pH, and the semiconductor preparation. Galoppini and co-workers [114] have tested the linking modes for porphyrin sensitizers with carboxylic

acid anchoring groups. Fennie *et al.* [115] have also studied dyes binding on metal oxides and suggested three possible carboxylate binding modes, as shown in Figure 1.17.

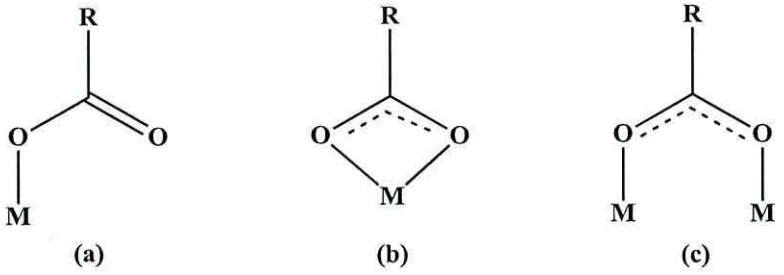

Figure 1.17. The possible carboxylate coordination modes: (a) unidentate, (b) bidentate chelating and (c) bridging. [115]

The strong electronic withdrawing properties makes cyanoacrylic acid another commonly used as acceptor group. The electronic withdrawing properties of the nitrile group affect the acidity of the carboxylic acid leading to stronger linking to the TiO_2. Researchers have developed new organic dyes using different types of acceptor, [116, 117] like those shown in Figure 1.18 which have been linked with indoline dyes to investigate as the DSC performance. [118]

Figure 1.18. Example of different acceptor groups of thiophene carboxylic acid or cyanoacrylic acid. [118]

There is another study reported by Hagberg *et al.* [119] which studied the influence of the linker groups on the HOMO and LUMO energy levels, using different type of linkers (Figure 1.19). They observed dyes **L0-L4** showed satisfactory efficiencies on TiO_2 and the longer linker increased conjugation and spectral response. The **L2** dye shows the highest efficiency (3.08%). In contrast, **L3** and **L4** showed lower efficiency which could be due to the orientation on the surface and/or structure.

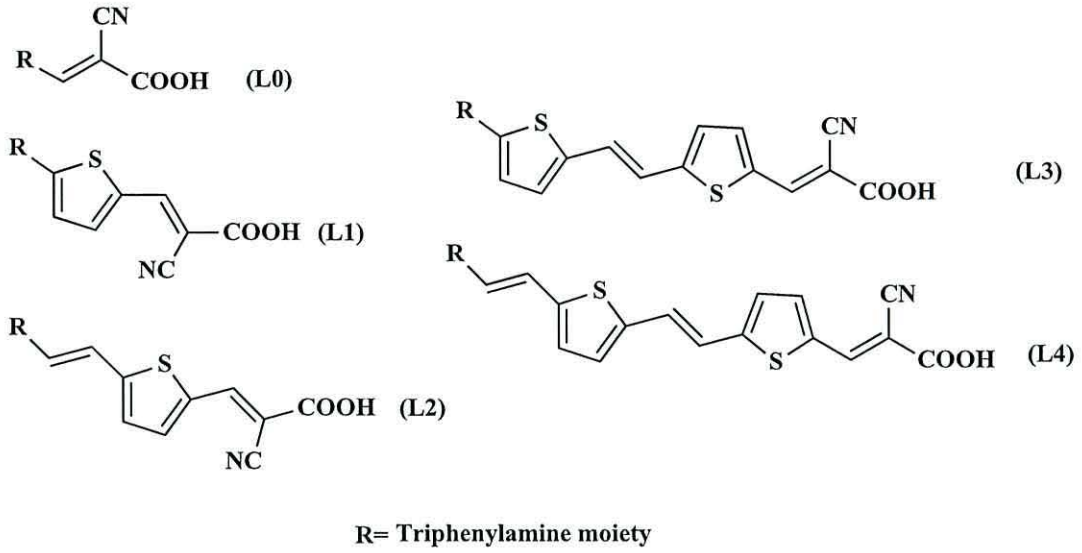

Figure 1.19. Molecular structure of different linker groups **L0**, **L1**, **L2**, **L3** and **L4** with cyanoacrylic acid as acceptor group. [119]

Wei Xu *et al.* [120] studied the influence of the acceptor group by synthesizing two different types of dyes 2-(4-oxo-5-(4-(phenyl (4-styrylphenyl) amino) benzylidene)-2-thioxothiazolidin-3-yl) acetic acid **TPAR11** (**1.22**) and 2-cyano-3-(4-(phenyl (4-styrylphenyl) amino) phenyl) acrylic acid **TC12 (1.23)**, Figure 1.20.

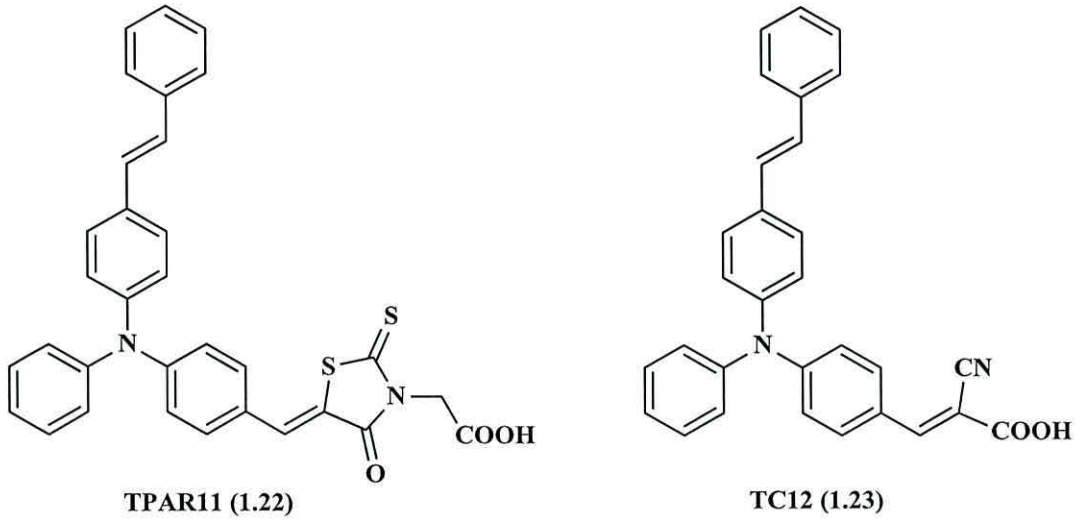

Figure 1.20. Molecular structure of **TPAR11** (**1.22**) and **TC12** (1.23) dyes. [120]

These workers also reported that, the addition of CDCA increased the performance for both dyes, (Table 1.3). The UV-Vis spectrum showed the maximum absorption for **TPAR11** (1.22) was higher than **TC12** (**1.23**), due to rodanine-3-acetic acid

extending the π-conjugated system. Finally, this study showed that **TPAR11 (1.22)** produced higher photocurrent while **TC12 (1.23)** produced higher photovoltage.

Table 1.3. Photovoltaic performance of DSCs based on **TPAR11 (1.22)** and **TC12 (1.23)** with or without addition of CDCA. [120]

Dye	CDCA (mM)	V_{oc} (mV)	J_{sc} (mA cm^{-2})	FF	η (%)
TPAR11 (1.22)	0	560	13.5	0.62	4.67
	1	569	16.1	0.60	5.46
TC12 (1.23)	0	638	12.6	0.63	5.05
	1	734	12.9	0.63	5.96

Similar studies on the influence of the acceptor groups have been done before. Ito *et al.* [49] utilized rhodanine-3-acetic acid as acceptor group with the indoline-based dyes and gained a conversion efficiency 9.03%. Also Hara *et al.* [121, 44] employed cyanoacrylic acid as an acceptor group with coumarin-based dyes. They obtained a range of overall conversion efficiencies (3.1% - 7.7%).

The highest conversion efficiency for metal-free organic dyes (10.3%) was obtained by Zeng *et al.* [122] for the **C219 (1.24)** dye as shown in Figure 1.21. This dye is composed of a π-conjugated spacer, a lipophilic alkoxy-substituted triphenylamine electron donor moiety and hydrophilic cyanoacrylic acid electron acceptor group. In this design, the 3,4-ethylenedioxythiophene (EDOT) is linked to the donor moiety to lift up the HOMO, and they introduced dihexyl-substituted dithienosilole (DTS) to reduce the π-π stacking of dye molecules on the semiconductor surface and linked this with the acceptor group to keep a suitable LUMO.

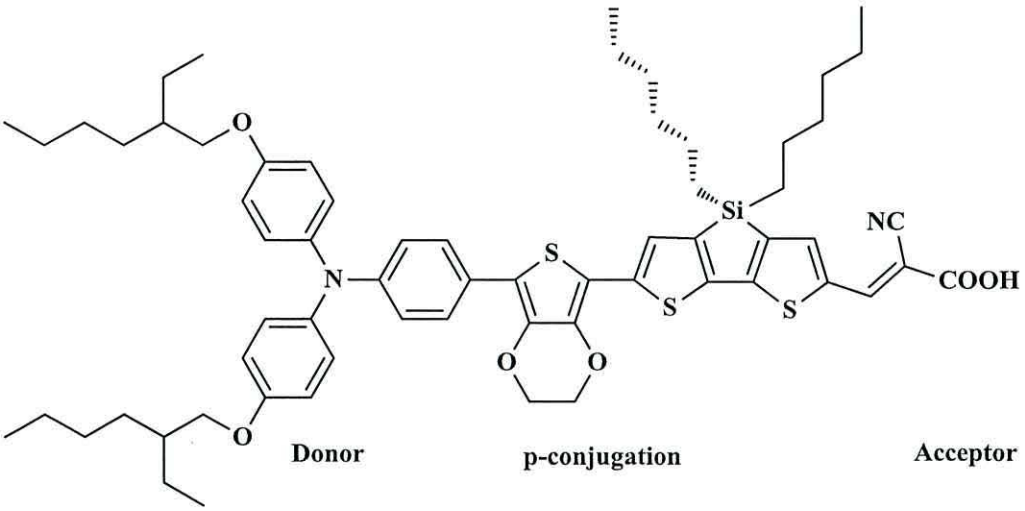

C219 (1.24)

Figure 1.21. Molecular structure of **C219 (1.24)**. [122]

Hwang *et al.* [123] reported a new DSC dye **TA-St-CA (1.27),** (Scheme 1.4) which gave of η = 9.1 %. This dye was based on a triphenylamine donor group, a p-conjugated oligo-phenylenevinylene spacer and a cyanoacrylic acid acceptor moiety.

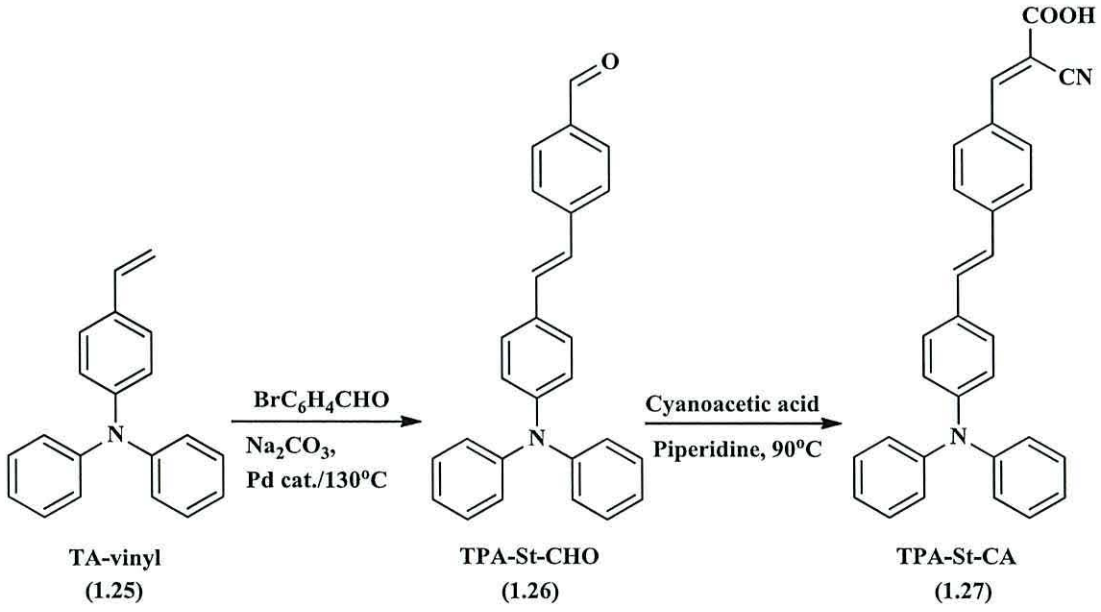

Scheme 1.4. The synthetic pathway of the **TA-St-CA (1.27)** dye. [123]

They synthesized this dye by three steps, started with prepared TA-vinyl (**1.25**) by a Wittig reaction of 4(N,N-diphenylamino)benzaldehyde, followed by a Heck-coupling reaction between TA-vinyl with 4-bromobenzaldehyde to produce **TPA-St-CHO (1.26)**, and finally used a Knoevenagel reaction to produced **TPA-St-CA (1.27)**. The

UV-Vis of **TA-St-CA (1.27)** shows a maximum absorption at 386 nm in ethanol (ε= 31600 $M^{-1}cm^{-1}$).

Chen *et al.* [124] synthesised a new type of organic sensitizers by using 1, 3-cyclohexadiene as a conjugated spacer moiety to link the acceptor group with the donor group leading to efficiency of 4.4%. **(1.28)**, **(1.29)**, **(1.30)** and **(1.31)** dyes show λ_{max} at 391, 387, 379 and 404 nm, respectively. The device performances of these dyes are in Table 1.4. The structures of these dyes are shown in Figure 1.22. They reported that the benefit of using the 1, 3-cyclohexadiene group was that it gave a planar conformation which yield more dense packing of the adsorbed dye on the TiO_2 surface.

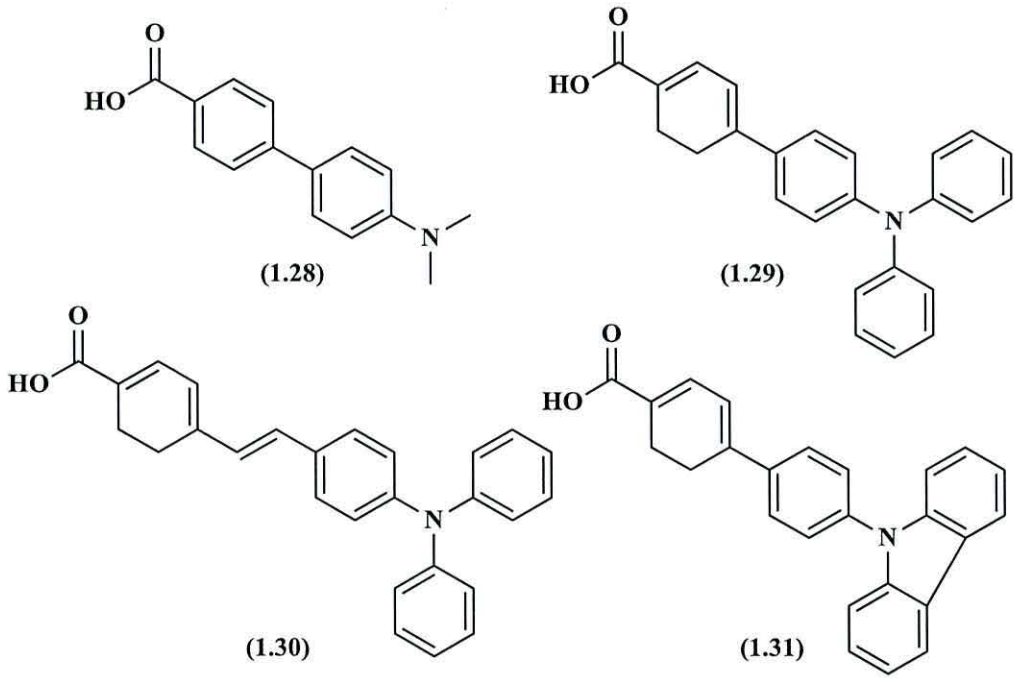

Figure 1.22. Structure of organic dyes reported by Chen *et al.* [124]

Scheme 1.5 explains the pathways to synthesize, dyes **(1.28)**, **(1.29)** and **(1.30)** by an elimination reaction of 4-bromo-N-carbazoyl-benzenamine, 4-bromo-N, N-dimethylbenzeneamine or 4-bromo-N, N-diphenylbenzeneamine with 3-ethoxycyclohex-2-enone to first produce **1a**, **1b** and **1c**. Then esterification with ethyl chloroformate produced **2a**, **2b** and **2c**. The ester compounds **3a-c** were obtained by consecutive steps of reduction of cyclohexenone, methanesulfonylation and elimination. The last step was to hydrolyze the ester to the carboxylic acid to get

compounds (**1.28**), (**1.29**) and (**1.30**). They followed the same synthetic route to prepare compound (**1.31**).

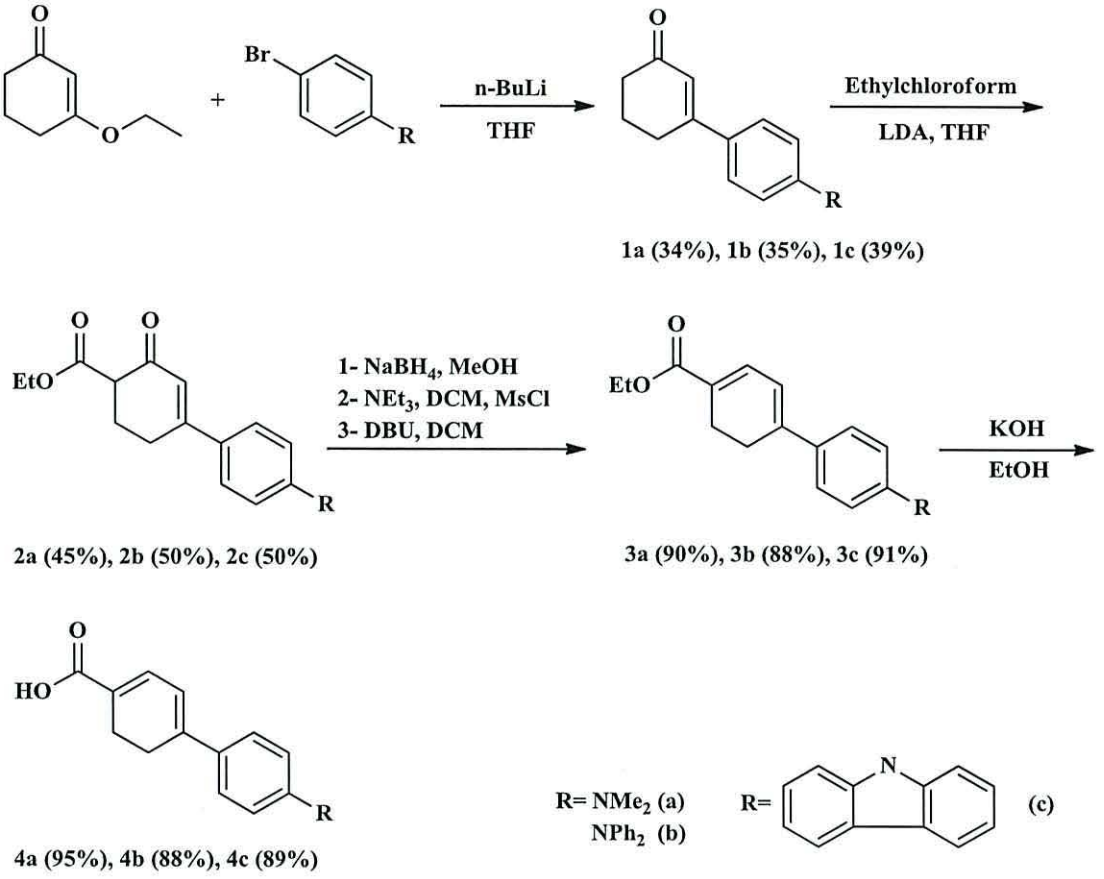

Scheme 1.5. Synthetic pathway of the dipolar dyes **4a-c**. [124]

Table 1.4. Photovoltaic Performance of (**1.28**), (**1.29**), (**1.30**), (**1.31**) and **N719** dyes. [124]

Dye	V_{oc} (mV)	J_{sc} (mA cm^{-2})	FF	η (%)
(1.28)	577	7.89	0.59	2.69
(1.29)	660	9.40	0.65	4.03
(1.30)	626	7.92	0.66	3.27
(1.31)	660	7.39	0.64	3.33
N719	695	11.9	0.71	5.87

Recently, theoretical and practical studies have shown the nonplanar structure of the TPA-group plays important role in DSCs and prevents aggregation. [125] Also there is

another study which has proven linking the spacer to lateral alkyl chains can increase efficiency. [50, 126]

Bo *et al.* [127] reported four types of metal-free organic dyes based on triphenylamine as a donor moiety as shown in Figure 1.23. These were designed based on the following factors. Firstly, they have a donor-π- acceptor design which consists of three components; (the triphenylamine group could be prevent I^-/I_3^- from reaching the TiO_2 film, a semi-rigid conjugated phenylethyne linker to favour electron injection, and a cyanoacrylic or carboxylic acid acceptor and anchor group).
Also they designed (**1.32**) and (**1.35**) with two dodecyloxy chains on the phenylethyne linker unit, to increase the electron lifetime and produce a higher V_{oc}.

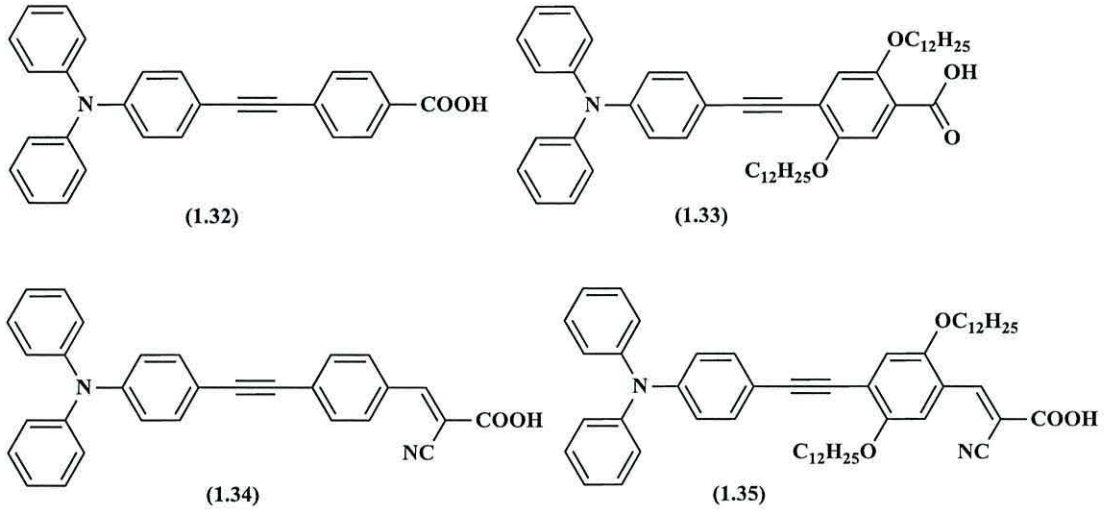

Figure 1.23. Molecular structure of (**1.32**), (**1.33**), (**1.34**) and (**1.35**). [127]

The UV-Vis spectrum of these dyes showed maximum absorption at 376, 399, 393 and 407 nm, respectively. Also (**1.34**) and (**1.35**) which included a cyanoacrylic acid group showed broader absorption than (**1.32**) and (**1.33**) which only have carboxylic acids. In addition the extra conjugation for (**1.34**) and (**1.35**) led to a red shift. Table 1.5 shows efficiency of 2.0-3.6% for these dyes.

Table 1.5. Photovoltaic performance of dye (**1.32**), (**1.33**), (**1.34**), (**1.35**) and **N719** devices. [127]

Dye	V_{oc} (V)	J_{sc} (mA/cm^2)	FF	η (%)
N719	0.66	14.82	0.47	4.54
(1.32)	0.70	4.62	0.62	2.00
(1.33)	0.71	8.56	0.47	2.89
(1.34)	0.79	6.64	0.59	3.06
(1.35)	0.73	9.30	0.49	3.61

Humbae *et al.* [128] synthesised other metal-free organic dyes based on the donor-π-acceptor model, **TA-DM-CA (1.36)**, **TA-TM-CA (1.37)** and **TA-HM-CA (1.38)**, (Figure 1.24).

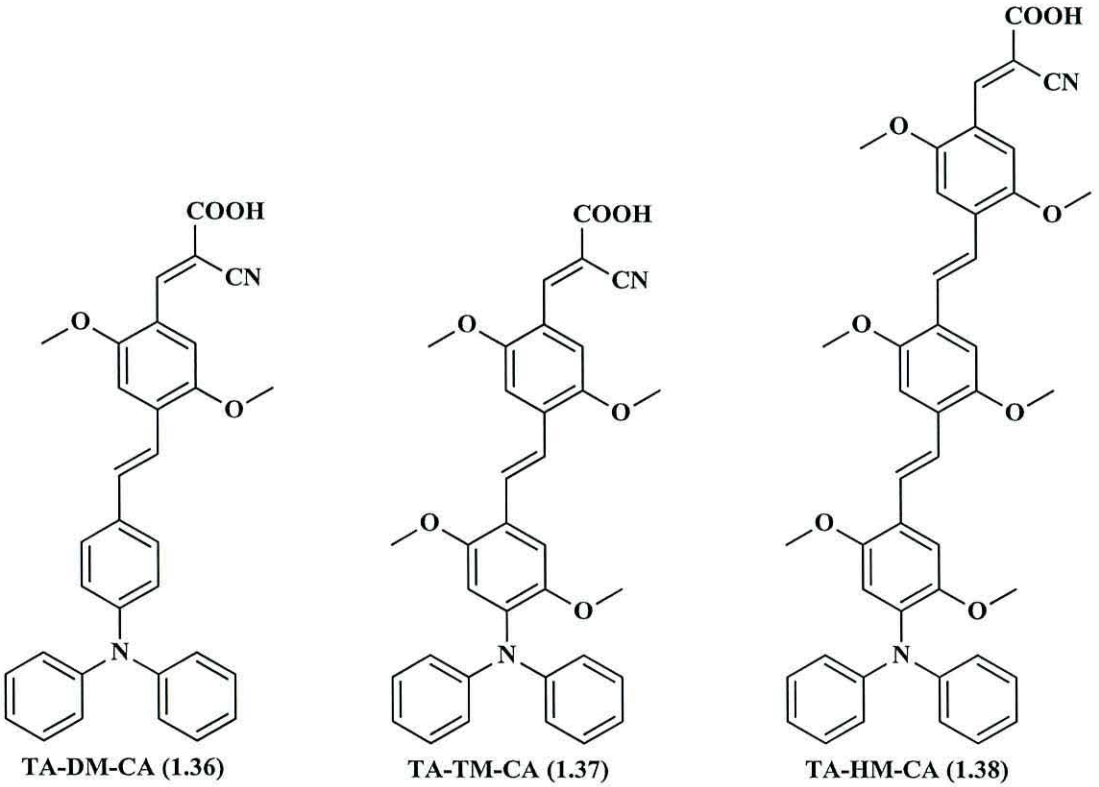

Figure 1.24. Molecular structure of the organic dyes **TA-DM-CA (1.36)**, **TA-TM-CA (1.37)** and **TA-HM-CA (1.38)**. [128]

These were similar to the Hwang dyes, but included an oligo-phenylenevinylene spacer with methoxy-substitution to increase electron donation into the π-conjugation

and to red shift the absorption. [129] **TA-HM-CA (1.38)** shows an absorption at 451 nm (ε= 39500 $M^{-1}cm^{-1}$) which is a slight red shift more than other dyes due to the extended π-conjugated spacer unit, whilst the **TA-DM-CA (1.36)** and **TA-TM-CA (1.37)** dyes show absorption at 433 nm (ε= 46100 $M^{-1}cm^{-1}$) and 432nm (ε= 23200 $M^{-1}cm^{-1}$), respectively.

The **TA-DM-CA (1.36)** dyes show higher conversion efficiency (9.67%) compared with the two other dyes, which was ascribed to more efficient electron injection.

Park *et al.* [130] synthesized two dyes with different types of donor group to investigate the influence on photovoltaic performance; the first one consist of cyanoacetic acid as acceptor group with a phenylthiophene bridge and diethylamino group as a donor group (**1.39**), whilst the second dye used an ethoxy group as a donor group (**1.40**), Figure 1.25.

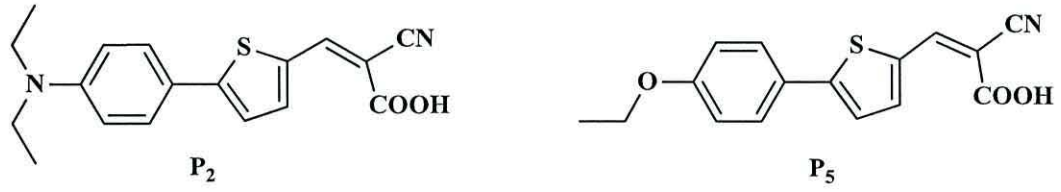

Figure 1.25. Molecular structure of (**1.39**) and (**1.40**) dye. [130]

The UV-Vis spectrum of (**1.39**) shows λ_{max} at 456 nm compared to (**1.40**) (386 nm), respectively due to the diethylamino which decreases the HOMO-LUMO gap. The molar absorption coefficients of (**1.39**) and (**1.40**) dyes were 33000 and 32000 M^{-1} cm^{-1}, respectively. They found that the HOMO level is more sensitive to changing the donor moiety, so P_2 shows higher HOMO energy and lower HOMO-LUMO gap. Other studies have focussed on the relationship between the length of π-conjugation and the energy levels [119] or between the substituents on the amino moiety and the energy levels. [131, 132]

Pei *et al.* [105] reported two new types of organic (D-π-A) dyes (**TPAR3 (1.43)** and **TPAR6 (1.46)**) containing two rhodanine-3-acetic acid groups as acceptors and based on triphenylamine as a donor linked through variety of alkene spacers (Figure 1.26).

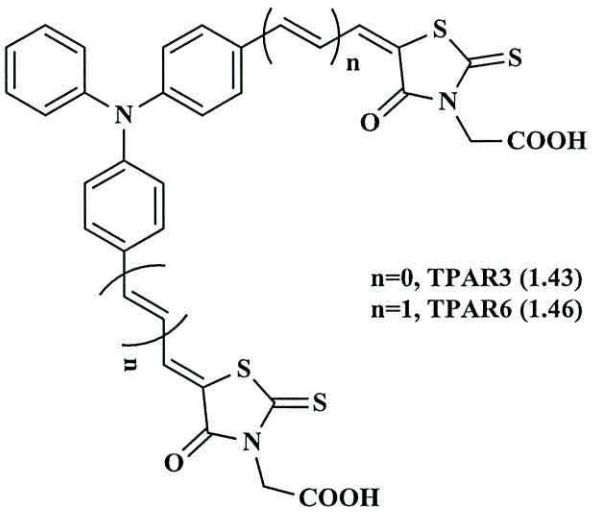

Figure 1.26. Structure of triphenylamine-based **TPAR3** (**1.43**) and **TPAR6** (**1.46**). [105]

Pei *et al.* [105] reported that **TPAR6** (**1.46**) showed longer wavelength λ_{max} higher than **TPAR3** (**1.43**) which corresponded to extended π-conjugation but higher conversion efficiency was obtained with **TPAR3** (**1.43**) of 3.27% compared with **TPAR6** (**1.46**), which shows very low efficiency (0.61%). The effect of additives like guanidinium thiocyanate GuSCN (GT) was also investigated (Table 1.6), and **TPAR3** (**1.43**) shows efficiency up to 4.02%. Increasing GT concentration up to 0.05 $mol.L^{-1}$ increased V_{oc} and FF but decreased J_{sc}, so efficiency increased to 4% at 0.100 $mol.L^{-1}$ of GT. They concluded the reason of superior performance results due to; the electron injection efficiency was increased due to the more negative LUMO energy level of **TPAR3** (**1.43**), and the electron injection into the semiconductor was competing with photoisomerization in electron transfer. Triphenylamine (**1.41**), the main precursor in this synthesis reaction, was prepared from diphenylamine and iodobenzene. Compound (**1.42**) was prepared using classical Vilsmeier-Haack reaction between (**1.41**) and $POCl_3$ in DMF. While compound (**1.44**) was produced using Wittig reaction, **1.45** was prepared using the same preparation as (**1.42**). Rhodanine-3-acetic acid was introduced to (**1.42**) and (**1.45**) with ammonium acetate and acetic acid to produce **TPAR3** (**1.43**) and **TPAR6** (**1.46**) as shown in Scheme 1.6.

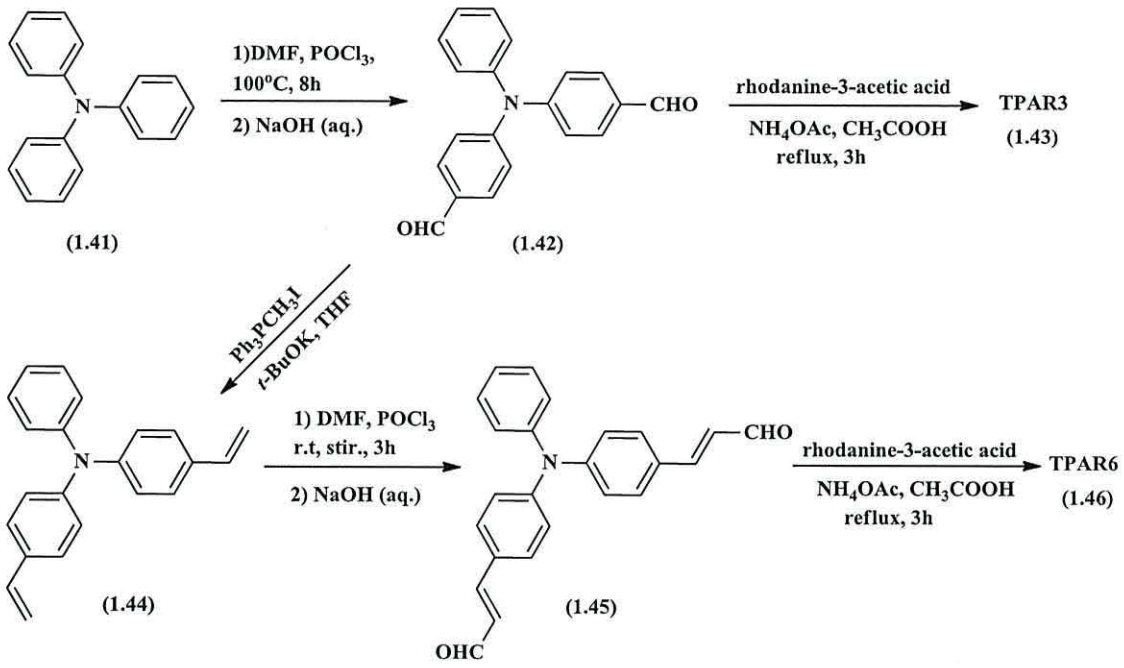

Scheme 1.6. Synthetic pathway of **TPAR3 (1.43)** and **TPAR6 (1.46)** dyes. [105]

Table 1.6. Parameters of DSCs based on **TPAR3 (1.43)** and **TPAR6 (1.46)** containing 1 mmol.L^{-1} **CDCA.** [105]

Dye	(GT) (mol L^{-1})	V_{oc} mV	J_{sc} (mA cm^{-2})	FF	η (%)
TPAR3 (1.43)	0.000	555.4	8.74	0.67	3.27
	0.025	593.5	8.51	0.68	3.43
	0.050	622.5	8.38	0.70	3.65
	0.100	696.8	8.25	0.70	4.02
	0.200	702.4	7.30	0.70	3.58
TPAR6 (1.46)	0.000	450	2.02	0.67	0.61

Hagberg *et al.* [131] reported new metal-free organic dyes (**1.47**), (**1.48**), (**1.49**) and (**1.50**) as shown in Figure 1.27. They synthesized these dyes to investigate the effect of substituted donor groups on the DSC performance. The thiophene group of (**1.48**) and (**1.50**) linked to the donor moiety using the Hornor-Wadsworth-Emmons reaction while the thiophene of (**1.47**) and (**1.49**) was linked using the Wittig reaction. Formylation of the thiophene moiety was then followed by condensation of the aldehyde to cyanoacrylic acid by using a Knoevenagel reaction in the presence of

piperidine. The UV-Vis spectrum of (**1.49**) dyes shows a maximum absorption at 462 nm (ε= 33000 M^{-1} cm^{-1}) while (**1.50**) shows absorption at 458 nm (ε= 38000 M^{-1} cm^{-1}). (**1.48**) shows the same absorption as (**1.47**) at 441 nm (33000 $M^{-1}cm^{-1}$). (**1.49**) and (**1.50**) show higher λ_{max} than (**1.48**) and (**1.50**), with a red shift in spectral absorption due to the presence of methoxy groups in the molecular structure.

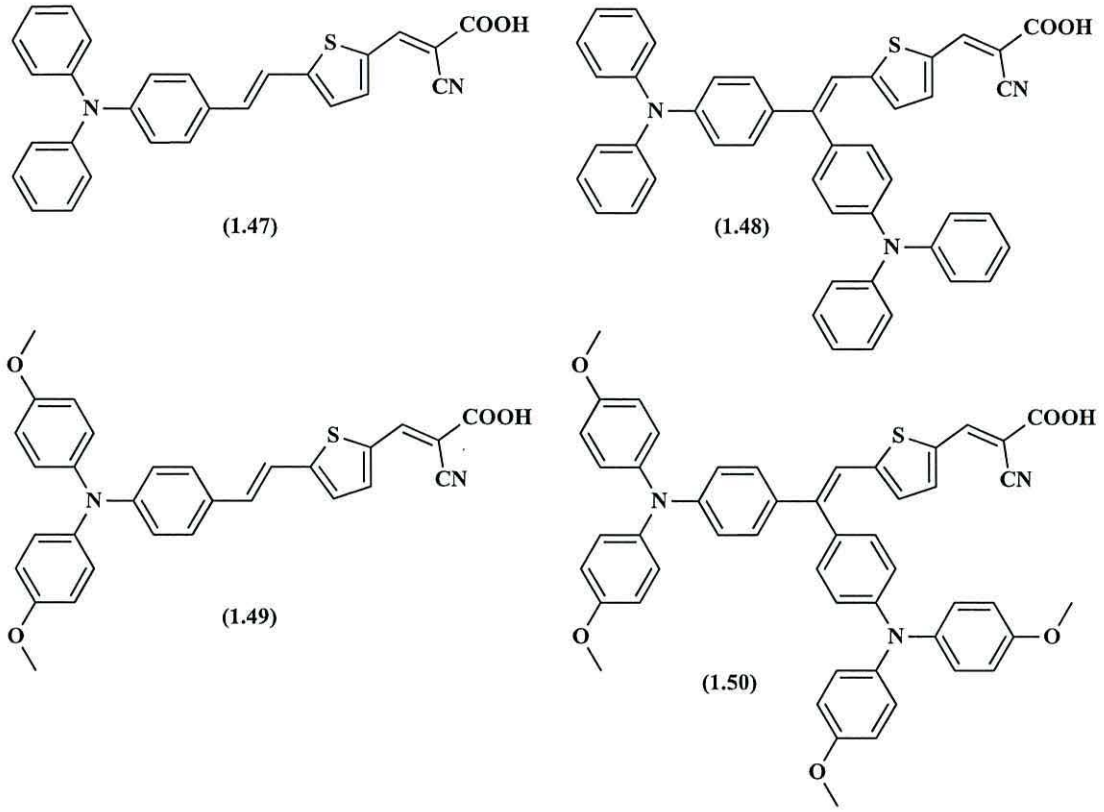

Figure 1.27. Molecular structures of (**1.47**), (**1.48**), (**1.49**) and (**1.50**). [131]

Compounds (**1.49**) and (**1.50**) produced higher photovoltage and photocurrent with efficiencies of 6.90% and 7.03%. (**1.50**) has four methoxy groups in the molecule structure compared with (**1.47**). It was suggested that the methoxy groups increased the red response and the lifetime of the conduction band electrons by preventing triiodide from recombining with the injected electrons in the TiO_2 conduction band, leading to increased V_{oc}.

Long term stability is one of the features of ruthenium dyes; e.g. ruthenium polypyridyl complexes can withstand thermal or light-soaking for at least 1000 h while keeping efficiency above 7%. [133, 134] Coumarin is a metal-free organic dye with good photovoltaic properties. Wang *et al.* [133] investigated the long term stability of

the new coumarin dye 2-cyano-3-{52-[1-cyano-2-(1,1,6,6- tetramethyl-10-oxo-2,3,5,6-tetrahydro-1*H*,4*H*,10*H*-11-oxa-3aazabenzo[*de*]anthracen-9-yl)-vinyl]-[2,22]bithiophenyl-5-yl}- acrylic acid (**1.51**), as shown in Figure 1.28.

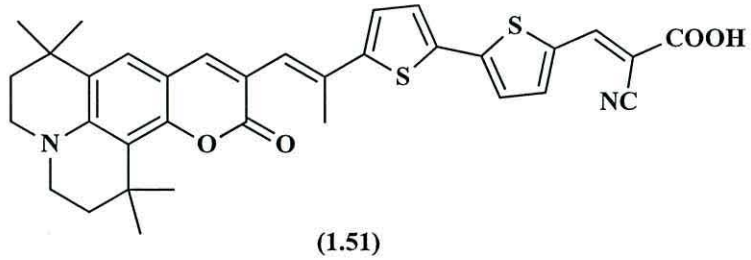

(1.51)

Figure 1.28. Molecular structure of the coumarin dye (**1.51**). [133]

This dye shows a broad absorption at 552 nm (ε= 97400 M^{-1} cm^{-1}). They investigated the stability of this coumarin dye by light soaking at 50-55°C using a non-volatile electrolyte and the dye showed good long term stability, as shown in Figure 1.29. Figure 1.29 shows that the J_{sc} increased up to 800 h and after that J_{sc} remained stable up to 1000 h. The V_{oc} decreased gradually from 0.53 V to 0.48 V, while FF increased slightly up to 150 h and followed dropped slowly up to 600 h; after that it remained stable up to 1000 h. Finally, the efficiency (η) increased slightly up to 150 h, and was then stable up to 1000 h. The stability data shown in Figure 1.29 prove that the organic dyes also have good photostability, similar to ruthenium polypyridine complexes which are used more frequently in DSC devices.

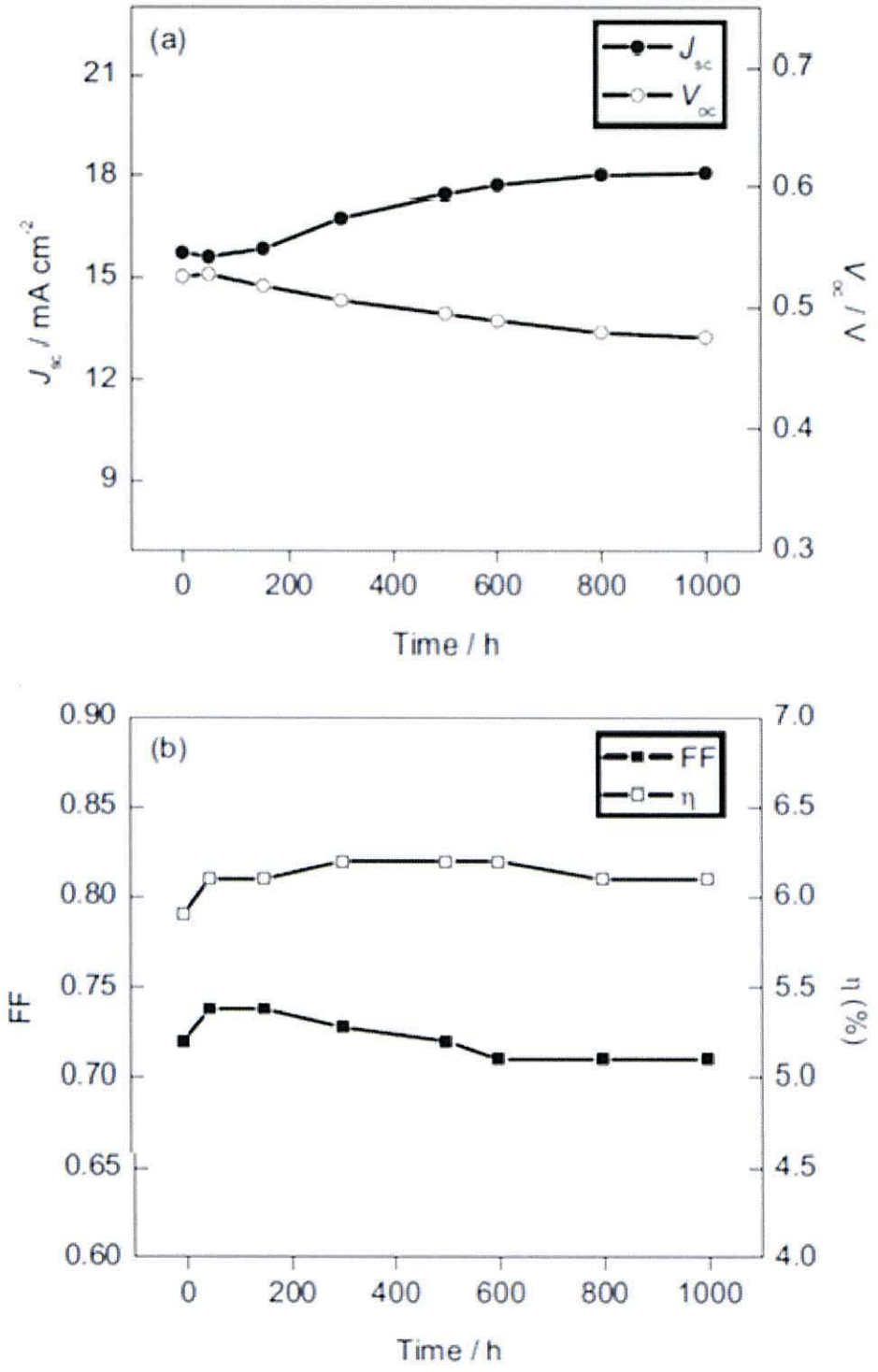

Figure 1.29. Evalution of solar cell parameters during visible-light soaking (AM 1.5G, 100 mWcm^{-2}) at 50-55°C A 420 nm cut-off filter was put on the cell surface during illumination. a) J_{sc} and V_{oc}, b) FF and η for coumarin dye (**1.51**). [133]

1.7.2.2 Cyanine dyes

The first cyanine dyes were synthesised by C.H.G. Williams in 1856. [135] He observed the tendency of quinolinium iodide to give intense colours on heating with silver oxide.

Recently, researchers have become interested in synthesizing organic dyes which absorb in the near infrared region such as cyanine dyes. Cyanines have high molar extinction coefficients and high fluorescence intensity leading to their use in applications such as silver halide photography, laser dyes, cosmetic ingredients and as fluorescent tags in DNA sequencing. [136] The main reason to develop near infrared DSC dyes is the lack of absorption of other DSC dyes in the near-infrared region. [137]

Usually cyanine dyes are prepared by condensation reactions between an unsaturated bisaldehyde with a heterocyclic group containing methyl group using a catalyst such as sodium acetate. Cyanine dyes are usually cationic compounds which contain two nitrogen heterocycles linked by a polymethine chain (Figure 1.30b). Their names depend on the number of methine group in the polyene chain (e.g. Figure 1.33a) when n=0 or n=3 is referred to as monomethine or heptamethine cyanine, respectively. [138]

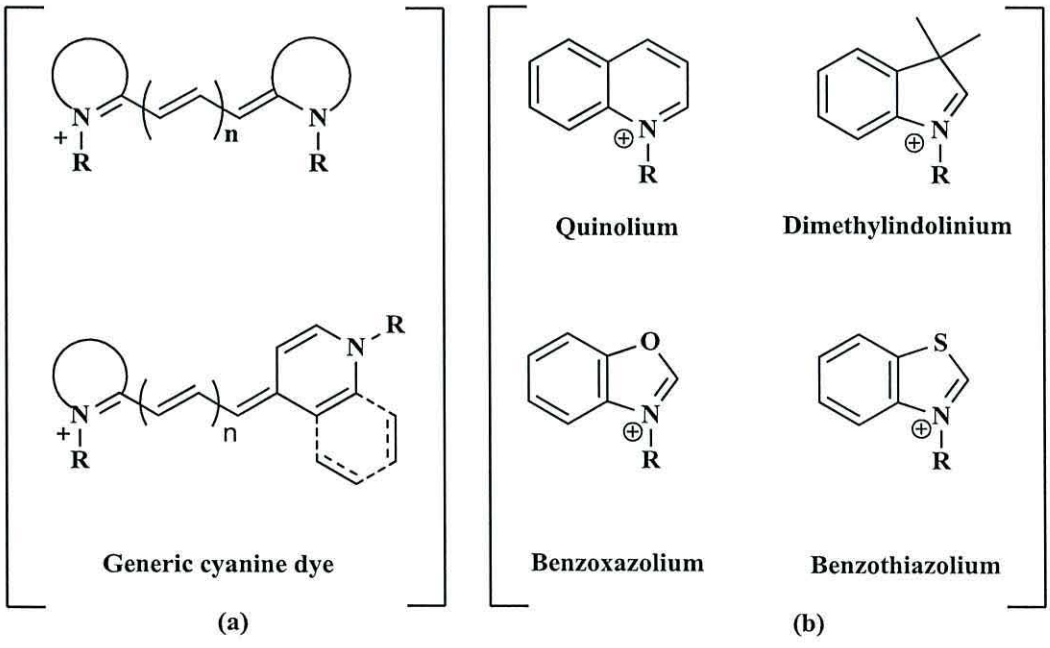

Figure 1.30. (a) The generic structure of cyanine dyes and (b) the typical heterocyclic components. [139]

Increasing the number of (CH=CH) units in the polymethine chain in cyanine dyes leads to an increase in the λ_{max} (bathochromic shift), of around 100 nm for each extension. Monomethine and trimethine cyanine compounds absorb light in the visible area of the solar spectrum, while pentamethines show absorption at around 700 nm in the near infrared region. [139] In these dyes, a chlorine on the cyclohexene (Figure 1.31) is reactive and can be replaced by nucleophiles. [136] By comparison, functional groups such as carboxylic and sulfonic acids are completely inert toward the reagents and reaction conditions used for achieving the condensation reaction. [136, 140]

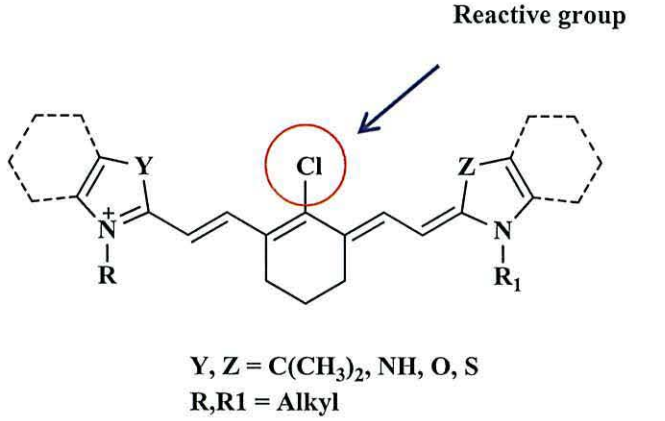

Figure 1.31. The general molecular structure of a cyanine dye showing the chlorine which can be replaced by nucleophiles.

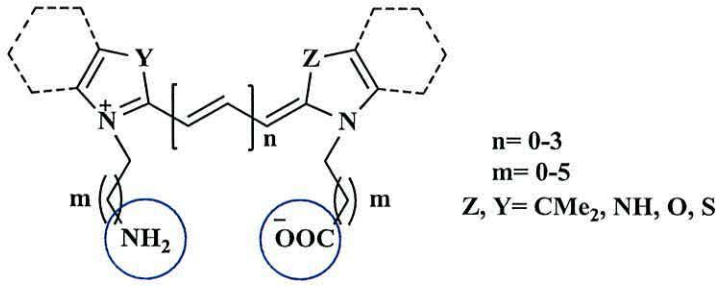

Figure 1.32. Functional groups (carboxyl or amino) which can be linked with the nitrogen of the indole by an alkyl chain.

Reichardt [141] studied the influence of substituents at the central carbon of the different type of pentamethine cyanine dyes. The results showed that an electron-withdrawing group caused a shift to shorter wavelengths. They observed the absorption also depends on the number of methine groups as discussed before. This made them expect that electron withdrawing substitutents at the central carbon of a

heptamethine dye should shift the absorption to longer wavelengths. To test this they repeated the work of Zemlicka and Arnold [141] and prepared the central units (**1.52**) and (**1.53**) (Figure 1.33). The dyes (**1.54**) and (**1.55**) synthesized from these precursors showed absorption shift to longer wavelengths. Also they used the precursors (**1.56**) and (**1.57**), to synthesize (**1.58**) and (**1.59**) (Figure 1.33). In contrast, (**1.58**) and (**1.59**) showed shorter λ_{max} despite the existence of a chlorine atom. Finally, after preparing several dyes they concluded the best way to get longer wavelength heptamethine dyes was through replacement of the chlorine atom with a more electronegative atom at the centre of the chain, but they only prepared with the bromo derivative.

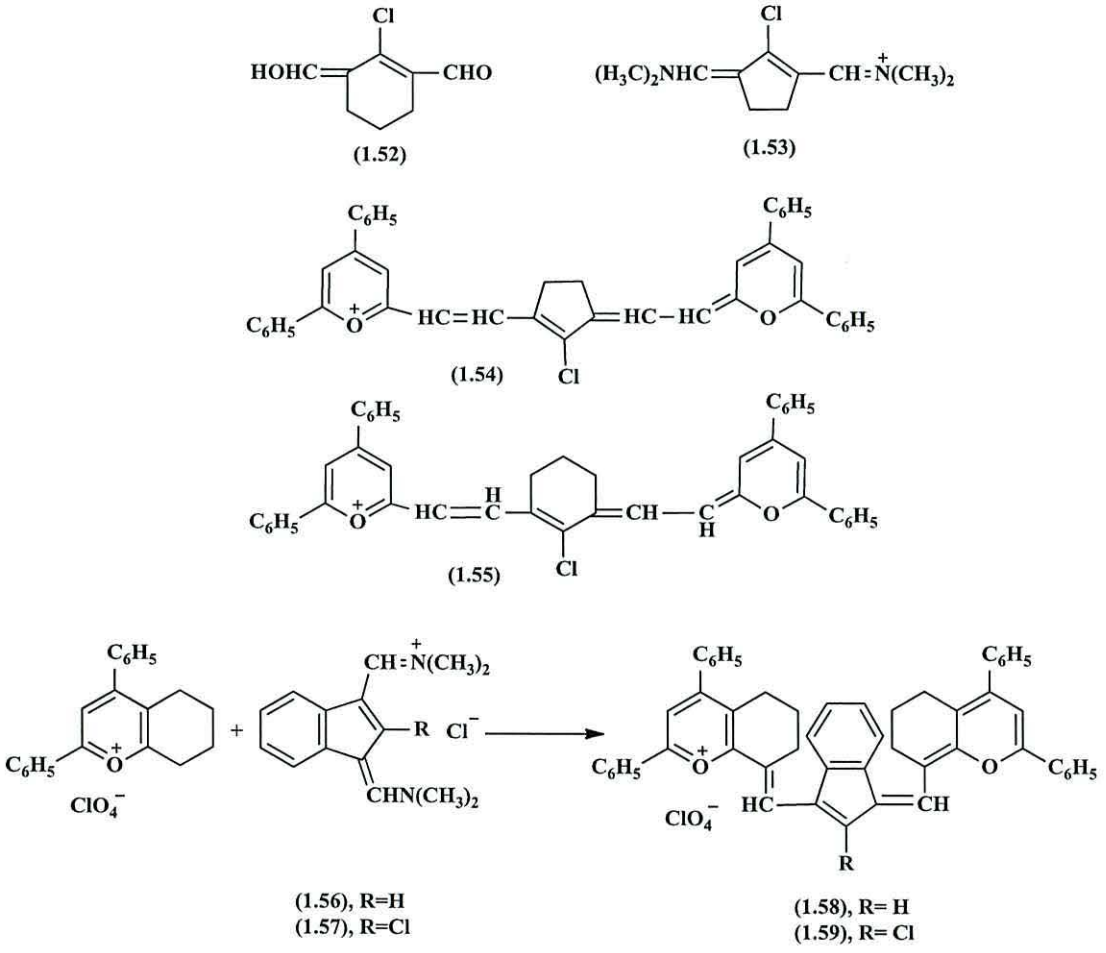

Figure 1.33. The molecular structure of the precursors (**1.52**), (**1.53**), (**1.56**) and (**1.57**) and the dyes (**1.54**), (**1.55**), (**1.58**) and (**1.59**). [141]

The effects of nucleophilic substitution of the chlorine atom on the central unit with other substituents, such as phenol and thiophenol showed the resultant compounds

were chemically unstable, which led to a failure to detect any fluorescence from them. [142]

In 1995, Narayanan *et al.* [136] developed a new method to synthesize heptamethine cyanine dye and derivatives without using a catalyst, (**1.60**) Figure 1.34. This reaction was carried out by refluxing a heterocyclic base containing an activated methyl group and an unsaturated bisaldehyde in a mixture of 1-butanol and benzene (7:3). The advantage of this method is that it produces high yields with enhanced purity, which allows scaling up. It can also allow the preparation of non-symmetric cyanines derived from two different heterocycles through a slower rate of reaction in a single pot without the use of a catalyst.

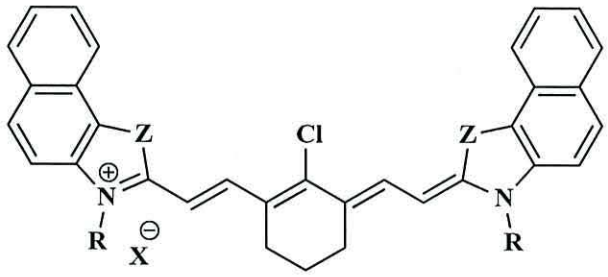

Z= CMe_2, O, S

R= alkyl or carboxylic acid with alkyl chain

X= Br^-, ClO_4^-, I^-

Figure 1.34. The molecular structures of heptamethine dye (**1.60**). [136]

In 2004 Song *et al.* [143] synthesized four water soluble heptamethine cyanine dyes which absorb in the near-infrared region for protein labelling. They investigated the influence of solvent on photostability and studied the spectral properties of these dyes (Figure 1.35). Photostability is an important factor for fluorescence dyes used in bioassays. Song *et al.* suggested two ways to improve photostability; adding sterically hindered N-benzyls to displace N-alkyl groups on the nitrogen atoms and by substituting the Cl on the cyclohexenylene by an electron-donor group such as a methoxyphenylamino group.

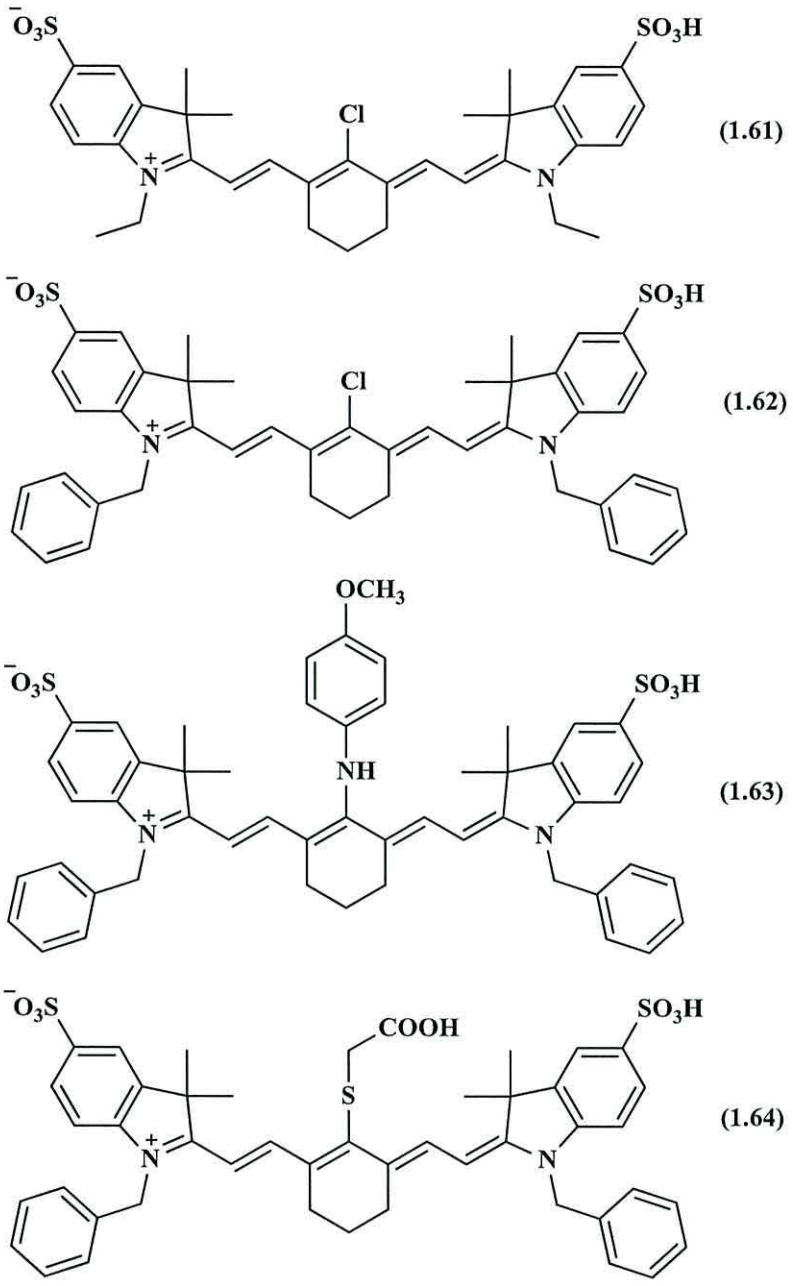

Figure 1.35. Molecular structure of heptamethine cyanine dyes (**1.61**), (**1.62**), (**1.63**) and (**1.64**) prepared by Song *et al.* [143]

The order of dye photostability was **1.63** > **1.62** > **1.61** > **1.64**. The difference of photostability between **1.62** and **1.61** was not large and **1.62** was better than **1.61** due to the extra steric hindrance and rigidity of the benzyl groups substituted on the nitrogen atoms. Dye **1.62** also had a slight bathochromic shift compared with **1.61**. Dye **1.63** showed better photostability than **1.62** and **1.64** which was due to the electron-donor property of the substituent groups.

In the same year, Zhang and Achilefu [144] synthesized a new carbocyanine dye containing galactose (**1.68**) (Scheme 1.7) which absorbs in the near infrared region (NIR) as a fluorescencent probe. This dye contained heptamethine group to increase fluorescence and stability. These worker followed the method developed by Narayanan *et al.* [136] to synthesize the intermediate compound (**1.67**). They introduced 1, 2, 3, 4-di-O-isopropylidene-D-galactopyranose in distilled THF to prepare (**1.68**).

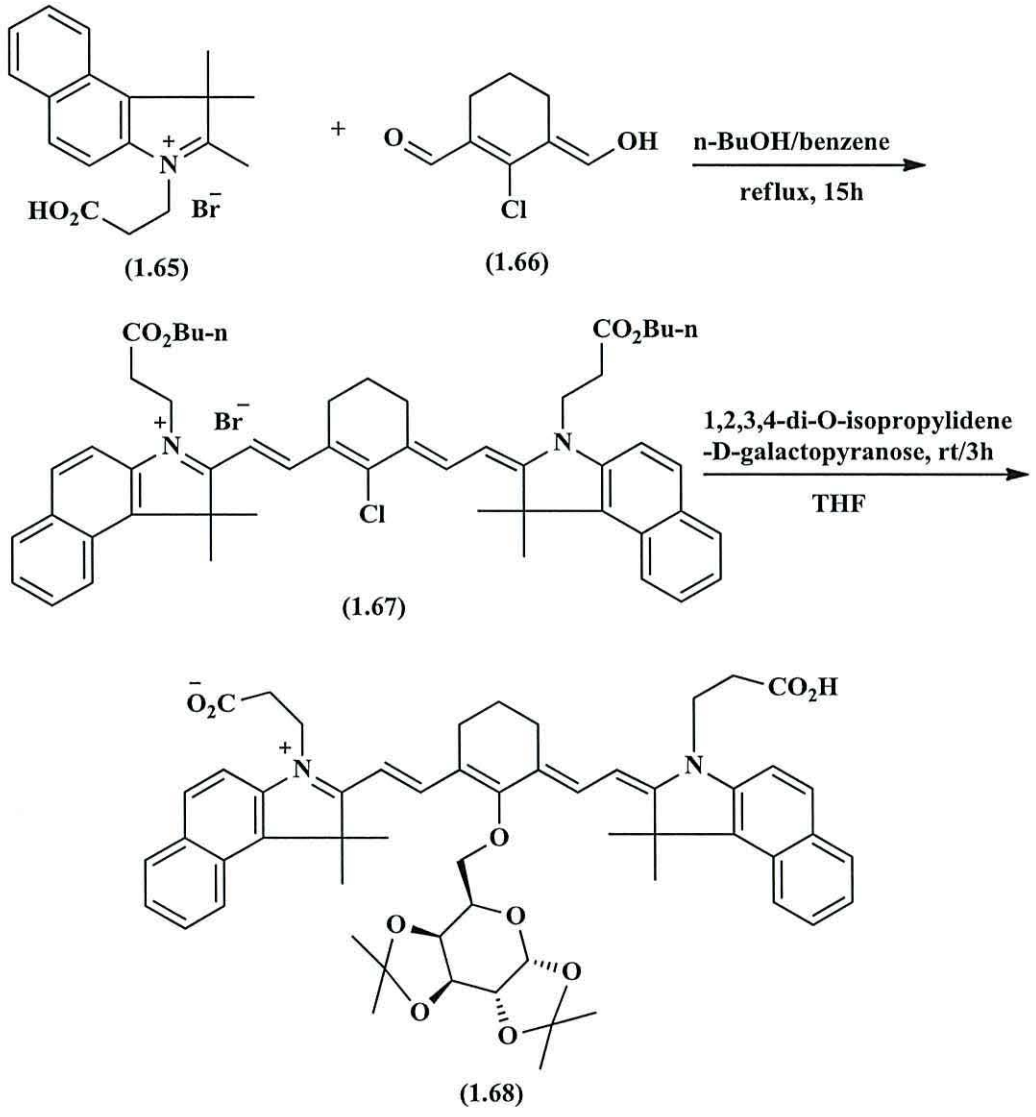

Scheme 1.7. The synthetic pathway of compound (**1.68**). [144]

In 2005, Peng *et al.* [145] synthesized and reported new heptamethine cyanine dyes (**1.70a** and **b**) prepared from compound (**1.69**) as shown in Scheme 1.8. The advantage of these dyes was strong fluorescence due to intramolecular charge transfer (ICT) between the donor and acceptor groups and high photostability due to

the benzoyl group replacing alkyl groups on the nitrogen atom of 3H-indole rings as discussed by Song *et al.* [143] Also there is another advantage of this dye; it is soluble in water due to the sulfonate groups, which is important for biological applications.

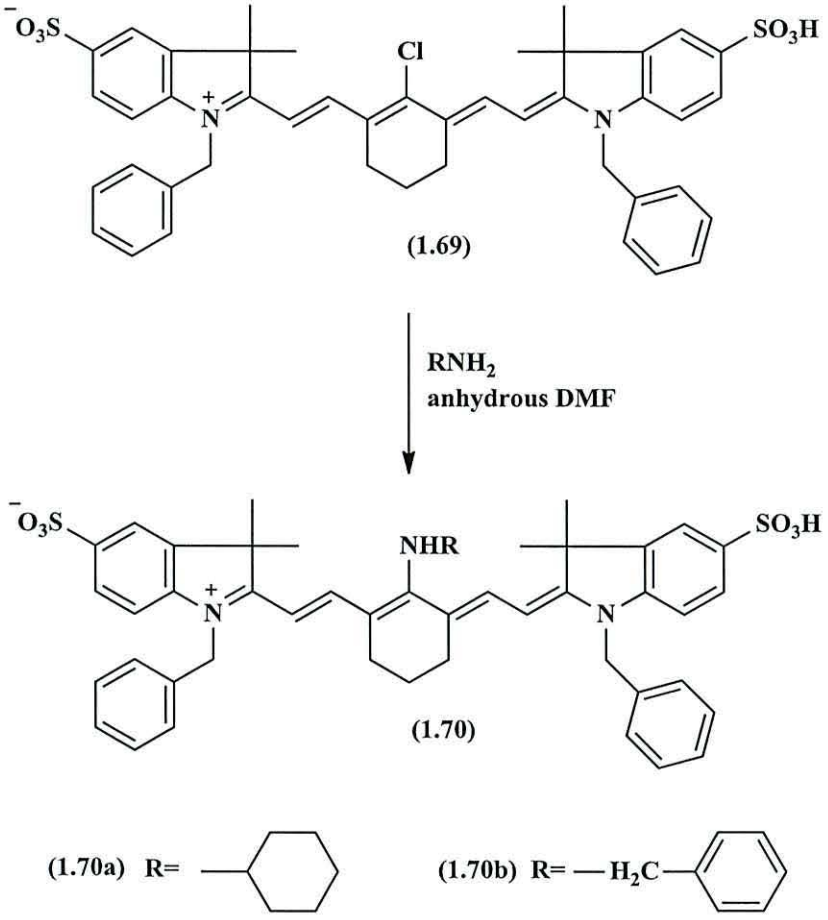

Scheme 1.8. Synthetic pathway of 1-benzyl-2-((E)-2-((E)-3-((E)-2-(1-benzyl-3,3-dimethyl-5-sulfoindolin-2-ylidene)ethylidene)-2-(benzylamino)cyclohex-1-en-1-yl)vinyl)-3,3-dimethyl-3H-indol-1-ium-5-sulfonate (**1.70**). [145]

In 2008 Ma *et al.* [146] reported the highest DSC conversion efficiency of 7.62% and 6.58% for cyanine dyes (**1.71** and **1.72**), Figure 1.36) using a triphenylamine group as donor, a carboxylic acid acceptor and a benzothiadiazole bridge. However, (**1.72**) had no benzothiadiazol group, to compare between these dyes. They introduced a triphenylamine unit to locate the cationic charge from the TiO_2 surface and to try to efficiently restrict recombination between conduction band electron and oxidized sensitizer. Dyes (**1.71**) and (**1.72**) show absorption at 590 nm (ε=150000 M^{-1} cm^{-1}) and 588 nm (ε= 120000 M^{-1} cm^{-1}), respectively. These dyes show higher efficiency than the cyanine dyes prepared previously. Also dye (**1.71**) shows a broader

absorption than dye (**1.72**), which means capture more light from solar spectrum, thus increased DSC performance.

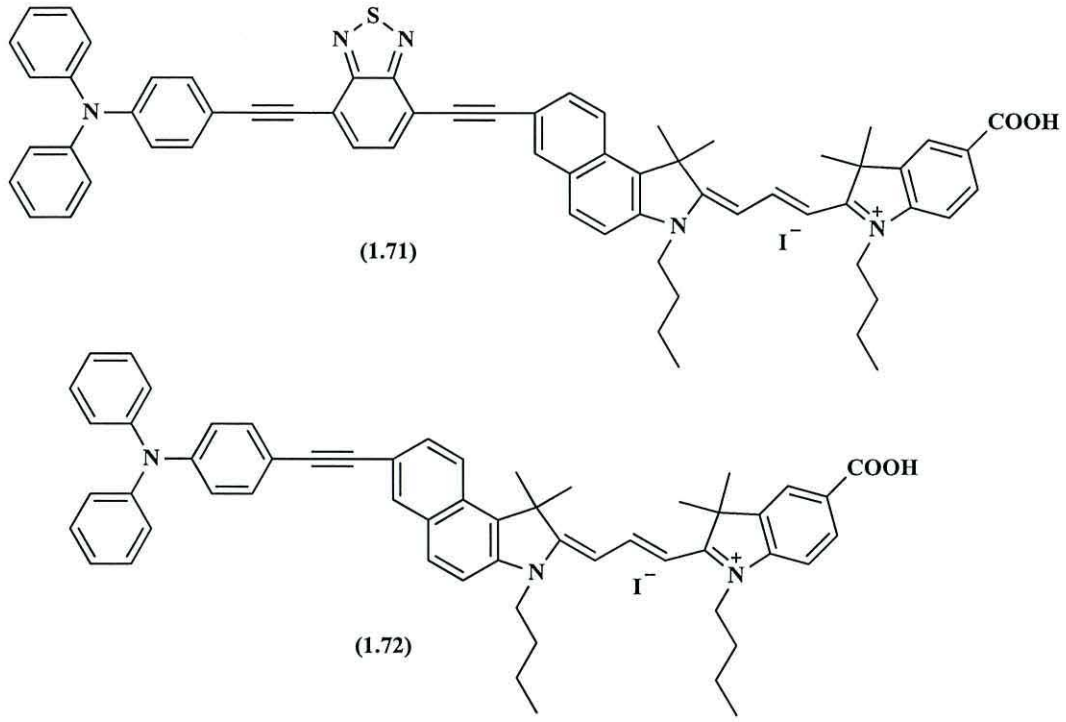

Figure 1.36. Molecular structure of (**1.71**) and (**1.72**) dyes. [146]

In 2009 Ono *et al.* [147] reported the synthesis, testing and characterization study of two new cyanine dyes for DSC (**NK6037 (1.73)** and **NK4432 (1.74)**) as shown in Figure 1.37. These two dyes showed λ_{max} at around 850 nm with high molar extinction coefficient (234,000 at 823 nm and 146,000 at 822 nm for **NK4432 (1.74)** and **NK6037 (1.73)**, respectively). This strong absorption was produced from the delocalized π- electrons of the cyanine structure.

They reported the influence of TiO_2 film thickness on the performance of **NK-6037 (1.73)** DSC and the effect of adding CDCA as a co-adsorbent. They found the best results with four layers of TiO_2 (η = 1.6%). The efficiency was increased further by a light-scattering layer (η= 1.9%). The best results were obtained at 100 mmol L^{-1} of CDCA (η= 2.3%).

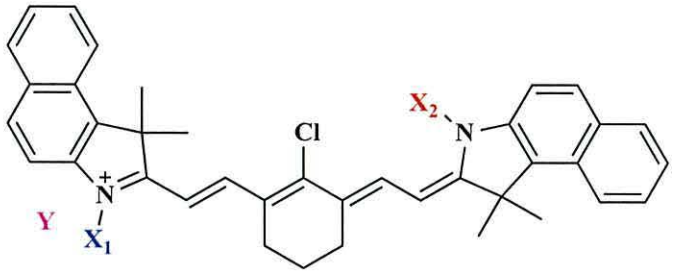

NK-4432 (1.74) = X1: C_2H_5: X2: C_2H_5, Y: $[BF_4]^-$

NK-6037 (1.73) = X1: CH_2COO^- : X2: CH_2COOH,

Figure 1.37. Molecular structure of **NK-4432 (1.74)** and **NK-6037 (1.73)**. [147]

In 2011 Funabiki *et al.* [137] reported the novel heptamethine cyanine dyes **KFH_2 (1.75)** and **KFH_3 (1.76)**, (Figure 1.38), for DSC devices using zinc oxide as the semiconductor prepared at low temperature 70°C achieving η = 1.2%, as shown in (Table 1.7). The UV-Vis spectra shows λ_{max} at 780 and 787 nm with molar extinction coefficient (ε= 263,000 and 280,000), respectively. These dyes show H-aggregation in dye solution, so chenodeoxycholic acid (CDCA) has been used as a co-sorbent to try to reduce this.

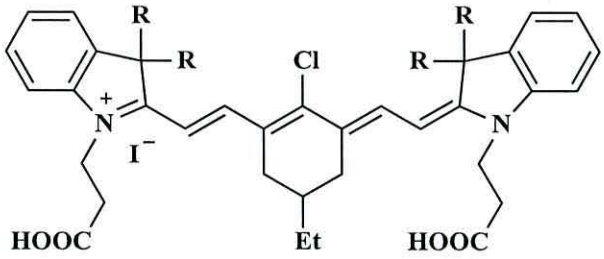

KFH2 (1.75): R= Me
KFH3 (1.76): R= Bu

Figure 1.38. Molecular structure of heptamethine cyanine dye **KFH-2 (1.75)** and **KFH-3 (1.76)**.

Table 1.7. Photovoltaic properties of DSC using **KFH-3 (1.76)** and **KFH-2 (1.75)** dyes with ZnO paste, deoxycholic acid (DCA) and tetrabutylammonium iodide (TBAI). [137]

Dye	Thickness of ZnO (μm)	DCA (M)	TBAI (M)	I_2 (M)	J_{sc} (mA cm^{-2})	V_{oc} (V)	FF	η (%)
KFH-3 (1.76)	3	0	0.5	0.05	0.30	0.04	0.56	0.08
	3	2	0.5	0.05	2.22	0.46	0.66	0.67
	7-9	0	1.0	0.10	1.20	0.46	0.78	0.43
	7-9	2	1.0	0.10	3.34	0.49	0.76	1.23
KFH-2 (1.75)	7-9	0	1.0	0.10	0.12	0.38	0.63	0.03
	7-9	10	1.0	0.10	1.59	0.45	0.68	0.49

1.8 Summary

Increasing global technology and demand on clean energy as a source of power energy to support the activities of modern society, has led to the appearance of solar cells as one feasible renewable energy technology. In recent years, dye-sensitized solar cells have been seen as an alternative to silicon PV due to their advantages of low cost etc as discussed earlier in this chapter. This thesis work has focused on the synthesis and design new dyes for three different types of organic dye-sensitized solar cells based on triphenylamine, cyanine and phthalocyanine as sensitizers, which absorb in the three different areas of the solar spectrum. The aim has been to study dyes which absorb complementary wavelengths of light to capture more light and enhancement the performance of DSC devices. Another area of this work has been co-sensitized these new dyes with existing DSC dyes (**N719** and **D149**) to improve the photovoltaic parameters.

1.9 References

1. M. Grätzel, *Chem. Lett.*, 2005, **34**, 8–13.
2. J. Chow, R. J. Kopp, and P. R. Portney, *Sci.*, 2003, **302**, 1528–1531.
3. Y. Ooyama and Y. Harima, *Eur. J. Org. Chem.*, **2009**, 2903–2934.
4. G. Boyle, in *Renewable Energy Power for a Sustainable Future*, 1996, Oxford University Press.
5. K. S. Brown, *Sci.*, 1999, **285**, 678–680.
6. M. Grätzel, *Nat.*, 2001, **414**, 338–344.
7. A. Hagfeldt, G. Boschloo, L. Sun, L. Kloo, and H. Pettersson, *Chem. Rev.*, 2010, **110**, 6595–6663.
8. R. Foster, in *Solar Energy Renewable Energy and the Environment*, 2009, CRC Press.
9. A. Geotzberger, H. Christopher, and H. W. Schock, *Mater. Sci. Eng.*, 2003, **40**, 1–46.
10. M. A. Green, *Phys. E*, 2002, **14**, 65–70.
11. P. J. Holliman, M. L. Davies, A. Connell, M. J. Carnie, and T. M. Watson, *Rapid, Low Temperature Processing of Dye Sensitized Solar Cells*, vol. Chapter in Functional Materials for Energy Applications, Eds. J.A. Kilner, S. J. Skinner, S.J.C. Irvine, P.P. Edwards 2012, Woodhead Publishers, Cambridge.
12. A. Hagfeldt and M. Grätzel, *Acc. Chem. Res.*, 2000, **33**, 269–277.
13. M. Liang, W. Xu, F. Cai, P. Chen, B. Peng, J. Chen, and Z. Li, *J. Phys. Chem. C*, 2007, **111**, 4465–4472.
14. B. O'Regan, M. Grätzel, *Nat.*, 1991, **353**, 737–740.
15. M. K. Nazeeruddin, A. Kay, I. Rodicio, R. Humphry-Baker, E. Mueller, P. Liska, N. Vlachopoulos, M. Grätzel, *J. Am. Chem. Soc*, 1993, **115**, 6382–6390.
16. M. K. Nazeeruddin, P. Péchy, T. Renouard, S. M. Zakeeruddin, R. Humphry-Baker, P. B. Deacon, C. A. Bignozzi, and M. Grätzel, *J. Am. Chem. Soc*, 2001, **123**, 1613.
17. W. Zeng, Y. Cao, Y. Bai, Y. Wang, Y. Shi, M. Zhang, F. Wang, C. Pan, and P. Wang, *Chem. Mater.*, 2010, **22**, 1915–1925.
18. M. V. Martínez-Díaz, G. de la Torre, and T. Torres, *Chem. Commun.*, 2010, **46**, 7090–7108.
19. M. A. Green, *Phys. E Low-Dimens. Syst. Nanostructures*, 2002, **14**, 11–17.
20. J. Nelson, in *The Physics of Solar Cells*, 2003, Imperial College Press.
21. R. D. Dupuis and M. R. Krames, *J. Light. Technol.*, 2008, **26**, 1154–1171.
22. D. M. Chapin, C. S. Fuller, and G. L. Pearson, *J. Appl. Phys.*, 1954, **25**, 676–677.

23. S.K. Deb, R. Ellingson, S. Ferrere, A.J. Frank, B.A. Gregg, A.J. Nozik, N. Park, and G. Schlichthörl Presented at, A National Laboratory of the U.S. Department of Energy, Vienna, Austria, 1998.
24. K. Keis, C. Bauer, G. Boschloo, A. Hagfeldt, K. Westermark, H. Rensmo, H. Siegbahn, *J. Photochem. Photobiol. Chem.*, 2002, **148**, 54–67.
25. M. Matsumura, Y. Nomura, and H. Tsubomura, *Chem. Soc. Jpn.*, 1977, **50**, 2533–2537.
26. H. Tsubomura, M. Matsumura, Y. Nomura, T. Amamiya, *Nat.*, 1976, **261**, 402–403.
27. D. Duonghond, N. Serpone, and M. Grätzel, *Helv. Chim. Acta*, 1984, **67**, 1012–1018.
28. J. Desilvestro, M. Graetzel, L. Kavan, J. Moser, and J. Augustynski, *J. Am. Chem. Soc.*, 1985, **107**, 2988–2990.
29. M. Grätzel, *J. Photochem. Photobiol. C Photochem. Rev.*, 2003, **4**, 145–153.
30. A. Yella, H. W. Lee, H. N. Tsao, C. Yi, A. K. Chandiran, M. K. Nazeeruddin, E. W. G. Diau, C. Y. Yeh, S. M. Zakeeruddin, and M. Grätzel, *Sci.*, 2011, **334**, 629–634.
31. S. Ito, in *Solar Cells - Dye-Sensitized Devices*, ed. L. A. Kosyachenko, 2011, InTech, Hyogo, Japan..
32. F. Z. Yang Jiao, in *Dye Sensitized Solar Cells Principles and New Design*, Beijing National Laboratory for Condensed Matter Physics and Institute of Physics, 2011, Chinese Academy of Sciences, China,.
33. A. C. Khazraji, S. Hotchandani, S. Das, and P. V. Kamat, *J. Phys. Chem. B*, 1999, **103**, 4693–4700.
34. K. Sayama, K. Hara, N. Mori, M. Satsuki, S. Suga, S. Tsukagoshi, Y. Abe, H. Sugihara, and H. Arakawa, *Chem. Commun.*, 2000, 1173–1174.
35. K. Sayama, S. Tsukagoshi, T. Mori, K. Hara, Y. Ohga, A. Shinpou, Y. Abe, S. Suga, and H. Arakawa, *Sol. Energy Mater. Sol. Cells*, 2003, **80**, 47–71.
36. K. Sayama, S. Tsukagoshi, K. Hara, Y. Ohga, A. Shinpou, Y. Abe, S. Suga, and H. Arakawa, *J. Phys. Chem. B*, 2002, **106**, 1363–1371.
37. Z. S. Wang, F. Y. Li, C. H. Huang, L. Wang, M. Wei, L. P. Jin, and N. Q. Li, *J. Phys. Chem. B*, 2000, **104**, 9676–9682.
38. Z. S. Wang, F. Y. Li, and C. H. Huang, *Chem. Commun.*, 2000, 2063–2064.
39. Z. S. Wang, F. Y. Li, and C. H. Huang, *J. Phys. Chem. B*, 2001, **105**, 9210–9217.
40. Y. S. Chen, C. Li, Z.-H. Zeng, W. B. Wang, X. S. Wang, and B. W. Zhang, *J. Mater. Chem.*, 2005, **15**, 1654–1661.

41. N. J. Cherepy, G. P. Smestad, M. Grätzel, and J. Z. Zhang, *J. Phys. Chem. B*, 1997, **101**, 9342–9351.
42. X. Chen, J. Guo, X. Peng, M. Guo, Y. Xu, L. Shi, C. Liang, L. Wang, Y. Gao, S. Sun, and S. Cai, *J. Photochem. Photobiol. Chem.*, 2005, **171**, 231–236.
43. W. Zhao, Y. Jun Hou, X. Song Wang, B. Wen Zhang, Y. Cao, R. Yang, W. Bo Wang, and X. Rui Xiao, *Sol. Energy Mater. Sol. Cells*, 1999, **58**, 173–183.
44. K. Hara, M. Kurashige, Dan-oh Yasufumi, C. Kasada, A. Shinpo, S. Suga, K. Sayama, and H. Arakawa, *New J. Chem.*, 2003, **27**, 783–785.
45. Z. S. Wang, K. Hara, Dan-oh Yasufumi, C. Kasada, A. Shinpo, S. Suga, H. Arakawa, and H. Sugihara, *J. Phys. Chem. B*, 2005, **109**, 3907–3914.
46. S. Ferrere, A. Zaban, and B. A. Gregg, *J. Phys. Chem. B*, 1997, **101**, 4490–4493.
47. S. Ferrere and B. A. Gregg, *New J. Chem.*, 2002, **26**, 1155–1160.
48. T. Horiuchi, H. Miura, and S. Uchida, *Chem. Commun.*, 2003, 3036–3037.
49. S. Ito, S. M. Zakeeruddin, R. Humphry-Baker, P. Liska, R. Charvet, P. Comte, M. K. Nazeeruddin, P. Péchy, M. Takata, H. Miura, S. Uchida, and M. Grätzel, *Adv. Mater.*, 2006, **18**, 1202–1205.
50. N. Koumura, Z. S. Wang, S. Mori, M. Miyashita, E. Suzuki, and K. Hara, *J. Am. Chem. Soc.*, 2006, **128**, 14256–14257.
51. S. Tan, J. Zhai, H. Fang, T. Jiu, J. Ge, Y. Li, L. Jiang, and D. Zhu, *Chem. Eur. J.*, 2005, **11**, 6272–6276.
52. S. L. Li, K. J. Jiang, K. F. Shao, and L. M. Yang, *Chem. Commun.*, 2006, 2792–2794.
53. K. Hara, T. Sato, R. Katoh, A. Furube, T. Yoshihara, M. Murai, M. Kurashige, S. Ito, A. Shinpo, S. Suga, and H. Arakawa, *Adv. Funct. Mater.*, 2005, **15**, 246–252.
54. T. Kitamura, M. Ikeda, K. Shigaki, T. Inoue, N. A. Anderson, X. Ai, T. Lian, and S. Yanagida, *Chem. Mater.*, 2004, **16**, 1806–1812.
55. M. Velusamy, K. R. Justin Thomas, J. T. Lin, Y. C. Hsu, and K. C. Ho, *Org. Lett.*, 2005, **7**, 1899–1902.
56. D. P. Hagberg, T. Edvinsson, T. Marinado, G. Boschloo, A. Hagfeldt, and L. Sun, *Chem. Commun.*, 2006, 2245–2247.
57. L. L. Li and E. W. G. Diau, *Chem. Soc. Rev.*, 2012, **42**, 291–304.
58. M. Liang and J. Chen, *Chem. Soc. Rev.*, 2013, **42**, 3453-3488.
59. M. J. Griffith, K. Sunahara, P. Wagner, K. Wagner, G. G. Wallace, D. L. Officer, A. Furube, R. Katoh, S. Mori, and A. J. Mozer, *Chem. Commun.*, 2012, **48**, 4145–4162.
60. R. Jose, V. Thavasi, and S. Ramakrishna, *J. Am. Ceram. Soc.*, 2009, **92**, 289–301.

61. D. Matthews, P. Infelta, and M. Grätzel, *Sol. Energy Mater. Sol. Cells*, 1996, **44**, 119–155.
62. T. Nagata and H. Murakami, *Ulvac Tech. J. Engl.*, 2009, N70E, 1-5.
63. T. N. Murakami and M. Grätzel, *Inorg. Chim. Acta*, 2008, **361**, 572–580.
64. A. Hagfeldt, B. Didriksson, T. Palmqvist, H. Lindström, S. Södergren, H. Rensmo, and S. E. Lindquist, *Sol. Energy Mater. Sol. Cells*, 1994, **31**, 481–488.
65. E. Olsen, G. Hagen, and S. Eric Lindquist, *Sol. Energy Mater. Sol. Cells*, 2000, **63**, 267–273.
66. N. Papageorgiou, *J. Electrochem. Soc.*, 1997, **144**, 876.
67. A. Kay and M. Grätzel, *Sol. Energy Mater. Sol. Cells*, 1996, **44**, 99–117.
68. K. Imoto, K. Takahashi, T. Yamaguchi, T. Komura, J. Nakamura, and K. Murata, *Sol. Energy Mater. Sol. Cells*, 2003, **79**, 459–469.
69. Z. Yu, N. Vlachopoulos, M. Gorlov, and L. Kloo, *Dalton Trans.*, 2011, **40**, 10289–10303.
70. G. Smestad, C. Bignozzi, and R. Argazzi, *Sol. Energy Mater. Sol. Cells*, 1994, **32**, 259–272.
71. O. Kohle, M. Grätzel, A. F. Meyer, and T. B. Meyer, *Adv. Mater.*, 1997, **9**, 904–906.
72. A. Hinsch, J. M. Kroon, R. Kern, I. Uhlendorf, J. Holzbock, A. Meyer, and J. Ferber, *Prog. Photovoltaics Res. Appl.*, 2001, **9**, 425–438.
73. G. Wolfbauer, A. M. Bond, J. C. Eklund, and D. R. MacFarlane, *Sol. Energy Mater. Sol. Cells*, 2001, **70**, 85–101.
74. H. Kusama and H. Arakawa, *J. Photochem. Photobiol. Chem.*, 2004, **165**, 157–163.
75. A. S. Polo, M. K. Itokazu, and N. Y. Murakami Iha, *Coord. Chem. Rev.*, 2004, **248**, 1343–1361.
76. E. Stathatos, in *Solar Cells - Dye-Sensitized Devices*, L. A. Kosyachenko, 2011, InTech.
77. J. Nelson, Rosemary E. Chandler, *Coord. Chem. Rev*, 2004, **48**, 1181–1194.
78. A. P. Uthirakumra, in *Solar Cells-Dye-Sensitized Devices*, L. A. Kosyachenko, 2011, InTech.
79. H. Tian, X. Yang, R. Chen, R. Zhang, A. Hagfeldt, and L. Sun, *J. Phys. Chem. C*, 2008, **112**, 11023–11033.
80. Y. Tachibana, K. Hara, K. Sayama, and H. Arakawa, *Chem. Mater.*, 2002, **14**, 2527–2535.

81. M. Liang, W. Xu, F. Cai, P. Chen, B. Peng, J. Chen, and Z. Li, *J. Phys. Chem. C*, 2007, **111**, 4465–4472.
82. Y. Qin and Q. Peng, *Int. J. Photoenergy*, 2012, **2012**.
83. M. K. Nazeeruddin, P. Péchy, and M. Grätzel, *Chem. Commun.*, 1997, 1705–1706.
84. M. K. Nazeeruddin, F. De Angelis, S. Fantacci, A. Selloni, G. Viscardi, P. Liska, S. Ito, B. Takeru, and M. Grätzel, *J. Am. Chem. Soc.*, 2005, **127**, 16835–16847.
85. P. Péchy, T. Renouard, S. M. Zakeeruddin, R. Humphry-Baker, P. Comte, P. Liska, L. Cevey, E. Costa, V. Shklover, L. Spiccia, G. B. Deacon, C. A. Bignozzi, and M. Grätzel, *J. Am. Chem. Soc.*, 2001, **123**, 1613–1624.
86. S. M. Zakeeruddin, M. K. Nazeeruddin, P. Pechy, F. P. Rotzinger, R. Humphry-Baker, K. Kalyanasundaram, M. Grätzel, V. Shklover, and T. Haibach, *Inorg. Chem.*, 1997, **36**, 5937–5946.
87. C. R. Rice, M. D. Ward, M. K. Nazeeruddin, and M. Grätzel, *New J. Chem.*, 2000, **24**, 651–652.
88. Z. S. Wang and F. Liu, *Front. Chem. China*, 2010, **5**, 150–161.
89. K. M. Kadish, K. M. Smith, and R. Guilard, in *The Porphyrin Handbook: Applications of Phthalocyanines*, 2003, Elsevier.
90. N. B. McKeown, in *Phthalocyanine Materials: Synthesis, Structure, and Function*, 1998, Cambridge University Press,.
91. R. P. Linstead, *J. Chem. Soc. Resumed*, 1934, 1016–1017.
92. L. L. Li and E. W. G. Diau, *Chem. Soc. Rev.*, 2012, **42**, 291–304.
93. H. Ali, R. Langlois, J. R. Wagner, N. Brasseur, B. Paquette, and J. E. VAN Lier, *Photochem. Photobiol.*, 1988, **47**, 713–717.
94. C. C. Leznoff, S. M. Marcuccio, S. Greenberg, A. B. P. Lever, and K. B. Tomer, *Can. J. Chem.*, 1985, **63**, 623–631.
95. L. Giribabu, C. Vijay Kumar, M. Raghavender, K. Somaiah, P. Yella Reddy, and P. Venkateswara Rao, *J. Nano Res.*, 2008, **2**, 39–48.
96. M. V. Martínez-Díaz, M. Ince, and T. Torres, *Monats. Chem.*, 2011, **142**, 699–707.
97. P. Y. Reddy, L. Giribabu, C. Lyness, H. J. Snaith, C. Vijaykumar, M. Chandrasekharam, M. Lakshmikantam, J. H. Yum, K. Kalyanasundaram, M. Grätzel, and M. K. Nazeeruddin, *Angew. Chem. Int. Ed.*, 2007, **46**, 373–376.
98. J. J. Cid, J. H. Yum, S. R. Jang, M. K. Nazeeruddin, E. Martínez-Ferrero, E. Palomares, J. Ko, M. Grätzel, and T. Torres, *Angew. Chem. Int. Ed.*, 2007, **46**, 8358–8362.

99. M. García-Iglesias, J. H. Yum, R. Humphry-Baker, S. M. Zakeeruddin, P. Péchy, P. Vázquez, E. Palomares, M. Grätzel, M. K. Nazeeruddin, and T. Torres, *Chem. Sci.*, 2011, **2**, 1145–1150.

100. J. J. Cid, M. García-Iglesias, J. H. Yum, A. Forneli, J. Albero, E. Martínez-Ferrero, P. Vázquez, M. Grätzel, M. K. Nazeeruddin, E. Palomares, and T. Torres, *Chem. Eur. J.*, 2009, **15**, 5130–5137.

101. S. Eu, T. Katoh, T. Umeyama, Y. Matano, and H. Imahori, *Dalton Trans.*, 2008, 5476.

102. J. H. Yum, S. Jang, R. Humphry-Baker, M. Grätzel, J. J. Cid, T. Torres, and M. K. Nazeeruddin, *Langmuir*, 2008, **24**, 5636–5640.

103. S. Mori, M. Nagata, Y. Nakahata, K. Yasuta, R. Goto, M. Kimura, and M. Taya, *J. Am. Chem. Soc.*, 2010, **132**, 4054–4055.

104. J. H. Yum, E. Baranoff, F. Kessler, T. Moehl, S. Ahmad, T. Bessho, A. Marchioro, E. Ghadiri, J. E. Moser, C. Yi, M. K. Nazeeruddin, and M. Grätzel, *Nat. Commun.*, 2012, **3**, 631.

105. J. Pei, M. Liang, J. Chen, Z. Tao, and W. Xu, *Acta Phys. Chim. Sin.*, 2008, **24**, 1950–1956.

106. J. Preat, C. Michaux, D. Jacquemin, and E. A. Perpète, *J. Phys. Chem. C 2009*, **113**, 16821–16833.

107. B. Liu, W. Zhu, Q. Zhang, W. Wu, M. Xu, Z. Ning, Y. Xie, and H. Tian, *Chem. Commun.*, 2009, 1766–1768.

108. P. Leriche, P. Frère, A. Cravino, O. Alévêque, and J. Roncali, *J. Org. Chem.*, 2007, **72**, 8332–8336.

109. S. Roquet, A. Cravino, P. Leriche, O. Alévêque, P. Frère, and J. Roncali, *J. Am. Chem. Soc.*, 2006, **128**, 3459–3466.

110. M. G. Kang, K. S. Rye, S. H. Chang, N. G. Park, J. S. Hong and K. J. Kim, *Bull. Kor. Chem. Soc.*, 2004, **25**, 742–744.

111. A. Solbrand, H. Lindström, H. Rensmo, A. Hagfeldt, S. E. Lindquist, and S. Södergren, *J. Phys. Chem. B*, 1997, **101**, 2514–2518.

112. Y. L. Ping Shen, *Dyes Pigments*, 187–197.

113. A. Mishra, M. K. R. Fischer, and P. Bäuerle, *Angew. Chem. Int. Ed.*, 2009, **48**, 2474–2499.

114. E. Galoppini, *Coord. Chem. Rev.*, 2004, **248**, 1283–1297.

115. K. S. Finnie, J. R. Bartlett, and J. L. Woolfrey, *Langmuir*, 1998, **14**, 2744–2749.

116. H. Otaka, M. Kira, K. Yano, S. Ito, H. Mitekura, T. Kawata, and F. Matsui, *J. Photochem. Photobiol. Chem.*, 2004, **164**, 67–73.

117. T. Horiuchi, H. Miura, K. Sumioka, and S. Uchida, *J. Am. Chem. Soc.*, 2004, **126**, 12218–12219.

118. T. Horiuchi, H. Miura, and S. Uchida, *J. Photochem. Photobiol. Chem.*, 2004, **164**, 29–32.

119. D. P. Hagberg, T. Marinado, K. M. Karlsson, K. Nonomura, P. Qin, G. Boschloo, T. Brinck, A. Hagfeldt, and L. Sun, *J. Org. Chem.*, 2007, **72**, 9550–9556.

120. W. Xu, J. Pei, J. Shi, S. Peng, and J. Chen, *J. Power Sources*, 2008, **183**, 792–798.

121. K. Hara, T. Sato, R. Katoh, A. Furube, Y. Ohga, A. Shinpo, S. Suga, K. Sayama, H. Sugihara, and H. Arakawa, *J. Phys. Chem. B*, 2003, **107**, 597–606.

122. W. Zeng, Y. Cao, Y. Bai, Y. Wang, Y. Shi, M. Zhang, F. Wang, C. Pan, and P. Wang, *Chem. Mater.*, 2010, **22**, 1915–1925.

123. S. Hwang, J. H. Lee, C. Park, H. Lee, C. Kim, C. Park, M. H. Lee, W. Lee, J. Park, K. Kim, N. G. Park, and C. Kim, *Chem. Commun.*, 2007, 4887–4889.

124. K. F. Chen, Y. C. Hsu, Q. Wu, M. C. P. Yeh, and S. S. Sun, *Org. Lett.*, 2009, **11**, 377–380.

125. W. Xu, B. Peng, J. Chen, M. Liang, and F. Cai, *J. Phys. Chem. C*, 2008, **112**, 874–880.

126. J. E. Kroeze, N. Hirata, S. Koops, M. K. Nazeeruddin, L. Schmidt-Mende, M. Grätzel, and J. R. Durrant, *J. Am. Chem. Soc.*, 2006, **128**, 16376–16383.

127. J. Song, F. Zhang, C. Li, W. Liu, B. Li, Y. Huang, and Z. Bo, *J. Phys. Chem. C*, 2009, **113**, 13391–13397.

128. H. Im, S. Kim, C. Park, S. H. Jang, C. J. Kim, K. Kim, N. G. Park, and C. Kim, *Chem. Commun.*, 2010, **46**, 1335.

129. C. L. Gettinger, A. J. Heeger, J. M. Drake, and D. J. Pine, *Mol. Cryst. Liq. Cryst. Sci. Technol. Sect. Mol. Cryst. Liq. Cryst.*, 1994, **256**, 507–512.

130. S. W. Park, K. I. Son, M. J. Ko, K. Kim, and N. G. Park, *Synth. Met.*, 2009, **159**, 2571–2577.

131. D. P. Hagberg, J. H. Yum, H. Lee, F. De Angelis, T. Marinado, K. M. Karlsson, R. Humphry-Baker, L. Sun, A. Hagfeldt, M. Grätzel, and M. K. Nazeeruddin, *J. Am. Chem. Soc.*, 2008, **130**, 6259–6266.

132. W. Xu, B. Peng, J. Chen, M. Liang, and F. Cai, *J. Phys. Chem. C*, 2008, **112**, 874–880.

133. Z. S. Wang, Y. Cui, K. Hara, Y. Dan-oh, C. Kasada, and A. Shinpo, *Adv. Mater.*, 2007, **19**, 1138–1141.

134. P. Wang, C. Klein, R. Humphry-Baker, S. M. Zakeeruddin, and M. Grätzel, *J. Am. Chem. Soc.*, 2005, **127**, 808–809.

135. B. A. Armitage, in *DNA Binders and Related Subjects*, M. J. Waring and J. B. Chaires, 2005, Springer Berlin Heidelberg, pp. 55–76.

136. N. Narayanan and G. Patonay, *J. Org. Chem.*, 1995, **60**, 2391–2395.

137. K. Funabiki, H. Mase, A. Hibino, N. Tanaka, N. Mizuhata, Y. Sakuragi, A. Nakashima, T. Yoshida, Y. Kubota, and M. Matsui, *Energy Environ. Sci.*, 2011, **4**, 2186–2192.

138. G. Patonay, J. Salon, J. Sowell, and L. Strekowski, *Molecules*, 2004, **9**, 40–49.

139. L. Strekowski, in *Heterocyclic Polymethine Dyes: Synthesis, Properties and Applications*, 2008, Springer.

140. H. Lee, J. C. Mason, and S. Achilefu, *J. Org. Chem.*, 2006, **71**, 7862–7865.

141. G. A. Reynolds and K. H. Drexhage, *J. Org. Chem.*, 1977, **42**, 885–888.

142. L. Strekowski, M. Lipowska, and G. Patonay, *J. Org. Chem.*, 1992, **57**, 4578–4580.

143. F. Song, X. Peng, E. Lu, R. Zhang, X. Chen, and B. Song, *J. Photochem. Photobiol. Chem.*, 2004, **168**, 53–57.

144. Z. Zhang and S. Achilefu, *Org. Lett.*, 2004, **6**, 2067–2070.

145. X. Peng, F. Song, E. Lu, Y. Wang, W. Zhou, J. Fan, and Y. Gao, *J. Am. Chem. Soc.*, 2005, **127**, 4170–4171.

146. X. Ma, J. Hua, W. Wu, Y. Jin, F. Meng, W. Zhan, and H. Tian, *Tetrahedron*, 2008, **64**, 345–350.

147. T. Ono, T. Yamaguchi, and H. Arakawa, *Sol. Energy Mater. Sol. Cells*, 2009, **93**, 831–835.

Chapter 2

Experimental section

2. Experimental section

2.1 Chemicals and instrumentation

2.1.1 Chemicals

All chemicals were purchased from Aldrich and Alfa Aesar Chemicals Company, and were used as supplied, unless otherwise stated. Anhydrous solvent were used as purchased except THF which was dried with sodium wire. Air sensitive reactions were carried out under inert conditions using either nitrogen or argon atmosphere and standard Schlenk techniques. Reactions carried out at low temperature (-70°C) were cooled by using bath of methylated spirit with liquid nitrogen. All reagents and solvents used were reagent grade unless otherwise stated. Anhydrous magnesium sulfate was used to dry organic solvents. For coupling reactions two types of palladium catalyst used; *trans*-di(μ-acetato)*bis*[0-(di-*O*-tolylphosphoino)benzyl] dipalladium (*II*) was used in Heck coupling reactions and palladium (II) acetate was used in Suzuki coupling reactions. Both were purchased from Alfa Aesar Chemicals. Fuming sulphuric acid 26-29% was purchased from Aldrich. Aluminium oxide activated, neutral Brockmann and silica gel were used for column chromatography. DMSO-d6 99.9% and CD_3OD were purchased from (CIL) Cambridge Iso Top Laboratories, Inc. while chloroform D 99.8% was purchased from Fluorochem.

2.1.2 Instrumentation

NMR spectra were recorded on a Bruker AC500 instrument operating at 500 MHz for ^1H and 125 MHz for ^{13}C and on a Bruker Ultrashield Plus 400 instrument operating at 400MHz for ^1H and 100 MHz for ^{13}C. Chemical shifts (δ) are given in ppm relative to tetramethylsilane (for ^1H and ^{13}C). *J* values are given in Hz and refer to $J_{H\text{-}H}$ unless otherwise indicated, with internal references of δ_H 7.27, δ_C 77, δ_H 2.5, δ_C 39.52 and δ_H 3.31, δ_C 49.00 ppm for $CDCl_3$, DMSO and CD_3OD respectively. Infrared spectra were measured on a Perkin-Elmer 1600 series FTIR spectrometer as KBr disc (solid). Elemental analysis was performed on a Carlo Erba EA1108 elemental analysis. UV-visible spectra were used on recorded on a UNICAM UV/Vis spectrometer UV4. Mass spectra were recorded using electron impact, chemical ionization (NH_3), fast atom bombardment, electrospray, matrix-assisted laser desorption ionization and laser desorption ionization at the EPSRC National

Mass Spectrometry Service at the University of Swansea. Current-voltage (*I-V*) data were measured using a Keithley 2400 Source meter. External quantum efficiency (EQE) was recorded on a QEX10 Quantum Efficiency Measurement System (measured by Dr Matthew Davies) at Swansea University. Single-crystal structures were measured and solved at the UK National Crystallography Service (NCS) Southampton.

2.2 Synthesis of triphenylamine dyes [TPA].

2.2.1 Synthesis of diphenyl-(4-vinyl-phenyl)-amine (1). [1]

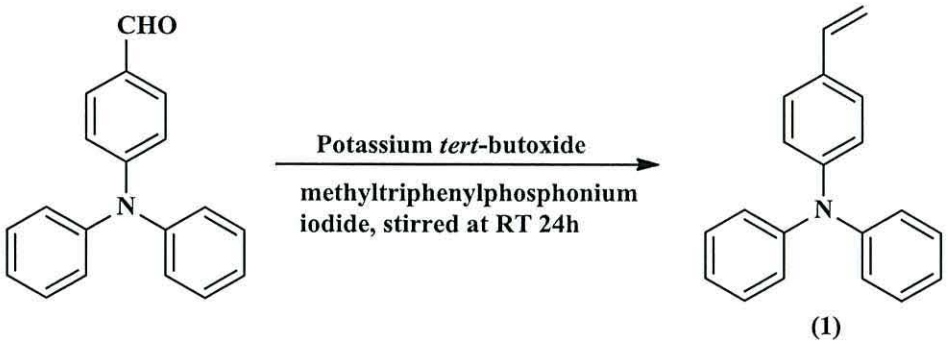

Scheme 2.1. Synthetic pathway of diphenyl-(4-vinyl-phenyl)-amine (**1**).

4-(N, N-diphenylamino)-benzaldehyde (7.5 g, 27.46 mmol) was dissolved in (20 ml) of distilled THF under N_2 and added to a mixture of potassium *tert*-butoxide (4.62 g, 41.19 mmol) and methyl triphenyl phosphonium iodide (16.65 g, 41.19 mmol). This reaction mixture was stirred at room temperature for 24 h under nitrogen. The solution was then poured into a mixture of distilled water / methylene chloride (1:1, v/v) and the organic layer separated in a separating funnel, dried over anhydrous magnesium sulfate and the solvent removed in *vacuo*. The product was purified by column chromatography on silica gel in n-hexane/ methylene chloride (95:5, v/v) as eluent. The pure product was identified by TLC and precipitated in methylene chloride/methanol (1:20, v/v) to give diphenyl-(4-vinyl-phenyl)-amine (**1**) as a white solid (yield 5.40 g, 72.5%), m.p. 92-93 °C (Lit 92-93°C). [1]

A suitable crystal for X-ray analysis was prepared by dissolving this compound in dichloromethane followed by slow evaporation.

$FTMS^+$-MS: Accurate Mass), reference compound: NH_4OAc, calcd. for $C_{20}H_{17}N$ 272.1437; found 272.1434 $[M+H]^+$. ^1H NMR (500 MHz, DMSO-d6) δ 5.15 (d, *J*=10.8 Hz, 1H, H-*CH*=CH-), 5.68 (d, *J*=17.5 Hz, 1H, *H*-CH=CH-), 6.66 (dd, *J*= 10.8, 17.5 Hz, 1H, CH_2=*CH*-), 6.92 (d, *J*=8.5 Hz, 2H, =CH-*Ph*-N-), 7.00 (d, *J*=8.5 Hz, 4H, -N-*Ph*$_2$), 7.04 (t, *J*=7.5 Hz, 2H, -N-*Ph*$_2$-), 7.29 (t, *J*=7.8 Hz, 4H, -N-*Ph*$_2$), 7.37 (d, *J*=8.2 Hz, 2H, =CH-*Ph*-N-). ^{13}C NMR (125 MHz, DMSO-d6) δ 112.46 (-CH=*CH*$_2$-), 123.03, 123.20, 124.03, 127.27, 129.57 (Ar-*C-H*), 131.50 (Ar-*C-C*), 136.02 (Ar-*CH*=CH_2), 146.95, 147.0(Ar-*C-N*).

The UV-Vis spectrum of (**1**) shows an absorption maximum at 324 nm (30864 cm^{-1}) in ethanol. For the FT-IR spectrum (KBr ν/cm^{-1}), the most important peaks at 3084, 3060 and 3032 cm^{-1} ν (C-H, m) aromatic; 2999, 2853 cm^{-1} ν (C-H, m) aliphatic; 1590, 1486 cm^{-1} ν (C=C, s) and 1175 cm^{-1} for ν (C-N, s).

Table 2.1. Crystal data and structure of (**1**).

Identification code	Compound (**1**)
Chemical formula (moiety)	$C_{20}H_{17}N$
Chemical formula (total)	$C_{20}H_{17}N$
Formula weight	271.35
Temperature	120(2) K
Radiation, wavelength	synchrotron, 0.6889 Å
Crystal system, space group	monoclinic, $P2_1/n$
Unit cell parameters	a = 10.000(2) Å $\alpha = 90°$
	b = 18.679(4) Å $\beta = 91.675(2)°$
	c = 15.789(4) Å $\gamma = 90°$
Cell volume	2948.0(11) $Å^3$
Z	8
Calculated density	1.223 g/cm^3
Absorption coefficient μ	0.071 mm^{-1}
F(000)	1152
Crystal colour and size	colourless, 0.05 × 0.04 × 0.01 mm^3
Reflections for cell refinement	9909 (θ range 2.2 to 27.5°)
Data collection method	Crystal Logic diffractometer and Rigaku Saturn 724+ detector thick-slice ω scans
θ range for data collection	1.6 to 25.5°
Index ranges	h −12 to 12, k −20 to 23, l −19 to 19
Completeness to θ = 25.5°	99.5 %
Reflections collected	25445
Independent reflections	5998 (R_{int} = 0.0530)
Reflections with $F^2>2\sigma$	4684
Absorption correction	none
Structure solution	direct methods
Refinement method	Full-matrix least-squares on F^2
Weighting parameters a, b	0.0613, 2.5596
Data / restraints / parameters	5998 / 0 / 380
Final R indices [$F^2>2\sigma$]	R1 = 0.0584, wR2 = 0.1633
R indices (all data)	R1 = 0.0732, wR2 = 0.1707
Goodness-of-fit on F^2	1.094
Extinction coefficient	0.008(3)
Largest and mean shift/su	0.000 and 0.000
Largest diff. peak and hole	0.26 and −0.24 e $Å^{-3}$

2.2.2 Synthesis of 4-[2-(4-Diphenylamino-phenyl)-vinyl]-benzaldehyde (2). [1]

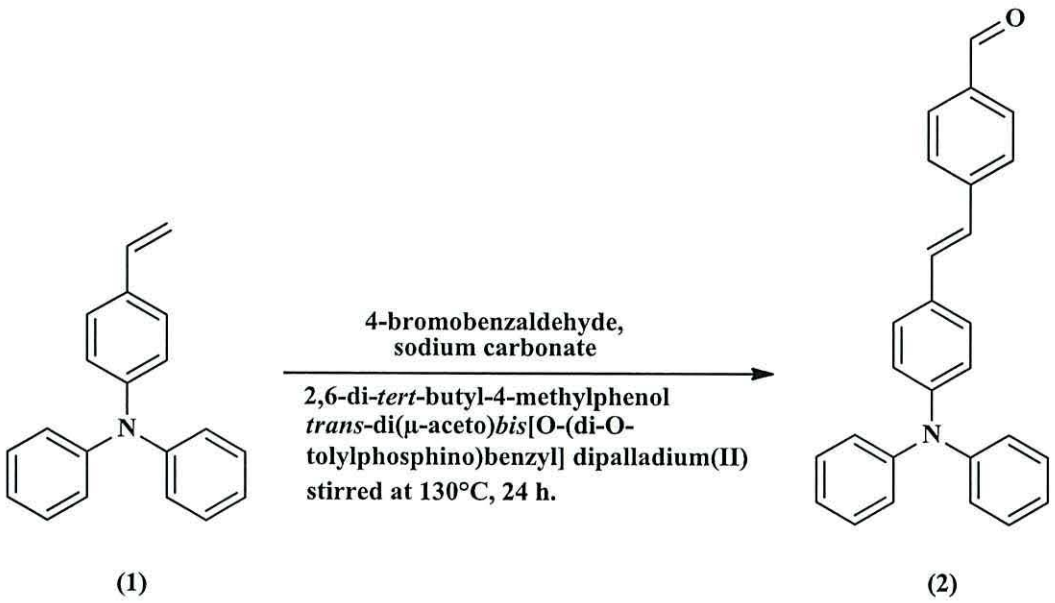

Scheme 2.2. Synthetic pathway of 4-[2-(4-diphenylamino-phenyl)-vinyl]-benzaldehyde (**2**).

A solution of diphenyl-(4-vinyl-phenyl)-amine compound (**1**) (3 g, 11.06 mmol) in anhydrous N,N-dimethylacetamide (DMAC) was added to a mixture of 4-bromobenzaldehyde (0.93g, 5.02 mmol), sodium carbonate (1.33 g, 12.56 mmol), 2,6 di-*tert*-butylcresol (0.22 g, 1.00 mmol), and *trans*-di(μ-acetato)*bis*[0-(di-0-tolylphosphoino)benzyl]dipalladium (*II*) (47.1 mg, 0.05 mmol) in 20 ml of anhydrous *N,N*-dimethylacetamide (DMAC) and the mixture was stirred at 130°C for 24 h. After cooling at room temperature, the solution was poured into a mixture of distilled water and methylene chloride (1:1, v/v). The mixture was separated using a separation funnel. The organic layer was taken and subsequently dried over anhydrous magnesium sulfate. After rotary evaporation of the solvent under reduced pressure and high vacuum under liquid nitrogen to remove solvent, the residue was purified by column chromatography on silica gel with petroleum spirit/ methylene chloride (95:5, v/v). The product was tested by TLC and the product collected after removed the solvent under reduced pressure. Precipitation was by using methanol to produce 4-[2-(4-diphenylamino-phenyl)-vinyl]-benzaldehyde (**2**) as a yellow solid (yield 2.0 g, 48%), m.p. 144-146°C (Lit 144-146°C). [1]

A suitable crystal for X-ray analysis was prepared by dissolving this compound in dichloromethane followed by slow evaporation.

FTMS+-MS: m/z (Accurate Mass), reference compound: NH_4OAc, calcd. for $C_{27}H_{21}NO$ 376.1696, found 376.1699 $[M+H]^+$.

^1H NMR (500 MHz, DMSO-d_6) δ 6.95 (d, *J*=8.5 Hz, 2H, -*Ph*-N-Ph_2), 7.05 (d, *J*=8.2 Hz, 4H, -Ph-N-*Ph_2*), 7.08 (t, *J*=8.2 Hz, 2H, -Ph-N-*Ph_2*), 7.19 (d, *J*=16.4 Hz, 1H, -*CH*=CH-Ph-), 7.32 (t, *J*=7.8 Hz, 4H, -Ph-N-*Ph_2*), 7.41 (d, *J*=16.4 Hz, 1H, -CH=*CH*-Ph-), 7.55 (d, *J*=8.5 Hz, 2H, -*Ph*-N-Ph_2), 7.77 (d, *J*=8.2 Hz, 2H, CHO-*Ph*-CH=), 7.88 (d, *J*=8.2 Hz, 2H, CHO-*Ph*-CH=), 9.97 (s, 1H, *CHO*-Ph-). ^{13}C NMR (125 MHz, DMSO-d_6) δ 122.40, 123.57, 124.47, 126.69, 128.16, 129.65, 130.43 (Ar-*C-H*), 125.43, 131.54 (-Ar-*CH*=*CH*-Ar-), 130.03, 134.73, 143.50 (Ar-*C-C*) 146.78, 147.48 (Ar-*C-N*), 192.28 (Ar-*C=O*).

The UV-Vis spectrum of (**2**) shows absorption maxima at 300 nm (33333 cm^{-1}) and at 400 nm (25000 cm^{-1}) in ethanol.

The FT-IR Spectrum (KBr) ν/cm^{-1} shows absorption peaks at 3060, 3029 cm^{-1} ν (C-H, m) aromatic; 2929, 2853 cm^{-1} ν (C-H, m) aldehyde; 1695 cm^{-1} ν (C=O, shp); 1580 cm^{-1} ν (C=C, str) aromatic; 1488 cm^{-1} ν (C=C, str); 1166cm^{-1} for ν (C-N, shp).

Table 2.2. Crystal data and structure details of (**2**).

Identification code	Compound (**2**)	
Empirical formula	$C_{27}H_{21}NO$	
Formula weight	375.45	
Temperature	120(2) K	
Wavelength	0.71073 Å	
Crystal system	Triclinic	
Space group	*P*–1	
Unit cell dimensions	a = 10.1895(10) Å	α = 102.487(5) °
	b = 11.4764(16) Å	β = 96.931(8) °
	c = 17.763(3) Å	γ = 101.360(8) °
Volume	1959.1(4) $Å^3$	
Z	4	
Density (calculated)	1.273 Mg / m^3	
Absorption coefficient	0.077 mm^{-1}	
F(000)	792	
Crystal	Block; yellow	
Crystal size	0.41 × 0.07 × 0.05 mm^3	
θ range for data collection	3.01 – 25.00°	
Index ranges	$-12 \le h \le 11$, $-13 \le k \le 13$, $-21 \le l \le 21$	
Reflections collected	30858	
Independent reflections	6734 [R_{int} = 0.1570]	
Completeness to θ = 25.00°	97.7 %	
Absorption correction	Semi–empirical from equivalents	
Max. and min. transmission	0.9962 and 0.9692	
Refinement method	Full-matrix least-squares on F^2	
Data / restraints / parameters	6734 / 0 / 523	
Goodness-of-fit on F^2	1.063	
Final *R* indices [$F^2 > 2\sigma(F^2)$]	*R1* = 0.1077, *wR2* = 0.2145	
R indices (all data)	*R1* = 0.1912, *wR2* = 0.2550	
Largest diff. peak and hole	0.258 and –0.278 e $Å^{-3}$	

2.2.3a Synthesis of 2-cyano-3-{4-[2-(4-diphenylamino-phenyl) vinyl]-phenyl}-acrylic acid (3). [1]

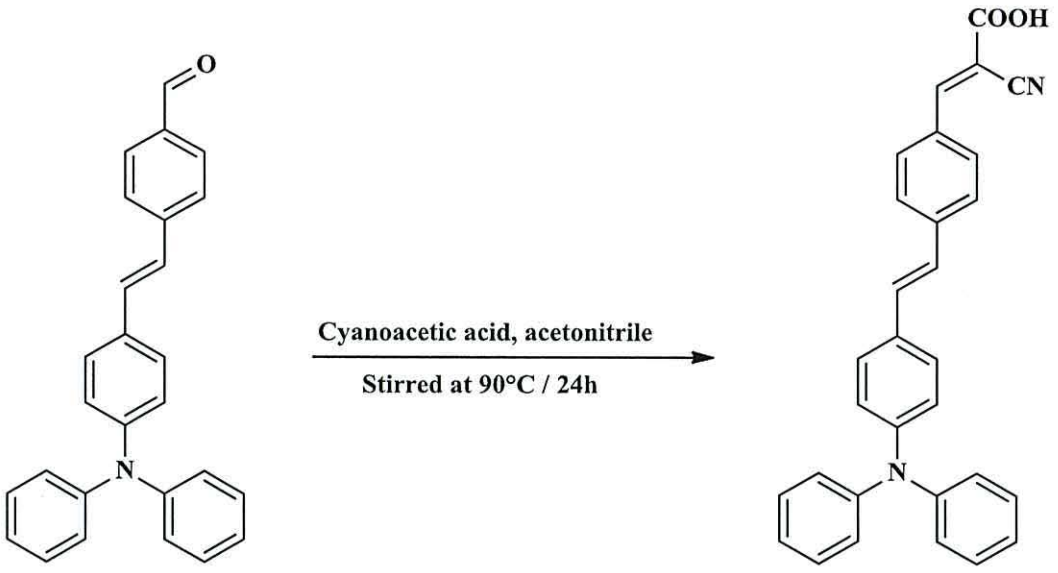

(2) (3)

Scheme 2.3. Synthetic pathway of 2-cyano-3-{4-[2-(4-diphenylamino-phenyl) vinyl]-phenyl}-acrylic acid (**3**).

4-[2-(4-Diphenylamino-phenyl)-vinyl]-benzaldehyde (**2**) (0.5 g, 1.33 mmol) was dissolved in 20 ml of acetonitrile and (2.27 g, 26.63 mmol) of cyanoacetic acid was added. The mixture was stirred at 90°C for 24 h under nitrogen. After cooling at room temperature, the solution was poured into a mixture of methylene chloride/ water (pH was adjusted to pH=2 by phosphoric acid). The mixture was separated by using separation funnel, and the organic layer removed in *vacuo* and subsequently dried over anhydrous sodium sulfate. The crude product was purified by column chromatography over silica gel using chloroform/methanol (9.7:0.3, v/v) as an eluent. The product was tested by TLC and the product collected after removal of the solvent under reduced pressure, followed by precipitation by using methanol to produce 2-cyano-3-{4-[2-(4-diphenylamino-phenyl)vinyl]-phenyl}-acrylic acid (**3**) as a red solid (yield 0.2 g, 34.5 %), m.p. 200-205°C (Lit 216-218°C). [1]

FTMS+-MS: m/z (Accurate Mass), reference compound: NH_4OAc, calcd for $C_{30}H_{22}N_2O_2$ 443.1754, found 443.1751 $[M+H]^+$.

Anal. Calcd for $C_{71}H_{76}O$: C, 81.43; H, 5.01; N, 6.33, Found: C, 62.91; H, 3.74; N, 6.74.

^{1}H NMR (500 MHz, DMSO-d_6) δ 6.96 (d, *J*=8.5 Hz, 2H, -*Ph*-N-Ph_2), 7.05 (d, *J*=8.2 Hz, 4H, Ph-N-*Ph_2*), 7.08 (t, *J*=8.2 Hz, 2H, Ph-N-*Ph_2*), 7.19 (d, *J*=16.4 Hz, 1H, -*CH*=CH-Ph), 7.33 (t, *J*=7.8 Hz, 4H,-Ph-N-*Ph_2*), 7.41 (d, *J*=16.4 Hz, 1H, -CH=*CH*-Ph), 7.55 (d, *J*=8.5 Hz, 2H, -*Ph*-N-Ph_2), 7.77 (d, *J*=8.2 Hz, 2H, =CH-*Ph*-CH=), 8.05 (d, *J*=8.2 Hz, 2H, =CH-*Ph*-CH=), 8.28 (s, 1H, -C=*CH*-Ph-). ^{13}C NMR (125 MHz, DMSO-d_6) δ 99.35 (Ar-C-*C*-CN), 118.52 (-*C≡N*), 122.30, 122.94, 123.21, 123.48, 124.09, 126.47, 127.59 (Ar-*CH*), 124.44, 129.58 (Ar-*CH=CH*-Ar), 127.70, 129.51, 131.18 (*Ar-C*-C), 136.93 (Ar-C-*CH*=C-CN), 138.46, 146.91 (*Ar-C*-N), 165.58 (*C=O*).

The UV-Vis spectrum of (**3**) shows an absorption peak at 300 nm (33333 cm^{-1}) and at 380 nm (26315 cm^{-1}) in ethanol.

The FT-IR spectrum (KBr) ν/cm^{-1} shows absorption peaks at 3300-2700 cm^{-1} ν (O-H, br) carboxylic acid; 2972 cm^{-1} ν (C-H, m) aromatic; 2270 cm^{-1} ν (C≡N, m) aliphatic; 1735 cm^{-1} ν (C=O, str); 1628 cm^{-1} ν (C=C, w); 1284 cm^{-1} ν (C-O, w).

2.2.3b Synthesis of 2-cyano-3-{4-[2-(4-diphenylamino-phenyl) vinyl]-phenyl}-acrylic acid (3b). [2]

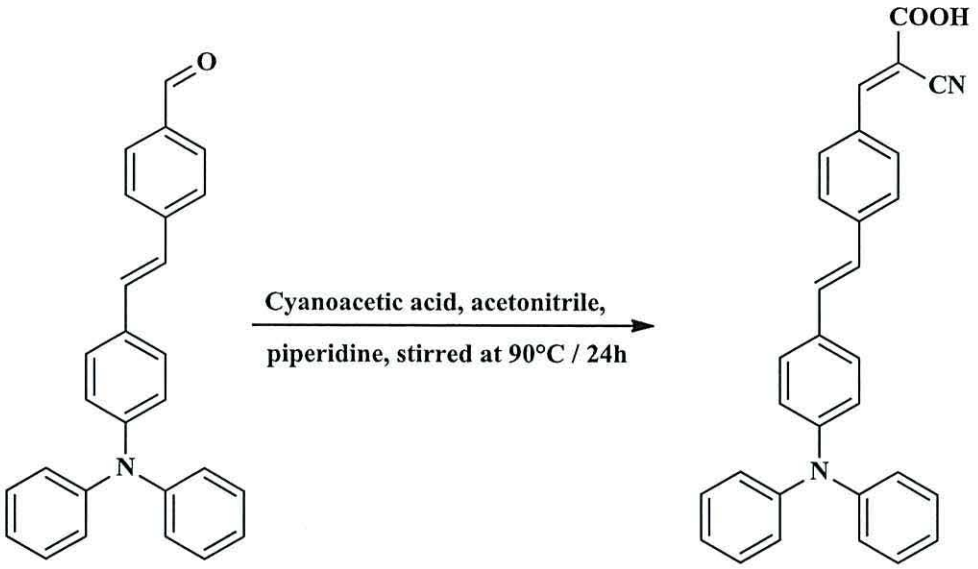

(2) (3b)

Scheme 2.4. Synthetic pathway of 2-cyano-3-{4-[2-(4-diphenylamino-phenyl) vinyl]-phenyl}-acrylic acid compound (**3b**).

In a modified procedure from 2-cyano-3-{4-[2-(4-diphenylamino-phenyl) vinyl]-phenyl}-acrylic acid (**3**), to a solution of 4-[2-(4-diphenylamino-phenyl)-vinyl]-benzaldehyde compound (**2**) (0, 5 g, 1.33 mmol) in 20 ml of acetonitrile was added (2.27 g, 26.63 mmol) cyanoacetic acid and (1 ml) of piperidine. The mixture stirred at 90°C for 24 h under nitrogen. After cooling at room temperature, the solution was poured into a mixture of methylene chloride/water (1:1, v/v). The pH was adjusted to pH=2 by phosphoric acid. The mixture was separated using a separation funnel, and the organic layer removed in *vacuo* and subsequently dried over anhydrous sodium sulfate. The crude product was purified by column chromatography over silica gel using chloroform/methanol (9.7:0.3, v/v) as eluent. The product was tested by TLC followed by precipitation in methanol to produce 2-cyano-3-{4-[2-(4-diphenylamino-phenyl) vinyl]-phenyl}-acrylic acid (**3b**) as a red solid (yield 0.35g, 60.3 %), m.p. 210-212°C (Lit 216-218°C). [1]

MS calcd. for $C_{30}H_{22}N_2O_2$ 442.1754, found 441.1603 $[M-H]^-$. Anal. Calcd. for $C_{30}H_{22}N_2O_2$; C, 81.43; H, 5.01; N, 6.33. Found: C, 81.46; H, 6.05; N, 8.66.

^{1}H NMR (500 MHz, DMSO-d_6) shows δ 6.96 (d, *J*=8.5 Hz, 2H, -*Ph*-N-Ph_2), 7.06 (m, 6H, -N-*Ph_2*), 7.22 (d, *J*=16.4 Hz, 1H, -*CH*=CH-Ph), 7.31 (t, *J*=7.6 Hz, 4H, -N-*Ph_2*)

7.39 (d, *J*=8.15 Hz, 1H, -CH=*CH*-Ph), 7.51 (d, *J*=8.5 Hz, 2H, -*Ph*-N-Ph_2), 7.76 (d, *J*=8.5 Hz, 2H, =CH-*Ph*-CH=), 8.04 (d, *J*=8.55 Hz, 2H, =CH-*Ph*-CH=), 8.28 (s, 1H, -C=*CH*-Ph-). ^{13}C NMR (125 MHz, DMSO-d_6) shows peaks at δ 95.86 (Ar-C-CH=*C*-CN), 118.66 (-*C*≡*N*), 122.63, 123.01, 124.37, 127.80, 128.25, 130.82, 131.27 (*Ar-C*-H), 126.56, 132.59 (Ar-*CH=CH*-Ar), 129.62, 137.00 150.10 (*Ar-C*-C), 138.52 (Ar-C-C-*CH*=C-CN), 140.16, 146.96 (*Ar-C*-N), 169.16 (*C=O*).

The UV-Vis spectrum of (**3b**) shows an absorption peak at 300 nm (33333 cm^{-1}) (ε = 26070 $M^{-1}cm^{-1}$) and at 368 nm (26315 $cm^{-1)}$ (ε = 33255 $M^{-1}cm^{-1}$) in ethanol.

The FT-IR spectrum (KBr) ν/cm^{-1} shows absorption peaks at 2700-3400 cm^{-1} ν (O-H, br) carboxylic acid; 3028 cm^{-1} ν (C-H, m) aliphatic; 2251 cm^{-1} ν (C≡N, m); 1732 cm^{-1} ν (C=O, str); 1587 cm^{-1} ν (C=C, shp) aromatic; 1490 cm^{-1} ν (C=C, shp) aliphatic; 1281 ν (C-O, str); and 1174 cm^{-1} for ν (C-N, shp).

2.2.4 Synthesis of 4-[2-(4-diphenylamino-phenyl)-vinyl]-benzoic acid ethyl ester (4).

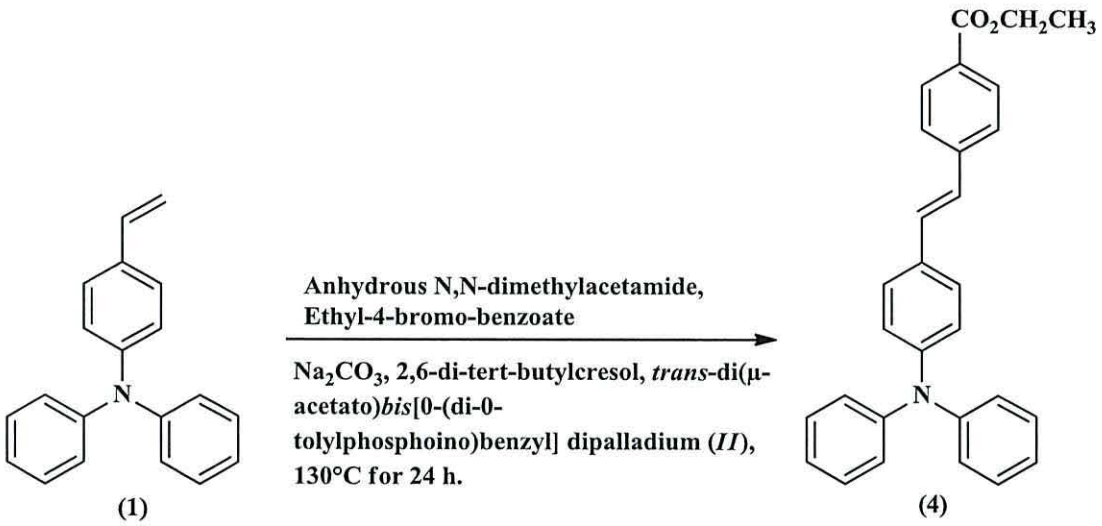

Scheme 2.5. Synthetic pathway of 4-[2-(4-diphenylamino-phenyl)-vinyl]-benzoic acid ethyl ester (**4**).

Diphenyl-(4-vinyl-phenyl)-amine (**1**) (1 g, 3.7 mmol) was dissolved in 20 ml of anhydrous N,N-dimethylacetamide (DMAC), ethyl- 4-bromobenzoate (0.38g, 1.66 mmol), sodium carbonate (0.44 g, 4.1 mmol), 2,6 di-*tert*-butylcresol (0.073 g, 0.33 mmol), and *trans*-di(μ-acetato)*bis*[o-(di-o-tolylphosphoino)benzyl] dipalladium (*II*) (0.015 g, 0.05 mmol) was added to the diphenyl-(4-vinyl-phenyl)-amine solution and the mixture was stirred at 130°C for 24h. After cooling, the solution was poured into a mixture of distilled water and methylene chloride (1:1, v/v). The mixture was separated using a separation funnel, and the organic layer was subsequently dried over anhydrous magnesium sulfate. After rotary evaporation of the solvent under a reduced pressure and high vacuum, the residue was purified by column chromatography on silica gel with petroleum spirit/diethyl ether (95:5, v/v) as an eluent. The product tested by using TLC and removed the solvent followed by precipitation in methanol to produce 4-[2-(4-diphenylamino-phenyl)-vinyl]-benzoic acid ethyl ester (**4**) as a yellow solid (yield 0.4 g, 26 %), m.p. 120-122 °C. A suitable crystal for X-ray analysis was prepared by dissolving this compound in mixture of (dichloromethane/diethyl ether) followed by slow evaporation.

FTMS$^+$-MS: m/z (Accurate Mass), reference compound: NH_4OAc, calcd for $C_{29}H_{25}NO_2$ 420.1958, found 420.1956 $[M+H]^+$. Anal. Calcd for $C_{29}H_{25}NO_2$: C, 83.03; H, 6.01; N, 3.34. Found: C, 82.99; H, 6.08; N, 3.36.

^{1}H NMR (400 MHz, DMSO-d6) δ1.32 (t, *J= 7.16 Hz*,3H, -Ph-OCH$_2$*CH$_3$*), 4.31 (q, *J= 7.04*, 2H, -Ph-O*CH$_2$*CH$_3$), 6.95 (d, *J=8.64* Hz, 2H, -*Ph*-N-Ph$_2$), 7.05 (d, *J=7.52* Hz, 4H, -N-*Ph$_2$*), 7.08 (t, *J=7.28* Hz, 2H, -N-*Ph$_2$*), 7.20 (br d, *J= 16.1*Hz, 1H, -*CH*=CH-Ph), 7.31-7.38 (m, 5H, -N-*Ph$_2$*, -CH=*CH*-Ph), 7.54 (d, *J=8.64*Hz, 2H, *Ph*-N-Ph$_2$), 7.69 (d, *J=8.4* Hz, 2H, -*Ph*-OCH$_2$CH$_3$), 7.93 (d, *J=8.4* Hz, 2H, -*Ph*-OCH$_2$CH$_3$).
^{13}C NMR (125 MHz, DMSO-d$_6$) δ 14.21 (-*CH$_3$*), 60.62 (-*CH$_2$*CH$_3$), 122.51, 123.53, 124.41, 126.29, 128.05, 129.58, 129.69, (*Ar-C*-H), 125.49, 130.00 (Ar-*CH=CH*-Ar), 128.11, 130.78, 142.13 (*Ar-C*-C), 146.83, 147.34 (*Ar-C*-N), 165.52 (*C=O*).
The UV-Vis spectrum of (**4**) shows an absorption peak at 296 nm (33783 cm^{-1}) and at 388 nm (25773 cm$^{-1)}$ in ethanol.
The FT-IR spectrum (KBr) ν/cm^{-1} shows absorption peaks at 3023 cm^{-1} ν (C-H, m) aromatic; 2984 cm^{-1} ν (C-H, m) aliphatic; 1709 cm^{-1} ν (C=O, shp); 1589 cm^{-1} ν (C=C, shp) aromatic; 1493 cm^{-1} ν (C=C, shp) aliphatic; 1278 cm^{-1} ν (C-O, shp); 1178 cm^{-1} ν (C-N, shp).

Table 2.3. Crystal data and structure refinement details of **(4)**.

Identification code	Compound (**4**)
Empirical formula	$C_{29}H_{25}NO_2$
Formula weight	419.50
Temperature	120(2) K
Wavelength	0.71073 Å
Crystal system	Monoclinic
Space group	*P*21/*c*
Unit cell dimensions	$a = 11.2472(4)$ Å $\quad \alpha = 90°$
	$b = 13.4462(4)$ Å $\quad \beta = 90.5670(10)°$
	$c = 30.0363(11)$ Å $\quad \gamma = 90°$
Volume	4542.2(3) $Å^3$
Z	8
Density (calculated)	1.227 Mg / m^3
Absorption coefficient	0.076 mm^{-1}
F(000)	1776
Crystal	Prism; Green
Crystal size	0.20 × 0.05 × 0.04 mm^3
θ range for data collection	3.03 – 25.00°
Index ranges	$-13 \le h \le 13, -15 \le k \le 14, -35 \le l \le 35$
Reflections collected	32084
Independent reflections	7961 [$R_{int} = 0.0685$]
Completeness to $\theta = 25.00°$	99.5 %
Absorption correction	Semi–empirical from equivalents
Max. and min. transmission	0.9970 and 0.9849
Refinement method	Full-matrix least-squares on F^2
Data / restraints / parameters	7961 / 0 / 595
Goodness-of-fit on F^2	1.165
Final *R* indices [$F^2 > 2\sigma(F^2)$]	*R1* = 0.0842, *wR2* = 0.1385
R indices (all data)	*R1* = 0.1306, *wR2* = 0.1606
Largest diff. peak and hole	0.264 and –0.255 e $Å^{-3}$

2.2.5 Synthesis of 4-[2-(4-diphenylamino-phenyl)-vinyl]-benzoic acid (5).

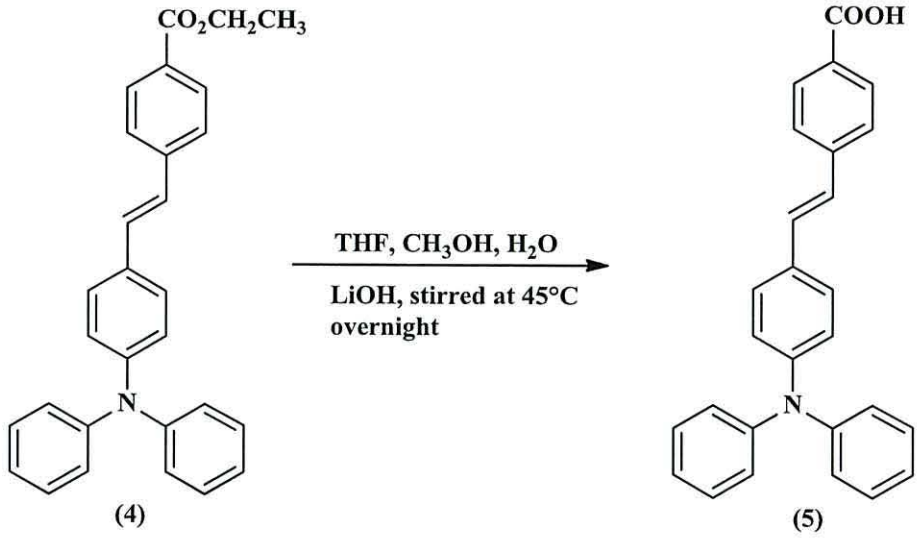

Scheme 2.6. Synthetic pathway of 4-[2-(4-diphenylamino-phenyl)-vinyl]-benzoic acid (**5**).

4-[2-(4-diphenylamino-phenyl)-vinyl]-benzoic acid ethyl ester (**4**) (0.35 g, 0.83 mmol) was dissolved in 10 ml THF with 1 ml methanol, 1 ml H_2O (10:1:1) and LiOH (0.699 g, 0.83 mmol, 20 eq.). Thus was stirred overnight at 45°C. After that a 5% of hydrochloric acid solution was added and the pH adjusted to between 6-5 using 5% HCl. The solution was then quenched with water and was then extracted with ethyl acetate, and water removed using anhydrous magnesium sulfate. After that the solution was concentrated to produce 4-[2-(4-diphenylamino-phenyl)-vinyl]-benzoic acid (**5**) as a yellow solid (yield 0.30 g, 93 %), m.p. 214 - 216 °C. A suitable crystal for X-ray analysis was prepared by dissolving this compound in mixture of (dichloromethane/diethyl ether) followed by slow evaporation.

FTMS$^+$-MS: m/z (Accurate Mass), reference compound: NH_4OAc, calcd for $C_{27}H_{21}NO_2$, 392.1645, found 392.1641 $[M+H]^+$. Anal. Calcd for $C_{27}H_{21}NO_2$: C, 82.84; H, 5.41; N, 3.58. Found: C, 81.89; H, 5.60; N, 3.41.

^{1}H NMR (500 MHz, DMSO-d6) δ 6.95 (d, *J=8.5* Hz, 2H, -*Ph*-N-Ph_2), 7.05 (d, *J=7.9* Hz, 4H, -N-*Ph_2*), 7.08 (t, *J=7.25* Hz, 2H, -N-*Ph_2*), 7.17 (d, *J=16.4* Hz, 1H, -*CH*=CH-Ph), 7.28-7.40 (m, 5H, -N-*Ph_2*, -CH=*CH*-Ph), 7.54 (d, *J=8.85* Hz, 2H, *Ph*-N-Ph_2), 7.66 (d, *J=8.5* Hz, 2H, -*Ph*-COOH), 7.91 (d, *J=8.5* Hz, 2H, -*Ph*-COOH).

^{13}C NMR (125 MHz, DMSO-d_6) δ 122.66, 123.42, 124.30, 128.03, 128.34, 130.01, 130.72 (*Ar-C*-H), 124.97, 130.55 (Ar-*CH=CH*-Ar), 129.63, 131.85, 138.43 (*Ar-C*-C), 146.87, 147.20 (*Ar-C*-N), 166.62 (*C=O*).

The UV-Vis spectrum of (**5**) shows an absorption peak at 296 nm (33783 cm^{-1}) and at 384 nm (26041 cm^{-1}) (ε = 26981 $M^{-1}cm^{-1}$) in ethanol solution.

The FT-IR spectrum (KBr) ν/cm^{-1} shows absorption peak at 3300-2700 cm^{-1} ν (O-H, br) carboxylic acid; 3029 cm^{-1} ν (C-H, m) aromatic; 1681 cm^{-1} ν (C=O, shp); 1589 cm^{-1} ν (C=C, shp) aromatic; 1493 cm^{-1} ν (C=C, shp) aliphatic; 1283 cm^{-1} ν (C-O, shp); 1179 cm^{-1} ν (C-N, shp).

Table 2.4. Crystal data and structure refinement details of (**5**).

Identification code	Compound (**5**)	
Empirical formula	$C_{27}H_{21}NO_2$	
Formula weight	391.45	
Temperature	120(2) K	
Wavelength	0.71073 Å	
Crystal system	Monoclinic	
Space group	*P*21/*c*	
Unit cell dimensions	a = 17.1248(5) Å	α = 90°
	b = 9.6815(2) Å	β = 110.727(2) °
	c = 12.9988(3)	γ = 90°
Volume	2015.63(9) $Å^3$	
Z	4	
Density (calculated)	1.290 Mg / m^3	
Absorption coefficient	0.081 mm^{-1}	
F(000)	824	
Crystal	Block; Light Yellow	
Crystal size	0.20 × 0.14 × 0.06 mm^3	
θ range for data collection	3.14 – 27.48°	
Index ranges	$-22 \le h \le 22$, $-12 \le k \le 12$, $-16 \le l \le 16$	
Reflections collected	28268	
Independent reflections	4613 [R_{int} = 0.0564]	
Completeness to θ = 27.48°	99.7 %	
Absorption correction	Semi–empirical from equivalents	
Max. and min. transmission	0.9952 and 0.9840	
Refinement method	Full-matrix least-squares on F^2	
Data / restraints / parameters	4613 / 0 / 280	
Goodness-of-fit on F^2	1.057	
Final *R* indices [$F^2 > 2\sigma(F^2)$]	*R1* = 0.0481, *wR2* = 0.1030	
R indices (all data)	*R1* = 0.0682, *wR2* = 0.1131	
Largest diff. peak and hole	0.214 and –0.254 e $Å^{-3}$	

2.2.6 Synthesis of 5-bromo-1, 3-di-benzaldehyde (9).

(Two methods used), method A.

2.2.6.1 Synthesis of 1-bromo-3, 5-bis (bromomethyl) benzene (6a). [3]

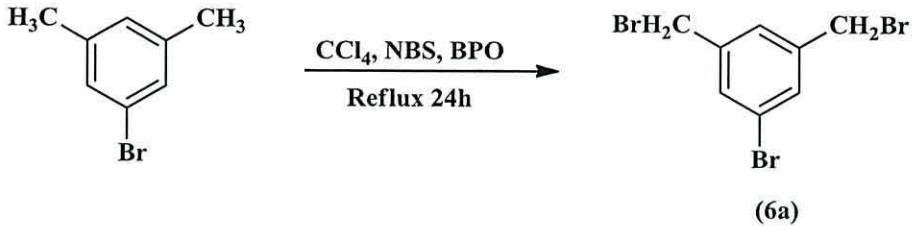

(6a)

Scheme 2.7. Synthetic pathway of 1-bromo-3, 5-*bis* (bromomethyl) benzene (**6a**).

Using a method developed from are reported previously, [3] 5-bromo-m-xylene (2.78 g, 15 mmol) and N-bromosuccinimide (NBS) (6.6 g, 37 mmol) were added to 150 ml CCl_4 and refluxed under nitrogen overnight in presence of benzoyl peroxide (BPO) (0.3 g). After refluxing the solution was treated with a mixture of petrol\ethylacetate (5:1, v\v), and then refluxed for 30 min, After cooling to room temperature and filtration to remove the solvent, the crude product was purified by column chromatography on silica gel by using petrol/ethyl acetate (5:2, v/v) as an eluent to produce white precipitate of 1-bromo-3, 5-*bis* (bromomethyl) benzene (**6a**) (yield 1.6g, 39%), m.p. 64-66°C. A suitable crystal for X-ray analysis was prepared by dissolving this compound in mixture of (dichloromethane/diethyl ether).
$FTMS^+$-MS: m/z (Accurate Mass), reference compound: NH_4OAc, calcd. for $C_8H_7Br_3$ 357.8436, found 357.8437 $[M+NH_4]^+$.

^1H NMR (500 MHz, $CDCl_3$) δ 4.41 (s, 4H, 2x -*CH_2*-Br), 7.34 (bs, 1H, *Ar-H*), 7.48 (d, *J*=1.55, 2H, *Ar-H*); ^{13}C NMR (125 MHz, $CDCl_3$) δ 31.04 (Ar-*CH_2*-Br), 122.71 (Ar-*C-Br*), 128.26, 133.30 (*Ar-C*-H), 140.30 (*Ar-C*-CH_2-).

Table 2.5. Crystal data and structure refinement details of **(6a).**

Identification code	Compound **(6a)**
Empirical formula	$C_8H_7Br_3$
Formula weight	342.87
Temperature	120(2) K
Wavelength	0.71073 Å
Crystal system	Triclinic
Space group	*P*–1
Unit cell dimensions	$a = 7.3267(2)$ Å $\quad \alpha = 66.856(2)°$
	$b = 8.8715(3)$ Å $\quad \beta = 69.377(2)°$
	$c = 8.9737(3)$ Å $\quad \gamma = 71.207(2)°$
Volume	490.40(3) $Å^3$
Z	2
Density (calculated)	2.322 Mg / m^3
Absorption coefficient	12.274 mm^{-1}
F(000)	320
Crystal	Prism; colourless
Crystal size	0.16 × 0.08 × 0.05 mm^3
θ range for data collection	3.29 – 27.50°
Index ranges	$-9 \le h \le 9, -11 \le k \le 11, -11 \le l \le 11$
Reflections collected	13935
Independent reflections	2253 [$R_{int} = 0.0372$]
Completeness to $\theta = 27.50°$	99.8 %
Absorption correction	Semi–empirical from equivalents
Max. and min. transmission	0.5789 and 0.2441
Refinement method	Full-matrix least-squares on F^2
Data / restraints / parameters	2253 / 0 / 100
Goodness-of-fit on F^2	1.128
Final *R* indices [$F^2 > 2\sigma(F^2)$]	*R1* = 0.0267, *wR2* = 0.0624
R indices (all data)	*R1* = 0.0311, *wR2* = 0.0649
Largest diff. peak and hole	0.643 and –0.784 e $Å^{-3}$

2.2.6.2 Synthesis of 5-bromo-1, 3-phenylene-bis (methylene) diacetate (7a). [3]

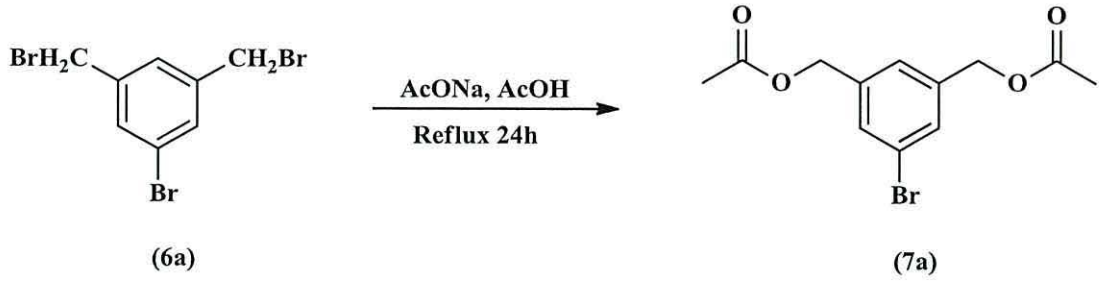

(6a) (7a)

Scheme 2.8. Synthetic pathway of 5-bromo-1, 3-phenylene-*bis* (methylene) diacetate (**7a**).

Sodium acetate (5 g) in (100 ml) of glacial acetic acid was added to a solution of (2 g, 0.0058 mmol) of compound (**6a**), which was then refluxed overnight. After cooling at room temperature, the solution was poured into a mixture of a saturated solution of sodium bicarbonate/dichloromethane, the aqueous and organic layers were separated by funnel separation and treated the organic layer with $MgSO_4$ anhydrous. The solvent was reduced under vacuum and the product extracted by column chromatography on silica gel by using petroleum spirit: ethyl acetate (5:2, v/v) as an eluent to produce compound (**7a**) as a white solid (yield 1.3g, 76%). FTMS+-MS: m/z (Accurate Mass), reference compound: NH_4OAc, calcd for $C_{12}H_{13}BrO_4$ 318.0335 found 318.0342 $[M+NH_4]^+$.

^1H NMR (500 MHz, $CDCl_3$) δ 2.09 (s, 6H, 2x-CH_2OCO-*CH_3*), 5.04 (s, 4H, 2x-*CH_2*-OCO-CH_3*)*, 7.22 (s, 1H, *Ar-H*) 7.43 (s, 2H, *Ar-H*). ^{13}C NMR (125 MHz, $CDCl_3$) δ 20.60 (-*CH_3*), 64.99 (-*CH_2*), 122.52 (*Ar-C*-Br), 126.16, 130.63 (*Ar-C*-H), 138.31 (*Ar-C*-CH_2-), 170.80 (*C=O*).

2.2.6.3 Synthesis of 5-bromo-1, 3-phenylene dimethanol (8a). [3]

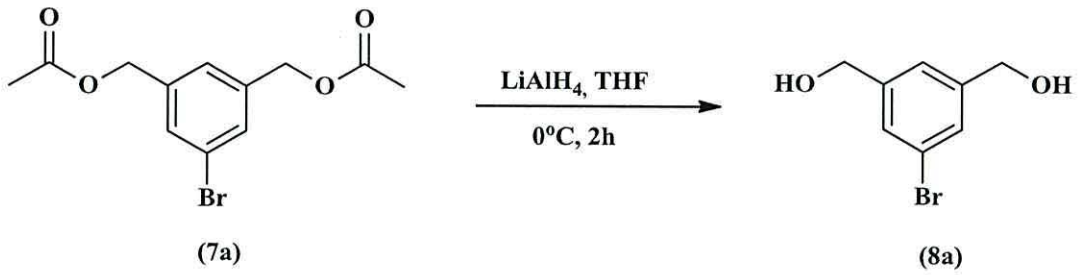

Scheme 2.9. Synthetic pathway of 5-bromo-1, 3-phenylene dimethanol (**8a**).

Compound (**7a**) (3.8g, 12.6 mmol) was added slowly (drop wise) to a solution of $LiAlH_4$ (0.95 g, 25.2 mmol) in THF (180 ml) at 0°C. This solution was stirred 1 h at 0°C, and then for 2 h at room temperature, before refluxing for 1 h. After cooling to room temperature a saturated aqueous solution of sodium sulfate decahydrate was added drop wise at 0°C. After filtration through celite, the filtrate was taken and the solvent reduced under vacuum, the product was purified by column chromatography on silica gel using petroleum spirit/ethyl acetate (5:2, v\v) as an eluent to produce 5-bromo-1, 3-phenylene dimethanol compound (**8a**) as a white precipitate (yield 2.4g, 88 %), m.p. 78-82°C. (GC) EI+: m/z, calcd for $C_8H_9BrO_2$ 215.98 found 215.9.
^1H NMR (500 MHz, DMSO-d_6) δ 4.48 (s, 4H, 2x-*CH*$_2$OH), 5.33 (bs, 2H, -CH$_2$*OH*), 7.24 (s, 1H, *Ar-H*), 7.35 (s, 2H, *Ar-H*); ^{13}C (125MHz, DMSO-d_6) δ 62.19 (*CH*$_2$-OH), 121.23 (*Ar*-*C*-Br), 123.32, 127.21 (*Ar*-*C*-H), 145.23 (*Ar*-*C*-CH$_2$OH). There are some traces of impurities with signal at (29.22, 48.65).

2.2.6.4 Synthesis of 5-bromoisophthalaldehyde (9a). [3]

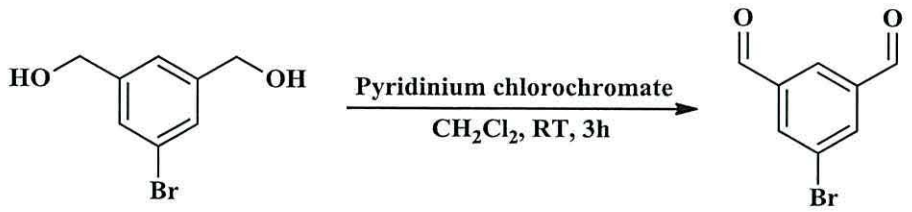

(8a) (9a)

Scheme 2.10. Synthetic pathway of 5-bromoisophthalaldehyde (**9a**).

To a solution of pyridinium chlorochromate PCC (7.39 g, 34.28 mmol) in 350 ml CH_2Cl_2 was added (2.8 g, 12.89 mmol) of the 5-bromo-1, 3-phenylene dimethanol (**8a**) which had been pre-dissolved in 120 ml CH_2Cl_2. This was added slowly (drop wise) over more than 60 minutes. After addition, the solution was left stirring at room temperature for 3 hours. It was then poured into a mixture of petroleum spirit/ethyl acetate (10:2, v/v) to form a precipitate, which was then filtered. The solvent was reduced under vacuum and the product purified by column chromatography on silica gel with petroleum spirit/ethyl acetate (5:2, v/v). The solvent was reduced under vacuum to produce a white precipitate of 5-bromoisophthalaldehyde (**9a**) (yield 1g, 37%), m.p. 100-104°C. A suitable crystal for X-ray analysis was prepared by dissolving this compound in dichloromethane followed by slow evaporation. GC mass calcd. for $C_8H_5BrO_2$ 213.03 found 213.9 M^+.

^{1}H NMR (500 MHz, $CDCl_3$) δ 8.28 (d, *J*= 0.95, 2H, *Ar-H*), 8.32 (t, *J*=1.25 Hz, 1H, *Ar-H*), 10.06 (s, 2H, 2x-*CHO*); ^{13}C (125 MHz, CDCl3) δ 124.42 (*Ar-C*-Br), 129.26, 137.23 (*Ar-C*-H), 138.45 (*Ar-C*-C=O), 189.50 (*C=O*).

Table 2.6. Crystal data and structure refinement details of (**9a**).

Identification code	Compound (**9a**)
Empirical formula	$C_8H_5BrO_2$
Formula weight	213.03
Temperature	120(2) K
Wavelength	0.71073 Å
Crystal system	Monoclinic
Space group	*P*21/*c*
Unit cell dimensions	$a = 7.9468(5)$ Å $\quad \alpha = 90°$
	$b = 13.9331(10)$ Å $\quad \beta = 114.587(4)°$
	$c = 7.4660(4)$ Å $\quad \gamma = 90°$
Volume	751.71(8) $Å^3$
Z	4
Density (calculated)	1.882 Mg / m^3
Absorption coefficient	5.406 mm^{-1}
F(000)	416
Crystal	Plate; colourless
Crystal size	0.16 × 0.10 × 0.02 mm^3
θ range for data collection	3.18 – 27.50°
Index ranges	$-10 \le h \le 10, -18 \le k \le 18, -9 \le l \le 9$
Reflections collected	8701
Independent reflections	1723 [$R_{int} = 0.0381$]
Completeness to $\theta = 27.50°$	99.7 %
Absorption correction	Semi–empirical from equivalents
Max. and min. transmission	0.8996 and 0.4783
Refinement method	Full-matrix least-squares on F^2
Data / restraints / parameters	1723 / 0 / 100
Goodness-of-fit on F^2	1.117
Final *R* indices [$F^2 > 2\sigma(F^2)$]	*R1* = 0.0397, *wR2* = 0.0825
R indices (all data)	*R1* = 0.0533, *wR2* = 0.0905
Largest diff. peak and hole	1.443 and –0.366 e $Å^{-3}$

2.2.7 Synthesis of 5-bromo-1, 3-di-benzaldehyde (9b).

Method B.

2.2.7.1 Synthesis of 1, 3-dimethyl 5-bromoisophthalate (10). [4]

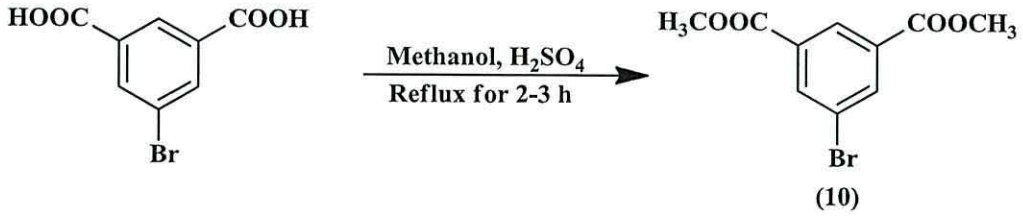

(10)

Scheme 2.11. Synthetic pathway of 1, 3-dimethyl 5-bromoisophthalate (**10**).

5-bromo-isophthalic acid (2 g) was dissolved in 60 ml of methanol, containing 1.4 ml of concentrate sulfuric acid, and this solution was refluxed for 3-4 h. After cooling at room temperature, 20 ml of a saturated aqueous solution of sodium bicarbonate was added drop wise followed by 100 ml of ethyl acetate. The mixture was separated using a separation funnel. The organic layer was taken and subsequently dried over anhydrous magnesium sulfate. After rotary evaporation of the solvent under reduced pressure, the residue was purified by column chromatography on silica gel with petroleum spirit/ethyl acetate (5:2, v/v). The product was tested using TLC and the product collected after rotary evaporation of the solvent under reduced pressure to produce a white solid of 1, 3-dimethyl 5-bromoisophthalate (**10**) (2.0 g, 90 %), m.p. 68-70°C. A suitable crystal for X-ray analysis was prepared by dissolving this compound in dichloromethane followed slow evaporation. $FTMS^{+}$-MS: m/z (Accurate Mass), reference compound: NH_4OAc, calcd. for $C_{10}H_9BrO_4$ 290.0022, found 290.0028 $[M+NH_4]^{+}$.

^1H NMR (400 MHz, $CDCl_3$) δ 3.97 (s, 6H, 2x-COO*CH*$_3$), 8.36 (d, *J*=1.4, 2H, *Ar-H*), 8.61 (t, *J*=1.4, 1H, *Ar-H*). ^{13}C NMR (100 MHz, $CDCL_3$) δ 52.66 (-*CH*$_3$), 122.57 (*Ar-C*-Br), 129.23, 132.30 (*Ar-C*-H), 136.63 (*Ar-C*-C=O), 164.96 (*C=O*).

Table 2.7. Crystal data and structure refinement details of (**10**).

Identification code	Compound (**10**)
Empirical formula	$C_{10}H_9BrO_4$
Formula weight	273.08
Temperature	100(2) K
Wavelength	0.71075 Å
Crystal system	Monoclinic
Space group	*P*21/*n*
Unit cell dimensions	$a = 7.578(3)$ Å $\quad \alpha = 90°$
	$b = 10.168(5)$ Å $\quad \beta = 90.240(8)°$
	$c = 13.190(6)$ Å $\quad \gamma = 90°$
Volume	1016.3(8) $Å^3$
Z	4
Density (calculated)	1.785 Mg / m^3
Absorption coefficient	4.034 mm^{-1}
F(000)	544
Crystal	Block; Colourless
Crystal size	0.22 × 0.20 × 0.18 mm^3
θ range for data collection	3.09 – 27.48°
Index ranges	$-6 \le h \le 9, -13 \le k \le 11, -17 \le l \le 17$
Reflections collected	6697
Independent reflections	2303 [$R_{int} = 0.0328$]
Completeness to $\theta = 27.48°$	99.1 %
Absorption correction	Semi–empirical from equivalents
Max. and min. transmission	0.5304 and 0.4706
Refinement method	Full-matrix least-squares on F^2
Data / restraints / parameters	2303 / 0 / 138
Goodness-of-fit on F^2	0.769
Final *R* indices [$F^2 > 2\sigma(F^2)$]	*R1* = 0.0298, *wR2* = 0.0812
R indices (all data)	*R1* = 0.0325, *wR2* = 0.0846
Largest diff. peak and hole	0.438 and –0.531 e $Å^{-3}$

2.2.7.2 Synthesis of (5-bromo-1, 3-phenylene) dimethanol (8b). [3]

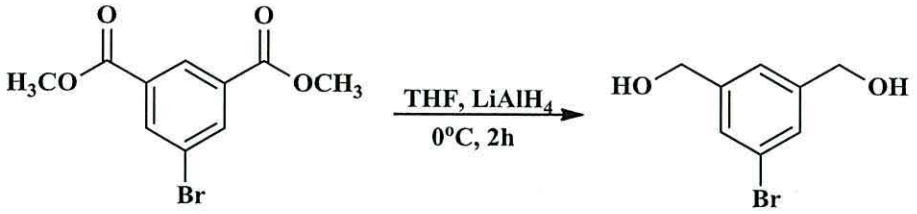

(10) (8b)

Scheme 2.12. Synthetic pathway of 5-bromo-1, 3-phenylene-dimethanol (**8b**).

Compound (**10**) (3.0 g, 11.0 mmol) was added slowly (drop wise) to a solution (0.83 g, 22 mmol) of $LiAlH_4$ in THF (150 ml) at 0°C, followed by stirring for one hour at 0°C. After that, the solution was stirred for 2 hours at room temperature and was then refluxed for 3-4 hours. It was then cooled to room temperature. Then a saturated aqueous solution of sodium sulphate decahydrate was added drop wise at 0°C, during which a white precipitate formed. This was filtered through C-light. The filtrate was collected and the solvent was reduced under vacuum. The solid product was then purified by column chromatography on silica gel using petrol/ethyl acetate (5:2, v/v) as an eluent to produce 5-bromo-1, 3-phenylene-dimethanol (**8b**) as a white precipitate (yield 2.0 g, 84 %), m.p. 78-82°C.

$FTMS^+$-MS: m/z (Accurate Mass), reference compound: NH_4OAc, calcd. for $C_8H_9BrO_2$ 234.0124, found 234.0126 $[M+NH_4]^+$.

^1H NMR (400 MHz, D_2O) δ 4.63 (s, 4H, -*CH_2*OH), 7.33 (s, 1H, *Ar-H*), 7.52 (s, 2H, *Ar-H*); DEPTQ (100 MHz, D_2O) δ 63.01 (-*CH_2*), 122.00 (*Ar-C*-Br), 124.76, 129.24 (*Ar-C*-H), 142.91 (*Ar-C*-CH_2OH).

Table 2.8. Crystal data and structure refinement details of (**8b**).

Identification code	Compound (**8b**)	
Empirical formula	$C_8H_9BrO_2$	
Formula weight	217.06	
Temperature	100(2) K	
Wavelength	0.71075 Å	
Crystal system	Orthorhombic	
Space group	*Pna*21	
Unit cell dimensions	$a = 24.3735(17)$ Å	$\alpha = 90°$
	$b = 4.5110(2)$ Å	$\beta = 90°$
	$c = 7.4416(5)$ Å	$\gamma = 90°$
Volume	818.20(9) $Å^3$	
Z	4	
Density (calculated)	1.762 Mg / m^3	
Absorption coefficient	4.968 mm^{-1}	
F(000)	432	
Crystal	Block; colourless	
Crystal size	0.09 × 0.08 × 0.04 mm^3	
θ range for data collection	3.21 – 27.48°	
Index ranges	$-31 \le h \le 23$, $-4 \le k \le 5$, $-9 \le l \le 9$	
Reflections collected	5511	
Independent reflections	1828 [$R_{int} = 0.0459$]	
Completeness to $\theta = 27.48°$	99.6 %	
Absorption correction	Semi–empirical from equivalents	
Max. and min. transmission	0.8260 and 0.6634	
Refinement method	Full-matrix least-squares on F^2	
Data / restraints / parameters	1828 / 1 / 102	
Goodness-of-fit on F^2	1.070	
Final R indices [$F^2 > 2\sigma(F^2)$]	$R1 = 0.0236$, $wR2 = 0.0570$	
R indices (all data)	$R1 = 0.0262$, $wR2 = 0.0580$	
Absolute structure parameter	0.011(11)	
Largest diff. peak and hole	0.290 and –0.326 e $Å^{-3}$	

2.2.7.3 Synthesis of 5-bromoisophthalaldehyde (9b). [3]

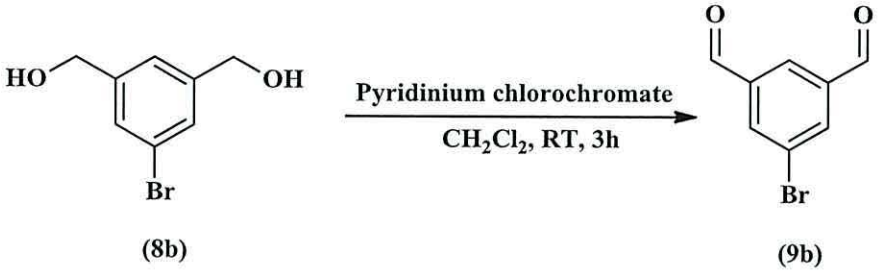

(8b) (9b)

Scheme 2.13. Synthetic path way of 5-bromoisophthalaldehyde (**9b**).

To a solution of pyridinium chlorochromate (PCC) (5.2 g, 24.5 mmol) in 130 ml CH_2Cl_2 was added drop wise (2.0 g, 9.2 mmol) of 5-(bromo-1, 3-phenylene)dimethanol (**8b**) which had been pre-dissolved in 120 ml CH_2Cl_2. This solution was left to stir at room temperature for 3 hours, and was then poured into a mixture of petroleum spirit/ethyl acetate (10:2, v/v), which formed a white precipitate. The solid was filtered and the filtrate solvent was reduced under vacuum and checked by TLC. The solid was then purified by column chromatography using petroleum spirit\ethyl acetate (5:2, v/v) as eluent. The solvent was then reduced under vacuum to produce a white precipitate of 5-bromoisophthalaldehyde (**9b**) (yield 0.9 g, 46 %), m.p. 100-104°C.

FTMS$^+$-MS: m/z (Accurate Mass), reference compound: ASAP (solid), calcd for $C_8H_5BrO_2$ 211.9546 found 212.9545 $[M+H]^+$.

^{1}H NMR (400 MHz, $CDCl_3$) δ 8.27 (d, *J*= 1.2, 2H, *Ar*-H), 8.31 (bs, 1H, *Ar-H*), 10.06 (s, 2H, *2x-CHO*); ^{13}C (100 MHz, $CDCl_3$) δ 124.39 (*Ar-C*-Br), 129.24, 137.20 (*Ar-C*-H), 138.42 (*Ar-C*-C=O), 189.48 (*C=O*).

2.2.8 Synthesis of (E)-5-(4-(diphenylamino) styryl) isophthalaldehyde (11).

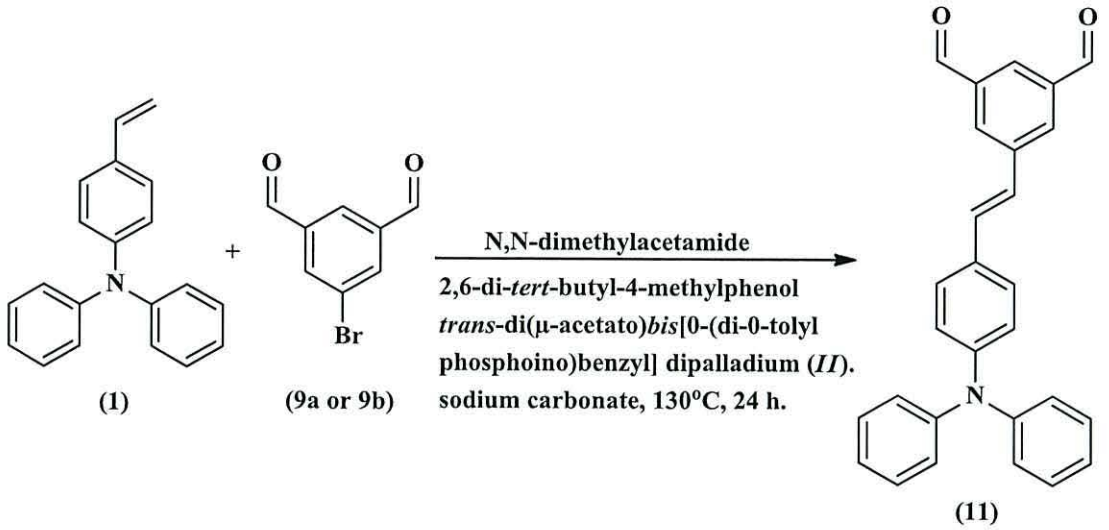

Scheme 2.14. Synthetic pathway of (E)-5-(4-(diphenylamino) styryl)isophthalaldehyde (**11**).

To a solution of diphenyl-(4-vinyl-phenyl)-amine (**1**) (1 g, 3.7 mmol) in N,N-dimethylacetamide (20 ml) was added 1,3-dimethyl 5-bromoisophthalate (**9a** or **9b**) (0.35 g, 0.453 mmol), 2,6-d-tert-butylmethyl phenol (0.073 gm, 0.09 mmol), anhydrous sodium carbonate (0.44 g, 1.13 mmol), and *trans*-di(μ-acetato)*bis*[0-(di-0-tolylphosphoino)benzyl] dipalladium (*II*) (0.015 g, 0.0045 mmol). The mixture was then stirred under nitrogen at 130°C for 24 h. The solution was cooled to room temperature and poured into a mixture of distilled water and methylene chloride (1:1, v/v). The resulting mixture was separated by using a separation funnel. The organic layer was taken and subsequently dried over anhydrous magnesium sulfate. Rotary evaporation of the solvent under a reduced pressure was followed by high vacuum to remove the solvent. The residue was purified by column chromatography on silica gel with petroleum spirit/diethyl ether (95:5, v/v). After that the product was tested by TLC and the product was collected after rotary evaporation of the solvent under reduced pressure to make (E)-5-(4-(diphenylamino) styryl)isophthalaldehyde (**11**) as a yellow solid (yield 0.4 g, 27%), m.p. 124-126°C. A suitable crystal for X-ray structural analysis was obtained by dissolving this compound in dichloromethane followed by slow evaporation.

$FTMS^{+}$-MS: m/z (Accurate Mass), reference compound: NH_4OAc, calcd. for $C_{28}H_{21}NO_2$ 404.1645, found 404.1645 $[M+H]^{+}$.

^{1}H NMR (400 MHz, DMSO) δ 6.97 (d, *J*=8.56 Hz, 2H, -*Ph*-N-Ph_2), 7.06 (d, *J*=8.5 Hz, 4H, -N-*Ph_2*), 7.10 (t, *J*=7.25 Hz, 2H, -N-*Ph_2*), 7.33 (t, *J*=7.92 Hz, 5H, -N-*Ph_2*), 7.48 (d, *J*=16.44 Hz, 1H, -*CH*=CH-Ph-), 7.58 (d, *J*=8.85 Hz, 2H, -*Ph*-N-Ph_2), 8.26 (s, 1H, -*Ph*-CHO), 8.39 (s, 2H, -*Ph*-CHO), 10.13 (s, 2H, -Ph-*CHO*); ^{13}C NMR (500 MHz, DMSO-d_6) shows peaks at δ 122.52, 123.56, 124.33, 126.11, 128.28, 130.370, 130.99 (*Ar-C*-H), 125.45, 131,84, (Ar-*CH=CH*-Ar), 129.68, 134.28, 143.48 (*Ar-C*-C), 146.83, 147.45 (*Ar-C*-N), 192.70 (*C=O*).

The UV-Vis spectrum of (**11**) shows an absorption peak at 296 nm (33783 cm^{-1}) and at 376 nm (26595 cm^{-1}) in ethanol.

The FT-IR spectrum (KBr) ν/cm^{-1} shows absorption peaks at 3038 cm^{-1} ν (C-H, m) aromatic; 2819, 2739 cm^{-1} ν (C-H, m) aldehyde; 1699 cm^{-1} ν (C=O, shp); 1588 cm^{-1} ν (C=C, shp) aromatic; 1492 cm^{-1} ν (C=C, shp) aliphatic; 1176 cm^{-1} ν (C-N, m) and 963 cm^{-1} for bending (C-N).

Table 2.9. Crystal data and structure refinement details of **(11)**.

Identification code	Compound **(11)**	
Empirical formula	$C_{28}H_{21}NO_2$	
Formula weight	403.46	
Temperature	100(2) K	
Wavelength	0.71075 Å	
Crystal system	Orthorhombic	
Space group	*Pna*21	
Unit cell dimensions	$a = 16.299(4)$ Å	$\alpha = 90°$
	$b = 16.668(4)$ Å	$\beta = 90°$
	$c = 7.6238(18)$ Å	$\gamma = 90°$
Volume	2071.2(9) $Å^3$	
Z	4	
Density (calculated)	1.294 Mg / m^3	
Absorption coefficient	0.081 mm^{-1}	
F(000)	848	
Crystal	Needle; yellow	
Crystal size	0.22 × 0.03 × 0.01 mm^3	
θ range for data collection	2.94 – 27.48°	
Index ranges	$-21 \le h \le 21$, $-21 \le k \le 21$, $-9 \le l \le 9$	
Reflections collected	25886	
Independent reflections	2548 [$R_{int} = 0.0863$]	
Completeness to $\theta = 27.48°$	99.8 %	
Absorption correction	Semi–empirical from equivalents	
Max. and min. transmission	0.9992 and 0.9824	
Refinement method	Full-matrix least-squares on F^2	
Data / restraints / parameters	2548 / 1 / 280	
Goodness-of-fit on F^2	1.316	
Final R indices [$F^2 > 2\sigma(F^2)$]	$R1 = 0.0640$, $wR2 = 0.1373$	
R indices (all data)	$R1 = 0.0663$, $wR2 = 0.1384$	
Largest diff. peak and hole	0.252 and –0.227 e $Å^{-3}$	

2.2.9 Synthesis of (2Z, 2′Z)-3, 3′-(5-((E)-4-(diphenylamino) styryl)-1, 3-phenylene) bis (2-cyanoacrylic acid) (12).

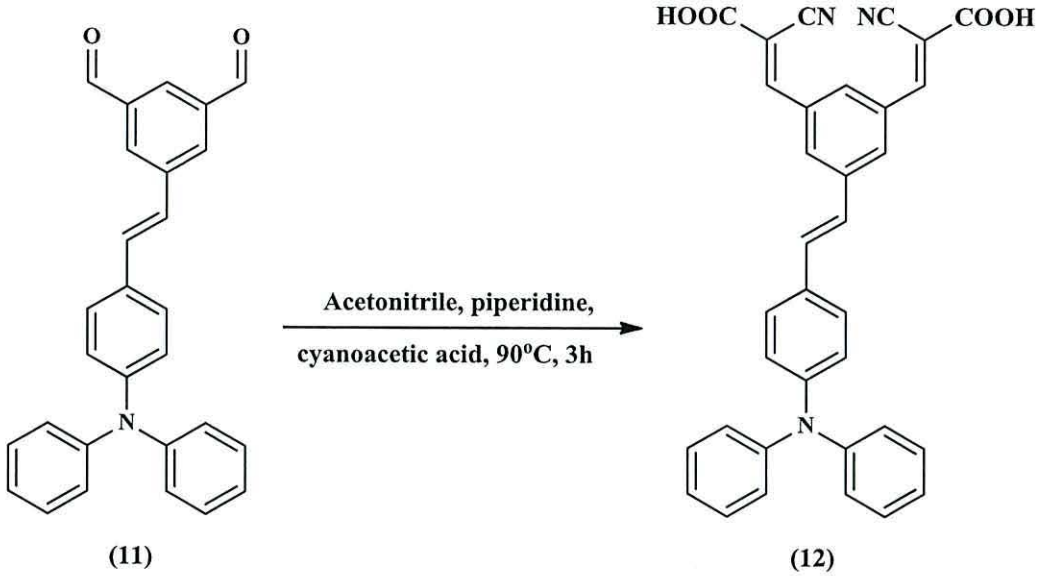

(11) (12)

Scheme 2.15. Synthetic pathway of (2Z, 2′Z)-3, 3′-(5-((E)-4-(diphenylamino) styryl)-1, 3-phenylene) *bis* (2-cyanoacrylic acid) (**12**).

To a solution of (E)-5-(4-(diphenylamino) styryl) isophthalaldehyde (**11**) (0. 3 g, 0.74 mmol) in 20 ml acetonitrile was added (1.2 g, 14.8 mmol) of cyanoacetic acid and 0.6 ml of piperidine. The mixture was then stirred at 90°C for 3 h under nitrogen. After cooling to room temperature, the solution was poured into a mixture of methylene chloride and water (1:1, v/v). The pH was adjusted to pH=2 by phosphoric acid. The mixture was extracted by using separation funnel and a red-orange precipitate formed in organic layer. This solid was filtered and purified by column chromatography over silica gel using petroleum spirit/dichloromethane (3:1, v/v) as an eluent. The product was identified using TLC and the product was collected after removing the solvent by rotary evaporation under reduced pressure to produce 2Z, 2′Z)-3, 3′-(5-((E)-4-(diphenylamino) styryl)-1, 3-phenylene) *bis* (2-cyanoacrylic acid) (**12**) as a red-orange solid (0.28g, 34.5 %), m.p. 262-264°C (decompose). FTMS^{+}-MS: m/z (Accurate Mass), reference compound: DEA, calcd. for $C_{34}H_{22}N_3O_4$ 536.1616, found 536.1612 $[M-H]^{-}$.

^{1}H NMR (400 MHz, DMSO) δ 6.96 (d, *J*= 8.56 Hz, 2H, -*Ph*-N-Ph_2), 7.08 (m, 6H, -N-*Ph*$_2$), 7.16 (br d, 1H, J= 16.04, -*CH*=CH-Ph), 7.24 (br d, 1H, J= 16.28, -CH=*CH*-Ph), 7.33 (t, *J*= 7.6 Hz, 4H, -N-*Ph*$_2$), 7.53 (d, *J*= 8.5 Hz, 2H, -*Ph*-N-Ph_2), 7.91 (s, 2H,

=CH-*Ph*-CH=), 8.01 (s, 1H, =CH-*Ph*-CH=), 8.10 (s, 2H, -C=*CH*-Ph-). ^{13}C NMR (100 MHz, DMSO-d_6) shows peaks at δ 115.99 (-*C*≡*N*), 122.06, 123.03, 123.92, 127.56, 129.14, 129.76, 129.84 (*Ar-C*-H), 124.07, 130.33 (Ar-*CH=CH*-Ar), 132.89, 138.58 (*Ar-C*-C), 146.32, 146.92 (*Ar-C*-N-), 150.97 (Ar-C-*CH*-C-CN), 162.16 (*C=O*).

The UV-Vis spectrum of (**12**) shows an absorption peak at 296 nm (33783 cm^{-1}) (ε = 35421 $M^{-1}cm^{-1}$) and at 376 nm (26595 cm^{-1}) (ε = 20869 $M^{-1}cm^{-1}$) in ethanol.

The FT-IR spectrum (KBr) ν/cm^{-1} shows absorption peaks at 3200-2700 cm^{-1} ν (O-H, br) carboxylic acid; 3032 cm^{-1} ν (C-H, m) aromatic; 2928 cm^{-1} ν (C-H, m) aliphatic; 2226 cm^{-1} ν (C≡N, m); 1723 cm^{-1} ν (C=O, str); 1587 cm^{-1} ν (C=C, shp) aromatic; 1493 cm^{-1} ν (C=C, str) aliphatic; 1273 cm^{-1} ν (C-O, str); 1177 cm^{-1} ν (C-N, str); 1050 cm^{-1} ν (C-H, str) bending and 963 cm^{-1} for (C-N, m) bending.

2.2.10 Synthesis of 5-[(2-diphenylamino-phenyl)-vinyl]-isophthalic acid dimethyl ester (13).

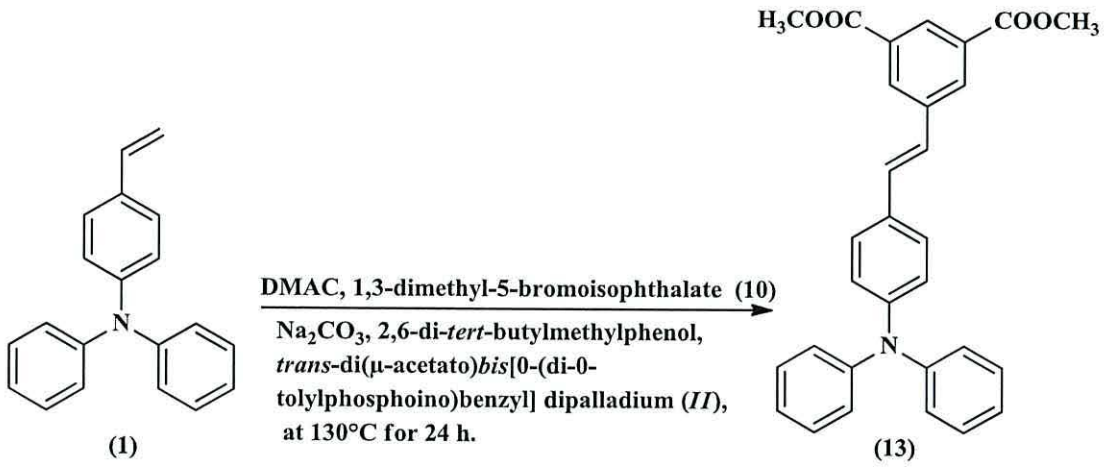

Scheme 2.16. Synthetic pathway of 5-[(2-diphenylamino-phenyl)-vinyl]-isophthalic acid dimethyl ester (**13**).

To a solution of diphenyl-(4-vinyl-phenyl)-amine (**1**) (1 g, 3.7 mmol) in N,N-dimethylacetamide (20 ml) was added 1,3-dimethyl-5-bromoisophthalate (**10**) (0.46 g, 0.453 mmol), 2,6-di-*tert*-butylmethyl phenol (0.073 g, 0.09 mmol), anhydrous sodium carbonate (0.44 g, 1.13 mmol), and *trans*-di(μ-acetato)*bis*[0-(di-0-tolylphosphoino)benzyl] dipalladium (*II*) (0.015 g, 0.0045 mmol). The mixture was stirred under nitrogen at 130°C for 24 h. The reaction was cooled to room temperature and poured into a mixture of distilled water and methylene chloride (v/v). The mixture was separated using separation funnel, and the organic layer was taken and dried over anhydrous magnesium sulfate then filtered. After rotary evaporation of the solvent under reduced pressure and high vacuum, the residue was purified by column chromatography on silica gel with petroleum spirit/diethyl ether (95:5, v/v). After that, the product was tested using TLC and the product collected after rotary evaporation of the solvent under a reduced pressure, to give 5-[(2-diphenylamino-phenyl)-vinyl]-isophthalic acid dimethyl ester (**13**) as a yellow solid (yield 0.16 g, 11%), m.p. 110-112°C. The suitable crystal for X-ray analysis was prepared by dissolving this compound in dichloromethane followed slow evaporation.

FTMS$^+$-MS: m/z (Accurate Mass), reference compound: NH_4OAc, calcd. for $C_{30}H_{25}NO_4$ 464.1856, found 464.1852 $[M+H]^+$.

^{1}H NMR (DMSO-d6) δ 3.91 (s, 6H, 2x-COO*CH$_3$*), 6.96 (d, *J= 8.8*, Hz, 2H, -*Ph*-N-Ph$_2$), 7.06 (d, *J=7.6* Hz, 4H, Ph-N-*Ph$_2$*), 7.09 (t, *J=7.25* Hz, 2H, Ph-N-*Ph$_2$*), 7.29-7.35 (m, 5H, Ph-N-*Ph$_2$*, -*CH*=CH-Ph), 7.42 (br d, J= 16.4, 1H, -CH=*CH*-Ph), 7.60 (d, *J=8.5*Hz, 2H, -*Ph*-N-Ph$_2$), 8.33 (bs, 1H, =CH-*Ph*-COOCH$_3$), 8.38 (bs, 2H, =CH-*Ph*-COOCH$_3$); ^{13}C NMR (125 MHz, DMSO-d$_6$) δ 52.54 (-*CH$_3$*), 122.51, 123.44, 123.90, 128.06, 129.49, 130,48, 130.60 (*Ar-C*-H), 124.34, 129.60 (Ar-*CH=CH*-Ar), 133.26, 138.89, 140.17 (*Ar-C*-C), 141.74, 146.84 (*Ar-C*-N), 165.43 (*C=O*).

The UV-Vis spectrum of (**13**) shows an absorption peak at 296 nm (33783 cm^{-1}) (ε = 20200 M^{-1}cm^{-1}) and at 376 nm (24580 cm^{-1}) (ε = 38700 M^{-1}cm^{-1}) in ethanol.

The FT-IR Spectrum (KBr) ν/cm^{-1} shows absorption peaks at 3041 cm^{-1} ν (C-H, m) aromatic; 2956, 2922 cm^{-1} ν (C-H, m) aliphatic; 1719 cm^{-1} ν (C=O, str (shp)); 1591 cm^{-1} ν (C=C, str) aromatic; 1494 cm^{-1} ν (C=C, shp) aliphatic; 1199 cm^{-1} ν (C-N, shp) and 963 cm^{-1} for ν (C-N, shp) bending.

Table 2.10. Crystal data and structure refinement details of (**13**).

Identification code	Compound (**13**)	
Empirical formula	$C_{30}H_{25}NO_4$	
Formula weight	463.51	
Temperature	120(2) K	
Wavelength	0.68890 Å	
Crystal system	Monoclinic	
Space group	*C*2/*c*	
Unit cell dimensions	$a = 18.49(2)$ Å	$\alpha = 90°$
	$b = 8.497(9)$ Å	$\beta = 92.706(12)°$
	$c = 30.62(4)$ Å	$\gamma = 90°$
Volume	4804(9) $Å^3$	
Z	8	
Density (calculated)	1.282 Mg / m^3	
Absorption coefficient	0.085 mm^{-1}	
F(000)	1952	
Crystal	Plate; yellow	
Crystal size	0.07 × 0.03 × 0.01 mm^3	
θ range for data collection	2.84 – 24.20°	
Index ranges	$-21 \le h \le 21, -8 \le k \le 10, -36 \le l \le 36$	
Reflections collected	17544	
Independent reflections	4171 [$R_{int} = 0.0733$]	
Completeness to $\theta = 24.20°$	98.3 %	
Absorption correction	Semi–empirical from equivalents	
Max. and min. transmission	0.9996 and 0.9941	
Refinement method	Full-matrix least-squares on F^2	
Data / restraints / parameters	4171 / 0 / 318	
Goodness-of-fit on F^2	1.089	
Final *R* indices [$F^2 > 2\sigma(F^2)$]	*R1* = 0.0715, *wR2* = 0.1751	
R indices (all data)	*R1* = 0.0970, *wR2* = 0.1952	
Largest diff. peak and hole	0.240 and –0.243 e $Å^{-3}$	

2.2.11 Synthesis of 5-[2-(4-diphenylamino-phenyl)-vinyl]-isophthalic acid (14).

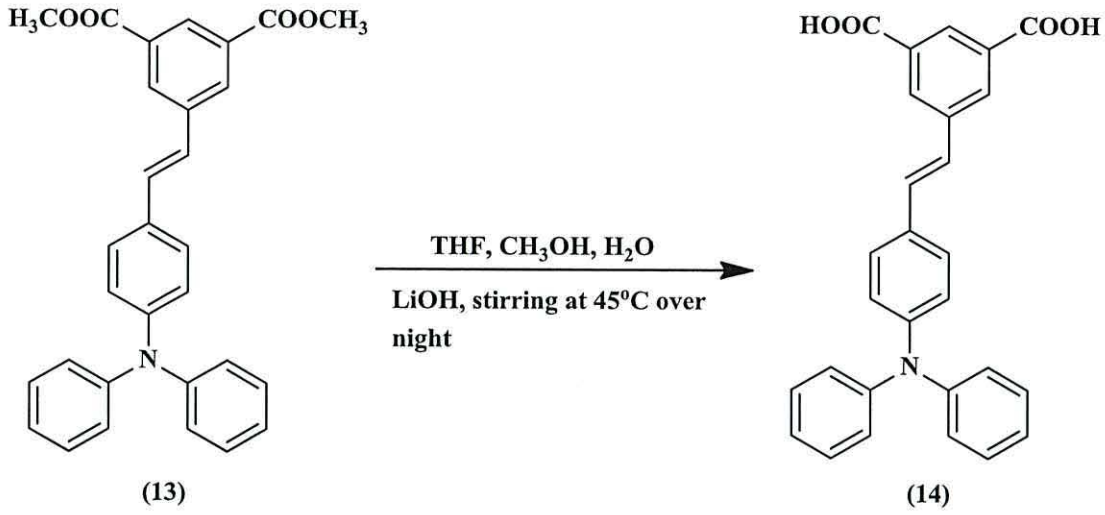

Scheme 2.17. Synthetic pathway of compound 5-[2-(4-diphenylamino-phenyl)-vinyl]-isophthalic acid (**14**).

5-[(2-diphenylamino-phenyl)-vinyl]-isophthalic acid dimethyl ester (**13**) (0.33 g, 0.71 mmol) was dissolved in 10 ml THF with 1.2 ml methanol and 1.3 ml H_2O and 30 eq. (0.85 g, 0.71 mmol) of LiOH. The mixture was stirred overnight at 45°C. After that, the solution was cooled to room temperature. A 5% solution of hydrochloric acid was added drop wise and the pH adjusted to between (5 and 6). The solution was then quenched with water. The product was extracted with ethyl acetate (3x 50 ml), and the organic layer dried using anhydrous magnesium sulfate. After that the solvent was evaporated using a rotary evaporator under vacuum to produce 5-[2-(4-diphenylamino-phenyl)-vinyl]-isophthalic acid (**14**) as a yellow solid (yield 0.27 g, 87 %) m.p. 300-302 °C. A suitable crystal for X-ray analysis was then prepared by dissolving this compound in mixture of dichloromethane/diethyl ether (v/v) followed by slow evaporation. $FTMS^+$-MS: m/z (Accurate Mass), reference compound: NH_4OAc, calcd. for $C_{28}H_{21}NO_4$, 436.1543, found 436.1542 $[M+H]^+$. Anal. Calcd. for $C_{28}H_{21}NO_4$: C, 77.23; H, 4.86; N, 3.22. Found: C, 76.07; H, 4.96; N, 3.11.

^1H NMR (500 MHz, DMSO-d6) δ 6.96 (d, *J=8.5* Hz, 2H, -*Ph*-N-Ph_2), 7.05 (d, *J=7.6* Hz, 4H, Ph-N-*Ph_2*), 7.08 (t, *J=7.25* Hz, 2H, -Ph-N-*Ph_2*), 7.28-7.39 (m, 6H, -Ph-N-*Ph_2*, Ph-*CH*=CH-Ph, Ph-CH=*CH*-Ph), 7.59 (d, *J=8.8*Hz, 2H, -*Ph*-N-Ph_2), 8.32 (s, 3H, =CH-*Ph*-COOH); ^{13}C NMR (125 MHz, DMSO-d_6) δ 122.17, 122.67, 123.19,

123.61, 126.09, 128.04, 129.11 (*Ar-C*-H), 124.31, 129.64 (Ar-*CH=CH*-Ar), 130.13, 130.54, 151.30 (*Ar-C*-C), 142.71, 146.89 (*Ar-C*-N), 166.66 (*C=O*). The UV-Vis spectrum of (**14**) shows an absorption peak at 296 nm (33783 cm^{-1}) (ε = 25718 $M^{-1}cm^{-1}$) and at 372 nm (26881 cm^{-1}) (ε = 35218 $M^{-1}cm^{-1}$) in ethanol.

The FT-IR spectrum (KBr) ν/cm^{-1} shoes absorption peaks at 3400-2700 cm^{-1} ν (O-H, br) carboxylic acid; 3041 cm^{-1} ν (C-H, m) aromatic; 2926 cm^{-1} ν (C-H, m) aliphatic; 1699 cm^{-1} ν (C=O, shp); 1589 cm^{-1} ν (C=C, shp) aromatic; 1492 cm^{-1} ν (C=C, shp) aliphatic; 1280 cm^{-1} ν (C-N, str); 961 cm^{-1} for (C-N, m) bending.

Table 2.11. Crystal data and structure refinement details of (**14**).

Identification code	Compound (**14**)	
Empirical formula	$C_{28}H_{21}NO_4$	
Formula weight	435.46	
Temperature	120(2) K	
Wavelength	0.71073 Å	
Crystal system	Monoclinic	
Space group	*P*21/*c*	
Unit cell dimensions	a = 11.8803(18) Å	α = 90°
	b = 15.9785(16) Å	β = 103.874(5)°
	c = 12.085(2) Å	γ = 90°
Volume	2227.2(5) $Å^3$	
Z	4	
Density (calculated)	1.299 Mg / m^3	
Absorption coefficient	0.087 mm^{-1}	
F(000)	912	
Crystal	Block; Yellow	
Crystal size	0.18 × 0.07 × 0.01 mm^3	
θ range for data collection	3.04 – 25.02°	
Index ranges	$-13 \le h \le 14$, $-18 \le k \le 18$, $-14 \le l \le 14$	
Reflections collected	18918	
Independent reflections	3927 [R_{int} = 0.0763]	
Completeness to θ = 25.02°	99.7 %	
Absorption correction	Semi–empirical from equivalents	
Max. and min. transmission	0.9991 and 0.9845	
Refinement method	Full-matrix least-squares on F^2	
Data / restraints / parameters	3927 / 0 / 300	
Goodness-of-fit on F^2	1.137	
Final R indices [$F^2 > 2\sigma(F^2)$]	*R1* = 0.0647, *wR2* = 0.1113	
R indices (all data)	*R1* = 0.1209, *wR2* = 0.1346	
Largest diff. peak and hole	0.264 and –0.258 e $Å^{-3}$	

2.3 Synthesis of 4, 5-diiodophthalonitrile (17).

2.3.1 Synthesis of 4, 5-diiodophthalimide (15a).

Method 1, (30% fuming sulphuric acid). [5]

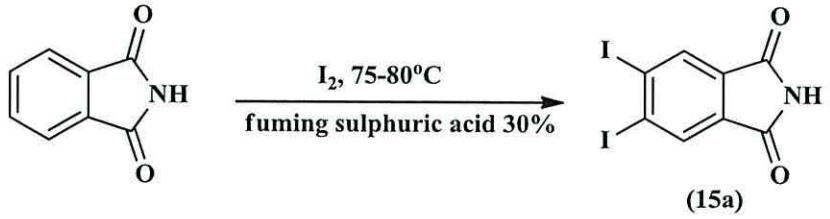

(15a)

Scheme 2.18. Synthetic pathway of (**15a**).

To 60 ml of fuming sulphuric acid 30% was added (14.7 g, 0.1 mol) of phthalimide and (25.4 g, 0.1 mol) of iodine. The reaction mixture was stirred and heated to 75-80°C for 24 h. the solution was cooled to room temperature and was poured onto 400 g of ice. The precipitated solids were washed twice with 30 ml of water, once with a 2% solution of K_2CO_3 30 ml, once with a saturated aqueous solution of $Na_2S_2O_3$ 30 ml, and finally washed with water and dried at room temperature to give a white powder.

Note: In this reaction we didn't get 4, 5-diiodophthalimide. No reaction.

Method 2, (periodic acid).

2.3.2 Synthesis of 4, 5-diiodophthalimide (15b). [6]

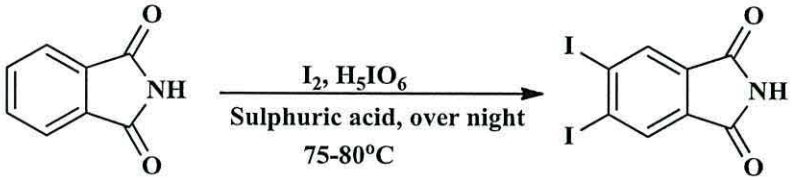

(15b)

Scheme 2.19. Synthetic pathway of 4, 5-diiodophthalimide (**15b**).

To a solution of periodic acid (5.75 g, 26.64 mmol) in concentrated sulphuric acid (120 ml) was added (7.75 g, 30.44 mmol) of iodine. The reaction mixture was stirred at room temperature for one hour. The solution was then heated to 40-50°C after which phthalimide (4.48 g, 30.44 mmol) was added slowly. The solution was then heated to 75-80°C for 24h. After cooling to room temperature the solution was poured onto ice (400 g), the solid product was then filtered and washed twice with water, once with 2% of K_2CO_3 solution (30 ml), once with saturated aqueous solution of $Na_2S_2O_3$ (30 ml), again with water and then was dried at room temperature to produce a yellow precipitate. The yellow precipitate was extracted with 500 ml of acetone using a Soxhlet extractor for 48 h. The yellow solid which formed in the flask was filtered, and then (80 ml) of water was added to the filtrate. The solution was concentrated to 250 ml and cooled to produce a bright yellow precipitate of 4, 5-diiodophthalimide (**15b**) (4.7 g, 39%) m.p. 213-215°C. FTMS$^+$-MS: m/z (Accurate Mass), reference compound: (solid) ASAP, calcd. for $C_8H_3I_2NO_2$, 398.8326, found 399.8324 $[M+H]^+$.

^{1}H NMR (500 MHz, DMSO-d6) δ 8.25 (s, 2H, *Ar-H*), 11.42 (s, 1H, *-NH*). ^{13}C NMR (125 MHz, DMSO-d6) δ 116.45 (2x*Ar-C*-C), 132.68 (2x*Ar-C*-H), 133.00 (2x*Ar-C*-I), 167.69 (2x*C=O*).

The FT-IR spectrum (KBr) ν/cm^{-1} shows absorption peaks at 3195 cm^{-1} ν (N-H, br); 3077 cm^{-1} ν (C-H, m) aromatic; 1770 cm^{-1} ν (C=O, str (shp)); 1719 cm^{-1} ν (C=O, str); 1594 cm^{-1} ν (C=C, m) benzene rings.

2.3.3 Synthesis of 4, 5-diiodophthalamide compound (16). [5]

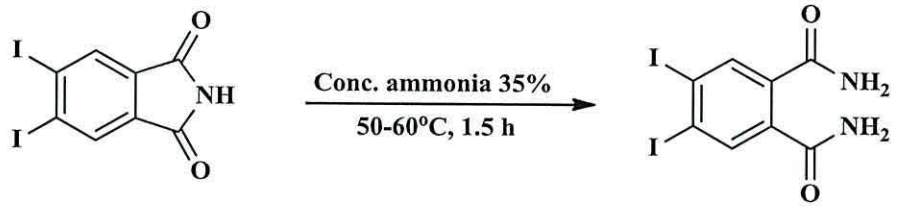

(15b) (16)

Scheme 2.20. Synthetic pathway of 4, 5-diiodophthalamide (**16**).

To a solution of ammonia (35%, d=0.88 g/cm^3, M= 17.03 g/mol, 42 ml) was added (3.7 g, 9.27 mmol) of 4, 5-diiodophthalimide (**15b**). The suspension was heated to 60°C for 2h. The white-yellow precipitate which formed was filtered and washed with ice cold water (60 ml) to remove any traces of ammonia. This was then washed with warmed ethanol (30ml) to remove any trace of 4, 5-diiodophthalimide starting material. The product dried in a desiccator under vacuum overnight to produce 4, 5-diiodophthalamide (**16**) (2.27 g, 59%) m.p. 212-214°C. FTMS$^+$-MS: m/z (Accurate Mass), reference compound: NH_4OAc, calcd. for $C_8H_6I_2N_2O_2$ 416.8591, found 416.8591 $[M+H]^+$. ^{1}H NMR (500 MHz, DMSO-d6) δ 7.41 (bs, 2H, -*NH$_2$*), 7.82 (bs, 2H, -*NH$_2$*), 7.91 (s, 2H, *Ar-H*); ^{13}C NMR (125 MHz, DMSO-d6) δ 109.89 (2x*Ar-C*-C), 137.03 (2x*Ar-C*-H), 137.65 (2x*Ar-C*-I), 167.93 (2x*C=O*).

The FT-IR spectrum (KBr) ν/cm^{-1} shows absorption peaks at 3430, 3327, 3175 cm^{-1} ν (N-H, br); 1692 cm^{-1} ν (C=O, str (br)); 1655 cm^{-1} ν (C=O, str (br)); 1604, 1562 cm^{-1} ν (C=C, m) aromatic.

2.3.4 Synthesis of 4, 5-diiodophthalonitrile compound (17). [5]

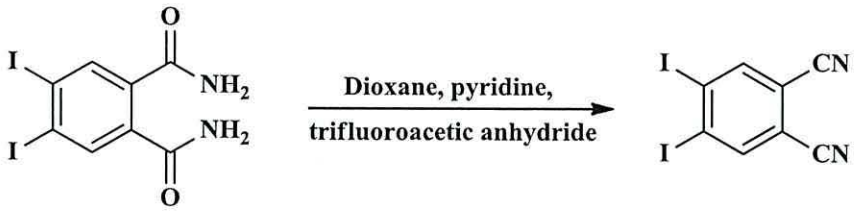

(16) (17)

Scheme 2.21. Synthetic pathway of 4, 5-diiodophthalonitrile (**17**).

To an anhydrous solution of 1, 4-dioxane (40 ml) was added (4 g, 9.6 mmol) of 4, 5-diiodophthalamide (**16**) and the solution was cooled at (0-5°C). To this solution was added 9 ml of anhydrous pyridine followed by 8 ml of trifluoroacetic anhydride whilst the reaction mixture was stirred under argon. After the addition was complete, the reaction mixture was allowed to warm to room temperature and left stirring overnight. The reaction mixture was then poured onto ice, and the product was extracted with ethyl acetate (3x 50 ml). The combined organic layer was washed with water (30 ml), 1M HCl (20 ml), saturated aqueous Na_2CO_3 (30 ml) then filtered and cooled water (30 ml). The organic layer was dried over anhydrous $MgSO_4$ and the solvent was reduced to dryness under vacuum, then further dried under high vacuum to produce 4, 5-diiodophthalonitrile (**17**) as a yellow solid (yield 2g, 53%) m.p. 170-172°C. A suitable crystal for X-ray analysis was then prepared by dissolving the compound in tetrahydrofuran followed by slow evaporation. MS EI^+ calcd. for $C_8H_2N_2I_2$ 379.8302, found 379.8302 M^+.

^1H NMR (500 MHz, $CDCl_3$) δ 8.23 (s, 2H, *Ar-H*). ^{13}C NMR (125 MHz, $CDCl_3$) δ 113.55 (2x*Ar-C*-I), 115.03 (2x*Ar-C*-C-N) 115.41 (2x-C≡N), 142.68 (2x*Ar-C*-H).

The FT-IR spectrum (KBr) ν/cm^{-1} shows the most important peak at 2231 cm^{-1} ν (C≡N, shp).

Table 2.12. Crystal data and structure refinement details of (**17**).

Identification code	Compound (**17**)	
Empirical formula	$C_{12}H_{10}I_2N_2O$	
Formula weight	451.94	
Temperature	100 K	
Wavelength	0.71075 Å	
Crystal system	Orthorhombic	
Space group	*Cmcm*	
Unit cell dimensions	$a = 10.781(4)$ Å	$\alpha = 90°$
	$b = 18.032(6)$ Å	$\beta = 90°$
	$c = 7.231(4)$ Å	$\gamma = 90°$
Volume	1405.7(10) $Å^3$	
Z	4	
Density (calculated)	2.135 Mg / m^3	
Absorption coefficient	4.461 mm^{-1}	
F(000)	840	
Crystal	Block; pale yellow	
Crystal size	0.40 × 0.08 × 0.08 mm^3	
θ range for data collection	3.58 – 27.50°	
Index ranges	$-13 \le h \le 14$, $-23 \le k \le 23$, $-9 \le l \le 7$	
Reflections collected	6080	
Independent reflections	901 [$R_{int} = 0.0473$]	
Completeness to $\theta = 27.50°$	97.9 %	
Absorption correction	Semi–empirical from equivalents	
Max. and min. transmission	0.7167 and 0.2685	
Refinement method	Full-matrix least-squares on F^2	
Data / restraints / parameters	901 / 9 / 55	
Goodness-of-fit on F^2	1.043	
Final *R* indices [$F^2 > 2\sigma(F^2)$]	*R1* = 0.0232, *wR2* = 0.0567	
R indices (all data)	*R1* = 0.0263, *wR2* = 0.0580	
Largest diff. peak and hole	1.807 and –0.672 e $Å^{-3}$	

2.3.5 Method 3, (Autoclave synthesis).

Synthesis of tetraiodophthalimide (18). [5]

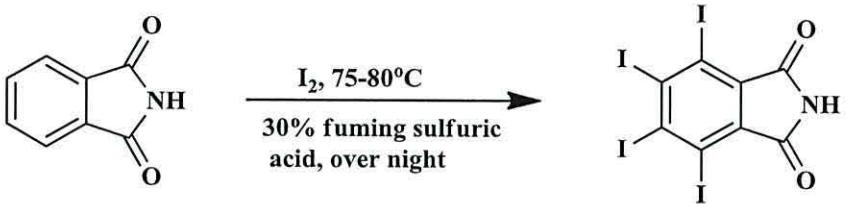

(18)

Scheme 2.22. Synthetic pathway of tetraiodophthalimide (**18**).

Iodine (25.4 g, 0.1 mol) was added to solution of phthalimide (14.7 g, 0.1 mol) in 60 ml of fuming sulphuric acid (30%). The reaction mixture was then placed in a PTFE-lined stirring autoclave and to heat 75-80°C for 24 h. the resulting solution was cooled to room temperature and poured onto 400 g of ice. The precipitate formed was then filtered and washed twice with water, once with 2% aqueous solution of K_2CO_3 (30 ml), once with a saturated aqueous solution of $Na_2S_2O_3$ (30 ml), again with water, and finally dried at room temperature. The yellow precipitate was then extracted with acetone (500 ml) in a Soxhlet extractor for 48 h. A yellow precipitate was then filtered from flask and 80 ml of water was added to the filtered solution, the solvent was reduced and cooled to produce a yellow precipitate of tetraiodophthalimide (**18**) (yield 5.6 g, 60%) m.p. 286-288°C. Acc. Mass, calcd. for $C_8HI_4NO_2$ 650.6181, found 650.6176 M^+. ^1H NMR (500 MHz, DMSO-d6) δ 11.68 (s, 1H, *-NH*). ^{13}C NMR (125 MHz, DMSO-d6) δ 103.89 (2x*Ar-C*-C), 134.88 (2x*Ar-C*-I), 135.50 (2x*Ar-C*-I), 165.17 (2x-*C=O*).

The FT-IR spectrum (KBr) ν/cm^{-1} shows absorption peaks 3271 cm^{-1} ν (N-H, br); 1780 cm^{-1} ν (C=O, str (shp)); 1718 cm^{-1} ν (C=O, str (shp)).

2.4 Synthesis of phthalocyanine dyes.

2.4.1 Synthesis of di-(4-methylbenzoate)-fumaronitrile (19). [7]

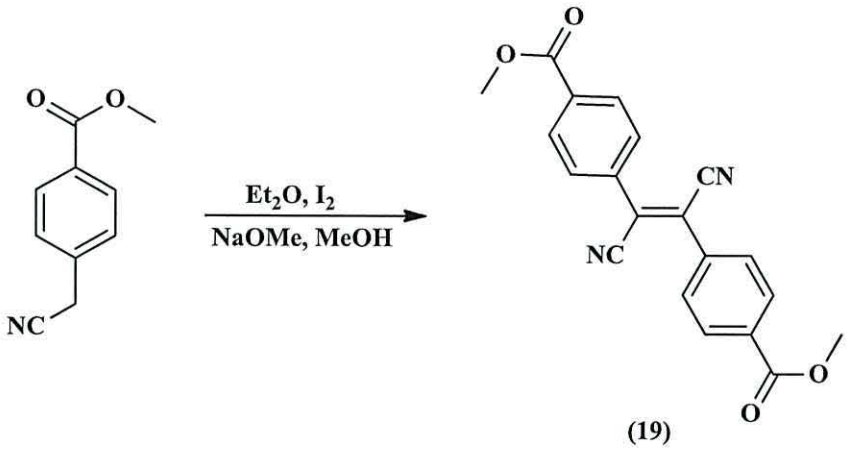

(19)

Scheme 2.23. Synthetic pathway of di-(4-methylbenzoate)-fumaronitrile (**19**).

Methyl-4-(cyanomethyl)-benzoate (5 g, 0.029 mol) and iodine (7.3 g, 0.029 mol) were dissolved in dry diethyl ether and cooled to -78°C. Sodium methoxide (3.2g, 0.06 mol) in anhydrous methanol (18 ml) was added drop wise into this solution under argon. The stirring black solution was then allowed to warm to 0-5°C, and then the colour of the solution changed from black to beige. The solution was kept at this temperature for 4 hours. The reaction was then quenched with 3-6% HCl at less than 10°C and the resultant solid then was filtered. The precipitate was then washed with a cold methanol-water solution to wash away ionic substances and dried over P_2O_5 to produce di-(4-methylbenzoate)-fumaronitrile (**19**) as an off white solid (4.24 g, 43%). A suitable crystal for X-ray analysis was then prepared by dissolving this compound in dichloromethane followed by slow evaporation. FTMS$^+$-MS: m/z (Accurate Mass), reference compound: NH_4OAc, calcd. for $C_{20}H_{14}N_2O_4$ 364.1292, found 364.1295 $[M+NH_4]^+$.

^{1}H NMR (500 MHz, $CDCl_3$) δ 3.98 (s, 6H, 2x-O*CH*$_3$), 7.93 (d, 4H, J= 8.85, *Ar-H*), 8.22 (d, 4H, J=8.85, *Ar-H*); ^{13}C NMR (125 MHz, $CDCl_3$) δ 52.60 (2x-*OCH*$_3$), 115.88 (2x*C*≡*N*), 125.92 (-*C*-*CN*), 128.83(*Ar*-*C*-H), 130.48 (*Ar*-*C*-H), 133.20 (*Ar*-*C*-C), 135.52 (*Ar*-*C*-C=O), 165.69 (2x*C*=*O*).

The FT-IR spectrum (KBr) ν/cm^{-1} shows absorption peaks at 3102, 3013 cm^{-1} ν (C-H, m) aromatic; 2962, 2850 cm^{-1} ν (C-H, m) aliphatic; 2222 cm^{-1} ν (C≡N, str (shp));

1726 cm^{-1} ν (C=O, str (shp)); 1608 cm^{-1} ν (C=C, shp); 1437 cm^{-1} δ_{as} CH_3, 1407 cm^{-1} δ_s CH_3.

Table 2.13. Crystal data and structure refinement details of compound (**19**).

Identification code	Compound (**19**)
Empirical formula	$C_{20}H_{14}N_2O_4$
Formula weight	346.33
Temperature	100 K
Wavelength	0.68890 Å (synchrotron)
Crystal system	Monoclinic
Space group	*P*21/*c*
Unit cell dimensions	$a = 23.3900(4)$ Å $\quad \alpha = 90°$ $b = 3.8000(6)$ Å $\quad \beta = 114.891(19)°$ $c = 20.5000(4)$ Å $\quad \gamma = 90°$
Volume	1652.8(3) $Å^3$
Z	4
Density (calculated)	1.392 Mg / m^3
Absorption coefficient	0.099 mm^{-1}
F(000)	720
Crystal	Needle; colourless
Crystal size	0.09 × 0.03 × 0.03 mm^3
θ range for data collection	3.36 – 24.21°
Index ranges	$-27 \le h \le 27, -4 \le k \le 4, -24 \le l \le 21$
Reflections collected	11084
Independent reflections	2829 [$R_{int} = 0.0840$]
Completeness to $\theta = 24.21°$	96.4 %
Absorption correction	Semi–empirical from equivalents
Max. and min. transmission	0.9970 and 0.9912
Refinement method	Full-matrix least-squares on F^2
Data / restraints / parameters	2829 / 0 / 237
Goodness-of-fit on F^2	1.058
Final *R* indices [$F^2 > 2\sigma(F^2)$]	*R1* = 0.0562, *wR2* = 0.1350
R indices (all data)	*R1* = 0.0787, *wR2* = 0.1566
Largest diff. peak and hole	0.276 and –0.292 e $Å^{-3}$

2.4.2 Synthesis of 4, 5-bis ([1, 1':3', 1''-terphenyl]-2'-yloxy) phthalonitrile (20). [8]

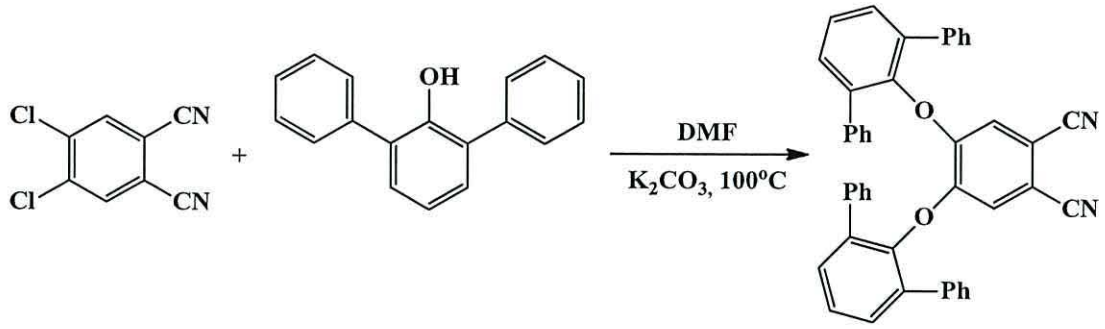

(20)

Scheme 2.24. Synthetic pathway of 4, 5-*bis* ([1, 1':3', 1''-terphenyl]-2'-yloxy) phthalonitrile (**20**).

2, 6-Diphenylphenol (1.88 g, 7.5 mmol), 4,5-dichlorophthalonitrile (0.5 g, 2.5 mmol) and potassium carbonate (3.5 g, 25.0 mmol) were dissolved in dry DMF (5 ml), and stirred under a nitrogen atmosphere at 100°C for 36 h. The reaction mixture was poured into water (50 ml), and was then extracted with 3x50 ml dichloromethane. The organic layer was collected and dried using anhydrous magnesium sulfate. The solvent was then evaporated and the residue was purified by column chromatography on silica gel by eluting with dichloromethane. The solvent was reduced to produce 4, 5-bis ([1, 1':3', 1''-terphenyl]-2'-yloxy) phthalonitrile (**20**) as a white solid (yield 0.7g, 47%) m.p. 240-244°C. A suitable crystal for X-ray analysis was then prepared by dissolving this compound in dichloromethane followed by slow evaporation. FTMS$^+$-MS: m/z (Accurate Mass), reference compound: NH_4OAc, calcd. for $C_{44}H_{28}N_2O_2$ 634.2489, found 634.2483 $[M+NH_4]^+$.

^{1}H NMR (500 MHz, $CDCl_3$) δ 6.20 (s, 2H, *Ar-H*), 7.04 (t, 8H, *J*= 7.5, *Ar-H*), 7.16 (t, 4H, *J*= 7.5 Hz, *Ar-H*), 7.42 (d, 8H, *J*= 7.25 Hz, *Ar-H*), 7.45 (s, 6H, *Ar-H*).

^{13}C NMR ($CDCl_3$, 125 MHz): δ (ppm) = 107.34 (*Ar-C*-C), 115.01 (-*C*≡*N*), 119.09, 126.69, 127.80, 128.40, 129.18, 131.27, (*Ar-C*-H), 134.94, 137.12, 146.81 and 148.48 (*Ar-C*-C).

The FT-IR spectrum (KBr) ν/cm^{-1} shows absorption peaks at 3056 cm^{-1} ν (C-H, m) aromatic; 2230 cm^{-1} ν (C≡N, str (shp)); 1595, 1579, 1566 cm^{-1} ν (C=C, shp) aromatic.

Table 2.14. Crystal data and structure refinement details of compound (**20**).

Identification code	Compound (**20**)	
Empirical formula	$C_{44}H_{28}N_2O_2$	
Formula weight	616.68	
Temperature	100(2) K	
Wavelength	0.71075 Å	
Crystal system	Triclinic	
Space group	*P*–1	
Unit cell dimensions	$a = 18.85(3)$ Å	$\alpha = 76.409(9)$ °
	$b = 19.35(2)$ Å	$\beta = 64.67(2)$ °
	$c = 21.33(3)$ Å	$\gamma = 89.96(2)$ °
Volume	6791(16) $Å^3$	
Z	8	
Density (calculated)	1.206 Mg / m^3	
Absorption coefficient	0.074 mm^{-1}	
F(000)	2576	
Crystal	Plate; yellow	
Crystal size	0.16 × 0.15 × 0.02 mm^3	
θ range for data collection	2.18 – 25.00°	
Index ranges	$-22 \le h \le 20$, $-22 \le k \le 22$, $-25 \le l \le 25$	
Reflections collected	41168	
Independent reflections	21336 [$R_{int} = 0.0943$]	
Completeness to $\theta = 25.00°$	89.2 %	
Absorption correction	Semi–empirical from equivalents	
Max. and min. transmission	0.9985 and 0.9883	
Refinement method	Full-matrix least-squares on F^2	
Data / restraints / parameters	21336 / 324 / 1725	
Goodness-of-fit on F^2	1.011	
Final *R* indices [$F^2 > 2\sigma(F^2)$]	*R1* = 0.1345, *wR2* = 0.3222	
R indices (all data)	*R1* = 0.2120, *wR2* = 0.4021	
Extinction coefficient	0.0031(6)	
Largest diff. peak and hole	0.527 and –0.466 e $Å^{-3}$	

2.4.3 Synthesis of methyl 3', 4'-dicyano-[1, 1'-biphenyl]-4-carboxylate (21). [8]

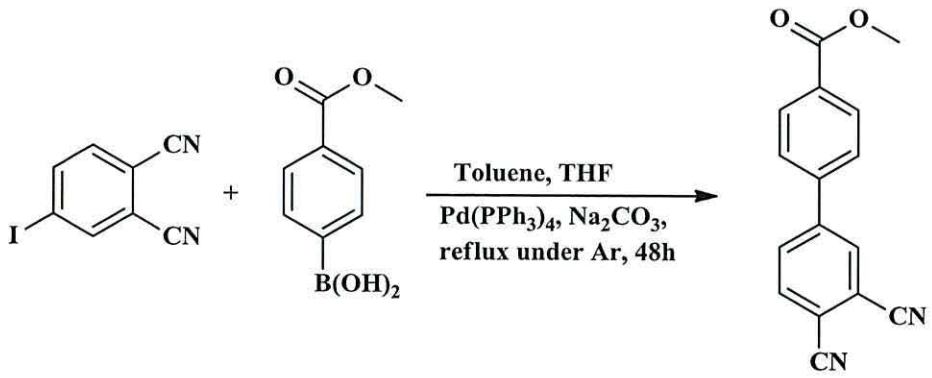

(21)

Scheme 2.25. Synthetic pathway of methyl 3', 4'-dicyano-[1, 1'-biphenyl]-4-carboxylate (**21**).

A Schlenk flask was charged with 4-iodophthalonitrile (0.15 g, 0.59 mmol) and $Pd(PPh_3)_4$ (10 mg, 12μmol) under an argon atmosphere. Solutions of 4-(methoxycarbonylphenyl) boronic acid (0.14 g, 0.71mmol) in THF (3 ml) and Na_2CO_3 (2M, 2ml) in H_2O were prepared these and deoxygenated toluene (4 ml) were added to the reaction vessel, and the mixture was refluxed under argon for 48 h. The reaction mixture was poured into a mixture of H_2O and diethylether (50:50 ml) (v/v). The crude product was purified using column chromatography on activated alumina by eluting with CH_2Cl_2, and resulting material was collected after removing the solvent to give methyl 3', 4'-dicyano-[1, 1'-biphenyl]-4-carboxylate (**21**) as an off-white solid (0.1 g, 67%) m.p. 186-188°C. FTMS$^+$-MS: m/z (Accurate Mass), reference compound: NH_4OAc, calcd for $C_{16}H_{10}N_2O_2$ 280.1081, found 280.1085 $[M+NH_4]^+$. ^{1}H NMR (500 MHz, $CDCl_3$) δ (ppm) 3.98 (s, 3H, *-OCH_3*), 7.67 (d, 2H, *J= 8.2, Ar-H*), 7.97 (d, 1H, *J= 8.2, Ar-H*), 7.92 (d, 1H, J= 8.2, *Ar-H),* 8.05(s, 1H, *Ar-H*), 8.2 (d, 2H, *J= 7.9* Hz, *Ar-H*). ^{13}C NMR (CDCl3, 125 MHz): δ (ppm) 52.48 (-*OCH_3*), 116.43 (-*C≡N*), 127.29, 130.71 (*Ar-C*-H), 131.63, 134.10, 141.06 (*Ar-C*-C), 170.19 (*C=O*). The FT-IR spectrum (KBr) ν/cm^{-1} shows absorption peaks at 3113, 3080 cm^{-1} ν (C-H, m) aromatic; 2925, 2855 cm^{-1} ν (C-H, m) aliphatic; 2233 cm^{-1} ν (C≡N, str (shp)); 1716 cm^{-1} ν (C=O, str (shp)); 1598 cm^{-1} ν (C=C, shp) aromatic and 1288 cm^{-1} ν (C-O, str).

2.4.4 Synthesis of 4, 5-bis (4-methoxycarbonylphenyl) phthalonitrile (22). [9]

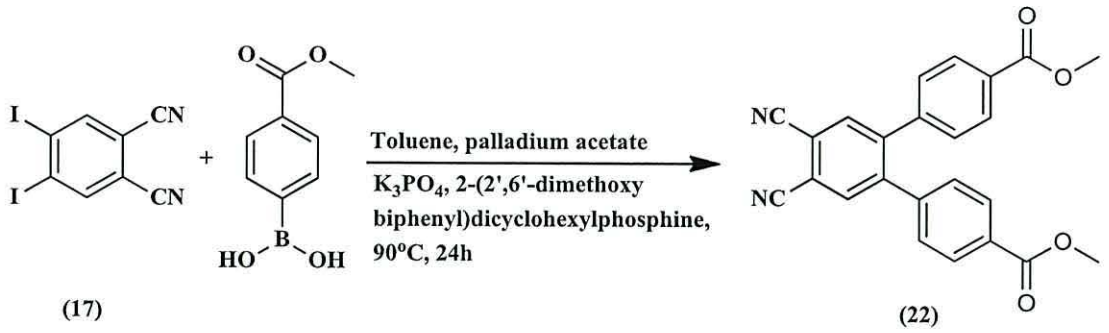

(17) (22)

Scheme 2.26. Synthetic pathway of 4, 5-*bis* (4-methoxycarbonylphenyl) phthalonitrile (**22**).

A Schlenk flask was charged with 4, 5-diiodophthalonitrile (**17**) (0.3 g, 0.79 mmol), 4-methoxycarbonylboronic acid (0.42 g, 2.3 mmol), anhydrous toluene 10 ml, palladium (*II*) acetate (20 mg), 2-(2`, 6`-dimethoxybiphenyl)dicyclohexylphosphine (20 mg) and K_3PO_4 (0.66 g, 3.15 mmol). The mixture was heated to 90°C for 2h under an argon atmosphere. The reaction was cooled to room temperature, and the solution was washed with water twice (2 x 25 ml) and separated using a separating funnel. The organic layer was collected and dried over anhydrous magnesium sulphate and the solvent removed to dryness. Then ethyl acetate was added to produce 4, 5-*bis* (4-methoxycarbonylphenyl) phthalonitrile (**22**) as an off-white solid (0.09 g, 30%) m.p. 184-186°C. MS calcd. for $C_{24}H_{16}N_2O_4$ 396.3948, found 412.8641 $[M+CH_3]^+$. ^1H NMR (500 MHz, $CDCl_3$) δ (ppm) 3.85 (s, 3H, -O*CH₃*), 3.90 (s, 6H, 2x -O*CH₃*), 6.94 (d, 1H, J= 8.5, *Ar-H*), 7.02 (d, 4H, J= 8.85, *Ar-H*), 7.69 (d, 1H, J= 8.5, *Ar-H*), 8.18 (d, 4H, J= 8.5, *Ar-H*), ^{13}C NMR (125 MHz, $CDCl_3$) δ 55.18 (-O*CH₃*), 113.50, 113.60 (*Ar-C*-C), 118.23 (-C≡N), 126.75 (*Ar-C*-H), 135.26, 137.49 (*Ar-C*-C), 163.20 (*C=O*).

The FT-IR spectrum (KBr) ν/cm^{-1} shows absorption peaks at 3046, 3000 cm^{-1} ν (C-H, m) aromatic; 2963, 2839 cm^{-1} ν (C-H, m) aliphatic; 2239 cm^{-1} ν (C≡N, w); 1603 cm^{-1}, 1570 cm^{-1} ν (C=C, br) aromatic; 1457 cm^{-1} δ_{as} (CH_3, w), 1340 cm^{-1} δ_s (CH_3, br) and 1246 cm^{-1} for ν (C-N, str).

2.4.5 Synthesis of 2, 3-di (4-pentoxybenzoate)-7^2, 12^2, 17^2-hexa (2, 6-diphenylphenoxy)-tribenzo-5, 10, 15, 20-tetrazaporphyrin zinc (23).

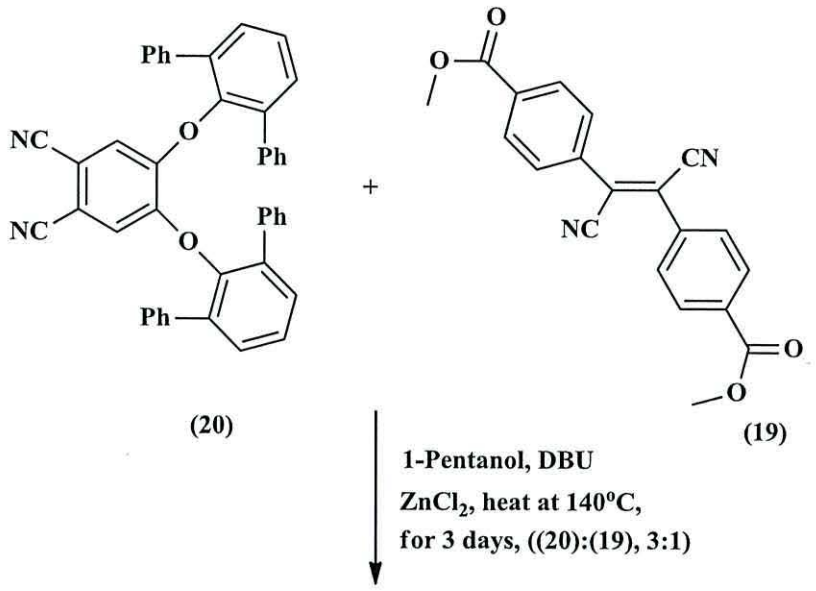

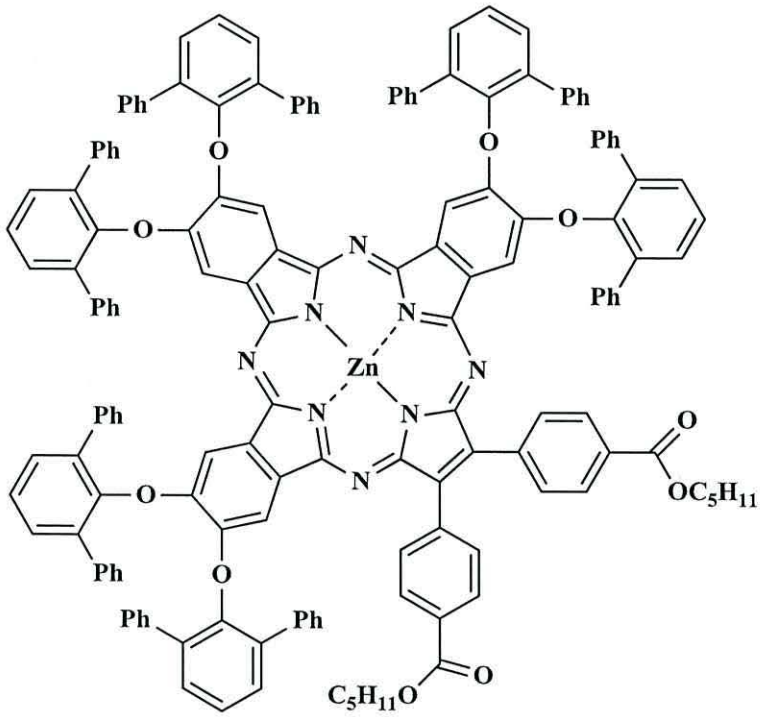

(23)

Scheme 2.27. Synthetic pathway of 2, 3-di (4-pentoxybenzoate)-7^2, 12^2, 17^2-hexa (2, 6-diphenylphenoxy)-tribenzo-5, 10, 15, 20-tetrazaporphyrin zinc (**23**).

Using a method developed from are reported previously, [8] fumaronitrile (**19**) (0.1 g, 0.289 mmol), (0.53g, 0.87 mmol) of 4,5-*bis*([1, 1′:3′, 1″-terphenyl]-2'-yloxy) phthalonitrile (**20**), $ZnCl_2$ (78mg, 0.58 mmol) and 0.3 ml of 1, 8-diazabicyclo [4, 5, 0] undec-7-ene (DBU) in 5 ml 1-pentanol was heated at 140°C with stirring for 72 h. After cooling to room temperature, the solvent was removed under reduced pressure and the product washed with methanol to remove excess $ZnCl_2$. The product was purified by column chromatography on activated alumina using dichloromethane as an eluent to produce 2, 3-di (4-pentoxybenzoate)-7^2, 12^2, 17^2-hexa (2, 6-diphenylphenoxy)-tribenzo-5, 10, 15, 20-tetrazaporphyrin zinc (**23**) as a dark green solid (yield 0.25 g, 36.5%).

MALDI-DCTB matrix mass calculate for $C_{160}H_{114}N_8O_{10}Zn$ 2373.07, found 2373.7 $[M]^+$.

^1H NMR (500 MHz, $CDCl_3$) δ (ppm) 0.94 (t, 6H, J= 7.25, -$(CH_2)_4CH_3$), 1.42 (m, 8H, 4x-CH_2), 1.79 (quint, 4H, 2x-CH_2), 4.35 (t, 4H, J= 6.6 Hz, 2x-OCH_2), 7.10-6.85 (m, 39H, *Ar-H*), 7.49-7.41 (m, 22H, *Ar-H*), 7.80-7.66 (m, 23H, *Ar-H*), 8.10 (br s, 4H, *Ar-H*), 8.26 (m, 4H, *Ar-H*); ^{13}C (125 MHz, $CDCl_3$) δ 13.96 ($\underline{CH_3}$-$(CH_2)_4$), 22.34, 28.17, 28.37 (CH_3-$(\underline{CH_2})_3$), 65.56 (-O$\underline{CH_2}$-), 117.47, 118.61, 121.61, 127.93, 128.14, 129.29, 129.47, (*Ar-C*-H) and (*Ar-C*-C), 165.92 (*C=O*). The UV-Vis spectrum of phthalocyanine shows an absorption peak at 684 nm (14619 cm^{-1}) (ε = 83672 $M^{-1}cm^{-1}$) in THF.

The FT-IR spectrum KBr ν/cm^{-1} shows absorption peaks at 3057 cm^{-1} ν (C-H, m) aromatic; 2956, 2929, 2869 cm^{-1} ν (C-H, m) aliphatic; 1717 ν (C=O, str (shp)); 1607 cm^{-1} ν (C=C, str) aromatic; 1271 cm^{-1} ν (C-O, shp) and 1199 cm^{-1} ν (C-N, str).

2.4.6 Synthesis of 2, 3-di (4-benzoic acid)-7^2, 12^2, 17^2-hexa (2, 6-diphenylphenoxy)-tribenzo-5, 10, 15, 20-tetrazaporphyrin zinc (24).

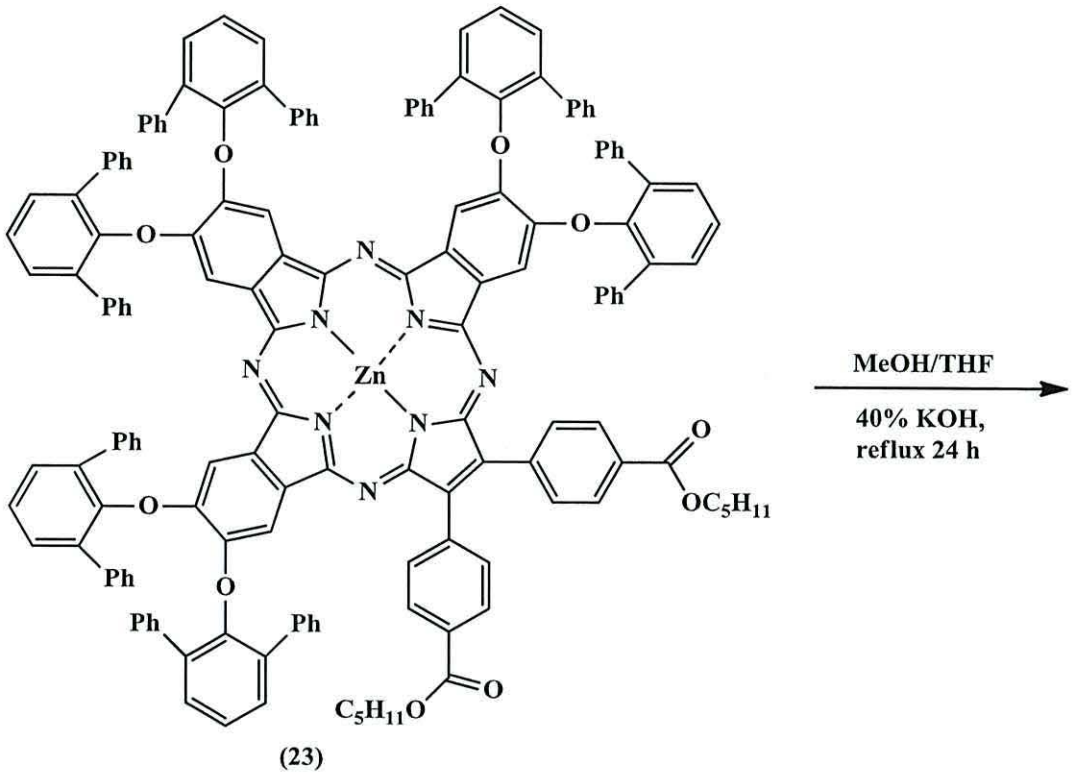

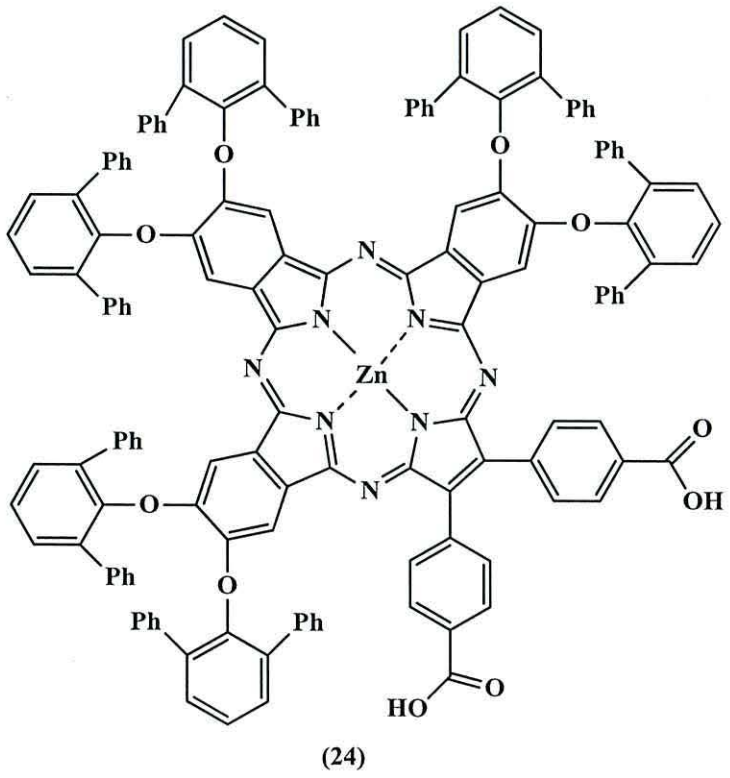

Scheme 2.28. Synthetic pathway of 2, 3-di (4-benzoic acid)-7^2, 12^2, 17^2-hexa (2, 6-diphenylphenoxy)-tribenzo-5, 10, 15, 20-tetrazaporphyrin zinc (**24**).

Using a method developed from are reported previously, [9] to a solution of the previously collected dark green solid (**23**) (0.1 g) in THF-methanol (2:1 v/v, 30 ml) was added 40% aqueous KOH solution (30 ml). The solution was stirred at reflux for 24 h and then was cooled at room temperature and the organic layer was removed under reduced pressure. The pH of the reaction mixture was adjusted to 4 by adding 6M HCl solution and a green precipitate was formed. The precipitate was collected and washed with copious amounts of water and dried. Then the green precipitate was suspended in 100 ml of chloroform and stirred at reflux for 1 h. It was then filtrated and dried under reduced pressure to produce 2, 3-di (4-benzoic acid)-7^2, 12^2, 17^2-hexa (2, 6-diphenylphenoxy)-tribenzo-5, 10, 15, 20-tetrazaporphyrin zinc (**24**) as a green solid (0.05 g, 53%). MALDI-DCTB matrix mass calculated for $C_{150}H_{94}N_8O_{10}Zn$ 2232.6, found 2232.6 $[M]^+$.

^1H NMR (500 MHz, $CDCl_3$) δ (ppm) 7.13-6.90 (m, 44H, *Ar-H*), 7.39-7.32 (m, 16H, *Ar-H*), 7.53-7.43 (m, 32H, *Ar-H*). ^{13}C NMR (125 MHz, $CDCl_3$) δ 127.93, 128.14, 129.29, 129.47, 154.00, 163.01. The UV-Vis spectrum of phthalocyanine shows an absorption peak at 708 nm (14124 cm^{-1}) (ε = 44726 $M^{-1}cm^{-1}$) in THF.

The FT-IR spectrum KBr ν/cm^{-1} shows absorption peaks at 3447 cm^{-1} ν (O-H, br) carboxylic acid; 3058 cm^{-1} ν (C-H, w) aromatic; 2919, 2851 cm^{-1} ν (C-H, m) aliphatic; 1659 cm^{-1} ν (C=O, br); 1584 cm^{-1} ν (C=C, w) aromatic; 1270 cm^{-1} ν (C-O, str) and 1199 cm^{-1} ν (C-N, str).

2.4.7 Synthesis of 2^2, 7^2, 12^2, 17^2 -octa (2, 6-diphenylphenoxy)-tetrazaporphyrin zinc (26).

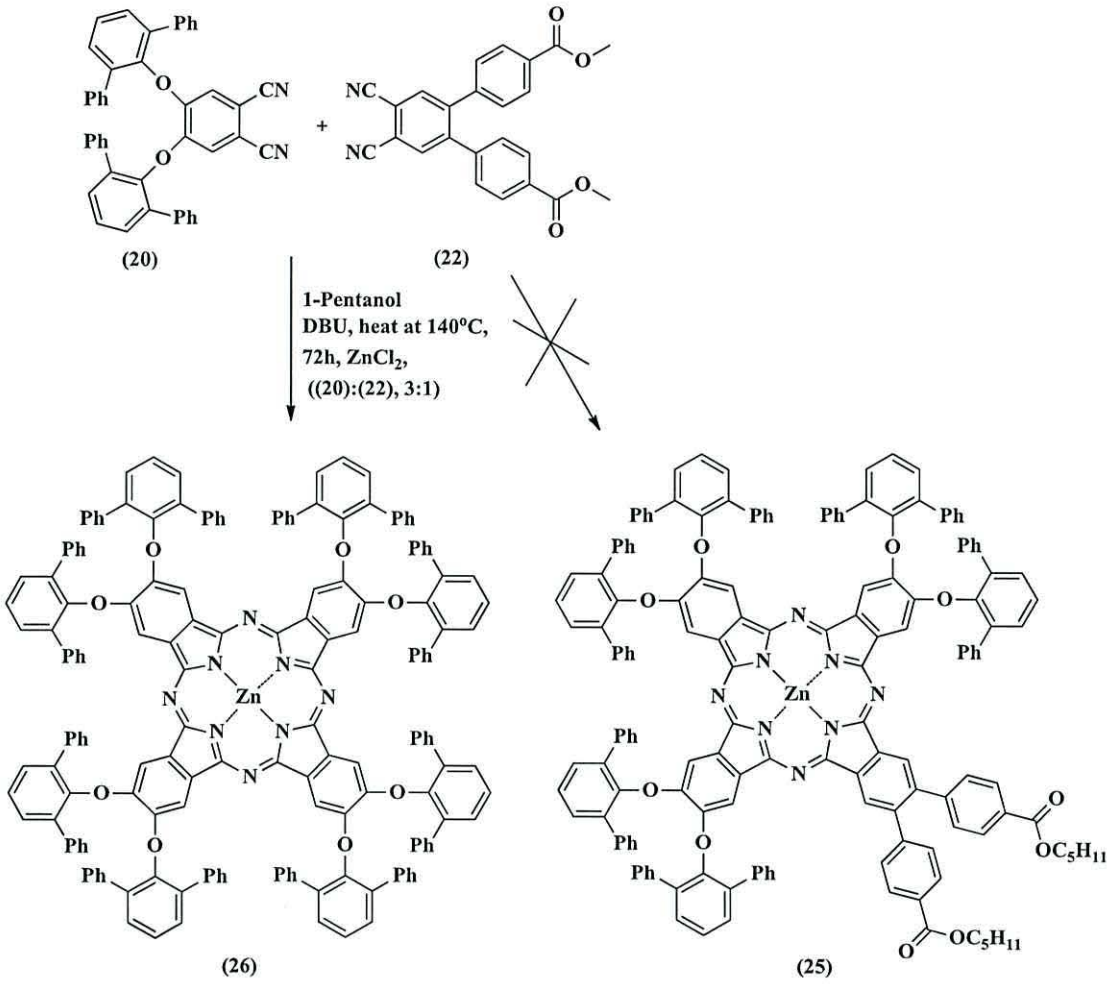

Scheme 2.29. Synthetic pathway of 2^2, 7^2, 12^2, 17^2- octa (2, 6-diphenylphenoxy)-tetrazaporphyrin zinc (**26**).

Using a method developed from are reported previously, [8] 4, 5-bis (4-methoxycarbonylphenyl) phthalonitrile (**22**) (0.08 g, 0.2 mmol), 4,5-*bis* ([1, 1′:3′, 1″-terphenyl]-2'-yloxy) phthalonitrile (**20**) (0.37 g, 0.6 mmol), $ZnCl_2$ (60 mg, 0.4 mmol) and 0.3 ml of 1, 8-diazabicyclo [4, 5, 0] undec-7-ene (DBU) in 5 ml 1-pentanol was heated at 140°C with stirring for 72 h. After cooling to room temperature, the solvent was removed under reduced pressure and the product washed with methanol to remove excess $ZnCl_2$. The product was purified by column chromatography on activated alumina using dichloromethane as an eluent to produce 2^2, 7^2, 12^2, 17^2 octa (2, 6-diphenylphenoxy)-tetrazaporphyrin zinc (**26**) as a dark green solid (yield 0.2 g,

41%). A suitable crystal for X-ray analysis was then prepared by dissolving the compound in tetrahydrofuran followed by slow evaporation.

MALDI-DCTB matrix mass calculated for $C_{176}H_{112}N_8O_8Zn$ 2529.79, found 2530.60.

^1H NMR (400 MHz, $CDCl_3$) δ (ppm) 6.36 (s, 8H, *Ar-H*), 6.72-7.13 (m, 40H, *Ar-H*), 7.40-7.53 (m, 48H, *Ar-H*), 7.72-7.78 (m, 16H, *Ar-H*); DEPTQ.^{13}C (100 MHz, $CDCl_3$) δ 109.52, 124.57, 126.11, 127.49, 127.64, 128.19, 129.28, 129.69, 131.24, 132.15, 135.09, 137.60, 150.26, (*Ar-C*-H), (*Ar-C*-C), (*Ar-C*-N) and (*Ar-C*-O).

The UV-Vis spectrum of compound (**26**) shows an absorption peak at 684 nm (14619 cm^{-1}) (ε = 206840 $M^{-1}cm^{-1}$) in THF.

The FT-IR spectrum KBr ν/cm^{-1} shows absorption peaks at 3057 cm^{-1} ν (C-H, m) aromatic; 2926, 2855 cm^{-1} ν (C-H, m) aliphatic; 1718 cm^{-1} ν (C=O, br); 1610 cm^{-1} ν (C=C, m) aromatic; 1271 cm^{-1} ν (C-O, shp) and 1200 cm^{-1} ν (C-N, shp).

Table 2.15. Crystal data and structure refinement details of (**26**).

Identification code	Compound (**26**)
Empirical formula	$C_{204}H_{168}N_8O_{15}Zn$
Formula weight	3036.83
Temperature	100(2) K
Wavelength	0.71075 Å
Crystal system	Triclinic
Space group	*P*–1
Unit cell dimensions	a = 11.8266(6) Å α = 65.139(5) °
	b = 19.9674(10) Å β = 74.370(5) °
	c = 20.2200(14) Å γ = 78.213(6) °
Volume	4149.5(4) $Å^3$
Z	1
Density (calculated)	1.215 Mg / m^3
Absorption coefficient	0.216 mm^{-1}
F(000)	1598
Crystal	Column; Green
Crystal size	0.07 × 0.04 × 0.02 mm^3
θ range for data collection	3.03 – 25.00°
Index ranges	$-14 \le h \le 14$, $-23 \le k \le 22$, $-24 \le l \le 22$
Reflections collected	44763
Independent reflections	14452 [R_{int} = 0.0772]
Completeness to θ = 25.00°	99.0 %
Absorption correction	Semi–empirical from equivalents
Max. and min. transmission	0.9957 and 0.9851
Refinement method	Full-matrix least-squares on F^2
Data / restraints / parameters	14452 / 35 / 1004
Goodness-of-fit on F^2	0.987
Final *R* indices [$F^2 > 2\sigma(F^2)$]	*R1* = 0.1044, *wR2* = 0.2846
R indices (all data)	*R1* = 0.1787, *wR2* = 0.3240
Largest diff. peak and hole	1.424 and –0.474 e $Å^{-3}$

2.4.8 Synthesis of 2-(propoxybenzoate)-3-(4-benzoic acid)-7^2, 12^2, 17^2-hexa (diphenylphenoxy)-tetrabenzo-5, 10, 15, 20-tetrazaporphyrin zinc (27).

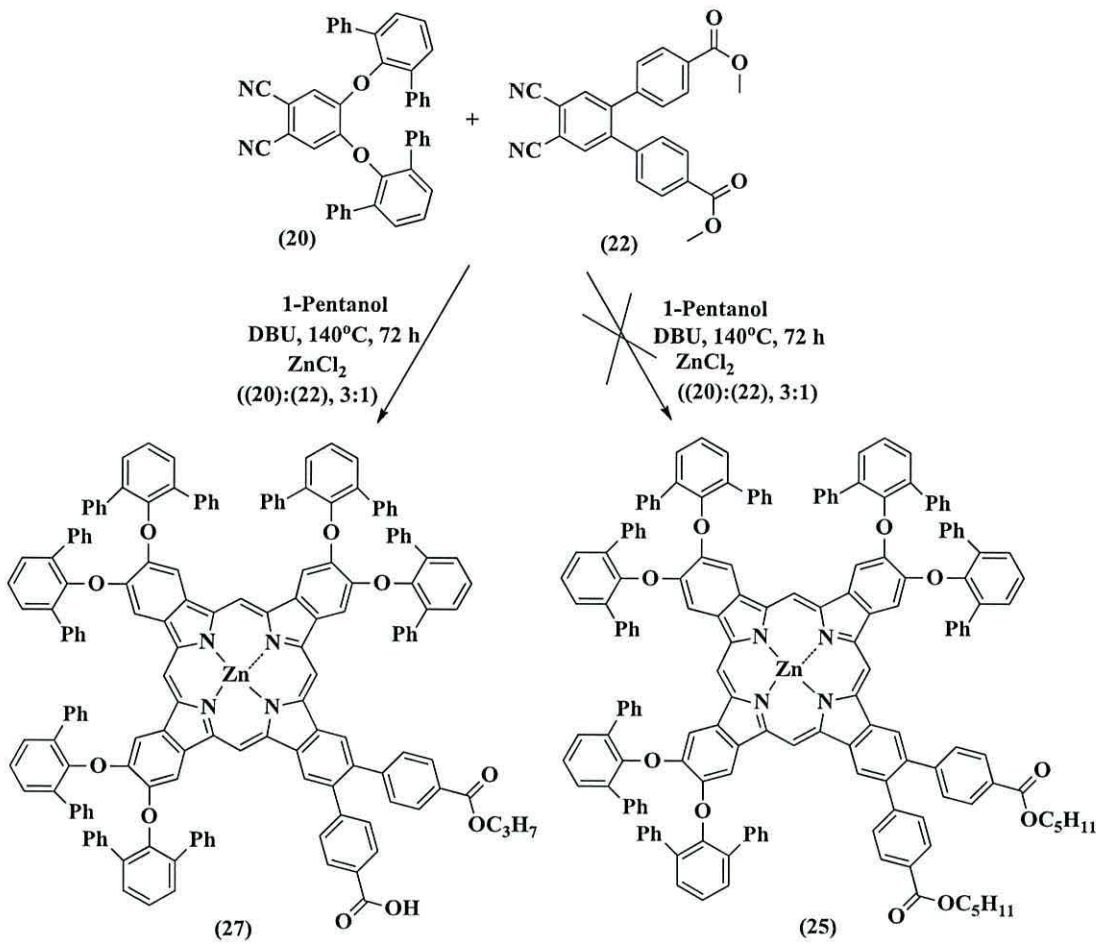

Scheme 2.30. Synthetic pathway of 2-(propoxybenzoate)-3-(4-benzoic acid)-7^2, 12^2, 17^2-hexa (diphenylphenoxy)-tetrabenzo-5, 10, 15, 20-tetrazaporphyrin zinc (**27**).

Using a method developed from a previous report, [8] 4, 5-bis (4-methoxycarbonylphenyl) phthalonitrile (**22**) (0.08 g, 0.2 mmol), 4,5-*bis* ([1, 1′:3′, 1″-terphenyl]-2'-yloxy) phthalonitrile (**20**) (0.37 g, 0.6 mmol), $ZnCl_2$ (60 mg, 0.4 mmol) and 0.3 ml of 1, 8-diazabicyclo [4, 5, 0] undec-7-ene (DBU) in 5 ml 1-pentanol was heated at 140°C with stirring for 72 h. After cooling to room temperature, the solvent was removed under reduced pressure and the product washed with methanol to remove excess $ZnCl_2$. The product was purified by column chromatography on activated alumina using dichloromethane as an eluent to produce the unexpected compound 2- (propoxybenzoate)-3-(4-benzoic acid)-7^2,12^2,17^2-hexa

(diphenylphenoxy)-tetrabenzo-5, 10, 15, 20-tetrazaporphyrin zinc (**27**) as a dark green solid (yield 0.2 g, 41%).

MALDI-DCTB matrix mass calculated for $C_{164}H_{116}N_8O_{10}Zn$ 2424.24 not found, found two peaks at 2321.4 and 2531.5 calculated for (**27**) and (**26**), respectively.

The ^1H NMR (400 MHz, $CDCl_3$) δ (ppm) 0.84-0.95 ppm (m, 3H, *CH₃*-CH_2-CH_2-O-), 1.86 (pentate, 2H, CH_3-*CH₂*-CH_2-O-), 3.75 (t, 2H, CH_3-CH_2-*CH₂*-O-), 6.35-7.56 ppm (m, 40H, *Ar-H*), 7.40-7.53 (m, 36H, *Ar-H*), 7.72-7.78 (m, 16H, *Ar-H*); ^{13}C NMR (100 MHz, $CDCl_3$) δ 27.78 (-*CH₃*CH_2-CH_2-O-), 29.68 (CH_3-*CH₂*-CH_2-O-), 69.41 (CH_3-CH_2-*CH₂*-O-), 109.53, 124.67, 126.12, 127.50, 127.80, 128.04, 128.20, 129.07, 129.29, 129.72, 130.94, 131.25, 135.11, 137.51, 137.67, 147.65, 150.27 (*Ar-C-H*), (*Ar-C*-C) and (*Ar-C*-N), 167.25 (*C=O*).

The UV-Vis spectrum of compound (**27**) shows an absorption peak at 360 nm and at 684 nm ($\varepsilon = 83672\ M^{-1}cm^{-1}$) in THF.

The FT-IR spectrum KBr ν/cm^{-1} shows absorption peaks at 3058 cm^{-1} ν (C-H, m) aromatic; 2926, 2855 cm^{-1} ν (C-H, m) aliphatic; 1718 cm^{-1} ν (C=O, br); 1610 cm^{-1} ν (C=C, m) aromatic and 1271 cm^{-1} ν (C-O, shp).

2.4.9 Synthesis of 2, 3-di(4-benzoic acid)-7^2, 12^2, 17^2-hexa(2,6-diphenylphenoxy)-tetrabenzo-5, 10, 15, 20-tetrazaporphyrin zinc (28).

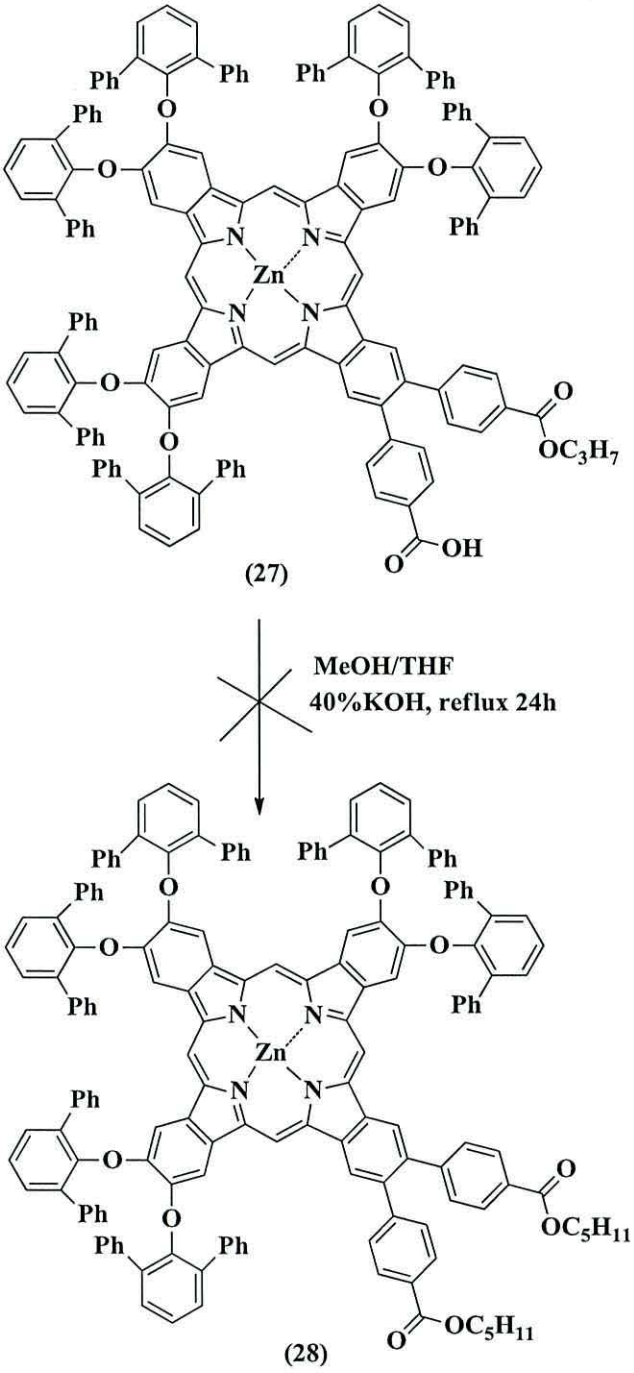

Scheme 2.31. synthetic pathway of 2,3-di(4-benzoic acid)-7^2,12^2,17^2-hexa(2,6-diphenylphenoxy)-tetrabenzo-5,10,15,20-tetrazaporphyrin zinc (**28**).

Note: In this reaction, 2,3-di(4-benzoic acid)-7^2,12^2,17^2-hexa(2,6-diphenylphenoxy)-tetrabenzo-5,10,15,20-tetrazaporphyrin zinc (**28**) was not formed. Compound (**27**) was recovered unreacted.

2.5 Synthesis of cyanine dyes.

2.5.1 Synthesis of 1-carboxyethyl-2, 3, 3-trimethylindolenium iodide (29). [10]

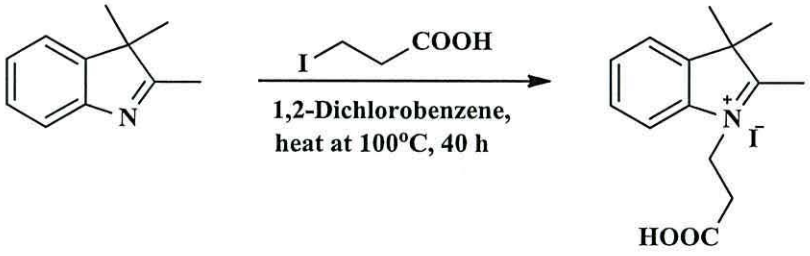

(29)

Scheme 2.32. Synthetic pathway of 1-carboxyethyl-2, 3, 3-trimethylindolenium iodide (**29**).

To a solution of 2, 3, 3-trimethyl-3H-indole (1 g, 1 ml, 6.3 mmol) in 5 ml of 1, 2-dichlorobenzene was added iodopropionic acid (1 g, 5.2 mmol). The mixture was left stirring at 100°C for 40 h under nitrogen. It was then cooled to room temperature and the solvent was removed under vacuum. Ethyl acetate was then added to give yellow-orange solid. The product was dried by high vacuum, to give a yellow-orange solid of 1-carboxyethyl-2, 3, 3-trimethylindolenium iodide (**29**) (1.4 g, 96 %), m.p. 167-169°C. A suitable crystal for X-ray analysis was then prepared by dissolving this compound in methanol followed by slow evaporation. MS: m/z (Accurate Mass), reference compound: NH_4OAc, calcd for $C_{14}H_{18}NO_2$, 232.1332, found 232.1333.
^{1}H NMR (500 MHz, DMSO-d6) δ 1.52 (s, 6H, 2x-*CH*$_3$), 2.84 (s, 3H, -*CH*$_3$), 2.97 (t, 2H, *J*= 6.95, -*CH*$_2$-COOH), 4.64 (t, 2H, J= 6.9, -N-*CH*$_2$), 7.61 (m, 2H, *Ar-H*), 7.83 (m, 1H, *Ar-H*), 7.98 (m, 1H, *Ar-H*), 12.73 (br s, 1H, -CH_2-*COOH*). ^{13}C (125 MHz, DMSO-d6) δ 14.26 (-*CH*$_3$), 21.84 (2x-*CH*$_3$), 31.07 (-*CH*$_2$-COOH), 43.48 (*C*-$(CH_3)_2$), 54.23 (N-*CH*$_2$), 115.52, 123.43, 128.90, 129.33 (*Ar-C*-H), 140.80, 141.73 (*Ar-C*-C), 171.47 (*C*=*O*), 197.89 (*C*-CH_3).

The FT-IR spectrum KBr ν/cm^{-1} shows absorption peaks at 3300-2700 cm^{-1} ν (O-H, br) carboxylic acid; 3046 cm^{-1} ν (C-H, m) aromatic; 2972, 2920 and 2863 cm^{-1} ν (C-H, m) aliphatic; 1730 cm^{-1} ν (C=O, str); 1627, 1606 cm^{-1} ν (C=C, shp) aromatic and 1594 cm^{-1} ν (C=C, shp) aliphatic.

Table 2.16. Crystal data and structure refinement details of (**29**).

Identification code	Compound (**29**)	
Empirical formula	$C_{14}H_{18}INO_2$	
Formula weight	359.19	
Temperature	100(2) K	
Wavelength	0.71075 Å	
Crystal system	Orthorhombic	
Space group	*Pbca*	
Unit cell dimensions	$a = 7.4137(5)$ Å	$\alpha = 90°$
	$b = 13.6430(12)$ Å	$\beta = 90°$
	$c = 29.756(3)$ Å	$\gamma = 90°$
Volume	3009.7(5) $Å^3$	
Z	8	
Density (calculated)	1.585 Mg / m^3	
Absorption coefficient	2.123 mm^{-1}	
F(000)	1424	
Crystal	Chip; colourless	
Crystal size	$0.01 \times 0.01 \times 0.01$ mm^3	
θ range for data collection	2.99 – 24.99°	
Index ranges	$-8 \le h \le 8$, $-16 \le k \le 13$, $-35 \le l \le 22$	
Reflections collected	11997	
Independent reflections	2636 [$R_{int} = 0.1644$]	
Completeness to $\theta = 24.99°$	99.6 %	
Absorption correction	Semi–empirical from equivalents	
Max. and min. transmission	0.9895 and 0.9791	
Refinement method	Full-matrix least-squares on F^2	
Data / restraints / parameters	2636 / 6 / 167	
Goodness-of-fit on F^2	0.860	
Final R indices [$F^2 > 2\sigma(F^2)$]	$R1 = 0.0486$, $wR2 = 0.0685$	
R indices (all data)	$R1 = 0.1294$, $wR2 = 0.0847$	
Largest diff. peak and hole	0.968 and –0.587 e $Å^{-3}$	

2.5.2 Synthesis of 1-carboxyethyl-2, 3, 3-trimethyl-1H-benzo [0]-indolium iodide (30). [10]

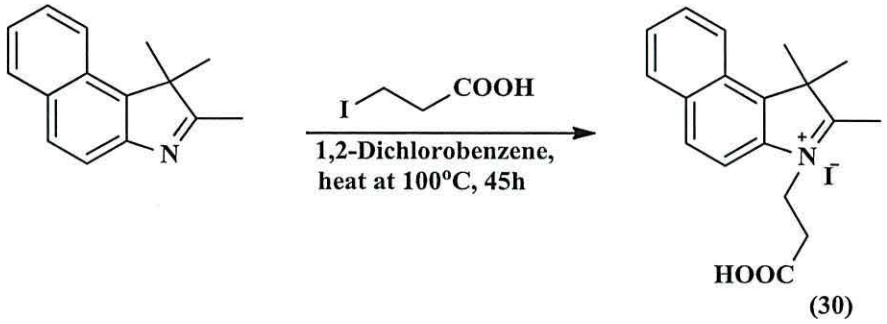

(30)

Scheme 2.33. Synthetic pathway of 1-carboxyethyl-2, 3, 3-trimethyl-1H-benzo [0]-indolium iodide (**30**).

To a solution of 2, 3, 3-trimethylbenzoindolenine (1 g, 4.78 mmol) in 5 ml of 1, 2-dichlorobenzene was added (0.9 g, 4 mmol) of iodopropionic acid. The mixture was left stirring at 100°C for 45 h under nitrogen. It was cooled to room temperature, and the solvent was removed under reduced pressure and ethyl acetate was added to give a solid. The product was filtrated and dried by high vacuum, to give a beige solid of 1-carboxyethyl-2, 3, 3-trimethyl-1H-benzo [*0*]-indolium iodide (**30**) (1.3 g, 96%), m.p. 215-217°C. A suitable crystal for X-ray analysis was then prepared by dissolving this compound in methanol followed by slow evaporation. FTMS$^+$-MS: m/z (Accurate Mass), reference compound: NH_4OAc, calcd. for $C_{18}H_{20}NO_2$, 282.1489, found 282.1491.

^{1}H NMR (500 MHz, DMSO-d6) δ 1.74 (s, 6H, 2x-*CH*$_3$), 2.95 (s, 3H, -*CH*$_3$), 3.03 (t, 2H, J= 6.95, -*CH*$_2$-COOH), 4.76 (t, 2H, J= 6.65, -N-*CH*$_2$), 7.73 (t, 1H, J= 7.55, *Ar-H*), 7.78 (t, 1H, J= 6.9, *Ar-H*), 8.16 (d, 1H, J= 9.15, *Ar-H*), 8.21 (d, 1H, J= 8.5, *Ar-H*), 8.28 (d, 1H, J= 8.85, *Ar-H*), 8.36 (d, 1H, J= 8.2, *Ar-H*), 12.73 (bs, 1H, -CH$_2$-*COOH*); ^{13}C NMR (125 MHz, DMSO-d6) δ 14.11 (-*C*H$_3$), 21.45 (2x-*C*H$_3$), 31.32 (-*C*H$_2$-COOH), 43.75 (*C*-(CH$_3$)$_2$), 55.59 (-N-*C*H$_2$), 113.41, 123.40, 127.20, 128.42, 129.72, 130.64 (*Ar-C*-H), 131.12, 133.00, 138.32, 143.89 (*Ar-C*-C), 171.52 (-*C*=*O*), 197.75 (*C*-CH$_3$).

The FT-IR spectrum KBr ν/cm^{-1} shows absorption peaks at 3300-2700 cm^{-1} ν (O-H, br) carboxylic acid; 3045 cm^{-1} ν (C-H, m) aromatic; 2973, 2927 and 2780 cm^{-1} ν (C-

H,m) aliphatic; 1727 cm^{-1} ν (C=O, str (shp)); 1582 cm^{-1} ν (C=C, str) aromatic and 1180 cm^{-1} ν (C-N, str).

Table 2.17. Crystal data and structure refinement details of (**30**).

Identification code	Compound (**30**)	
Empirical formula	$C_{18}H_{20}INO_2$	
Formula weight	409.25	
Temperature	100 K	
Wavelength	0.71075 Å	
Crystal system	Orthorhombic	
Space group	*Pbca*	
Unit cell dimensions	$a = 7.530(2)$ Å	$\alpha = 90°$
	$b = 13.635(3)$ Å	$\beta = 90°$
	$c = 34.164(8)$ Å	$\gamma = 90°$
Volume	3507.9(15) $Å^3$	
Z	8	
Density (calculated)	1.550 Mg / m^3	
Absorption coefficient	1.832 mm^{-1}	
F(000)	1632	
Crystal	Plate; Colourless	
Crystal size	0.20 × 0.15 × 0.01 mm^3	
θ range for data collection	2.96 – 27.48°	
Index ranges	$-9 \le h \le 7, -17 \le k \le 13, -44 \le l \le 39$	
Reflections collected	21886	
Independent reflections	3992 [$R_{int} = 0.0666$]	
Completeness to $\theta = 27.48°$	99.3 %	
Absorption correction	Semi–empirical from equivalents	
Max. and min. transmission	0.9819 and 0.7108	
Refinement method	Full-matrix least-squares on F^2	
Data / restraints / parameters	3992 / 0 / 203	
Goodness-of-fit on F^2	1.245	
Final *R* indices [$F^2 > 2\sigma(F^2)$]	*R1* = 0.0596, *wR2* = 0.0821	
R indices (all data)	*R1* = 0.0717, *wR2* = 0.0858	
Largest diff. peak and hole	0.905 and –0.629 e $Å^{-3}$	

2.5.3 Synthesis of 4, 6-dibromo-2, 3, 3-trimethyl-1-octyl-3H-indolium iodid (31).

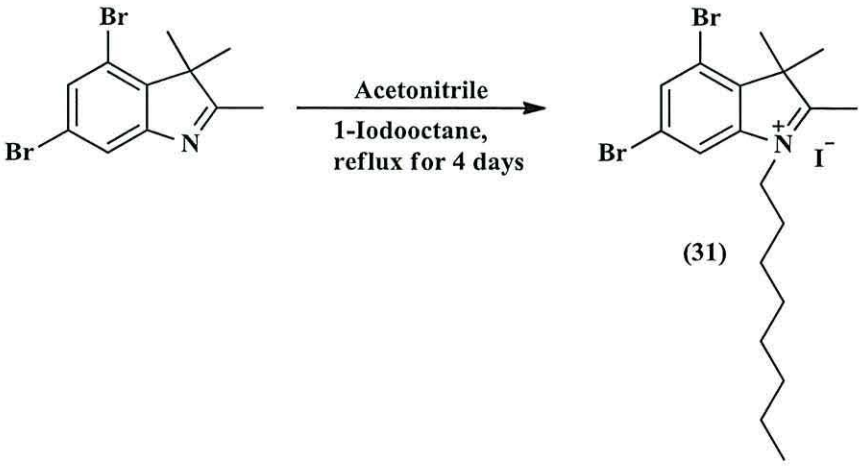

Scheme 2.34. Synthetic pathway of 4, 6-dibromo-2, 3, 3-trimethyl-1-octyl-3H-indolium iodide (**31**).

Using a method developed from are reported previously, [11, 12] dibromo-2, 3, 3-trimethyl-3H-indole was synthesized by Dr Arthur Connell at Bangor University and used as supplied (2.5 g, 7.885 mmol) was dissolved in 30 ml of dry acetonitrile, and then 5ml of 1-iodooctane was added. The mixture reaction was left to stir at 100° C for 45 h. the solution was cooled to room temperature and the solvent removed using a flash distillation method to give a brown solid of (**31**) (1.9 g, 56 %). FTMS^{+}-MS: m/z (Accurate Mass), reference compound: NH_4OAc-ASAP, calcd. for $C_{19}H_{28}Br_2N$, 428.0583, found 428.0581 M^{+}.

^{1}H NMR (500 MHz, $CDCl_3$) δ 0.89 (t, 3H, J= 6.95, -$(CH_2)_7$*CH_3*), 1.33 (m, 10H, 5x-*CH_2*), 1.57 (s, 6H, 2x-*CH_3*), 1.8 (pentate, 2H, -*CH_2*), 2.31 (s, 3H, -*CH_3*), 3.19 (t, 2H, J= 6.9, -N-*CH_2*-), 7.63 (d, 1H, J= 1.6, *Ar-H*), 7.33 (d, 1H, J= 1.6, *Ar-H*).

^{13}C (125 MHz, $CDCl_3$) δ 7.30 (C-*$\underline{C}H_3$*), 14.07 (*$\underline{C}H_3$*-$(CH_2)_7$), 15.65, 22.62, , 28.51, 29.08, 30.52, 31.76 (CH_2-*$(\underline{C}H_2)_6$*), 22.90 (C-*$(\underline{C}H_3)_2$*), 33.59 (*$\underline{C}$*-$(CH_3)_2$), 56.01 (N-*$\underline{C}H_2$*), 114.28, 119.15 (*Ar-C*-Br), 123.93, 133.34 (*Ar-C*-H), 148.79, 151.23 (*Ar-C*-C), 189.95 (*$\underline{C}$*-CH_3).

2.5.4 Synthesis of 2, 3, 3-trimethyl-3H-indole-6-carboxylic acid (32). [12]

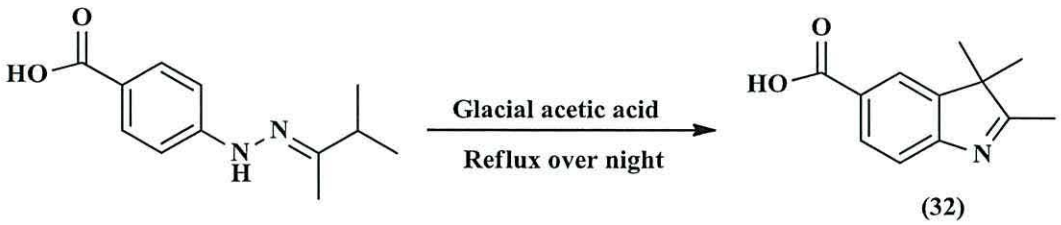

(32)

Scheme 2.35. Synthetic pathway of 2, 3, 3-trimethyl-3H-indole-6-carboxylic acid (**32**).

4-[(1,2-dimethylpropylidene) hydrazino]-benzoic acid was synthesized by Dr Arthur Connell at Bangor University and used as supplied (4 g, 18.15 mmol) was dissolved in 100 ml of glacial acetic acid and the resulting solution was refluxed under nitrogen overnight. This was then cooled to room temperature, and the glacial acetic acid was removed by using flash distillation. The product was washed with a mixture (50:50, v/v) toluene:methanol and the crude product was recrystallized from ethyl acetate:petroleum (3:1) to produce 2, 3, 3-trimethyl-3H-indole-6-carboxylic acid (**32**) as an orange-yellow solid (0.8 g, 22 %). FTMS+-MS: m/z (Accurate Mass), reference compound: DEA, calcd. for $C_{12}H_{12}NO_2$ 202.0874 found 202.0872 $[M-H]^-$. ^1H NMR (500 MHz, DMSO-d6) δ 1.27 (s, 6H, 2x-*CH*$_3$), 2.25 (s, 3H, -*CH*$_3$), 7.5 (d, 1H, *Ar-H*), 7.9 (d, 1H, *Ar-H*), 7.98 (s, 1H), 12.78 (bs, 1H, -*COOH*); ^{13}C (125 MHz, DMSO-d6) δ 15.31 (C-*C*H$_3$), 22.22 (C-x2 *(C*H$_3$*)*), 53.42 (*C*-(CH$_3$)$_2$), 119.05, 122.66, 127.23 (*Ar-C*-H), 129.55, 146.07, 157.37 (*Ar-C*-C), 167.42 (*C=O*), 191.63 (*C*-CH$_3$).

2.5.5 Synthesis of (E)-2-chloro-3-(hydroxymethylene)cyclohex-1-enecarbaldehyde (33). [13]

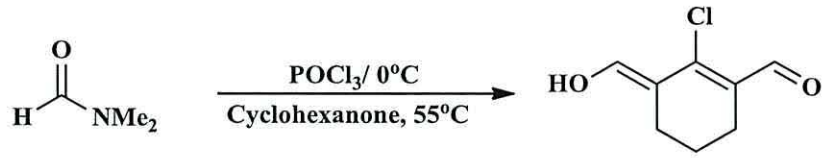

(33)

Scheme 2.36. Synthetic pathway of (E)-2-chloro-3-(hydroxymethylene)cyclohex-1-enecarbaldehyde (**33**).

$POCl_3$ (3.378 g, 22.0 mmol) was added to 4 ml of DMF at 0°C and the reaction mixture was gradually warmed to room temperature. Then a solution of cyclohexanone (0.99 g, 5.04 mmol) in 5 ml DMF was added slowly drop wise. The resulting mixture was heated at 55°C for 4 h. After that it was cooled to room temperature. Then water was added with crushed ice and the solution was stored in a refrigerator overnight to give a yellow precipitate which was filtered to produce (**33**) as a yellow precipitate (1.4 g, 80%), m.p. 108-110°C (Lit 125-127°C). [14] $FTMS^+$-MS: m/z (Accurate Mass), reference compound: NH_4OAc, calcd. for $C_8H_9ClO_2$, 173.0364, found 173.0362 $[M+H]^{+\cdot}$

^1H NMR (400MHz, DMSO-d6) δ (ppm) 1.57 (quint, 2H, -*CH_2* -cyclohexene), 2.35 (t, 4H, *J= 6.16*, 2x-*CH_2* -cyclohexene), 4.02 (br s, 1H, =CH*OH*), 8.81 (br s, 1H, =*CH*OH), 10.84 (br s, 1H, -*CHO*). ^{13}C NMR (100 MHz, DMSO-d6) δ (ppm) 16.86, 19.22, 23.66 (3x-*$\underline{C}H_2$*-cyclohexene), 146.02 (*$\underline{C}$*-Cl), 182.93 (*$\underline{C{=}O}$*). Residual two carbons could not be found in ^{13}C NMR.

The FT-IR spectrum KBr ν/cm^{-1} shows absorption peaks at 3197 cm^{-1} ν (OH, br) alcohol; 3066 cm^{-1} ν (C-H, m) aromatic; 2952, 2883 and 2753 cm^{-1} ν (C-H, m) aliphatic; 1794 cm^{-1} ν (C=O, str (shp)); 1603 cm^{-1} ν (C=C, br) aromatic; 1540 cm^{-1} ν (C=C, br) aliphatic; 1276 cm^{-1} ν (C-O, shp).

2.5.6 Synthesis of 3-(2-((E)-2-((E)-3-((E)-2-(1-(2-carboxyethyl)-3, 3-dimethyl indolin-2-ylidene) ethylidene)-2-chlorocyclohex-1-en-1-yl) vinyl)-3, 3-dimethyl-3 H-indol-1-ium-1-yl) propanoate (34).

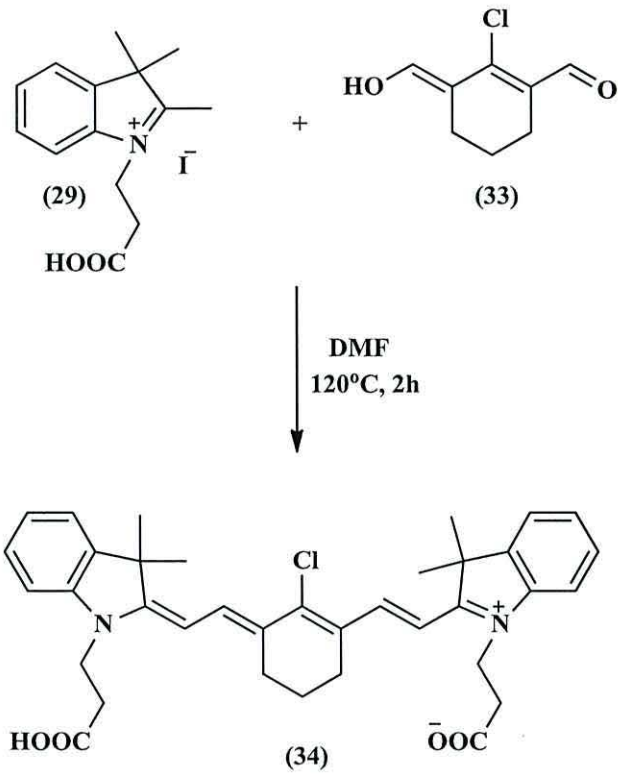

Scheme 2.37. Synthetic pathway of 3-(2-((E)-2-((E)-3-((E)-2-(1-(2-carboxyethyl)-3, 3-dimethylindolin-2-ylidene) ethylidene)-2-chlorocyclohex-1-en-1-yl) vinyl)-3, 3-dimethyl-3H-indol-1-ium-1-yl) propanoate (**34**).

Using a method developed from Funabiki *et al.*[13] to a solution of (E)-2-chloro-3-(hydroxymethylene)cyclohex-1-enecarbaldehyde (**33**) (0.1 g, 0.5 mmol) in 15 ml DMF was added (0.27 g, 1.16 mmol, 2 eq.) of 1-carboxyethyl-2, 3, 3-trimethylindolium iodide (**29**). The reaction mixture was heated at 120°C for 2 h. It was cooled to room temperature and 50 ml H_2O was added. The resulting precipitate was purified by column chromatography on silica gel with dichloromethane/methanol as the eluent (3:1, v/v). The solvent was removed under vacuum to produce (**34**) as a green solid (0.3 g, 43%). A suitable crystal for X-ray analysis was prepared by dissolving this compound in dichloromethane followed by slow evaporation.

MS: m/z (Accurate Mass), calcd. for $C_{36}H_{38}ClN_2O_4$, 597.2526, found $C_{36}H_{38}ClN_2O_4$, 597.2520 $[M-H]^-$.

^{1}H NMR (400 MHz, CD_3OD) δ 1.73 (s, 12H, 4x-*CH_3*), 1.96 (pentate, 2H, -*CH_2*-cyclohexene), 2.70 (t, 4H, J= 7.08, 2x-*CH_2* cyclohexene), 2.76 (t, 4H, J= 6.24, 2x-*CH_2*-COOH), 4.42 (t, 4H, J= 7.2, 2x-N-*CH_2*), 6.45 (d, 2H, J= 14.04, -*CH=CH*-), 7.27 (t, 2H, J= 7.32, 2x*Ar-H*), 7.40 (dt, 4H, J= 8.04, 6.72, *Ar-H*), 7.50 (d, 2H, J= 7.36, 2x*Ar-H*), 8.42 (d, 2H, J= 14.08, -*CH=CH*-). ^{13}C (100 MHz, CD_3OD) δ (ppm) 22.16-*$\underline{C}H_2$*-cyclohexene), 27.37 (2x-*$\underline{C}H_2$*-cyclohexene), 28.30 (4x-*$\underline{C}H_3$*), 34.96 (-*$\underline{C}H_2$*-COOH), 42.45 (*$\underline{C}$*-$(CH_3)_2$), 50.60 (N-*$\underline{C}H_2$*), 102.90, 103.77 (-*$\underline{CH=CH}$*-), 112.36, 123.42, 126.46, 128.52 (*$\underline{Ar}$*-*$\underline{C}$*-H), 129.86 (-*$\underline{CH}$*=C-), 142.64, 143.39 (*$\underline{Ar}$*-*$\underline{C}$*-C), 144.43 (-*CH=CH*-), 145.52, 151.01 (*$\underline{Ar}$*-*$\underline{C}$*-C), 174.16 (C-N) and 176.39 *$\underline{(C=O)}$*. The UV-Vis spectrum of (**34**) shows an absorption at 780 nm (12820 cm^{-1}) (ε = 173314 $M^{-1}cm^{-1}$) in methanol.

The FT-IR spectrum KBr ν/cm^{-1} shows absorption peaks at 3500-270 cm^{-1} ν (O-H, br) carboxylic acid; 2967 cm^{-1} ν (C-H, m) aromatic; 2930, 2865 cm^{-1} ν (C-H, m) aliphatic; 1732 cm^{-1} ν (C=O, br); 1637 cm^{-1} ν (C=O, shp); 1618 cm^{-1} ν (C=C, shp) aromatic; 1496 cm^{-1} ν (C=C, shp) aliphatic; 1196 cm^{-1} ν (C-N, m).

Table 2.18. Crystal data and structure refinement details of (**34**).

Identification code	Compound (**34**)
Empirical formula	$C_{37}H_{43}ClN_2O_5$
Formula weight	631.18
Temperature	100(2) K
Wavelength	0.71075 Å
Crystal system	Monoclinic
Space group	*P*21/*c*
Unit cell dimensions	$a = 6.5317(13)$ Å $\quad \alpha = 90°$
	$b = 26.615(5)$ Å $\quad \beta = 90.629(4)°$
	$c = 19.290(4)$ Å $\quad \gamma = 90°$
Volume	3353.2(12) $Å^3$
Z	4
Density (calculated)	1.250 Mg / m^3
Absorption coefficient	0.159 mm^{-1}
F(000)	1344
Crystal	Fragment; green
Crystal size	0.08 × 0.04 × 0.04 mm^3
θ range for data collection	3.06 – 27.39°
Index ranges	$-8 \le h \le 6, -34 \le k \le 33, -24 \le l \le 24$
Reflections collected	28704
Independent reflections	7617 [$R_{int} = 0.0382$]
Completeness to $\theta = 27.39°$	99.7 %
Absorption correction	Semi–empirical from equivalents
Max. and min. transmission	0.9937 and 0.9874
Refinement method	Full-matrix least-squares on F^2
Data / restraints / parameters	7617 / 0 / 413
Goodness-of-fit on F^2	1.035
Final *R* indices [$F^2 > 2\sigma(F^2)$]	*R1* = 0.0420, *wR2* = 0.1010
R indices (all data)	*R1* = 0.0542, *wR2* = 0.1073
Largest diff. peak and hole	0.335 and –0.324 e $Å^{-3}$

2. 5.7 Synthesis of 3-(2-((E)-2-((E)-3-((E)-2-(3-(2-carboxyethyl)-1,1-dimethyl-1H-benzo[e]indol-2(3H)-ylidene)ethylidene)-2-chlorocyclohex-1-en-1-yl)vinyl)-1,1-dimethyl-1H-benzo[e]indol-3-ium-3-yl)propanoate (35).

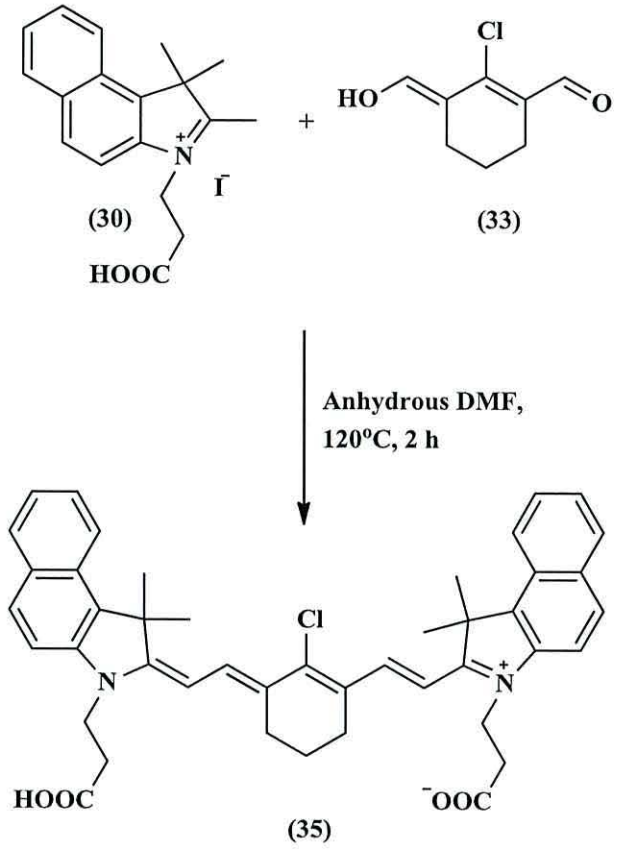

Scheme 2.38. Synthetic pathway of 3-(2-((E)-2-((E)-3-((E)-2-(3-(2-carboxyethyl)-1,1-dimethyl-1H-benzo[e]indol-2(3H)-ylidene)ethylidene)-2-chlorocyclohex-1-en-1-yl)vinyl)-1,1-dimethyl-1H-benzo[e]indol-3(2H)-yl)propanoic acid (**35**).

Using a method developed from Funabiki *et al.* [13], to a solution of (E)-2-chloro-3-(hydroxymethylene)cyclohex-1-enecarbaldehyde (**33**) (0.1g, 0.58 mmol) in 15 ml anhydrous DMF was added 1-carboxy-ethyl-2, 3, 3-trimethyl-1H- benzo[0] indolium iodide (**30**) (0.33 g, 1.6mmol). The reaction mixture was heated at 120°C for 2 h. The mixture was cooled at room temperature and 50 ml of H_2O was added. The resulting precipitate was filtered and was then purified by column chromatography on silica gel with dichloromethane/methanol as the eluent (3:1, v/v). The solvent was removed under vacuum to give (**35**) as a green solid (0.35 g, 85%), m.p. 224-226°C. MS: m/z (Accurate Mass), calcd. for $C_{44}H_{42}ClN_2O_4$, 697.2839, found 697.2835 $[M-2H]^-$. ^1H NMR (400 MHz, CD_3OD) δ 1.60 (s, 2H, -CH_2-cyclohexene), 2.03 (s, 12H, 4x-CH_3),

2.71 (t, 4H, *J= 7.28*, -CH_2-cyclohexene), 2.81 (t, 4H, *J= 6.04*, 2x-CH_2-COOH), 4.53 (t, 4H, *J= 7.16*, 2x-N-CH_2-), 6.49 (d, 2H, *J= 14.2*, *-CH=CH-*), 7.48 (t, 2H, J= 8.04, 2x *Ar-H*), 7.66 (dt, 4H, J= 8.76, 8.16, *Ar-H*), 8.00 (t, 4H, *J= 9.12*, *Ar-H*), 8.26 (d, 2H, *J= 8.4*, *Ar-H*), 8.55 (d, 2H, *J= 14.16*, *-CH=CH-*). ^{13}C NMR (100 MHz, CD_3OD) δ 24.13 (-$\underline{CH_2}$-cyclohexene), 27.43 (2x-$\underline{CH_2}$-cyclohexene), 27.86 (4x-$\underline{CH_3}$), 36.16 (-$\underline{CH_2}$-COOH), 43.07 (2x$\underline{C}$-$(CH_3)_2$), 52.42 (-N-$\underline{CH_2}$-), 102.39, 128.69, 144.58 (-CH=CH-), 112.37, 123.43, 126.11, 128.35, 129.41, 131.13, (Ar-C-H), 131.78, 132.91, 133.55, 135.22, 139.60, 140.98, 141.98, 150.30 ($\underline{Ar\text{-}C}$-C), 175.38 ($\underline{C\text{-}N}$-indole) and 177.40 (C=O).

The UV-Vis spectrum of **(35)** shows an absorption at 820 nm (12195 cm^{-1}) (ε = 173314 $M^{-1}cm^{-1}$) in methanol.

The FT-IR spectrum KBr ν/cm^{-1} shows absorption peaks at 3600-2700 cm^{-1} ν (O-H, br) carboxylic acid; 2927, 2862 cm^{-1} ν (C-H, m) aliphatic; 1732 cm^{-1} ν (C=O, str (shp)); 1624 cm^{-1} ν (C=O, m); 1547 cm^{-1} ν (C=C, str) aromatic; 1465 cm^{-1} ν (C=C, w) aliphatic; 1271 cm^{-1} ν (C-O, m).

2.5.8 Synthesis of 3-(2-((E)-2-((E)-2-chloro-3-((E)-2-(1-ethyl-3,3-dimethyl-1H-benzo[g]indol-2(3H)-ylidene)ethylidene)cyclohex-1-en-1-yl)vinyl)-1,1-dimethyl-1H-benzo[e]indol-3(2H)-yl)propanoic acid (37).

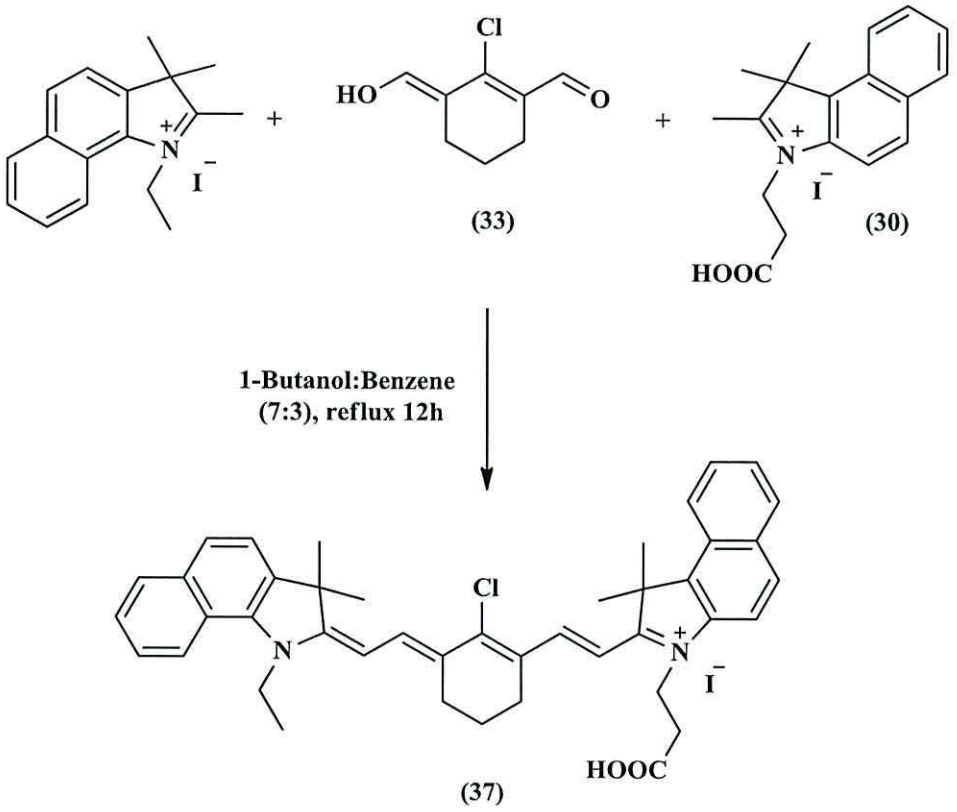

Scheme 2.39. Synthetic pathway of 3-(2-((E)-2-((E)-2-chloro-3-((E)-2-(1-ethyl-3,3-dimethyl-1H-benzo[g]indol-2(3H)-ylidene)ethylidene)cyclohex-1-en-1-yl)vinyl)-1,1-dimethyl-1H-benzo[e]indol-3(2H)-yl)propanoic acid (**37**).

Using a method developed from are reported previously, [15] (0.1 g, 0.58 mmol) of (E)-2-chloro-3-(hydroxymethylene)cyclohex-1-enecarbaldehyde (**33**) and (0.138 g, 0.58mmol) of 1-ethyl-2, 3, 3-trimethylindolenium iodide was synthesized by Dr Arthur Connell at Bangor University and used as supplied were dissolved in 45 ml of a mixture of 1-butanol:benzene, (7:3, v/v). The mixture was refluxed with stirring for 2 h. It was cooled to room temperature and (0.16 g, 0.58 mmol) of 1-carboxy-ethyl-2, 3, 3-trimethyl-1H-benzo [0]-indolium iodide (**30**) dissolved in 15 ml mixture of 1-butanol: benzene, (7:3, v/v was added to the reaction mixture and refluxed for 12 h. The water which formed during the reaction was removed as an azeotrope by using a Dean-Stark condenser. The resulting solution was cooled to room temperature, and the solvent removed under vacuum. The solid product was purified by column

chromatograph on silica gel using methylene chloride/methanol (3:1, v/v) as eluent. Finally, the solvent was removed to dry to give (**37**) as a green solid (0.1 g, 37%). $FTMS^{+}$-MS: m/z (Accurate Mass), reference compound: NH_4OAc, calcd. for $C_{43}H_{43}ClN_2O_2$ 655.3086, found 655.3081 $[M+H]^{+}$.

^{1}H NMR (400 MHz, CD_3OD) δ 1.26 (br m, 2H, -*CH_2*-cyclohexene), 1.48 (t, 3H, J= 7.16, -N-CH_2-*CH_3*), 2.03 (s, 12H, 4x-*CH_3*), 2.79 (br t, 6H, J= 7.16, -*CH_2*-COOH, 2x-*CH_2*-cyclohexene), 4.35 (quartate, 2H, -N-*CH_2*-CH_3), 4.59 (br m, 2H, -N-*$(CH_2)_2$*-COOH), 6.41 (dd, 2H, J= 14.08, 13.96, -*CH=CH*-), 7.5 (m, 2H, *Ar-H*), 7.66 (m, 4H, *Ar-H*), 8.09 (m, 4H, *Ar-H*), 8.27 (t, 2H, J= 7.92, *Ar-H*), 8.5 (m, 2H, =*CH-CH*=).

^{13}C NMR (100 MHz, CD_3OD) δ 12.76 (*CH_3*-CH_2-), 22.21 (*CH_2*-cyclohexene), 24.36 ((*CH_2*)$_2$-cyclohexene), 27.77 *(-CH_3)$_2$*, 27.89 *(-CH_3)$_2$*, 31.66 (-*CH_2*-COOH), 37.34 (-*C*-$(CH_3)_2$), 40.63 (-*C*-$(CH_3)_2$), 52.37 (-N-*CH_2*-), 53.64 (-N-*CH_2*-), 111.97, 112.23, 126.14, 140.90 (-*CH=CH*-), 123.50, 126.31, 128.74, 128.88, 129.83, 131.18 (*Ar-C*-H), 131.82, 131.98, 133.54, 149.15 (*Ar-C*-C), 172.62 (*C-N*-Indole), 175.30 (*C=O*).

The UV-Vis spectrum of (**37**) shows an absorption peak at 820 nm (12195 cm^{-1}) (ε = 121980 $M^{-1}cm^{-1}$) in methanol.

2.5.9 Synthesis of 3-(2-carboxyethyl)-2-(4-(diphenylamino) styryl)-1, 1-dimethyl-1H-benzo[e]indol-3-ium (38).

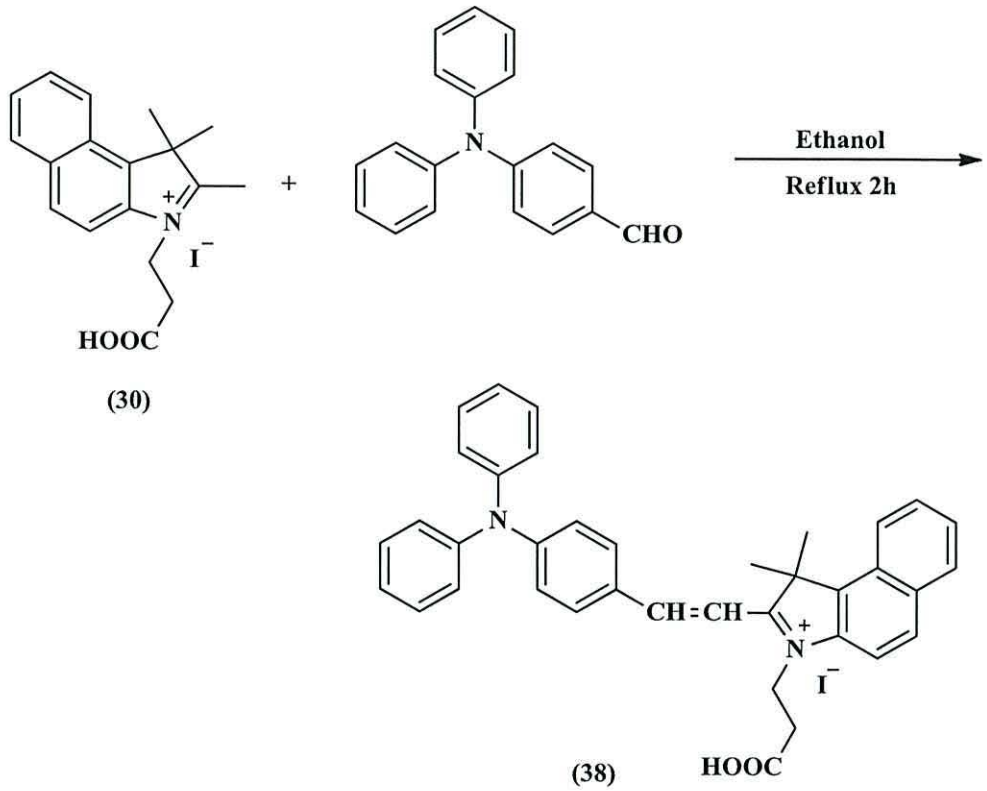

Scheme 2.40. Synthetic pathway of (3-(2-carboxyethyl)-2-(4-(diphenylamino) styryl)-1, 1-dimethyl-1H-benzo[e]indol-3-ium (**38**).

Using a method developed from Wang *et al.*[16], a mixture of 4-(N, N-diphenylamino)-benzaldehyde 0.2 g (0.73 mmol) and 1-carboxy-ethyl-2, 3, 3-trimethyl-1H-benzo [0]-indolium iodide (**30**) 0.23 g (0.8 mmol) was refluxed in 10 ml of ethanol for 2h. The solution was cooled to room temperature, and the red precipitate was filtered. This was purified by column chromatography on silica gel using methylene chloride/methanol (3:1, v/v) as an eluent to produce (**38**) as a purple precipitate (0.3 g, 77%), m.p. 210-212°C. FTMS$^+$-MS: m/z (Accurate Mass), reference compound: NH_4OAc, calcd. for $C_{37}H_{33}N_2O_2$ 537.2537, found 537.2530.

^{1}H NMR (400 MHz, CD_3OD) δ 1.94 (s, 6H, 2x-*CH$_3$*), 2.71 (t, 2H, J= 6.88, -*CH$_2$*-COOH), 4.5 (bs, 2H, -N-*CH$_2$*), 6.99 (d, 2H, J=8.88, *Ph*-N-Ph$_2$), 7.26 (dt, 6H, J= 7.56, 7.52, -N-*Ph$_2$*), 7.43 (t, 4H, J= 7.76, -N-*Ph$_2$*), 7.58-7.67 (m, 2H, -*CH=CH*-), 7.76 (t, 1H, J= 7.76, *Ar-H*), 7.93 (m 3H, *Ar-H*), 8.12 (d, 1H, J= 8.0, *Ar-H*), 8.18 (d, 1H, *Ar-H*), 8.35-8.43 (m, 2H, -*Ph*-N-Ph$_2$).

^{13}C NMR (100 MHz, CD_3OD) δ 26.90 (2x-*C*H_3, 35.72 (-*C*H_2-COOH), 44.59 (C-(*C*H_3)$_2$), 54.93 (N-*C*H_2-), 109.03, 113.50, 120.10, 123.97, 127.18, 127.92, 128.08, 128.75, 129.40, 131.08, 131.08, 131.28, 132.44 (Ar-*C-H*), (*CH=CH-*), 133.92, 134.97, 139.17 (Ar-*C-C*), 139.68, 146.94 (Ar-*C-N*), 154.61, 154.89, 175.32 (Indole *C-C*), 183.84 (*C=O*).

The UV-Vis spectrum of (**38**) shows an absorption peak at 548 nm (18248 cm^{-1}) (ε = 45506 $M^{-1}cm^{-1}$) in methanol.

The FT-IR spectrum KBr ν/cm^{-1} shows absorption peaks at 3600-2800 cm^{-1} ν (O-H, m) carboxylic acid; 3018 cm^{-1} ν (C-H, m) aromatic; 2927, 2861 cm^{-1} ν (C-H, m) aliphatic; 1733-1717 cm^{-1} ν (C=O, br); 1612 cm^{-1} ν (C=C, w) aromatic; 1571 cm^{-1} ν (C=C, shp) aliphatic; 1452 cm^{-1} δ_{as} CH_3; 1403 cm^{-1} δ_s CH_3; 1277 cm^{-1} ν (C-O, shp) and 1172 cm^{-1} ν (C-N, m).

2.6 Fabrication of dye-sensitized solar cells (DSC)

Conducting glass plates (TEC 15, 15Ω $\square^{-1}$) were used to deposit TiO_2 films on the surface of the conducting glass. The glass was masked with adhesive tape and a TiO_2 film was spread using glass road to form a film, film thickness could be controlled by the number of applications. Typically 1 cm^2 of the conducting glass plate was coated of TiO_2 paste, and the thin film allowed drying for a few minutes. After removal of the adhesive tape the applied paste substrate was calcined at 450°C for 30 minutes, and allowed to cool to room temperature. The film was then soaked in an aqueous solution 0.3 M of $TiCl_4$ for 30 minutes at 70°C. After that, it was washed with distilled water, and calcined again at 450°C for 30 minutes. [17] The TiO_2 electrode was then cooled to 100°C and soaked in dye solution for 24 hour in a closed chamber (passive dyed), or (fast dyed) by injecting the solution of dye and dying the TiO_2 electrode through 5 minutes after making the counter electrode and complete device. The TiO_2 electrode was washed with isopropanol and dried under nitrogen, a platinum counter electrode was also prepared by making hole in the conductive glass (TEC 8, 8Ω $\square^{-1}$) then coating the surface of the glass with 40 μL of H_2PtCl_6. After heating in the tube furnace at 400 °C for 30 min, the Pt electrode and the dye-coated TiO_2 electrode were sealed together by using hot melt gasket. The two electrodes were pressed and heating together at 120°C. Then the edge of the Pt counter electrode and the dye –coated TiO_2 electrode were coated with Ag paint. A small quantity of electrolyte was introduced into the porous structure of the dye-covered TiO_2 film by capillary action. The internal space was filled with a liquid electrolyte. The electrolyte-injecting hole on the counter electrode was made with a drill and was sealed with sheet and thin glass cover by heating as shown in Figure 2.1.

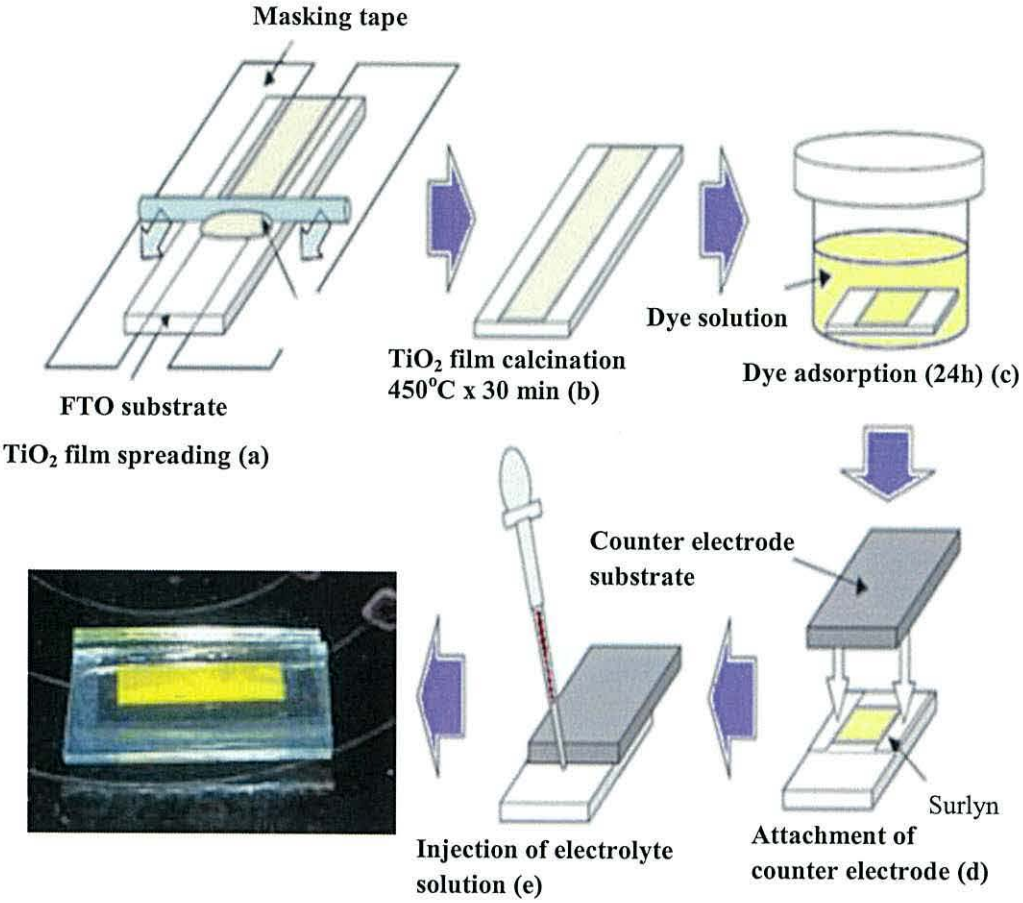

Figure 2.1. DSC fabrication steps, (a) printing of TiO_2 paste onto FTO conductive glass, (b) TiO_2 film calcination at 450°C, (c) TiO_2 film immersed in dye solution, (d) sealing of the TiO_2 electrode with the Pt counter electrode and (e) injection of electrolyte solution. [18]

2.7 References

1. S. Hwang, J. H. Lee, C. Park, H. Lee, C. Kim, C. Park, M. H. Lee, W. Lee, J. Park, K. Kim, N. G. Park, and C. Kim, *Chem. Commun.*, 2007, 4887–4889.
2. P. J. Holliman, M. Mohsen, A. Connell, M. L. Davies, K. Al-Salihi, M. B. Pitak, G. J. Tizzard, S. J. Coles, R. W. Harrington, W. Clegg, C. Serpa, O. H. Fontes, C. Charbonneau, and M. J. Carnie, *J. Mater. Chem.*, 2012, **22**, 13318–13327.
3. A. Osuka, B. L. Liu, and K. Maruyama, *J. Org. Chem.*, 1993, **58**, 3582–3585.
4. M. Okanuma, Y. Ishida, Y. Hase, N. Higashida, T. Enoki, *Aromatic carboxylic acids, acid halides thereof and processes for preparing both,* US Patent, 2005.
5. D. S. Terekhov, K. J. M. Nolan, C. R. McArthur, and C. C. Leznoff, *J. Org. Chem.*, 1996, **61**, 3034–3040.
6. D. L. Mattern, *J. Org. Chem.*, 1984, **49**, 3051–3053.
7. E. G. Sakellariou, A. G. Montalban, S. L. Beall, D. Henderson, H. G. Meunier, D. Phillips, K. Suhling, A. G. Barrett, and B. M. Hoffman, *Tetrahedron*, 2003, **59**, 9083–9090.
8. S. Mori, M. Nagata, Y. Nakahata, K. Yasuta, R. Goto, M. Kimura, and M. Taya, *J. Am. Chem. Soc.*, 2010, **132**, 4054–4055.
9. S. Eu, T. Katoh, T. Umeyama, Y. Matano, and H. Imahori, *Dalton Trans.*, 2008, 5476–5483.
10. Z. Zhang and S. Achilefu, *Org. Lett.*, 2004, **6**, 2067–2070.
11. M. V. Reddington, *Bioconjug. Chem.*, 2007, **18**, 2178–2190.
12. J. H. Yum, P. Walter, S. Huber, D. Rentsch, T. Geiger, F. Nüesch, F. De Angelis, M. Grätzel, and M. K. Nazeeruddin, *J. Am. Chem. Soc.*, 2007, **129**, 10320–10321.
13. K. Funabiki, H. Mase, A. Hibino, N. Tanaka, N. Mizuhata, Y. Sakuragi, A. Nakashima, T. Yoshida, Y. Kubota, and M. Matsui, *Energ. Environ. Sci.*, 2011, **4**, 2186.
14. G. A. Reynolds and K. H. Drexhage, *J. Org. Chem.*, 1977, **42**, 885–888.
15. N. Narayanan and G. Patonay, *J. Org. Chem.*, 1995, **60**, 2391–2395.
16. J. Wang, W. F. Cao, J. H. Su, H. Tian, Y. H. Huang, and Z. R. Sun, *Dyes and Pigments*, 2003, **57**, 171–179.
17. S. W. Park, K. I. Son, M. J. Ko, K. Kim, and N. G. Park, *Synth. Met.*, 2009, **159**, 2571–2577.
18. T. Nagata and H. Murakami, *ULVAC Tech. J*, 2009, **N70E**, 1-5.

Chapter 3

Triphenylamine Dyes

3.1 Triphenylamine dyes

This chapter describes the synthesis of three new metal-free organic dyes, designed using a donor-spacer-acceptor (donor-π-acceptor) model (Figure 3.1) which comprises a triphenylamine moiety (TPA) as the electron donor group, a phenylenevinyl group as the spacer or bridging moiety (π system) and either cyanoacrylic acid or a carboxylic acid moieties as the electron acceptor or anchoring group to chemisorb the dye to the TiO_2. This chapter consists of two parts; the first part was to synthesize single-linker triphenylamine dyes which contain a single carboxylic or cyanoacrylic acid as the acceptor group. Two dyes were made and tested in this piece of work; single-linker red dye (**3a, 3b**) and single-linker yellow dye (**5**). The second part was to synthesize and test new di-linker triphenylamine dyes which either include two cyanoacrylic acids as acceptor groups to produce a di-linker red dye (**12**) or two carboxylic acids to produce di-linker yellow dye (**14**).

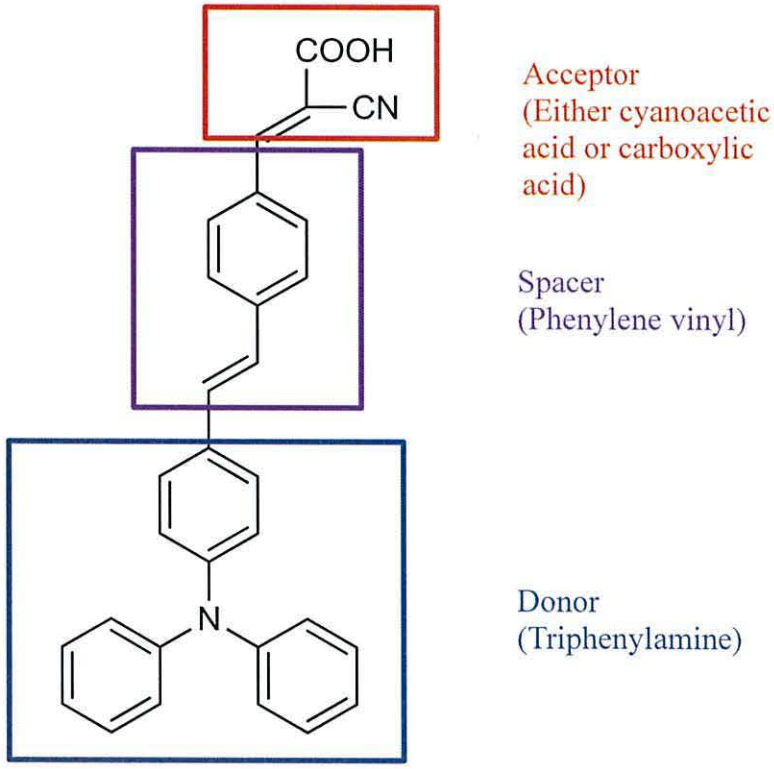

Figure 3.1. Schematic of a (D-π-A) system of the type applied to the triphenylamine dyes studied as dye-sensitizers in this chapter.

3.2 Synthesis of triphenylamine dyes-based one anchoring group

3.2.1 2-Cyano-3-{4-[2-(4-diphenylamino-phenyl) vinyl]-phenyl}-acrylic acid (3a and 3b).

Scheme 3.1 shows the synthesis of 2-cyano-3-{4-[2-(4-diphenylamino-phenyl) vinyl]-phenyl}-acrylic acid compound (**3a**) which was attempted using the conditions reported by Hwang and co-workers in the literature. [1] By comparison (**3b**) was synthesized by using modified conditions developed from the literature [1] particularly using piperidine as a base in the reaction. Compounds (**3a, 3b**) were synthesized by four steps as shown in Scheme 3.1.

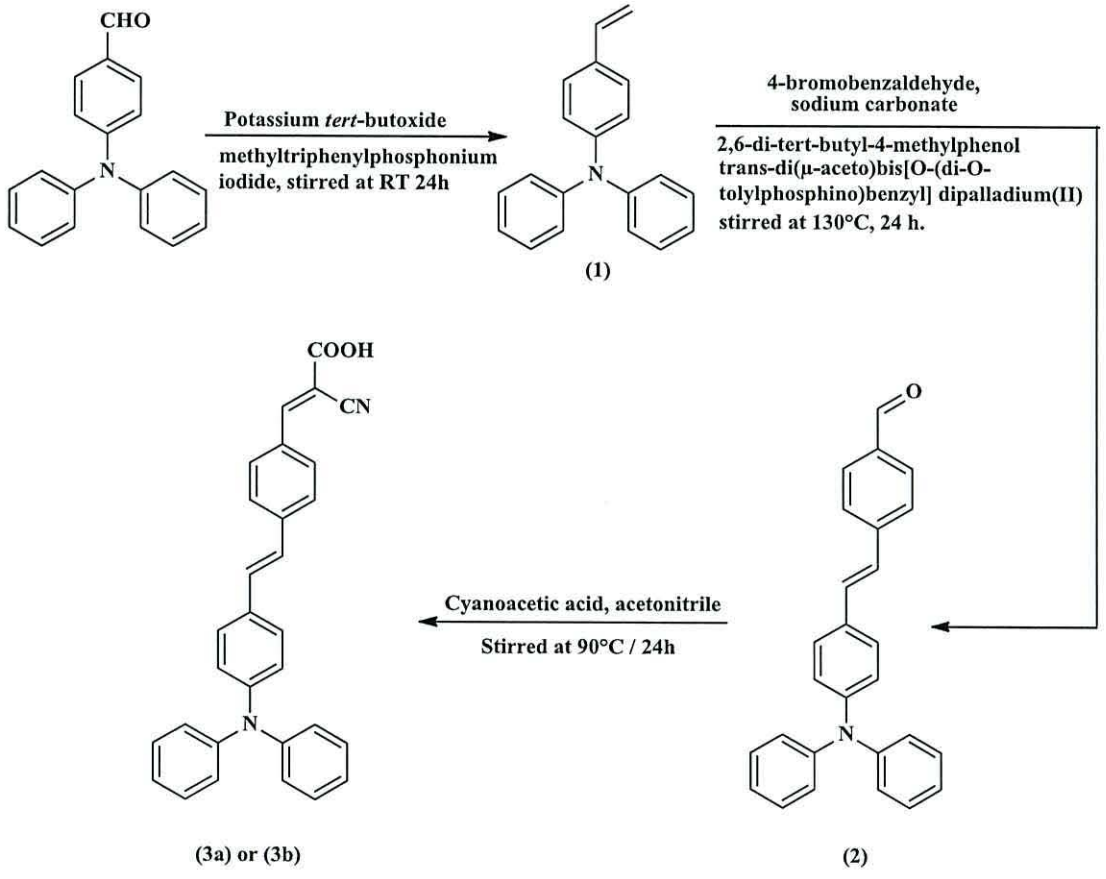

Scheme 3.1. Pathway for the synthesis of the single cyanoacrylic acid linker red dye (**3**).[1]

Hwang and co-workers did not report using piperidine to synthesize (**3**), they used cyanoacetic acid and acetonitrile in a condensation reaction to convert (**2**) to (**3**) at 90°C. However, using piperidine as a base improved the yield in this work to (0.35 g, 60% yield) compared to (0.2 g, 34% yield) without using piperidine but by following Hwang's method. [1] In this work diphenyl-(4-vinyl-phenyl)-amine compound (**1**) was

the synthesized by a Wittig reaction (Scheme 3.2) of 4-(N, N-diphenylamino)-benzaldehyde with potassium *tert*-butoxide and methyl triphenyl phosphonium iodide in dry THF to produced compound (**1**) [1] which was confirmed by UV-Vis spectroscopy which showed a an absorption peak at 308 nm (32467 cm^{-1}) in ethanol which is due to a (π-π^*) transition. [2] The FT-1R spectrum of (**1**) shows bands at 3084, 3060 and 3032 cm^{-1} due to ν (C-H) stretching modes of the aromatic rings, 2999 and 2853 cm^{-1} which are assigned to υ (C-H) aliphatic stretching , a sharp peak at 1590 cm^{-1} which is due to υ (C=C) benzene ring stretching while the band at 1486 cm^{-1} is assigned to (C=C) stretching and the band at 1175cm^{-1} is due to (C-N) stretching of the triphenylamine moiety.

Inspection of the ^{1}H NMR spectrum, as shown in Figure 3.2, shows the presence signals at δ 5.15 (Hb) and δ 5.69 (Hc) ppm as a doublet due to (H-*CH*=CH-) and (*H*-CH=CH-) respectively, and signal at 6.62-6.70 (Ha) ppm as a double doublet due to (*-CH*=CH_2). The ^{13}C NMR data also confirms the ^{1}H NMR data and shows 10 signals for 10 environments. Signals at δ112.60 and 135.99 ppm are due to (Ph-CH=*CH_2*) and (Ph-*CH*=CH_2) respectively, the signals at 122.99, 123.16, 124.00, 127.24 and 129.53 ppm are due to aromatic rings and the peak at 131.47 ppm is due to (-*Ph*-CH=CH_2). Finally, the peaks at 146.91 and 146.96 ppm are due to (-*Ph*-N-) and (-*Ph_2*-N-) respectively. [1]

Mass spectrometry shows the most prominent peak occurs at 272.1434, which corresponds to diphenyl-(4-vinyl-phenyl)-amine (**1**), $[M+H]^+$.

Scheme 3.2 shows the mechanism of Wittig reaction which is useful for C-C bond formation. Triphenylphosphine is the nucleophile which attacks the carbon of the aldehyde to form phosphonium ion, which attack the carbon of carbonyl again as a nucleopile to form an alkoxide. The alkoxide attacks the phosphorus in an intramolecular closure reaction to form four-membered ring. Then the ring fragments to form triphenylphosphine oxide and the desired alkene. [3]

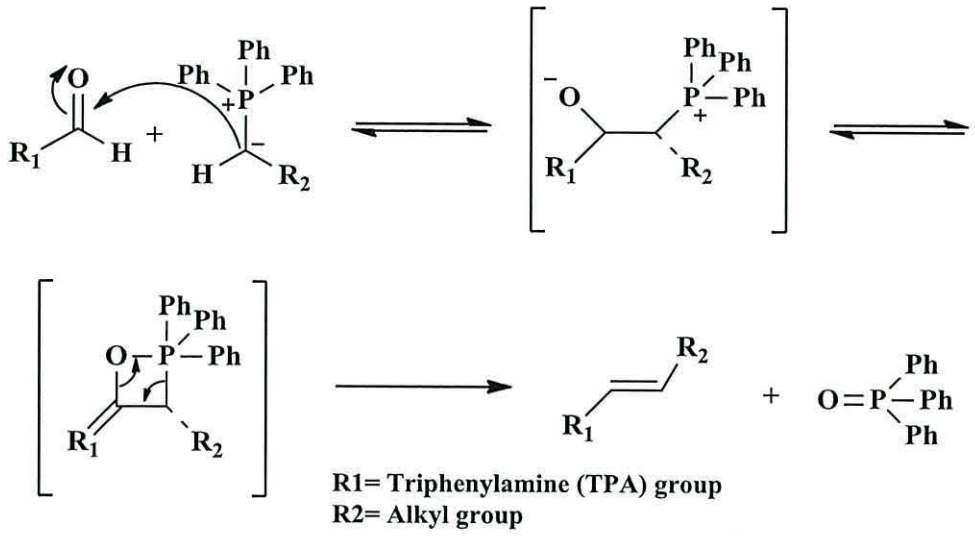

Scheme 3.2. Mechanism of the Wittig reaction. [3]

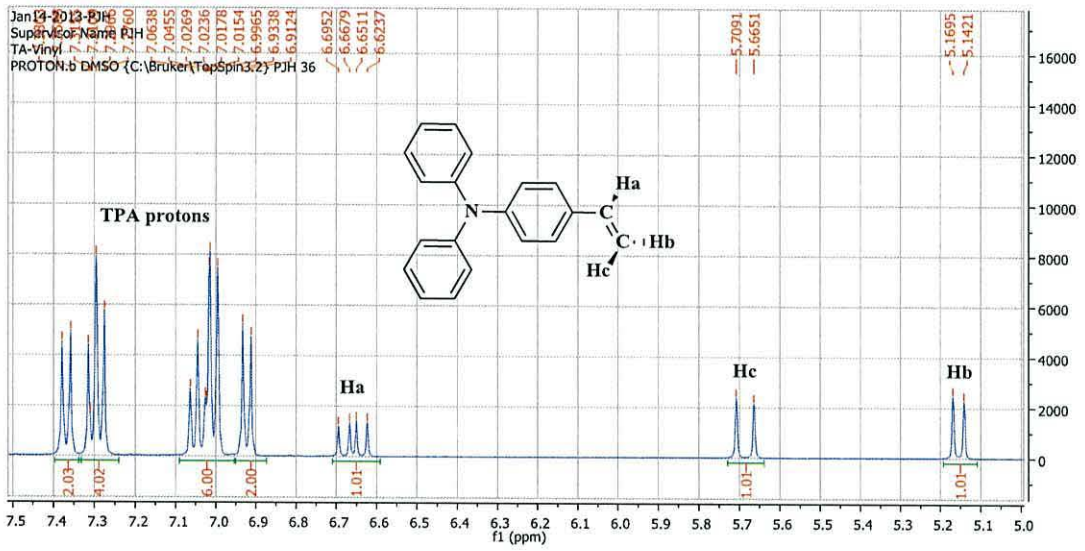

Figure 3.2. ^{1}H NMR spectrum of diphenyl-(4-vinyl-phenyl)-amine (**1**) between 5.0 and 7.5 ppm.

Suitable crystals for x-ray structure determination were obtained by the evaporation method, in which methylene chloride was used as the solvent. These crystals were then sent to the National Crystallography Centre (NCS) at Southampton University. The molecular structure of compound (**1**) is shown in Figure 3.3. The compound crystallised as two molecules in the asymmetric unit. Figure 3.4 shows the packing arrangement of the molecules in the unit cell. Details of the determination and selected bond lengths (Å) and angles (°) are listed in Table 3.1. The data show the

triphenylamine group introduced as an electron donor. The three phenyl rings (C1-C6), (C9-C14) and (C15-C20) are confirmed as being like blades of a propeller and the dihedral angle between the benzene ring are close to 120°. The bond angles values of (C1-N1-C9), (C1-N1-C15) and (C9-N1-C15) for the first molecule and (C21-N2-C35), (C21-N2-C29) and (C29-N2-C35) for the second molecule are close to 120°. The data also shows there are no significant differences between the bond lengths for the first molecule (NI-C1), (N1-C15), (N1-C9) and the second molecule (N2-C21), (N2-C35) and (N2-C29). The bond length values of (C-N) bonds mentioned above are in good agreement with values reported previously for the triphenylamine moiety. [4]

Table 3.1. Selected bond lengths [Å] and angles [°] for compound (**1**).

NI-C1	1.411(3) Å	C1-N1-C9	122.67(8) °
N1-C9	1.424(3) Å	C1-N1-C15	119.47(17) °
N1-C15	1.428(3) Å	C9-N1-C15	117.55(17) °
N2-C21	1.412(3) Å	C21-N2-C35	121.19(18) °
N2-C35	1.424(3) Å	C21-N2-C29	121.21(17) °
N2-C29	1.430(3) Å	C29-N2-C35	117.24(18) °

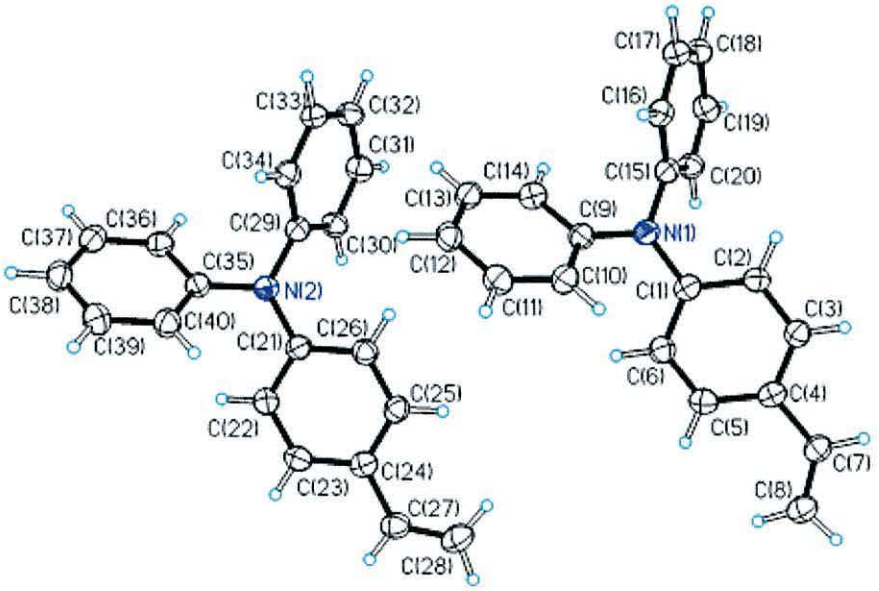

Figure 3.3. The two independent molecules of (**1**) in the asymmetric unit.

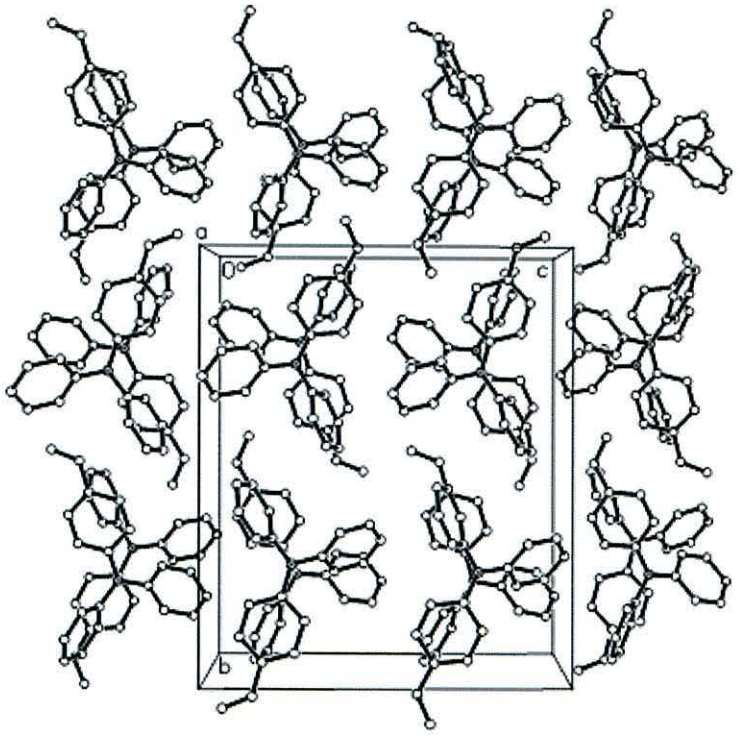

Figure 3.4. A packing diagram of compound (**1**), viewed along the (*a*) axis. H atoms have been omitted for clarity.

Then compound (**1**) was then coupled with 4-bromobenzaldehyde. This reaction carried out using a Heck coupling reaction [1] using sodium carbonate, 2,6 di-*tert*-butylcresol and *trans*-di(μ-acetato)bis[0-(di-0-tolylphosphoino)benzyl] dipalladium (*II*) as a catalyst to give compound (**2**). The mechanism of reaction is shown in Scheme 3.3. The successful formation of (**2**) is confirmed by the UV-Vis spectrum in ethanol Figure (3.5) which shows absorption peak at 300 nm (I) corresponds to a (π-π*) transition [2] and an absorption at 400 nm (II) which is due to (π-π*) intra-molecular charge transfer. [5]

The successful synthesis was achieved using Heck-coupling reaction to form C-C bond using palladium as a catalyst. The reaction carried out by reacting an aryl halide (4-bromobenzaldehyde) with an olefin (diphenyl-(4-vinyl-phenyl)-amine (**1**)) and the mechanism of reaction is shown in Scheme 3.3. The mechanism composes transmetallation and migratory insertion steps. The first step is the oxidative addition of the aryl halide to the Pd (II) complex. In the next step the alkene coordinates and inserts into the aryl-Pd bond. The elimination of the alekene occurs *via* a β-hydride and the next step is regeneration of Pd by deprotonation.

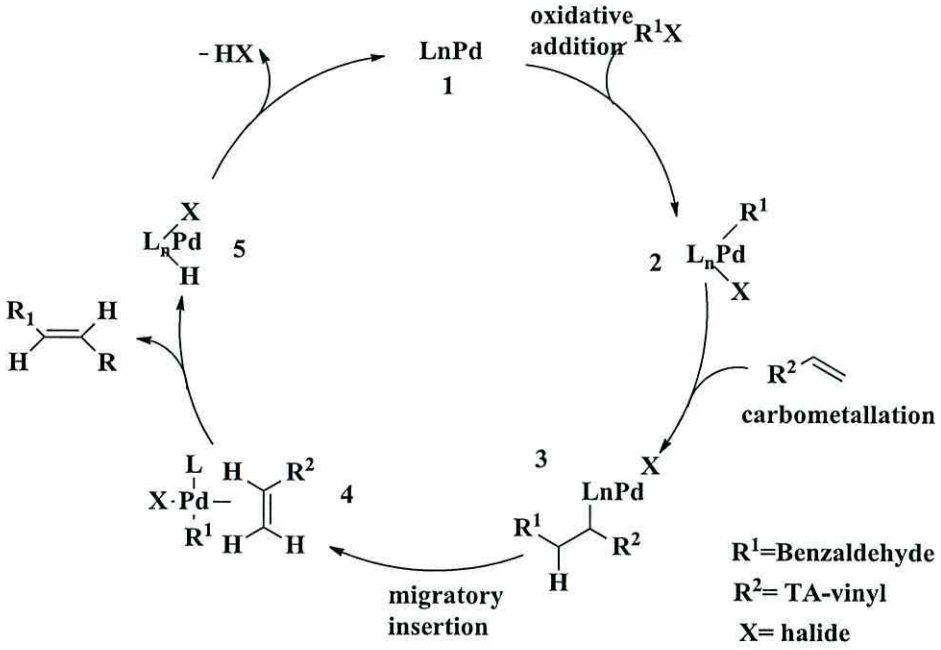

Scheme 3.3. Mechanism of the Heck-coupling reaction. [6]

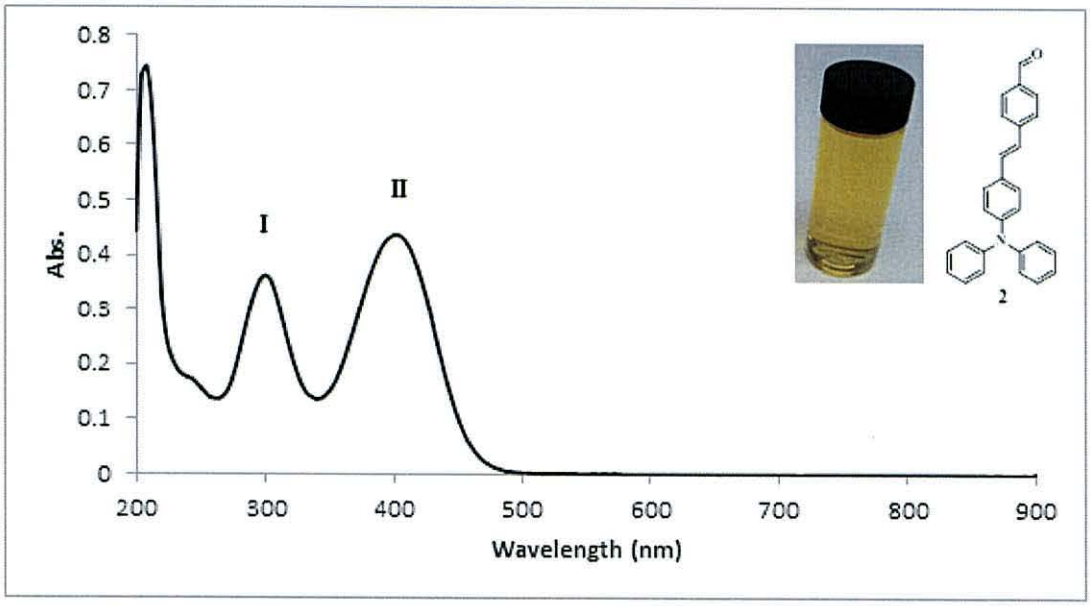

Figure 3.5. UV-Vis spectrum of 4-[2-(4-diphenylamino-pheny vinyl]-benzaldehyde (**2**) in ethanol ($1x10^{-4}$ M) and vial containing a 0.1 mmol solution of (**2**) in ethanol and the molecular structure of (**2**).

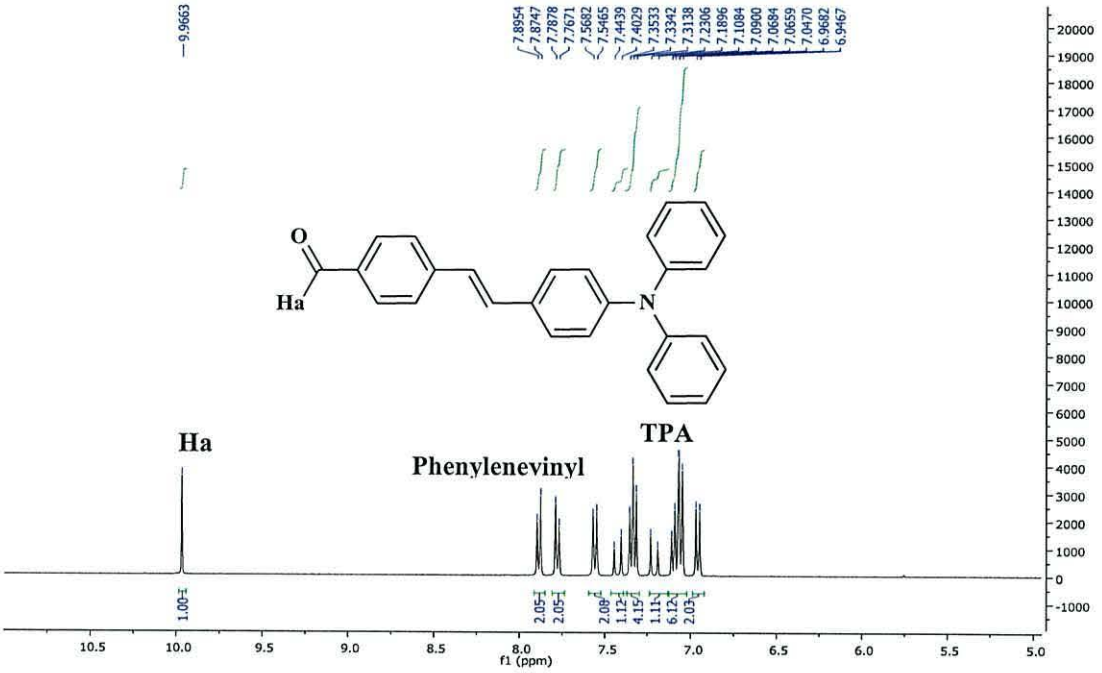

Figure 3.6. ^{1}H NMR spectrum of (**2**), between 5.0 and 11.0 ppm.

For the FT-IR spectrum the most important peaks occur at 3060 and 3029 cm^{-1} due to ν (C-H) aromatic stretching and at 2929 cm^{-1} ν (C-H) for aldehyde stretching. A sharp and strong peak at 1695 cm^{-1} is obtained for the (C=O) stretching of the carbonyl aldehyde, a strong and sharp peak at 1580 cm^{-1} for ν (C=C) benzene ring stretching, 1283 cm^{-1} due to (C-O), and 1166 cm^{-1} for the (C-N) of the triphenylamine moiety. [7] As expected for (**2**), the ^{1}H NMR data (500 MHz, DMSO-d_6) shows the disappearance of peaks in the area of δ 5.0-6.7 ppm which are due to (*CH_2*=CH-) and (CH_2=*CH*-) which appeared in compound (**1**). This confirmed the addition of the benzene aldehyde group. A triplet peak at δ 7.32 (4H, *J*=7.87Hz) is due to (Ph-N-*Ph_2*). This peak should appear as a double doublet (dd) but it appears as a triplet due to overlapping peaks because they have same (*J*) value. Signals at 7.19 and 7.41 ppm due to (*CH=CH*). A singlet peak at δ 9.97 ppm is due to the aldehyde proton on the benzene ring, Figure 3.6. The ^{13}C NMR data showed 15 signals due to 15 environments. The important characteristic peaks at δ 125.9 and 132.1 ppm are due to the double bond of (Ph-*CH=CH*-Ph) and at δ 192.28 ppm due to the carbonyl (Ph-*CHO*) of the benzene aldehyde group. [1] The data from mass spectrometry also confirm compound (**2**) with the most prominent peak at 376.16, which corresponds to (**2**) $[M+H]^{+}$.

Single crystals were again obtained by evaporation method, using dichloromethane as the solvent. The molecular structure of (**2**) is shown in Figure 3.7. The details of the determination and selected bond lengths (Å) and angles (°) are listed in Table 3.2. The data show the angles of (C1-N1-C7), (C13-N1-C1) and (C13-N1-C7) are close to 120°. [8] There are no significant differences between the bond lengths of (N1-C13), (N1-C1) and (N1-C7) which are in good agreement with (C-N) bond lengths reported for the triphenylamine moiety. [4] All the carbon-carbon bond lengths are between single bond (C-C) and double bond (C=C). [9]

Table 3.2. Selected bond lengths [Å] and angles [°] for (**2**).

N1-C13	1.412(6) Å	C13-N1-C1	122.0(4) °
N1-C1	1.413(6) Å	C13-N1-C7	116.9(4) °
N1-C7	1.425(6) Å	C1-N1-C7	120.7(4) °
C16-C19	1.472(6) Å	C101-N101-C107	122.8(4) °
C19-C20	1.331(6) Å	C101-N101-C113	119,4(4) °
O1-C27	1.205(7) Å	C107-N101-C113	117.7(4) °
O101-C127	1.99(5) Å	N101-C113	1.418(6) Å
N101-C101	1.418(6) Å	N101-C107	1.426(6) Å

Torsion angles confirm that the phenyl bridge is coplanar with the first phenyl unit of the triphenylamine moiety, as represented by (C19-C20-C21-C22) and (C16-C19-C20-C21) dihedral angle, Figure 3.7. While the phenylvinyl group which is linked by a single bond with nitrogen shows co-planarity with the other diphenylamine unit which is represented by the (N1-C13-C14-C15) dihedral angle. Figure 3.7 also shows the phenyl groups of the diphenylamine moiety twisted in a propeller-like confirmation as represented by the (C6-C1-N1-C7) and (C8-C7-N1-C1) dihedral angles.

Table 3.3. Selected torsion angles (°) of compound (**2**).

C27-C24-C25-C26	179.7 (4)	C27-C24-C25-C26	179.7 (4)
C19-C20-C21-C22	177.6 (4)	C6-C1-N1-C7	-29.9 (6)
C16-C19-C20-C21	178.7 (4)	C8-C7-N1-C1	-48.2 (6)
N1-C13-C14-C15	178.2 (4)	C19-C20-C21-C26	-2.0 (7)

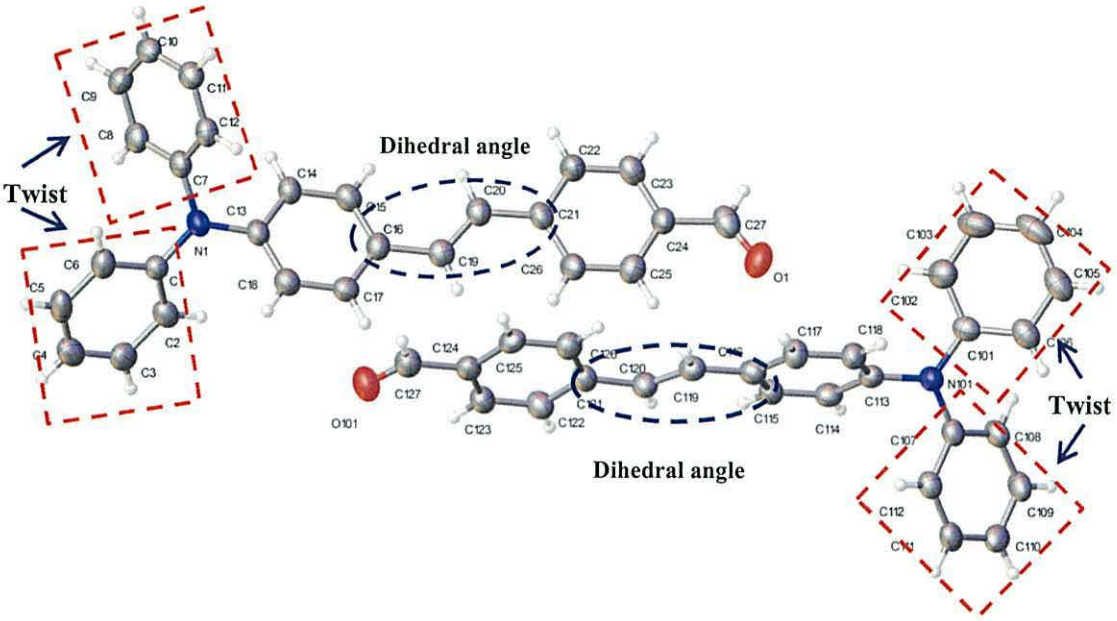

Figure 3.7. Single-crystal structure of 4-[2-(4-diphenylamino-phenyl)-vinyl]-benzaldehyde (**2**), the square red dashed show the twist and the blue dashed circle.

Following this, the target dye (**3**) was synthesized by a Knoevenagel condensation reaction of (**2**) using one of two methods. The first one was using (**2**) with cyanoacetic acid and acetonitrile as the solvent to produce (**3a**). The second one, used (**2**) with cyanoacetic acid and piperidine as a base in the presence of acetonitrile as the solvent to produce compound (**3b**). Both methods produced same compound but the second method gave a greater yield compared to the first one.

Formation of the target dye (**3**) was confirmed by UV-Vis spectroscopy (Figure 3.8) and (Figure 3.9) which shows an absorption band at 300 nm (ε = 25013 $M^{-1}cm^{-1}$) (I) which is due to a (π-π^*) electron transition. The absorption peak at 368 nm (ε = 33376 $M^{-1}cm^{-1}$) (II) and the shoulder at 440 nm (III) can be assigned to intra-molecular charge transitions between the triphenylamine-based donor and the cyanoacetic acid acceptor moiety, [2, 3] The FT-IR spectrum shows a broad peak around 2700-3700 cm^{-1} due to an ν (O-H) stretch for the CO_2H of the cyanoacrylic acid linker, a peak at 1732 cm^{-1} assigned to the carbonyl carboxylic acid, and a peak at 2251 cm^{-1} assigned to a (C≡N) stretch.[7] The ^{1}H NMR data of (**3**) show the absence of aldehyde signal at 9.97 ppm which appeared in (**2**). The data also show a multiplet at 7.06 ppm with six protons. This should be appearing as a doublet and triplet but it appears a multiplet due to overlapping peaks. The ^{13}C NMR results confirm the ^{1}HNMR results and show 18 signals due to 18 carbon environments. There is a new

signal at 118 ppm due to (C≡N), and the carbonyl signal for the aldehyde in (**2**) was shifted from 192.25 ppm to 165 ppm for the carbonyl of the cyanoacetic acid group in (**3**). The data from mass spectrometry of (**3**) also shows the most prominent peak at m/z 443.17, which corresponds to (**3**), $[M+H]^+$.

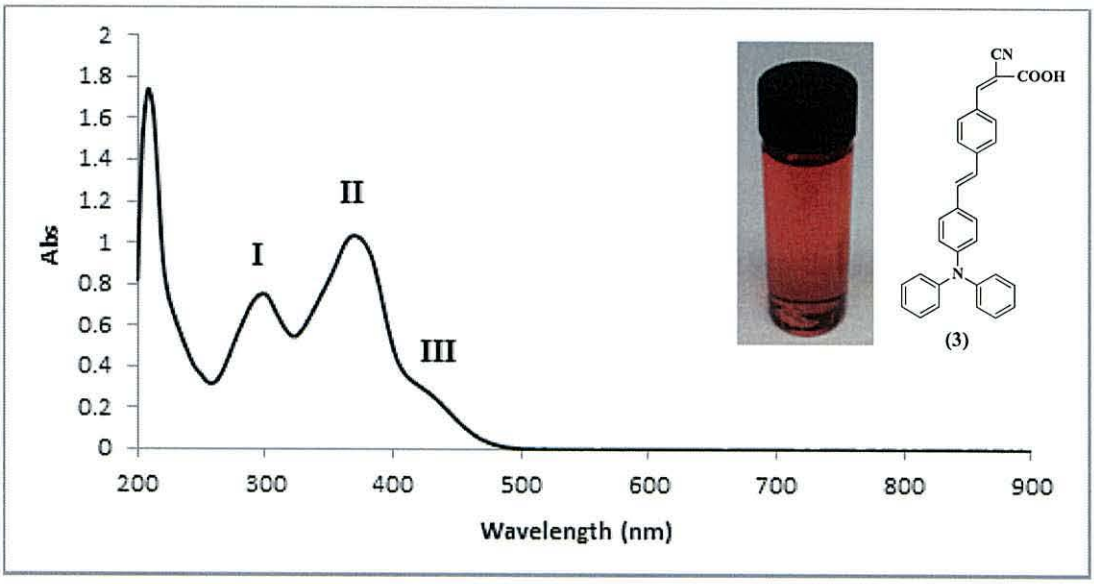

Figure 3.8. The UV-Vis spectroscopy of 2-cyano-3-{4-[2-(4-diphenylamino-phenyl) vinyl]-phenyl}-acrylic acid (**3**) in ethanol $3x10^{-5}$ M, $\varepsilon = 33376\ M^{-1}cm^{-1}$ at 368 nm. Vial containing a 0.1mM solution of (**3**) in ethanol and the molecular structure of (**3**).

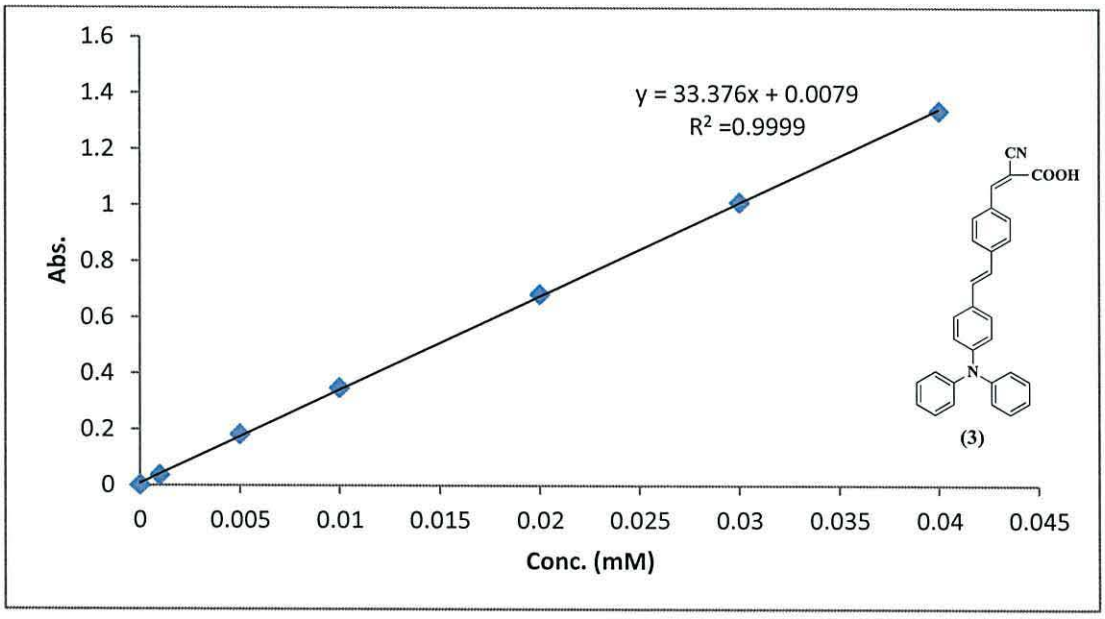

Figure 3.9. Calibration curve show plot absorbance *versus* concentration (mol L^{-1}) for 2-cyano-3-{4-[2-(4-diphenylamino-phenyl) vinyl]-phenyl}-acrylic acid (**3**) at 368 nm in ethanol.

3.2.2 Fabrication of devices

Dye-sensitized solar cells were fabricated using compound (**3**) as a sensitizer, with an effective area (1 cm^2). The metal oxide semiconductor electrode was prepared using either of the commercial TiO_2 anatase pastes DSL18 NRT (Dyesol), Ti-nano oxide HT (Solaronix)) or an in-house prepared P25 TiO_2 paste on TEC 8 conducting glass (FTO, $8\Omega\square^{-1}$). All films were sintered at 450°C for 30 minutes. The influence of post treatment with $TiCl_4$ solution was also investigated. Table 3.4 shows higher J_{sc} and η for Device A prepared using TiO_2 DSL 18NRT paste compare with Devices B and C which used TiO_2 H-T Solaronix and TiO_2 P25, respectively.

Table 3.4. Photovoltaic Performance Parameters of compound (**3**) or **N719** using two layers of different types of TiO_2 paste either with or without $TiCl_4$ treatment.

No	Dye	TiO_2	$TiCl_4$	V_{oc} (V)	J_{sc} (mA cm^{-2})	η (%)	FF
A	(3)	DSL 18NRT	-	0.65	7.11	2.8	0.60
		DSL 18NRT	+	0.66	8.94	3.5	0.59
B		HT-Solaronix	-	0.61	6.61	2.4	0.58
		HT-Solaronix	+	0.63	8.35	3.2	0.59
C		P25	-	0.61	7.41	2.7	0.59
		P25	+	0.65	8.02	3.2	0.61
D	**N719**	DSL 18NRT	-	0.71	11.44	4.5	0.55
		DSL 18NRT	+	0.77	13.10	5.6	0.56

Table 3.4 shows $TiCl_4$ improved the solar cells performance. The main result of using $TiCl_4$ was to improve the photocurrent density. Some studies have suggested post treatment with $TiCl_4$ can lead to an increase in the surface area of TiO_2 layer and this can increase the amount of dye adsorbed. This increase in dye adsorption may be assigned to the availibilty of more binding sites on TiO_2 surface, leading to increased photocurrent. Also treating with $TiCl_4$ due to a shift of the conduction band of TiO_2 and leading to longer electron lifetimes. [10, 11] Device make with **N719** (Device D), show the J_{sc} improved after post treatment with $TiCl_4$ from (11.44 to 13.10 $mAcm^{-2}$). Figure 3.10 shows the photocurrent-voltage I-V curves of the cells.

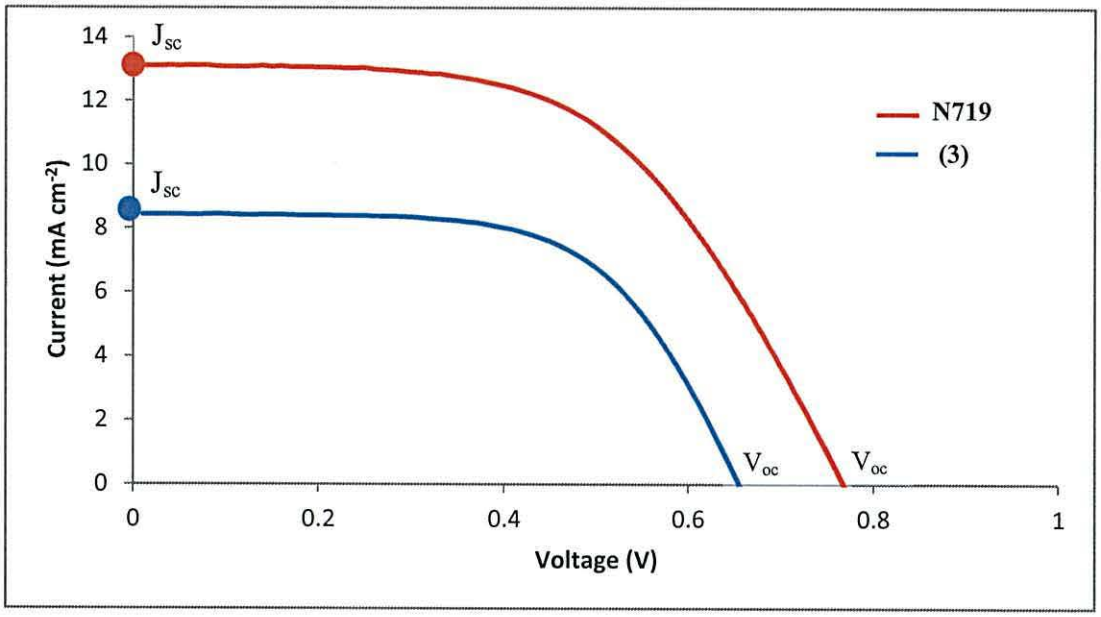

Figure 3.10. IV data for (**3**) and **N719** at (100 mW cm^{-2}).

The **N719** data are included here as a reference to compare with the new dyes. Here, **N719** shows photocurrent and open-circuit voltage (J_{sc}= 13.10 mA cm^{-2} and V_{oc}= 0.77 V) leading to a conversion efficiency of 5.6% which is higher than (**3**), which shows (J_{sc}= 8.42 mA cm^{-2} and V_{oc} = 0.65 V) with conversion efficiency of 3.4%. Both dyes show the same value of (FF) approximately. The significant differences in results between these dyes are believed to be due to **N719** having wider spectral response than (**3**) leading to it capturing and converting more photons into electricity. Table 3.5 shows the photovoltaic performance of (**3**) using different TiO_2 paste when first made and then after leaving for 21 days. The data shows the J_{sc} and η for Device A, B and D decreased slightly for all devices. By comparison, Device C showed a significant decline in J_{sc} and η value 8.02 to 4.29 mA cm^{-2} and 3.20 to 1.7% respectively. This suggests that (**3**) shows more stability with the DSL18-NR-T paste from Dyesol and HT-Solaronix pastes than with P25.

Table 3.5. Photovoltaic Performance Parameters of compound (**3**) and **N719,** the blue reading represent devices re-measured after 21 days blue).

No.	Dye	TiO_2	V_{oc} (V)	J_{sc} (mA cm^{-2})	η (%)	FF
A	(3)	DSL 18NRT	0.65	8.43	3.4	0.63
A	(3)	DSL 18NRT	0.67	7.92	3.3	0.62
B	(3)	HT-Solaronix	0.63	8.79	3.0	0.54
B	(3)	HT-Solaronix	0.68	6.78	2.7	0.58
C	(3)	P25	0.65	8.02	3.2	0.61
C	(3)	P25	0.66	4.29	1.7	0.59
D	N719	DSL 18NRT	0.77	13.10	5.6	0.55
D	N719	DSL 18NRT	0.78	11.70	4.7	0.51

3.2.3 Synthesis of 4-[2-(4-Diphenylamino-phenyl)-vinyl]-benzoic acid (5).

Compound (**5**) was synthesized in two steps (Scheme 3.4). The first step was to synthesize (**4**) by coupling ethyl-4-bromobenzoate to diphenyl (4-vinyl) amine (**1**) using a Heck coupling reaction with Na_2CO_3, 2, 6-di-*tert*-butyl-4-methylphenol and palladium (*II*) as a catalyst in dimethylacetamide (DMAC) as a solvent to produce compound (**4**). The second step was to synthesize (**5**) by de-esterifying compound (**4**) using THF, CH_3OH with some drops of water and 30 eq. of LiOH before acidification with 5% HCl to adjust the pH to 5-6 to produce compound (**5**) as a yellow solid (0.27 g, 87% yield). The UV-Vis spectrum of (**4**) in ethanol shows an absorption at 300 nm (I) which is believed to be due to a (π-π*) transition of the conjugated molecule. The absorption peak at 388nm (II) is assigned to intra-molecular charge transfer between the triphenyl amine moiety and the ester group. [5]

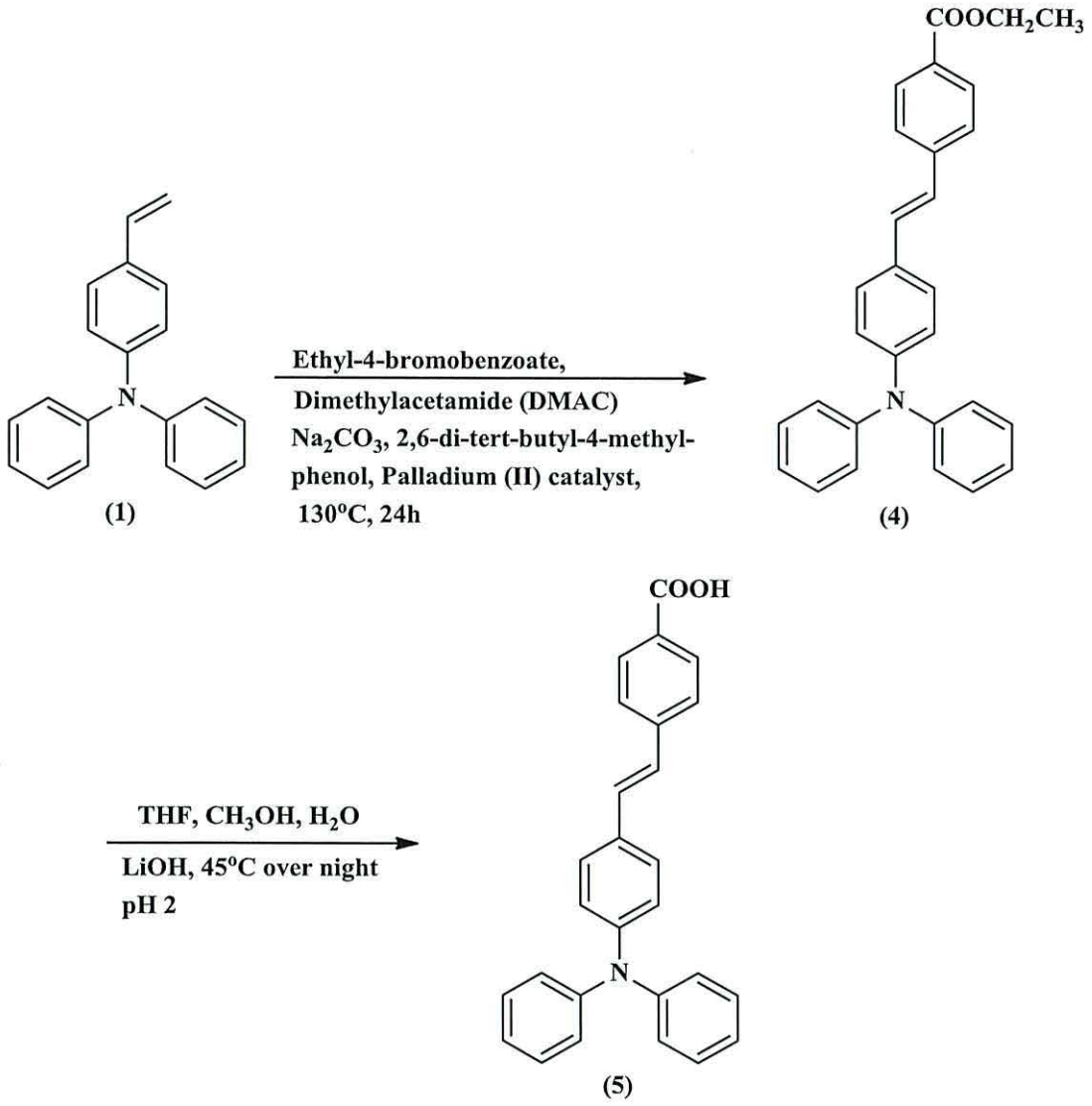

Scheme 3.4. Synthetic pathway of 4-[2-(4-diphenylamino-phenyl)-vinyl]-benzoic acid (**5**).

The FT-IR spectrum shows a medium peak at 3023 and 2984 cm^{-1} due to ν (C-H) benzene ring and aliphatic stretches, respectively. A sharp and intense peak at 1707 cm^{-1} is due to the (C=O) carbonyl group of the ester and peaks at 1589 and 1493 cm^{-1} are due to ν (C=C) benzene ring and ν (C=C) stretches, respectively. Sharp peaks at 1278 and 1178 cm^{-1} are due to ν (C-O) and ν (C-N) stretches. The mass spectrum of (**4**) confirms was present with the most prominent peak at 420.1956 m/z, which corresponds to 4-[2-(4-diphenylamino-phenyl)-vinyl]-benzoate ethyl ester (**4**), $[M+H]^+$.

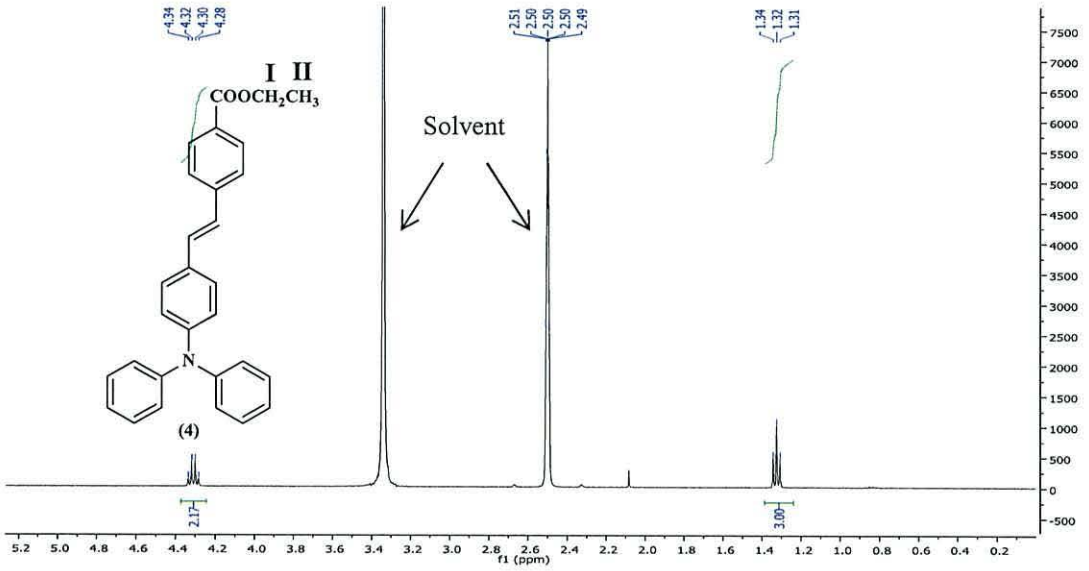

Figure 3.11. The ^{1}H NMR of 4-[2-(4-diphenylamino-phenyl)-vinyl]-benzoate ethyl ester (**4**).

The ^{1}H NMR Figure 3.11 shows alkyl ester signal for the ethyl group as a triplet at δ 1.32 ppm and a quartet at δ 4.31 ppm due to the $-CH_3$ and $-CH_2$ group, respectively. Signals at 7.38-7.31 ppm appear as a multiplet with five protons (-Ph-N-Ph_2 and Ph-CH=*CH*-Ph). This should appear as a double doublet, but the overlapping peaks causes the multiplet peak. ^{13}C NMR shows 17 signals due to 17 environments. Considering the symmetry of the molecule, the number of carbon environments equals the number of carbon signals, and confirms the ^{1}H NMR data with signals at 14.21 and 60.62 ppm due to the ethyl ester group along with a signal at 165.52 ppm for the carbon of the ester carbonyl. Elemental analysis also confirms the desired compound as mentioned in the experimental section.

Single crystals for x-ray structure determination were obtained by the evaporation method, using methylene chloride/diethyl ether as the solvent. The molecular structure of (**4**) is shown in Figure 3.12. The compound crystallised as a two molecules in the asymmetric unit cell. The hydrogen atoms are omitted of clarity. The details of the determination and selected bond lengths (Å) and angles (°) are listed in Table 3.6. The data show the angles of (**4**) (C1-N1-C7), (C7-N1-C13) and (C1-N1-C13) close to 120°. [8] The bond lengths of (C1-N1), (C7-N1) and (C13-N1) are in a good agreement with (C-N) values reported for the triphenylamine moiety. [4]

Whilst the bond length of (C19-C20) are shorter than (C16-C19) and (C24-C27) because these are double bond. [12]

Table 3.6. Selected bond lengths [Å] and angles [°] for ESTA compound (**4**).

N1-C1	1.443(4) Å	C27 -O1	1.209(4)
N1-C7	1.413(4) Å	C27-O2	1.336(4)
N1-C13	1.417(4) Å	C1-N1-C7	120.2(3)
C16-C19	1.464(5) Å	C1-N1-C13	116.1(3)
C19-C20	1.343(5) Å	C7-N1-C13	121.5(3)
C20-C21	1.458(5) Å	C16-C19-C20	127.4(3)
C24-C27	1.485(5) Å	C19-C20-C21	125.7(3)
C28-C29	1.495(5) Å	C21-C22-C23-C24	-0.1(6)

The torsion angles show the co-planarity of the molecule. The ester group is found to be co-planar with the phenyl bridge, as represented by (C29-C248-O2-C27) dihedral angle. Figure 3.12 shows the phenyl bridge is co-planar with the first phenyl unit of the triphenylamine moiety, as represented by (C16-C19-C20-C21) and (C21-C22-C23-C24) dihedral angles. The phenylvinyl group is coplanar with the diphenylamine which is represented by the (C18-C13-N1-C1) dihedral angle. Also Figure 3.12 show the two rings of diphenylamine are twisted into a propeller-like configuration as seen for (**3**). Selected torsion angles for (**4**) are listed in Table 3.7.

Table 3.7. Selected torsion angles [°] for (**4**).

C16-C19-C20-C21	-179.2 (3)	C29-28-O2-C27	-164.3 (3)
C20-C21-C22-C23	179.9 (3)	C18-C13-N1-C1	56.6 (4)
C19-C16-C17-C18	178.5 (3)	C8-C7-N1-C1	17.1 (5)
C22-C23-C24-C27	-178.6 (3)	C6-C1-N1-C7	82.7 (4)
C27-C24-C25-C26	179.2 (3)	C14-C13-N1-C7	41.1 (5)

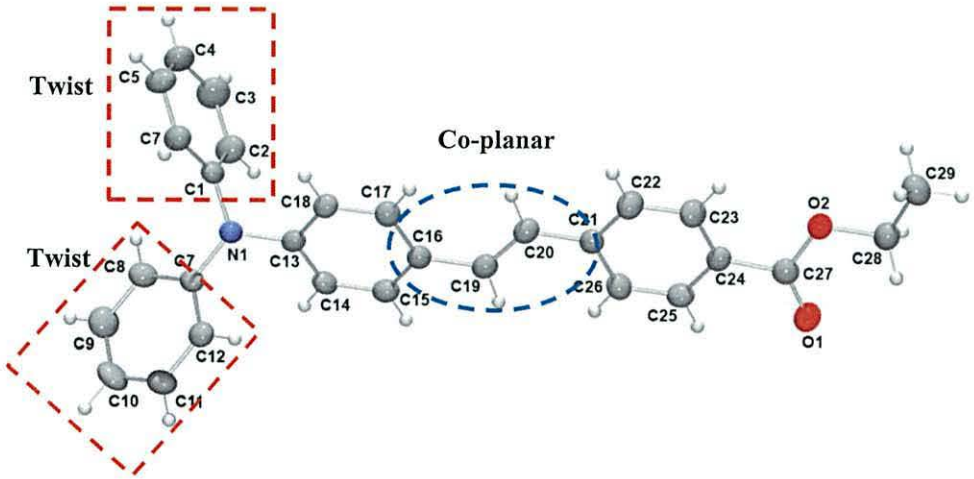

Figure 3.12. Single-crystal molecular structure of (**4**). The square red dashed shows the twist groups and the blue dashed circle co-planar group.

De-esterification of (**4**) led to the new single carboxylate linker yellow dye (**5**). This dye has reduced conjugation compared to the literature [1] single cyanoacrylate linker red dye (**3**) because the cyanoacrylic acid, has been replaced with a carboxylate linker. However, (**5**) has increased conjugation compared to the literature yellow dye [13] because it has a benzene ring in place of a 1,3-cyclohexadiene unit closest to the linker.

The UV-Vis spectrum of (**5**) (Figure 3.13) shows an absorption peak at 296 nm (I) which is due to (π-π^*) electron transition. [2] The absorption peak at 384 nm (ε = 26979 $M^{-1}cm^{-1}$) (II) can be assigned to the intramolecular charge transfer between the triphenylamine donor and the carboxylic acid acceptor, [13, 14] (Figure 3.14).

The data from the mass spectrum of (**5**) shows that, the most prominent peak occurs at 392.1641, which corresponds to (**5**) $[M+H]^+$. The formation of (**5**) is also confirmed by the absence of alkyl ester signals at δ 1.32 and δ 4.31pp in the ^1H NMR data and a shift of the ^{13}C NMR carbonyl ester signal from 192.25 ppm for (**4**) to 183.00 ppm for the carbonyl of the acid in (**5**). Considering the symmetry of (**5**), the number carbon environment equals the number of ^{13}C signals. The FT-IR spectrum shows shift the signal of carbonyl ester from 1709 to 1681 cm^{-1} for the acid in (**5**). A broad peak in (**5**) at 3300-2700 cm^{-1} is due to a ν (OH) carboxylic acid stretch, 3029 cm^{-1} due to ν (C-H) aromatic stretching. Elemental analysis confirms the desired compound.

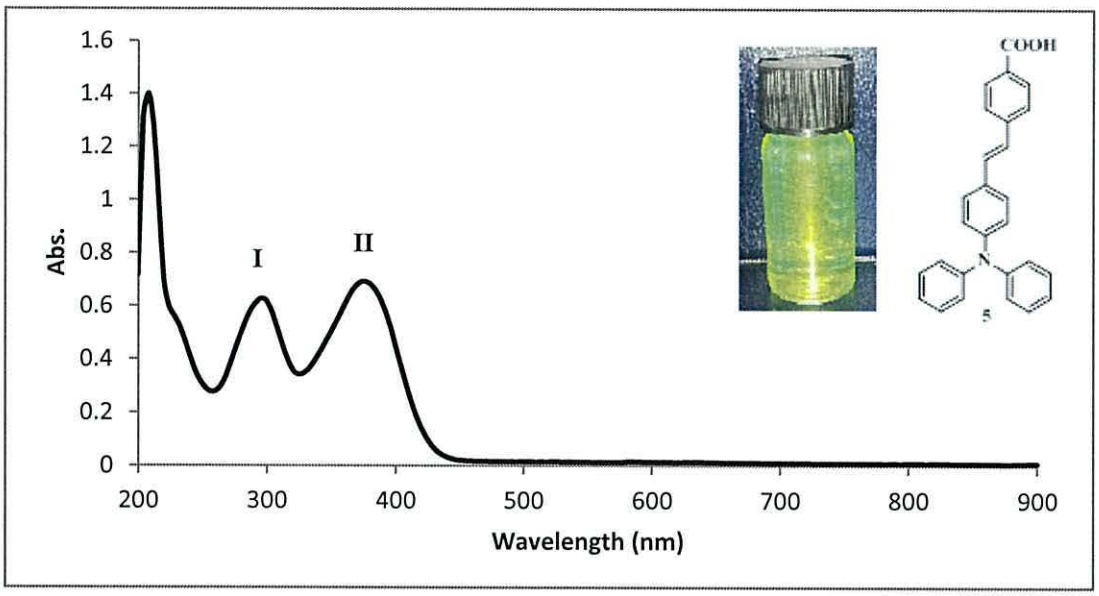

Figure 3.13. UV-Vis spectrum of 4-[2-(4-diphenylamino-phenyl)-vinyl]-benzoic acid (**5**) in ethanol $1x10^{-5}$ M, $\varepsilon = 26979\ M^{-1}cm^{-1}$ at 384 nm, a photograph of a vial containing 0.1 mM ethanolic solution of (**5**) and the molecular structure of (**5**).

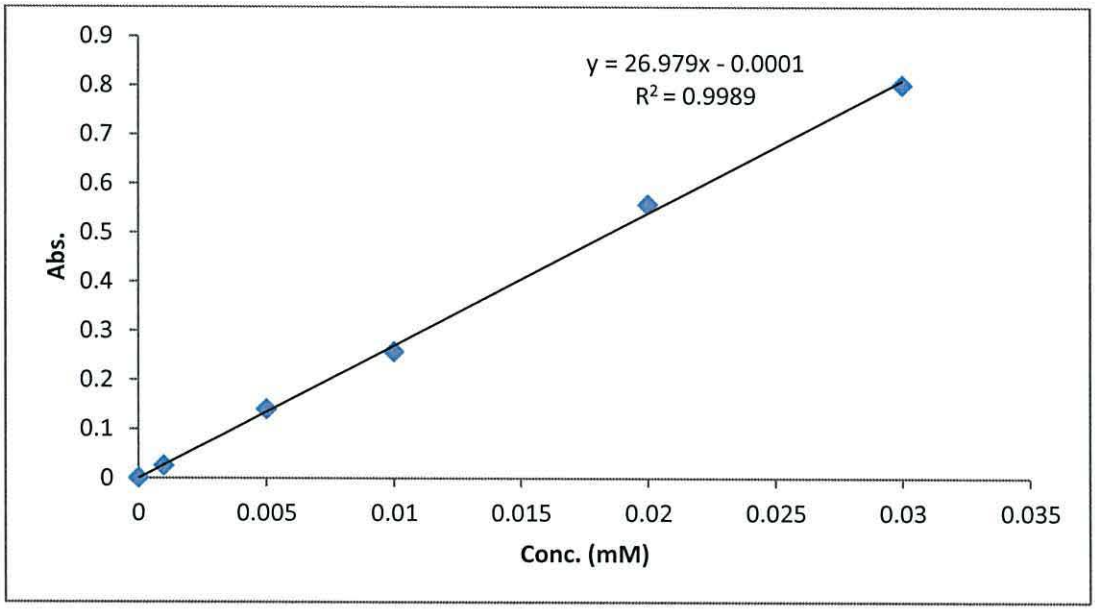

Figure 3.14. Calibration curve show plot absorbance *versus* concentration (mM) for 4-[2-(4-diphenylamino-phenyl)-vinyl]-benzoic acid (**5**) at 384 nm in ethanol.

Single crystals for x-ray structure determination were again obtained by evaporation from dichloromethane/diethyl ether. The molecular structure of (**5**) is shown in Figure 3.15. Figure 3.16 and 3.17 shows the crystal packing arrangement of the molecules in the unit cell along b and c-axis respectively. The details of the selected

bond lengths (Å) and angles (°) are listed in Table 3.8. The x-ray data shows that the angles of (C1-N1-C7), (C1-N1-C13) and (C7-N1- C13) are close 120°. There are no significant difference in the (C-N) values of (N1- C1), (N1- C13) and (N1-C7) and these are agreement with triphenylamine moiety values reported previously. [8] All C-C bonds in phenyl groups are between a single (C-C) and (C=C) double bonds. Figure 3.16 shows hydrogen bonds are formed between two carboxylic acid molecules. Importantly this confirms the desired donor-linker-acceptor arrangement for (**5**) with the strongly donating triarylamine group separated from the adsorbing carboxylate group by the vinyl spacer. In addition the x-ray data also show that the target compound (**5**) with (D-π-A) concept are approximately co-llinear and the conjugated nature of the bonding suggests this type of molecule should be preferable to optimize efficient electron injection into TiO_2. [15] The torsion angles (Table 3.9 show) that the triphenylamine is planar with the phenyl bridge, as represented by (C16-C19-C20-C21) and (C21-C22-C23-C24) dihedral angle. Also the carboxylic acid group is coplanar with the phenyl bridge group, as represented C27-C24-C23-C22 dihedral angle. Figure 3.15 also shows the two rings of the diphenylamine are twisted and fixed to be coplanar as represented by (C8-C7-N1-C1) and (C2-C1-N1-C7) dihedral angles.

Table 3.8. Selected bond lengths [Å] and angles [°] for (**6**).

N1-C1	1.4152(19)	C1-N1-C7	119.35(12)
N1-C13	1.4156(18)	C7-N1- C13	117.79 (12)
N1- C7	1.4350(18)	C1-N1-C13	122.80(12)
C16-C19	1.471(2)	C16-C19-C20	122.65(14)
C19-C20	1.337(2)	C19-C20-C21	128.66(14)
C20-C21	1.467(2)	O1-C27-O2	122.89(13)
C24-C27	1.477(2)	O1-C27-C24	120.68(13)
C27-O1	1.2492(18)	O2-C27-C24	116.43(13)
C27-O2	1.2976(18)	C27-O2-H2A	109.5

Table 3.9. Selected torsion angles [°] for (**5**).

C16-C19-C20-C21	-173.49 (14)	N1-C13-C18-C17	177.89 (13)
C27-C24-C23-C22	178.85 (14)	C28-C21-C26-C25	174.21 (14)
N1-C7-C12-C11	178.68 (14)	C8-C7-N1-C1	-58.7 (8)
C14-C15-C16-C19	178.07 (14)	C2-C1-N1-C7	-25.4 (2)

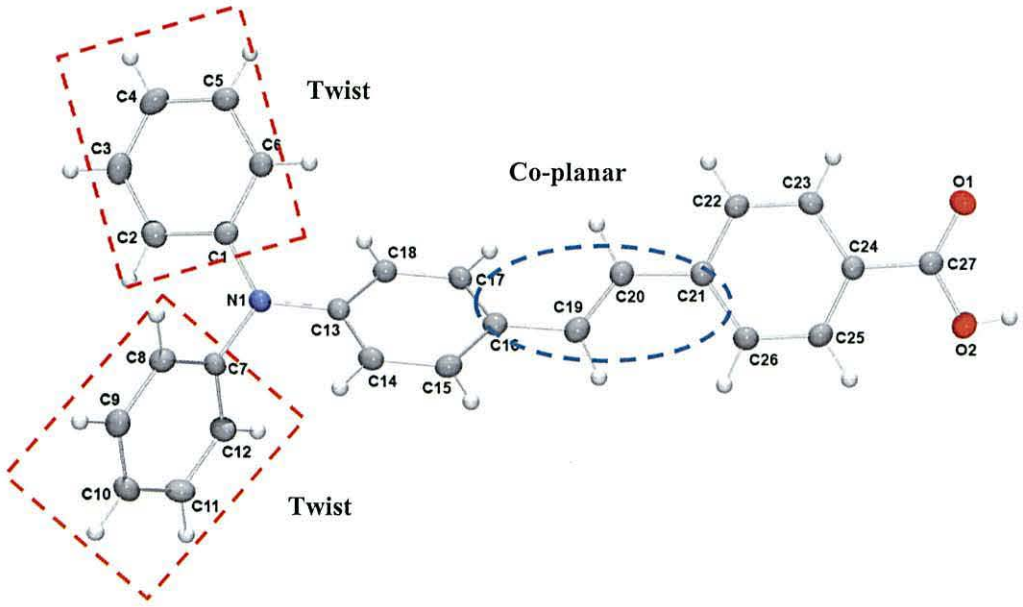

Figure 3.15. An Ortep representation of (**5**). Thermal ellipsoids are drawn at 50% probability level.

Table 3.10 and Figure 3.16 show hydrogen bonding between two molecules of (**5**); O2-H2A….O1, which is representing head to head bonding.

Table 3.10. Hydrogen bonds [Å] and [°] of (**5**).

D–H···*A*	*d*(*D*–H)	*d*(H···*A*)	*d*(*D*···*A*)	∠(*DHA*)
O2–H2A···O1^{i}	0.84	1.80	2.6346(15)	174.5
Symmetry transformations used to generate equivalent atoms:				
(i) –x,–y,–z+2				

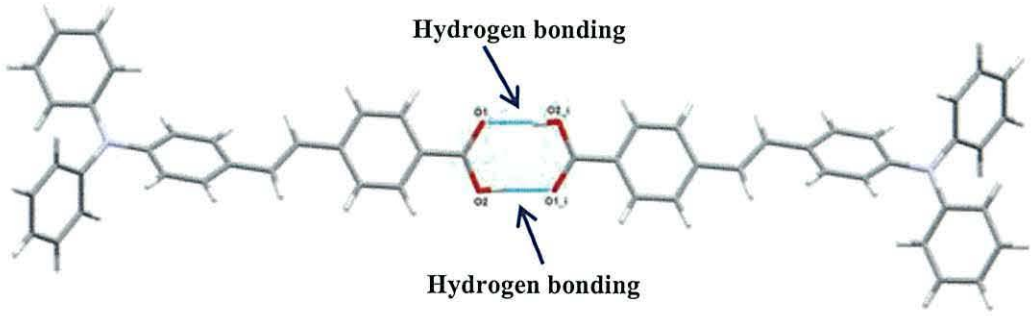

Figure 3.16. Hydrogen bonding between two molecules of (**5**).

In addition, Figure 3.17 shows the crystal packing along b and c axes, respectively. Which appear in multi layers of (**5**) molecules with hydrogen bonding between every two molecules, as a layer top of each other.

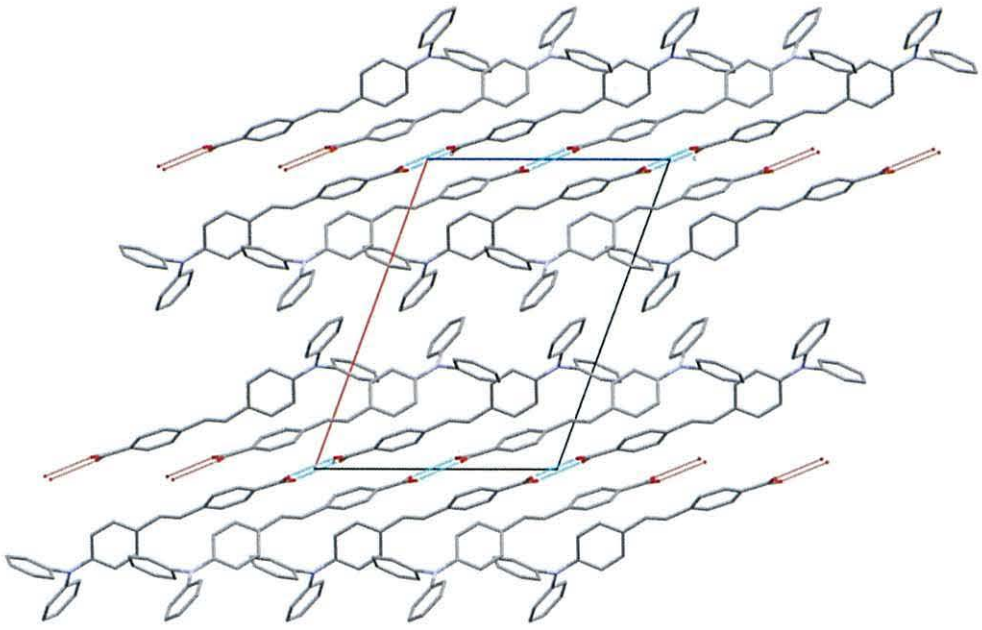

Figure 3.17. Show the crystal packing of (**5**) molecules along b-axis, and the hydrogen bonding between two molecules of (**5**) in "herning bone" packing design.

The detailed photovoltaic parameters (J_{sc}, V_{oc}, FF, and η) for (**5**) are listed in Table 3.11, after passive dyeing with dye (**5**) in dye solution overnight, while Figure 3.18 shows the photocurrent-voltage (I-V) curves of the cells.

Table 3.11. Photovoltaic performance parameters of the ESTCA compound (**5**) two layers of DSL 18NRT TiO_2 paste.

Dye	$TiCl_4$	V_{oc} (V)	J_{sc} (mA cm^{-2})	η (%)	FF
Compound (**5**)	+	0.70	2.64	1.2	0.65

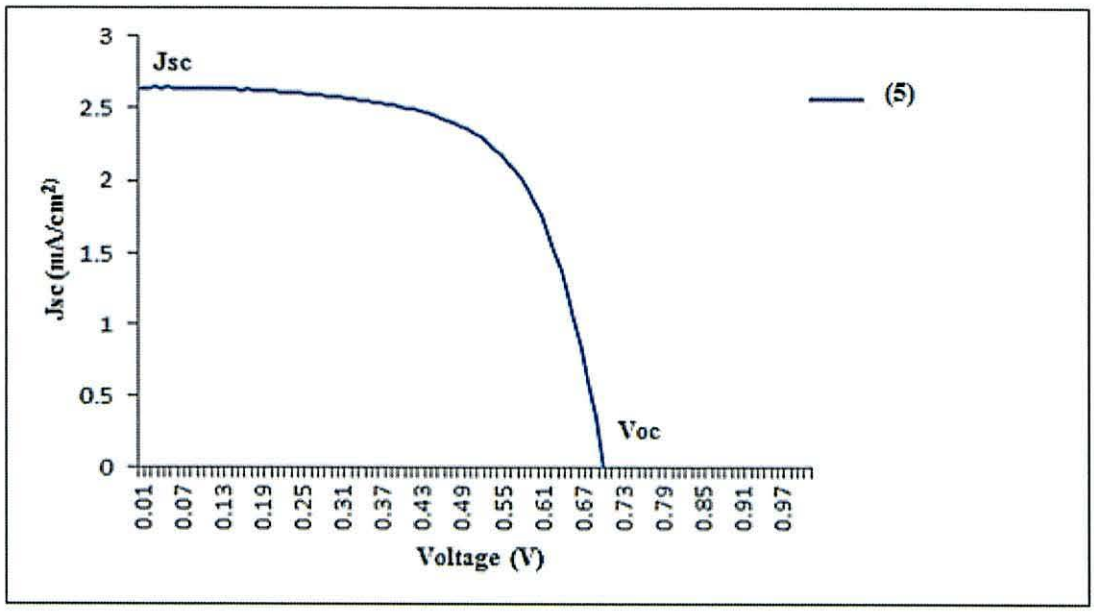

Figure 3.18. IV data for (**5**) under 1 sun (100 mW cm^{-2}).

The stability of the new single-linker yellow dye (**5**) was investigated with time, and shows excellent stability during thermal and light soaking. Figure 3.19 shows the light soaking data for **(5)** and also the ruthenium dye **(N719)** as a standard for comparison under same conditions over 1800 h. The short-circuit current (J_{sc}), circuit open-voltage (V_{oc}), fill factor (FF) and efficiency (η) data are listed in Table 3.12. The efficiency of both dyes increased from 0 to 200 h (which is ascribed to improved electrolyte pore filling) after that the efficiency remains fairly stable up to 1800 h. Slight changes in the short-circuit current, which decreased slightly from 200 to 536 h followed by slight decreases up to 1800 h, whilst V_{oc} and fill factor (FF) remained fairly constant over the time period measured.

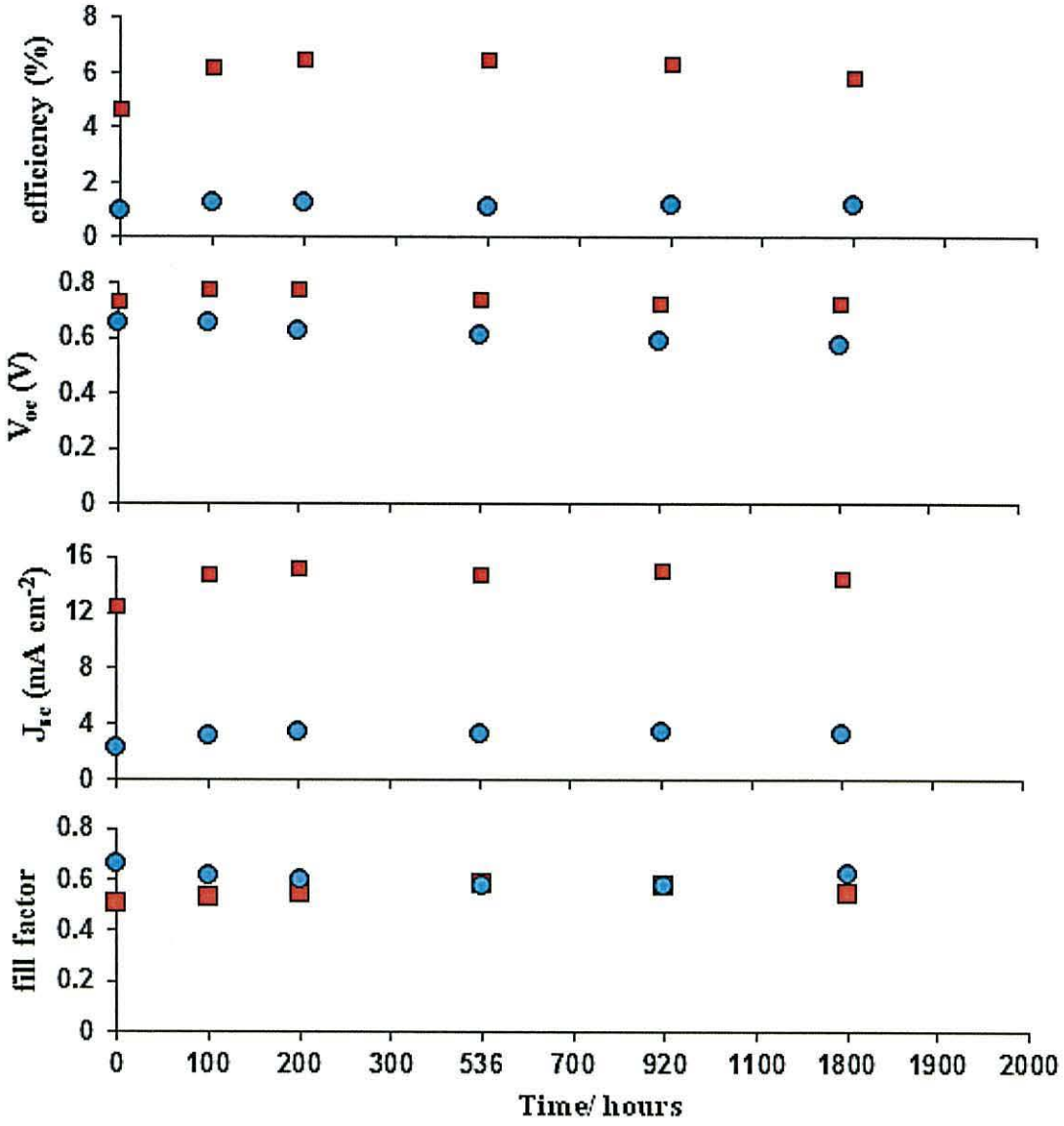

Figure 3.19. Light soaking of DSC devices for up to 1800 h at 1 Sun for **N719** (blue circles) and compound (**5**) (red squares) showing η, V_{oc}, J_{sc} and fill factor (FF).

Table 3.12. Photovoltaic parameter of (**5**) and **N719**.

Dye	Time hours	FF	V_{oc} (V)	J_{sc} (mA cm^{-2})	J_{sc} (EQE mA cm^{-2})	η (%)
N719	0	0.51	0.74	12.48	7.55	4.7
	100	0.53	0.78	14.88	9.82	6.2
	200	0.55	0.78	15.30	9.23	6.5
	536	0.59	0.75	14.76	9.18	6.5
	920	0.58	0.73	15.10	10.50	6.4
	1800	0.55	0.73	14.49	11.40	5.8
(5)	0	0.67	0.66	2.25	3.74	1.0
	100	0.61	0.66	3.16	4.27	1.3
	200	0.60	0.63	3.40	4.09	1.3
	536	0.58	0.61	3.27	4.45	1.5
	920	0.58	0.59	3.51	4.41	1.2
	1800	0.63	0.58	3.34	4.89	1.2

3.3 Studies of the co-sensitization of (3), (5) N719 and SQ1 dyes.

The aim of this section of work was to study the co-sensitization of a combination of two or more dyes together in a single photoelectrode using the ultra-fast dye sensitization technique developed by the Holliman group. [16] One benefit of this method is to reduce the dyeing time from the standard overnight passive dyeing to 5-10 min. It also reduces the amount of dye solution from around 50 ml of dye solution to 1-2 ml per device. [16] In this work devices were co-sensitized with the literature red, triphenylamine dye (**3**), the new single-linker yellow triphenylamine dye (**5**), **N719** (λ_{max}= 550 nm) and/ or with **SQ1** (λ_{max}= 640 nm). UV-Visible spectroscopy (Figure 3.20) shows that (**3**) and (**5**) have maxima absorption at 388 and 384 nm, respectively, but that single-linker red dye (**3**) has an additional shoulder compared to (**5**) which appears at *ca.* 440 nm. This shoulder has a red shift due to presence of a (-CN) group in the cyanoacetic acid linker group which increases the conjugation causing red shift absorbance which should increase the spectral response.

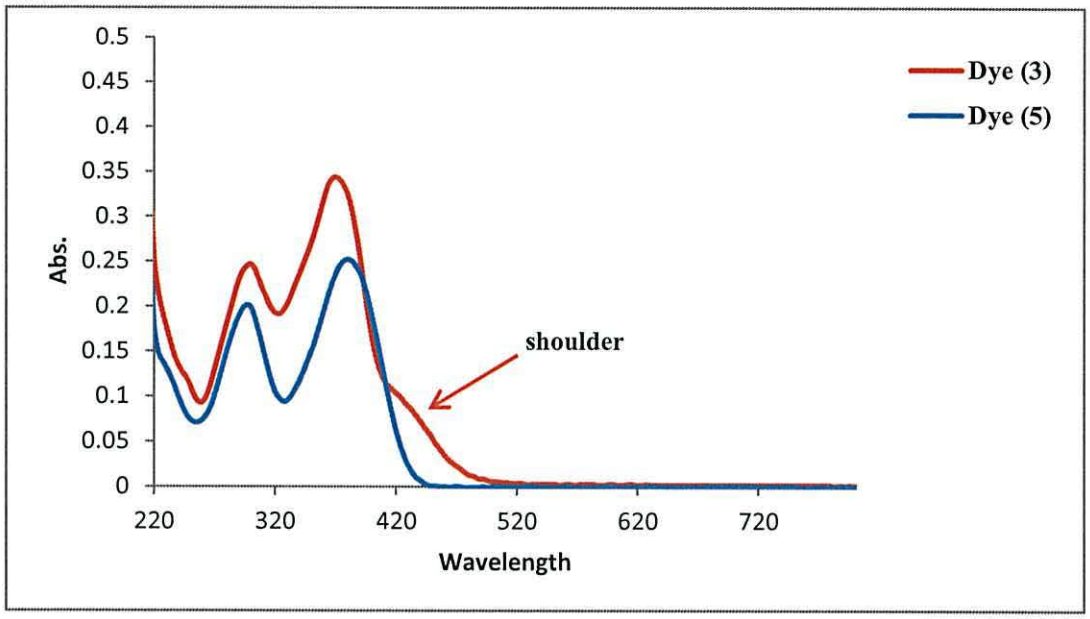

Figure 3.20. UV-Vis spectra of 2-cyano-3-{4-[2-(4-diphenylamino-phenyl) vinyl]-phenyl}-acrylic acid (**3**) and 4-[2-(4-diphenylamino-phenyl)-vinyl]-benzoic acid (**5**). Both dyes at $1x10^{-5}$ M in ethanol.

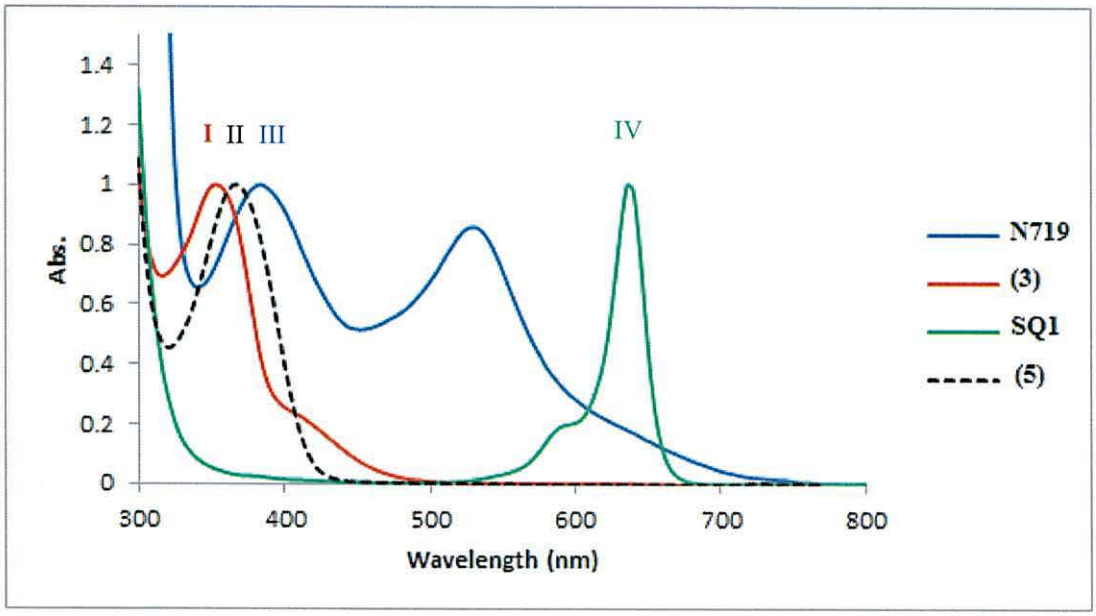

Figure 3.21. UV-Vis spectra of **N719** (blue line) $6x10^{-5}$ M in acetonitrile:*t*-butanol, (**3**) (red line) $1x10^{-5}$ M in ethanol, **SQ1** (green line) $0.6x10^{-5}$ M in ethanol and (**5**) (dashed line) $1x10^{-5}$ in ethanol.

Figure 3.21 shows the UV-Visible spectra of (**3**), (**5**), **N719** and **SQ1**. The bands at around 400 nm (I) for (**3**) and at (II) for (**5**) appear at similar wavelengths to the

secondary band (III) of **N719**. The band at around 650 nm (IV) corresponds to **SQ1**. Furthermore, the EQE data Figure 3.22 shows that **N719** harvests photons less efficiently than (**3**) or (**5**) in this region at around 400 nm of the spectrum.

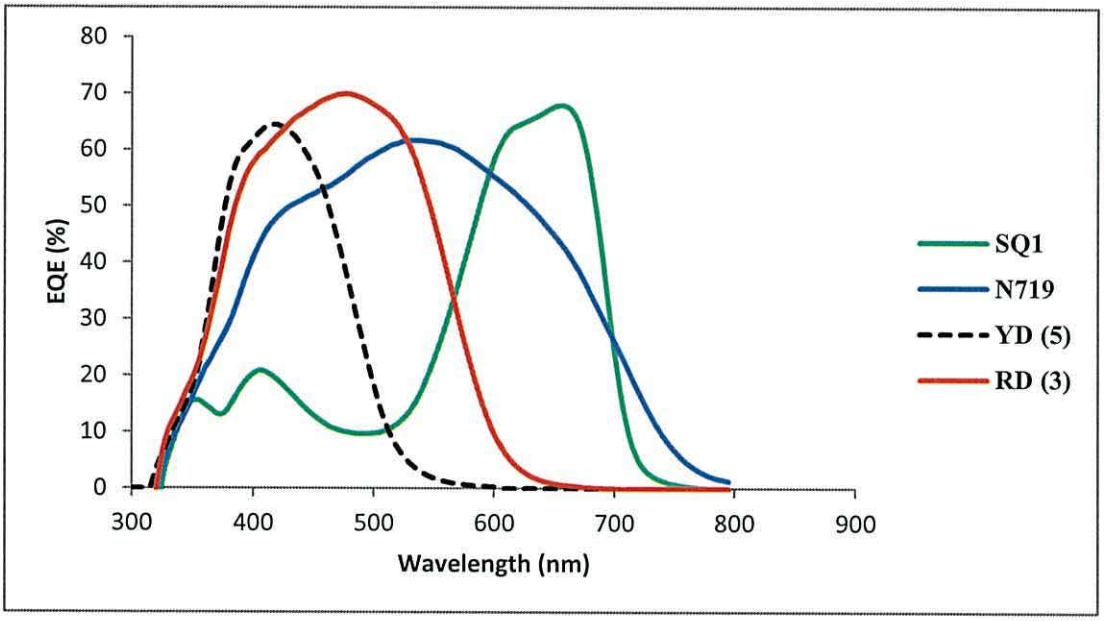

Figure 3.22. External quantum efficiency (EQE) data. The dashed black line is for (**5**), the red line (**3**), the blue line is for **N719** and the green line is for squaraine (**SQ1**).

Interestingly, a comparison of the EQE data of **(3)**, **(5)** and **SQ1**, as shown in Figure 3.22, shows greater differences than the UV data (Figure 3.21). For instance, compound **(3)** show harvesting of photons across a much wider range (320-650 nm) than **(5)** which absorbs in the range 320-550 nm. Also SQ1 harvests photons in the range 325-500 nm with low (%EQE) but with higher EQE from 600-720 nm. Hence, the co-sensitization of (**3**) or (**5**) with **N719** does not seem promising because the EQE shows (**3**), (**5**) and **N719** have an absorption band in the same region of the solar spectrum. However, **(3)** and **(5)** have significantly higher molar extinction coefficient than **N719**, (33,255 and 26,981 L cm^{-1} mol^{-1} respectively, compared to *ca.* 13,000 L cm^{-1} mol^{-1} for **N719**). In theory, this means less (**3**) or (**5**) could absorb as much light as **N719**.

Table 3.13 shows photovoltaic parameters for Devices A, B and C which were dyed passively, showing efficiencies of 3.4% *versus* 1.2% for **(3)** and **(5),** respectively.

Devices D, E, F and G were prepared using ultra-fast dying of (**3**), (**5**), **N719** and **SQ1** in 5 min as described previously. [16] Devices D and E show improved conversion efficiencies for (**5**) and (**3**) (η = 2.6% and 4.4%), mainly due to increased J_{sc} (6.2 and 8.8 mA cm^{-2}).

Fast dying works by pumping dye solution through the mesoporous TiO_2 film to overcome the mass transfer issues of passive diffusion, [16] and Figure 3.23 explains this process. This is become fast dying electrodes is controlled by the rate of adsorption so the whole process can be completely finished within a few minutes.

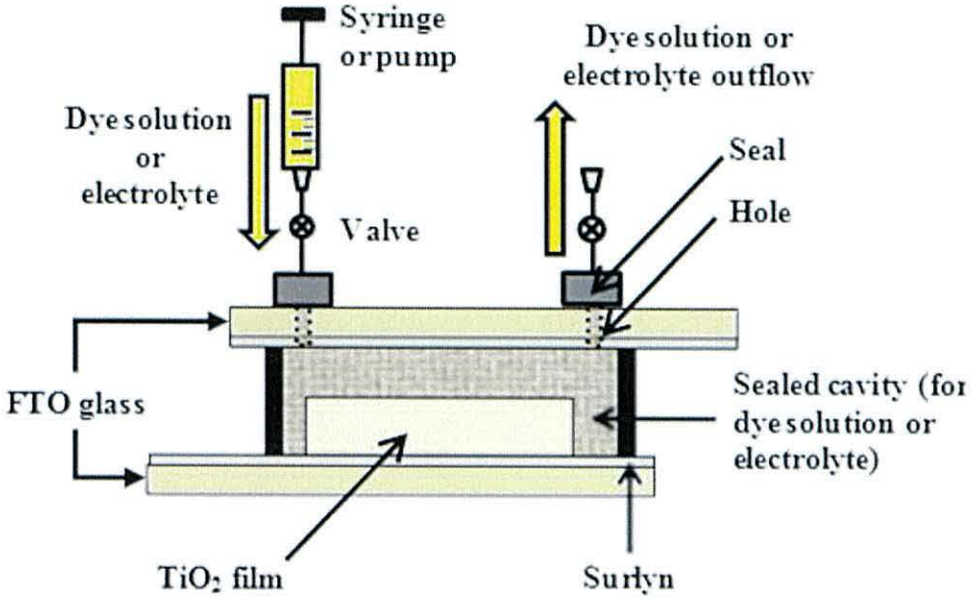

Figure 3.23. Device configuration used for ultra-fast dyeing in DSC devices. [16]

Ultra-fast co-sensitization has also been applied to combinations of (**3**), (**5**) and **N719**. That co-sensitization of (**5**) with **N719** confirms the beneficial effects of ultra-fast co-sensitization in terms of the EQE for these dyes. The EQE data for (**5**) Figure 3.22 shows high spectral response between 350-550 nm. On the other hand, **N719** is most effective between *ca.* 350 and 650 nm. The combination (**5**) with **N719** works because the EQE of (**5**) is more effective at 410 nm. In contrast, **N719** is relatively poor in this region. This combination improved the overall EQE and led to the capture of more photons than either single dye on its own.

Table 3.13. I-V testing data for 2-cyano-3-{4-[2-(4-diphenylamino-phenyl) vinyl]-phenyl}-acrylic acid (**3**), 4-[2-(4-diphenylamino-phenyl)-vinyl]-benzoic acid (**5**), **N719** and **SQ1** devices.

	Device	η (%)	FF	J_{sc} (mA cm^{-2})	V_{oc} (V)
	Passive dyed				
A	Compound (**5**)	1.2	0.65	2.64	0.70
B	Compound (**3**)	3.4	0.63	8.43	0.65
C	**N719**	5.6	0.56	13.10	0.77
	Fast dyed				
D	Compound (**5**)	2.6	0.66	6.19	0.64
E	Compound (**3**)	4.4	0.72	8.80	0.70
F	**SQ1**	3.5	0.67	8.16	0.64
G	**N719**	6.0	0.63	12.42	0.77
H	Compound (**5**) + **N719**	7.5	0.65	15.45	0.74
I	Compound (**3**) + **N719**	7.2	0.63	14.92	0.77
J	Compound (**3**) + (**5**)	3.2	0.57	8.89	0.63
K	Compound (**5**) + **SQ1**	3.7	0.63	9.23	0.64
L	Compound (**5**) + **N719** + **SQ1**	6.5	0.55	16.05	0.73
M	Compound (**5**) + (**3**) + **SQ1**	4.4	0.51	13.56	0.64
N	(**5**) + (**3**) + **N719**	6.5	0.68	13.04	0.73

The photovoltaic data are listed in Table 3.13, and confirm successful co-sensitization with increased J_{sc} from 12.42 to 15.45 mA cm^{-2} and η from 6.0% to 7.5% for Devices G and H. However, the combination of (**3**) and (**5**) (Device J) does not show a significant increase in η value. This is expected as both dyes absorb at similar wavelengths and they have similar molar extinction coefficients. Table 3.13 and Figure 3.24 show that mixing (**5**) and blue **SQ1** (Device K) gives a green device and a small increase in η and J_{sc} from 3.5 to 3.7% and from 8.16 to 9.23 mA cm^{-2} respectively with similar V_{oc} for both devices. In addition, co-sensitization with three dyes together was attempted. Devices L and M were prepared using (**5**), (**N719**), and **SQ1** or (**5**), (**3**) and **SQ1**, respectively. These devices were a good example of successful ultra-fast tri-sensitization, which show increased J_{sc} and η arising from 3 dyes within the photo-electrode. Device L shows the highest J_{sc} (16.05 mA cm^{-2}) compared with the other devices reported here, due to the addition of (**5**) which

absorbs around 400 nm, close to N719 absorption which absorbs at 535 nm, extending response along with SQ1. Finally, Device M shows J_{sc} increased from 8.89 to 13.56 (mA cm^{-2}) with η increasing from 3.2% to 4.4%.

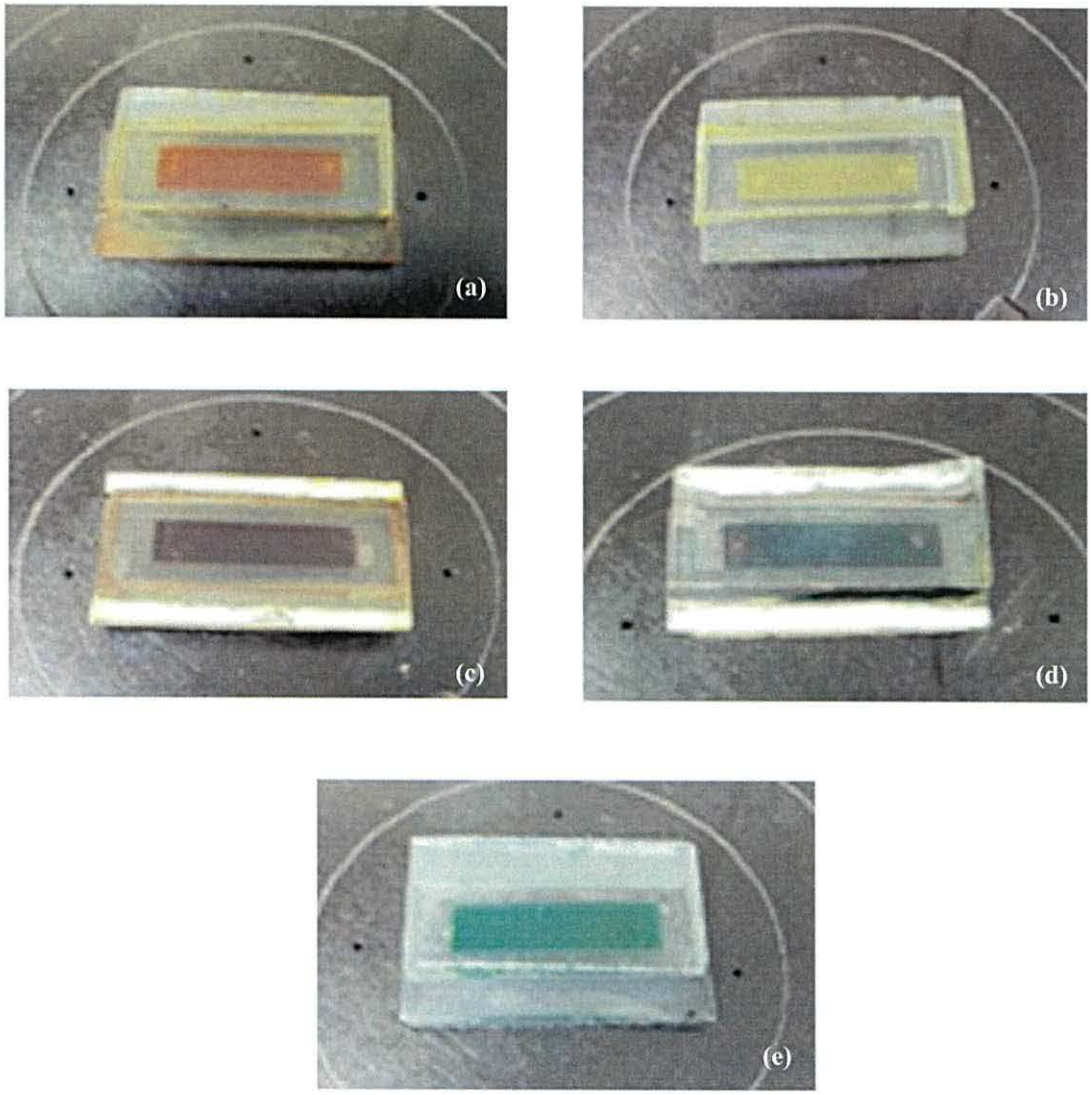

Figure 3.24. Photographs of DSC devices dyed (a) with (**3**), (b) with (**5**), (c) with (**3**), (**5**) and **N719**, (d) with (**5**) and **N719**, (e) with (**5**) and **SQ1**.

3.4 Synthesis of triphenylamine dyes-based two anchoring group

The second part of this chapter includes the synthesis and characterization of new triphenylamine dyes containing two acceptors or anchoring groups; either two cyanoacrylic acids as a red dye (**12**) or two carboxylic acids as a yellow dye (**14**).

The aim of this work was to investigate the effect of increasing the number of anchoring groups on the dye properties and on the photovoltaic performance of dye sensitized solar cells

3.4.1 (2Z, 2'Z)-3, 3'-(5-((E)-4-(diphenylamino) styryl)-1, 3-phenylene) bis (2-cyanoacrylic acid) (12).

The successful synthesis of (2Z, 2'Z)-3, 3'-(5-((E)-4-(diphenylamino) styryl)-1, 3-phenylene) *bis* (2-cyanoacrylic acid) (**12**) was attempted by using three steps. Scheme 3.5 shows the synthetic pathway used to synthesize (**12**).

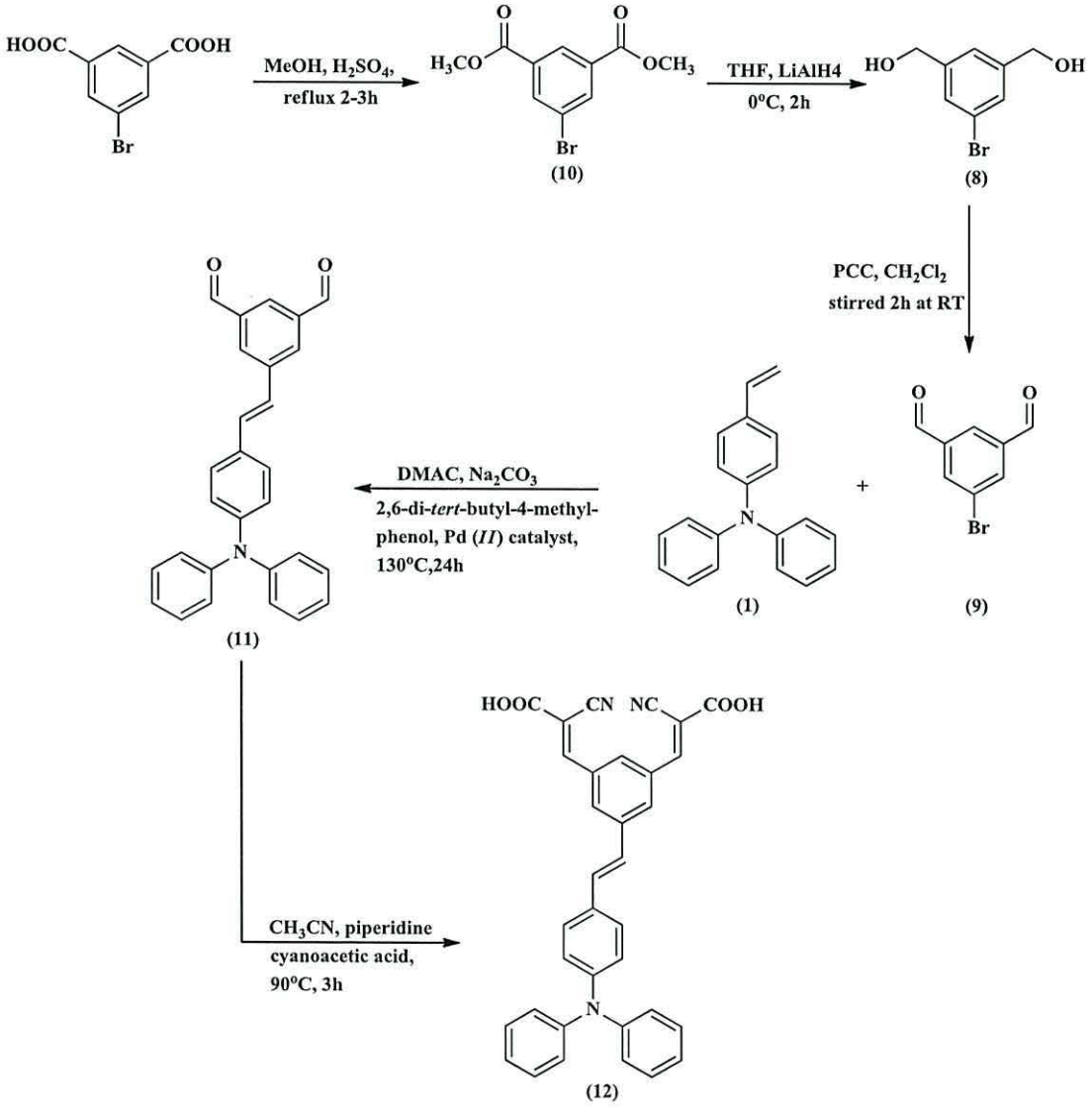

Scheme 3.5. Synthetic pathway of (2Z, 2′Z)-3, 3′-(5-((E)-4-(diphenylamino) styryl) - 1, 3-phenylene) bis (2-cyanoacrylic acid) compound (**12**).

The longest section in this synthetic route was the synthesis of (**9**). We have reduced the pathway to synthesize (**9**) from four steps to three steps compared to the literature. [17] Previous reports started with m-xylene with CCl_4 as a solvent to synthesize (**9**). In contrast, this work started with isophthalic acid as a precursor which avoided the use of CCl_4. The synthesis of (**9**) was achieved by first esterifying isophthalic acid using methanol and sulphuric acid and refluxing for 2-3 h to produce compound (**10**). The esterification mechanism is shown in Scheme (3.6). The treatment of a carboxylic acid with an alcohol in the presence of acid as the catalyst, leads to the formation of an ester. The addition of the acid helps to make the carbonyl carbon more electrophilic, then the alcohol introduces the (-OR) group which is a nucleophilic which adds to the carbonyl carbon to form a new bond and positively charged. The acid again protonaties the OH gives (OH_2), which is displaced to form the ester.

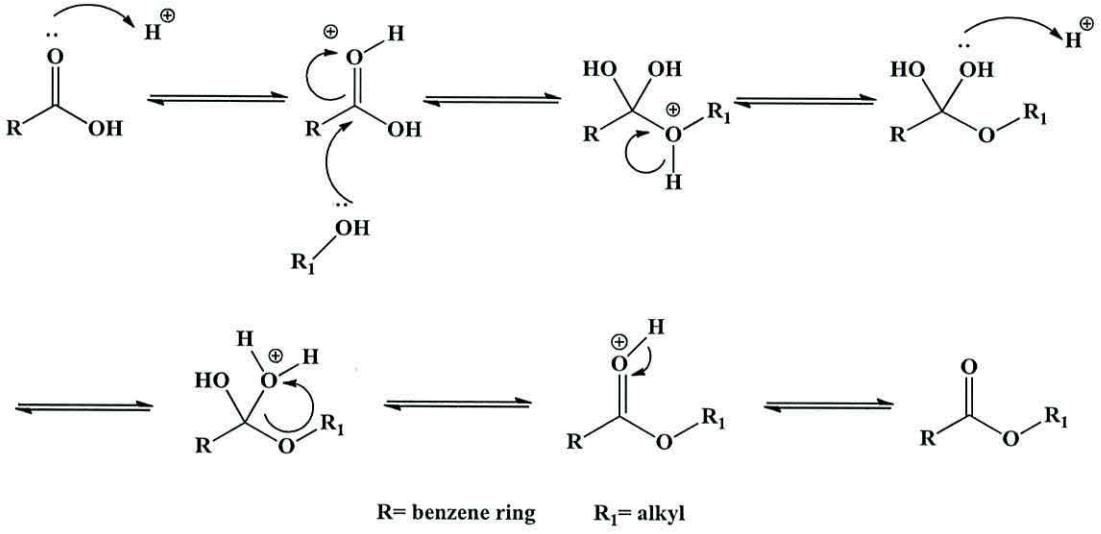

Scheme 3.6. General mechanism of esterfication carboxylic acid. [6]

As expected for (**10**), the ^1H NMR spectrum shows a signal at 3.97 ppm as a singlet due to methyl ester group. The singlet is shifted down field due to its close proximity to the oxygen of the ester group. ^{13}C NMR confirms the formation of (**10**) and shows 6 signals due to 6 carbons environment with a signal at 52.70 ppm due to the methyl ester carbon, and a signal at 164.96 ppm due to carbonyl carbon of the ester group. The data from mass spectrometry also confirm compound (**10**) with a peak at 290.0028, which corresponds to $[M+NH_4]^+$. Single crystals for x-ray structure determination were obtained by evaporation from dichloromethane. The molecular

structure of (**10**) is shown in Figure 3.25. Details of the determination and selected bond lengths (Å) and angles (°) are listed in Table 3.14.

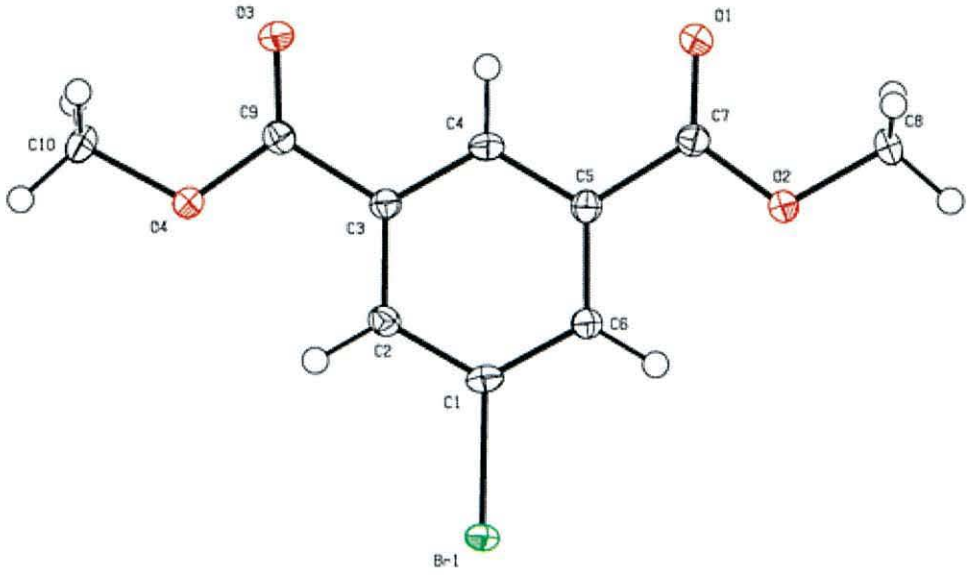

Figure 3.25. Crystal structure of (**10**) with displacement ellipsoids shown at 50% probability.

Table 3.14. Selected bond lengths (Å) and angles (°) of (**10**).

C1-C2	1.385 (5)	C7-O2	1.339 (3)
C5-C6	1.396 (3)	C8-O2	1.448 (3)
C3-C9	1.494 (3)	C10-O4	1.452 (3)
C5-C7	1.499 (3)	C2-C1-C6	121.8 (2)
C7-O1	1.202 (3)	C3-C4-C5	119.7 (2)
C1-Br	1.893 (3)		

All the C-C bonds of the benzene ring are between single (C-C) and double bonds (C=C) and are between 1.385-1.396 (Å). There are no significant differences between the angles of the benzene ring which are all close to 120°. There are differences between the bond lengths of (C7-O1) and (C7-O2) which are 1.202 and 1.339 Å corresponding to C=O and C-O, respectively.

The next step was to synthesize compound (**8**) by reducing (**10**) with $LiAlH_4$ in THF at 0°C for 2 h to produce compound (**8**). The progress of the reduction was followed

carefully by TLC. The reaction was then quenched with a saturated aqueous solution of sodium sulphate decahydrate drop wise at 0°C to protonate on the alkoxide oxygen to produce alcohol. The crude solution was reduced and the product purified by column chromatography used petroleum spirit:ethyl acetate (5:2, v/v) to produce a white solid of compound (**8**) (2 g, 84 yield). Scheme 3.7 shows the mechanism of reduction to convert the ester to an alcohol using $LiAlH_4$. The nucleophilic hydride ion attacks the carbonyl carbon group to give a tetrahedral intermediate. Re-arrangment of the intermediate compound and displacement of (OR) forms the aldehyde. The nucleophilic hydride again attacks the carbonyl carbon and water is added to form an alcohol.

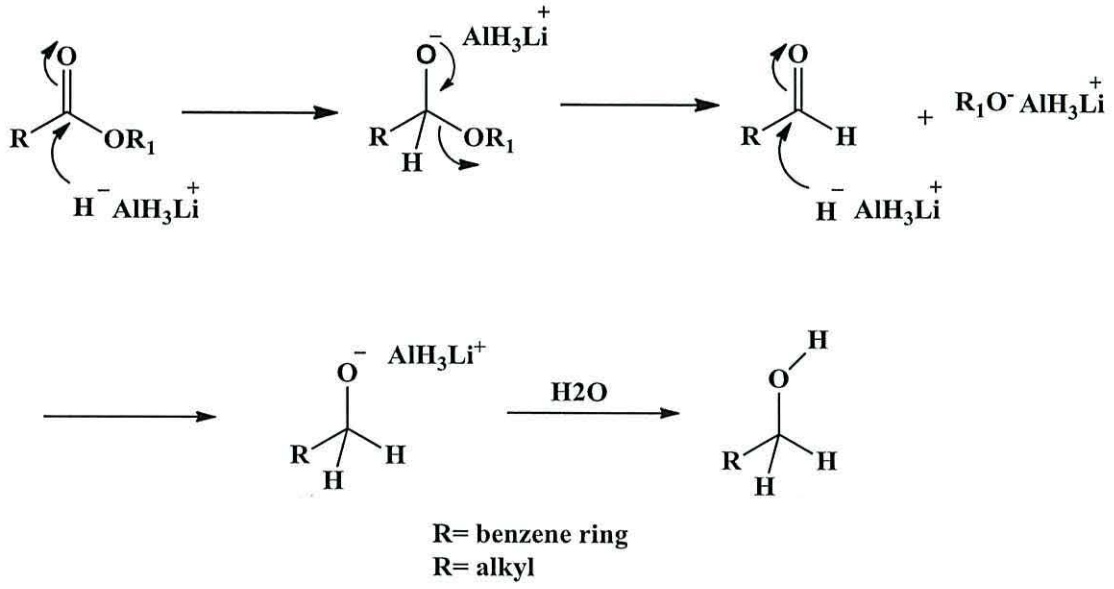

Scheme 3.7. Mechanism reduction of ester by $LiAlH_4$. [18]

^1H NMR data showed a signal for the protons in an alcohol group (2x-CH_2OH) at 4.63 ppm as a singlet which integrates (4H). The DEPTQ of ^{13}C shows 5 signals due to 5 carbon environments and shows an important new signal at 63.01 ppm due to (-$\underline{C}H_2$-OH). Also the data from mass spectrometry confirm (**8**) with the most prominent peak at 234.0126 which corresponds to compound (**8**) $[M+NH_4]^+$.

Compound (**8**) was oxidized with pyridinium chlorochromate (PCC) [19] in methylene chloride to produce the di-aldehyde (**9**). The crude product was purified by column chromatography using petroleum spirit\ethylacetate (5:2, v\v) as an eluent to give a white solid of (**9**) (0.9 g, 46 % yield).

Scheme 3.8 shows the mechanism of oxidation of an alcohol to an aldehyde. The alcohol coordinates to the chromium (VI) atom. The first step is attack of oxygen on the chromium to form a (Cr-O) bond. Then the proton of OH is transferred to one of the oxygens on the chromium and the chloride ion is then displaced, which then acts as a base. The C=O is formed after removing the proton on the carbon adjacent to the oxygen.

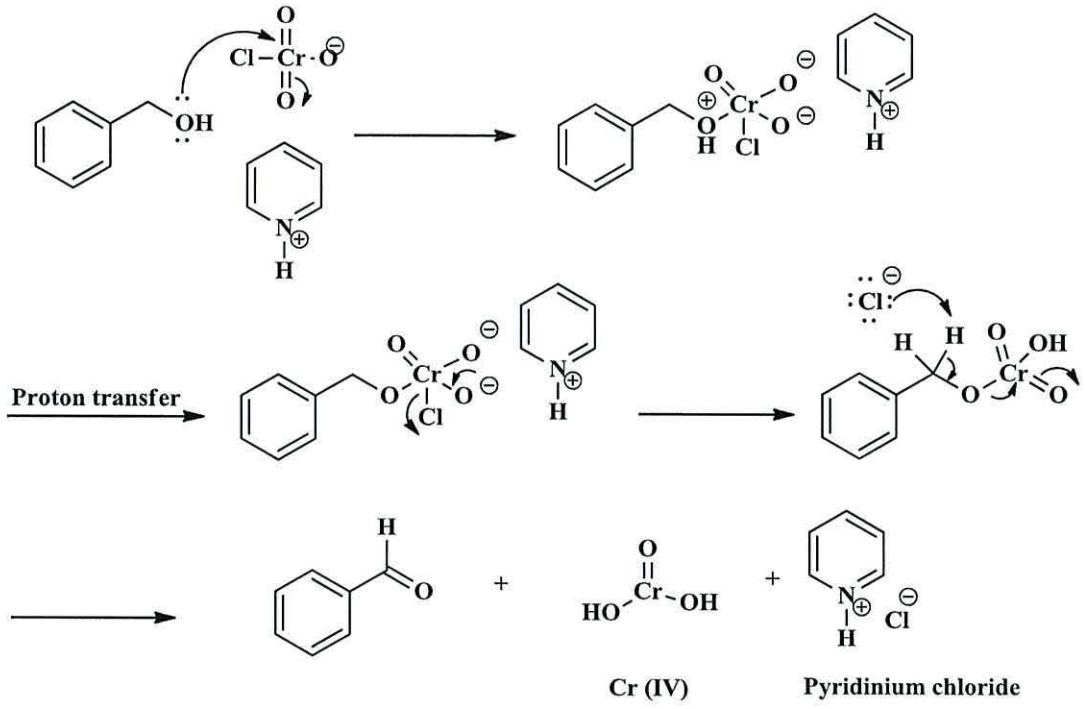

Scheme 3.8. The mechanism reaction of oxidation compound (**8**) to produce (**9**) using PCC, redrawn from. [18]

The synthesis of (**9**) has been confirmed by the absence of CH_2OH signals in the ^1H NMR data and the appearance a signal at 10.06 ppm corresponding to an aldehyde group. ^{13}C NMR data show a signal at 189.48 ppm due to an aldehyde carbon. Mass spectrometry also confirms (**9**). The most prominent peak at m/z 212.9546 corresponds to compound (**9**) $[M+H]^+$. Single crystals of (**9**) for x-ray structure determination were obtained by evaporation from dichloromethane. The molecular structure of (**9**) is shown in Figure 3.26. Details of the determination and selected bond lengths (Å) and angles (°) are listed in Table 3.15.

Table 3.15. Selected bond lengths (Å) and angles (°) of (**9**).

C1-C2	1.388 (5)	C5-C8-O2	124.1(4)
C1-C6	1.380 (5)	O1-C7-H7	118.0
C2-C3	1.387 (5)	O2-C8-H8	118.0
C5-C6	1.398 (5)	C6-C5-C8	119.9
C3-C7-O1	123.9 (4)	C2-C3-C7	119.2

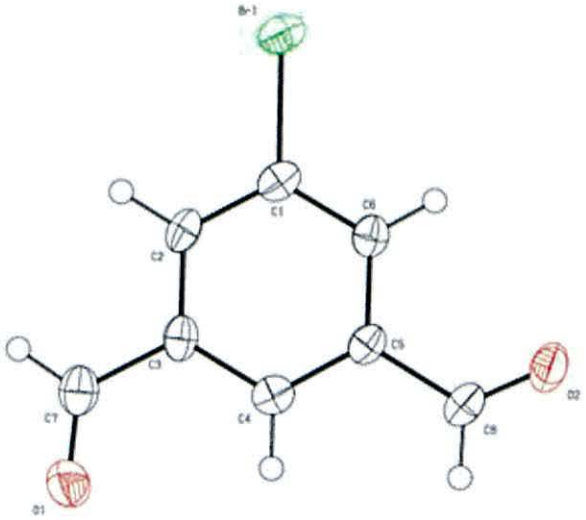

Figure 3.26. Crystal structure of (**9**). Displacement parameters are drawn at 50% probability.

After producing compound (**9**) this was then reacted with (**1**) in a Heck coupling using sodium carbonate, 2,6-di-*tert*-butyl-4-methylphenol and *trans*-di(μ-acetato)*bis*[0-(di-0-tolylphosphoino)benzyl] dipalladium (*II*) in dimethylacetamide (DMAC) as a solvent to produce (**11**) as a yellow solid (0.4 g, 27% yield). The ^{1}H NMR confirmed the presence signals at 6.97-8.39 ppm due to the triphenylamine-vinyl group, along with a signal at 10.13 ppm as a singlet corresponding to aldehyde group from the addition of the benzene aldehyde group. The ^{13}C NMR data shows 15 signals due to 15 carbon environments. The aldehyde signal of (**9**) is shifted from 189.48 to 192.70 ppm in (**11**). The UV-Vis spectrum of (**11**) in ethanol (Figure 3.27) shows an absorption peak at 296 nm (I) is due to a (π-π*) transition [2] and at 376 nm (II) which is due to (π-π*) transition of the conjugated molecule. [5] The FT-IR spectrum also confirms of (**11**) and a shows sharp and intense peak at 1699 cm^{-1}

which is assigned to the ν (C=O) stretch of the aldehyde, a peak at 3038 cm^{-1} is assigned to ν (C-H) of the aromatic groups, 1588 cm^{-1} is assigned to (C=C) benzene ring stretch and the peak at 1176 cm^{-1} is assigned to ν (C-N) stretching. [7] Mass spectrometry identified (**11**) and shows a peak at 404.1645 which corresponds to compound (**11**) $[M+H]^+$.

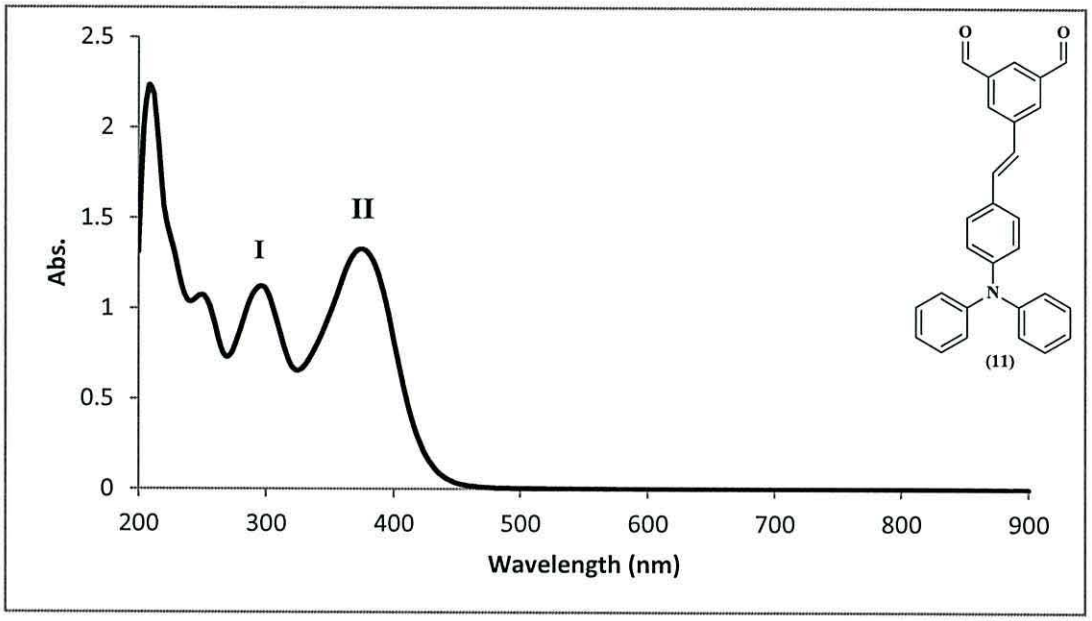

Figure 3.27. The UV-Vis spectrum of 5-[(2-diphenylamino-phenyl)-vinyl]-benzene-1, 3-dicarbaldehyde (**11**) $1x10^{-4}$ M in ethanol and the molecular structure of (**11**).

Single crystals for x-ray structure determinations were obtained by evaporation of solvent from column chromatography vials overnight as shown in Figure 3.28b.

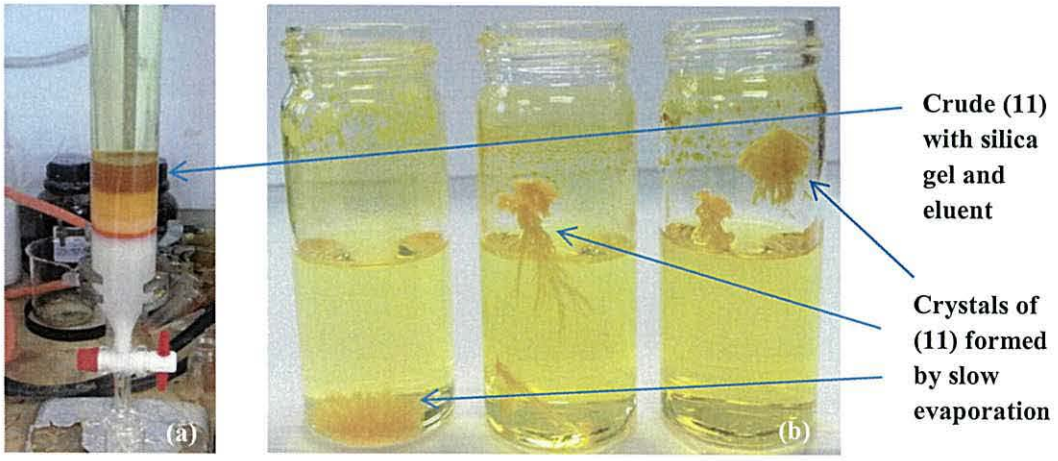

Figure 3.28. (a) Column chromatography of (**11**) and (b) crystallization of 5-[(2-diphenylamino-phenyl)-vinyl]-benzene-1, 3-dicarbaldehyde (**11**) by evaporation of the eluent petrol:methylenechloride (7:3, v/v).

The details of selected bond lengths (Å) and angles (°) are listed in Table 3.16. The molecular structure of (**11**) is shown in Figure 3.29. Table 3.16 shows there are no different between the angles of (C1-N1-C7), (C7-N1-C13) and (C7-N1- C13) for the triphenylamine moiety and are close 120°. [12] The bond lengths of (N1- C1), (N1-C13) and (N1-C7) are (1.434(4), 1.426 (4) Å and 1.419 (4) Å), respectively and are in a good agreement with the (C-N) values of the triphenylamine moiety. [8] There are no significant differences in the bond lengths of (C16-C19) and (C20-C21) 1.474(4) Å and 1.472 Å but these are longer than (C19-C20) 1.335(5) Å. These are agreement with triphenylamine moiety values reported previously. [14]

Table 3.16. Selected bond lengths [Å] and angles [°] for compound (**11**).

N1-C1	1.434(4)	C16-C19	1.474(4)
N1-C7	1.419(4)	C20-C21	1.472(4)
N1-C13	1.426(4)	C1-N1C7	120.1(2)
C23-C27	1.476(4)	C1-N1-C13	119.6(2)
C25-C28	1.479(4)	C7-N1-C13	120.0(2)
C19-C20	1.335(5)		

The torsion angle data (Table 3.17) prove the planarity of the skeleton of (**11**), with the phenyl bridge coplanar with the triphenylamine moiety, represented by (C16-C19-C20-C21) and (C19-C20-C21-C22) dihedral angles. The phenylvinyl group is co-planar with diphenylamine group, as represented by the (N1-C13-C18-C17) and (C18-C13-N1-C1) dihedral angles. On other hand, the co-planarity of phenyl bridge with triphenylamine moiety has been destroyed due to steric repulsion between the phenyl bridge and the triphenylamine moiety. [20] The two rings in diphenylamine are twisted as represented by (C8-C7-N1-C1) and (C6-C1-N1-C7) dihedral angles.

Table 3.17. Selected torsion angles (°) of compound (**11**).

C16-C19-C20-C21	-177.5 (4)	C27-C23-C22-C21	175.7 (3)
C19-C20-C21-C22	155.2 (4)	C18-C13-N1-C1	40.9 (5)
N1-C13-C18-C17	178.6 (5)	C8-C7-N1-C1	32.8 (6)
C14-C15-C16-C19	175.8 (3)	C6-C1-N1-C7	43.0 (6)

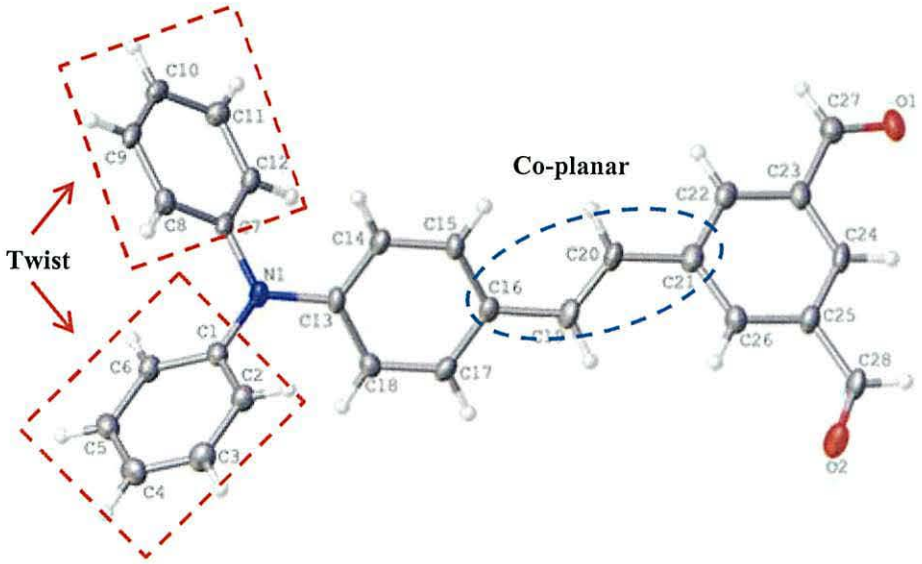

Figure 3.29. Single-crystal structure of 5-[(2-diphenylamino-phenyl)-vinyl]-benzene-1, 3-dicarbaldehyde (**11**). The square red dashed shows the twist groups and the blue dashed circle the co-planar group.

To synthesize two-linker red dye (2Z, 2′Z)-3, 3′-(5-((E)-4-(diphenylamino) styryl)-1, 3-phenylene) bis (2-cyanoacrylic acid) (**12**) several unsuccessful attempts were made before the successful method produced the target compound. At the beginning the main reasons for failure were not clear, so it was decided to check the reaction every 10 min by TLC to know when the reaction started and completed. Through the observing reaction closely with time, it was found that the reaction needed just 3-4 h to complete which was associated with a change in colour for the reaction from yellow to dark red-orange. Thus the successful synthesis of (**12**) was achieved by a Knoevenagel condensation reaction of (**11**) with cyanoacetic acid in the presence of piperidine in acetonitrile at 90°C for 3h to produce a red-orange solid of (2Z, 2′Z)-3, 3′-(5-((E)-4-(diphenylamino) styryl)-1, 3-phenylene) bis(2-cyanoacrylic acid) (**12**).

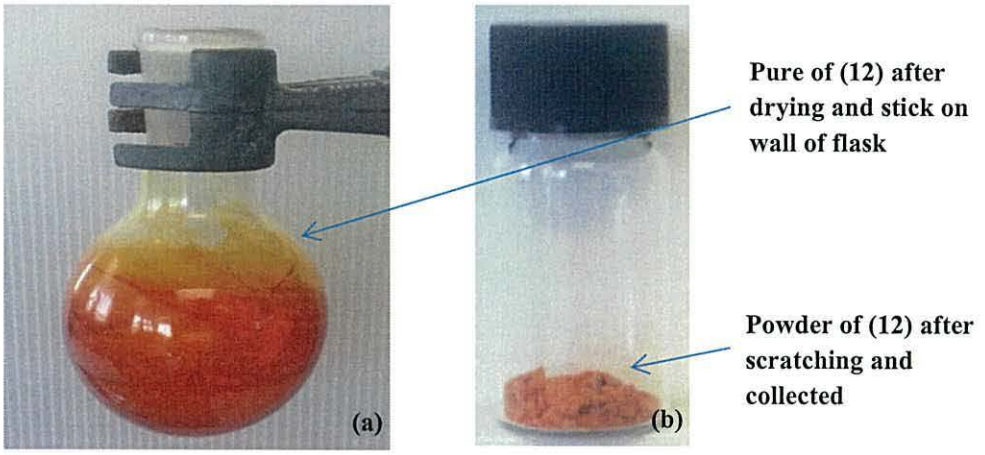

Figure 3.30. Photographs show (a) flask contains (**12**) after drying under high vacuum, (b) (**12**) after scratching from the flask and collecting in a vial.

The UV-Vis spectrum of the (**12**) shown in Figure 3.31 shows an absorption peak at 296 nm (ε= 35421 $M^{-1}cm^{-1}$) (I) which is assigned to a (π-π^*) electron transition and 376 nm (ε= 21077 $M^{-1}cm^{-1}$) (II) which is assigned to intra-molecular charge transfer between the triphenylamine donor and the cyanoacrylic acid acceptor. [2, 21]

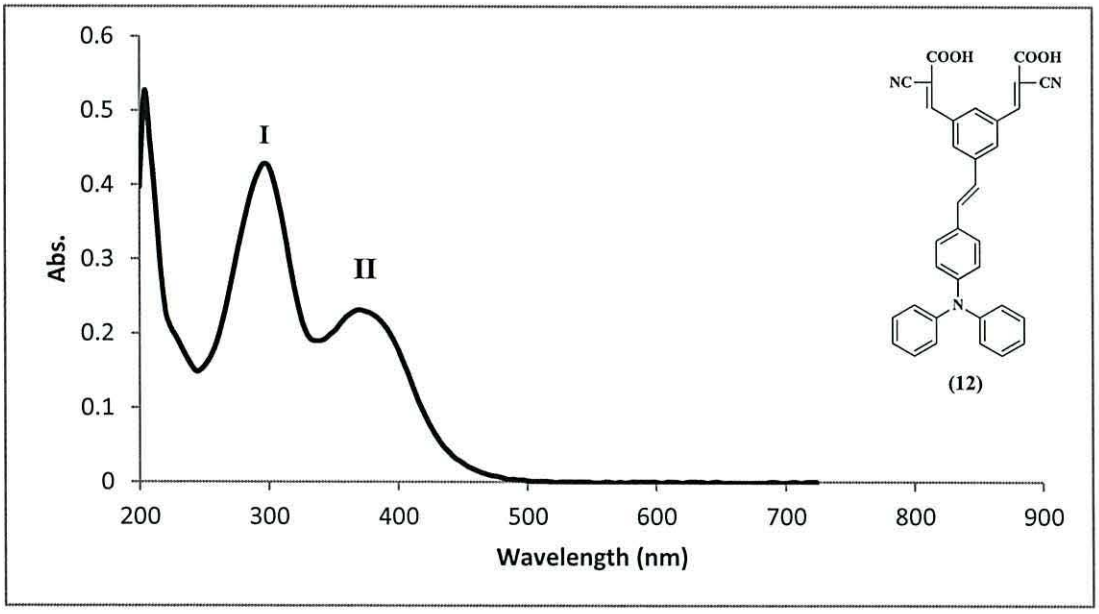

Figure 3.31. UV-Vis spectrum of (2Z, 2′Z)-3, 3′-(5-((E)-4-(diphenylamino) styryl)-1, 3-phenylene) bis (2-cyanoacrylic acid) (**12**) $1x10^{-5}$ M in methanol, ε = 21077 $M^{-1}cm^{-1}$ at 376 nm and the molecular structure of (**12**).

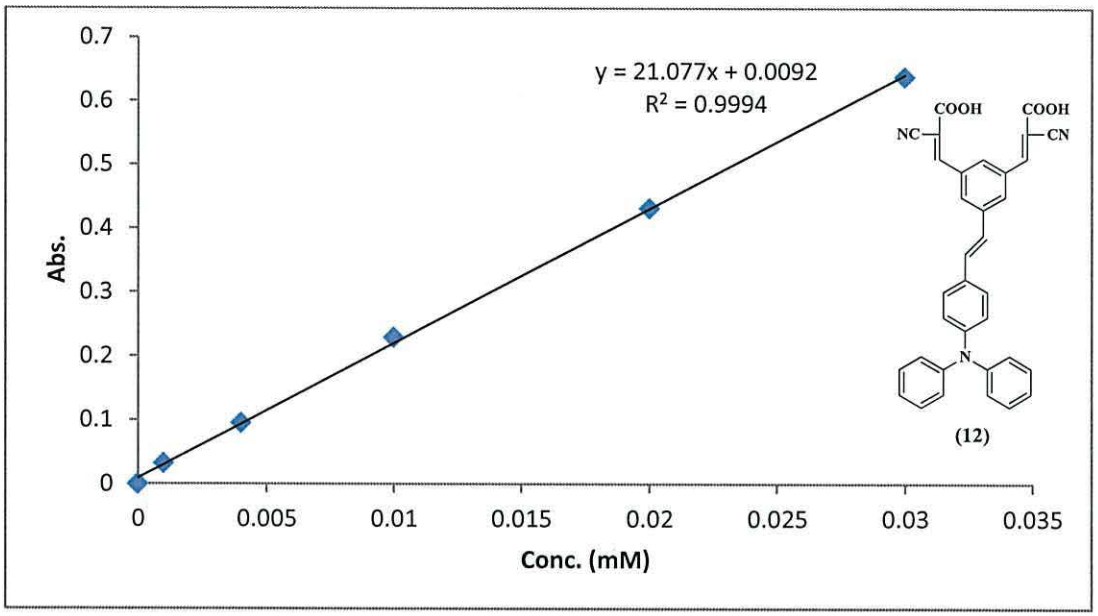

Figure 3.32. Calibration curve show plot absorbance *versus* concentration (mM) for (2Z, 2′Z)-3, 3′-(5-((E)-4-(diphenylamino) styryl)-1, 3-phenylene) *bis* (2-cyanoacrylic acid) (**12**) at 384 nm in ethanol.

The ^{1}H NMR of (**12**) confirmed the absence of an aldehyde signal and the presence of three singlets at 8.11 ppm assigned to (–C=*CH*-Ph-), 8.01 ppm assigned to (=CH-*Ph*-CH=) and 7.91 ppm assigned to (=CH-*Ph*-CH=). Also ^{13}C NMR data shows 18 signals due to 18 environments in line with the molecule's symmetry. The data show a shifted carbonyl signal from 192.70 ppm in (**11**) to 162.16 ppm in (**12**), and a signal at 115.99 ppm due to (C≡N). The FT-IR spectrometry shows a broad peak at 3200-2700 cm^{-1} which is assigned to ν (OH) stretching for the CO_2H of the cyanoacrylic acid linker, ν (C-H) stretch of the aromatic ring at 3032 cm^{-1}, a carbonyl stretch at 1723 cm^{-1} and the presence of a peak at 2226 cm^{-1} assigned to a ν (C≡N) stretch, in addition to peaks at 1493 and 1177 cm^{-1} are due to a ν (C=C) stretch and ν (C-N) stretch, respectively. [8,7] Compound (**12**) was also confirmed by mass spectrometry which shows a peak at m/z 536.1612 corresponding to (**12**) [M-H]$^{-}$.

3.4.2 Synthesis of 5-[2-(4-diphenylamino-phenyl)-vinyl]-isophthalic acid (14).

The synthesis of 5-[2-(4-diphenylamino-phenyl)-vinyl]-isophthalic acid (**14**) (Scheme 3.9) is generally similar to the method for (**5**). The successful synthesis has been achieved by following a similar synthetic pathway to (**5**) but starting with a

different precursor. The synthesis of (**14**) was carried out by using three steps; the first step was the esterification of 5-bromo isophthalic acid to 5-bromo-isophthalic acid dimethyl ester (**10**), using methanol, some drops of sulphuric acid, and then refluxing for 2-3h. The reaction was worked up using a saturated solution of sodium bicarbonate. The crude product was purified by column chromatography using petroleum spirit:ethylacetate (5:2, v/v) to produce (**10**) as a white solid (1 g, 90% yield).

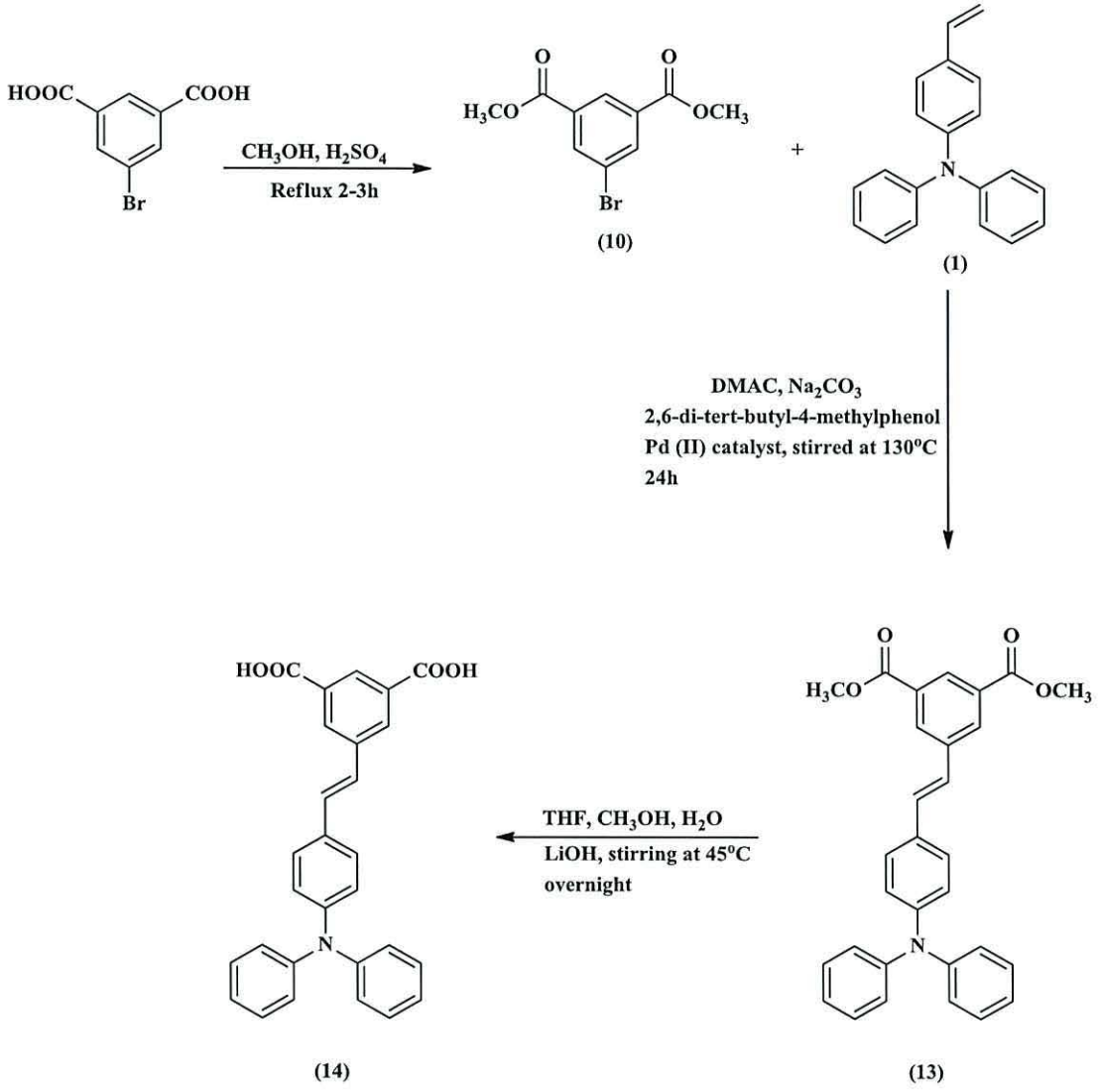

Scheme 3.9. Synthetic pathway of 5-[2-(4-diphenylamino-phenyl)-vinyl]-isophthalic acid compound (**14**).

The ^{1}H NMR, ^{13}C NMR and mass spectrometry data of (**10**) were discussed earlier in this section. The next step was to synthesize (**13**). This was achieved by coupling compound (**1**) with (**10**) in dimethylacetamide (DMAC) as a solvent, with sodium

carbonate, 2,6-di-*tert*-butylcrysol and palladium (*II*) catalyst at 130°C overnight to produce compound (**13**). The UV-Vis spectrum shows a maximum absorption at 296 nm (I) which is assigned to a (π-π^*) transition, and at 376 nm (ε = 38700 $M^{-1}cm^{-1}$) (II) can be assigned to a (π-π^*) intera-molecular charge transfer. [5] The FT-IR data show the important peaks of (**13**) at 3041 cm^{-1} assigned to a ν (C-H) stretch of the benzene rings at 2956 and 2853 cm^{-1} due to ν (CH_3) stretching vibrations, 1719 cm^{-1} assigned to the ν (C=O) stretch of the carbonyl ester groups. Also the peak at 1591 cm^{-1} is due to ν (C=C) of the benzene ring and 1199 cm^{-1} is due to a ν (C-N) stretch. The ^1H NMR spectrum confirms a signal at 3.91 ppm for methyl ester groups as a singlet and signals from 6.96 to 8.38 ppm for the triphenylamine group linked with the addition of the diester benzoate group. The ^{13}C NMR data also confirm the ^1H NMR data and show a signal at 165.34 ppm due to the carbonyl carbon of the ester group. Also the Mass spectrometry data confirmed (**13**) and shows the most prominent peak at 464.1852, which corresponds to (**13**) $[M+H]^+$.

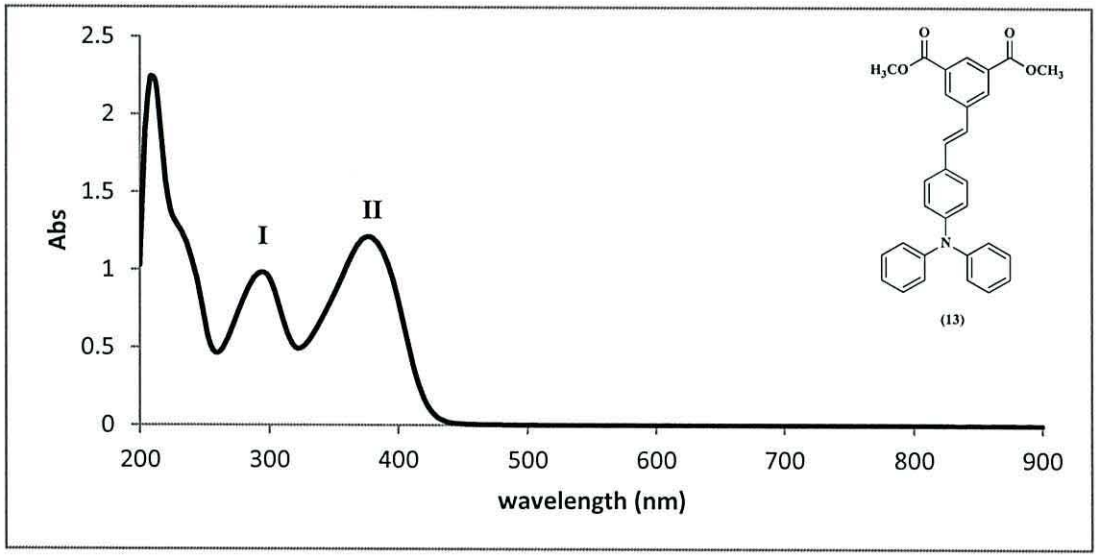

Figure 3.33. UV-Vis spectrum of 5-[(2-diphenylamino-phenyl)-vinyl]-isophthalic acid dimethyl ester (**13**) in ethanol $1x10^{-5}$ M, and the molecular structure of (**13**).

Single crystals for x-ray structure determination were again obtained by evaporation from dichloromethane. The molecular structure of 5-[2-(4-Diphenylamino-phenyl)-vinyl]-isophthalic acid dimethyl ester (**13**) is shown in Figure 3.34. The selected bond lengths (Å) and angles (°) are listed in Table 3.18. The angles of triphenylamine moiety (C1-N1-C7), (C1-N1-C13) and (C7-N1- C13) close to 120° are in the range

reported previously. [8] The (C-N) bond lengths of (N1-C1), (N1-C13) and (N1-C7) are also in agreement with reported values for the triphenylamine moiety. [12] All the C-C bonds of the benzene ring are between single bond (C-C) and double bonds (C=C).

Table 3.18. Selected bond lengths [Å] and angles [°] for compound (**13**).

N1-C1	1.433 (4) Å	C1-N1-C13	117.9 (2) °
N1-C13	1.432 (3) Å	C7-N1-C13	119.9 (2) °
N1-C7	1.424 (4) Å	C1-N1-C7	122.0 (2) °
C16-C19	1.466 (4) Å	C27-O1-C28	114.7 (2) °
C19-C20	1.339 (4) Å	C29-O3-C30	115.9 (2) °
C25-C29-O3	111.6 (2)°	C23-C27-O1	112.5 (2) °

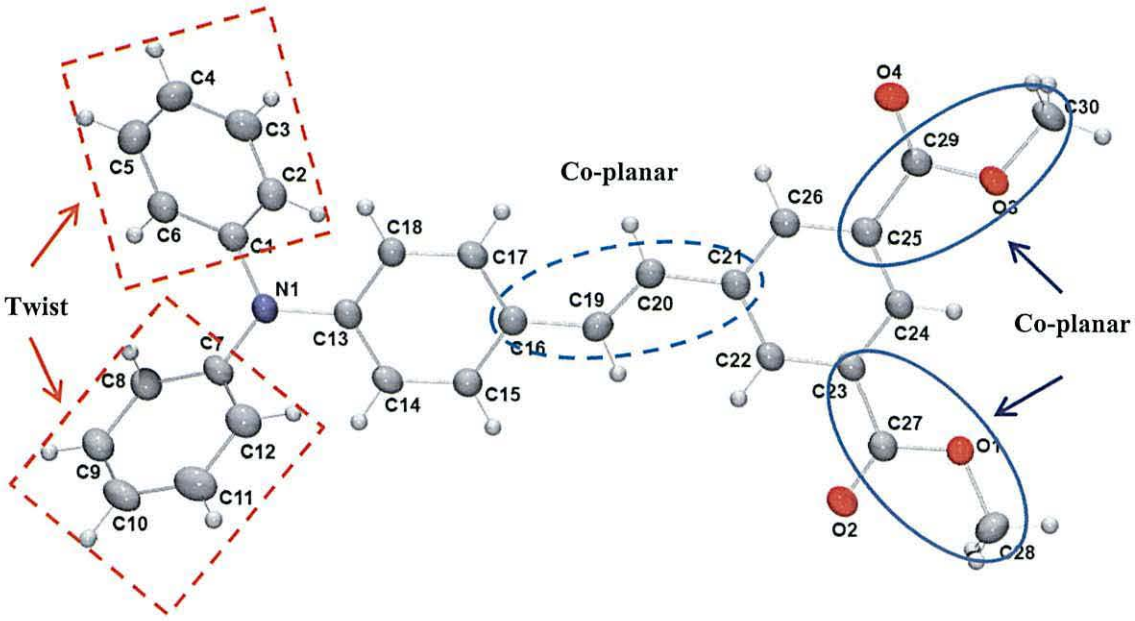

Figure 3.34. Single-crystal x-ray structure of 5-[(2-diphenylamino-phenyl)-vinyl]-isophthalic acid dimethyl ester (**13**). The square red dashed shows the twist groups and the blue dashed circles co-planar groups.

Table 3.19. Selected torsion angles (°) for compound (**13**).

C16-C19-C20-C21	175.4 (3)	C30-O3-C29-C25	174.7 (2)
N1-C7-C12-C11	179.9 (3)	C8-C7-N1-C1	34.7 (4)
N1-C1-C6-C5	179.1 (3)	C6-C1-N1-C7	31.5 (4)
C28-O1-C27-C23	174.4 (2)	C13-N1-C7-C12	29.5 (4)

Figure 3.34 is shows the ester group is co-planar with the phenyl bridge, as represented by (C28-O1-C27-C23) and (C30-O3-C29-C25) dihedral angles. The phenyl bridge is coplanar with the triphenylamine moiety as represented by the (C16-C19-C20-C20) and (C19-C20-C21-C22) dihedral angles.

Finally, the synthesis of (**14**) was achieved by hydrolysis (**13**) with methanol:water and LiOH in THF. Then the pH was adjusted to 5-6 with 5% of hydrochloric acid to produce 5-[2-(4-diphenylamino-phenyl)-vinyl]-isophthalic acid (**14**) as a yellow solid (0.3 g, 93% yield).

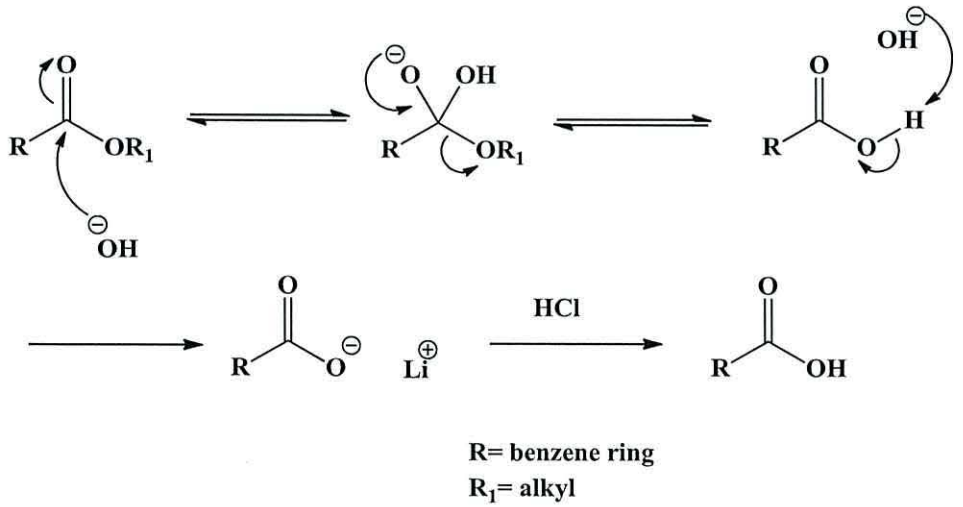

Scheme 3.10. General mechanism for the hydrolysis of an ester. [6]

Schem 3.10 shows the mechanism of ester hydrolysis using base as the catalyst. The hydroxide nucleophile attacks carbonyl carbon of the ester to form a tetrahedral intermediate. Then the C=O reforms with the loss of the leaving group (RO^-), which then deprotonaties the carboxylic acid.

Indications of the successful transformation were observed in both the ^{1}H NMR and ^{13}C NMR spectra which confirmed the absence of a signal for the methyl ester groups and a shift of the carbonyl carbon from 165.34 to 166.63 ppm for the carboxylic acid. The FT-IR spectrum displayed a broad peak from 3400-2700 cm^{-1} which is assigned to ν (OH) carboxylic acid stretch and a sharp peak at 1699 cm^{-1} due to the ν (C=O) stretch of the carbonyl of the carboxylic acid. Confirmation of the desired compound was achieved by using mass spectrometry which detected an ion at 436.1542 which corresponds to (**14**) $[M+H]^{+}$. The UV-Vis spectrum (Figure 3.35) shows two absorption peaks at 296 nm (ε= 25718 $M^{-1}cm^{-1}M^{-1}cm^{-1}$) (I) which is assigned to (π-π*) electron transition and at 372 nm (ε= 35196 $M^{-1}cm^{-1}$) (II) which is assigned to intra-molecular charge transfer between the triphenylamine donor and the carboxylic acid acceptor. [21, 22] Figure 3.36 shows the calibration curve of (**14**)

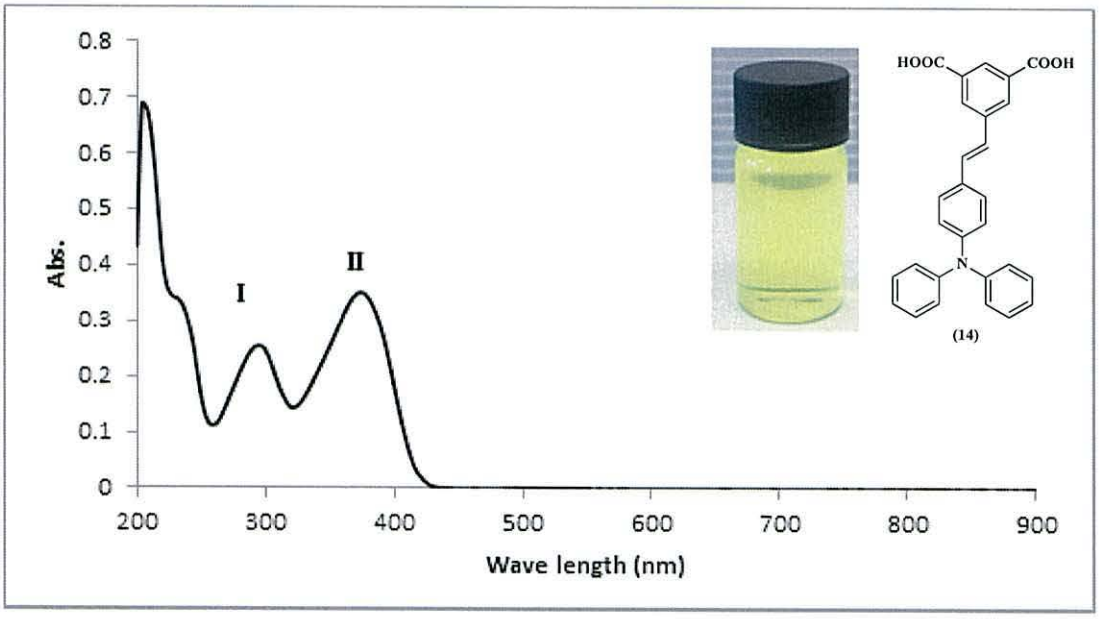

Figure 3.35. UV-Vis spectrum of 5-[2-(4-diphenylamino-phenyl)-vinyl]-isophthalic acid (**14**) in ethanol $1x10^{-5}$ M, ε = 35196 $M^{-1}cm^{-1}$ at 372 nm, and vial containing a 0.1 mM solution of (**14**) in ethanol and the molecular structure of (**14**).

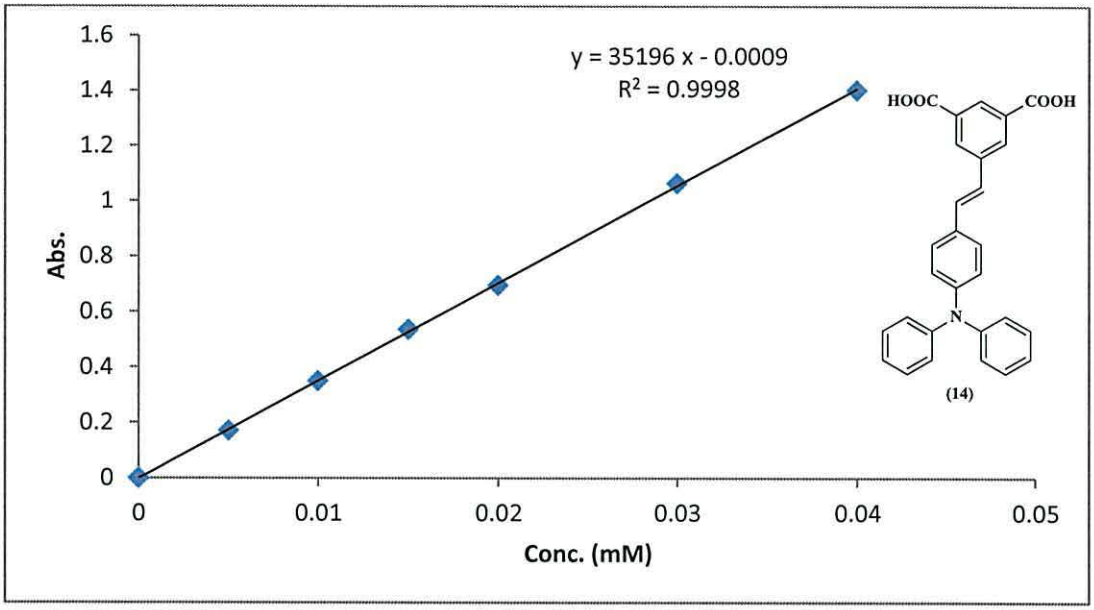

Figure 3.36. Calibration curve show plot absorbance *versus* concentration (mM) for 5-[2-(4-diphenylamino-phenyl)-vinyl]-isophthalic acid (**14**) at 372 nm in ethanol.

Single crystals for x-ray determination were again obtained by the evaporation method, using dichloromethane/ diethyl ether as the solvent. The molecular structure of 5-[2-(4-diphenylamino-phenyl)-vinyl]-isophthalic acid (**14**) is shown in Figure 3.37. Table 3.20 shows the selected values for bond length (Å) and angles (°). The bond lengths of (N1-C1), (N1-C7) and (N1-C13) are in a good agreement with the bond length of (C-N) values of the triphenylamine moiety previously reported. [4] The angles (C1-N1-C7), (C1-N1-C13) and (C7-N1- C13) are in the range of (118.5 (2) ° – 121.9 (2) °, which are agreement with triphenylamine previously reported. [12] All the carbon-carbon lengths in the phenyl bridge and triphenylamine group are between the distance of a single bond (C-C) and a double bond (C=C). [9]

Table 3.20. Selected bond length (Å) and angles (°) for compound (**14**).

N1-C1	1.430 (4)	C20-C21	1.459 (4)
NI-C7	1.421 (4)	C1-N1-C7	118.5 (2)
N1-C13	1.411 (3)	C1-N1-C13	119.5 (2)
C16-C19	1.454 (4)	C7-N1-C13	121.9 (2)
C19-C20	1.336 (4)	C23-C27-O1	115.5 (3)
C23-C27	1.482 (4)	C25-C28-O3	115.0 (2)

The torsion angles show that the carboxylic acid group is coplanar with the phenyl bridge and the first phenyl group of the triphenylamine moiety, as represented by (C28-C25-C26-C21) and (C27-C23-C22-C21) dihedral angles. The phenyl bridge is coplanar with triphenylamine moiety as represented by (C16-C19-C20-C21) dihedral angle. Also Figure 3.37 shows the phenyl groups of the diphenylamine moiety twisted in a propeller-like confirmation as represented by the (C8-C7-N1-C1) and (C2-C1-N1-C7) dihedral angles. Table 3.21 is shown selected value of torsion angles for compound (**14**).

Table 3.21. Selected torsion angles (°) for compound (**14**).

C16-C19-C20-C21	177.7 (3)	N1-C13-C18-C17	-177.1 (3)
C28-C25-C26-C21	177.9 (3)	C8-C7-N1-C1	-38.1 (4)
C21-C22-C23-C27	-177.0 (3)	C2-C1-N1-C7	-46.7 (4)
N1-C13-C14-C15	177.8 (3)		

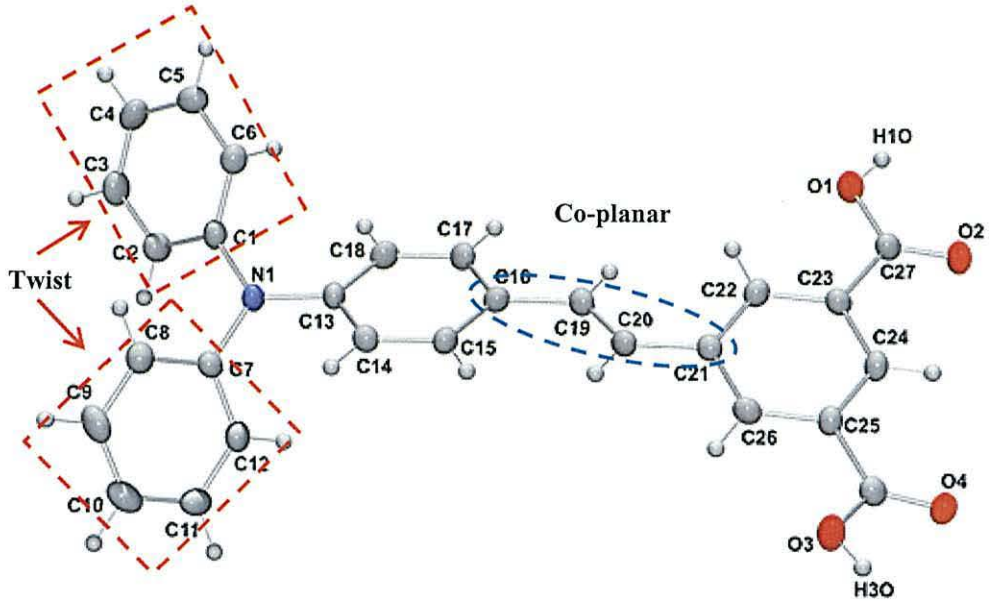

Figure 3.37. An ortep single crystal structure of 5-[2-(4-diphenylamino-phenyl)-vinyl]-isophthalic acid (**14**). The square red dashed shows the twisted phenyl groups and of triphenylamine moiety and the blue dashed circle shows the co-planar groups.

Figure 3.38 and Table 3.22 show the hydrogen bonding of (**14**) for the molecule with other two molecules through carboxylic acid O1-H1O...O4 and O3-H3O…O2.

Table 3.22. Hydrogen bonds [Å and °] of (**14**).

D–H···*A*	*d*(*D*–H)	*d*(H···*A*)	*d*(*D*···*A*)	∠(*DHA*)
O1–H1O···O4^{i}	0.84	1.80	2.634(3)	175.7
O3–H3O···O2^{ii}	0.84	1.76	2.600(3)	177.2

Symmetry transformations used to generate equivalent atoms:

(i) –x,y+1/2,–z+1/2 (ii) –x,y–1/2,–z+1/2

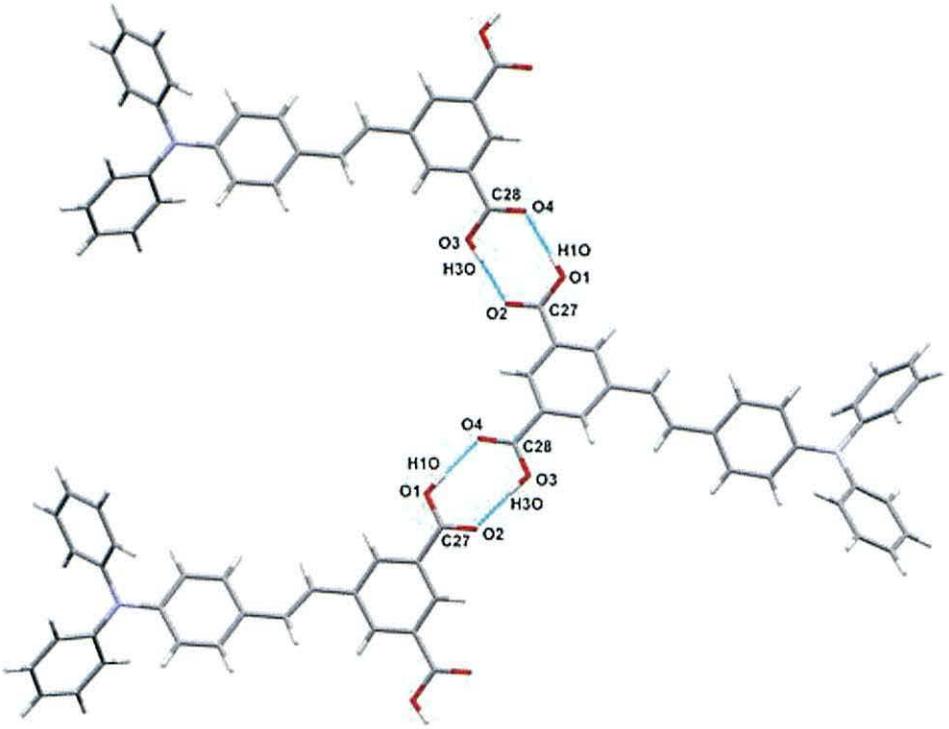

Figure 3.38. Hydrogen bonding in 5-[2-(4-diphenylamino-phenyl)-vinyl]-isophthalic acid (**14**).

Overall, the successful synthesis of new double linker triphenylamine-based metal-free organic dyes was achieved using two different types of acceptor moiety, (carboxylic acids and cyanoacrylic acids). The main reason for this work was to focus on the acceptor group and its influence on the photovoltaic properties in DSC devices. In theory, the carboxylic acid anchor group should link strongly to the semiconductor surface, whilst the presence of the cyano (CN) group should increase

the electron-withdrawing nature of the linker moiety which can shift the oxidation potentials positively but does not take part in the adsorption process. [23]

3.5 Fabrication of devices

The same method mentioned previously was used to fabricate DSC devices but using, (2Z, 2'Z)-3, 3'-(5-((E)-4-(diphenylamino) styryl)-1, 3-phenylene) *bis* (2-cyanoacrylic acid) (**12**) and 5-[(2-diphenylamino-phenyl)-vinyl]-isophthalic acid (**14**) as new sensitizers.

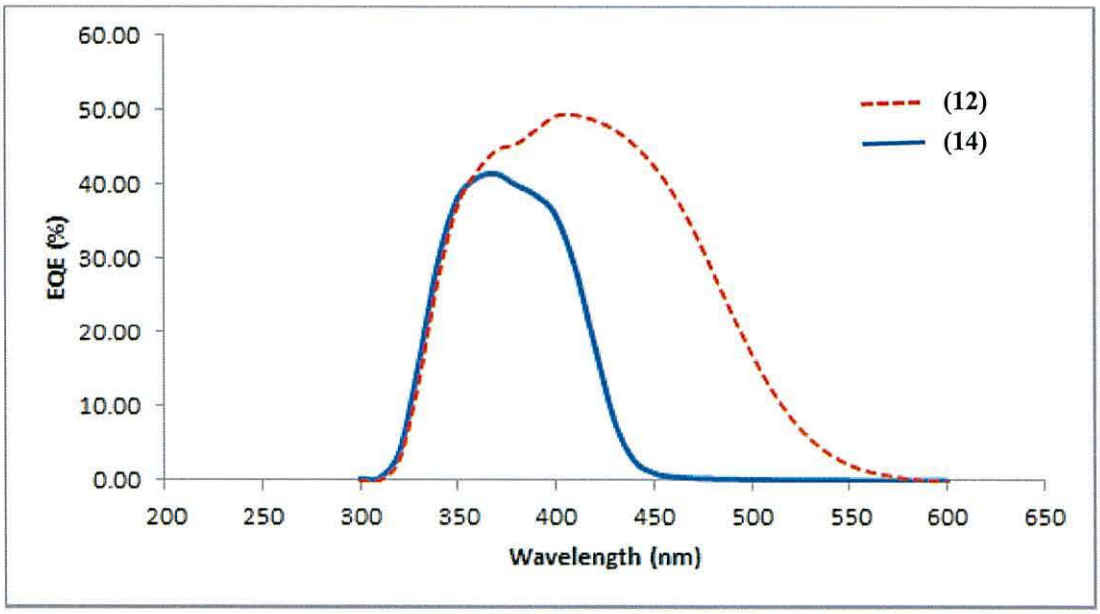

Figure 3.39. External quantum efficiency (EQE) *versus* wavelength. The solid blue line is for 5-[2-(4-diphenylamino-phenyl)-vinyl]-isophthalic acid compound (**14**) and the dashed red line is for (2Z, 2'Z)-3, 3'-(5-((E)-4-(diphenylamino) styryl)-1, 3-phenylene) bis (2-cyanoacrylic acid) (**12**)

The EQE data in Figure 3.39 show that (**12**) harvests more photons than (**14**) and shows an EQE response from 330 to just over 500 nm whilst (12) absorbs from 330 to 430 nm. Interestingly, a comparison of the EQE and UV-Vis data for both dyes shows that they behave significantly differently in that both dyes show red shift when absorbed on TiO_2 compared to the UV-Vis data in solution.

Table 3.23. I-V testing data for (2Z, 2'Z)-3, 3'-(5-((E)-4-(diphenylamino) styryl)-1, 3-phenylene) bis (2-cyanoacrylic acid) (**12**), 5-[2-(4-diphenylamino-phenyl)-vinyl]-isophthalic acid (**14**), **N719** and **D149** devices.

Device	η (%)	FF	J_{sc} (mA cm^{-2})	V_{oc} (V)
Passive dyed				
A (**12**)	2.4	0.63	5.37	0.71
B (**14**)	1.2	0.67	2.82	0.63
C **D149**	4.4	0.54	13.50	0.60
Fast dyed				
D **N719**	4.2	0.62	9.32	0.73
E (**12**)	2.6	0.72	4.53	0.76
F (**14**)	1.0	0.58	2.50	0.67
G **D149**	4.3	0.53	13.34	0.61
H (**12**) + **D149**	5.4	0.59	14.69	0.58
K (**14**) + **D149**	4.4	0.54	12.63	0.58
L (**12**) + **N719**	2.1	0.58	5.82	0.62
M (**14**) + **N719**	2.6	0.78	4.41	0.74

Table 3.23 shows the photovoltaic parameters data (J_{sc}, V_{oc}, FF and η) for DSCdevices prepared from the individual dyes (**12**), (**14**), **D149** and **N719** and also combinations of these dyes. For instance, Devices A, B and C were prepared using a single dye only (**12**), (**14**) and **D149,** respectively and by passive dyeing (overnight), showing conversion efficiencies of 2.4, 1.2 and 4.4% with J_{sc} values (5.37, 2.82 and 13.50 mA cm^{-2}), respectively. Devices D, E, F and G were prepared using fast dying with using the same dyes in addition to **N719** (Device D), showing conversion efficiencies of 4.2, 2.6, 1.0 and 4.3%, respectively. When comparing between the passive and fast dying data there are no significant differences between (**12**) and (**14**) except that the J_{sc} is decreased slightly for the fast dyed devices. Devices H and K were prepared by co-sensitizing dyes (**12**+**D149**) and (**14**+**D149**), respectively. Device H shows improved data for co-sensitization compared with Device C with an

increase in efficiency from 4.3 to 5.4% and J_{sc} from 13.34 to 14.69 mA cm^{-2}. The EQE data for a combination of (**12**) and **D149** (Device H) Figure 3.40, shows a maximum EQE of 72% at 540 nm for **D149** (II) and of 62% at 410 nm (I) for (**12**). Overall these EQE data show higher spectral response and wider photon capture across solar spectrum for the co-sensitized devices leading to increase of J_{sc}. In contrast, Device K did not show as good a result compared with Device H or C.

Figure 3.41 shows a maximum EQE of 71% at 540 nm for **D149** (II) and of 55% at 400 nm (I) for (**14**). The EQE data for Devices L and M which were made by co-sensitizing (**12**+**N719**) or (**14**+**N719**), Figures 3.42 and 3.43 respectively, were much lower and did not show as promising results which suggests that either the lower (ε) of **N719** reduced photon harvesting so that more adsorbed dye was required which too up surface sites or that **N719** did not work cooperatively with these dyes.

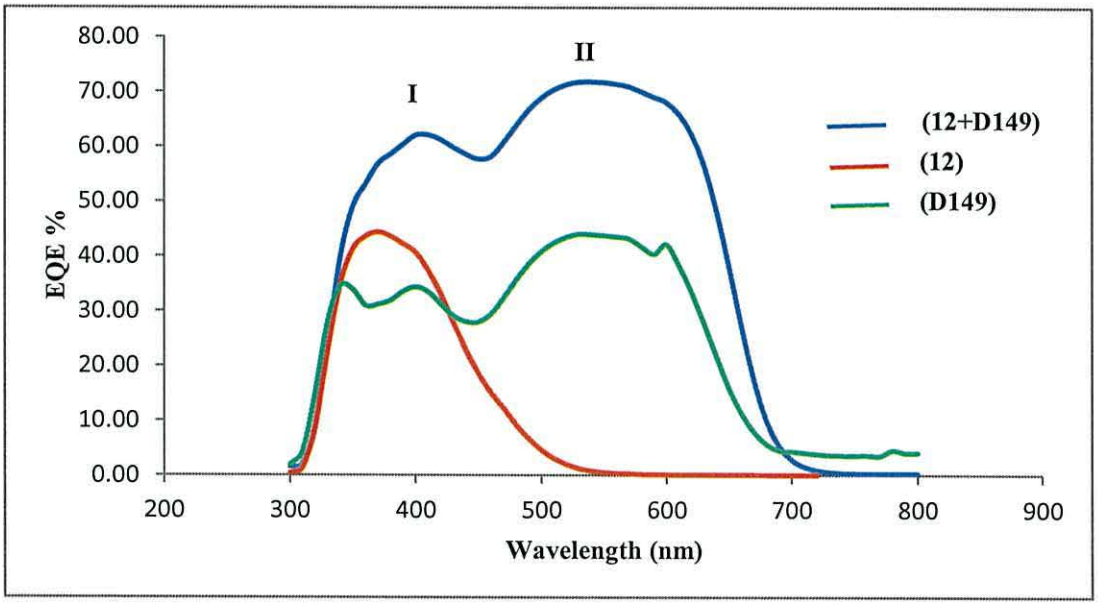

Figure 3.40. External quantum efficiency (EQE) *versus* wavelength. The red line is for (**12**), the green line is for **D149** and the blue line is for co-sensitized (**12**) + **D149**.

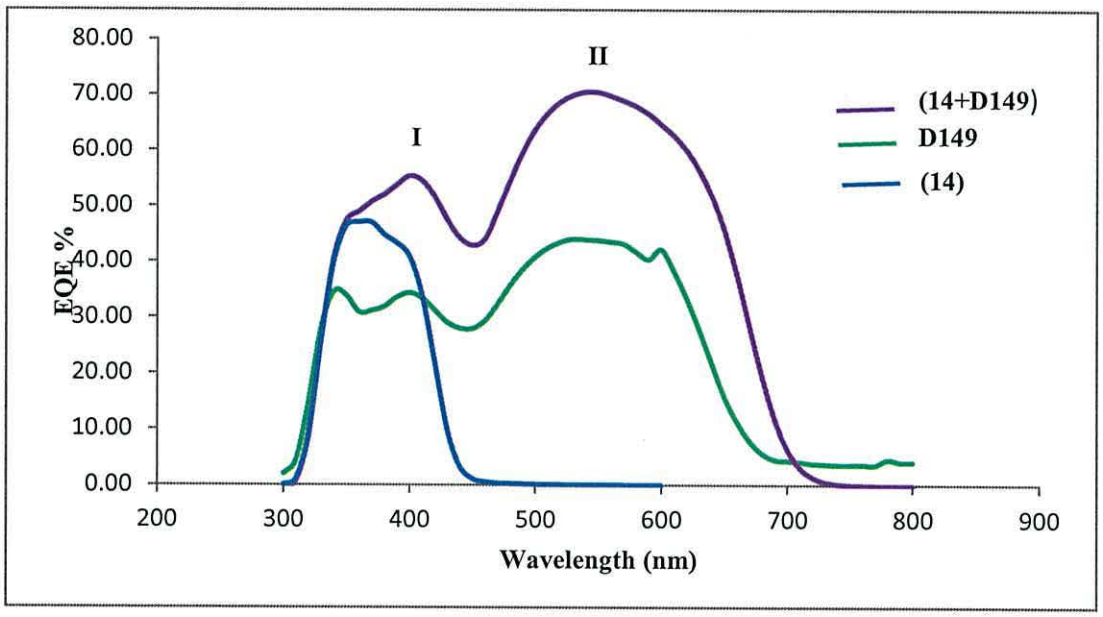

Figure 3.41. External quantum efficiency (EQE) *versus* wavelength. The blue line is for (**14**), the green line is for **D149** and the purple line is for co-sensitized (**14**) + **D149**.

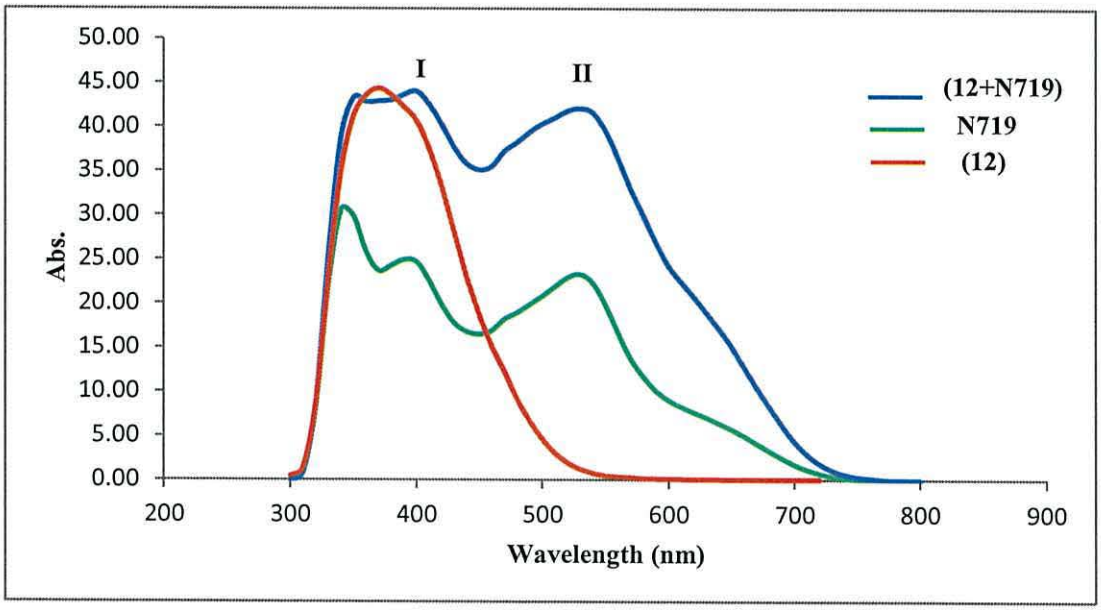

Figure 3.42. External quantum efficiency (EQE) *versus* wavelength. The red line is for (**12**), the green line is for **N719** and the blue line is for co-sensitized (**12**) + **N719.**

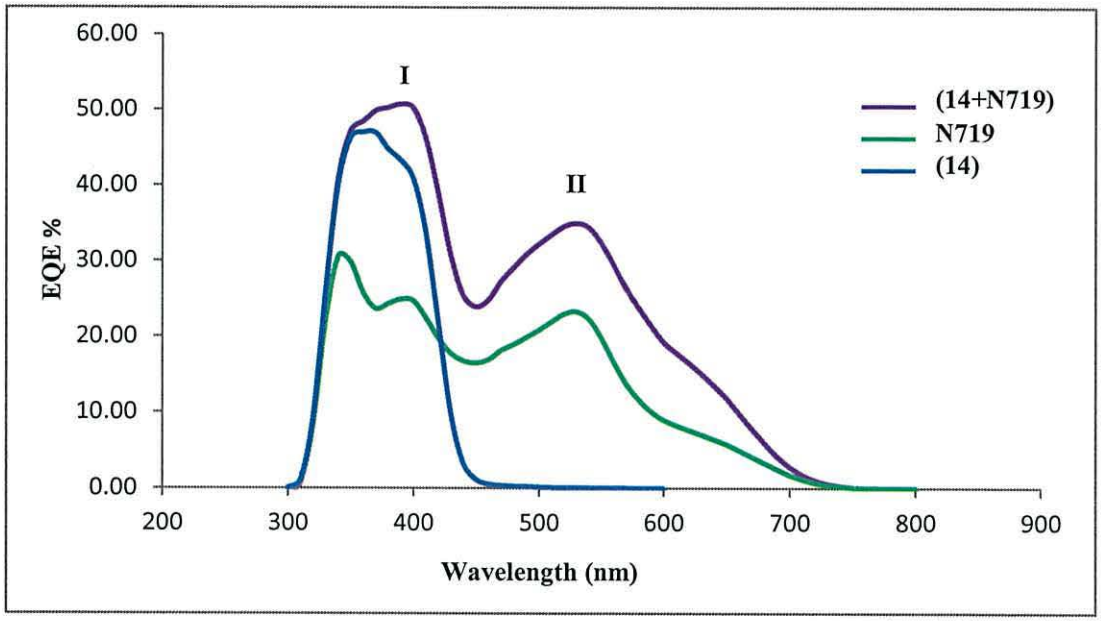

Figure 3.43. External quantum efficiency (EQE) *versus* wavelength. The blue line is for (**14**), the green line is for **N719** and the purple line is for co-sensitized (**14**) + **N719**.

Device L shows a maximum EQE of 42% at 530 nm for **N719** (II) and of 44% at 400 nm (I) for (**12**), while Device M shows a maximum EQE of 35% at 530 nm for **N719** (II) and of 51% at 390 nm (I) for (**14**).

Figure 3.44 confirms these dyes was adsorbed on the TiO_2 surface and changed the coulor of TiO_2 paste from white to yellow for single or double linkers dyes (**5**) and (**14**) devices , dark brown devices for **N719** (individual and co-sensitized), dark red for **D149** devices (individual and co-sensitized).

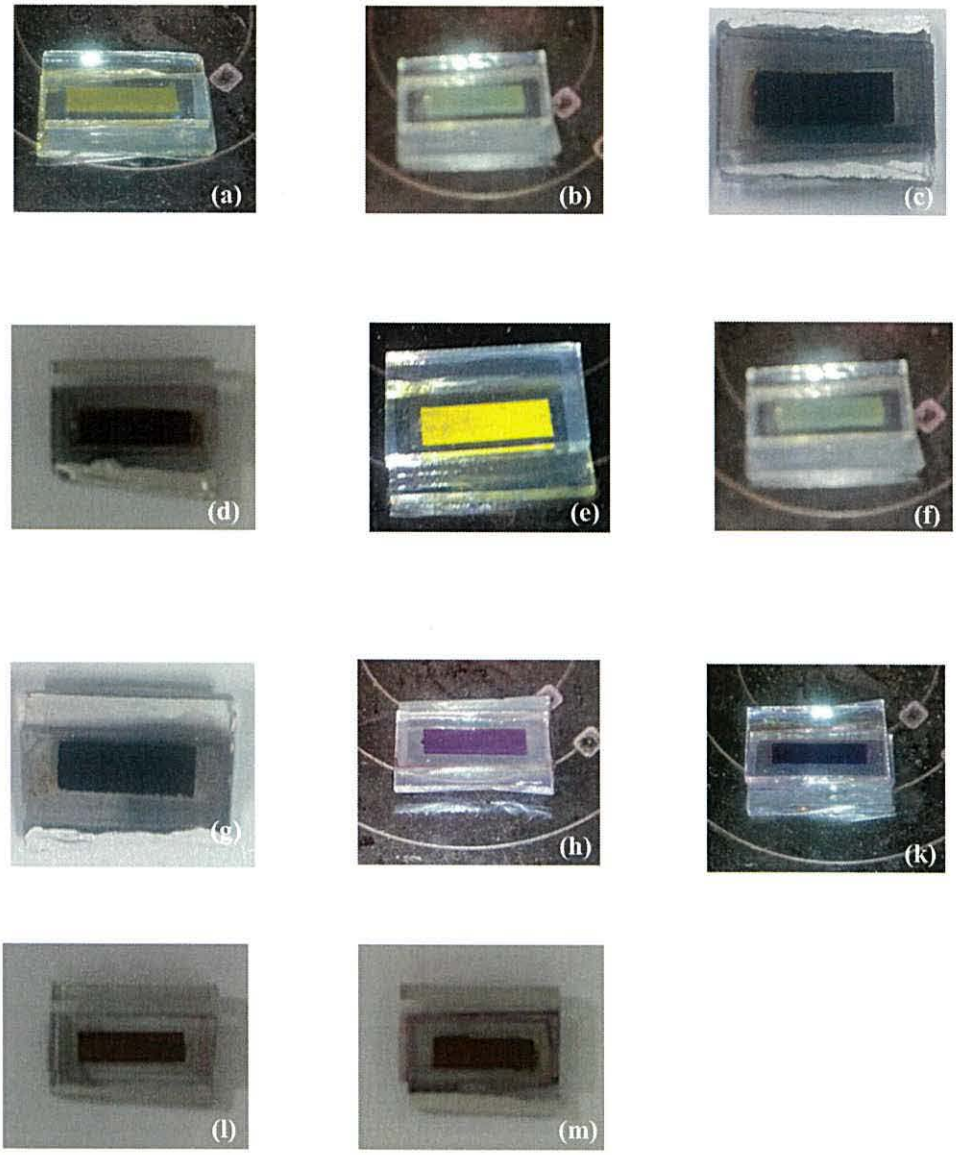

Figure 3.44. Photographs of DSC devices passive dyed (a) with (**12**), (b) with (**14**), (c) with **D149**, (d) **N719**, (e) (**12**), (f) (**14**), (g) **D149**. Meanwhile other cells were dyed as follows: - (h) (**12**) with **D149**, (k) (**14**) with **D149**, (l) (**12**) with **N719** and (m) (**14**) with **N719**.

Figure 3.44 confirms these dyes adsorb on TiO_2 by showing colour changes of the TiO_2 electrode from white to the according colour of each dye.

3.6 Conclusions

This chapter describe the synthesis of different types of triphenylamine-based dyes, and includes three new dyes ((**5**), (**12**) and (**14**)) and one re-synthesis. The purpose of re-synthesizing the red dye (**3**) was to measure (I-V) data to co-sensitize with other dyes and also to compare with the new dyes. The dyes can be divided into two groups: the first group uses single linkers (either cyanoacrylic or carboxylic acids), while the second group uses double linkers of either cyanoacrylic or carboxylic acids. The main purpose of synthesizing these dyes was to investigate the influence of the number of acceptor groups on the photocurrent and performance efficiency of D-π-A dyes.

The data obtained for these dyes showed that DSL 18NRT is the best TiO_2 paste. Also it has been proved that fast dying is better than passive dying, to reduce dyeing time and amount of dye used. However, the single-linker yellow dye shows a great stability compared N719 dye.

Dyes (**12**) and (**14**) gave results contrary to what was expected. The reason for not getting better results than (**3**) and (**5**) could be due to the molecular structures of these dyes. Looking carefully to the molecular structures of (**12**) and (**14**) it could be that the second acceptor group is not bound and that may reduce efficiency and weaken the dye bond strength with the semiconductor surface. The binding of molecules on TiO_2 surface by one acceptor group as shown in Figure 3.45 makes these dyes occupy more space on TiO_2 surface, which means fewer molecules linked to the surface, and that leads to a decrease in the amount of dye which adsorbs on TiO_2, decreasing the performance of devices. On other hand, there is another reason for reduce the performance photovoltaic and conversion efficiency, Xu *et al.* [20] studied the effects of increasing anchoring groups of triphenylamine sensitizers. They concluded that the charge of the donor shows a remarkable decrease with an increase in the numbers of anchoring groups, and observed that substituting more anchoring or acceptor groups led to a decrease in the electron donating ability of the donor group. [20]

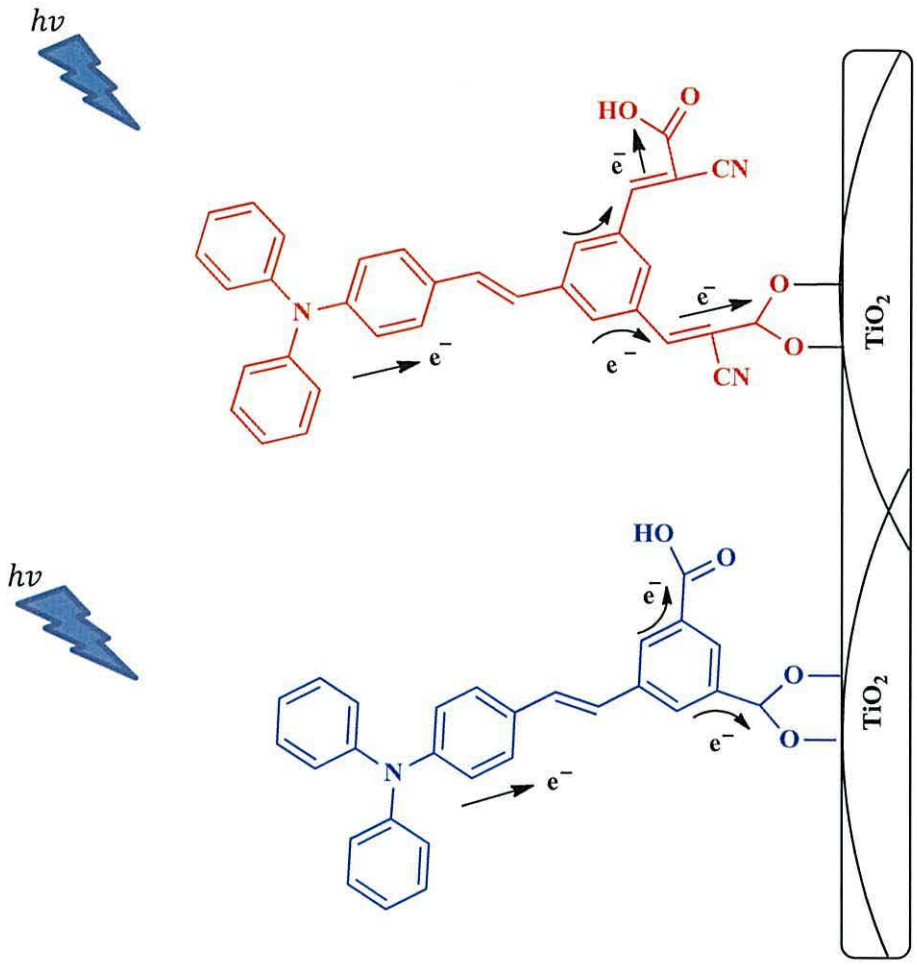

Figure 3.45. Show the possibility of two linkers dyes (**12**) and (**14**) to link on the semiconductor surface by anchoring group (carboxylic or cyanoacrylic acid).

3.7 References

1. S. Hwang, J. H. Lee, C. Park, H. Lee, C. Kim, C. Park, M. H. Lee, W. Lee, J. Park, K. Kim, N. G. Park, and C. Kim, *Chem. Commun.*, 2007, 4887.
2. J. Song, F. Zhang, C. Li, W. Liu, B. Li, Y. Huang, and Z. Bo, *J. Phys. Chem. C*, 2009, **113**, 13391–13397.
3. B. E. Maryanoff, A. B. Reitz, M. S. Mutter, R. R. Whittle, and R. A. Olofson, *J. Am. Chem. Soc.*, 1986, **108**, 7664–7678.
4. J. C. Sancho-García, C. L. Foden, I. Grizzi, G. Greczynski, M. P. de Jong, W. R. Salaneck, J. L. Brédas, and J. Cornil, *J. Phys. Chem. B*, 2004, **108**, 5594–5599.
5. D. P. Hagberg, J. H. Yum, H. Lee, F. De Angelis, T. Marinado, K. M. Karlsson, R. Humphry-Baker, L. Sun, A. Hagfeldt, M. Grätzel, and M. K. Nazeeruddin, *J. Am. Chem. Soc.*, 2008, **130**, 6259–6266.
6. J. Clayden, N. Greeves, S. Warren and P. Wothers, *in Organic Chemistry*, 2001, Oxford University Press.
7. S. W. Park, K.-I. Son, M. J. Ko, K. Kim, and N. G. Park, *Synth. Met.*, 2009, **159**, 2571–2577.
8. J. Baldenebro-López, J. Castorena-González, N. Flores-Holguín, J. Almaral-Sánchez, and D. Glossman-Mitnik, *Int. J. Mol. Sci.*, 2012, **13**, 4418–4432.
9. J. Xu, L. Wang, G. Liang, Z. Bai, L. Wang, W. Xu, and X. Shen, *Bull. Kor. Chem. Soc.*, 2010, **31**, 2531–2536.
10. D. Saxena, Manmeeta, Mridul Kumar Mathur, G. D. Sharma, and M. S. Roy, *International Conference on Electrical and Electronics Engineering (ICEEE'2012) June 16-17, 2012, Bangkok*, 2012, 5–9.
11. P. M. Sommeling, B. C. O'Regan, R. R. Haswell, H. J. P. Smit, N. J. Bakker, J. J. T. Smits, J. M. Kroon, and J. A. M. van Roosmalen, *J. Phys. Chem. B*, 2006, **110**, 19191–19197.
12. M. Malagoli and J. L. Brédas, *Chem. Phys. Lett.*, 2000, **327**, 13–17.
13. K.-F. Chen, Y. C. Hsu, Q. Wu, M. C. P. Yeh, and S. S. Sun, *Org. Lett.*, 2009, **11**, 377–380.
14. J. Preat, C. Michaux, D. Jacquemin, and E. A. Perpe`te, *J. Phys. Chem. C 2009*, 2009, **113**, 16821–16833.
15. P. J. Holliman, M. Mohsen, A. Connell, M. L. Davies, K. Al-Salihi, M. B. Pitak, G. J. Tizzard, S. J. Coles, R. W. Harrington, W. Clegg, C. Serpa, O. H. Fontes, C. Charbonneau, and M. J. Carnie, *J. Mater. Chem.*, 2012, **22**, 13318–13327.

16. P. J. Holliman, M. L. Davies, A. Connell, B. V. Velasco, and T. M. Watson, *Chem. Commun.,* 2010, **46**, 7256.
17. A. Osuka, B. L. Liu, and K. Maruyama, *J. Org. Chem.*, 1993, **58**, 3582–3585.
18. D. Z. Al-Kremawi, PhD thesis, Bangor University, 2011.
19. E. J. Corey and J. W. Suggs, *Tetrahedron Lett.*, 1975, **16**, 2647–2650.
20. J. Xu, L. Zhu, L. Wang, L. Liu, Z. Bai1, L. Wang and W. Xu, *J. Mol. Model.*, 2012, **18**.
21. W. Xu, B. Peng, J. Chen, M. Liang, and F. Cai, *J. Phys. Chem. C*, 2008, **112**, 874–880.
22. W. Xu, J. Pei, J. Shi, S. Peng, and J. Chen, *J. Power Sources*, 2008, **183**, 792–798.
23. M. P. Balanay, S. Kim, M. J. Lee, S. H. Lee, and D. H. Kim, *Bull. Kor. Chem. Soc.*, 2009, **30**, 2077–2082.

Chapter 4
Cyanine dyes and derivatives

4.1 Cyanine dyes and derivatives

The aim of this chapter was to synthesize and characterize new symmetric and unsymmetric cyanine dyes which can absorb light in the visible and near-infrared (NIR) regions of the electro-magnetic spectrum and to investigate their performance as sensitizers in DSC devices. There is not much literature on the synthesis and study of these dyes which contain an indole moiety and a methine group. A common feature of all the symmetric and unsymmetric cyanine dyes studied is a chlorocyclohexene group as a central unit. The chlorinated central unit substitutes at the *meso* carbon for cyanine dyes which have been synthesized.

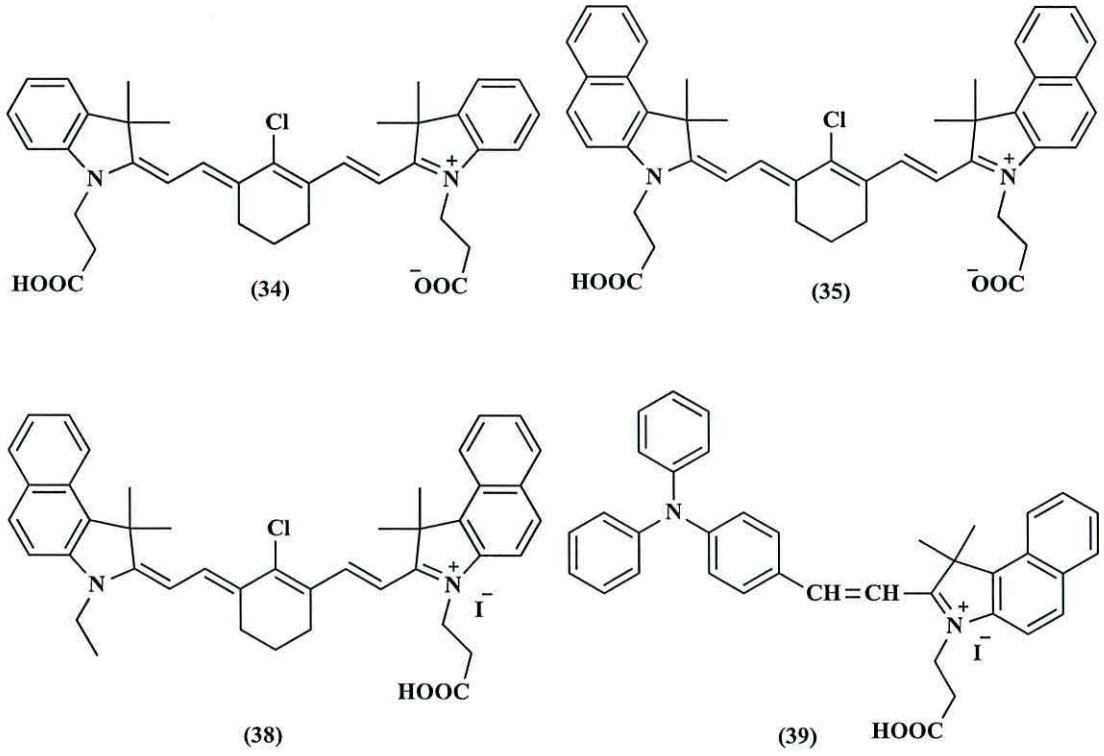

Figure 4.1. The molecular structure of symmetrical and unsymmetrical cyanine dyes, (**34**), (**35**), (**38**) and (**39**).

In general, the literature reports that there are two common methods used to synthesize symmetric and unsymmetric cyanine dyes; both of which need heating. [1] The first method uses sodium acetate as a catalyst and involves a condensation reaction of a heterocyclic base with an active methyl group with an unsaturated *bis*-aldehyde using a mixture of acetic acid and acetic anhydride or ethanol as the solvent in the reaction. [1, 2] The second method, does not involve a catalyst and instead

refluxes the reactants in a mixture of 1-butanol: benzene (7:3, v\v) or DMF as solvent. [1, 3]

In this thesis, the second method has been studied to synthesize cyanine dyes and derivatives using either DMF or a mixture of 1-butanol: benzene (7:3, v\v) as a solvent in the reaction. The water which formed during the reaction using (1-butanol: benzene, v/v), was removed and collected by using Dean-Stark condenser. [1, 3] Despite, the first method being faster than the second method it suffers from some disadvantages like the purification of the product being more difficult because of the catalyst which interferes with the purity of the product. Also this method cannot be used to synthesize unsymmetric cyanine dyes because the rate of reaction is too fast to control. However, the second (uncatalyzed) method is slower and allows unsymmetric cyanines to form from two different heterocycles attaching to the central unit in a single pot with a good yield. [1]

4.1.1 Synthesis of 3-((E)-2-((E)-2-(3-((E)-2-(1-(2-carboxyethyl)-3, 3-dimethylindolin-2-yl) vinyl)-2-chlorocyclohex-2-en-1-ylidene) ethylidene)-3, 3-dimethylindolin-1-yl) propionic acid compound (34).

The synthesis of compound (**34**) was attempted using the uncatalyzed method by using different solvents to study the effect on the purity and yield. The successful synthesis of symmetrical (**34**) was achieved using DMF as the solvent by two steps as shown in Scheme 4.1.

The first step was to synthesize 1-carboxyethyl-2, 3, 3-trimethyl indolium iodide (**29**) as shown in Figure 4.2 by reacting 2, 3, 3-trimethyl-3H-indole with iodopropionic acid in 1, 2-dichlorobenzene (as described in the experimental section) to produce a yellow-orange solid of (**29**) (1.4 g, 96 % yield). Since the solvent was difficult to remove using a rotary evaporator instead it was removed by flash distillation under high vacuum due to the high boiling point of 1, 2-dichlorobenzene (180.5 °C).

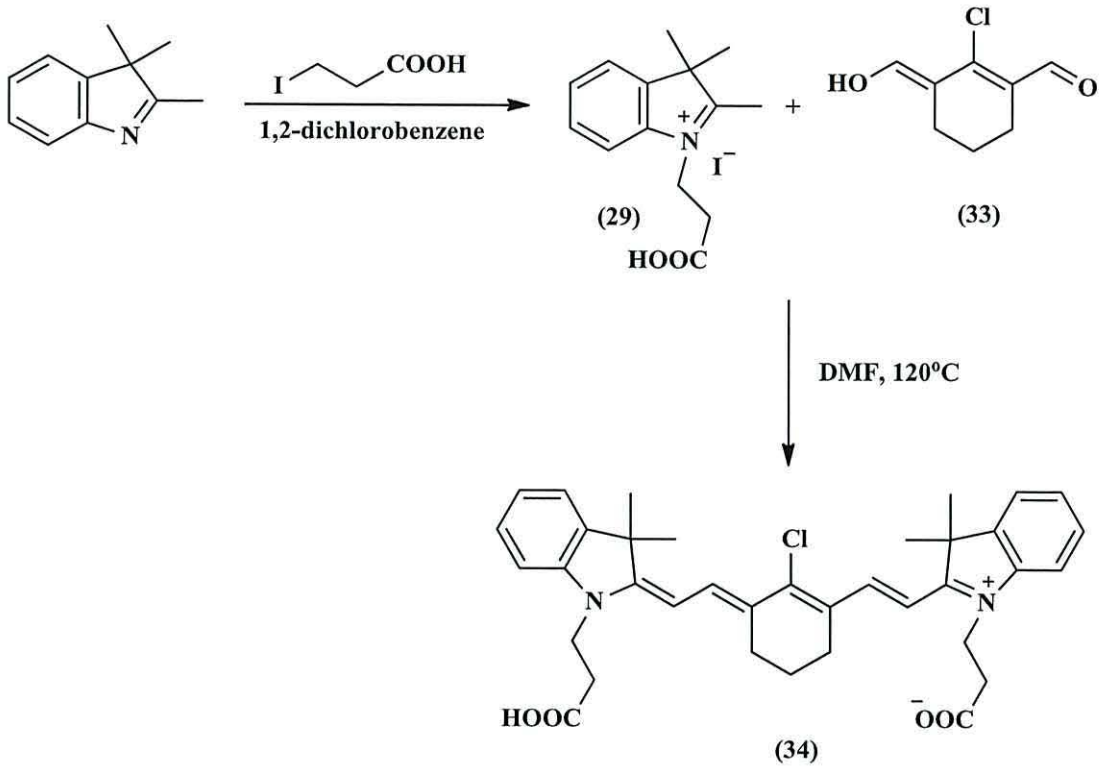

Scheme 4.1. Synthetic pathway of 3-((E)-2-((E)-2-(3-((E)-2-(1-(2-carboxyethyl)-3, 3dimethylindolin-2-yl) vinyl)-2-chlorocyclohex-2-en-1-ylidene) ethylidene)-3, 3-dimethylindolin-1-yl) propionic acid (**34**).

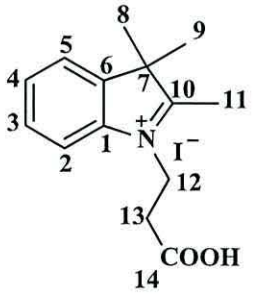

Figure 4.2. The molecular structure of 1-carboxyethyl-2, 3, 3-trimethyl indolium iodide (**29**) showing atom labelling to aid NMR assignments.

Inspection of the ^{1}H NMR spectrum of (**29**) shows the presence of signals at 1.52 and 2.84 ppm due to methyl groups H-8, H-9, H-11. A triplet at 2.97 ppm is due to (*CH_2*-COOH, H-13), and the signal at 4.64 ppm (a triplet) is due to (-N-*CH_2*-, H-12). This CH_2 signal is shifted to down field due to the electron withdrawing effect of neighbouring nitrogen deshielding these protons. Multiplet signals at 7.62, 7.38 and 7.98 ppm are assigned to (*Ar-H*, H-2, H-3, H-4 and H-5). The singlet at 12.73 ppm is

due to CH_2-*COOH* (H-14). ^{13}C NMR shows signals at 14.26, 21.84 ppm due to the methyl groups (3x-CH_3, C-11, C-8 and C-9), and signals at 39.01 and 54.23 ppm due to (-CH_2-CO_2H, C-13) and (-N-CH_2, C-12), respectively. The signals at 115.52, 123.44, 128.89 and 129.33 ppm are due to (*Ar-C-H*), whilst the signals at 140.80 and 141.73 ppm due to (*Ar-C*-C). Finally, the signal at 171.47 ppm is due to (-*COOH*, C-14), whilst the last signal at 197.89 ppm is assigned to (Indole *C*-CH_3, C-10). [3] The most important characteristics of the FTIR spectrum are a broad peak around 3400 cm^{-1} due to ν (OH) of the carboxylic acid, peaks at 3046 and 3034 cm^{-1} which are assigned to ν (C-H) from the aromatic ring, along with peaks at 2972, 2920 and 2863 cm^{-1} which are assigned to ν (C-H) either from the aromatic ring or from the CH_3 and CH_2 groups. In the remainder of the spectrum, a sharp peak at 1730 cm^{-1} is assigned to the carbonyl of carboxylic acid, and a weaker peak at 1594 cm^{-1} which is ascribed to ν (C=C) benzene ring stretches. The mass spectrometry data confirm the target compound (**29**) and show the most prominent peak at 232.1333, which corresponds to an accurate mass for (**29**) $[M+H]^+$. The data obtained from mass spectrometry confirms the purity of (**29**) by showing the absence of other peaks and showed only the peaks of (**29**).

Single crystal X-ray structural analysis confirms the target compound (**29**) has been synthesized, and the molecular structure is shown in Figure 4.3. This shows the molecule structure of an indole with a 1-carboxyethyl group linked to N with an iodide counter ion located between the methyl groups in proximity to the positive charged N of the indole confirming that an iodide salt had been formed. Selected bond lengths (Å) and angles (°) are listed in Table 4.1. All the angles in the benzene ring are close to 120° as expected for a hexagonal arrangement whilst those within the five membered rings are close to 112° as expected for pentagonal arrangement of atoms. [4] The (C-N) bond lengths are a mixture in values normally reported for single (C-N) bonds and double (C=N) bonds for (N1-C1) and (N1-C10) with bond lengths of 1.411 (9) Å and 1.291 (9) Å, respectively. The carbon-carbon bond lengths of the molecular skeleton show values consistent with both (C-C) and (C=C) bonds; 1.533 (6) Å and 1.372 (10) Å, respectively. The bond lengths of benzene ring are around 1.372 and 1.400 Å. [5]

Table 4.1. Selected bond lengths [Å] and angles [°] for (**29**).

N1-C1	1.411 (9) Å	C3-C4	1.392 (10) Å
N1-C12	1.479 (9) Å	C4-C5	1.394 (10) Å
N1-C10	1.291 (9) Å	C5-C6	1.400 (10) Å
C1-C2	1.372 (10) Å	C12-C13	1.505 (10) Å
C1-C6	1.381 (10) Å	C13-C14	1.506 (10) Å
C7-C8	1.533 (10) Å	C1-N1-C12	123.1 (6) °
C7-C9	1.522 (10) Å	C10-N1-C12	124.5 (7) °
C10-C11	1.472 (11) Å	C1-N1-C10	112.4 (7) °

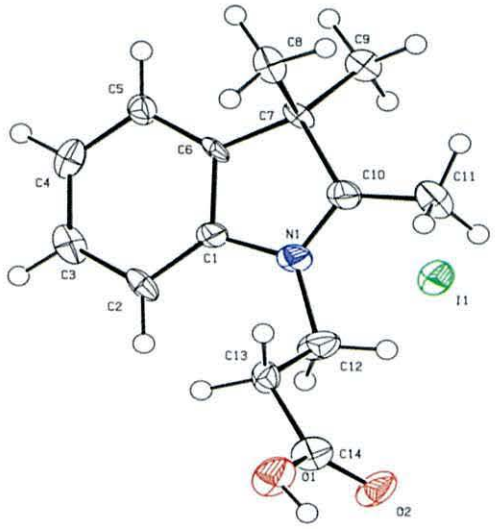

Figure 4.3. Single crystal X-ray structure of 1-carboxyethyl-2, 3, 3-trimethyl indolium iodide (**29**).

The central unit of the cyanine (**33**) was then synthesized by following a literature method developed from Funabiki *et al.* [3] The central unit (**33**) was found to be unstable at room temperature (as reported in the literature for related compounds) and so needed careful with handling and storage in the fridge at *ca.* 5 °C. [6] The central unit which was reported by Funabiki *et al.* actually contained an ethyl group substituted on the cyclohexene ring para to the chlorine. This is different from (**33**) which had no ethyl group. Compound (**33**) was synthesized by Vilsmeier-Haak formylation of cyclohexanone with dimethylformamide (DMF) and phosphoryl

chloride $POCl_3$, and then hydrolyzed to give (**33**) as the central unit, (Figure 4.4). It has been reported [3] that the chlorine group in the bis-aldehyde (**33**) plays important role in this reaction especially in the absence of a catalyst, because the electron withdrawing nature of the chlorine makes the aldehydic protons more acidic and so more reactive. It has also been reported that the chlorine can be replaced with variety nucleophiles to produce many heptamethine cyanine dyes. [1] In addition, the delocalization of π-electron makes (**33**) a more reactive compound for the subsequent cyanine dyes synthesis as shown in Figure 4.5.

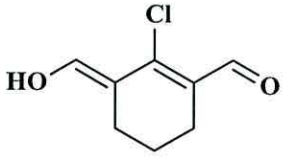

Figure 4.4. The molecular structure of 2-chloro-1-formyl-3-(hydroxymethylene) cyclohex-1-ene (**33**).

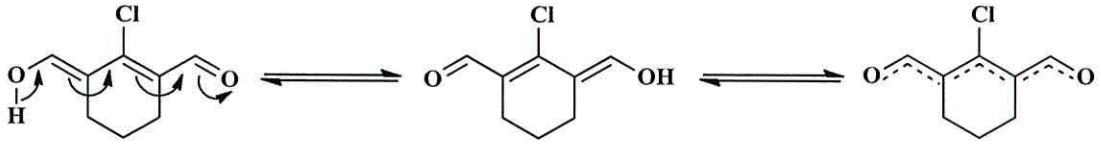

Figure 4.5. The delocalization of electrons in 2-chloro-1-formyl-3-(hydroxymethylene) cyclohex-1-ene (**33**).

The final step was to synthesize the cyanine dye 3-((E)-2-((E)-2-(3-((E)-2-(1-(2-carboxyethyl)-3, 3dimethylindolin-2-yl) vinyl)-2-chlorocyclohex-2-en-1-ylidene) ethylidene)-3, 3-dimethylindolin-1-yl) propionic acid (**34**). The successful synthesis was achieved using a method developed from Funabiki *et al.* [3] The synthesis was carried out by reacting 1-carboxyethyl-2, 3, 3-trimethyl-1-indolium iodide compound (**29**) (2 eq) with 2-chloro-1-formyl-3-(hydroxymethylene) cyclohex-1-ene (**33**) as a central unit. DMF was used as a solvent without any catalyst. The mixture reaction was heated at 120°C for 2 h. After finishing the reaction, the solution was cooled to RT, and then the solvent was removed using rotary evaporator. The resulting product (**34**) was purified by using column chromatography on silica gel eluting with methylene chloride/methanol (10:1, v/v). The solvent was reduced after collecting compound (**34**) vials. The solutions were treated by bubbling nitrogen through them to slowly reduce the solvent and also in order to remove any oxygen or water from

the flask in order to grow crystals in the mother liquor under a nitrogen atmosphere. After this the product was left at ambient temperature to form crystals as shown in Figure 4.7. A photograph of the purification of (**34**) by column chromatography is shown in Figure 4.6 b. The purification of this cyanine dye was not easy and required the column chromatography to be repeated twice to obtain pure cyanine dye because after checking by TLC, the product of the first column showed more than one spot. Repeating the column again gave a pure product of (**34**).

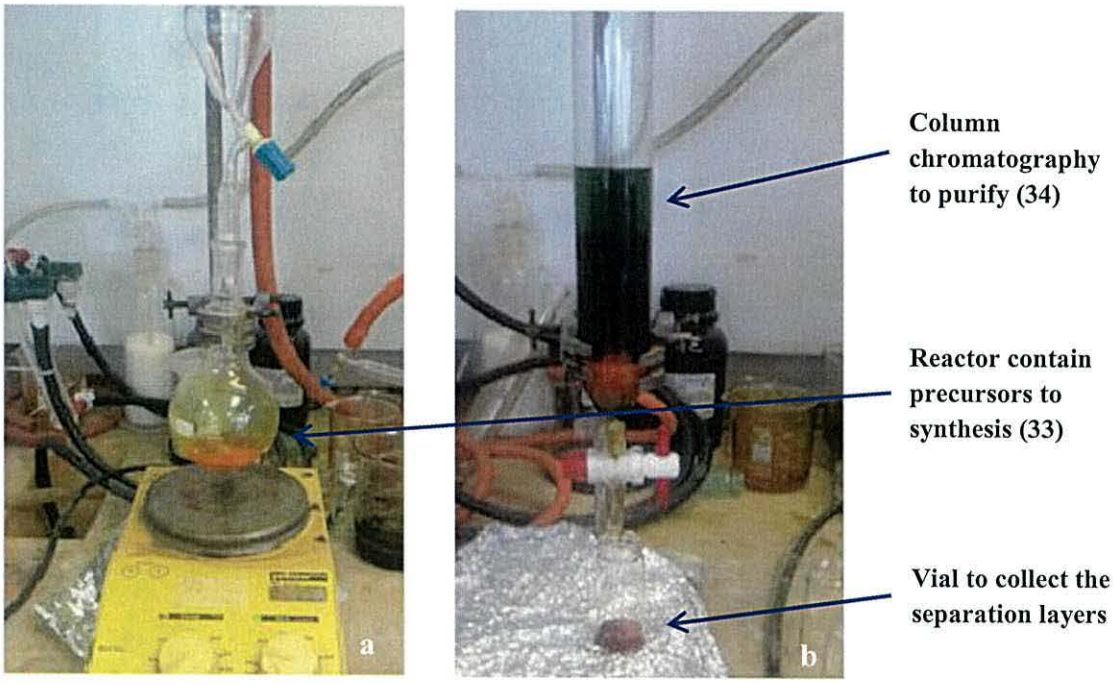

Figure 4.6. Photographs showing (a) the synthesis reaction of (**33**) and (b) the first column chromatography of the purification of (**34**).

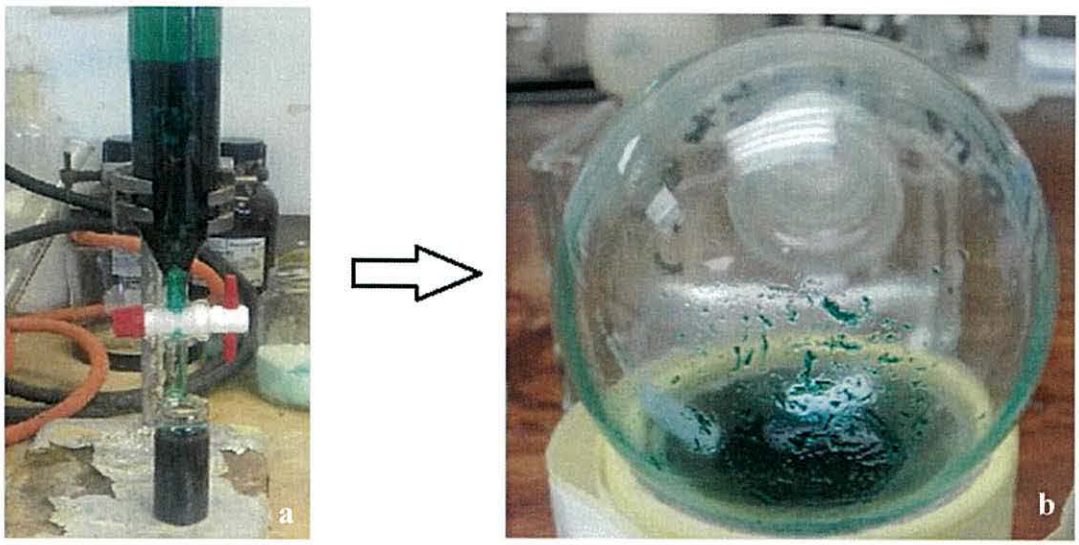

Figure 4.7. Photographs of (a) the second column chromatography to purify (**34**) and (b) crystals of (**34**) formed after slow evaporation.

Both ^{1}H NMR (Figure 4.9b) and ^{13}C NMR confirm the successful synthesis of (**34**). The signal at 1.73 ppm in the ^{1}H NMR is a singlet and is due to the methyl groups (H-12, H-13, H-26, H-27), the triplets at 1.96 and 2.70 ppm are due to CH_2 groups on the central unit (H-18 and H-17, H-19), respectively. Triplet signals at 2.76 and 4.42 ppm are due to (-CH_2-COOH, H-8 and H-35) and (-N-CH_2-, H-7 and H-34), respectively (see Figure 4.8). The signals at 6.45 and 8.42 ppm are doublets due to (-*CH=CH*-, H-7, H-10, H-8 and H-11) with the coupling constants J= 14.04 and 14.08 Hz, respectively which confirms a *trans* arrangement. The data also show signals at 7.27, 7.40 and 7.50 ppm as triplet, doublet triplet and doublet which are assigned to protons on the aromatic ring (H-3, H-31), (H-2, H-32), (H-4, H-30) and (H-5, H-29), respectively. The ^{13}C NMR data show signals at 22.16 ppm due to (CH_2-cyclohexene, C-18), and signal at 27.37 ppm which is assigned to (2x-CH_2-cyclohexene, C17, C-19), 28.30 ppm which is due to (4x-CH_3, C-12, C-13, C-26, C27), a signal at 34.96 ppm due to (2x-CH_2-COOH, C-8, C-35), one at 42.45 ppm due to (*C*-$(CH_3)_2$, C-11, C-25) and, a signal at 50.60 ppm which is ascribed to (2x-N-CH_2-, C-7, C-34). The signals at 102.89 and 103.98 ppm are due to (-*CH=CH*-, C-14, C-23), whilst the signals at 112.36, 123.42, 126.46, 128.52 ppm are assigned to (*Ar-C-H*, C-2, C-3, C-4, C-5, C-29, C-30, C-31 and H-32). Another signal at 129.85 ppm is assigned to (*Ar-C*-Cl-, C-21). Also signals at 142.64, 143.39 ppm due to (*Ar-C*-C, C-1, C-6, C-28 and C-33), and a signal at 144.43 ppm is assigned to (-*CH=CH*-

, C-15, C-22), with the signals at 145.52, 151.01 ppm ascribed to (*Ar-C*-C, C-20 and C-16). The signals at 174.16 and 176.39 ppm due to (C-N) and (C=O*)*, respectively. The UV-Vis spectrum of (**34**) (Figure 4.10) shows a strong and sharp absorption beak at 780 nm (I) with a high molecular coefficient (ε = 180,414 $M^{-1}cm^{-1}$) in methanol, along with a shoulder at 712 nm (II) corresponding to dye aggregation. [7, 8]

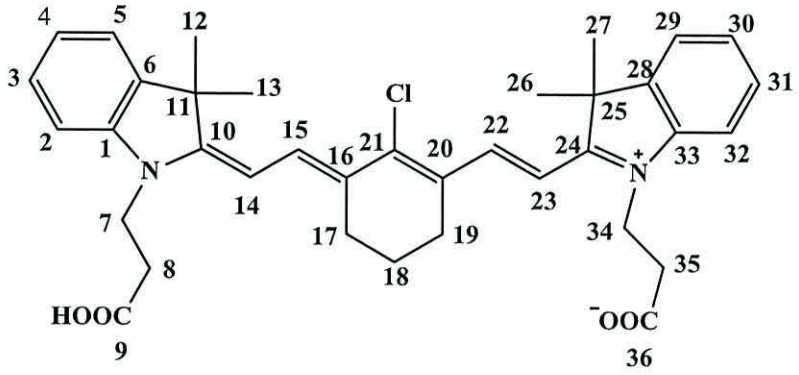

Figure 4.8. Molecular structure of 3-((E)-2-((E)-2-(3-((E)-2-(1-(2-carboxyethyl)-3, 3dimethylindolin-2-yl) vinyl)-2-chlorocyclohex-2-en-1-ylidene) ethylidene)-3, 3-dimethylindolin-1-yl) propionic acid **(34)** showing labelling for NMR assignments.

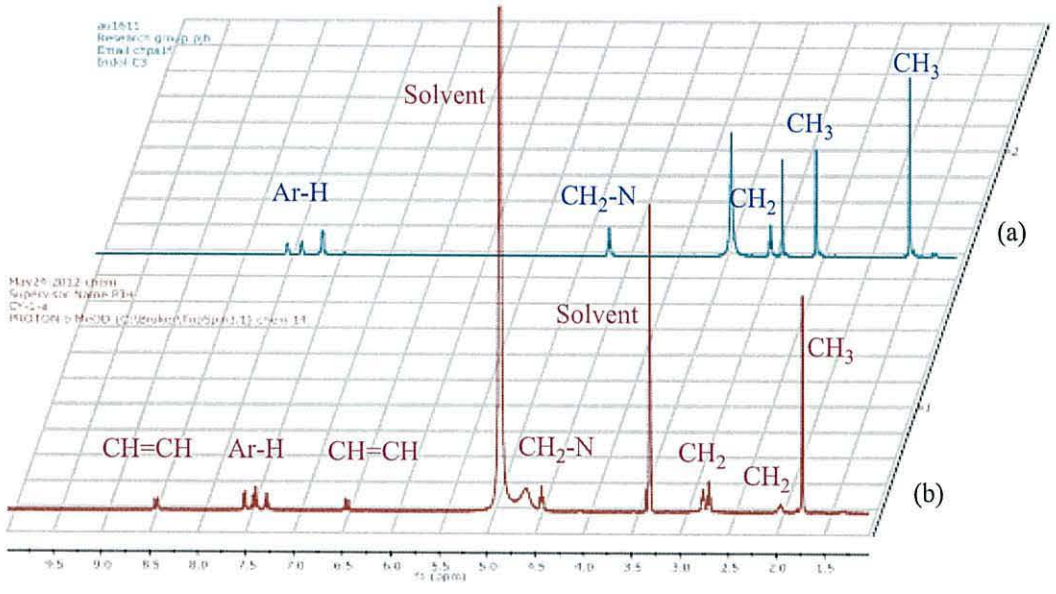

Figure 4.9. ^{1}H NMR spectra showing of (a) the blue line is for (**29**) and (b) the red line is for (**34**).

The comparison of (**34**) with the Funabiki paper [3] (Figure 4.11) shows that (**34**) absorbs at the same λ_{max} (780 nm) as the literature. The molar extinction coefficient of (**34**) was lower than the literature analogue and that could be assigned to the additional ethyl group on the cyclohexene ring of the central unit which increases the absorption intensity. The Funabiki compound also shows H-aggregation which represented by the shoulder at 730 nm. [3]

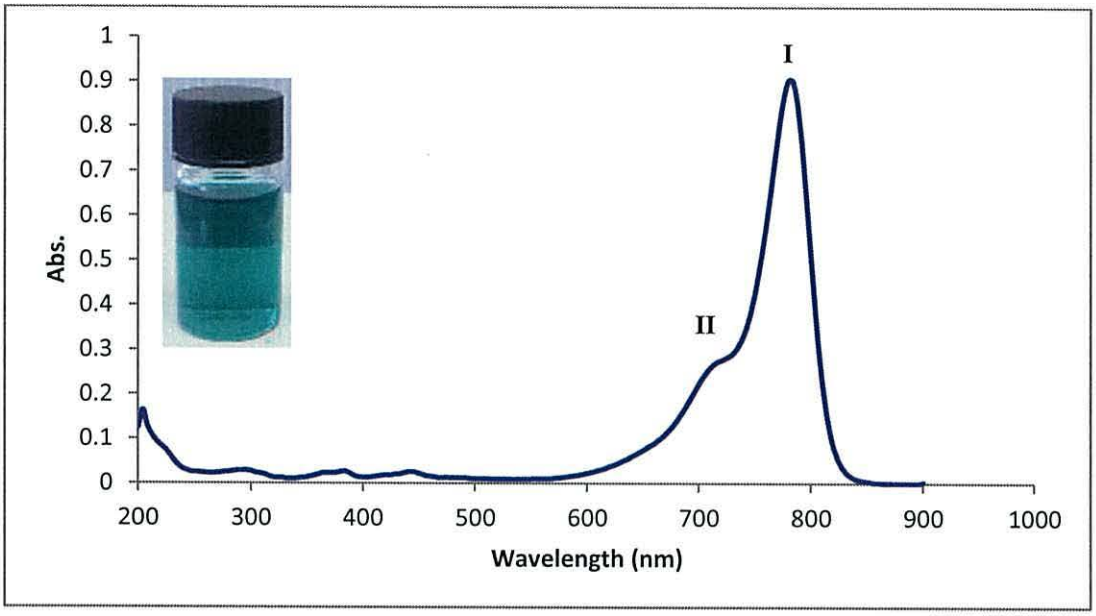

Figure 4.10. UV-Vis spectrum of 3-((E)-2-((E)-2-(3-((E)-2-(1-(2-carboxyethyl)-3, 3dimethylindolin-2-yl) vinyl)-2-chlorocyclohex-2-en-1-ylidene) ethylidene)-3, 3-dimethylindolin-1-yl)propanoic acid (**34**) in MeOH $0.5x10^{-5}$ M. The data show ε = 180,414 $M^{-1}cm^{-1}$ at 780 nm, in set (**34**) in solution.

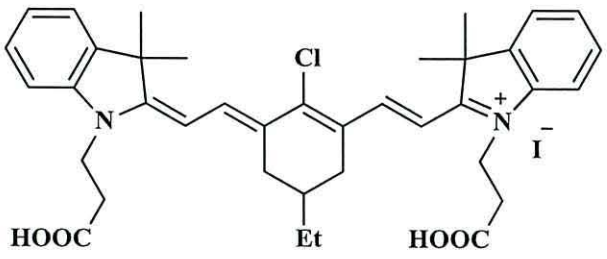

Figure 4.11. The molecular structure of the Funabiki compound **KFH-2**, ε= 263,000 $M^{-1}cm^{-1}$ at 780 nm. [3]

This aggregation is in line with the previous reports that cyanine molecules interact strongly with each other in solution and thus have a strong tendency to aggregate. [9]

The molar extinction coefficient (ε) of (**34**) has been found by measuring the absorbance for a variety of different dye concentrations in solution. Figure 4.12 shows the UV-Vis spectra for different concentrations of (**34**). The molar extinction coefficient for (**34**) was found by drawing calibration curve between absorbance *versus* concentration (mol L^{-1}), as shown in Figure 4.21 and from the slope can be found ε= 180,414 $M^{-1}cm^{-1}$.

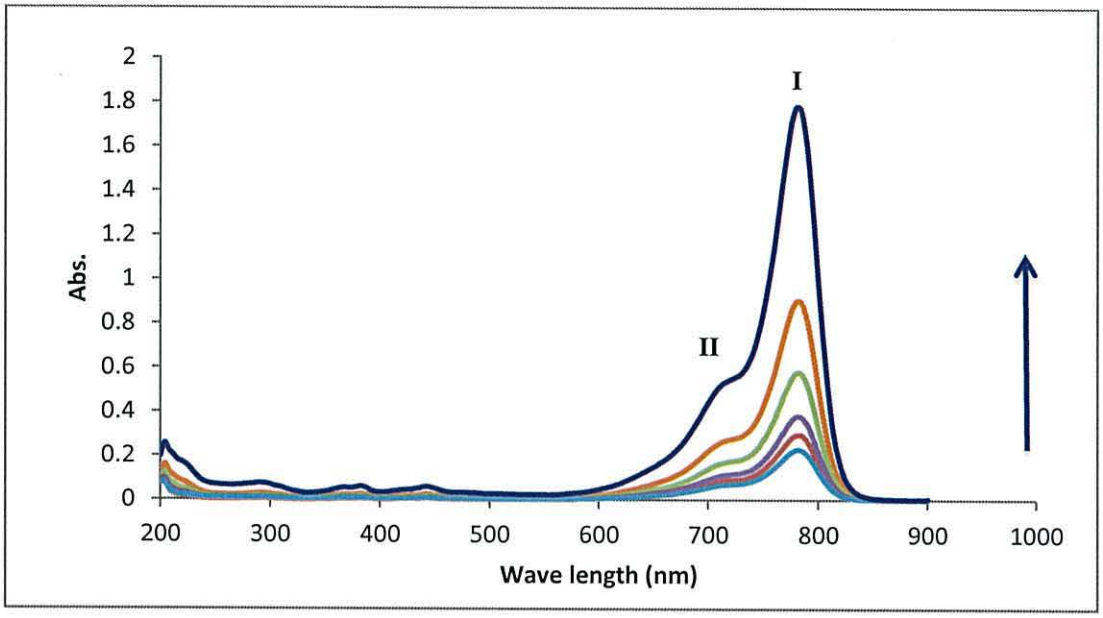

Figure 4.12. UV-Vis spectrum of 3-((E)-2-((E)-2-(3-((E)-2-(1-(2-carboxyethyl)-3, 3dimethylindolin-2-yl) vinyl)-2-chlorocyclohex-2-en-1-ylidene) ethylidene)-3, 3-dimethylindolin-1-yl)propanoic acid (**34**) at different dye concentrations ($0.5x10^{-5}$, $1x10^{-}5$, $1x10^{-6}$, $1.5x10^{-6}$, $2x10^{-6}$, $3x10^{-6}$ M) in MeOH.

Figure 4.12 shows that the relative ratio of intensities between peaks I and II remained the same despite the changes in dye concentration, at 0.29 (found by dividing λ_{max} for (I) on λ_{max} for (II)). This suggests that the amount of dye aggregation is relatively the same across the range of dye concentrations tested.

The data from mass spectrometry using accurate mass measurements also confirm the target compound (**34**) has been successfully synthesized. Figure 4.13 shows the most prominent peak at 597.2520, which corresponds to (**34**), $[M-H]^+$. In addition the data also shows a small peak at 631.2560 which corresponds to compound (**34**) $[M+CH_3OH]^+$, which is believed to be produced from strong solvent-dye interactions (presumably based around hydrogen bonding) between compound (**34**) and methanol

molecules which were used as the solvent for recrystallization. This is interesting and was not reported previously for similar dyes. [3] On other hand, the mass data gives good evidence of the purity of (**34**) by showing only peaks for (**34**).

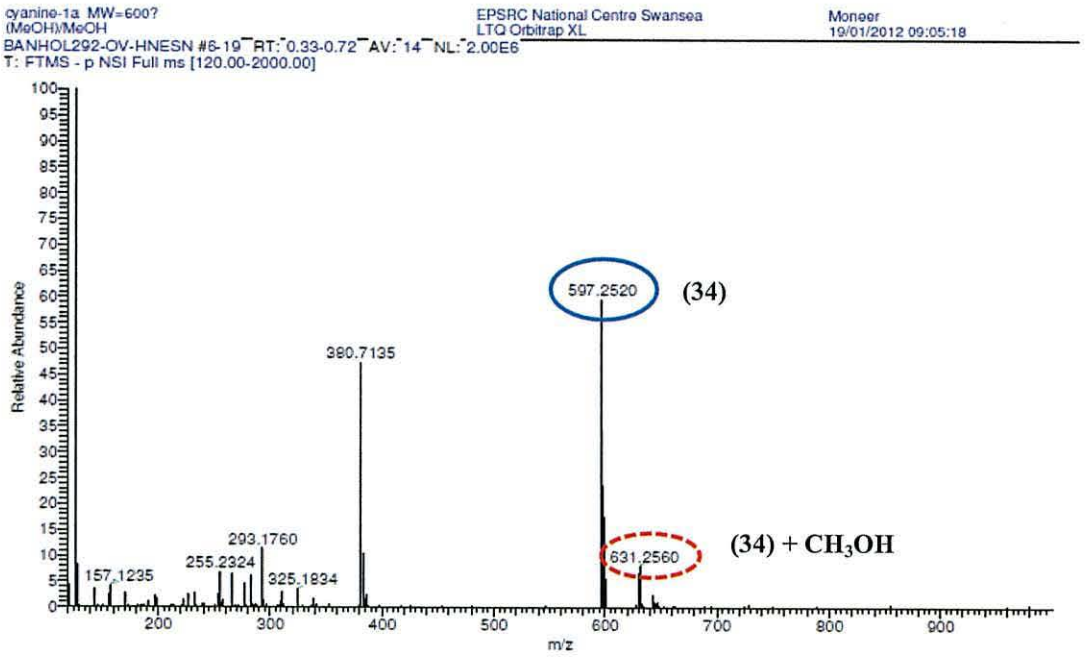

Figure 4.13. Electrospray negative mass spectrum of 3-((E)-2-((E)-2-(3-((E)-2-(1-(2-carboxyethyl)-3, 3dimethylindolin-2-yl) vinyl)-2-chlorocyclohex-2-en-1-ylidene) ethylidene)-3, 3-dimethylindolin-1-yl) propanoic acid (**34**).

Single crystals for X-ray structure determination were again obtained by the evaporation method, using methanol as the solvent. The molecular structure of (**34**) is shown in Figure 4.14. The data show monoclinic crystals of (**34**) in the space group *P*21/*c*. Details of the determination and selected bond lengths (Å) and angles (°) are listed in Table 4.2. The molecular structure confirms that two indole molecules are linked symmetrically to the central unit. In the unit cell (Figure 4.16), two molecules of (**34**) are assembled in a centro-symmetric dimer by means of two intermolecular hydrogen bonds created by H-bonding interaction between H4a from one cyanine molecule linking with the carboxylate group for another cyanine molecule. As was observed in the crystal structure data for the indole (**29**), the carbon-carbon bond angles for the indole units of (**34**) are close to 120° in the benzene ring and close to 111° in the indole moiety (a five-membered ring), [4] as shown by the angles (C6-N1-C7), (C7-N1-C10), (C6-N1-C10), (C42-N2-C34),

(C33-N2-C34) and (C24-N2-C33). These data are in the good agreement with indole moiety angles which have been reported previously. [5]

Table 4.2. Selected bond lengths [Å] and angles [°] for cyanine-1-compound (**34**).

C6-N1	1.4176 (19) Å	C23-C24	1.390 (2) Å
C7-N1	1.4728 (18) Å	C7-C8	1.517 (2) Å
C10-N1	1.3539 (18) Å	C8-C9	1.527 (2) Å
C24-N2	1.3564 (18) Å	C34-C35	1.530 (2) Å
C33-N2	1.4119 (18) Å	C35-C36	1.514 (2) Å
C34-N2	1.4676 (18) Å	C6-N1-C10	111.52 (12) °
C10-C14	1.393 (2) Å	C6-N1-C7	122.46 (12) °
C14-C15	1.390 (2) Å	C7-N1-C10	126.02 (12) °
C15-C16	1.399 (2) Å	C24-N2-C33	111.44 (12) °
C20-C22	1.391 (2) Å	C24-N2-C34	124.35 (12) °
C22-C23	1.395 (2) Å	C33-N2-C34	123.25 (12) °

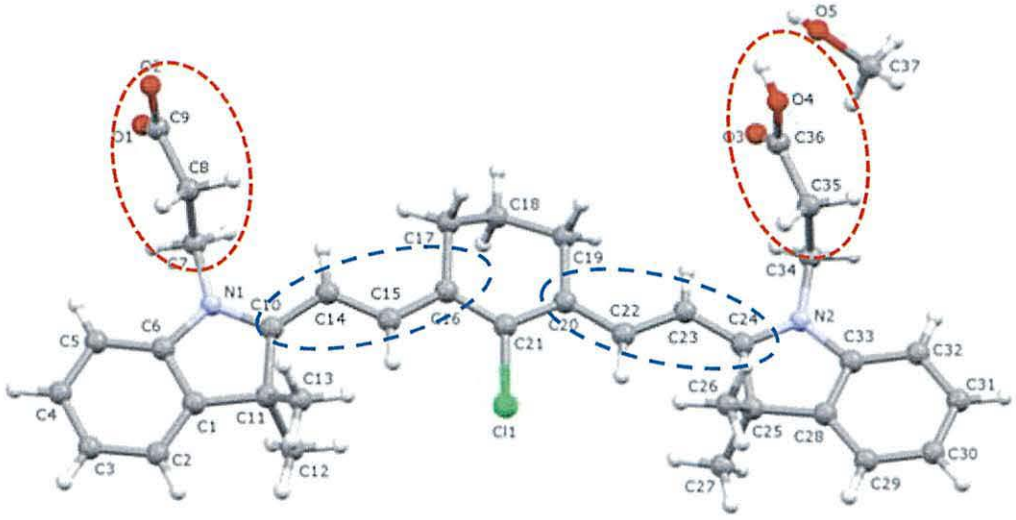

Figure 4.14. The molecular structure (**34**). The blue dashed cycle represent the planarity of the indole groups with molecule skeleton and the red dashed cycle represent the co-linearity of carboxylic and alkyl chains with the molecule skeleton.

The torsion angles data have also been investigated to investigate the planarity and linearity of the molecule. This is important in the context of DSC devices because the longer term aim of this work has been to study these dyes as titania sensitizers. For

this end-use, the molecules will be adsorbed on the metal oxide surface (see section 4.2 and 4.3) and the mode of adsorption (e.g. linear, monodentate bonding or "gate-leg" bidentate bonding) are believed to potentially be important factors affecting dye performance, as shown in Figure 4.15.

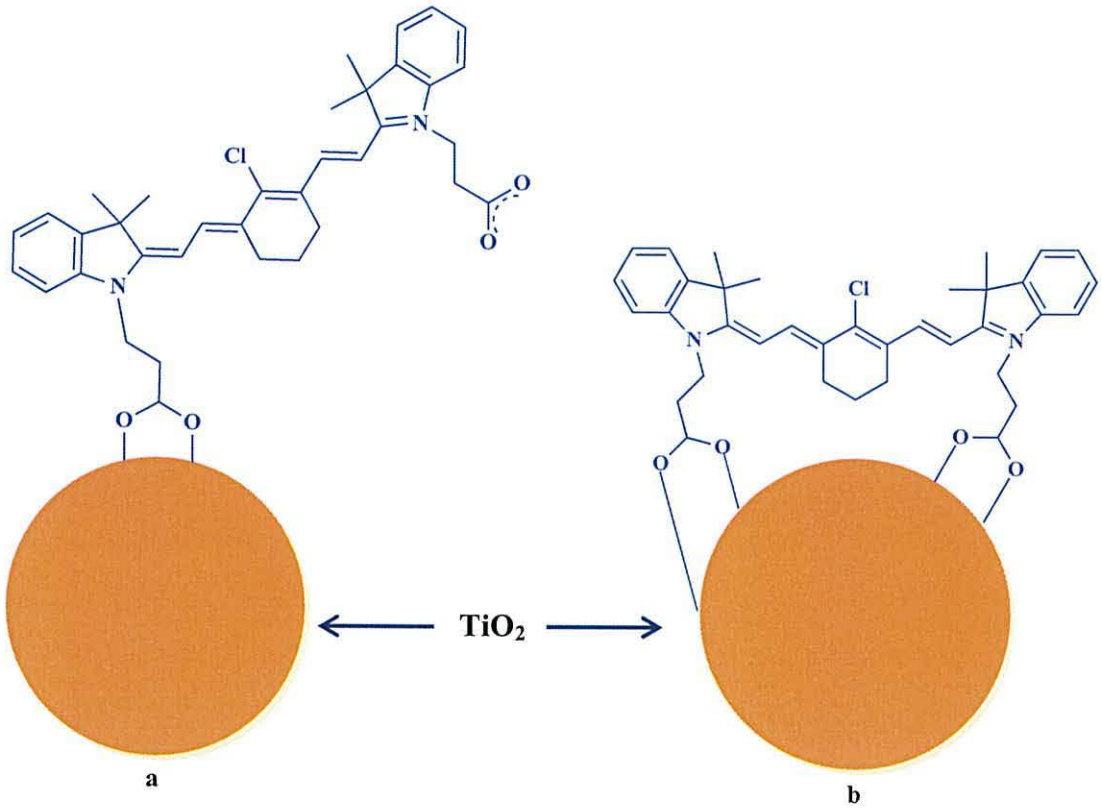

Figure 4.15. Possibile (**34**) binds on metal oxide surfaces, (a) monodentate bonding or (b) "gate-leg" bidentate bonding.

The torsion angles obtained confirmed the planarity of (**34**). Thus, Table 4.3 shows selected torsion angles (°) between, the conjugated six-membered and five-membered rings of the indole moieties and the central linker unit of (**34**). Thus the carboxylic acid groups are co-linear with a plane running through the long axis of the cyanine molecule as represented by O4-C36-C35-C34 and O2-C9-C8-C7 dihedral angles which are all close to 180.0° and both of the indole groups are coplanar as represented by the C10-C14-C15-C16 and C20-C22-C23-C24 dihedral angles.

Table 4.3. Selected torsion angles (°) of (**34**).

C10-C14-C15-C16	172.03 (15)	C11-C10-C14-C15	8.8 (2)
C20-C22-C23-C24	176.76 (15)	C25-C24-C23-C22	-2.5 (3)
O4-C36-C35-C34	179.69 (13)	C14-C10-N1-C7	3.1 (2)
O2-C9-C8-C7	177.23 (15)	C23-C24-N2-C34	8.1 (2)
C1-C11-C10-C14	176.94 (14)	N1-C6-C1-C11	-0.28 (16)
C32-C33-C28-C25	-179.86 (13)	C32-C31-C30-C29	1.2 (2)
C23-C24-C25-C28	176.98 (15)	N2-C33-C28-C25	0.29 (16)
C5-C6-C1-C11	178.66 (13)	C2-C3-C4-C5	0.4 (2)

In addition to the points mentioned above, Figure 4.16 and Table 4.4 show two sets of hydrogen bonding between two cyanine molecules; O4-H4a....O2 and also between O5-H5a....O1 and methanol molecules which are present as a solvent of crystallisation because methanol was used as the solvent to grow the crystals. This is in line with the mass spectrometry data which shows a small peak for cyanine-methanol complex. This is also important because hydrogen bonding is likely to increase aggregation between cyanine molecules in solution (see UV-Vis data) and potentially also for adsorbed molecules on titania surface within DSC devices.

The H-bonding between the two cyanine molecules and cyanine molecule with methanol molecule suggests a strong tendency for H-bonding which could be the cause of the increase in the aggregation of cyanine molecule. Table 4.4 shows the hydrogen bond lengths and bond angles of (**34**).

Table 4.4. Hydrogen bonds with H...A < r (A) + 2.000 Å and <DHA > 110 deg.

D-H	d(D-H)	d(H..A)	<DHA	d(D..A)	A
O4-H4A	0.840	1.616	171.37	2.450	O2 [-x-1, -y+1, -z+1]
O5-H5A	0.840	1.946	156.62	2.737	O1 [-x-1, -y+1, -z+1]

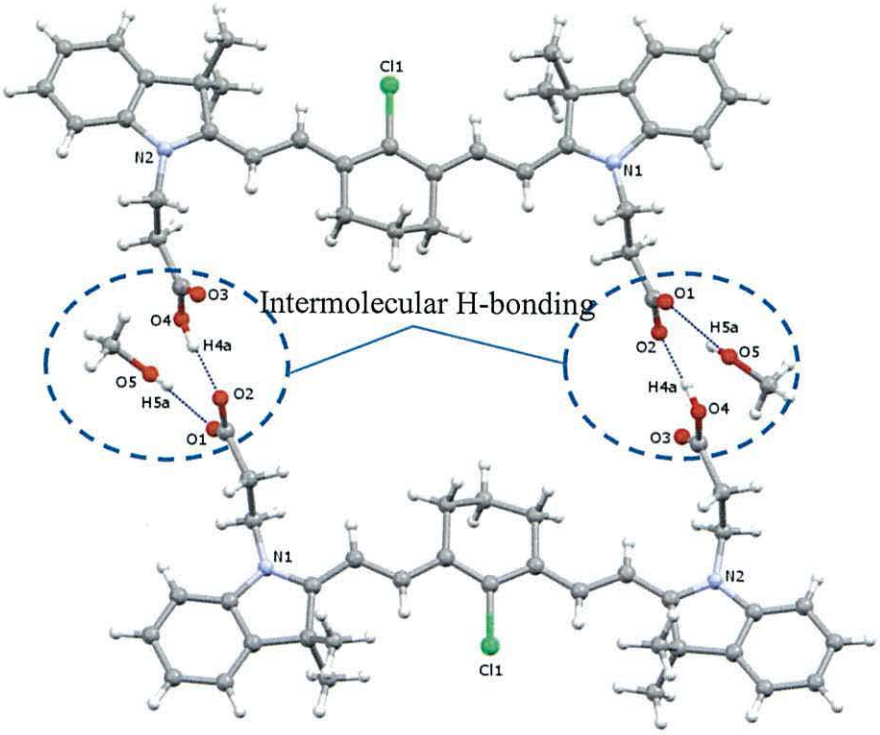

Figure 4.16. Molecular structural data showing interamolecular hydrogen bonding of (**34**). The blue dashed cycle show the H-bonding between cyanine molecules and cyanine with methanol molecules.

Before the successful synthesis of (**34**) discussed above, the synthesis had previously been attempted using the same method but with a different solvent. In detail, the synthesis was attempted by reacting 1-carboxyethyl-2, 3, 3-trimethyl indolium iodide (**29**) (2 eq) with 2-chloro-1-formyl-3-(hydroxymethylene) cyclohex-1-ene compound (**33**) in a mixture of 1-butanol:benzene (7:3, v/v) as the solvent but without a catalyst. A Dean-Stark condenser was again used to collect the water which formed during the reaction. [1, 3] The reaction was refluxed for 5-6 h and the crude product of (**34**) was purified by column chromatography on silica gel with dichloromethane/methanol (3:1, v/v) to give a green solid which contained two compounds, a di-n-butyl-ester (**34a**) and a di-ester which included both a mono-methyl and a mono butyl-ester (**34b**), as shown in (Scheme 4.2). Attempts to purify this mixture by column chromatography were carried out twice to try to get a pure compound and try to remove the butanoate ester but without success.

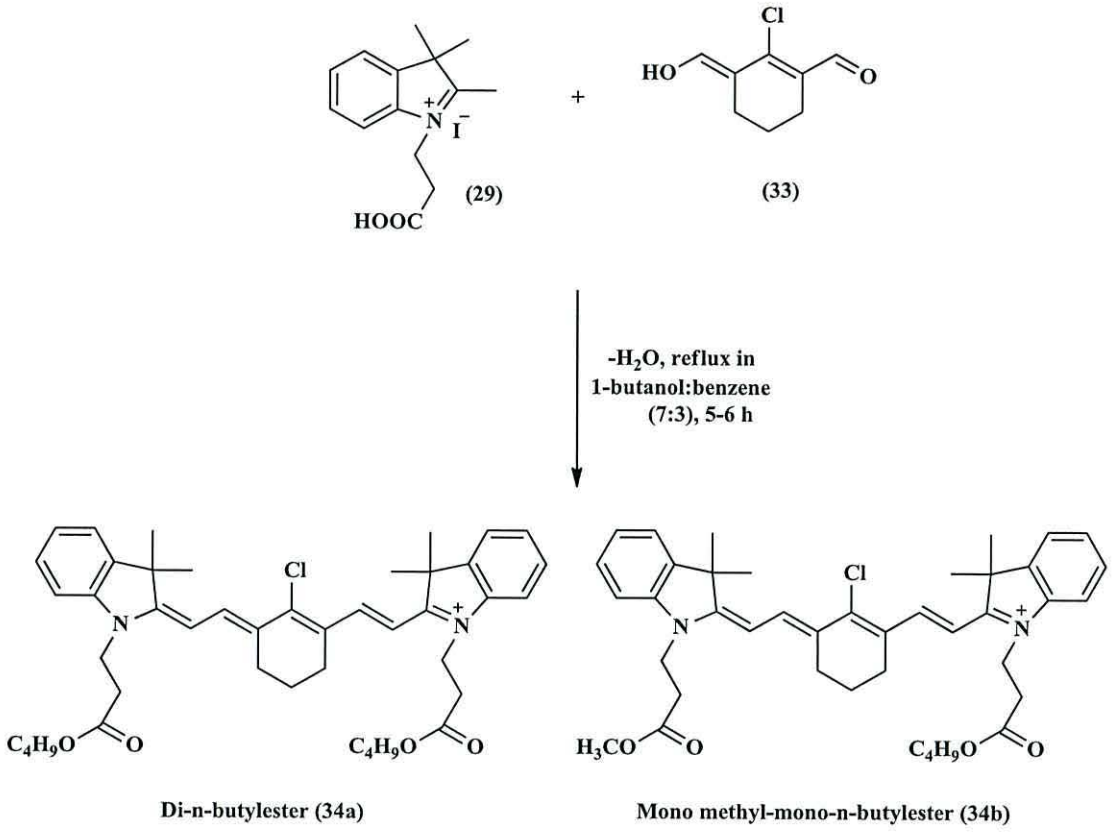

Scheme 4.2. Synthetic pathway of 1-(3-butoxy-3-oxopropyl)-2-((E)-2-((E)-3-((E)-2-(1-(3-butoxy-3-oxopropyl)-3,3-dimethylindolin-2-ylidene)ethylidene)-2-chlorocyclohex-1-en-1-yl)vinyl)-3,3-dimethyl-3H-indol-1-ium (**34a**) and 1-(3-butoxy-3-oxopropyl)-2-((E)-2-((E)-2-chloro-3-((E)-2-(1-(3-methoxy-3-oxopropyl)-3,3-dimethylindolin-2-ylidene)ethylidene)cyclohex-1-en-1-yl)vinyl)-3,3-dimethyl-3H-indol-1-ium (**34b**)

Initial inspection of the ^{1}H NMR data (Figure 4.17) confirms this product is a mixture. The presence of butanoate ester groups in addition to the cyanine signals can be seen with an additional triplet observed at 0.88 ppm for the (CH_3) of the ester alkyl chain, and a multiplet between 1.29 and 1.47 ppm due to (2xCH_2) moieties of the alkyl ester chain next to the methyl group. An additional triplet at 4.04 ppm is due to the methyl ester group (CH_2-O) of the butanoate which is shifted downfield due to its proximity to the electron withdrawing oxygen of the ester group. The presence of butanoate group was further confirmed by ^{13}C NMR data which show additional signals at 13.99, 28.35, and 33.00 ppm for the terminal CH_3 and the methyl alkyl chain, respectively while the signal at 66.22 ppm is due to the methyl

alkyl chain next to oxygen.

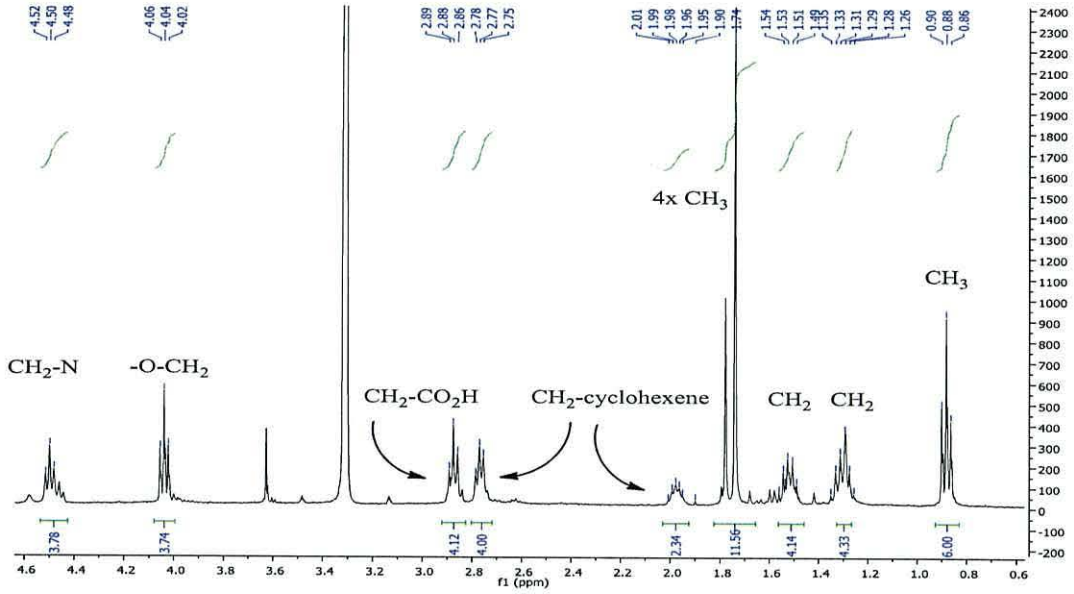

Figure 4.17. ^{1}H NMR of 1-(3-butoxy-3-oxopropyl)-2-((E)-2-((E)-3-((E)-2-(1-(3-butoxy-3-oxopropyl)-3,3-dimethylindolin-2-ylidene)ethylidene)-2-chlorocyclohex-1-en-1-yl)vinyl)-3,3-dimethyl-3H-indol-1-ium (**34a**), data shown between 0-4.6 ppm.

Confirmation that (**34**) contains mixture of two ester products is also given by the mass spectrometry data. Figure 4.18 shows peaks at 711.4 and a small peak at 669.3 which are assigned to di-n-butyl ester (**34a**) and mono-methyl-mono-n-butyl ester (**34b**), respectively. The NMR data didn't show peaks for (**34b**). This is believed to be due to the small amount of (**34b**) and the lower sensitivity of NMR relative to mass spectrometry. The results obtained confirm the presence of butyl ester in the final product due to the mixture of butanol:benzene which using as the solvent in the reaction. Butanol reacts at the carboxylate group to produce a mixture of products which explained the present of butyl ester.

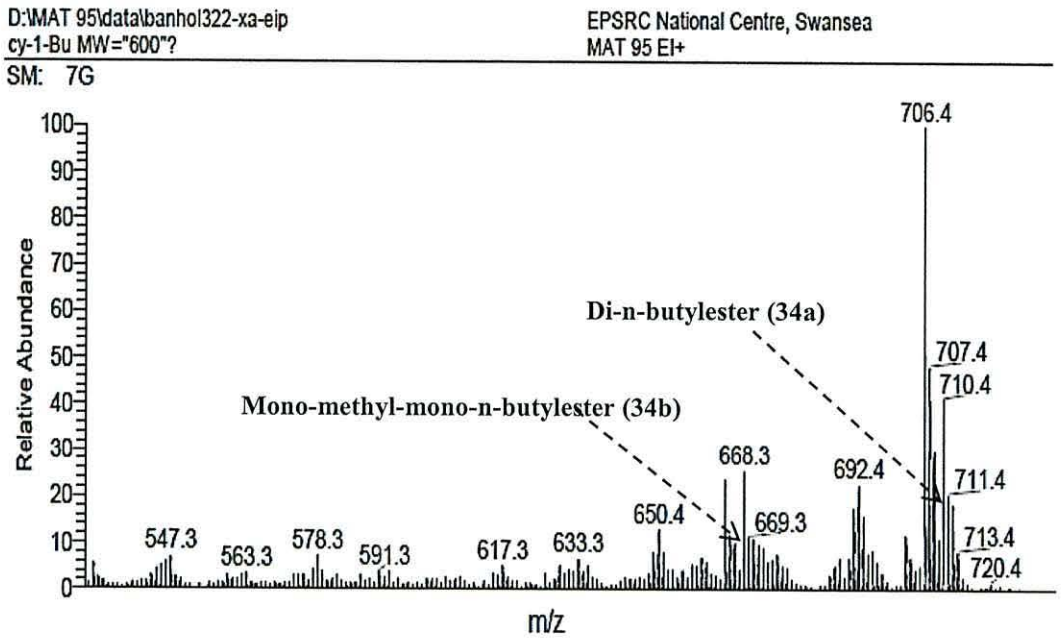

Figure 4.18. Electron impact mass spectrum of a mixture of 1-(3-butoxy-3-oxopropyl)-2-((E)-2-((E)-3-((E)-2-(1-(3-butoxy-3-oxopropyl)-3,3-dimethylindolin-2-ylidene)ethylidene)-2-chlorocyclohex-1-en-1-yl)vinyl)-3,3-dimethyl-3H-indol-1-ium **(34a)** and 1-(3-butoxy-3-oxopropyl)-2-((E)-2-((E)-2-chloro-3-((E)-2-(1-(3-methoxy-3-oxopropyl)-3,3-dimethylindolin-2-ylidene)ethylidene)cyclohex-1-en-1-yl)vinyl)-3,3-dimethyl-3H-indol-1-ium (**34b**).

The decision to use DMF as the solvent to synthesize the cyanine dye was based on the results obtained above which confirm that the using a mixture of 1-butanol/benzene as the solvent results in esterification.

4.1.2 Synthesis of 3-(2-((E)-2-((E)-3-((E)-2-(3-(2-carboxyethyl)-1,1-dimethyl-1H-benzo[e]indol-2(3H)-ylidene)ethylidene)-2-chlorocyclohex-1-en-1-yl)vinyl)-1,1-dimethyl-1H-benzo[e]indol-3-ium-3-yl)propanoate (35).

In this part of work we attempted to synthesize another type of symmetrical cyanine dye with additional benzene ring compared to (**34**), to try to capture longer wavelength light by increasing the conjugation of the molecule. In this part we also attempted to synthesize (**35**) by following the second (uncatalyzed) method was used in a mixture of 1-butanol/benzene as the solvent but trying to change the conditions of the reaction. The synthesis of (**35**) Scheme 4.3 was attempted by reacting 1-carboxyethyl-2, 3, 3-trimethyl-benzo [0]indolenium iodide (**30**) with the same 2-

chloro-1-formyl-3-(hydroxymethylene) cyclohex-1-ene central unit (**33**) used in the synthesis of (**34**). This reaction again involved two steps. The first step was to synthesize 1-carboxyethyl-2, 3, 3-trimethyl benzo[0] indolenium iodide (**30**) (see Figure 4.19). This was achieved by reacting 2, 3, 3-trimethyl-1H-benzo [0] indole with iodopropionic acid in 1, 2-dichlorobenzene as a solvent. [1, 4] After flash distillation of the solvent, the product was dried under high vacuum producing a beige solid of (**30**) (1.3 g, 96% yield). The yield was improved of (**30**) compared with literature which reports 90%. [6]

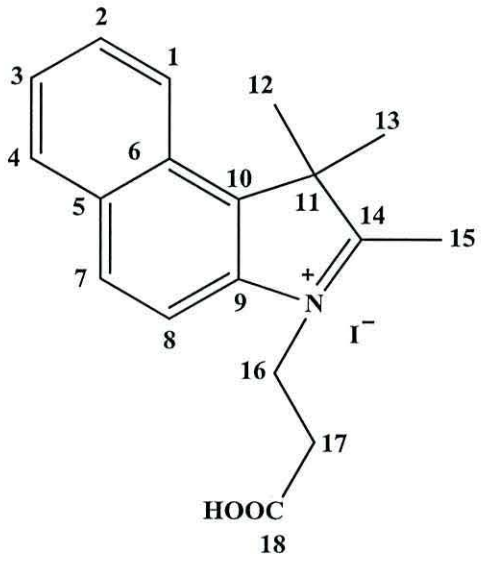

Figure 4.19. The molecular structure of 1-carboxyethyl-2, 3, 3-trimethyl-benzo [0]indolenium iodide (**30**) showing atom labelling to aid NMR assignments.

The ^{1}H NMR spectrum of (30) confirms the presence of the propionic acid group linked to the nitrogen of pyrrole ring with triplets at 3.03 and 4.64 ppm due to (*CH_2*-COOH, H-17) and (-N-*CH_2*-, H-16), respectively. The presence of the signals at 1.66 and 2.97 ppm (9H) are ascribed to the three methyl groups in the molecule (*CH_3*, H-12, H-13 and H-15). The doublet signals at 8.16, 8.21, 8.28 and 8.36 ppm are assigned to (*Ar-H*, H-1, H-4, H-7 and H-8), whilst the signals at 7.73 and 7.78 ppm are assigned to (*Ar-H*, H-3 and H-4) and the presence of a signal at 12.77 ppm is due to (*COOH*, H-18). The corresponding carbon signals are also observed in the ^{13}C NMR. The signals at 14.10 and 21.45 ppm are due to the (*CH_3*, C-12, C-13, C-15), 31.32 and those 55.58 ppm are due to (*CH_2*, C-17 and C-16), respectively. The signals at 113.41, 123.40, 127.42, 128.42, 129.72 and 130.64 ppm are due to (*Ar-C-H*, C-1, C-2, C-3, C-4, C-7 and C-8), whilst the signals at 131.12, 133.00, 138.32 and

143.89 ppm due to (*Ar-C*-C, C-5, C-6, C-9 and C-10). Finally, the signal at 171.47 ppm is due to (*-COOH*, C-18), and the signal at 197.75 ppm corresponds to (*C=N*, C-14).

The FT-IR spectrum shows bands at 3046 and 3034 cm^{-1} due to the OH stretch associated with carboxylic acid, along with peaks at 2972, 2920 and 2863 cm^{1} which are assigned (C-H) stretching of the aromatic rings and CH_3 and CH_2 stretching associated with the alkyl ester groups. A sharp peak at 1730 cm^{-1} assigned to carbonyl of the carboxylic acid and a weaker peak at 1594 cm^{-1} is ascribed to C=C benzene ring stretching. Finally the band at 1176 cm^{-1} is believed to be due to (C-O) bending. The mass spectrometry data confirm the target compound (**30**) has been synthesized and shows the most prominent peak occurs at an accurate mass of 232.1333, which corresponds to (**30**) $[M+H]^+$. Single crystal structural analysis also confirms the target compound and the molecular structure of (**30**) is shown in Figure 4.20. Selected bond lengths (Å) and angles (°) are also listed in Table 4.5. The carbon-carbon bond lengths of the molecular skeleton show values consistent with both (C-C) and (C=C) bonds; 1.523 (6) Å and 1.392 (10) Å, respectively. Also the carbon-nitrogen bond lengths also show data consistent with (C-N) and (C=N) bonds; 1.442 (5) Å and 1.303 (6) Å, respectively. [4] All the angle bonds in the benzene ring close 120°, while in the five-membered rings close 110°, which are agreements with the literature as observed for the previous indole (**29**). The X-ray data also show the iodide counter ion in the molecular structure of (**30**).

Table 4.5. Selected bond lengths [Å] and angles [°] for (**30**).

N1-C9	1.442 (5) Å	C11-C14	1.511 (6) Å
N1-C16	1.463 (5) Å	C9-N1-C14	126.4 (4) °
N1-C14	1.303 (6) Å	C9-N1-C16	123.0 (4) °
C10-C11	1.523 (6) Å	C14-N1-C16	101.7 (4) °
C11-C12	1.539 (6) Å	C10-C11-C14	110.6 (4) °
C11-C13	1.551 (6) Å		

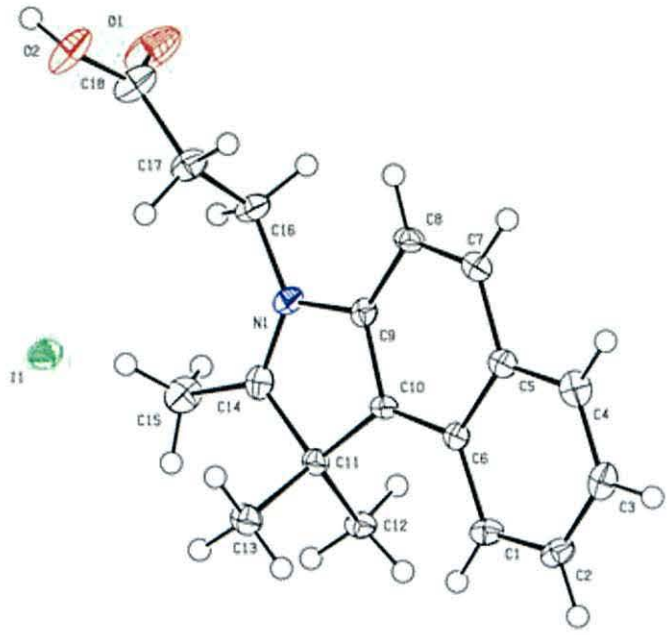

Figure 4.20. An ortep molecular structure of 1-carboxyethyl-2, 3, 3-trimethyl benzo[0] indolenium iodide (**30**).

The second step was the synthesis of (**35**) which was carried out by reacting 1-carboxyethyl-2, 3, 3-trimethyl-benzo[*0*]indolenium iodide (**30**) with 2-chloro-1-formyl-3-(hydroxymethylene) cyclohex-1-ene as a central unit (**33**). The reaction scheme to synthesize (**35**) is shown in Scheme 4.3. Compound (**33**) was synthesized using a method developed from the literature and presented in the previous section. [2, 3] To make (**35**), (**30**) and (**33**) were dissolved in a solvent mixture consisting of 1-butanol: benzene (7:3, v\v). This solution was then refluxed without the addition of a sodium acetate catalyst. The water formed during the reaction was removed using Dean-Stark condenser which is shown in Figure 4.21. After the reaction had been refluxed for 3 hours, the solution was allowed to cool to room temperature. The solvent was removed to give a crude product as a green solid of (**35**). The crude product of (**35**) was then purified using column chromatography on silica gel with dichloromethane: methanol (10:1, v/v) as an eluent. In this synthesis, the reaction conditions were changed from (**34**) by reducing the reflux time from 6 to 3 h and keeping the reflux at a lower temperature 100-105°C to try to reduce the esterified by products from the reaction compared with first time which was refluxed at 115°C.

During this attempt to synthesize (**35**), a mixture of three compounds was obtained; a mono-n-butyl ester, a di-n-butyl ester and the target compound (**35**) as a dicarboxylic acid. This confirmed partial success in synthesizing the target compound (**35**) with reduced amounts of the butyl-esters (**35a**) and (**35b**). In contrast, during the synthesis of (**34**) using the same solvent no target compound was obtained and all the product was esterified, which means this type of reaction needs lower temperature and shorter time. This is in line with the literature. [6] Zhang and Achilefu, reported that they obtained a mixture of esterified products and they stated that the formation of the carboxylic acid compound in the mixture can be increase of at lower temperature and shorter reaction times.

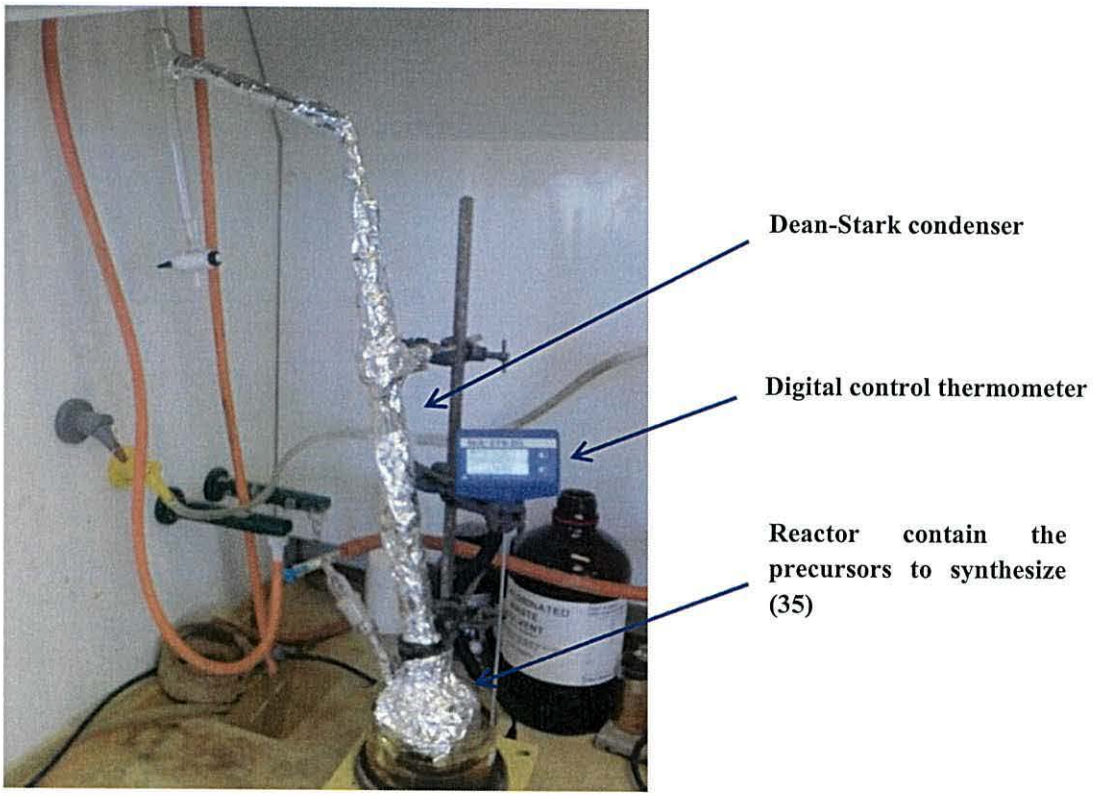

Figure 4.21. Photograph of a Dean-Stark condenser used in the synthesis of (**35**), to remove the water formed during the condensation reaction.

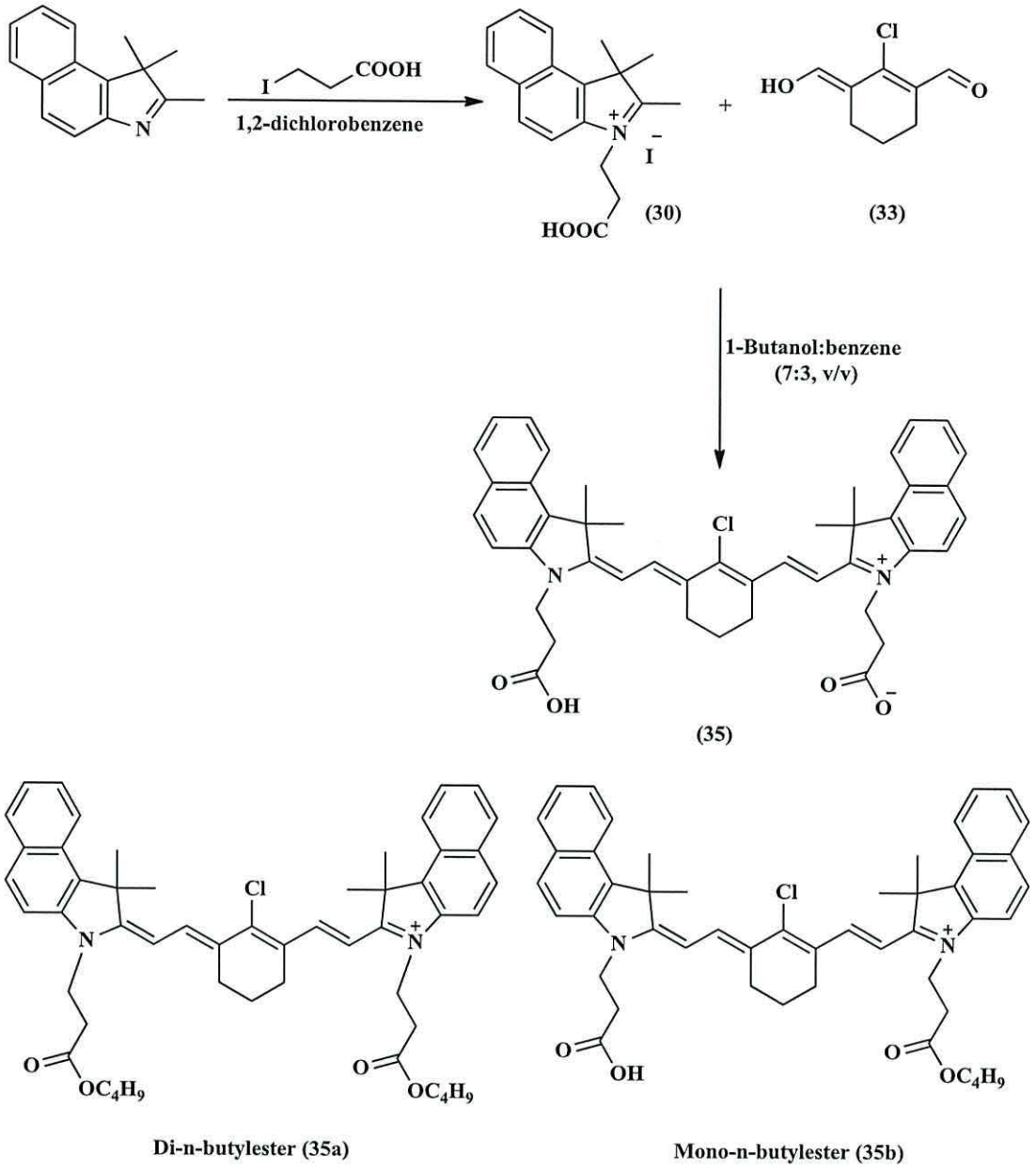

Scheme 4.3. Synthetic pathway of a mixture compound of 3-(2-((E)-2-((E)-3-((E)-2-(3-(2-carboxyethyl)-1,1-dimethyl-1H-benzo[e]indol-2(3H)-ylidene)ethylidene)-2-chlorocyclohex-1-en-1-yl)vinyl)-1,1-dimethyl-1H-benzo[e]indol-3-ium-3-yl)propanoate (**35**), 3-(3-butoxy-3-oxopropyl)-2-((E)-2-((E)-3-((E)-2-(3-(3-butoxy-3-oxopropyl)-1,1-dimethyl-1H-benzo[e]indol-2(3H)-ylidene)ethylidene)-2-chlorocyclohex-1-en-1-yl)vinyl)-1,1-dimethyl-1H-benzo[e]indol-3-ium (**35a**) and 3-(3-butoxy-3-oxopropyl)-2-((E)-2-((E)-3-((E)-2-(3-(2-carboxyethyl)-1,1-dimethyl-1H-benzo[e]indol-2(3H)-ylidene)ethylidene)-2-chlorocyclohex-1-en-1-yl)vinyl)-1,1-dimethyl-1H-benzo[e]indol-3-ium (**35b**).

Initial characterization of a mixture (**35**) was achieved using mass spectrometry which confirmed a peak at an accurate mass of 699.2970, for the dicarboxylic acid. There were two other peaks at 755.3598 and 811.4215 as shown in Figure 4.22, which correspond to the mono-n-butyl ester and the di-n-butyl ester, respectively. The ratio of the mixture product was 10:7.6:1.2 for di-n-butyl ester (**35 a**), mono-n-butyl ester (**35 b**) and (**35**), respectively.

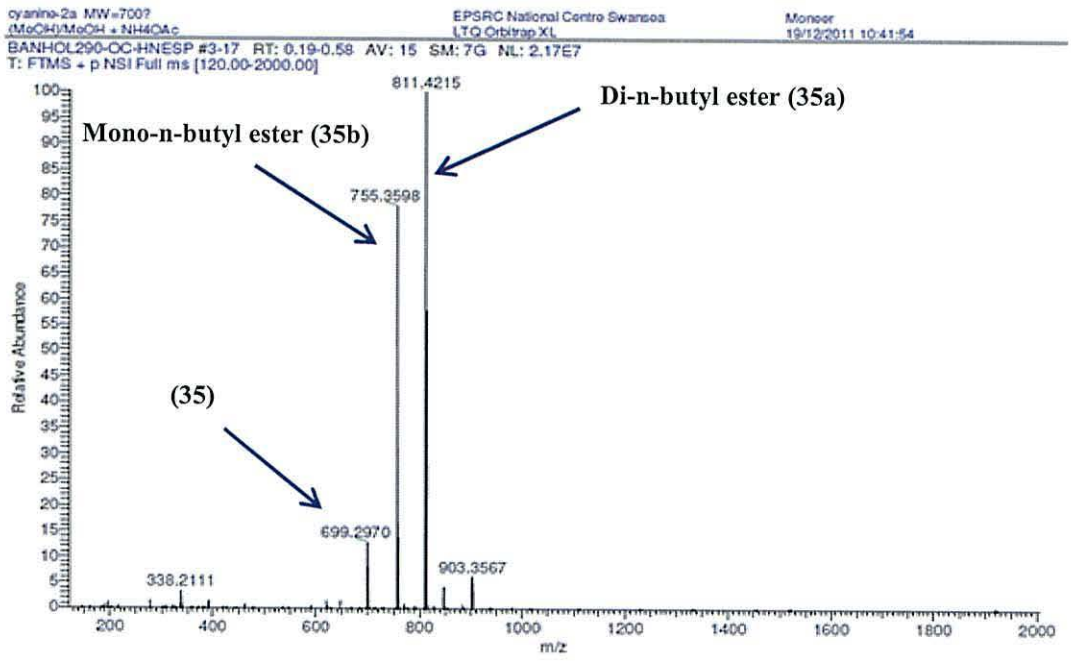

Figure 4.22. Electrospray mass spectrum of the crude, mixed product of **(35)**.

The ^{1}H NMR of the reaction mixture of (**35**) (Figure 4.23) shows additional peaks to the cyanine dye and confirms the presence of alkyl ester butanoate groups with a triplet observed at 0.81 ppm for the methyl group, and signals at 1.25 and 1.48 ppm representing the alkyl chain. The data also show a triplet at 4.03 due to methyl group next oxygen which was shifted down field. ^{13}C NMR also show additional peaks and confirms the presence of the butanoate group and shows signals at 13.93, 20.06, 33.22 and 66.19 are due to carbons of the alkyl chain $(-CH_2)_3$-CH_3, and $(-CH_2)_3$-CH_3 and the ($-OCH_3$) respectively.

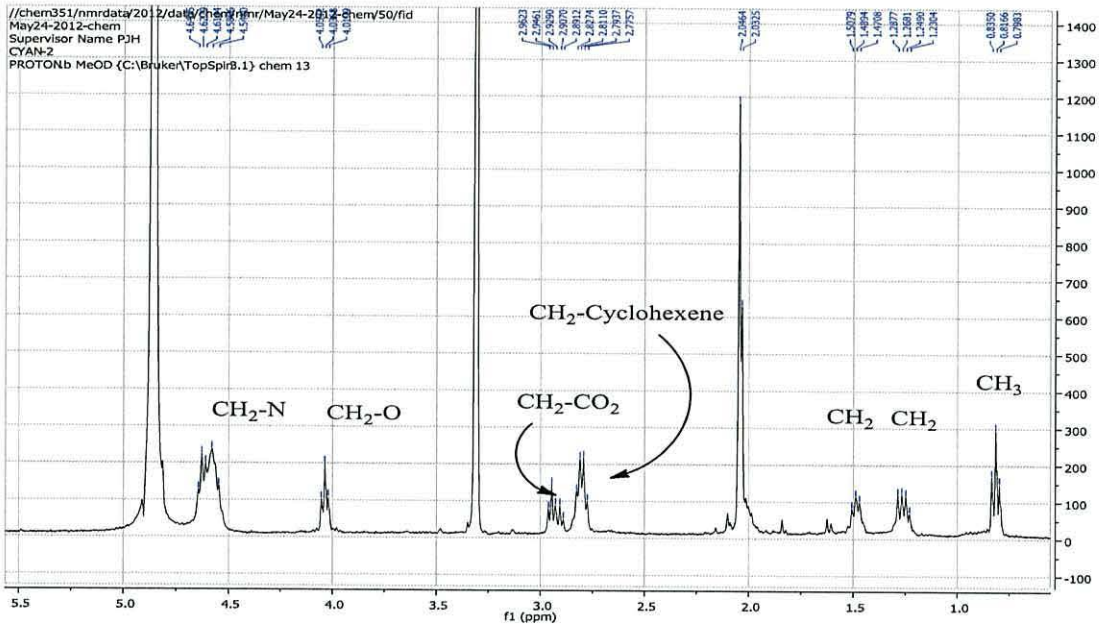

Figure 4.23. Partial ^{1}H NMR spectrum of the mixed products of the reaction to produce **(35)** between 0 and 5.5 ppm.

To avoid forming esterified mixtures of products another method was used to synthesize compound (**35**) by using DMF as a solvent and following the same procedure which had been used to synthesize compound (**34**). This approach avoided by use of an alcoholic solvent and aimed to avoid producing esterified by-products as a result. In this approach the successful synthesis of (**35**) was achieved by reacting 1-carboxyethyl-2, 3, 3-trimethyl-benzo[*0*] indolenium iodide (**30**) with 2-chloro-1-formyl-3-(hydroxymethylene) cyclohex-1-ene (**33**) in DMF and heating for 2 h at 120°C. The crude compound was purified by using column chromatography on silica gel with dichloromethane: methanol (10:1, v/v) as an eluent. The mass spectrum results (Figure 4.24) confirm the target compound and show a single peak at an accurate mass of 697.2853 for compound **(35)** $[M-2H]^{-}$.

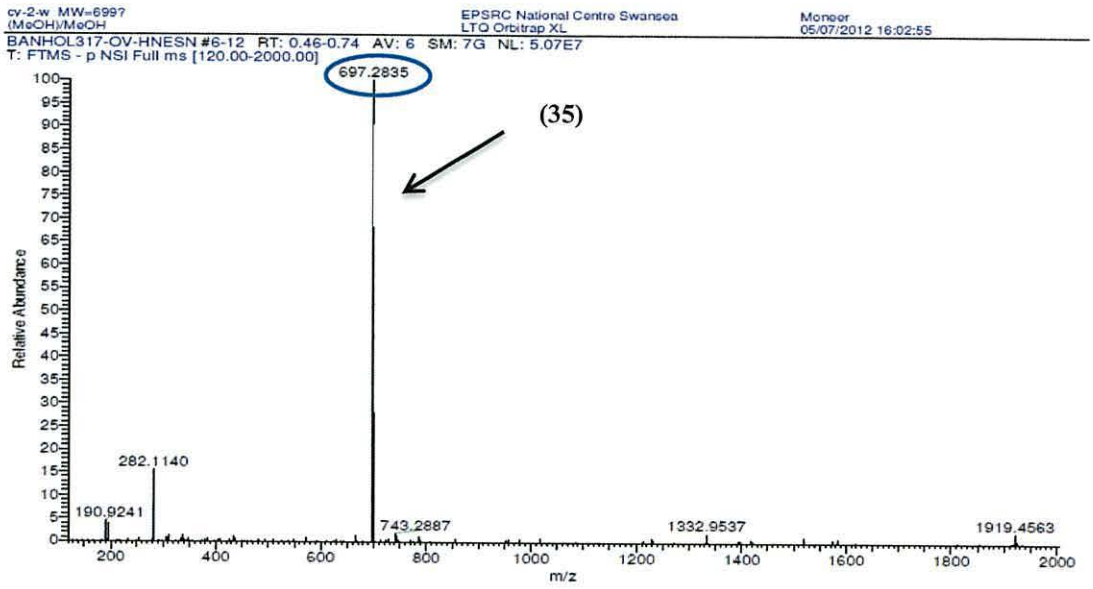

Figure 4.24. Electrospray mass spectrum of 3-(2-((E)-2-((E)-3-((E)-2-(3-(2-carboxyethyl)-1,1-dimethyl-1H-benzo[e]indol-2(3H)-ylidene)ethylidene)-2-chlorocyclohex-1-en-1-yl)vinyl)-1,1-dimethyl-1H-benzo[e]indol-3(2H)-yl)propanoic acid (**35**).

This confirms that the product was not a mixture with any esters. Formation of the target dye compound (**35**) was also confirmed by UV-Vis spectroscopy (Figure 4.25) which shows a peak at 820 nm (12195 cm^{-1}) (I) with a high molecular coefficient (ε = 150,100 $M^{-1}cm^{-1}$) in methanol. The data also shows an absorption shoulder at 750 nm (II) which is ascribed to dye aggregation. [7, 8] As discuss previously, cyanine dyes have been reported to have a strongly tend to aggregate [9] and to interact with each other in solution. The molar extinction coefficient (ε) for (**35**) was found by preparing a variety concentration of cyanine (**35**) solutions started from $1x10^{-5}$ to $3x10^{-6}$ mol L^{-1} and then measured the absorption at λ_{max} 820 nm by using UV-Vis spectra, the calibration curve was drawn between absorbance *versus* concentration (mol L^{-1}), as shown in Figure 4.26. The molar extinction coefficient for (**35**) (ε= 150,100 $M^{-1}cm^{-1}$) is higher than the molar extinction coefficient of the analogue compound NK-6037 which reported by Ono *et al.* [9]

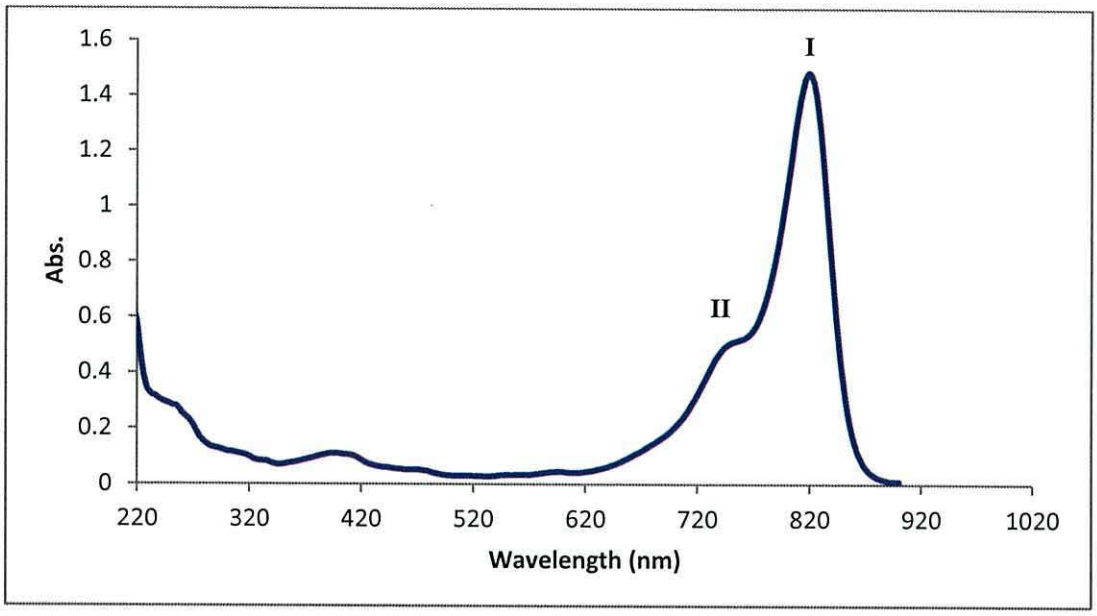

Figure 4.25. UV-Vis spectrum of 3-(2-((E)-2-((E)-3-((E)-2-(3-(2-carboxyethyl)-1,1-dimethyl-1H-benzo[e]indol-2(3H)-ylidene)ethylidene)-2-chlorocyclohex-1-en-1-yl)vinyl)-1,1-dimethyl-1H-benzo[e]indol-3(2H)-yl)propanoic acid (**35**) in MeOH $1x10^{-5}$ M, ε =150,100 $M^{-1}cm^{-1}$ at 820 nm.

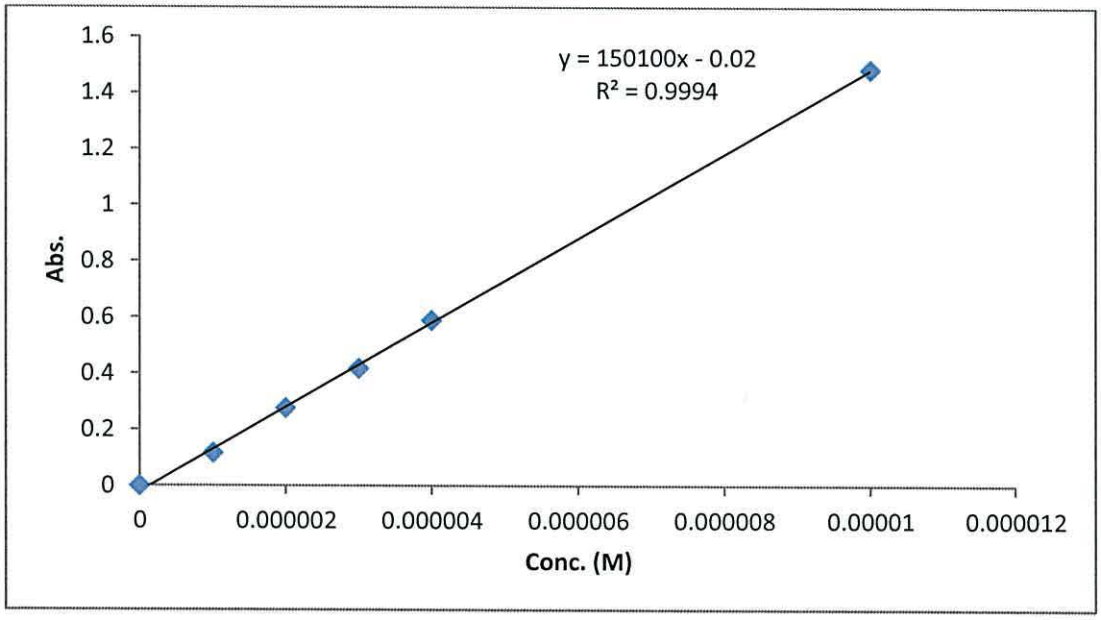

Figure 4.26. Calibration curve show plot absorbance *versus* concentration (mol L^{-1}) for (**35**) at wavelength 820 nm in MeOH.

The UV-Vis spectra in Figure 4.27 show that the ratio of relative intensities between I and II remained the same despite changes in dye concentration, and the ratio data was fixed for all concentrations at 0.33 (by dividing λ_{max} for (I) on λ_{max} for (II)). This suggests that the amount of dye aggregation is relatively the same across the range of dye concentrations tested. To obtain optimized DSC, it is important to minimize/eliminate dye aggregation, which can led to a lower dye loading on the TiO_2 surface and/or an increase in recombination losses.

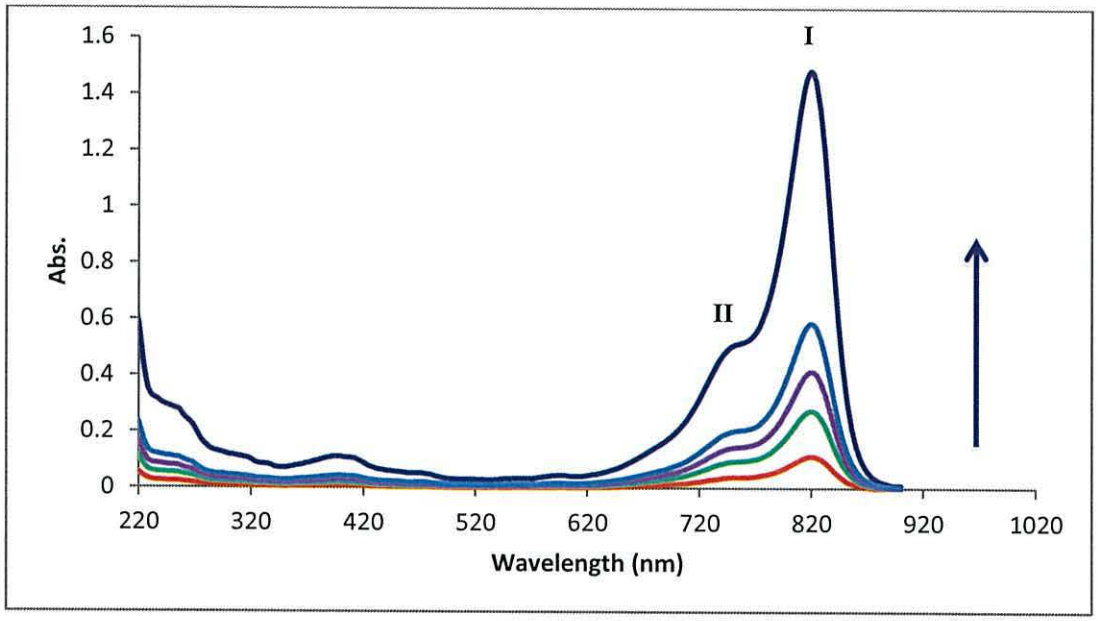

Figure 4.27. UV-Vis spectrum of 3-(2-((E)-2-((E)-3-((E)-2-(3-(2-carboxyethyl)-1,1-dimethyl-1H-benzo[e]indol-2(3H)-ylidene)ethylidene)-2-chlorocyclohex-1-en-1-yl)vinyl)-1,1-dimethyl-1H-benzo[e]indol-3(2H)-yl)propanoic acid (**35**) in different concentrations ($1x10^{-5}$, $1x10^{-6}$, $2x10^{-6}$, $3x10^{-6}$ and $4x10^{-6}$ M) in MeOH.

The FT-IR spectrum of (**35**) shows a broad peak at 3432 cm^{-1} due to the OH stretch of the carboxylic acid. Peaks at 2955, 2928 and 2868 cm^{-1} are assigned to (C-H) stretches of the aromatic ring and CH_3 and CH_2 aliphatic stretches. A sharp peak at 1727 cm^{-1} is assigned to the carbonyl of the carboxylic acid and a weaker peak at 1584 cm^{-1} assigned to C=C benzene ring stretching while the band at 1176 cm^{-1} is due to (C-O) bending.

The ^1H NMR of (**35**) (Figure 4.29) confirms the absence of any signals for a butanoate group and the presence of a singlet at 2.03 ppm is assigned to methyl groups (4x-CH_3) for (H-38, H-39, H-40, H-41), whilst signals at 2.71 and 2.81 ppm

are assigned to (-CH_2-cyclohexene) and (-CH_2-COOH) for (H-2, H-3, H-4) and (H-43, H-46), respectively. In addition the data show a triplet at 4.53 ppm due to (-N-CH_2-, H-42, and H-45). The signals at 6.49 and 8.55 ppm are doublets due to (-*CH=CH*-, H-7, H-10, H-8 and H-11) with the coupling constant (J= 14.20 and 14.16 Hz), respectively which confirms *trans* arrangement. The data also show signals at 7.48 and 7.66 ppm as triplet are assigned to (H-28, H-35) and (H-27, H-36), respectively. Signals at 7.69 and 8.00 ppm as doublet and triplet are assigned to (H-23, H-32) and (H-34, H-37, H-26, H-29), respectively. The doublet signal at 8.26 ppm is assigned to (H-22 and H-33). The ^{13}C NMR data show signals at 24.13 ppm due to (CH_2-cyclohexene, C-3), and signals at 27.43 ppm which is assigned to (2x-CH_2-cyclohexene, C2, C-4), signal at 27.86 ppm which is due to (4x-CH_3, C-38, C-39, C-40, C-41), a signal at 34.96 ppm due to (2x-CH_2-COOH, C-43, C-46), one at 42.45 ppm due to (C-$(CH_3)_2$, C-17, C-18) and, a signal at 50.60 ppm which is ascribed to (2x-N-CH_2-, C-14, C-21). The signals at 102.39, 128.69 and 144.58 ppm are due to (-*CH=CH-*, C-7, C-8, C-10 and C11), whilst the signals at 112.37, 123.43, 126.11, 128.35, 129.41, 131.13 ppm are assigned to (*Ar-C-H*, C-22, C-23, C-26, C-27, C-29, C-30, C-32, C34, C-35, C-36 and H-37). Also signals at 131.78, 132.91, 133.55, 135.22, 139.60, 140.98, 141.98 and 150.30 ppm due to (*Ar-C*-C). The signals at 175.38 and 177.40 ppm due to (*C-N*) and *(C=O)*, respectively.

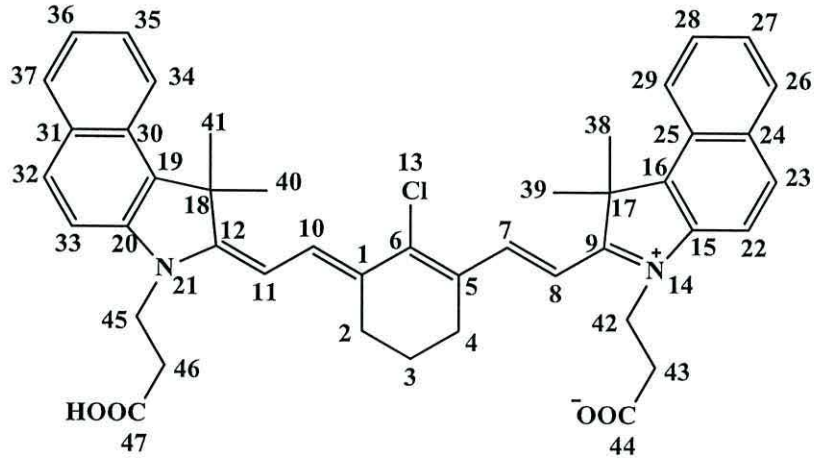

Figure 4.28. the molecular structure of 3-(2-((E)-2-((E)-3-((E)-2-(3-(2-carboxyethyl)-1,1-dimethyl-1H-benzo[e]indol-2(3H)-ylidene)ethylidene)-2-chlorocyclohex-1-en-1-yl)vinyl)-1,1-dimethyl-1H-benzo[e]indol-3(2H)-yl)propanoic acid **(35)** labelling for NMR.

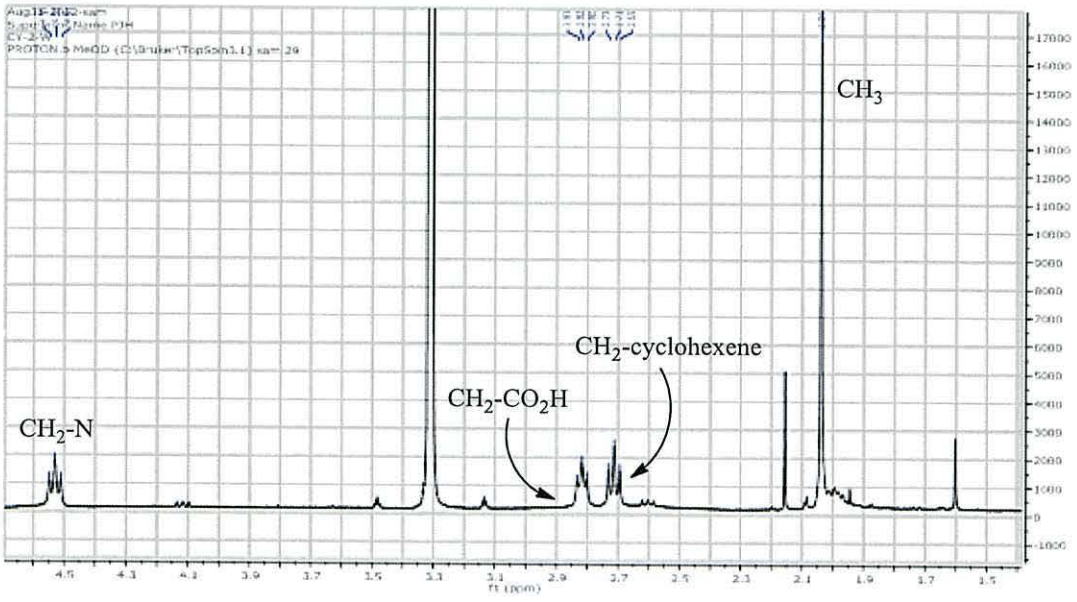

Figure 4.29. The partial ^{1}H NMR spectrum from 1.4 to 4.7 ppm of 3-(2-((E)-2-((E)-3-((E)-2-(3-(2-carboxyethyl)-1,1-dimethyl-1H-benzo[e]indol-2(3H)-ylidene)ethylidene)-2-chlorocyclohex-1-en-1-yl)vinyl)-1,1-dimethyl-1H-benzo[e]indol-3(2H)-yl)propanoic acid (**35**).

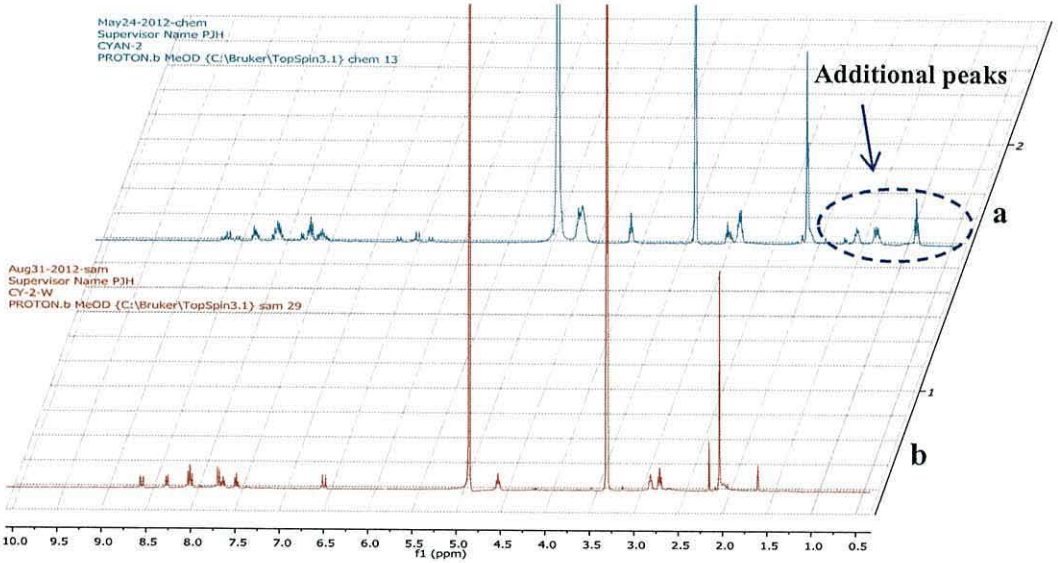

Figure 4.30. The whole ^{1}H NMR spectra of a) a mixture (**35**), (**35a**) and (**35b**) and (b) pure (**35**) from 0-10 ppm.

4.2 Synthesis of cyanine derivatives

The aim of synthesizing unsymmetrical cyanine dyes has been to investigate the influence of different the indole groups to vary light absorption in the near-infrared

region the bonding mode and the effect on DSC devices. In this part of work the synthesis and characterization of two new unsymmetrical cyanine dyes is described. These dyes are structural variations depending on the nature of the heteroaromatic ring and the length of the N, N-dialkyl groups. The first one was 3-(2-((E)-2-((E)-2-chloro-3-((E)-2-(1-ethyl-3,3-dimethyl-1H-benzo[g]indol-2(3H)-ylidene)ethylidene)cyclohex-1-en-1-yl)vinyl)-1,1-dimethyl-1H-benzo[e]indol-3(2H)-yl)propanoic acid (**37**), while the second was diphenyl-{4-[2-(1,3,3-trimethyl-1Hbenzo[e]indolinum-2yl)-vinyl]-phenyl}-amine iodide (**38**).

4.2.1 Synthesis of 3-(2-((E)-2-((E)-2-chloro-3-((E)-2-(1-ethyl-3,3-dimethyl-1H-benzo[g]indol-2(3H)-ylidene)ethylidene)cyclohex-1-en-1-yl)vinyl)-1,1-dimethyl-1H-benzo[e]indol-3(2H)-yl)propanoic acid (37).

The synthesis of unsymmetrical cyanine compounds was attempted using two methods. The first method was attempted by reacting two different hetroaromatic moieties with the central chlorocyclohexene unit in a procedure analogous to that used previously. The second method was by condensation reactions of two different heteroaromatic moieties in ethanol as the solvent.

The synthesis of 3-(2-((E)-2-((E)-2-chloro-3-((E)-2-(1-ethyl-3,3-dimethyl-1H-benzo[g]indol-2(3H)-ylidene)ethylidene)cyclohex-1-en-1-yl)vinyl)-1,1-dimethyl-1H-benzo[e]indol-3(2H)-yl)propanoic acid (**37**) was attempted as shown in (Scheme 4.4). The synthesis involved two steps. The first step was attempted by reacting the central unit 2-chloro-1-formyl-3-(hydroxymethylene) cyclohexene-1-ene (**33**) with (1 eq) of the quaternary salt of (1-ethyl-2, 3, 3-trimethylindoleniumiodide in 45 ml a mixture of 1-butanol: benzene, (7:3, v/v). The mixture reaction was refluxed with stirring for 2 h. The intermediate compound (**36**) was produced after cooling to room temperature, as shown in Scheme (4.4).

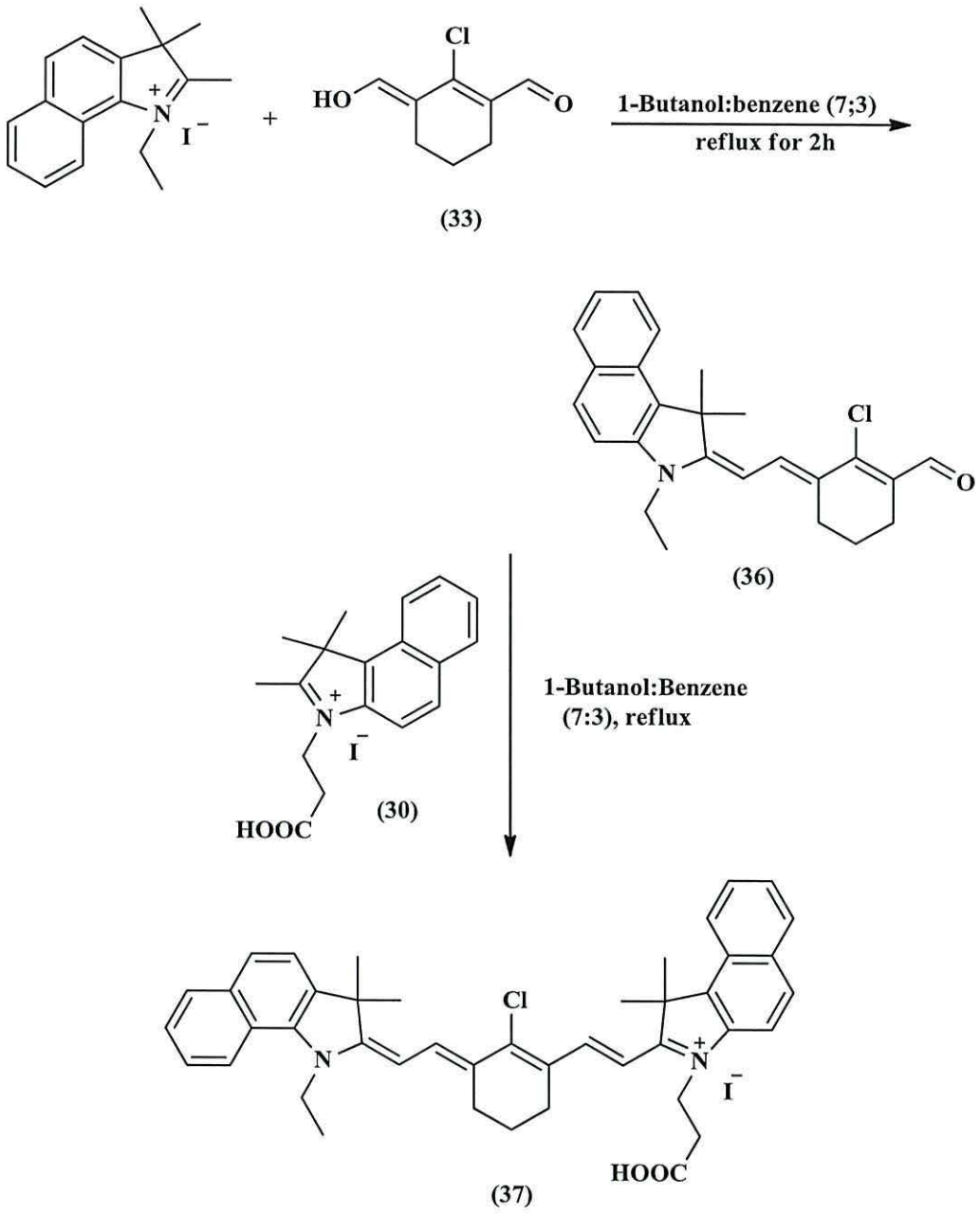

Scheme 4.4. Synthetic path way of (E)-2-chloro-3-((E)-2-(3-ethyl-1,1-dimethyl-1H-benzo[e]indol-2(3H)-ylidene)ethylidene)cyclohex-1-enecarbaldehyde (**36**) towards the formation of 3-(2-((E)-2-((E)-2-chloro-3-((E)-2-(1-ethyl-3,3-dimethyl-1H-benzo[g]indol-2(3H)-ylidene)ethylidene)cyclohex-1-en-1-yl)vinyl)-1,1-dimethyl-1H-benzo[e]indol-3(2H)-yl)propanoic acid (**37**).

A solution of (1 eq) of 1-carboxy-ethyl-2, 3, 3-trimethyl-1H-benzo [0]-indolium iodide **(30)** in 15 ml mixture of 1-butanol: benzene (7:3, v/v) was added to the reaction mixture and this was refluxed for 12 h. The water formed during the reaction was removed as an azeotrope by using a Dean-Stark condenser to produce a green

solid of (**37**) (0.1 g, 37% yield). This material was then purified by column chromatography on silica gel used dichloromethane/methanol (3:1, v/v) as eluent. The purification of (**37**) was not easy and, because of the difficulty in resolving the different compounds from the column, this process needed to be repeated more than once. In this reaction the second (uncatalyzed) method has been used as reported previously. [1] It is believed that the alcoholic solvent used esterified the carboxylic acid making purification difficult.

The mass spectrometry data for the purified reaction product shows an intense peak at 655.3081 corresponding to an accurate mass of (**37**) $[M+H]^+$. In addition, there is a much weaker peak at 711.3703 which represents the presence of a trace amount of the butanoate-ester of (**37**). The ^1H NMR spectrum of (**37**) also confirms the presence of a trace amount of the butanoate-ester with a triplet observed at 0.80 ppm assigned to CH_3 of the alkyl butanoate chain. However the integration of this peak shows only one proton (1H), whilst is supposed to be 3H whilst there are also some noisy peaks at 4.03 ppm which again is ascribed to the small amount of the ester in the product.

The ^1H NMR of target compound (**37**) shows a signal at 1.26 ppm as a broad multiplate for (CH_2-cyclohexene, H-3), a triplet at 1.48 ppm for (-N-CH_2-CH_3, H-46), a signal at 2.03 ppm assigned to (4x-CH_3, H-38, H-39, H-40 and H-41) and a broad triplet at 2.79 ppm which is ascribed to (-CH_2-COOH, H-43) and (2x-CH_2-cyclohexene, H-2, H-4). A quartet at 4.35 ppm is ascribed to (N-CH_2-CH_3, H-45), whilst the signal at 4.59 ppm is assigned to (-N-CH_2, H-42). The data also show signals at 7.50, 7.66, 8.09, and 8.27 ppm which are assigned to protons on the aromatic rings (H-22, H-23, H-26, H-27, H-28, H-29, H-32, H-33, H-34, H-35, H-36 and H-37). The signals at 6.41 and 8.5 ppm are double doublet and multiplet due to -*CH*=*CH*- (H-8, H-9) and (H-11 and H-12), respectively.

The ^{13}C NMR data shows signals at 12.76, 22.21 and 24.36 ppm are due to (-N-CH_2-$\underline{CH_3}$-C-46) and (CH_2-cyclohexene, C3, C-2 and C-4), respectively. Signals at 27.77 and 27.89 ppm are assigned to (4xCH_3, C-38, C-39, C-40 and C-41), and a signal at 34.67 ppm due to (-CH_2-COOH, C-43), whilst the signal at 37.34 ppm is due to (-*C*-CH_3, C-17 and C-18). Further signals at 52.37 and 53.64 ppm are assigned to (-N-CH_2-CH_3, C-45) and (-N-CH_2-, C-42), respectively. The signals at 111.97, 112.23, 126.14, 140.90 ppm are due to (-*CH*=*CH*-, C8, C-9, C-11 and C-12). Signals at

123.50, 126.31, 128.74, 128.88, 129.83, 131.18 ppm are assigned to (*Ar-C*-H, C-22, C-23, C-26, C-27, C-28, C-29, C-32, C-33, C-34, C-35, C-36 and C-37), while the signals at 131.82, 131.98, 133.54, 149.15 ppm which are assigned to (*Ar-C*-C, C-1, C-5, C-6, C-15, C-16, C-19, C-20). Finally, the signals at 172.62 and 175.30 ppm are due to. (C-N-Indole, C-10, C-13) and (C=O, C-44), respectively.

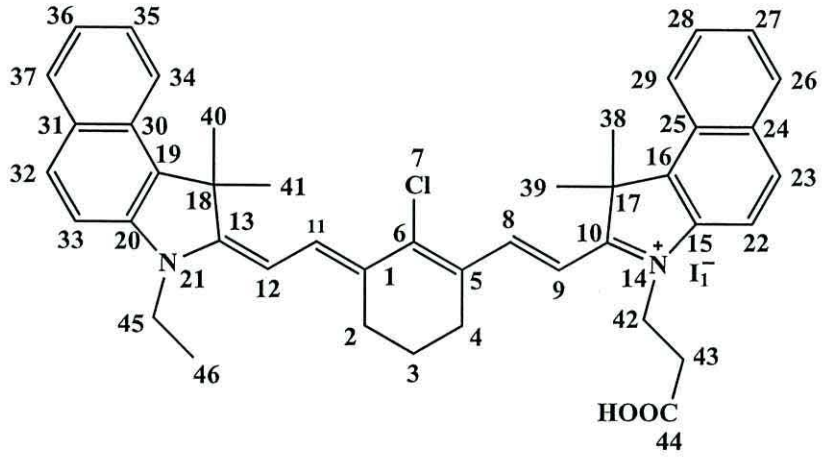

Figure 4.31. The molecular structure of 3-(2-((E)-2-((E)-2-chloro-3-((E)-2-(1-ethyl-3,3-dimethyl-1H-benzo[g]indol-2(3H)-ylidene)ethylidene)cyclohex-1-en-1-yl)vinyl)-1,1-dimethyl-1H-benzo[e]indol-3(2H)-yl)propanoic acid (**37**) showing atomic labelling for assignment of the NMR data.

The UV-Vis spectrum of (**37**) (Figure 4.32) shows an absorption peak at 816 nm (I) with a high molecular coefficient (ε= 122,800 $M^{-1}cm^{-1}$) in methanol. There is also a shoulder at 740 nm (II) which may be due to dye aggregation [7, 8] because, as discussed previously, cyanine molecules tend to aggregate in solution. [9] From these data, this also seems to happen with cyanine derivatives.

The molar extinction coefficient (ε) for (**37**) was found by preparing a variety concentration of (**37**) solutions as described above, which started from $1x10^{-5}$ to $5x10^{-6}$ mol L^{-1} and then measured the absorption at λ_{max} 816 nm by using UV-Vis spectra, the calibration curve was drawn between absorbance *versus* concentration (mol L^{-1}), as shown in Figure 4.33. The molar extinction coefficient (ε) for **(37)** is less than symmetrical cyanine (**34**) and (**35**) which may be due to the additional carboxylic group (electron withdrawing substituents) in (**34**) and (**35**) compared with (**37**). This (COOH) group contains lone pair on oxygen which effectively increases the length of the chromophore.

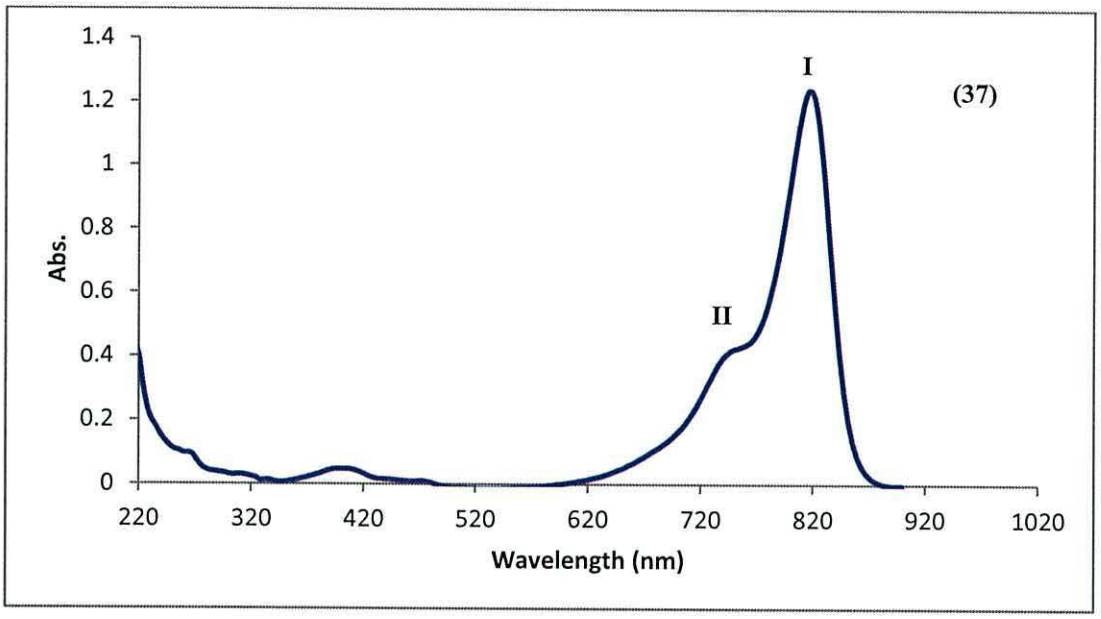

Figure 4.32. UV-Vis spectrum of 3-(2-((E)-2-((E)-2-chloro-3-((E)-2-(1-ethyl-3,3-dimethyl-1H-benzo[g]indol-2(3H)-ylidene)ethylidene)cyclohex-1-en-1-yl)vinyl)-1,1-dimethyl-1H-benzo[e]indol-3(2H)-yl)propanoic acid (**37**) $1x10^{-5}$M in MeOH, ε =122,800 $M^{-1}cm^{-1}$ at 816 nm.

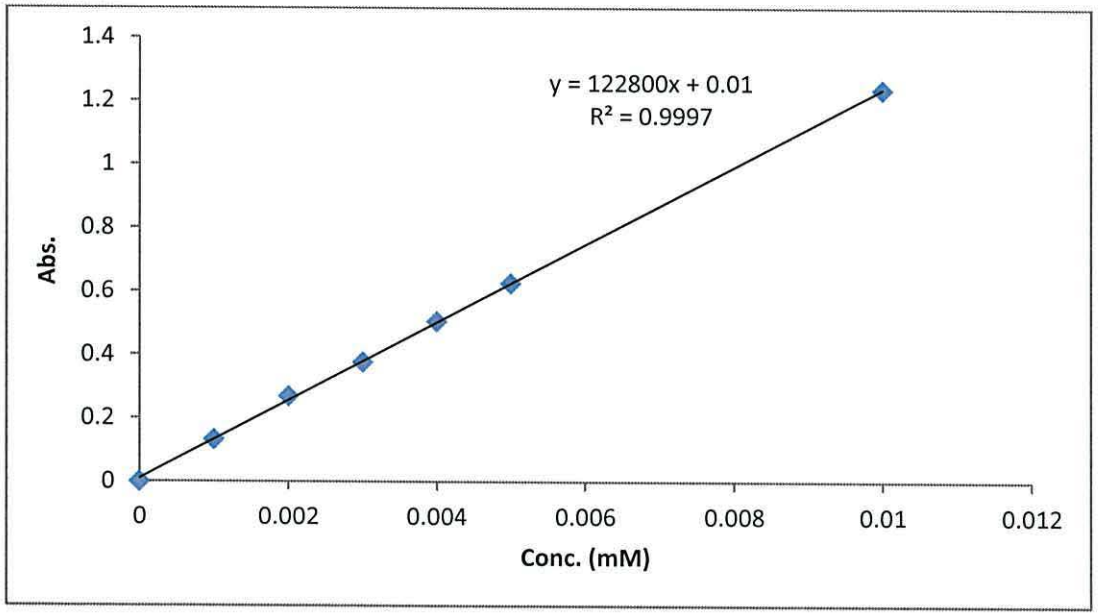

Figure 4.33. Calibration curve show plot absorbance *versus* concentration (mol L^{-1}) for (**37**) at wavelength 816 nm in MeOH.

The UV-Vis spectra in Figure 4.34 show that the relative intensities ratio between I and II remain the same despite changes in dye concentration, with a ratio around 0.30 for all concentrations between (I) and (II), which found (by dividing λ_{max} for (I) on

λ_{max} for (II)) . This suggests that the amount of dye aggregation is relatively the same across the range of dye concentrations tested.

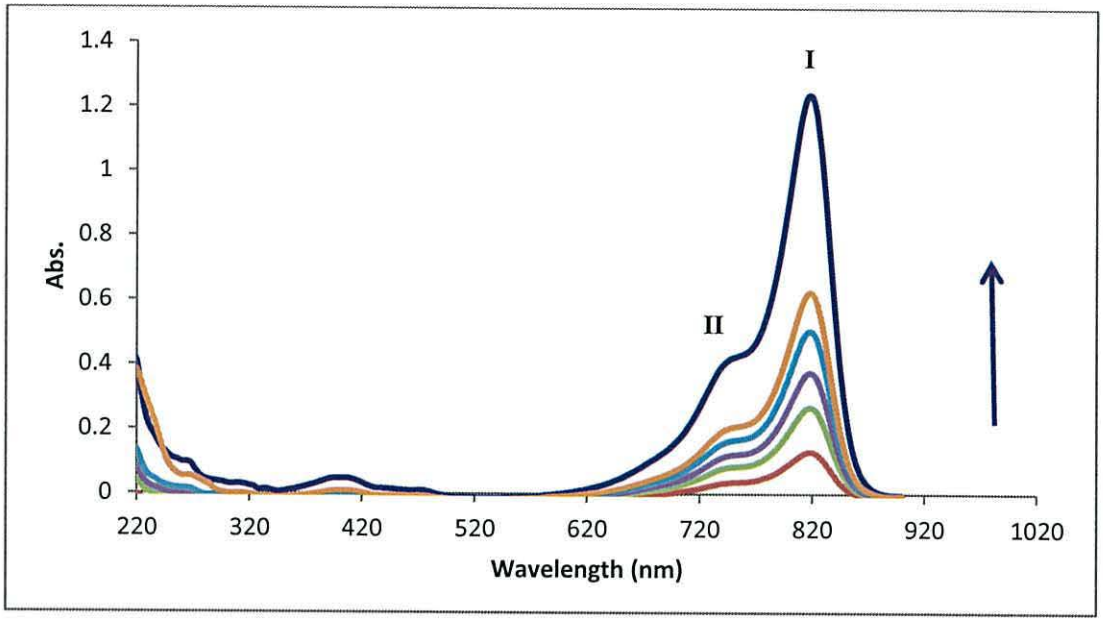

Figure 4.34. UV-Vis spectrum of 3-(2-((E)-2-((E)-2-chloro-3-((E)-2-(1-ethyl-3,3-dimethyl-1H-benzo[g]indol-2(3H)-ylidene)ethylidene)cyclohex-1-en-1-yl)vinyl)-1,1-dimethyl-1H-benzo[e]indol-3(2H)-yl)propanoic acid (**37**) in different concentrations ($1x10^{-5}$, $1x10^{-6}$, $2x10^{-6}$, $3x10^{-6}$ and $4x10^{-6}$, $5x10^{-6}$ M) in MeOH.

In order for (**37**) to be suitable to act as a sensitizer for TiO_2 in DSC devices, it was necessary to prove that compound (**37**) can adsorb onto TiO_2 electrode surfaces. To test this TiO_2 photoelectrodes which had been prepared using HT-Solaronix paste were sintered and immersed overnight in a 10^{-4} solution of M (**37**) dissolved in methanol. The HT-Solaronix paste was used because, when sintered, it produces transparent films which can then be studied using UV-visible spectroscopy in transmission mode. Figure 4.35 confirms that the compound (**37**) is adsorbed on the TiO_2 surface by showing a broad absorbance at 824 nm which shows a slight red-shift (8 nm) compared to the dye in methanol solution. This may be due to the interactions between dye molecules and the TiO_2 surface, or dye-dye interactions, or both. [10] The UV-Vis spectra (Figure 4.35) also show that the relative intensities ratio of peak I and II of (**37**) on HT-Solaronix is higher than for (**37**) in the solution (0.61 to 0.32, respectively). This suggests that the amount of dye aggregation on HT-Solaronix is more than in solution, which may be due to increase interactions

between dye molecules on the semiconductor surface. This might be reflected in the DSC performance.

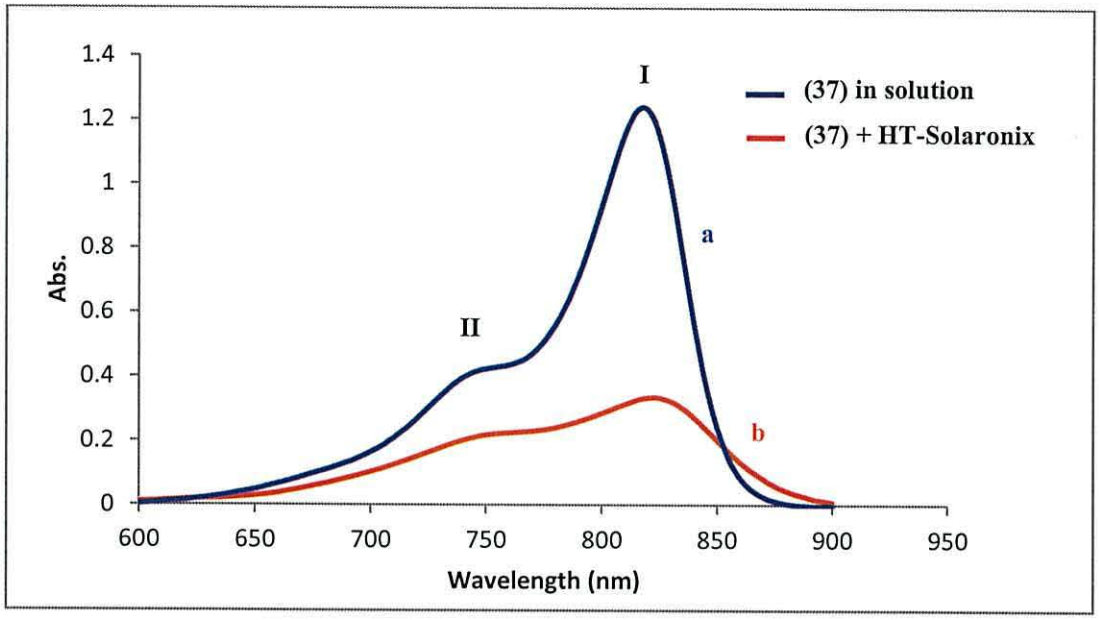

Figure 4.35. UV-Vis spectra of (a) (**37**) $1x10^{-5}$ M in methanol solution shown by the blue line and (b) (**37**) on an HT-Solaronix photo-electrode shown by the red line.

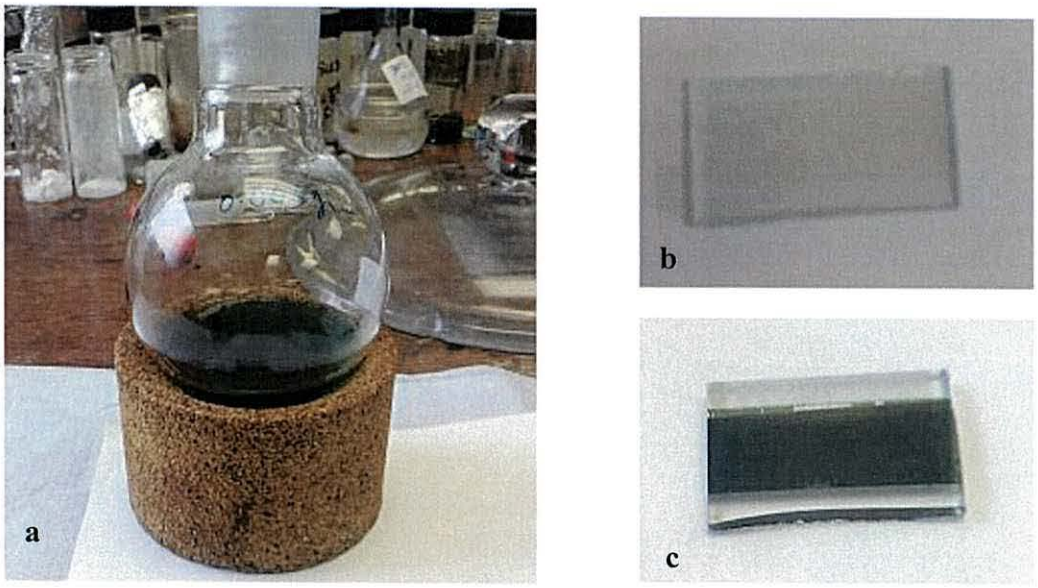

Figure 4.36. Photographs of (a) (**37**) in methanol solution $1x10^{-4}$ M, (b) TiO_2 electrode before dyeing and (c) TiO_2 electrode after dyeing with (**37**).

4.2.2 Synthesis of diphenyl-{4-[2-(1, 3, 3-trimethyl-1H-benzo[e]indolinum-2yl)-vinyl]-phenyl}-amine iodide unsymmetrical cyanine (38).

The next step was the synthesis of a new type of unsymmetrical cyanine dye with a shorter methine chain, which contains a triphenylamine moiety as donor and a carboxylic acid as an acceptor linked by (CH=CH) linker. The reason for using triphenlamine as donor due to the greatly located the cationic charge from TiO_2 surface and efficiently restrict recombination between conduction band electron and oxidized sensitizer. [11] This synthesis was carried out by reacting 4-(N, N-diphenylamino)-benzaldehyde with 1-carboxy-ethyl-2, 3, 3-trimethyl-1H-benzo [0]-indolium iodide (**30**). The synthesis of (**38**) was achieved by reacting 4-(N, N-diphenylamino)-benzaldehyde with 1-carboxy-ethyl-2, 3, 3-trimethyl-1H-benzo [*0*]-indolium iodide (**30**) and refluxing in 10 ml of ethanol for 2 h to produce a purple solid of (**38**) (0.3 g, 77% yield) as shown in (Scheme 4.5). The additional benzene rings on indole increase the polarity of the unsymmetrical cyanine dye and make it more soluble in organic solvents.

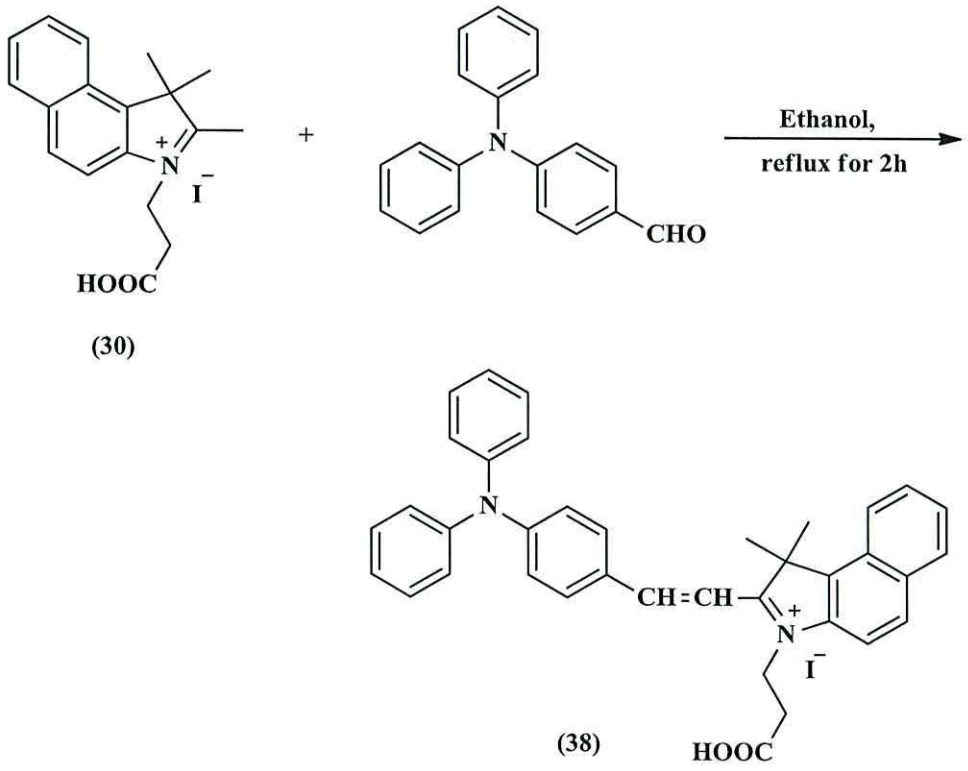

Scheme 4.5. Synthetic pathway for the synthesis diphenyl-{4-[2-(1, 3, 3-trimethyl-1Hbenzo[e]indolinum-2yl)-vinyl]-phenyl}-amine iodide (**38**).

After purification using column chromatography on silica gel with dichloromethane: methanol (3:1, v/v) as eluent, the described unsymmetrical product (**38**) was obtained after drying by high vacuum and then collecting the product by scratching off the wall of the flask, as shown in Figure 4.37.

Figure 4.37. Photographs of (a) solid (**38**) after drying under high vacuum, (b) a solution of (**38**) $1x10^{-4}$ M dissolved in MeOH.

An accurate mass of 537.2530 was shown for the desired molecular ion $[M+H]^+$ by mass spectrometry (Figure 4.38) with little evidence for any impurities.

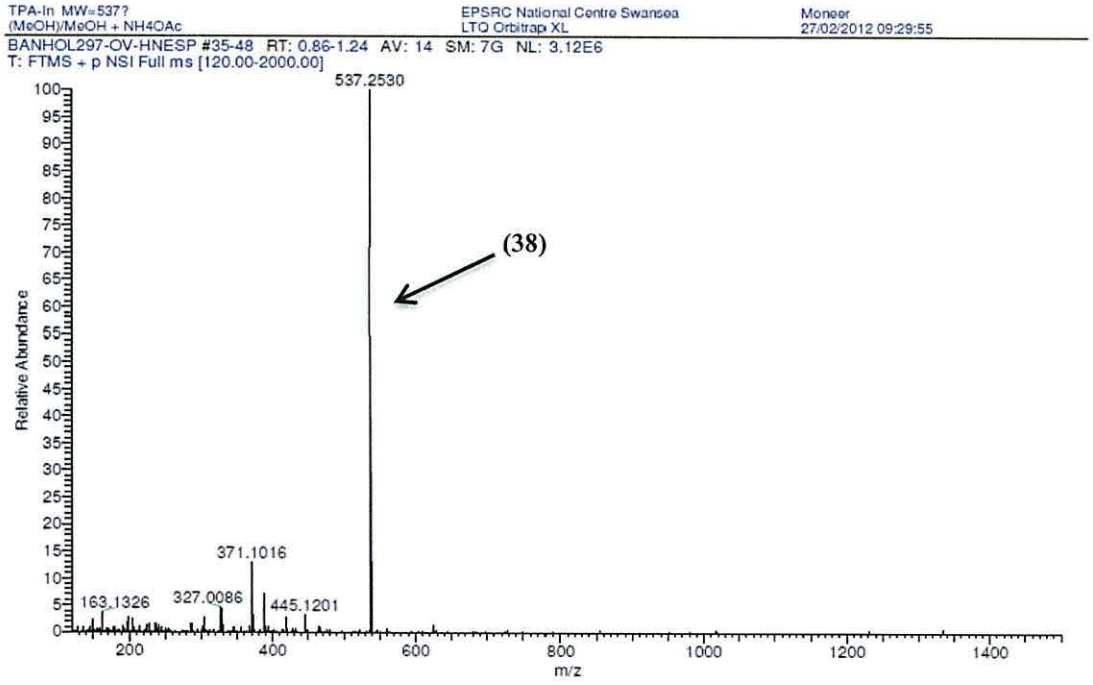

Figure 4.38. Electrospray mass spectrum of diphenyl-{4-[2-(1, 3, 3-trimethyl-1Hbenzo[e]indolinum-2yl)-vinyl]-phenyl}-amine iodide (**38**).

The UV-Vis spectrum of (**38**) (Figure 4.39) shows an absorption peak at 548 nm (ε =45506 $M^{-1}cm^{-1}$) (I) which is ascribed to (π-π^*) conjugated transitions. [12]

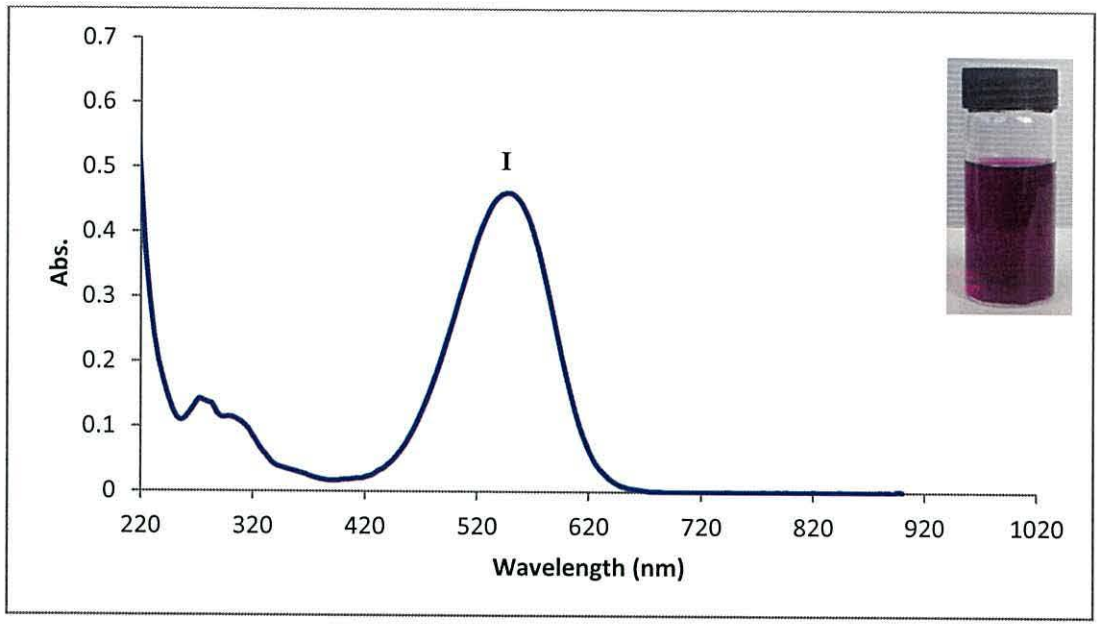

Figure 4.39. UV-Vis spectrum of diphenyl-{4-[2-(1, 3, 3-trimethyl-1H-benzo[e]indolinum-2yl)-vinyl]-phenyl}-amine iodide unsymmetrical cyanine compound (**38**) $1x10^{-5}$M in MeOH, ε = 45506 $M^{-1}cm^{-1}$ at 548 nm.

The successful synthesis of (**38**) has also been confirmed by ^{1}H NMR data which shows the absence of an aldehyde signal for the precursor compound 4-(N, N-diphenylamino)-benzaldehyde along with the presence of signals for (-CH=CH-) as a doublet doublet at 7.79 and 7.82 ppm with coupling constants of J= 8.8 and 8.92 Hz (*cis*-arrangment), which confirms a link between the donor triphenylamine and acceptor indole groups. Signals at 1.94 and 2.71 ppm (singlet and triplet, respectively) are due to CH_3 and CH_2 substituents on the indole and (-CH_2-COOH), respectively. The newly formed link between the donor and acceptor moiety are also observed in the ^{13}C NMR, which shows signals at 113.50 and 132.45 ppm corresponding to (-*CH*=*CH*-). The data also shows signals at 54.93 and 44.59 ppm due to (-N-CH_2-) and (-CH_2-COOH), respectively. Also the ^{1}H NMR show signals at 7.26 and 7.43 ppm are due to (*N*-Ph_2), while the signals at 6.99 and 8.39 ppm due to (*Ph*-N-Ph_2). The signals at 7.64, 7.76, 7.93, 8.12 and 8.18 ppm are assigned to the indole group. The ^{13}C NMR data also have signals at 109.03, 120.10, 123.97, 127.18, 127.92, 128.08, 128.75, 129.40, 131.08, and 131.28 ppm which are assigned to (*Ar*-

H), signals at 133.92, 134.97 and 139.17 ppm are due to (*Ar-C*-C), whilst the signals at 139.68 and 146.94 (*Ar-C*-N). Finally, the signals at 154.61, 154.89 ppm are assigned to (Indole *C-C*), the signal at 175.32 ppm due to (*C=O*) and the signal at 183.84 ppm due to (*C=N*).

The FT-IR spectrum shows a broad peak at 3438 cm^{-1} due to the OH stretch of the carboxylic acid, the peak at 3018 cm^{-1} is assigned to (C-H) stretches of the aromatic ring, 2927 and 2861 cm^{-1} are due to CH_2 and CH_3 stretches, and a broad peak at 1733 cm^{-1} ppm due to (C=O) stretch. A weak peak at 1607 is assigned to (C=C) benzene ring stretching.

4.3 Adsorption dyes on TiO_2 electrode

The aim of this part of work was to investigate the activity of cyanine dyes as sensitizers for DSC and, in particular, to study dye adsorption on the semiconductor surface. Also this study investigates the influence of co-adsorbents and film thickness on photovoltaic performance. This study successfully shows the adsorption of cyanine dyes and derivatives on the titania surface. Figure 4.40 shows HT-TiO_2 Solaronix electrodes which have been soaked in solutions of either (**34**) or (**35**) overnight. The data suggest that both dyes adsorb on the TiO_2 surface. Both spectra show H-aggregation at 704 and 712 nm for (**34**) and (**35**), respectively. [8, 10]

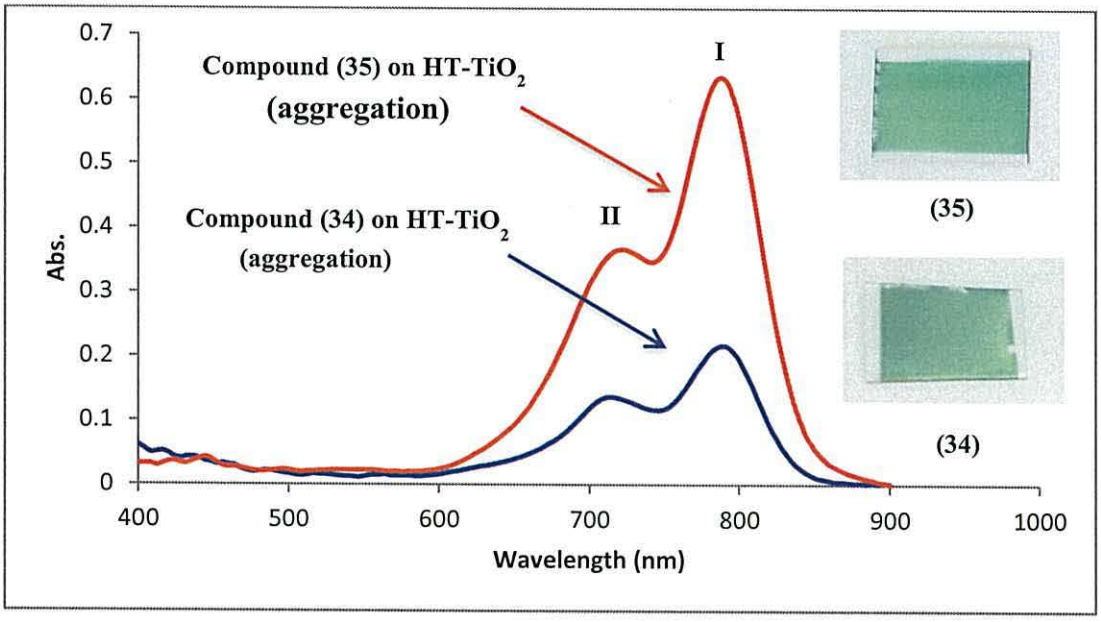

Figure 4.40. UV-Vis spectrum of (a) blue line of (**34**) sorbed on HT-TiO_2 Solaronix, (b) red line of (**35**) sorbed on HT-TiO_2 Solaronix, $1x10^{-5}$ M overnight.

Given that (**34**) has a higher (ε) than (**35**) suggests that there is a higher dye loading in the case of (**35**). Figure 4.40 show that the relative intensities ratio of peak I and II of (**34**) on HT-Solaronix is slightly higher than for (**35**) on HT-Solaronix (0.59 to 0.52), respectively. This suggests that the amount of ggregation of (**34**) on HT-Solaronix is slightly more than (**35**). As expected the performance of DSC devices of (**34**) are lower than (**35**), (Table 4.8).

The UV-Vis spectrum of compound (**34**) and (**35**) either in solution or sorbed onto a TiO_2 film are shown in Figures 4.41 and 4.42. These data show that both dyes have adsorbed on the titania surface with broad absorption bands. Also Figure 4.41 shows that the relative intensities ratio of peak I and II of (**34**) on HT-Solaronix more than (**34**) in the solution, which is 0.28 to 0.65, respectively. This suggests that the amount of dye aggregation on HT-Solaronix is higher than in solution, which may be due to increase interactions of dye molecules on the semiconductor surface. Figure 4.42 also shows the relative intensities ratio of peaks I:II on HT-Solaronix is more than (**35**) in the solution. Interestingly both peaks I and II shift to lower wavelength (blue shift) after adsorbing dye on HT-Solaronix.

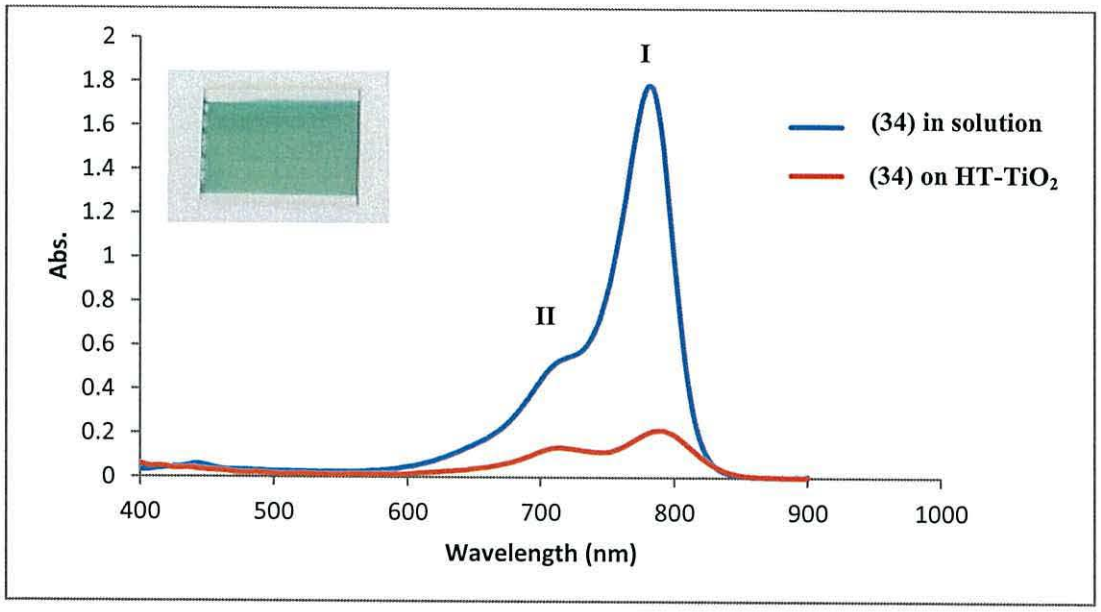

Figure 4.41. UV-Vis spectrum of (a) (**34**) in methanol solution 10^{-5} M, (blue line) and (b) (**34**) adsorbed on HT-TiO_2 (red line).

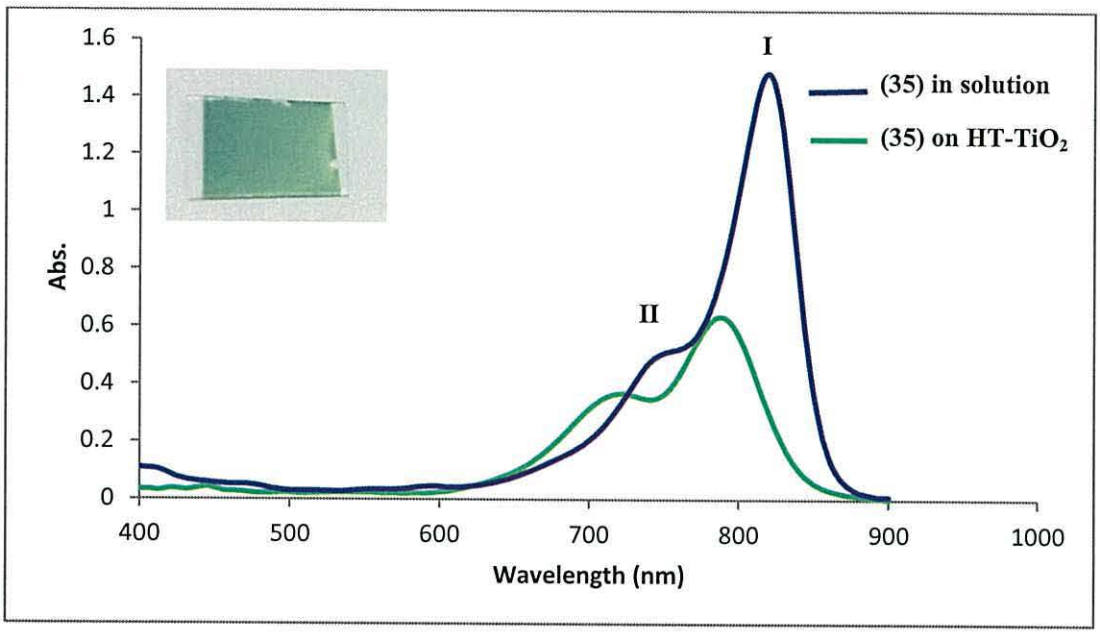

Figure 4.42. UV-Vis spectrum of (a) (**35**) in methanol 10^{-5} M, (a) the (blue line) and (b) (**35**) adsorbed on HT-TiO_2 (red line).

The issues of aggregation led to a study of the use of chenodeoxycholic acid (CDCA) as a co-adsorbent to try to improve device performance of these cyanine dyes. CDCA is a white powder which is transparent in the visible range in solution (Figure 4.43). It is also the most popular co-adsorbent used to improve the solar cell performance. [10, 13] This is because it is believed to prevent dye aggregation through its ability to strongly bind to the semiconductor surface and, therefore displace dye molecules on TiO_2 surface. That can lead to the formation of a mixed mono-layer which should be more tightly packed and more effective for electron injection. [10] Here UV-Vis studies have been used to study the influence adding chenodeoxycholic acid (CDCA) as co-adsorbent into cyanine dye solutions. The main purpose of adding CDCA was to try to solve the dye aggregation problem.

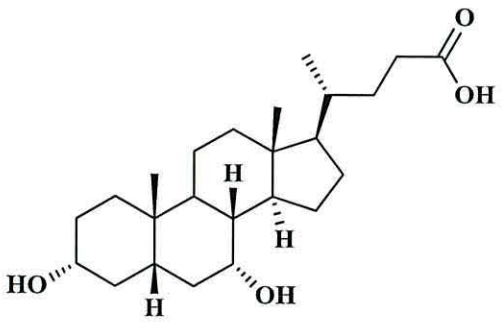

Figure 4.43. Molecular structure of chenodeoxycholic acid **(CDCA)** co-adsorbent.

Figures 4.44 and 4.45 show UV-Vis spectra before and after adding CDCA for compounds (**34**) and compound (**35**), respectively. The data show that adding CDCA to (**34**) shows the absorbance of the dye become broader and captures more light compared without CDCA.

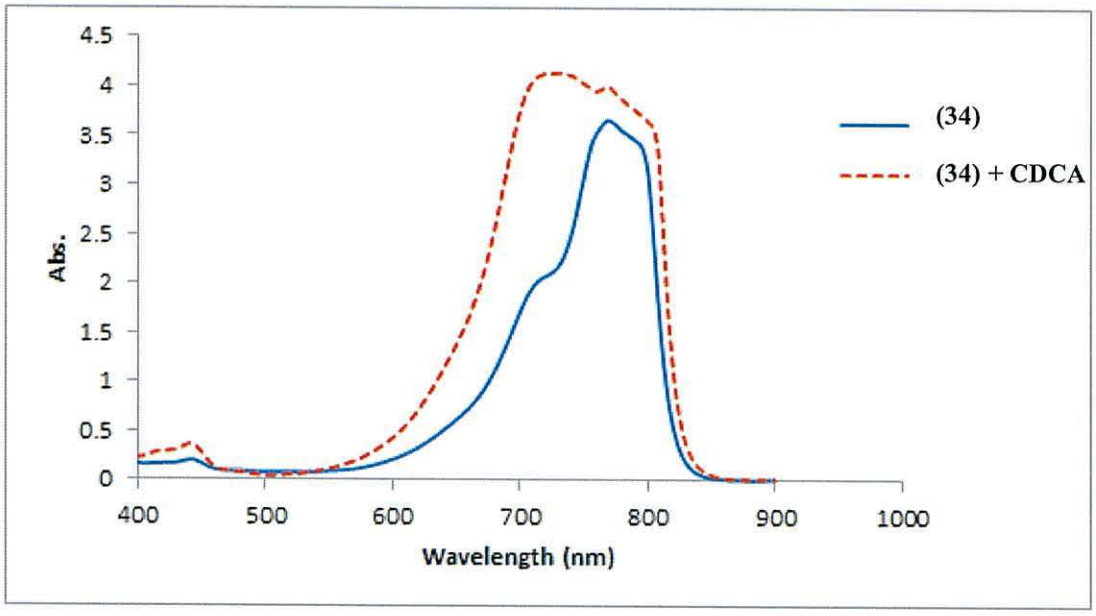

Figure 4.44. UV-Vis spectrum of compound (**34**) in methanol $1x10^{-4}$M, (a) the blue line before adding CDCA, (b) the dashed red line after adding 10 mM CDCA.

Figure 4.45 shows the UV-Vis spectrum of (**35**) in solution at different concentrations of CDCA under the same experimental conditions which shows that increasing the CDCA concentration led to a slight decrease in the intensity of absorbance and also a slight red shift in wave length.

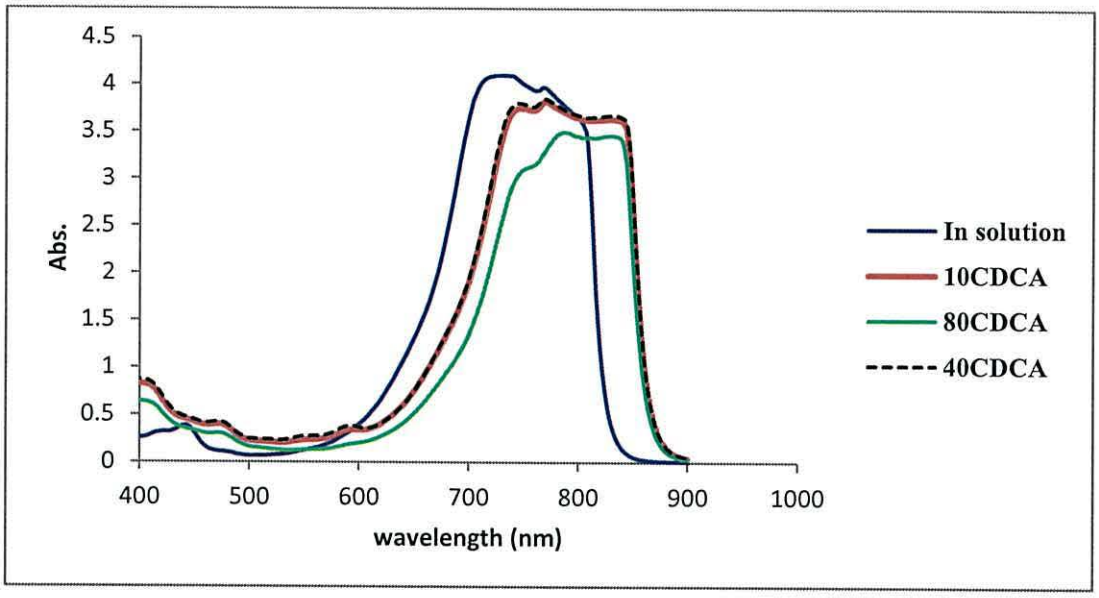

Figure 4.45. UV-Vis spectra of (**35**) in methanol $1x10^{-4}$M, the blue line = before adding CDCA, the red line = (**35**) +10 mM CDCA, the black dashed line = (**35**) + 40 mM CDCA and the green line = (**35**) + 80 mM CDCA.

Having shown the effect of chenodeoxycarboxylic acid (CDCA) as a co-adsorbent to prevent the aggregation of cyanine dyes on the TiO_2 surface. The next step was to prepare and investigate a suitable electrolyte to use it in DSC for cymmetric and unsymmetric cyanine dyes and their derivatives.

4.4 Electrolyte

The electrolyte is a key component of all DSC, [14] and plays an important role in enhancing DSC device performance. As mentioned in Chapter One, the iodide /triiodide redox couple has been most widely used to date and was used in this work as a standard electrolyte redox couple. Attempts were then made to try to prepare a suitable electrolyte for the cyanine dyes by investigating the effect of adding different additives to a standard electrolyte; namely lithium iodide LiI and 4-*tert*-butylpyridine (TBP) both of which are known to play role in the enhancement of DSC performance. [15] Table 4.6 shows several kinds of electrolyte which have been studied. The stock electrolyte was composed of a mixture of (0.8 M imidazolium iodide and 0.1M iodine) in 3-methylpropionitrile. The additives were then added to this as shown in Table 4.6. The investigation carried out using (**35**) as the dye. The reason for using (**35**) in this investigation was due to the high λ_{max} absorption and the

additional benzene ring which makes it more conjugated than (**34**). (**35**) also has two carboxylic acids compared with (**37**) and (**38**).

Table 4.6. Electrolytes which used to investigate the performance DSC devices of (**35**).

Electrolyte	Imidazolium iodide (mol L^{-1})	Iodine (mol L^{-1})	LiI (mol L^{-1})	TBA (mol L^{-1})
A	0.8	0.1	-	-
B	0.8	0.1	0.1	-
C	0.8	0.1	1	-
D	0.8	0.1	-	0.1
E	0.8	0.1	-	0.5
F	0.8	0.1	0.1	0.5
G	0.8	0.1	1	0.5

Table 4.7. Photovoltaic parameters of DSC devices made using (**35**) investigated with different types of electrolyte. The working electrode based on DSL18-NRT paste.

Dye	Electrolyte	FF	J_{sc} (mA cm^{-2})	V_{oc} (V)	η (%)
(35)	A	0.44	0.22	0.31	0.03
	B	0.43	0.27	0.36	0.04
	C	0.50	0.28	0.43	0.06
	D	0.60	0.24	0.48	0.07
	E	0.48	0.29	0.37	0.05
	F	0.59	0.26	0.46	0.08
	G	0.62	0.33	0.50	0.10

Table 4.7 shows that the photovoltaic performance started to improve when electrolyte (C) was used which consisted of electrolyte (A) + 1M of LiI. A further slight increase was observed with electrolyte (D) which was composed of the components of electrolyte (A) + 0.1 M of *tert*-butylpyridine (TBP). The increase in

the open circuit voltage (V_{oc}) using TBP additive matches with the literature. [16] The efficiency (η) and V_{oc} decreased slightly when electrolyte (E) was used which was composed of electrolyte (A) + 0.5M of *tert*-butylpyridine (TBP). This suggests that too much TBP has a negative effect on the performance of the device. The best result for the efficiency (η) and the photocurrent density (J_{sc}) were achieved by using electrolyte (G) which compose of electrolyte (A) + 1M LiI + 0.5M TBP. This increase is attributed to the small size of Li^+ cations which can more easily interact with the TiO_2 particles to enhance electron transfer from the excited dye molecules into the conduction band of TiO_2. [17, 18] Also the 4-*tert*-butylpyridine increased the open-circuit voltage which could have affected on the rate of electron transfer from the conduction band of the semiconductor to the triiodide in the electrolyte and that led to a decrease in the rate constant for triiodide reduction. [19] 4-*tert*-butylpyridine TBP is known to shift the TiO_2 conduction band which would also help dye injection. [16]

Table 4.8. Photovoltaic parameters of DSC devices prepared using (**34**), (**35**), (**37**) and (**38**) based on electrolyte G and TiO_2 18-NRT paste.

Dye	CDCA mM	FF	V_{oc} (V)	J_{sc} (mA cm^{-2})	η (%)
(**34**)	-	0.55	0.47	0.35	0.09
	10	0.58	0.47	0.51	0.14
	40	0.65	0.52	0.54	0.18
	80	0.69	0.57	0.58	0.06
(**35**)	-	0.62	0.33	0.5	0.10
	10	0.57	0.54	0.41	0.13
	40	0.57	0.58	0.44	0.14
(**35**)-3 layers TiO_2	40	0.70	0.48	0.75	0.25
(**35**)-4 layers TiO_2	40	0.65	0.56	0.50	0.18
(**37**)	-	0.42	0.40	0.31	0.05
(**38**)	-	0.47	0.56	0.44	0.12

The DSC photovoltaic performances for all cyanine dyes have been investigated and Table 4.8 shows the data before and after adding the co-adsorbent chenodeoxycholic acid (CDCA). Firstly, photovoltaic parameters were investigated for devices based on 2 screen-printed layers of DSL18-NRT pastes sensitized using (**34**), (**35**), (**37**) and (**38**). These gave a maximum efficiency of 0.09% with J_{sc} (0.35 mA cm^{-2}), 0.1% (0.5 mA cm^{-2}), 0.05% (0.31 mA cm^{-2}) and 0.12% (0.44 $mAcm^{-2}$), respectively without CDCA. To solve the problem of aggregation, studies were carried out using CDCA as a co-adsorbent in dye solutions of (**34**) or (**35**) because CDCA has been used to supress dye aggregation. [10, 20] Table 4.8 shows (η, J_{sc}, V_{oc} and FF) increased gradually with increased CDCA concentration and gave the best result at 40 mM (η= 0.18%, J_{sc}= 0.54 mA cm^{-2}), which suggests that CDCA binds to the TiO_2 surface competitively and displaces some dye molecules on the semiconductor surface to prevent the formation of dye aggregates. [10] In contrast, the conversion efficiency was much lower (0.06%) when too much CDCA (80 mM) was used, which was believed to reduce the dye loading. The influence of TiO_2 film thickness and CDCA concentration on device performance was investigated for compound (**35**) devices. As discussed above, the best result obtained for (**35**) when applying two layers of TiO_2 with 40 mM of CDCA was 0.14%, while (**35**) showed enhanced device performance after increasing the TiO_2 film thickness to 3 layers and using 40 mM CDCA. Here the conversion efficiency and photocurrent increased from 0.14 to 0.25% and from 0.44 to 0.75 mA cm^{-2}, respectively. However for similar conditions, increasing the film thickness to 4 layers dropped the conversion efficiency and photocurrent to 0.18% and 0.50 mA cm^{-2}, which is believed to reflect greater recombination due to the longer distances electrons need to travel. [21]

4.5 Conclusions

In this chapter, symmetrical ((**34**) and (**35**)) and unsymmetrical ((**37**) + (**38**)) cyanine dyes have been synthesized. This aim was to use these dyes in DSC devices in an attempt to capture more light in the near infrared region (NIR). This has not been widely reported in the literature. In this work, an uncatalyzed method was used to synthesize cyanine dyes with different solvent. The data show that DMF is a better solvent for this type of reaction than a 1-butanol: benzene mixture because DMF avoids the formation of a mixture butyl-ester by-product which are hard to separate

from the target compounds. The mass spectrum and single crystal structure data obtained have confirmed that the molecular structure of (**34**) does not include iodine as a counter ion. The first compound (**34**) was an analogue of the Funabiki compound **KFH-2** which was reported in 2011. [3] However, there were differences in the central unit as shown in Figure 4.46. Interestingly, in both compounds (**34**) and (**35**) there appears to be an internal transfer of a hydrogen ion from one of the carboxylic acid (COOH) groups to the amine group to leave an ion with both a negative charge and positive charge (a zwitterion). For KFH-2, this would only possible on one side of the molecule because an iodide ion is coordinated to the other (positively charged) N atom.

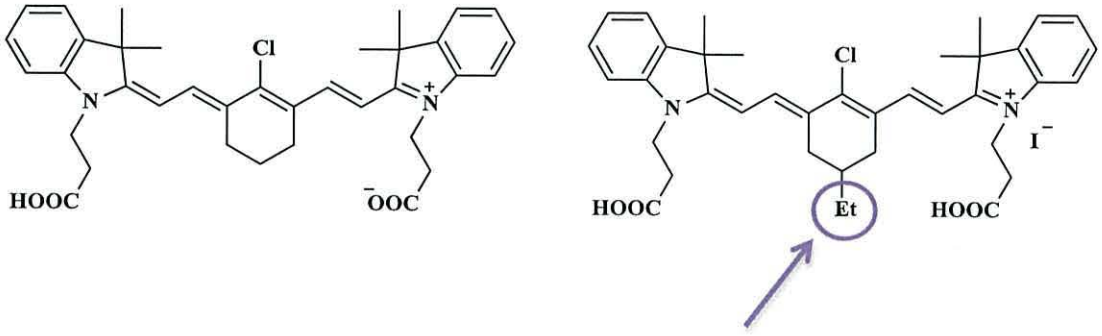

Figure 4.46. Molecular structure of compound (**34**) and **KFH-2.**

Funabiki *et al.* investigated KFH-2 dye on porous ZnO at low temperature with different ZnO film thicknesses, while we investigated with DSL18-NRT TiO_2 sintered at high temperature and also with different film thickness. When Funabiki *et al.* used a ZnO film prepared from 7-9 μm of paste they got an overall conversion efficiency 0.03% without using CDCA and 0.49% by using 10 M CDCA, while we used 2 layers of TiO_2 to get conversion efficiencies of 0.09% and 0.18% with and without using 40 mM CDCA, respectively. The results show these compounds do not currently work well in these DSC devices. However, we were able to prove that these compounds are optically active as sensitizers.

The molecular structure of these compounds is believed to play an important role in enhancement of performance photovoltaic and optical properties. This can be seen for these compounds, if the λ_{max} of (**35**) which absorbs at 820 nm is compared with (**34**) which has a maximum absorbance at 780 nm. This is due to the additional

benzene rings in (**35**) which lead to an increase in the conjugation of the molecule and shift the absorbance to a longer wavelength. (**37**) Shows a maximum absorption at λ_{max} 816 nm, whilst (**38**) shows a maximum absorption at λ_{max} 548 nm. In addition, (**34**) show the highest molar extinction coefficient ε =180,414 $M^{-1}cm^{-1}$ compared with other cyanine dyes (**35**), (**37**) and (**38**) which were 150100, 122980 and 45506 $M^{-1}cm^{-1}$, respectively.

In the context of DSC it was found that one of the most important features of the cyanine dyes are that they suffer from aggregation due to strong inter-dye interactions between molecules.

When considering the DSC devices prepared from these compounds. (**35**) Shows slightly better data than (**34**). Also 3 layers of TiO_2 gave slightly better results than 2 or 4 layers. The results which were obtained from investigating different types of electrolyte show that, LiI and/or TBP additives could both improve device performance with the biggest improvement after adding 1 M of LiI with 0.5 M of TBP in line with the literature. [19] The electron injection lifetimes of these dyes are being tested.

4.6 References

1. N. Narayanan and G. Patonay, *J. Org. Chem.*, 1995, **60**, 2391–2395.
2. G. A. Reynolds and K. H. Drexhage, *J. Org. Chem.*, 1977, **42**, 885–888.
3. K. Funabiki, H. Mase, A. Hibino, N. Tanaka, N. Mizuhata, Y. Sakuragi, A. Nakashima, T. Yoshida, Y. Kubota, and M. Matsui, *Energy Environ. Sci.*, 2011, **4**, 2186–2192.
4. X. H. Zhang, Y. H. Zhan, D. Chen, F. Wang, and L. Y. Wang, *Dyes and Pigments*, 2012, **93**, 1408–1415.
5. B. Morzyk-Ociepa, D. Michalska, and A. Pietraszko, *J. Mol. Struct.*, 2004, **688**, 79–86.
6. Z. Zhang and S. Achilefu, *Org. Lett.*, 2004, **6**, 2067–2070.
7. G. Janssens, F. Touhari, J. W. Gerritsen, H. van Kempen, P. Callant, G. Deroover, and D. Vandenbroucke, *Chem. Phys. Lett.*, 2001, **344**, 1–6.
8. K. Sayama, S. Tsukagoshi, T. Mori, K. Hara, Y. Ohga, A. Shinpou, Y. Abe, S. Suga, and H. Arakawa, *Sol. Energy Mater. Sol. Cells*, 2003, **80**, 47–71.
9. T. Ono, T. Yamaguchi, and H. Arakawa, *Sol. Energy Mater. Sol. Cells*, 2009, **93**, 831–835.
10. J. Li, W. Wu, J. Yang, J. Tang, Y. Long, and J. Hua, *Sci. China Chem.*, 2011, **54**, 699–706.
11. X. Ma, J. Hua, W. Wu, Y. Jin, F. Meng, W. Zhan, and H. Tian, *Tetrahedron*, 2008, **64**, 345–350.
12. J. Wang, W. F. Cao, J. H. Su, H. Tian, Y. H. Huang, and Z. R. Sun, *Dyes and Pigments*, 2003, **57**, 171–179.
13. J. H. Yum, S. J. Moon, R. Humphry-Baker, P. Walter, T. Geiger, F. Nüesch, M. Grätzel, and M. d K. Nazeeruddin, *Nanotechnol.*, 2008, **19**, 424005.
14. J. Gong, J. Liang, and K. Sumathy, *Renew. Sustain. Energy Rev.*, 2012, **16**, 5848–5860.
15. A. Hagfeldt, G. Boschloo, L. Sun, L. Kloo, and H. Pettersson, *Chem. Rev.*, 2010, **110**, 6595–6663.
16. S. A. Haque, Y. Tachibana, R. L. Willis, J. E. Moser, M. Grätzel, D. R. Klug, and J. R. Durrant, *J. Phys. Chem. B*, 2000, **104**, 538–547.
17. J. Wu, Z. Lan, S. Hao, P. Li, J. Lin, M. Huang, L. Fang, and Y. Huang, *Pure Appl. Chem.*, 2008, **80**, 2241–2258.
18. D. F. Watson and G. J. Meyer, *Coord. Chem. Rev.*, 2004, **248**, 1391–1406.

19. M. K. Nazeeruddin, A. Kay, I. Rodicio, R. Humphry-Baker, E. Mueller, P. Liska, N. Vlachopoulos, and M. Graetzel, *J. Am. Chem. Soc.*, 1993, **115**, 6382–6390.
20. W. Wu, F. Guo, J. Li, J. He, and J. Hua, *Synth. Met.*, 2010, **160**, 1008–1014.
21. A. Solbrand, H. Lindström, H. Rensmo, A. Hagfeldt, S. E. Lindquist, and S. Södergren, *J. Phys. Chem. B*, 1997, **101**, 2514–2518.

Chapter 5

Phthalocyanine dyes

5.1 Introduction

Phthalocyanine compounds have been synthesized using several methods, as described in chapter one. Phthalocyanine compounds are either metalated or metal-free macrocyclic rings. They have been used industrially as dyes for biological applications, [1] as photocatalysts and in chemical sensors. [2]

This chapter describes the design and synthesis of new types of unsymmetrical and symmetrical phthalocyanines by reacting 4, 5-bis ([1, 1', 3', 1''-terphenyl]-2'-yloxy) phthalonitrile (**20**) with di-(4-methylbenzoate)-fumaronitrile (**19**) or with 4, 5-bis (4-methoxycarbonylphenyl) phthalonitrile (**22**), while the synthesis of symmetrical phthalocyanine has been carried out by the cyclisation of 4, 5-bis ([1, 1', 3', 1''-terphenyl]-2'-yloxy) phthalonitrile (**20**).

The results obtained showed varying the ratio of phthalonitrile precursors affects the phthalocyanine compounds formed in this work. Also the solubility and reactivity of the phthalonitrile substitutes play important role in formed a variety ratio of product. Purification is the main problem for the phthalocyanine compounds, which means forming a mixture of products is a bigger problem. Scheme 5.1 shows the statistical mixture of phthalocyanine product that can occur through attempt to cyclisation used two different phthalonitrile precursors as substitutes. It's of course there is a possibility to form all the possibilities depending on the ratio of substituted phthalonitrile as a precursor. On other hand, the desired compound can be produce by manipulation of the reactant ratio and the reaction condition.

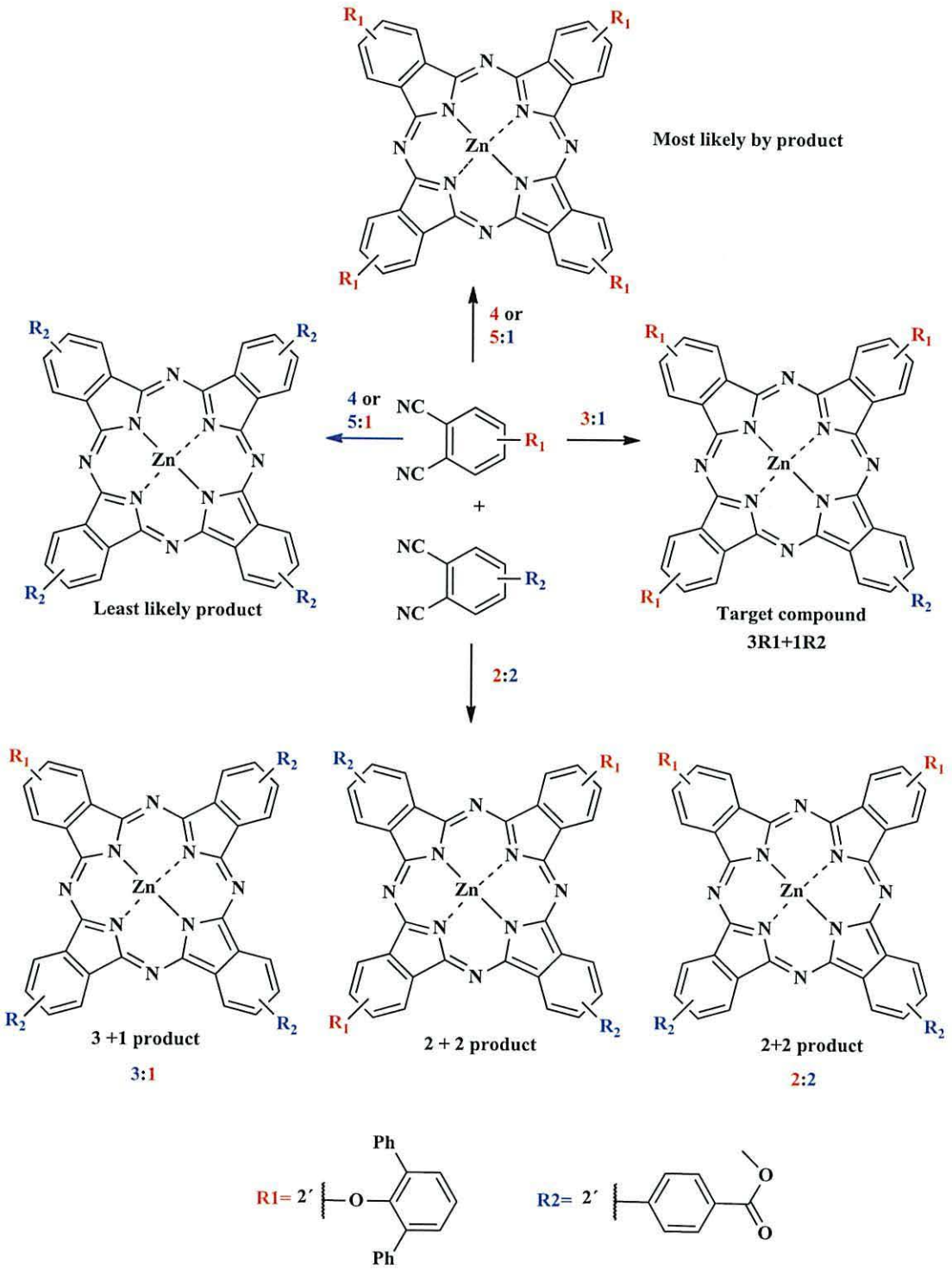

Scheme 5.1. Statistical mixture of possible phthalocyanine products formed by reacting two different phthalonitrile precursors.

5.2 Synthesis of unsymmetrical phthalocyanine 2, 3-di (4-benzoic acid)-7^2, 12^2, 17^2-hexa (2, 6-diphenylphenoxy)-tribenzo-5, 10, 15, 20-tetrazaporphyrin zinc (24).

The strategy of this part of work was to synthesize and design a new unsymmetrical phthalocyanine compound containing two carboxylic acids as linker groups, to anchor to the semiconductor surface. We have also prepared the precursors needed to obtain these molecules. In this work a new unsymmetrical phthalocyanine with six 2, 6-diphenylphenol groups substituted on the outer Pc benzene rings have been studied to prevent aggregation. The successful synthesis of unsymmetrical phthalocyanine (**24**) (Scheme 5.2) was achieved by reacting 4, 5-bis ([1, 1', 3', 1''-terphenyl]-2'-yloxy) phthalonitrile (**20**) with di-(4-methylbenzoate)-fumaronitrile (**19**) in a ratio of 1:3 and zinc chloride in 1-butanol as solvent in the presence of 1, 8-diazabicyclo [4, 5, 0] undec-7-ene (DBU) at 140°C for 72 h to produce a green solid of phthalocyanine-ester (**23**). Hydrolysis of (**23**) produced the desired compound (**24**).

This synthetic pathway was achieved by four steps. The first step was to synthesize the precursor (**19**), which was prepared by dissolving methyl-4-(cyanomethyl)-benzoate and iodine in dry diethyl ether. Then the reaction was stirred at -78°C, and sodium methoxide in dry methanol was added drop wise under nitrogen before quenching with 3-6% HCl. After the temperature of reaction increased to 0-5°C and the colour changed from black to beige to produce a beige solid of di-(4-methylbenzoate)-fumaronitrile (**19**) (4.24g, 43%). Identification of the resultant (**19**) was initially achieved using the diagnostic C≡N stretch in the FT-IR spectrum at 2222 cm^{-1} and a sharp peak at 1726 cm^{-1} due to the carbonyl of the methyl ester group.

The ^1H NMR confirmed (**19**) with a signal at 3.98 ppm as a singlet due to methyl ester group, and signals at 7.93 and 8.22 ppm as a doublet due to (*Ar-H*). ^{13}C NMR confirmed (**19**) with signals at 52.60 ppm for the methyl ester group, and a signal at 115.88 ppm assigned to (C≡N). A signal at 125.92 ppm was due to (-*C*-CN), whilst the signals at 128.83 and 130.48 ppm are assigned to (*Ar-H*). Finally, the signals at 133.20 and 135.52 ppm are due to (*Ar-C*-C=O, C-3 and C-3a) and (*Ar-C*-C, C-6 and C-6a), respectively and the signal at 165.69 ppm due to carbonyl ester group.

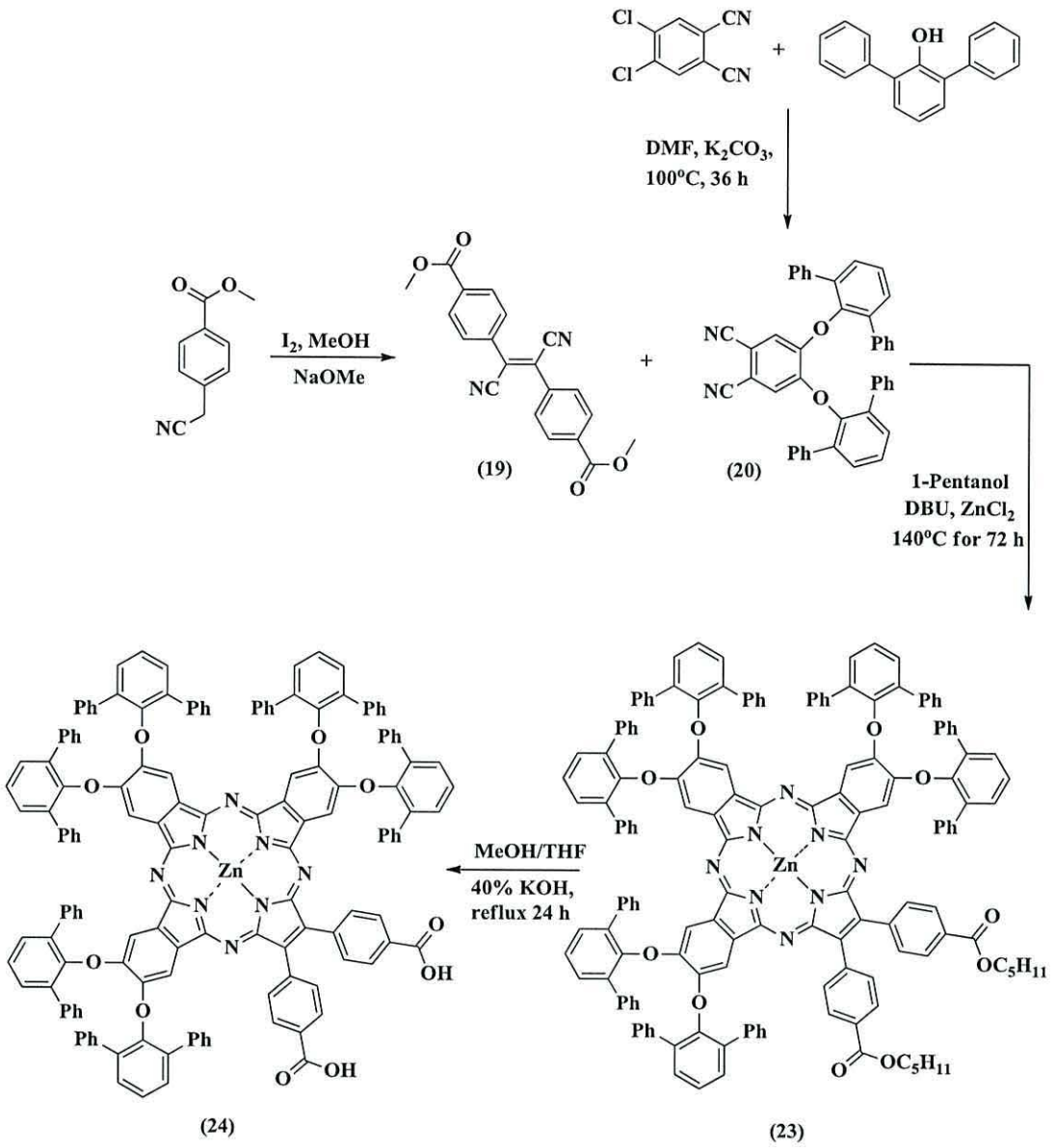

Scheme 5.2. Synthetic pathway of 2, 3-di (4-benzoic acid)-7^2, 12^2, 17^2-hexa (2, 6-diphenylphenoxy)-tribenzo-5, 10, 15, 20-tetrazaporphyrin zinc (**24**).

The data from mass spectrometry also confirm compound (**19**) with the most prominent peak at 364.1295, which corresponds to (**19**) $[M+NH_4]^+$. Single crystals for X-ray structure determination were obtained by the evaporation method, using dichloromethane as the solvent. The resultant molecular structure of di-(4-methylbenzoate)-fumaronitrile (**19**) is shown in Figure 5.1. The details selected bond length (Å) and angles (°) are listed in Table 5.1. All the C-C bonds in the benzene rings are between single (C-C) and double (C=C) bond lengths and are between 1.393 and 1.412 (Å). There are no significant differences between the bond angles of

the benzene rings which are close to 120°, [3] while the bond length for C≡N is between 1.135-1.139 (Å) while indicates that this is a triple bond. The figure also shows the nitrile groups are in a *trans*- position in the molecule structure.

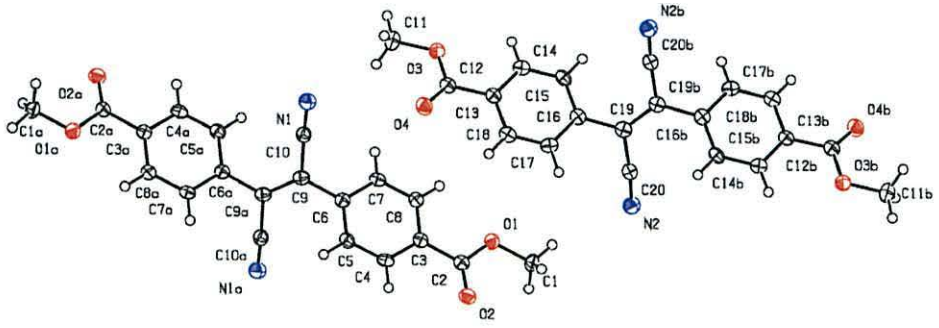

Figure 5.1. Molecular structure of two molecules of di-(4-methylbenzoate)-fumaronitrile **(19)** in unit cell.

Table 5.1. Selected bond length (Å) and angles (°) for **(19)**.

C6-C9	1.499 (3)	C2-O1	1.356 (3)
C2-C3	1.501 (3)	C2-O2	1.210 (3)
C9-C10	1.453 (3)	C9-C9a	1.372 (5)
C10-N1	1.149 (3)	C5-C6-C7	119.5 (2)
C1-O1	1.462 (3)	C4-C3-C8	119.5 (2)

The torsion angle data also confirm that the phenyl groups are co-planar with each other in the molecule as represented by C8-C7-C6-C9 and C14-C15-C16-C19 dihedral angles which are closed to 180°. The carboxylate methyl groups are co-linear with the molecule skeleton as represented by C2-C3-C4-C5 and C12-C13-C18-C17 dihedral angles which are also close to 180°.

The second step was to synthesize the precursor compound **(20)**. The reaction carried out by mixing 2, 6-diphenylphenol and 4, 5-dichlorophthalonitrile in DMF as solvent in the presence of potassium carbonate at 100°C for 36 h under a nitrogen atmosphere. The crude product purified by column chromatography on silica gel with dichloromethane as an eluent to produce **(20)** as a white solid (yield 0.7 g, 47%).

The ^{1}H NMR spectrum in $CDCl_3$ showed signals at 6.20 ppm as a singlet due to (*Ar-H*, H-3, H-6), and at 7.04 ppm as a triplet due to (*Ar-H*, H-18, H-20, H-24, H-26, H-36, H-38, H-42, H-44). This should be appearing as a double doublet but it appeared as a triplet due to peak overlap and with the same J value. A triplet signal at 7.16 ppm is due to (*Ar-H*, H-19, H-25, H-37 and H-43), the signal at 7.42 ppm as a doublet is due to (*Ar-H*, H-17, H-21 H-23, H-27, H-35, H-39, H-41 and H-45). A singlet at 7.45 ppm is due to (*Ar-H*, H-12, H-13, H-14, H-30, H-31 and H-32). The ^{13}C NMR shows 12 signals due to 12 environments with signals at 107.34 ppm due to (*Ar-C*-C, C-2 and C-7), and a signal at 115.01 ppm due to (*C≡N*). These results match with the literature. [4] The signals at 119.09, 126.69, 127.80, 128.40, 129.18, 131.27 are due to (*Ar-C*-H), and signals at 134.94, 137.12, 146.81 and148.48 ppm are due to (*Ar-C*-C).

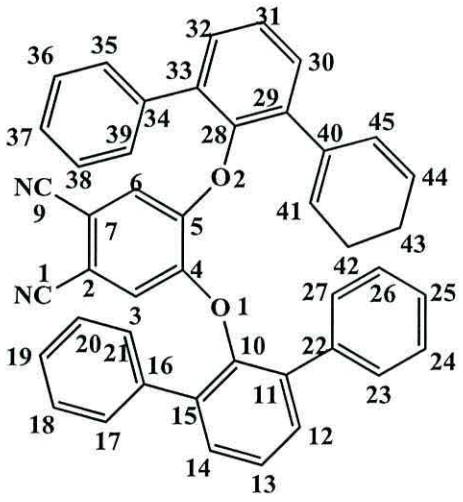

Figure 5.2. Molecular structure of 4, 5-bis ([1, 1', 3', 1''-terphenyl]-2'-yloxy) phthalonitrile (**20**). Showing atom labelling to aid NMR assignments.

The initial ^{1}H and ^{13}C NMR spectra were measured in $CDCl_3$. However, the data were re-measured in deuterated benzene to better characterize the peaks. HSQC was also measured. The re-run ^{1}H NMR data show signals at 6.15 ppm as a singlet (integrated to 2H) due to (*Ar-H*, H-3, H-6), a signal at 6.87 ppm as a multiplet with 12H due to (*Ar-H*, H-17, H-21, H-23, H-27, H-35, H-39, H-41, H-45 and H-19, H-25, H-37, H-43), a triplet at 6.97 ppm with 2H due to (*Ar-H*, H-13, H-31), a signal at 7.10 ppm as a doublet with 4H due to (*Ar-H*, H-12, H-14, H-30, H-32), and signal at 7.28 as a double doublet with 8H due to (*Ar-H*, H-18, H-20, H-24, H-26, H-36, H-38,

H-42, H-44). The DEPTQ data show 12 carbon signals due to 12 environments. The HSQC data for carbon-proton correlation shows signal at 108.72 ppm due to (*Ar-C*-C, C-2,C-7), 115.07 ppm (*Ar-C*-C, C-1,C-9), 119.48 ppm (*Ar-C*-C, C-3,C-6), 126.79, 127.82, 128.70, 129.55 and 131.55 ppm for (*Ar-H*), 135.29 ppm (*Ar-C*-C, C-11, C-15, C-29, C-33), 137.73 ppm for (*Ar-C*-C, C-16, C-22, C-34, C-40), 147.34 ppm for (*Ar-C*-C, C-10, C-28) and 148.66 ppm for (*Ar-C*-C, C-4, C-5). The FT-IR data show the most important characteristic peaks at 2230 cm^{-1} assigned to a (C≡N) stretch. The mass spectrum confirmed (**20**) was present with the most prominent peak at 634.2483 corresponding to (**20**), $[M+NH_4]^+$.

Single crystals for X-ray structure determination were obtained by the evaporation method, using dichloromethane/diethylether as the solvent. The resulting molecular structure of 4, 5-bis ([1, 1', 3', 1''-terphenyl]-2'-yloxy) phthalonitrile (**20**) is shown in Figure 5.3.

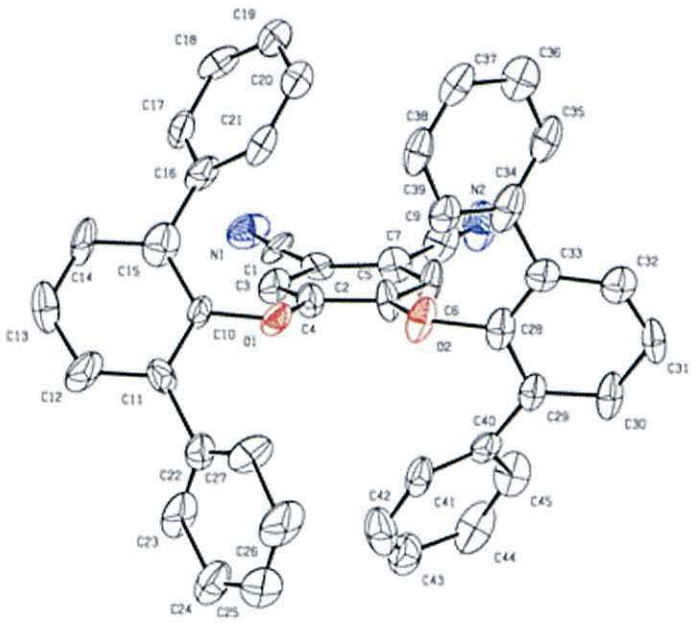

Figure 5.3. Molecular structure of 4, 5-bis ([1, 1', 3', 1''-terphenyl]-2'-yloxy) phthalonitrile (**20**).

The details of selected bond length (Å) and angles (°) are listed in Table 5.2. As expected, all the C-C bonds in the benzene rings are between single (C-C) and double (C=C) bonds between 1.438 and 1.356 (Å). [3] There are no significant

differences between the angles of benzene rings which are close to 120°, while the bond lengths for C≡N are between 1.135 and 1.139 (Å) which indicates triple bonds.

Table 5.2. Selected bond length (Å) and angles (°) for 4, 5-bis ([1, 1', 3', 1''-terphenyl]-2'-yloxy) phthalonitrile (**20**).

C15-C16	1.500 (15)	C28-O2	1.432 (10)
C11-C22	1.535 (13)	C4-O1	1.391 (10)
C29-C40	1.474 (13)	C5-O2	1.374 (9)
C33-C34	1.539 (14)	C1-N1	1.135 (11)
C10-O1	1.388 (9)	C9-N2	1.139 (12)

The next step after preparation of the precursor compounds, was to attempt to synthesize an unsymmetrical phthalocyanine ester 2, 3-di (4-pentoxybenzoate)-7^2, 12^2, 17^2-hexa (2, 6-diphenylphenoxy)-tribenzo-5, 10, 15, 20-tetrazaprophyrin zinc (**23**). The successful synthesis was achieved by condensation of 4, 5-bis ([1, 1', 3', 1''-terphenyl]-2'-yloxy) phthalonitrile (**20**) and di-(4-methylbenzoate)-fumaronitrile (**19**) in a 3:1 ratio with zinc chloride in 1-pentanol as solvent in the presence of 1, 8-diazabicyclo [4, 5, 0] undec-7-ene (DBU) at 140°C for 72 h to produce a dark green solid of the unsymmetrical phthalocyanine-ester (**23**). The crude product was purified by column chromatography on silica gel with methanol as an eluent to produce (**23**) as a dark green solid (yield 0.25 g, 37%), as shown in Figure 5.6. However, the expected unsymmetrical phthalocyanine product with methyl ester groups was not obtained. Instead mass spectrometry (Figure 5.4) identifies a molecular ion at 2372.7 for an unsymmetrical phthalocyanine with pentyl ester groups. It is believed that an exchange reaction between methanoate and pentanoate groups present in the pentanol solvent occurred during the cyclisation reaction. [5] After repeating the reaction to scale up, a mixture of products of the unsymmetrical pentyl-ester (**23**) and the symmetrical phthalocyanine (**26**) were obtained. Mass spectrum data Figure 5.5 also has showed two molecular ions peaks at 2373.8 and 2531.8 which correspond to the unsymmetrical phthalocyanine pentyl-ester (**23**) and symmetrical phthalocyanine (**26**), respectively.

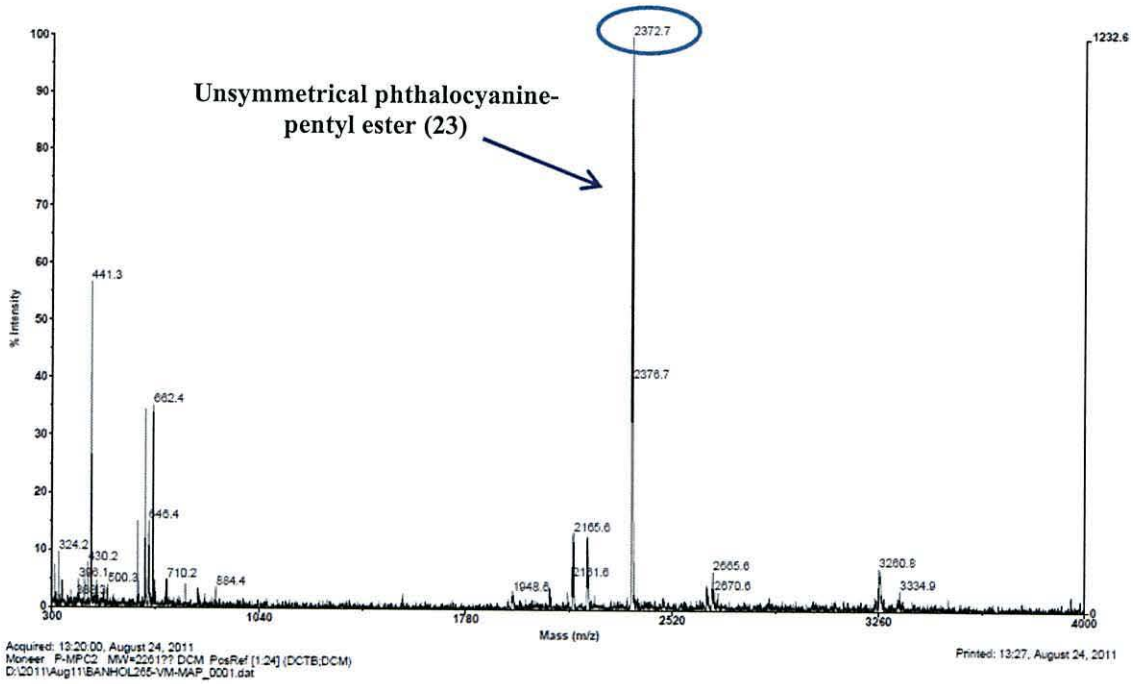

Figure 5.4. MALDI-DCTB matrix mass spectrum of 2, 3-di (4-pentoxybenzoate)-7^2, 12^2, 17^2-hexa (2, 6-diphenylphenoxy)-tribenzo-5, 10, 15, 20-tetrazaporphyrin zinc (**23**).

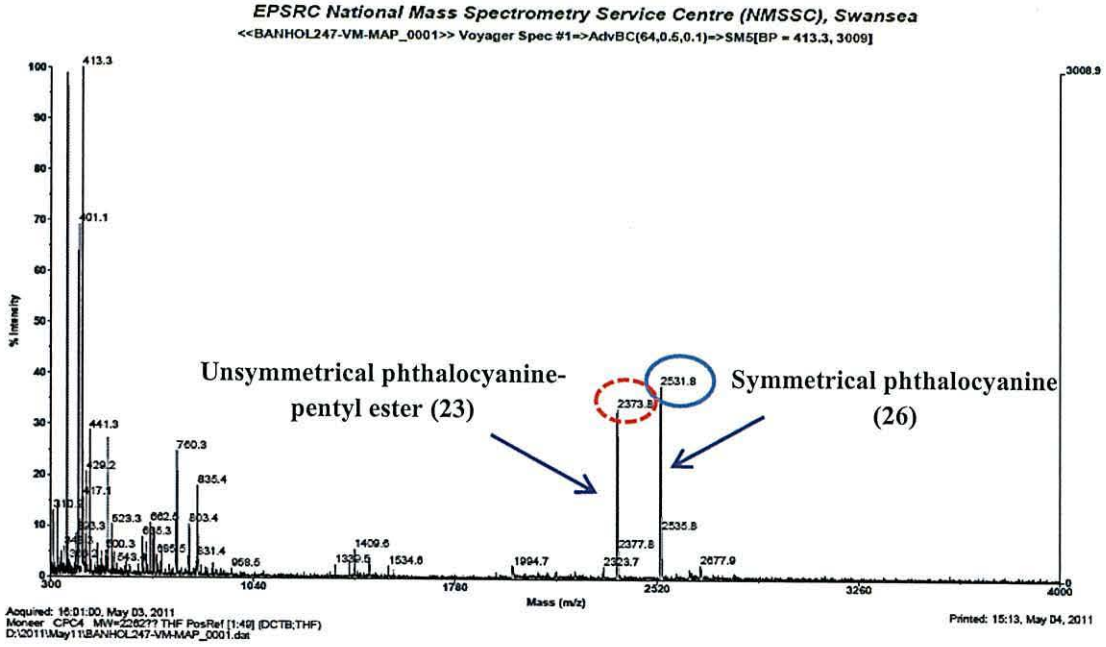

Figure 5.5. MALDI-DCTB matrix mass spectrum of a mixture 2, 3-di (4-pentoxybenzoate)-7^2, 12^2, 17^2-hexa (2, 6-diphenylphenoxy)-tribenzo-5, 10, 15, 20-tetrazaprophyrin zinc **(23)** and 2^2, 7^2, 12^2, 17^2 octa (2, 6-diphenylphenoxy)-tetrabenzo-5, 10, 15, 20-tetrazaporphyrin zinc (**26**).

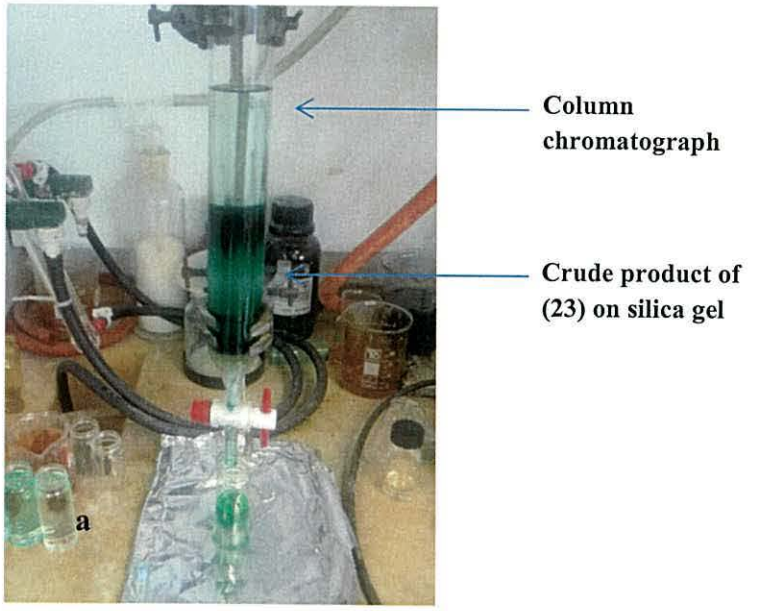

Figure 5.6. Photograph showing the purification of (**23**) using column chromatography.

The UV-Vis spectrum of the unsymmetrical phthalocyanine-pentyl ester (**23**) is shown in Figure 5.7 in THF solution. The data show a Soret band absorption at 360 nm (I) and a sharp and intense a Q-band absorption at 684 nm (II) (ε= 83672 $M^{-1}cm^{-1}$) due to a (π-π^*) transition of the conjugated macrocycle. [2]

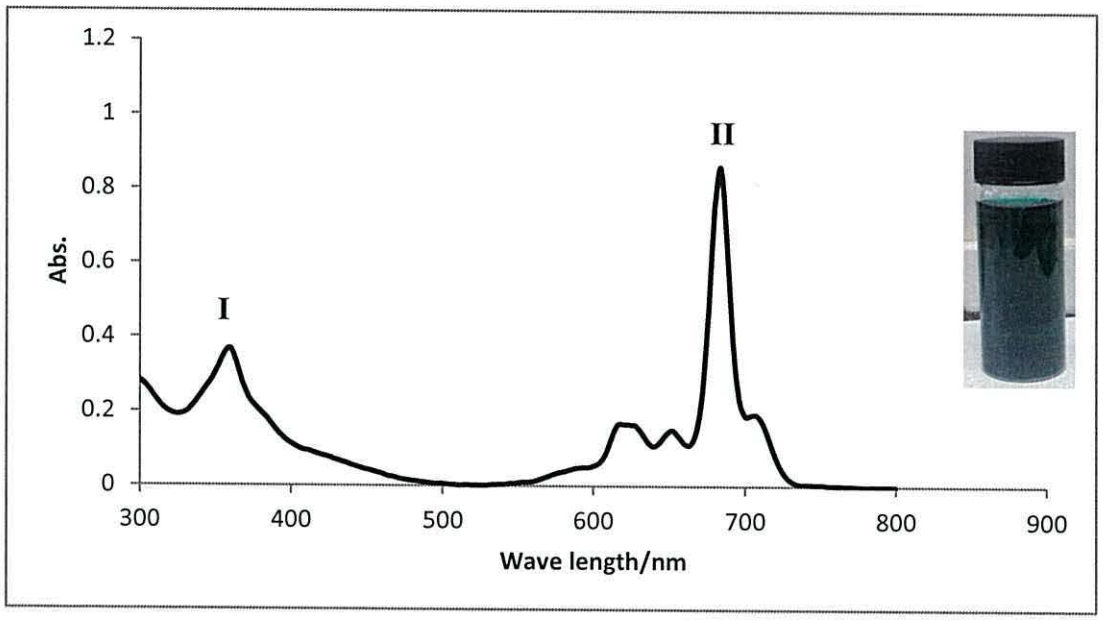

Figure 5.7. UV-Vis spectrum of 2, 3-di (4-pentoxybenzoate)-7^2, 12^2, 17^2-hexa (2, 6-diphenylphenoxy)-tribenzo-5, 10, 15, 20-tetrazaporphyrin zinc (**23**), in THF 10^{-5} M, ε= 83672 $M^{-1}cm^{-1}$ at 684 nm. Vial containing a 0.1mM solution of (23) in THF.

It's difficult to fully characterize these types of phthalocyanine by NMR because the bulky groups show large numbers of overlapping signals. However, the ^{1}H NMR confirms the presence of pentanoate groups which are observed as a triplet at 0.94 ppm due to the methyl pentanoate chain group and signals at 1.42 and 1.79 ppm representing the alkyl chain. A signal at 4.35 ppm is a triplet due to the methyl pentanoate group close to the oxygen, which is shifted to down field due to the deshielding effect of the oxygen. The signals from 6.85- 8.29 ppm appear as a multiplet and represent the benzene groups which includes 6H for the benzene groups A, 8H due to the benzene linkers B, 18H for the outer of the "butterfly" ligands C and finally 60 H for the side groups of the "butterfly" ligands for the benzene rings D. ^{13}C NMR also confirms the present of pentanoate groups with signals at 13.96 ppm due to (-O-CH_2 $(CH_2)_3CH_3$), signals at 22.34, 28.17and 28.37 ppm due to (-O-CH_2 $(CH_2)_3CH_3$) and 65.56 ppm for (-O-CH_2 $(CH_2)_3CH_3$), respectively. Signals at 117.47, 118.61, 121.61, 127.93, 128.14, 129.29, 129.47 ppm due to (*Ar-H*) and (*Ar-C*-C). A signal at 165.92 ppm is due to (*C=O*). The FT-IR spectrum shows the most important characteristic peaks at 2956 and 2929 cm^{-1} due to (CH_3) stretches, 2869 cm^{-1} assigned to a (CH_2) stretch, and a sharp and strong peak at 1717 cm^{-1} due to the carbonyl ester group.

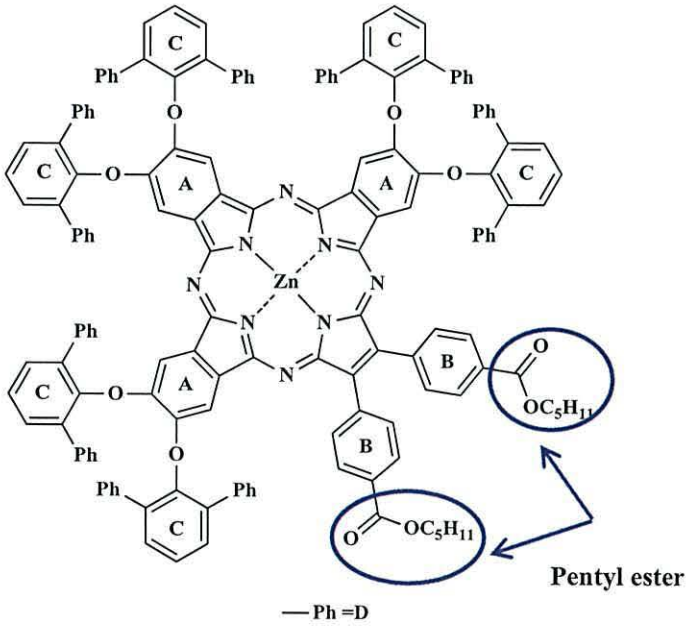

Figure 5.8. The molecular structure of 2, 3-di (4-pentoxybenzoate)-7^2, 12^2, 17^2-hexa (2, 6-diphenylphenoxy)-tribenzo-5, 10, 15, 20-tetrazaporphyrin zinc (**23**) showing selected labelling (A to D) for assignment of the NMR data.

The final step was to synthesize the target compound (**24**), by hydrolysis of (**23**). Initial unsuccessful attempts to hydrolyze (**23**) used a method developed by Shogo Mori [4] which was based on adding 1ml of aqueous solution NaOH (1M) to a solution of the zinc-pentyl ester unsymmetrical phthalocyanine of the (**23**) in THF, which was refluxed overnight, followed by removal of the solvent and refluxing again with H_2O for 1 h. The pH was then adjusted to 4 with acetic acid, which formed a green precipitate. Initial inspection of this product by mass spectrometry still showed a peak at 2373.8 corresponds to the pentyl ester. So it was decided to test another method of hydrolysis. The successful hydrolysis was a achieved using the method developed by Eu *et al.* [5] Here, a mixture of THF-methanol containing aqueous potassium hydroxide solution (40%) was added to 0.1 g of (**23**) and refluxed for 24 h. After removing the solvent the pH was adjusted to 4 using 6M HCl to produce a green precipitate. This was filtered and dried at room temperature to afford a green solid corresponding to unsymmetrical phthalocyanine zinc with two carboxylic acid groups (**24**) as shown in Figure 5.9.

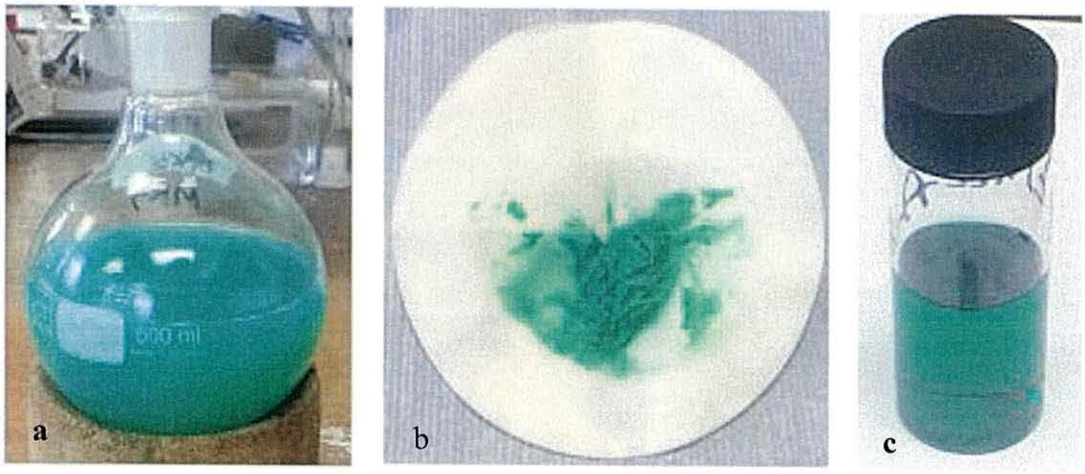

Figure 5.9. Photographs show the hydrolysis process of (**23**) to produce (**24**), (a) shows a solution of (**24**) adjusted to pH 4 by using (6) mol L^{-1} HCl, (b) filtration of the precipitate and (c) (**24**) dissolved in THF solution $1x10^{-4}$ M.

The UV-Vis spectrum of (**24**) is shown in Figure 5.10 and shows a Soret band absorption at 360 nm (I), with Q band absorptions at 684 nm (III), $\varepsilon = 44726\ M^{-1}cm^{-1}$ and 704 nm (IV) which are due to a (π-π^*) transitions of a conjugated macrocycle. [2, 6] The absorption band at 628 nm (II) is believed to be due to the aggregation of phthalocyanine molecules in solution. Aggregation is known to cause problems for

DSC dyes by reducing device efficiency, [7] which is due to the large π-conjugate system. [8]

Mass spectrometry (Figure 5.11) shows two molecular ion peaks at 2233.6 due to the target compound (**24**) and at 2531.8 corresponds to symmetrical phthalocyanine (**26**).

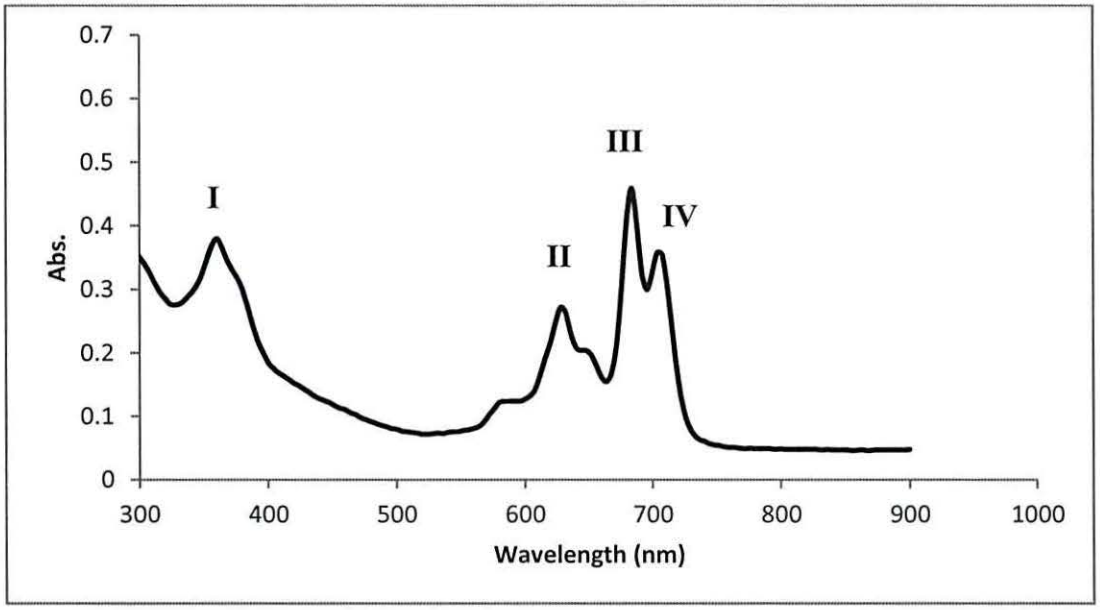

Figure 5.10. UV-Vis spectrum of unpurified 2, 3-di (4-benzoic acid)-7^2, 12^2, 17^2-hexa (2, 6-diphenylphenoxy)-tribenzo-5, 10, 15, 20-tetrazaporphyrin zinc (**24**) in THF 10^{-5} M, $\varepsilon = 44726\ M^{-1}cm^{-1}$ at 684 nm.

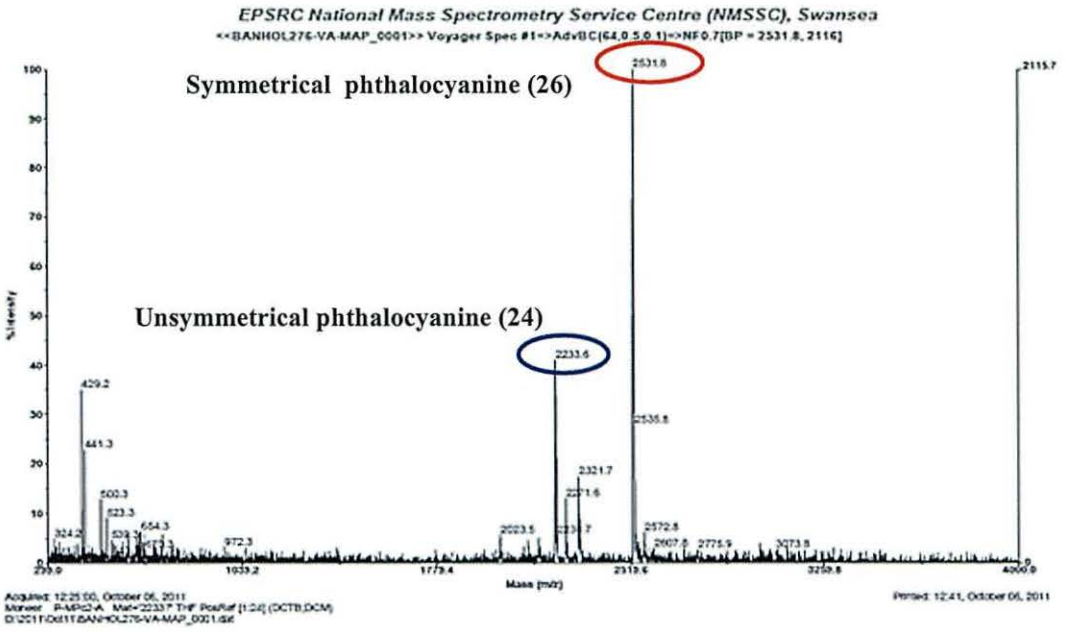

Figure 5.11. MALDI-DCTB matrix mass spectrum of 2, 3-di (4-benzoic acid)-7^2, 12^2, 17^2-hexa (2, 6-diphenylphenoxy)-tribenzo-5, 10, 15, 20-tetrazaporphyrin zinc (**24**) and symmetrical phthalocyanine (**26**).

Purification was attempted using column chromatography with silica gel and dichloromethane as eluent and was repeated twice but the mass spectral data still showed two molecular ions representing a mixture of (**24**) and the symmetrical product (**26**). A new method was therefore developed and tested to solve the purification problem of the unsymmetrical phthalocyanine (**24**) by dissolving 0.1 g of (**24**) in 50 ml of THF. Then 1.5 g of TiO_2 (P25) was added and the mixture left stirring for 10 min. Then the mixture was filtered. If the filtrate was green, more TiO_2 (P25) was added to obtain a colourless solution. After filtration 0.1 M of aqueous ammonium hydroxide solution NH_4OH was added with the aim of desorbing the unsymmetrical phthalocyanine from the TiO_2 surface. This was collected in vials. The aim was that the symmetrical phthalocyanine and unreacted ester should remain on the TiO_2 surface, because the NH_4OH (aq) would only desorb chemisorbed dye (i.e. dye bound to the TiO_2 through carboxylate group).

The purification process for the unsymmetrical phthalocyanine (**24**) is summarized in Scheme 5.3. This shows how the unsymmetrical phthalocyanine ester and

symmetrical phthalocyanine are believed to attach to the TiO_2 surface by Van der Waals forces, while the unsymmetrical phthalocyanine **(24)** links by ester linkages.

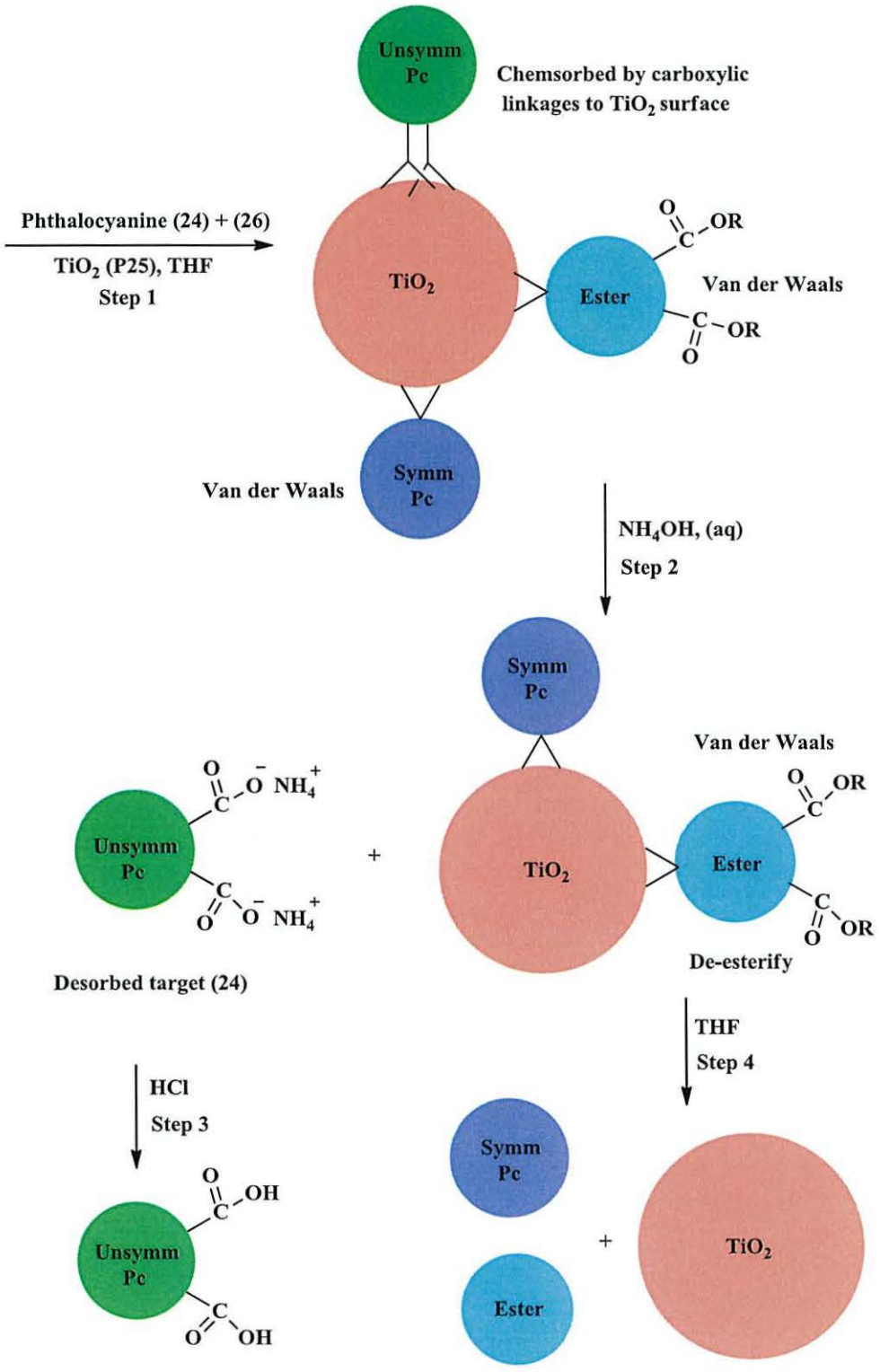

Scheme 5.3. The purification process of 2, 3-di (4-benzoic acid)-7^2, 12^2, 17^2-hexa (2, 6-diphenylphenoxy)-tribenzo-5, 10, 15, 20-tetrazaporphyrin zinc (**24**).

Figure 5.12a shows the first step of this process by dissolving (**24**) in THF. Figure 5.12b shows the unsymmetrical phthalocyanine solution after adding 0.1 M aqueous solution of NH_4OH. Finally, (Figure 5.12 c and d) show the symmetrical phthalocyanine and unconverted ester still on the TiO_2 surface.

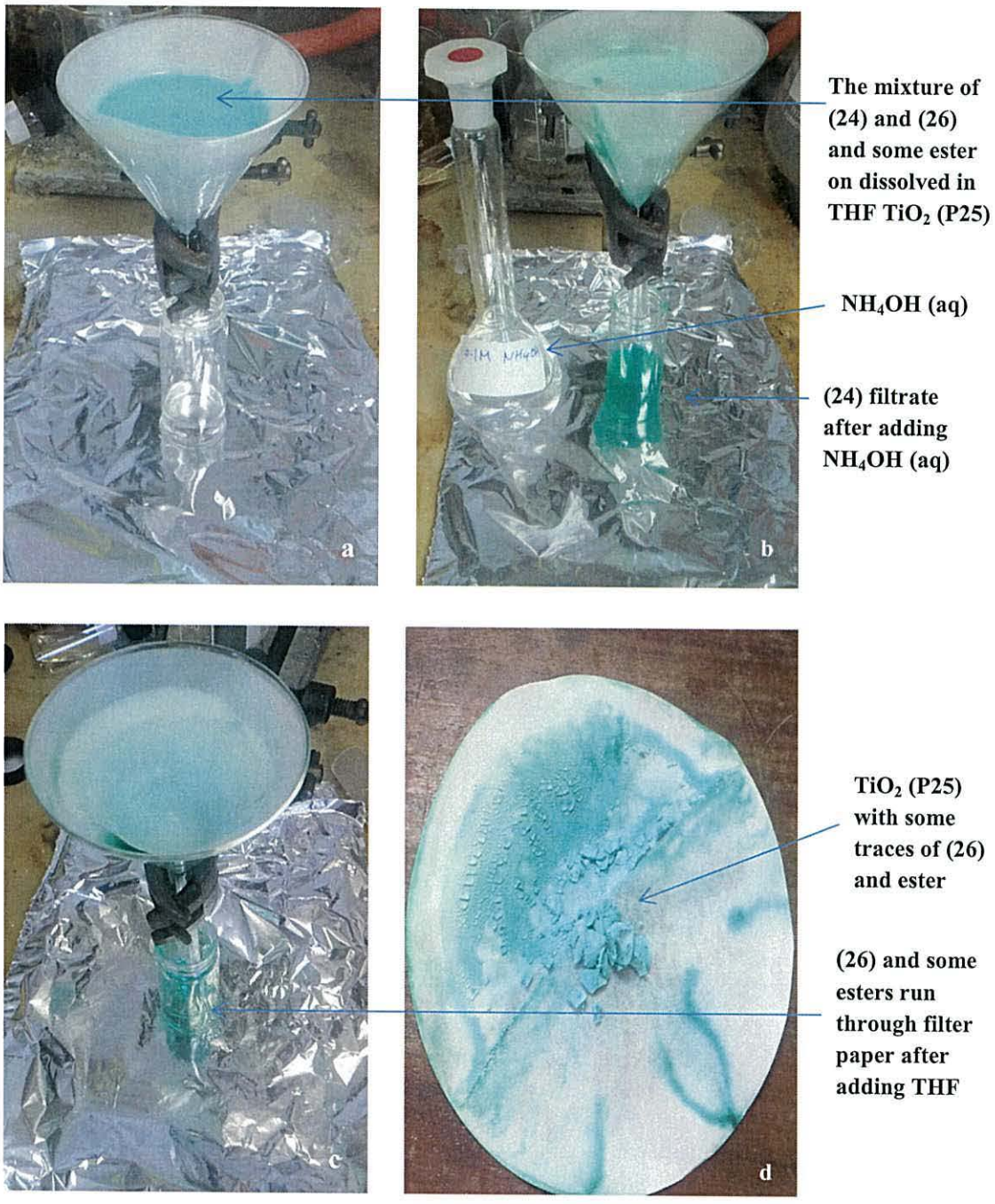

Figure 5.12. Photographs show the purification of (**24**) using TiO_2 (P25) and 0.1 M of NH_4OH (aq). (a) mixture of (**24**), (**26**) and some traces of Pc esters dissolved in THF, (b) collect (**24**) after adding NH_4OH, (c) collect (**26**) and some Pc esters after adding THF and (d) TiO_2 (P25) after finishing purification process.

The mass spectrum data (Figure 5.13) confirms purified unsymmetrical phthalocyanine (**24**) with a molecular ion at 2232.6 as a single peak with no evidence for the ester of (**24**) or the symmetrical Pc.

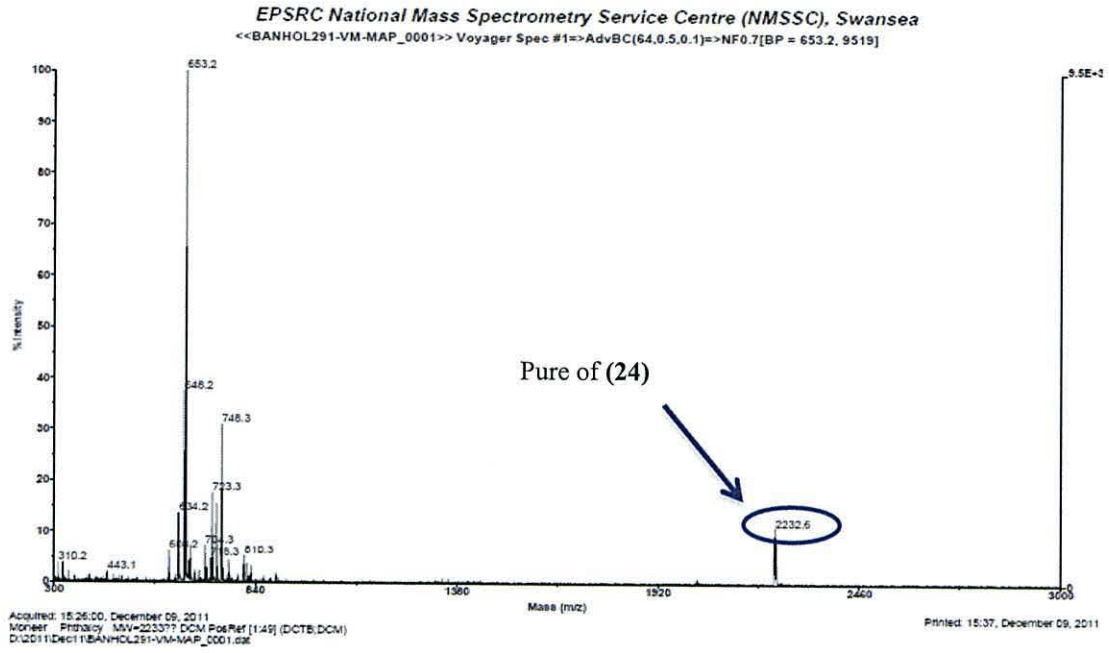

Figure 5.13. MALDI-DCTB matrix mass spectrometry of pure 2, 3-di (4-benzoic acid)-7^2, 12^2, 17^2-hexa (2, 6-diphenylphenoxy)-tribenzo-5, 10, 15, 20-tetrazaporphyrin zinc (**24**).

The absence of peaks for the pentanoate group was further confirmed by ^{1}H NMR which didn't show any peaks from 0.8-6.0 ppm. Instead the data showed signals at 6.88-7.51 ppm as a multiplet due to (*Ar-H*) and which are distributed into four environment groups such as described for (**23**); 6H for the benzene groups A, 8H due to benzene linker groups B, 18H for central benzene rings of the "butterfly" ligands C and finally 60 H for phenyl groups which form the sides of the "butterfly" ligands D. ^{13}C NMR also confirms the successful conversion of ester to acid and shows a shift of the carbonyl signal from 165.92 ppm for an ester group to 163.11 ppm for acid groups. The FT-IR spectrum shows a broad peak at 3447 cm^{-1} assigned to OH stretching of carboxylic acid, a peak at 3058 cm^{-1} for (C-H) stretching of benzene ring, a broad peak at 1659-1580 cm^{-1} due to (C=O) stretching of carboxylic acid, and a sharp peak at 1199 cm^{-1} assigned to (C-O) stretching.

The UV-Vis spectrum of the purification process of a mixture (**24**) is shown in Figure 5.14. The pure unsymmetrical phthalocyanine (**24**) was obtained after desorption from TiO_2 using of 0.1 M NH_4OH. Pure (**24**) shows absorption peaks at 372 nm and 704 nm of the Soret and Q bands, respectively. Also Figure 5.14 shows the remaining phthalocyanine (ester and symmetrical, black dotted line) absorb at 684 nm.

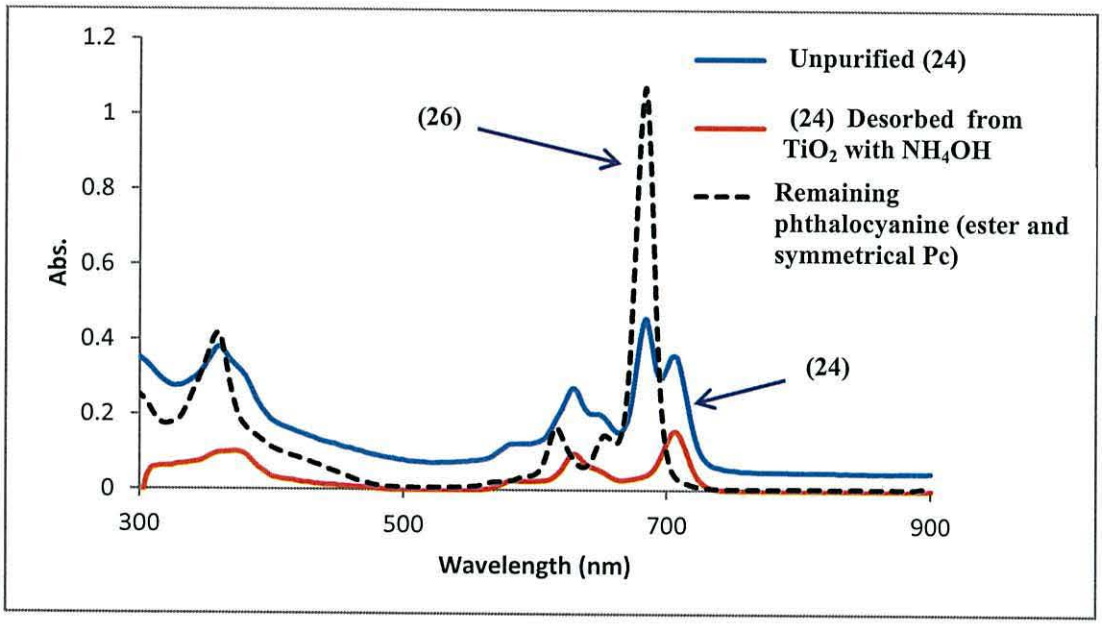

Figure 5.14. UV-Vis spectrum of; the blue sold line of unpurified 2, 3-di (4-benzoic acid)-7^2, 12^2, 17^2-hexa (2, 6-diphenylphenoxy)-tribenzo-5, 10, 15, 20-tetrazaporphyrin zinc (**24**), the sold red line of (**24**) desorbed from TiO_2 with NH_4OH and the black dashed line of ester and symmetrical phthalocyanine.

The mechanism of cyclotetramerisation of phthalonitrile to form phthalocyanine is similar to the mechanism of Linstead cyclo-tetramerisation of phthalonitrile. [9] This reaction occurs in 1-pentanol or N,N-dimethylaminoethanol (DMAE), as a high boiling point solvent with 1,8-diazabicyclo[5,4,0]undec-7-ene (DBU) as a strong organic base. The mechanism involves nucleophilic attack on carbon of the one of nitrile groups by an alkoxide anion, which is formed by deprotonation of the solvent by DBU. Figure 5.15 shows that phthalonitrile (1) as the starting material to form phthalocyanine and cyclization after converting to alkoxyiminoisoindolenine as an intermediate (2). Then the nucleophilic attack of the anionic nitrogen of the intermediate (2) on the nitrile group with another molecule of phthalonitrile forms a

dimeric intermediate (3), which can be subsequently react with another phthalonitrile molecule to give the final product of cyclic phthalocyanine compound, as shown in Scheme 5.4.

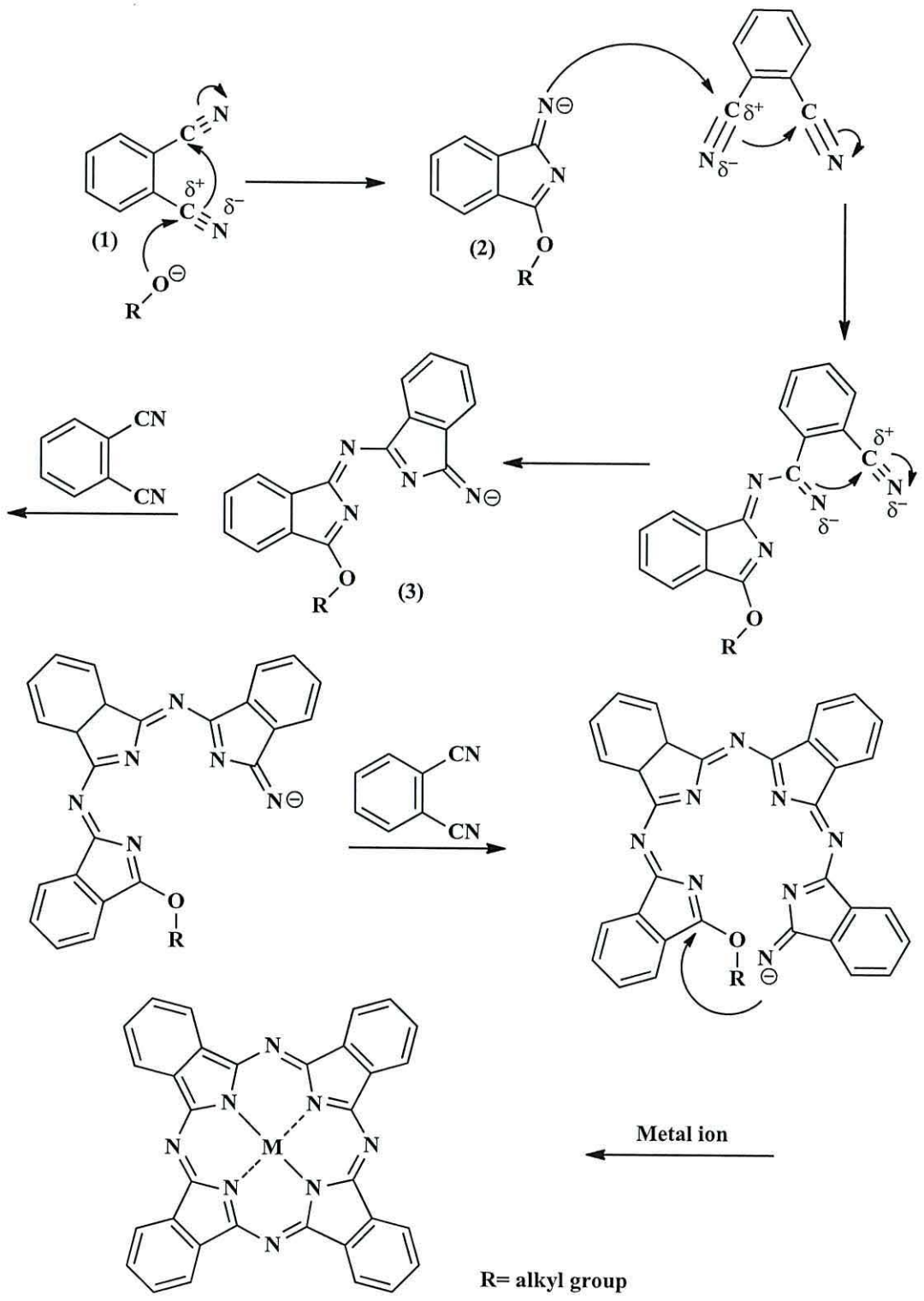

Scheme 5.4. The general mechanism of phthalocyanine formation. [10]

5.3 Device fabrication

The same method which was mentioned previously to fabricate devices in Chapters 3 and 4 was followed. After dying the TiO_2 electrode (two layers of DSL18NRT paste) with phthalocyanine (**24**), the device was assembled. Table 5.3 shows that the efficiency (η) and short circuit density (J_{sc}) increased gradually for different devices. Devices (A, B and C) were made and measured before (**24**) had been purified, while device (D) which was made using purified (**24**) shows the highest conversion efficiency of 0.73% with J_{sc} (2.40 mA/cm^{-2}). This is believed to be the reason for the increase of the photovoltaic parameters for device (D). Despite these data, (**24**) did not show remarkable performance. Device E made by co-sensitizing phthalocyanine (**24**) with **D149** dye shows conversion efficiency 1.82% with J_{sc} (6.54 mA/cm^{-2}). This efficiency value is not good and it is different compared with the literature data reported previously [11] for **D149** and also is different with **D149** data which obtained earlier in chapter 3.

Table 5.3. Photovoltaic parameters of DSC using phthalocyanine (**24**).

Dye	Device	η (%)	FF	J_{sc} ($mA\ cm^{-2}$)	V_{oc} V
(24)	A	0.49	0.61	1.48	0.55
	B	0.52	0.55	1.57	0.60
	C	0.66	0.65	2.03	0.50
	D	0.73	0.56	2.40	0.54
D149 + (24)	E	1.82	0.50	6.54	0.56

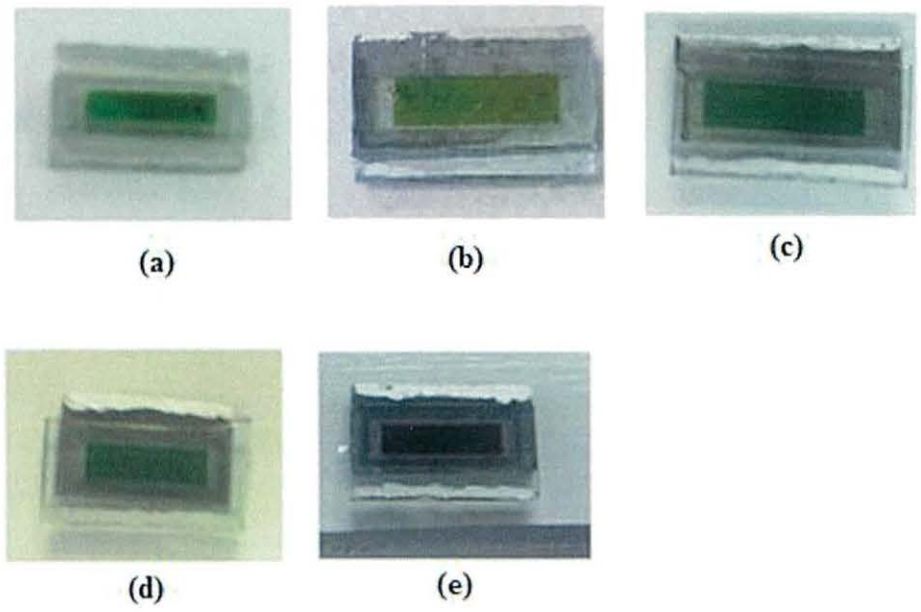

Figure 5.15. Photographs of DSC devices dyed (a), (b) and (c) with unpurified (**24**), (d) with purified (**24**) and (e) dyed with (**24**) and **D149**.

Figure 5.16 show the progress that was achieved to improve the solar cell performance of (**24**) before and after purifying, while Figure 5.17 show the I-V curve of (**24**) after mixing with **D149** and individual **D149** and (**24**) , **D149** shows results better than co-sensitized (**24**) with **D149**.

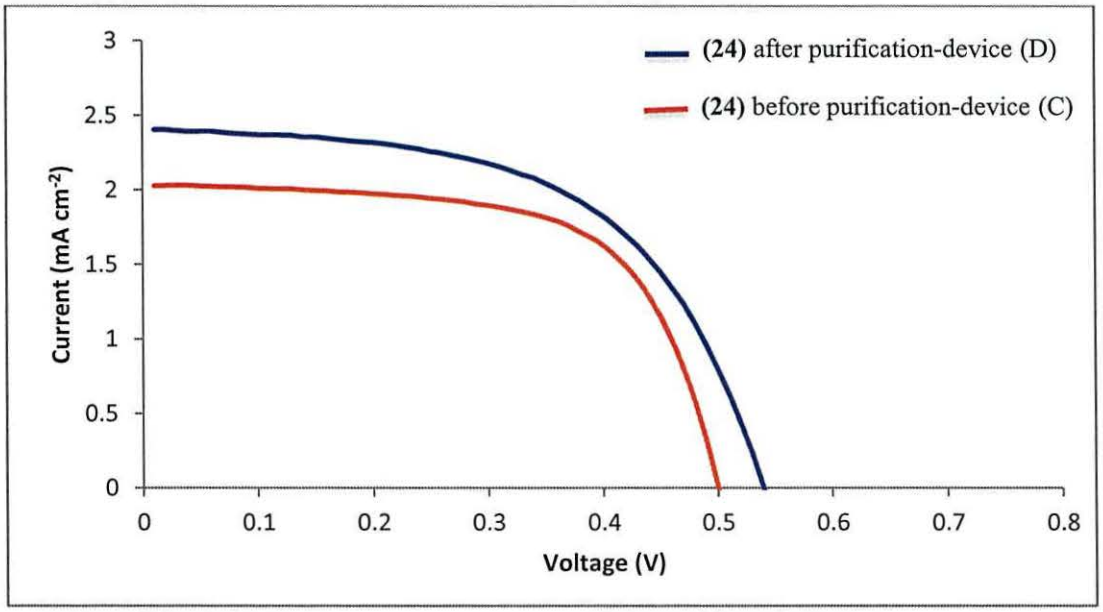

Figure 5.16. Photocurrent density-photovoltage curve of (**24**) under AM 1.5 G radiation.

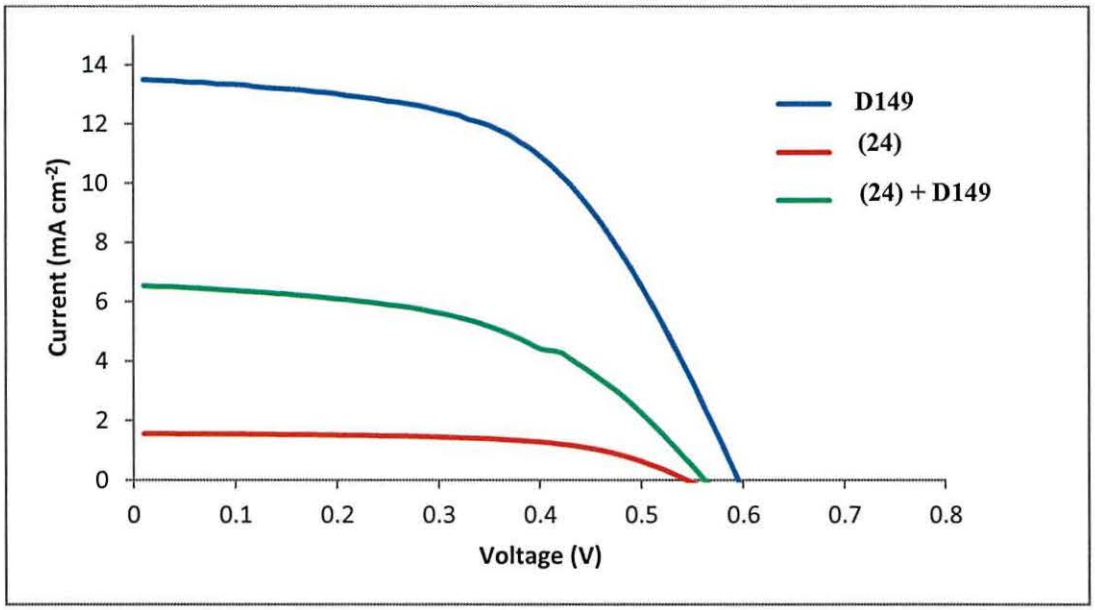

Figure 5.17. Photocurrent density-photovoltage curve of **D149** (blue line), co-sensitized (**24**) and **D149** (green line), and individual (**24**) (red line) under AM 1.5 G radiations (100 Mw cm^{-2}).

External quantum efficiency (EQE) (Figure 5.18) shows **(24)** has an EQE response at 340 nm (I) which is 17% and at 700 nm (II) of 10%. A comparison of the EQE of phthalocyanine (**24**) with the UV-Vis spectrum (Figure 5.1), show that the harvesting of photon from sorbed dye on TiO_2 electrodes (300-750) nm is broader in solution.

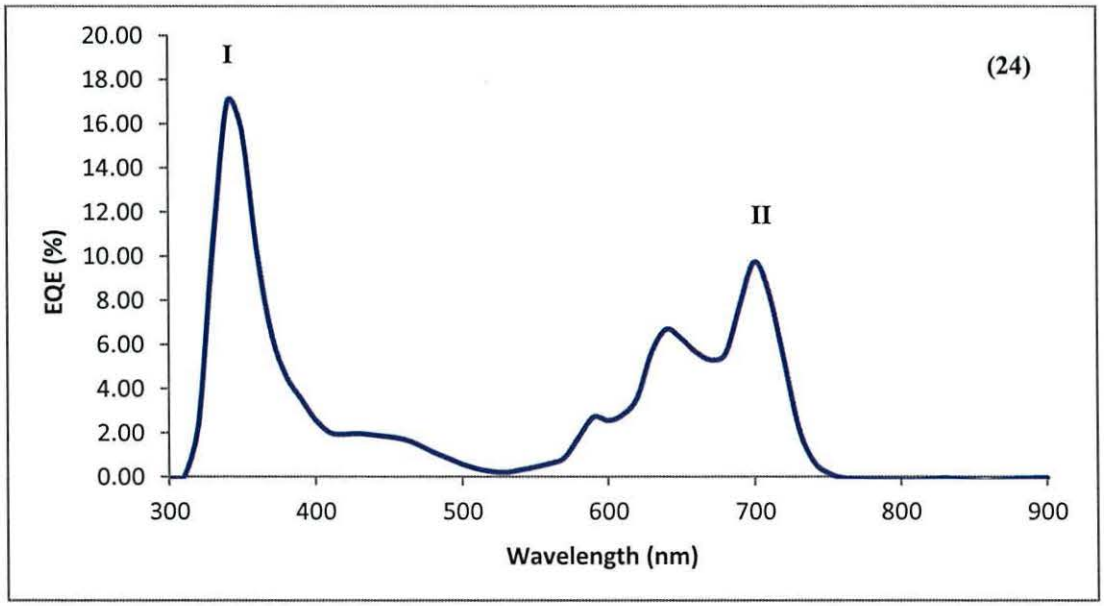

Figure 5.18. External quantum efficiency (EQE) of 2, 3-di (4-benzoic acid)-7^2, 12^2, 17^2-hexa (2, 6-diphenylphenoxy)-tribenzo-5, 10, 15, 20-tetrazaporphyrin zinc (**24**).

5.4 Unsymmetrical phthalocyanine 2, 3-di (4-pentoxybenzoate)-7^2,12^2,17^2-hexa (diphenylphenoxy)-tetrabenzo-5, 10, 15, 20-tetrazaporphyin zinc (25).

The synthesis of unsymmetrical phthalocyanine zinc (**25**) was attempted by reacting 4, 5-*bis* ([1, 1':3', 1''-terphenyl]-2'-yloxy) phthalonitrile (**20**) with 4, 5-*bis* (4-methoxycarbonylphenyl) phthalonitrile (**22**) in a ratio of 5:1, $ZnCl_2$ was added in the presence of 1, 8-diazabicyclo [4, 5, 0] undec-7-ene (DBU) in 5 ml of 1-pentanol as the solvent, the synthetic path way is shown in (Scheme 5.5).

The precursor 4,5-*bis*(4-methoxycarbonylphenyl) phthalonitrile compound (**22**) used to synthesize (**25**) was synthesized by using a Suzuki-Miyura cross-coupling reaction between 4,5-diiodophthalonitrile (**17**) with 4-methoxycarbonylboronic acid 2-(2`,6`-dimethoxybiphenyl)dicyclohexylphosphine and K_3PO_4 in toluene in the presence of a palladium (II) acetate catalyst under an argon atmosphere to produce compound (**22**) as a yellow-white (0.16 g, yield 52%).

The Suzuki-Miyura coupling reaction is most widely used for this type of reaction, [12, 13] In this reaction 2-(2,6-dimethoxybiphenyl)dicyclohexyl phosphine (S-Phos), [14] was used which is electron-rich and sterically hindered. The main reason for that, because this will make the palladium (0) coordinatively unsaturated. The reaction proceeded smoothly with moderate to good yield. [15]

The ^1H NMR of (**22**) confirmed the presence of the acetate group with a singlet observed at 3.90 ppm due to methyl ester group, signals between 6.94 and 8.18 ppm for benzene rings. The additional singlet at 3.85 ppm integrates to 3 protons for a methyl group and is assigned to 4-methoxycarbonylboronic acid starting material, so it was suggested this reaction needed more time than 2 h to complete. The signals at 6.94, 7.02, 7.69 and 8.18 ppm are assigned to (*Ar-H*). ^{13}C NMR also shows signals at 55.17 and 56.12 ppm due to the additional methyl and methyl ester groups, respectively. The signals at 113.52 and 163.23 ppm are for cyanine (C≡N) and carbonyl ester groups, respectively.

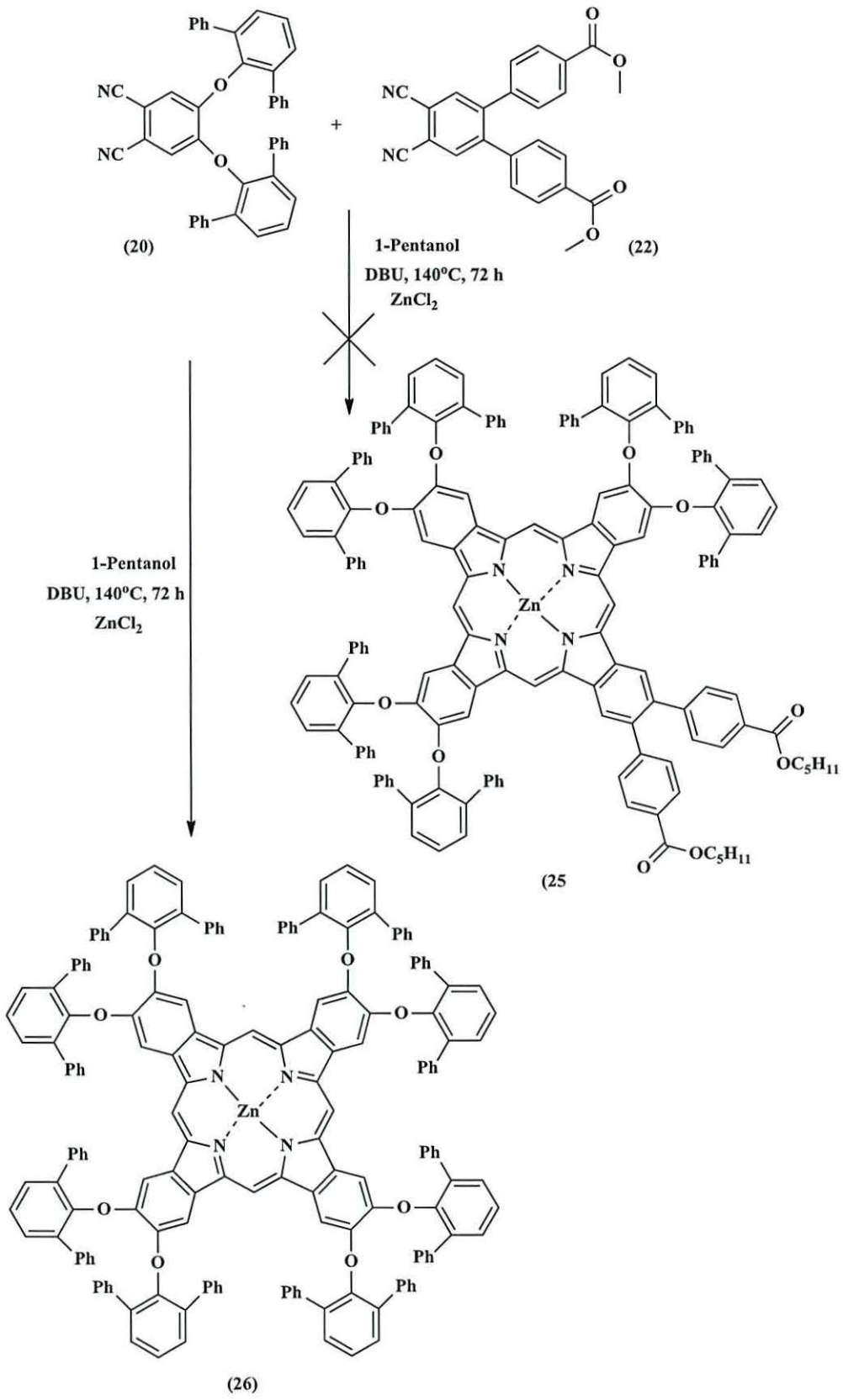

Scheme 5.5. Show the unsuccessful synthesis of 2, 3-di (4-pentoxybenzoate)-7^2,12^2,17^2-hexa (diphenylphenoxy)-tetrabenzo-5, 10, 15, 20-tetrazaprophyin zinc (**25**) and form 2^2, 7^2, 12^2, 17^2 octa (2, 6-diphenylphenoxy)-tetrazaporphyrin zinc (**26**).

The mass spectrometry data also confirms the ^{1}H and ^{13}C NMR results and shows a peak at 412.8641 which confirmed an impurity in this compound which contains an additional lone methyl group, which corresponds to $[M+CH_3]^+$.

The diiodophthalonitrile precursor (**17**) was prepared in four steps. An unsuccessful attempt was carried out using the conditions reported by Leznoff *et al.* [16] by adding iodine to a solution of phthalimide in fuming sulfuric acid at 70-75°C for 24 h. During the reaction, the mixture splashed up the sides of the flask and formed a black solid which covered the inner wall of the reaction flask, (Figure 5.19). The reaction was repeated using the same starting materials but this time with a closed system in an autoclave reactor, (Figure 5.20). After cooling to room temperature, the mixture reaction was poured onto ice and the precipitate washed twice with water, once with 2% K_2CO_3 solution and once with a saturated solution of $Na_2S_2O_3$. The solid was then extracted with acetone to produce the unexpected compound 4, 5, 6, 7-tetraiodoisoindoline-1, 3-dione (**18**) instead of the desired diiodophthalonitrile (**17**).

Figure 5.19. Iodine splashing on the inner wall flask during synthesis of 4,5-diiodophthalimide (**17**) reaction using fuming sulfuric acid.

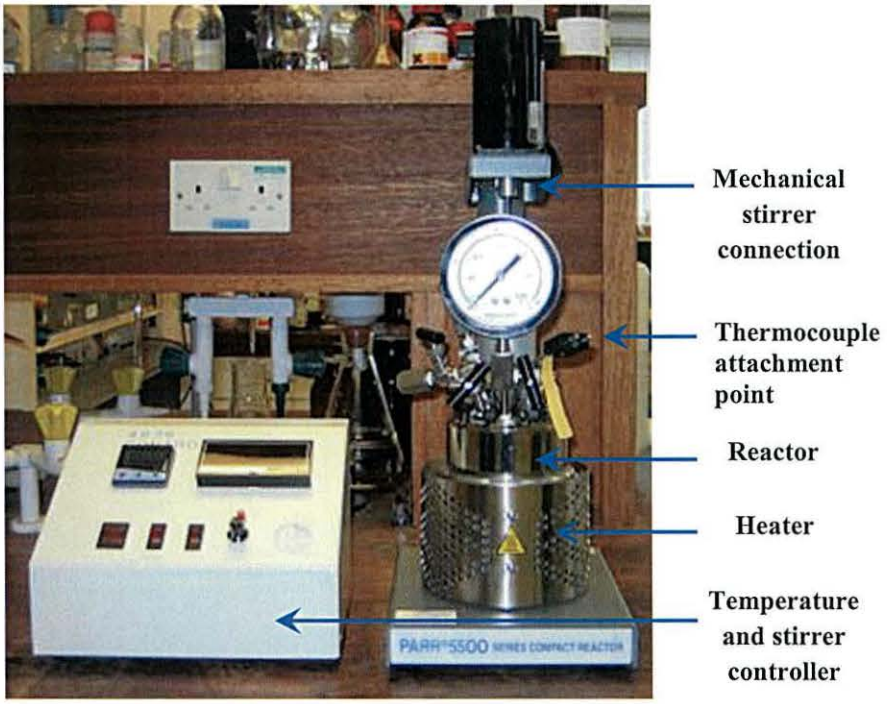

Figure 5.20. Autoclave reactor equipped with stirring mechanism and temperature controller used to synthesize tetraiodoisoindoline-1, 3-dione (**18**).

The reason was thought to be due to the lack of control over temperature at the start of the reaction which rose to more than 100°C. This matched with Leznoff's explaination [16] who formed triiodophthalimide when trying to prepare 4,5-diiodophthalonirile because the reaction proceeded at 85-90°C. Mass spectrometry data confirms tetraiodoisoindoline-1, 3-dione (**18**) with a peak at 650.6176 for (**18**). ^{1}H NMR shows one signal at 11.68 ppm as a singlet due to the (*-NH*) group. The ^{13}C NMR data show signals at 103.89 and 134.88 ppm due to C-I, and a signal at 165.17 ppm due to the carbon carbonyl group.

Due to unsuccessful attempts to synthesize diiodophthalimide by the two methods mentioned above, it was decided to employ periodic acid instead of fuming sulfuric acid. [17] This was used to convert the iodine to a more powerful electrophile (I^{+}). Mattern reported [17] using periodic acid instead of fuming sulfuric acid and iodine. It was that using a stoichiometric amount of I^{+} was necessary to avoid iodination on all aromatic sites. In this work a stoichiometric amount of I^{+} achieved the successful synthesis of diiodophthalonitrile (**17**) in three steps as shown in Scheme 5.6.

Theoretically in this process the iodine is converted to iodonium (I^+) as shown in eq 1. The (I^+) is an ideal electrophile for the iodination process through electrophilic aromatic substitution. [17]

$$^1/_7\, H_5 IO_6 + {}^3/_7\, I_2 + H^+ \rightarrow I^+ + {}^6/_7\, H_2O \qquad \text{Eq. 1}$$

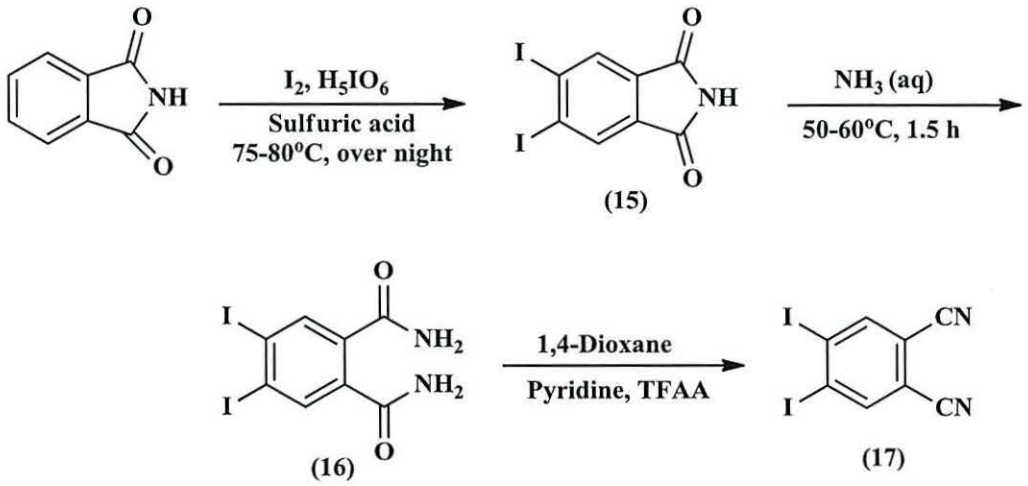

Scheme 5.6. The synthetic pathway of 4, 5-diiodophthalonitrile (**17**).

The first step was to synthesize diiodophthalimide (**15**) by adding iodine to a solution of periodic acid in concentrated sulphuric acid, and stirring for 1 h at ambient temperature. Then phthalimide was added to the reaction mixture after heating to 40°C and the mixture was heated to 75-80°C for 24h. The crude product of reaction (Figure 5.21a) was washed twice with 2% K_2CO_3 solution to get rid of any acid residues, once with a saturated solution of $Na_2S_2O_3$ to get rid of any iodine residues, and once with water. The crude solid extracted by a Soxhlet extractor using acetone (Figure 5.21b) for 48 h to produce a yellow solid of 4, 5-diiodophthalimide (**15**) (39% yield). Leznoff *et al.* reported a yield of 80% for the synthesis of 4, 5-diiodophthalimide (**15**).

The next step was to convert (**15**) to 4, 5-diiodophthalamide (**16**) using concentrated ammonia to produce a diamide *via* nucleophilic addition which produced a white-yellow precipitate. Again a Soxhlet extractor was used to extract 4, 5-diidophthalamide from the crude reaction by using acetone as the solvent for 24h.

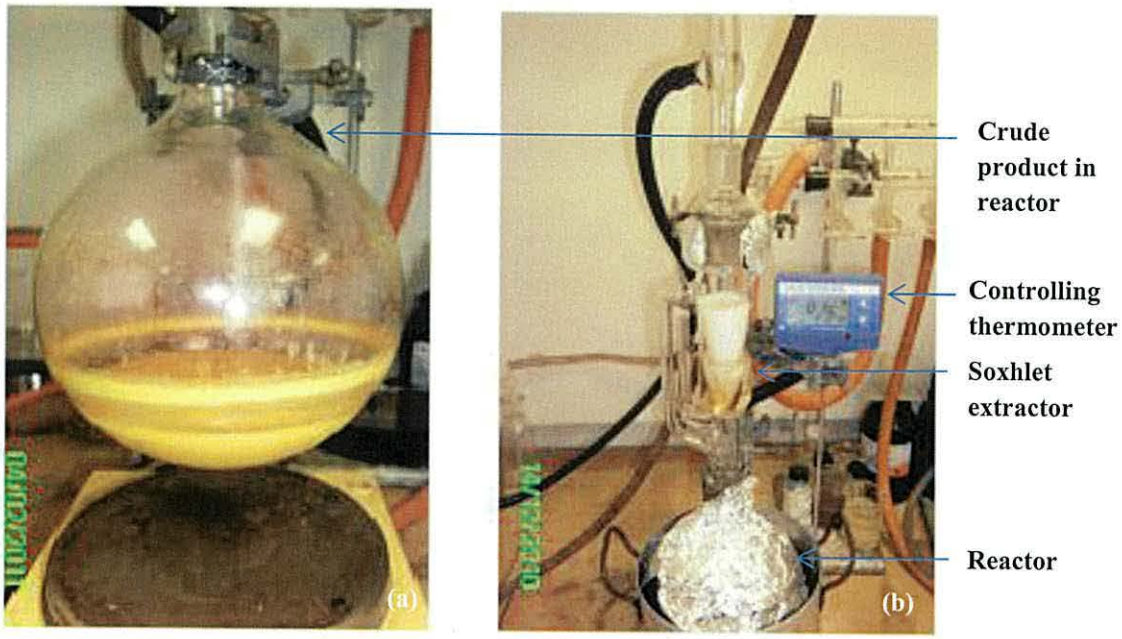

Figure 5.21. Photographs of synthesis 4, 5-diiodophthalimide (**16**), on the left the crude product, on the right extracted by Soxhlet extractor.

The ^{1}H NMR of (**15**) shows a signal at 11.42 ppm as singlet due to the (-*NH*) group and a singlet at 8.25 ppm for the benzene ring protons (H2 and H2a). By comparison, (**16**) shows a shift up field for the amide group protons to 7.82 and 7.41 ppm as a broad singlet peaks and a signal at 7.91 ppm as a singlet for the benzene ring protons (H2 and H2a). (**15**) shows signals at 116.45, 132.68 and 133.00 ppm due to (*Ar-C*-C, C-3 and C-3a), (*Ar-C*-H, C-2 and C-2a) and (*Ar-C*-I, C-1 and C-1a), respectively. (**16**) Also shows signals at 109.89, 137.03 and 137.65 ppm due to (*Ar-C*-C, C-3 and C-3a), (*Ar-C*-H, C-2 and C-2a) and (*Ar-C*-I, C-1 and C-1a), respectively. Both (**15**) and (**16**) show signals for a carbon carbonyl group around 167.69 and 167.93 ppm due to (C4 and C4a) in both compounds. The FT-IR spectrum of (**15**) shows a broad band at 3195 cm^{-1} assigned to (NH) group, and two bands at 1719 and 1770 cm^{-1} due to the carbonyl of the amide group. By comparison (**16**) shows three bands assigned to (NH) stretches of the amide group at 3430, 3327 and 3175 cm^{-1} respectively, and two peaks for carbonyl amide group at 1692 and 1655 cm^{-1}, respectively. ^{1}H NMR and infrared data were consistent with literature data. [16]

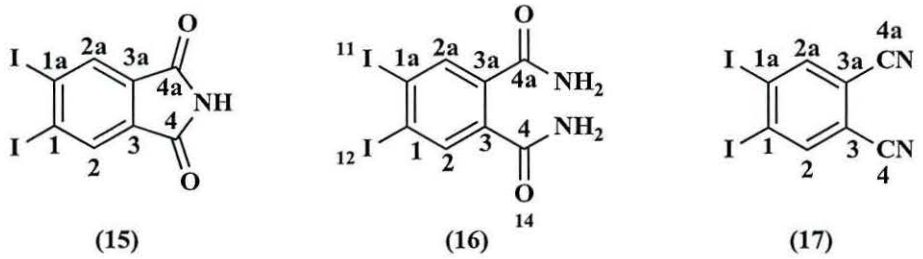

Figure 5.22. Labelled hydrogen and carbon atoms for compound (**15**), (**16**) and (**17**) used for NMR assignments.

The final step was to synthesize 4, 5-diiodophthalonitrile (**17**) which was achieved by dehydration of (**16**) to produce a yellow precipitate of (**17**). Identification of was achieved by ^{1}H NMR which shows a signal at 8.23 ppm as a singlet due to (H2 and H2a) for the benzene ring protons and the disappearance of the amide signals. ^{13}C NMR shows a signal at 113.55 ppm due to (*Ar-C*-C, C-3 and C-3a), a signal at 115.03 ppm due to (*Ar-C*-C-N). The signal at 115.41 ppm was due to the (C≡N) group, and a signal at 142.68 ppm was due to (*Ar-C*-H, C-2 and C-2a). Evidence for conversion to the nitrile was also seen in the FTIR by the observation a peak at 2231 cm^{-1} which is consistent with literature data. [16] Mass spectral data confirms (**17**) with a molecular ion at 379.8302 corresponding to (**17**) [M^{+}]. Single crystals were obtained by evaporation method, using THF the solvent, and the molecular structure of (**17**) is shown in Figure 5.23. The selected bond lengths (Å) and angles (°) are listed in Table 5.4.

Table 5.4. Selected bond lengths (Å) and angles for 4, 5-diiodophthalonitrile (**17**).

C1-C1a	1.416 (8)	C1-C2-C3	121.4 (3)
C1-C2	1.391 (5)	C2-C3-C4	121.6 (4)
C3-C4	1.387 (5)	C2-C1-C1a	119.3 (2)
C3-C3a	1.418 (8)	C2-C3-C3a	119.3 (2)
C4-N1	1.150 (6)	C1-I1	2.093 (3)

There are no differences between the angles of the benzene ring (119-121°). The C-C bond lengths are between single and double bonds values (1.38-1.41 Å). Also the bond lengths of C≡N and C-I are 1.15 and 2.093 Å, respectively.

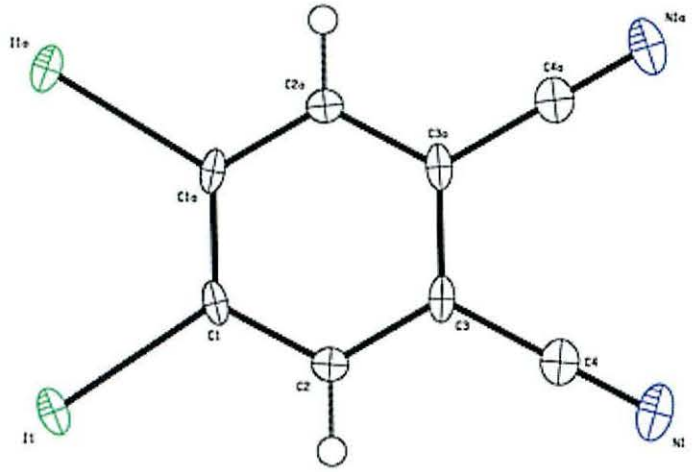

Figure 5.23. Molecular structure of 4,5-diiodophthalonitrile **(17)**.

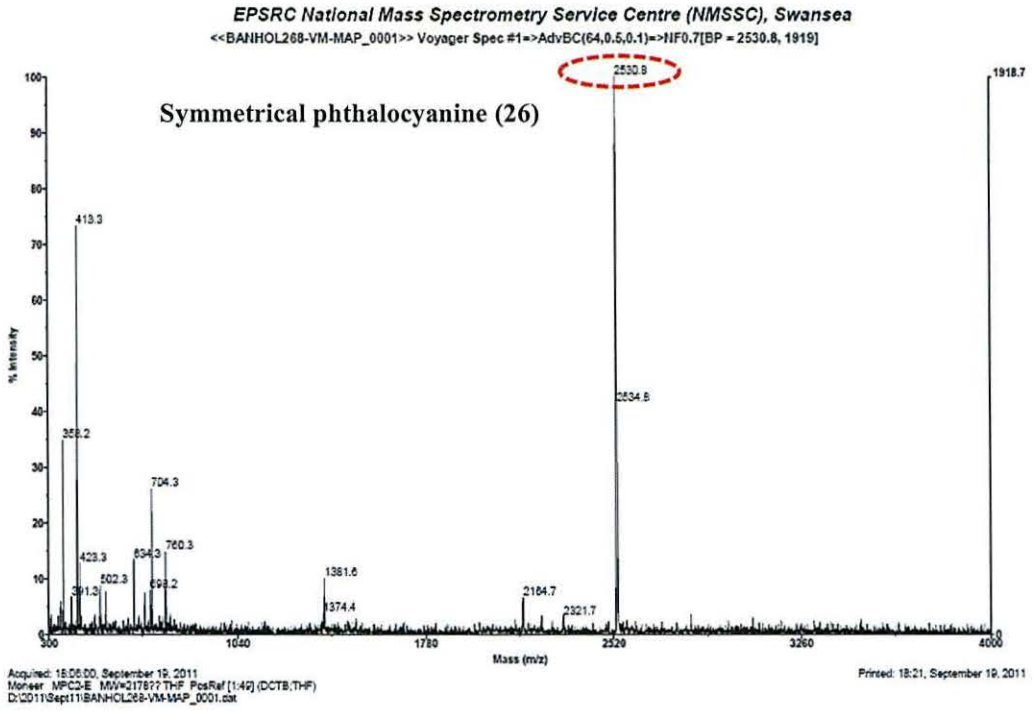

Figure 5.24. MALDI-DCTB matrix mass spectrometry of 2^2, 7^2, 12^2, 17^2 octa (2, 6-diphenylphenoxy)-tetrabenzo-5, 10, 15, 20-tetrazaporphyrin zinc (**26**).

The crystallization of symmetrical phthalocyanine zinc was achieved by dissolving the purified compound after further purification using column chromatography in THF. Slow evaporation and crystallization gave the molecular structure of symmetrical phthalocyanine zinc (**26**) with eight 2, 6-diphenylphenol groups. This hasn't reported before. The X-ray structural data Figure 5.25a and 25b show a

symmetrical phthalocyanine (**26**), with a central Zn atom 50:50 disordered over a centre of inversion. The crystal structure shows THF molecules as solvent of crystallisation. The crystal structure also contains small voids of heavily disordered solvent (1-pentanol) which was impossible to model. Figure 5.26 also has showed the crystal structure of (**26**) showing coordinated and uncoordinated of THF molecules.

Torsion angles confirm that the "butterfly" benzene rings for 2, 6-diphenyl phenol substituents are perpendicular as represented by O1-C1-C6-C5 and O1-C19-C20-C21, O2-C27-C28-C29 and O2-C27-C32-C31, O3-C53-C58-C57, O4-C49-C50-C51 and O4-C49-C48-C7 dihedral angles which close to 180.0 (°). Table 5.5 shows selected torsion angles (°).

Table 5.5. Selected torsion angles (°) of (**26**).

O1-C1-C6-C5	179.3 (4) Å	C4-C3-C2-C1	-0.9 (8) °
O1-C19-C20-C21	178.4 (5) Å	C24-C25-C26-C19	0.4 (8) °
O2-C27-C28-C29	176.8 (4) Å	C29-C30-C31-C32	-0.7 (10) °
O2-C27-C32-C31	-178.7 (5) Å	C31-C30-C29-C28	-1.3 (8) °
O3-C53-C58-C57	179.1 (4) Å	C55-C56-C57-C58	0.0 (9) °
O4-C49-C50-C51	-177.4 (5) Å	C51-C46-C47-C48	0.7 (8) °
O4-C49-C48-C7	177.4 (5) Å	C47-C46-C51-C50	-0.5 (8) °

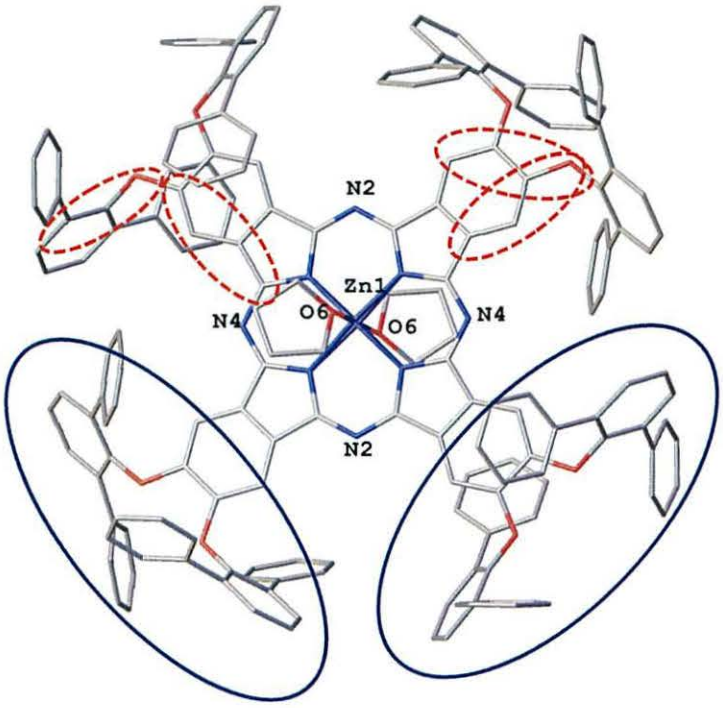

(a)

Butterfly groups

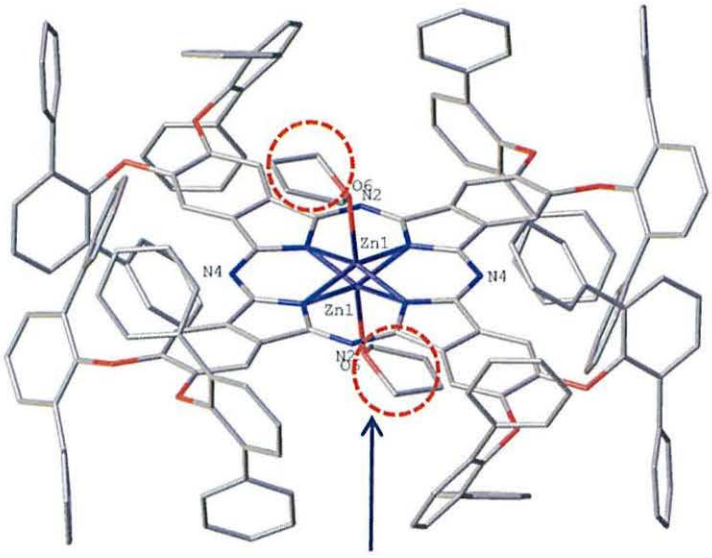

(b)

Coordinated THF molecules

Figure 5.25. Molecular structure of 2^2, 7^2, 12^2, 17^2 octa (2, 6-diphenylphenoxy)-tetrabenzo-5, 10, 15, 20-tetrazaporphyrin zinc (**26**), (a) top view shows the butterfly ligand and (b) side view shows the coordinated THF molecules.

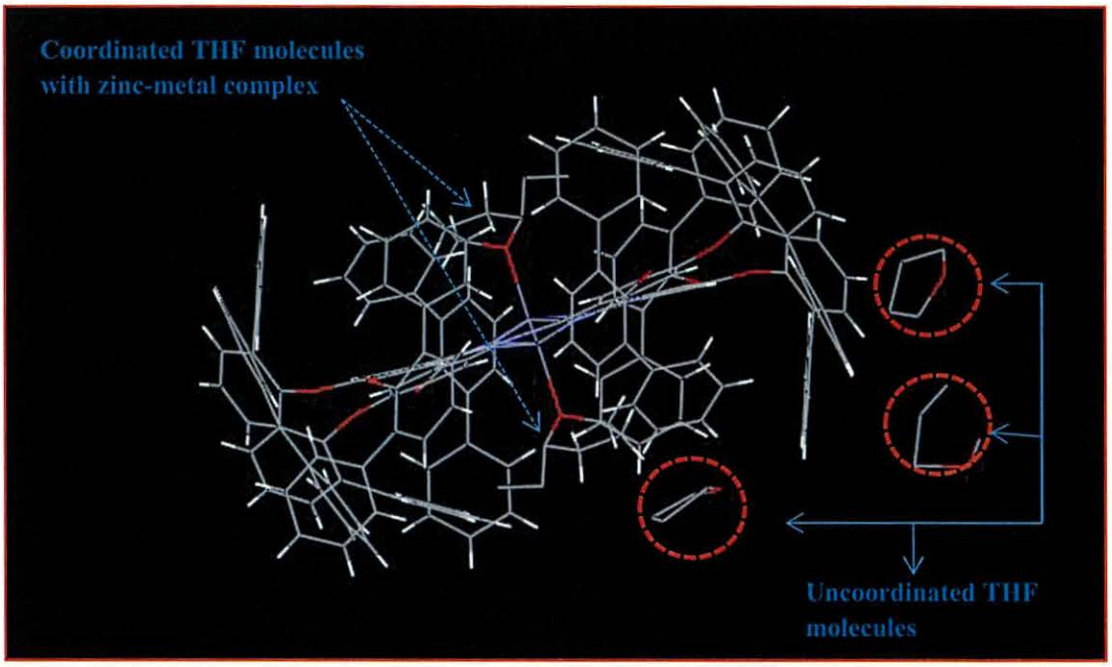

Figure 5.26. X-ray structure of 2^2, 7^2, 12^2, 17^2 octa (2, 6-diphenylphenoxy)-tetrabenzo-5, 10, 15, 20-tetrazaporphyrin zinc (**26**) showed uncoordinated THF molecules in red dashed cycle.

To try to improve the yield of (**25**) it was decided to change the ratio of the precursor reactants 4,5-bis ([1, 1':3', 1''-terphenyl]-2'-yloxy) phthalonitrile (**20**) and 4,5-bis (4-methoxycarbonylphenyl) phthalonitrile (**22**) to 3:1 instead of 5:1, respectively whilst still using $ZnCl_2$ in 1-pentanol in the presence of 1, 8-diazabicyclo [4, 5, 0] undec-7-ene (DBU) for 72h. The crude product was purified by column chromatography on silica gel using dichloromethane as an eluent to produce a dark green solid of (0.2 g, 41%). However, the expected product of 2, 3-di (4-pentoxybenzoate)-7^2,12^2,17^2-hexa (diphenylphenoxy)-tetrabenzo-5, 10, 15, 20-tetrazaprophyrine zinc (**25**) was not obtained, (Scheme 5.7).

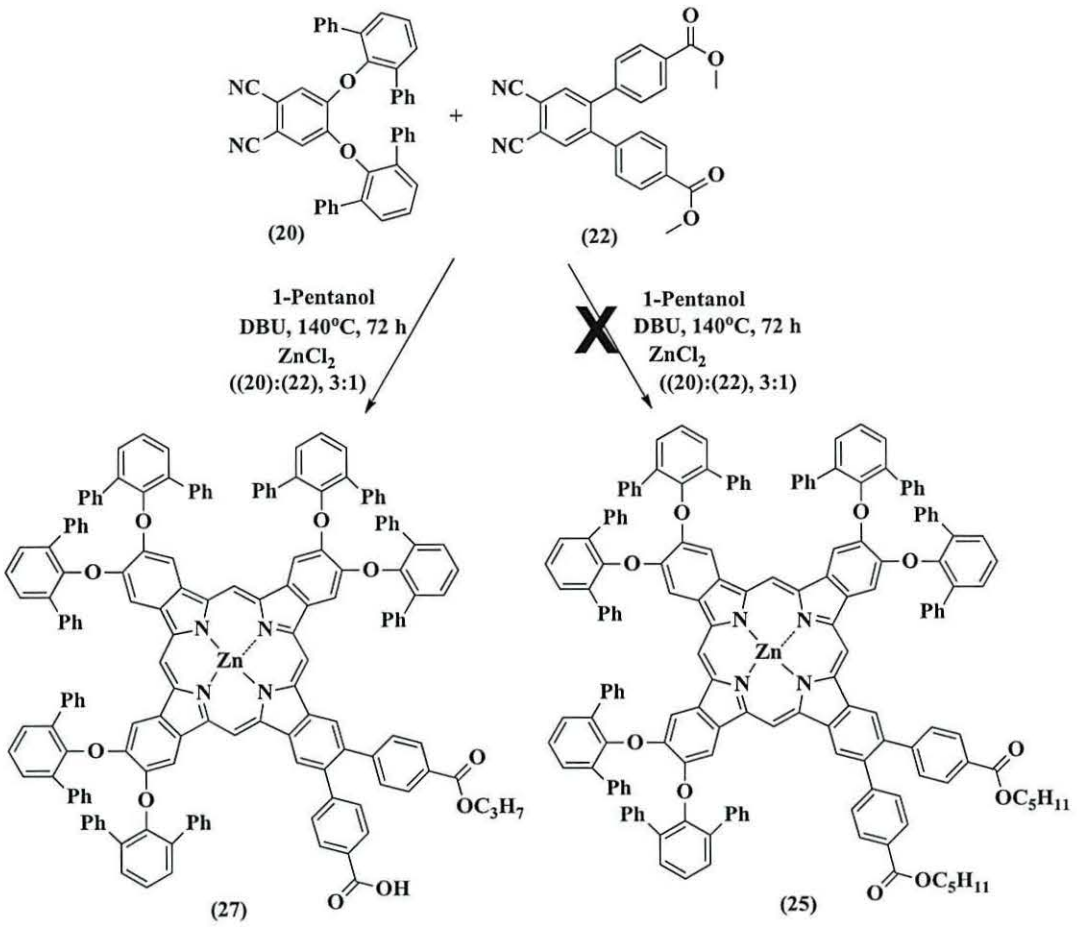

Scheme 5.7. The synthetic path way of 2- (propoxybenzoate)-3-(4-benzoic acid)-7^2,12^2,17^2-hexa (diphenylphenoxy)-tetrabenzo-5, 10, 15, 20-tetrazaporphyrin zinc (**27**).

The initial identification by mass spectrometry (Figure 5.27) shows two peaks; an intense peak at 2530.6 which corresponds to the symmetrical phthalocyanine zinc (**26**) 2530.5 M^+ and a peak at 2324.5 which is believed to correspond to 2-(propoxybenzoate)-3-(4-benzoic acid)-7^2, 12^2, 17^2-hexa (diphenylphenoxy)-tetrabenzo-5,10,15,20-tetrazaporphyrin zinc (**27**). Based on relative peak hights, thus represents approximately 30% of the yield.

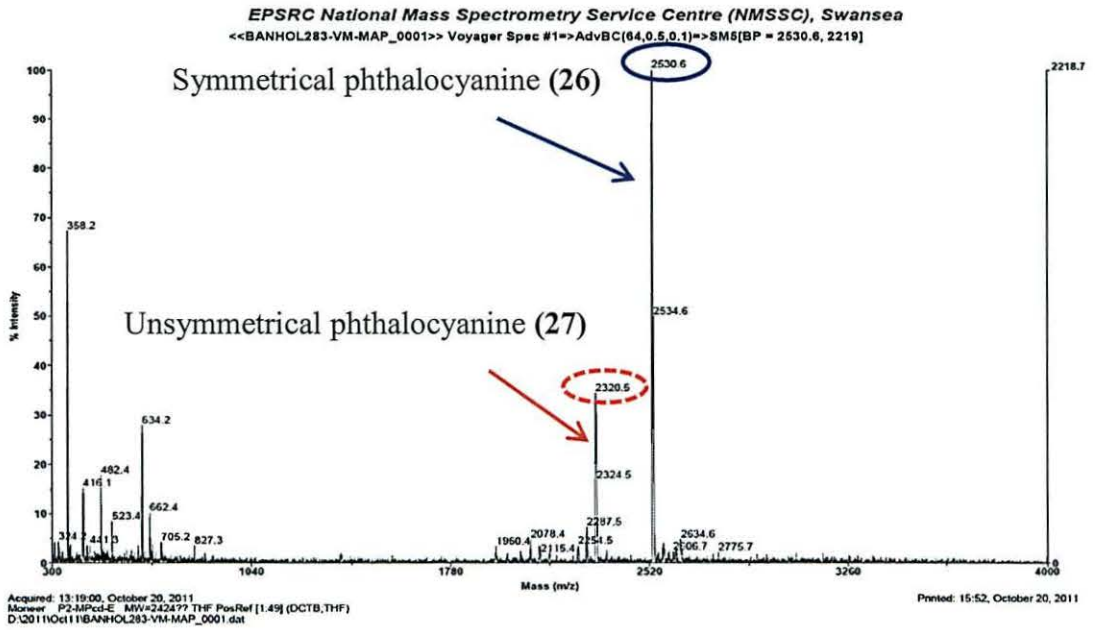

Figure 5.27. MALDI-DCTB matrix mass spectrometry of the reaction mixture containing the phthalocyanines (**26**) and (**27**).

The ^{1}H NMR data confirms the resultant (**27**) and shows a broad multiplet at 0.84-0.95 ppm due to (*CH*$_3$-CH$_2$-CH$_2$-O-), a pentet at 1.86 ppm due to (CH$_3$-*CH*$_2$-CH$_2$-O-) and a triplet at 3.75 ppm due to (-O-*CH*$_3$). There are also signals from 6.35-7.56 ppm due to (*Ar-H*). ^{13}C NMR shows signals at 27.78 and 29.68 ppm due to CH_3 and CH_2 from the alkyl chain, a signal at 69.41 ppm assigned to the methyl next oxygen (-O-*CH*$_3$). Finally, signals 109.53, 124.67, 126.12, 127.50, 127.80, 128.04, 128.20, 129.07, 129.29, 129.72, 130.94, 131.25, 135.11, 137.51, 137.67, 147.65, 150.27 ppm are assigned to (*Ar-H*) and (*Ar-C*-C) for the phthalocyanine macrocycle and the signal at 167.25 ppm to the carbonyl groups (*C=O*).

The UV-Vis spectrum of the mixture of phthalocyanines (**26**) and (**27**) is shown in Figure 5.28 in THF solution. The data show a Soret band absorption at 360 nm (I) and a sharp and intense a Q-band absorption at 684 nm (IV) (ε= 83672 $M^{-1}cm^{-1}$) due to a (π-π*) transition of the conjugated macrocycle. [2] There are also small peaks at 612 nm (II) and 648 nm (III) due to aggregation.

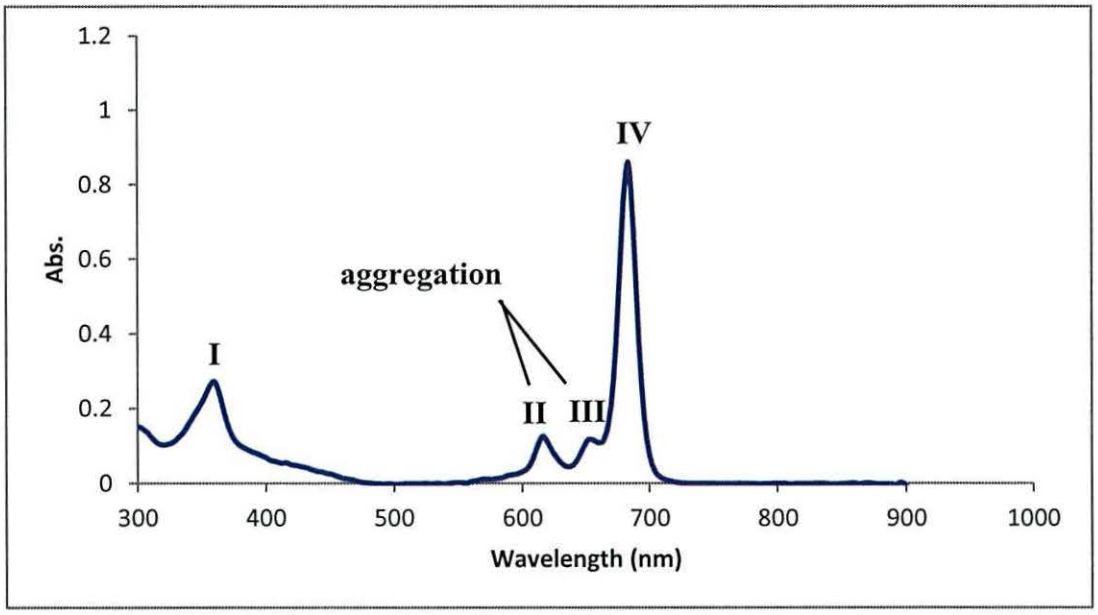

Figure 5.28. UV-Vis spectrum of mixture phthalocyanine ester (**26**) and (**27**), in THF $4x10^{-6}$ mol L^{-1}, ε= 206804 $M^{-1}cm^{-1}$ at 684 nm.

The FT-IR spectrum shows a peak at 3058 cm^{-1} for (C-H) stretch of benzene ring, medium peaks at 2926 and 2855 cm^{-1} due to (C-H) stretches for CH_3 and CH_2. A weak peak at 1718 cm^{-1} is due to (C=O) stretch of carbonyl carbon ester group, a sharp peak at 1271 cm^{-1} is assigned to (C-O) bending and a sharp peak at 1200 cm^{-1} is due to (C-N) stretch.

The hydrolysis of the ester of (**27**) in the mixed product was attempted to produce 2,3-di(4-benzoic acid)-7^2,12^2,17^2-hexa(2,6-diphenylphenoxy)-tetrabenzo-5,10,15,20-tetrazaprophyrin zinc (**28**). This was carried out by using a method developed from Eu *et al.* [5] To a mixture of THF-methanol containing aqueous potassium hydroxide solution (40%) was added 0.1 g of the phthalocyanine mixture which was then refluxed for 24 h. After removing the solvent, the pH was adjusted to 4 using 6M HCl to produce a green precipitate. Filtration and drying at room temperature gave a green solid. The initial inspection by mass spectrum (Figure 5.29) shows two peaks at 2531.5 due to the symmetrical phthalocyanine zinc (**26**) and a peak at 2324.5 assigned to 2-(propoxybenzoate)-3-(4-benzoic acid)-7^2, 12^2, 17^2,-hexa (diphenylphenoxy)-tetrabenzo-5, 10, 15, 20-tetrazaporphyrin zinc (**27**) unsymmetrical phthalocyanine-ester. This indicated that the hydrolysis reaction was not successfull.

Further attempts were also unsuccessful.

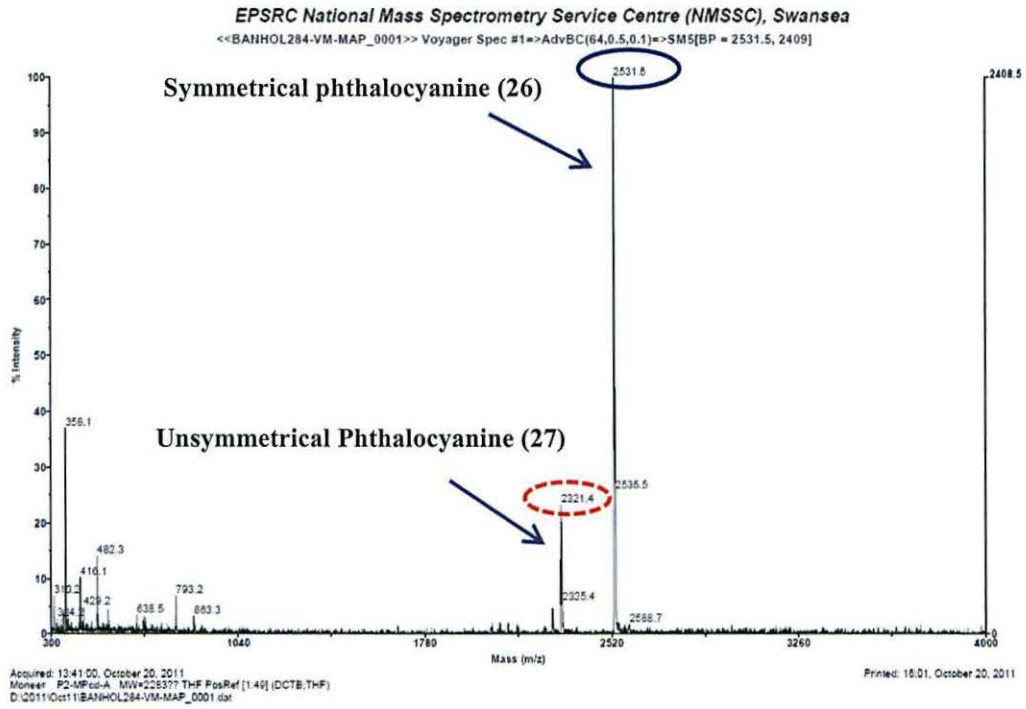

Figure 5.29. MALDI-DCTB matrix mass spectrometry of a mixture phthalocyanine zinc (**26**) and (**27**).

One possible reason for this reaction being unsuccessful is believed due to the impurity of the precursor of 4, 5-*bis* (4-methoxycarbonylphenyl) phthalonitrile (**22**). As a discussed previously, this starting material was prepared by a Suzuki coupling reaction. The initial inspection by ^{1}H NMR shows a singlet peak at 3.85 ppm with three protons present extra methyl group, in addition to the singlet peak at 3.90 ppm due to (2x $-OCH_3$). The mass results show that the observed weight was 412.8641 compared to the theoretical weight of 396.3948. This increase is believed to be due to an extra lone methyl group, $[M+CH_3]^+$ which may suggest the Suzuki-coupling reaction had gone wrong.

5.5 Conclusions

The strategy of this chapter was attempted to synthesize new unsymmetrical phthalocyanine zinc compounds as sensitizers for DSC devices which absorb light in the near infrared region (NIR). Unsymmetrical (**24**) and symmetrical (**26**) dyes were made but attempts to synthesize the unsymmetrical phthalocyanine (**25**) did not succeed.

Unsymmetrical phthalocyanine (**24**) was designed and synthesized as discussed above as a new sensitizer, synthesized from different phthalonitrile groups; six 2,6-diphenylphenoxy groups substituted on benzene ring represent a push unit and another substituent containing two carboxylic acids represents a pull unit to compose a push-pull dye overall, as shown in Figure 5.31a. The form this ratio depends on some factors such as the ratio of phthalonitrile substitutes which have been used and type of solvent which used in reaction.

The solar cell performance of compound (**24**) was investigated and showed conversion efficiency up to 0.7%, without any co-adsorbents. The effect of co-sensitization of (**24**) with **D149** was investigated to improve the photovoltaic performance giving efficiency of 1.5%. Mori *et al.* [18] synthesized phthalocyanine compound (**PcS6**) contain six 2, 6-diphenyphenoxy group but with different substituent contain one carboxylic acid group, as shown in Figure 5.30b.

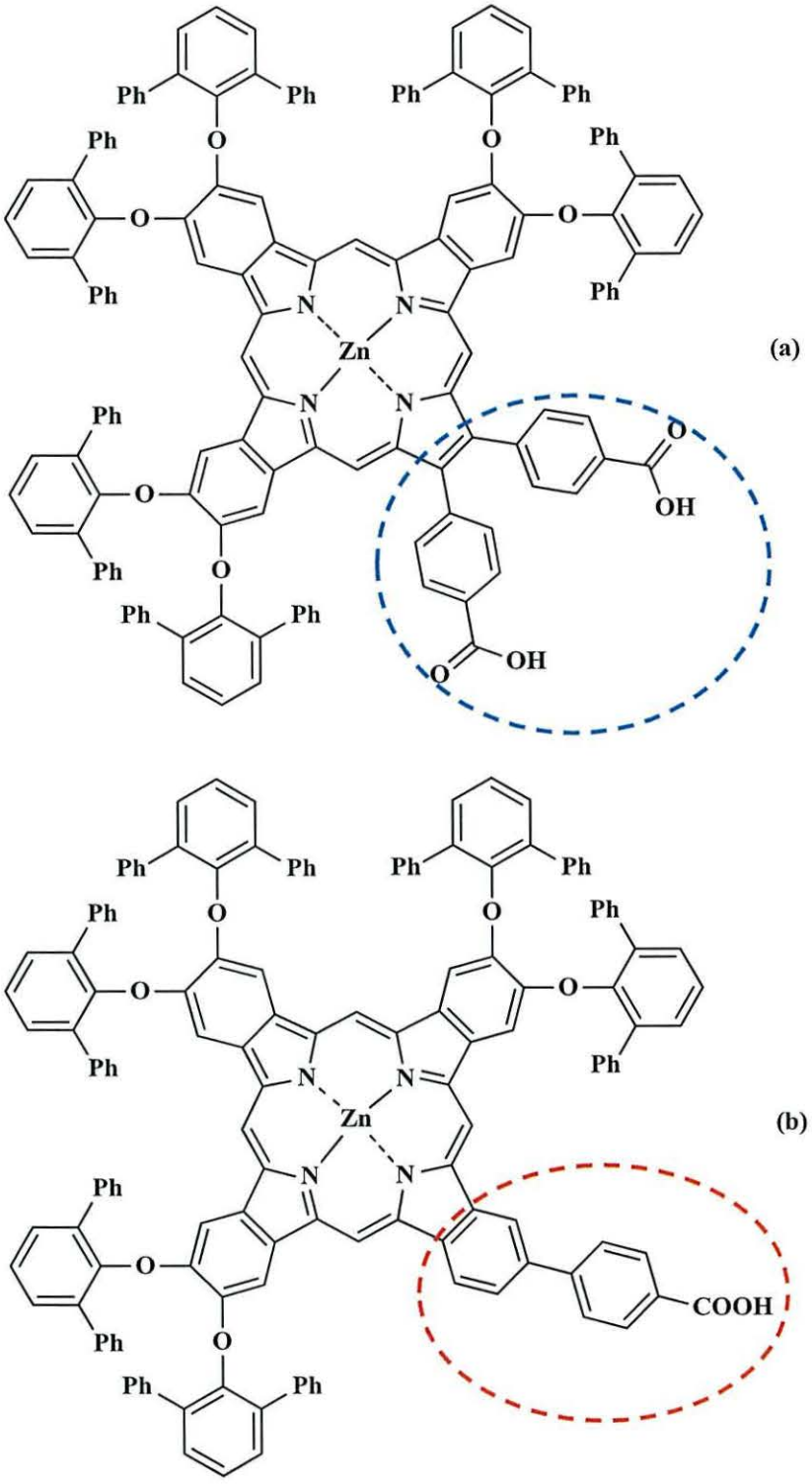

Figure 5.30. The molecular structure of (a) of (**24**) and (b) of (**PcS6**) which reported by Mori *et al.* [18]

5.6 References

1. D. S. Terekhov, K. J. M. Nolan, C. R. McArthur, and C. C. Leznoff, *J. Org. Chem.*, 1996, **61**, 3034–3040.
2. L. Giribabu, C. V. Kumar, M. Raghavender, K. Somaiah, P. Y. Reddy, and P. V. Rao, *J. Nano. Res.*, 2008, **2**, 39–48.
3. X. H. Zhang, Y. H. Zhan, D. Chen, F. Wang, and L. Y. Wang, *Dyes Pigments*, 2012, **93**, 1408–1415.
4. S. Mori, M. Nagata, Y. Nakahata, K. Yasuta, R. Goto, M. Kimura, and M. Taya, *J. Am. Chem. Soc.*, 2010, **132**, 4054–4055.
5. S. Eu, T. Katoh, T. Umeyama, Y. Matano, and H. Imahori, *Dalton Trans.*, 2008, 5476.
6. Y. Rio, M. S. Rodríguez-Morgade and T. Torres, *Org. Biomol. Chem.*, 2008, **6**, 1877–1894.
7. P. Y. Reddy, L. Giribabu, C. Lyness, H. J. Snaith, C. Vijaykumar, M. Chandrasekharam, M. Lakshmikantam, J. H. Yum, K. Kalyanasundaram, M. Grätzel, and M. K. Nazeeruddin, *Angew. Chem. Int. Ed.*, 2007, **46**, 373–376.
8. C. G. Claessens, U. Hahn, and T. Torres, *Chem. Rec.*, 2008, **8**, 75–97.
9. K. Kadish, R. Guilard, and K. M. Smith, in *The Porphyrin Handbook: Phthalocyanines: Synthesis*, 2006, Elsevier.
10. F. I. Bohrer, in *Gas Sensing Mechanisms in Chemiresistive Metal Phthalocyanine Nanofilms*, 2008, ProQuest.
11. S. Ito, S. M. Zakeeruddin, R. Humphry-Baker, P. Liska, R. Charvet, P. Comte, M. K. Nazeeruddin, P. Péchy, M. Takata, H. Miura, S. Uchida, and M. Grätzel, *Adv. Mater.*, 2006, **18**, 1202–1205.
12. N. Miyaura and A. Suzuki, *Chem. Rev.*, 1995, **95**, 2457–2483.
13. J. P. Corbet and G. Mignani, *Chem. Rev.*, 2006, **106**, 2651–2710.
14. J. Yin, M. P. Rainka, X. X. Zhang, and S. L. Buchwald, *J. Am. Chem. Soc.*, 2002, **124**, 1162–1163.
15. A. F. Littke, C. Dai, and G. C. Fu, *J. Am. Chem. Soc.*, 2000, **122**, 4020–4028.
16. D. S. Terekhov, K. J. M. Nolan, C. R. McArthur, and C. C. Leznoff, *J. Org. Chem.*, 1996, **61**, 3034–3040.
17. D. L. Mattern, *J. Org. Chem.*, 1984, **49**, 3051–3053.
18. S. Mori, M. Nagata, Y. Nakahata, K. Yasuta, R. Goto, M. Kimura, and M. Taya, *J. Am. Chem. Soc.*, 2010, **132**, 4054–4055.

Chapter 6

Conclusions and future work

6.1 Conclusion

In this thesis the synthesis and testing three different DSC dye families is discussed; triarylamine dyes which absorb with λ_{max} around 380 nm, cyanine dyes with λ_{max} around 820 nm and phthalocyanine dyes with λ_{max} absorb around 700 nm. The strategy of this work was to attempt to harvest visible and near infrared light (NIR) with multiple dyes to capture more light from the solar spectrum. Figure 6.1 shows the AM spectrum and the UV-Vis absorption regions of the synthesized dyes compared with commercial ruthenium dye.

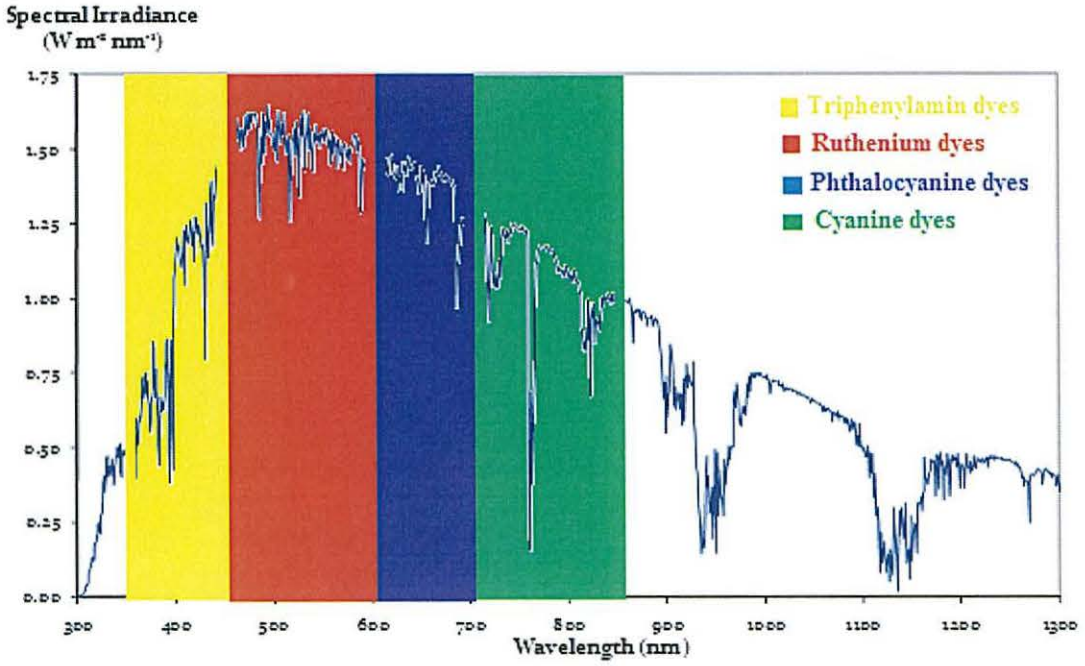

Figure 6.1. The light absorption of triphenylamine dyes (yellow colour), ruthenium dye (red colour), phthalocyanine dyes (blue colour) and cyanine dyes (green colour).

Triarylamine dyes have been synthesized with a donor-bridge-acceptor (D-π-A) concept, based on TPA as a donor moiety. The single-linker yellow dye (**5**) has been published in a journal paper during this thesis. [1] This dye was designed, synthesized and investigated as a DSC sensitizer with overall conversion efficiency of 2.6%. The improvements of photovoltaic performance of this dye were investigated by co-sensitizing with other dyes and achieved a conversion efficiency of 7.5%, J_{sc} (15.45 mA cm^{-2}) when co-sensitized with **N719** dye. The same thing was done with single-linker red dye (**3**) which is a known DSC dye and which was re-synthesized in this work. This dye was also investigated by co-sensitization with **N719** to give 7.2%

overall conversion efficiency and J_{sc}= 14.92 mA cm^{-2}. This is also related with the aim of this thesis to capture more light to try to enhance the performance devices.
The stability of the single-linker yellow dye (**5**) was examined with time, and shows excellent stability during thermal and light soaking when compared to the ruthenium dye **N719**. The efficiency of yellow dye (**5**) remains fairly stable up to 1800 h as described in the paper. [1] This chapter also reports the effect of increasing the number of acceptor groups on DSC performance. To test this, we synthesized red and yellow triarylamine dyes containing two cyanoacrylic acid or carboxylic acid acceptor groups (**12**) and (**14**), respectively. The strategy of synthesizing two-linker dyes was to try to make the binding between the anchoring group and the semiconductor stronger, and study the influence on DSC performance. The strategy for the synthesis of (**12**) depended on the synthesis of 5-bromoisophthalaldehyde (**9**) as the main precursor. This had been reported previously by Osuka *et al.* [2] They prepared this precursor by four steps starting with 5-bromo-*m*-xylene by using a Ziegler reaction with CCl_4 as the solvent. In this thesis, the synthetic pathway was reduced to three steps and did not use CCl_4 as the solvent. To do this, we started with 5-bromoisophthalic acid as the main raw material. However, many attempts to synthesize (**12**) failed. Finally, we were able to solve this problem which lay in reducing the refluxing time from overnight to 3 h. Both two-linker dyes (**12**) and (**14**) show overall conversion efficiency and photocurrent results of 2.6%, J_{sc} (4.35 mA cm^{-2}) and 1.2% (2.28 mA cm^{-2}), respectively. Co-sensitization with other dyes was again investigated with **D149** and **N719**. The solar cells devices of (**12**) showed efficiencies and photocurrents of 5.4% (14.69 mA cm^{-2}) and 2.1% (5.82 mA cm^{-2}) with **D149** and **N719**, respectively. While (**14**) shows 2.6% (4.41 mA cm^{-2}) and 4.4% (12.63 mA cm^{-2}) with **N719** and **D149**, respectively. The results which obtained above shows (**12**) and (**14**) dyes show a good result when mixing with **D149** better than **N719**.

Chapter 4 describes the synthesis of two symmetrical cyanine dyes which were synthesized to investigate their DSC device performance and to attempt to capture more near infrared light. New unsymmetrical cyanine dyes also have been synthesized and investigated DSC devices. The photovoltaic parameters result of the symmetrical and unsymmetrical cyanine dyes do not show promising data. The influence of co-adsorbent as additives to enhance the photovoltaic performance was

also investigated, and chenodeoxycholic acid (CDCA) was used as a co-adsorbent to try to prevent dye aggregation and to enhance the photovoltaic performance. However, the cyanine dyes still do not show promising results with CDCA co-adsorbent. It is believed that aggregation could be effecting the electron injection lifetimes of these dyes. The influence of effect TiO_2 film thickness was investigated and better results were obtained with three layers thickness which was better than 2 or 4 layers. This is believed to reflect greater recombination due to the longer distances electrons need to travel when the layers thickness increases.

Chapter 5 synthesized the final dye family tested in this thesis which also absorbs near-infrared light. Hence, we synthesized new the unsymmetrical phthalocyanine (**24**), and the symmetrical phthalocyanine (**26**). However, attempts to synthesize the unsymmetrical phthalocyanine (**27**) were not successful; which is believed to be due to the impurity of the precursor (**22**). Purification was a main problem in the phthalocyanine synthesis. This chapter also describes a method to solve this problem and produce a pure unsymmetrical phthalocyanine by using TiO_2 (P25) and ammonium solution 0.1M to adsorb impure dye solution and desorb the carboxylate dye. The symmetrical phthalocyanine (**26**) was then confirmed by an X-ray single crystal structure. The photovoltaic performance of unsymmetrical phthalocyanine (**24**) has been investigated without the use of any co-adsorbent which showed conversion efficiency and photocurrent of 0.7% (2.40 mA cm^{-2}). Co-sensitizing unsymmetrical phthalocyanine (**24**) with **D149** showed conversion efficiency and photocurrent 1.8% (6.54 mA cm^{-2}). During the synthesis of phthalocyanine compounds the data showed that there is a possibility to form a variety of phthalocyanine products which have been discussed in chapter 5.

6.2 Future work

The aim of this work was to synthesize three new different families' dyes, which absorb light in different area of the solar spectrum as discussed earlier. In this thesis were synthesized triphenylamine, phthalocyanine and cyanine dyes. These dyes were investigated as sensitizers for DSC and also have co-sensitized with other dyes. According to the results obtained, single-linker yellow dye (**5**) was the best dye due to the high stability, easy manufacturing, and low cost starting materials, external quantum efficiency (EQE) around 70% and shows high conversion efficiency when co-sensitized with **N719** dye.

During the period laboratory work and research for three years in this field of the synthesis of organic sensitizers for dye-sensitized solar cells can suggest many ideas for future work. If time was not a problem, one idea would be the synthesis of more yellow dye (scaled up) to make more devices to try to co-sensitize with other different types of dyes such **D149**, unsymmetrical cyanine dyes (**38**) or with phthalocyanine which have been synthesized in this thesis. Two-linker yellow and red dyes did not give promising results because they contain two acceptor groups which should have given better results than single-linker groups. Another suggestion is to re-synthesize these dyes again and do a wide study about the effect of the number of acceptor groups on the physical properties and performance of devices, in addition to a study about the way these molecules link on the TiO_2 surface. This work also needs more development to improve the performance of co-sensitization; e.g. two-linker dyes with **N719** and **D149** or with other dyes.

The phthalocyanine dyes are promising dyes due to their ability to absorb near infrared region (NIR) light. In this thesis, these dyes not work very well and show external quantum efficiency (EQE) around 17% at 340 nm and 10% at 700 nm. Failure in the synthesis of unsymmetrical phthalocyanine (**28**), which is believed due to impurity of the starting materials (**22**), suggests it is worth trying to re-synthesize the starting metrial again to try to get a pure compound and then synthesize the unsymmetrical phthalocyanine (**28**), using more characterization to check this compound and then doing more co-sensitization with other dyes.

Another suggestion based on the synthetic work would be to synthesize a new dye by using 4, 6-dibromo-2, 3, 3-trimethyl-1-octyl-3H-indolium iodide compound (**31**)

which has been synthesized in this thesis to produce 4,6-diformyl-2,3,3-trimethyl-1-octyl-3H-indol-1-ium iodide (**39**) with two aldehyde groups, and then using a Knoevenagel condensation reaction to produce 6-((E)-2-carboxy-2-cyanovinyl)-4-((Z)-2-carboxy-2-cyanovinyl)-2,3,3-trimethyl-1-octyl-3H-indol-1-ium (**40**) as a new dye with two acceptor groups as shown in Scheme 6.1. This could then be used as the linker group of new dyes (e.g. squaraine dyes which absorb NIR light) as shown in Scheme 6.4.

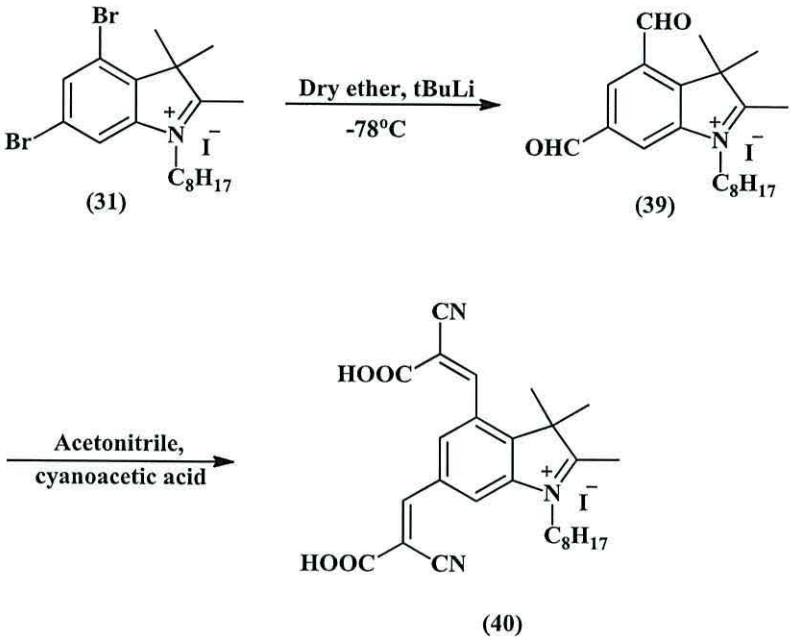

Scheme 6.1. The synthetic pathway to synthesize 6-((E)-2-carboxy-2-cyanovinyl)-4-((Z)-2-carboxy-2-cyanovinyl)-2, 3, 3-trimethyl-1-octyl-3H-indol-1-ium (**40**).

Another suggestion would be the synthesis of a new phthalocyanine dye with high molar extinction coefficient which absorbs in the near infrared region by synthesizing symmetrical phthalocyanine and linking the coordinated zinc with an isonicotinic acid unit to TiO_2. This should enable the dye to chemsorb to TiO_2 and improve the performance of this dye, as shown in Figure 6.2, but it would also be easier to synthesis and purify as this reaction would give only one phthalocyanine product.

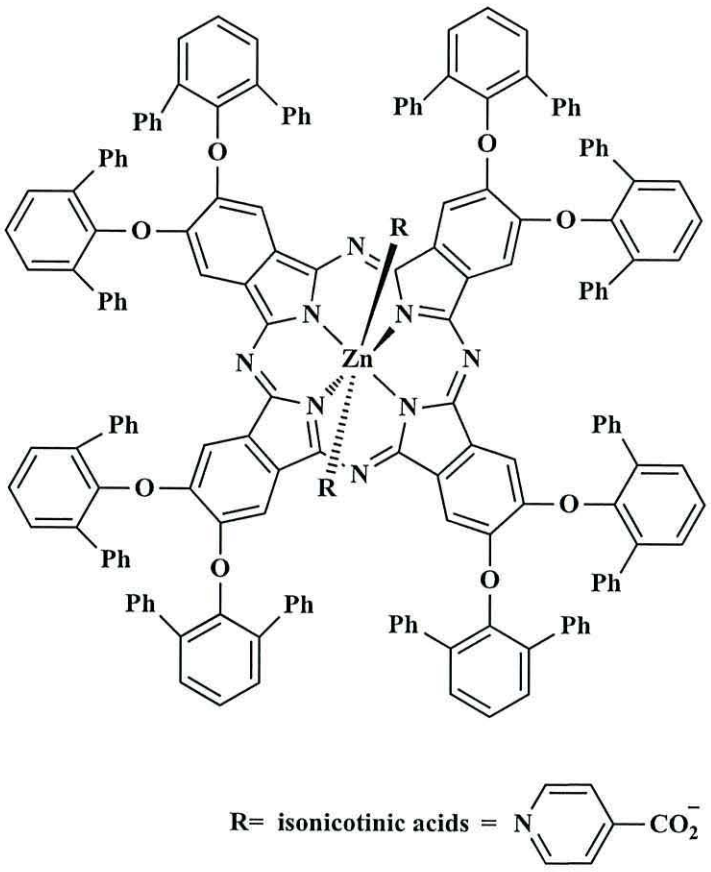

Figure 6.2. The molecular structure of 2^2, 7^2, 12^2, 17^2 octa (2, 6-diphenylphenoxy)-tetrazaprophyrin zinc with two isonicotinic acid groups linked to zinc atom.

As discussed previously, squaraine dyes absorb in the near infrared region. [3] Squaraine have received attention because of their strong absorption, high molar absorption coefficient and long-wavelength λ_{max}. [4] Squaraine can also be synthesized using similar indoline side groups and procedures to the cyanine dyes prepared in this thesis. Future work could use starting materials from this thesis. For instance, Scheme 6.3 shows the design of (SQ-In-TPA) compound as a sensitizer in DSC, which compose of two groups of triphenylamine as a donor and indolenine squaraine moiety which are electron-rich bridge. [5]

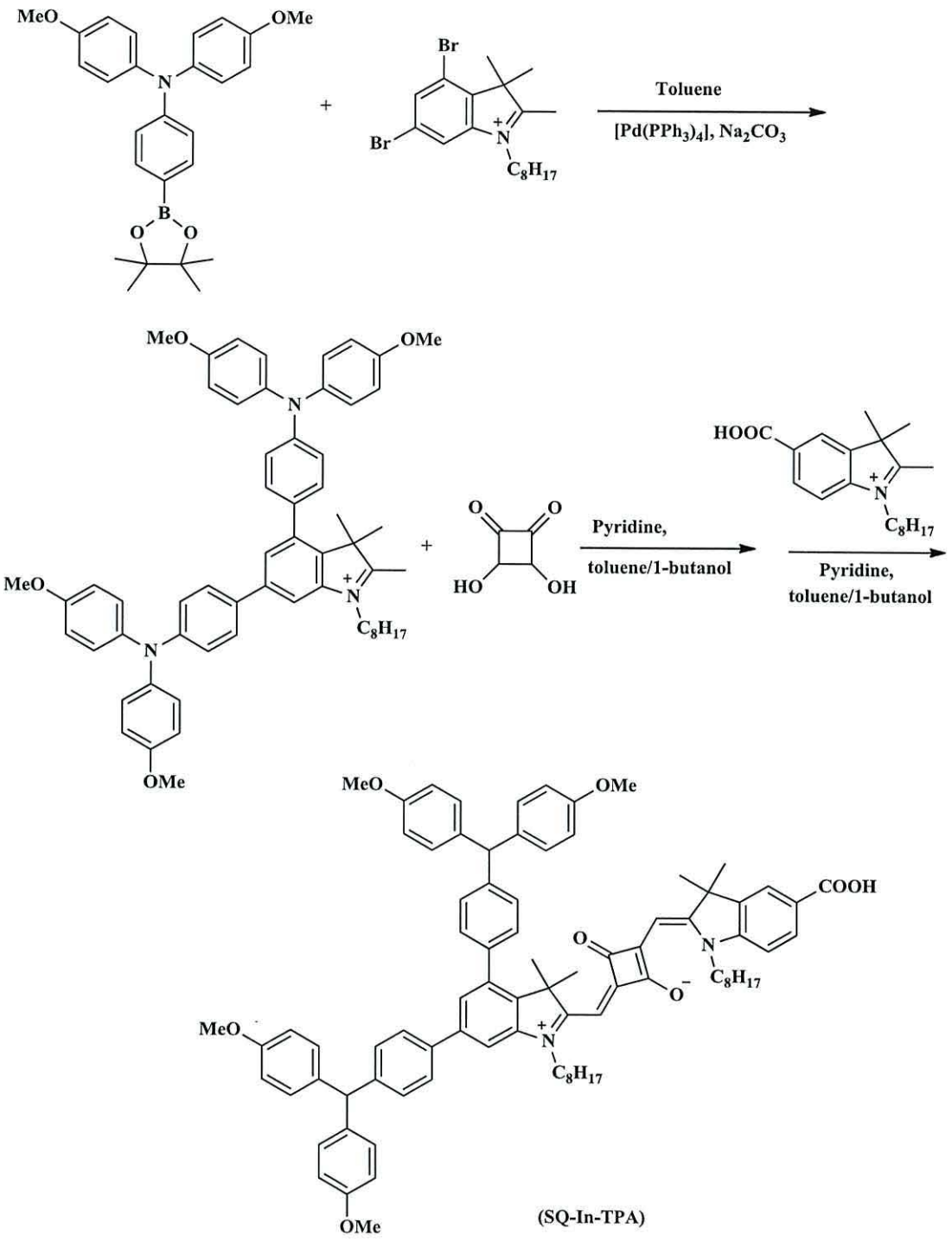

Scheme 6.3. Synthetic pathway of (**SQ-In-TPA**).

Another suggestion for squaraine dyes is shown in Scheme 6.4, which shows the design of squaraine dyes with two cyanoacrylic acid as acceptor group using compound (**30**).

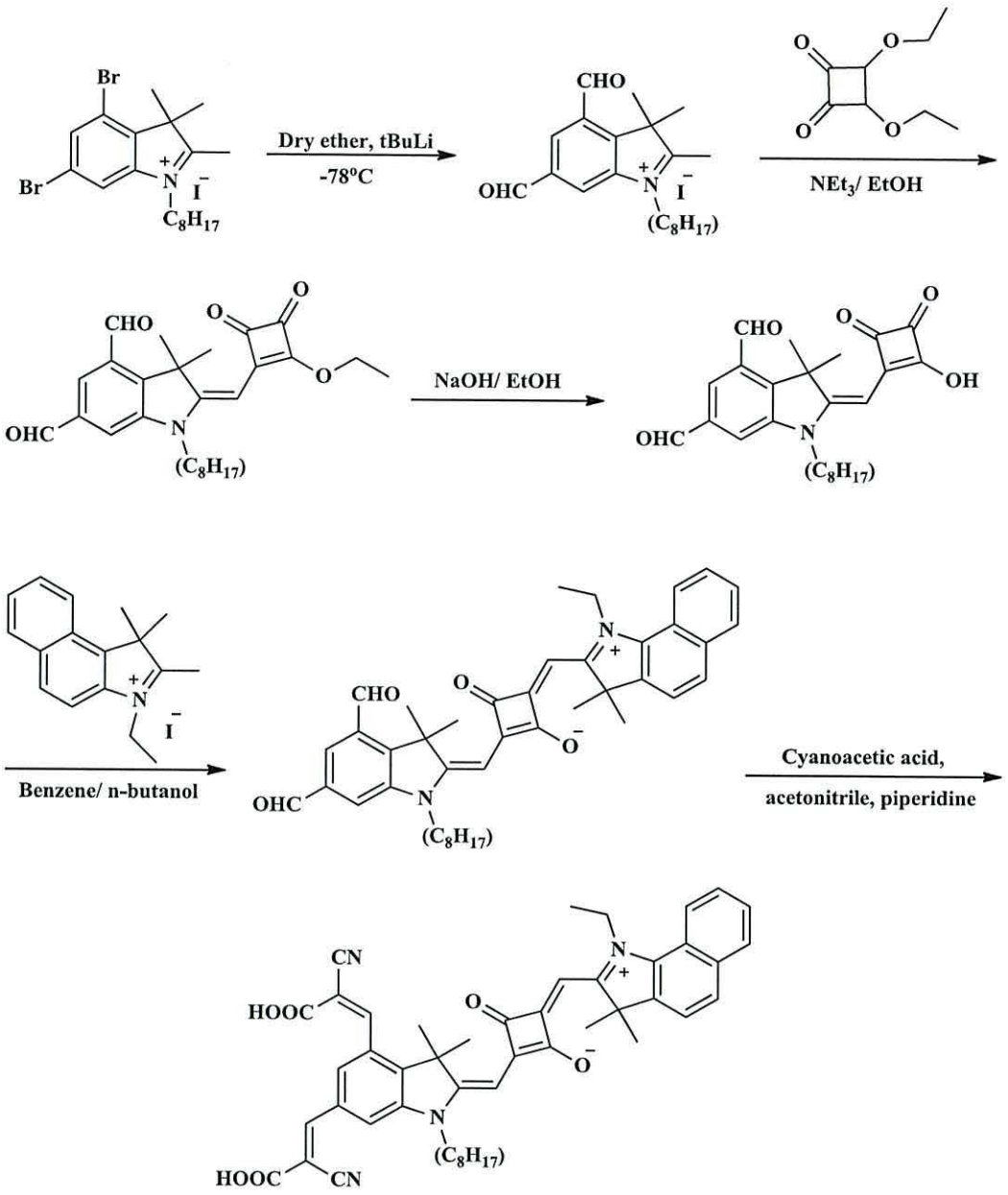

Scheme 6.4. Synthetic pathway of (**SQ-In-2CA**).

In addition, Figure 6.3 shows other possible ideas for the future work using squaric acid indolines and the triphenylamine moiety to synthesize and design new sensitizers for DSC.

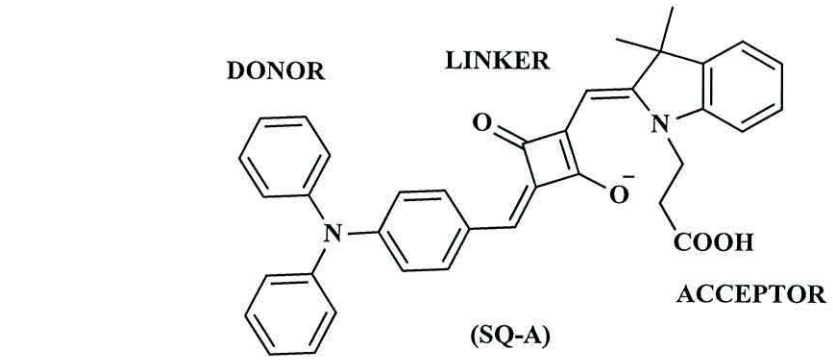

(SQ-A)

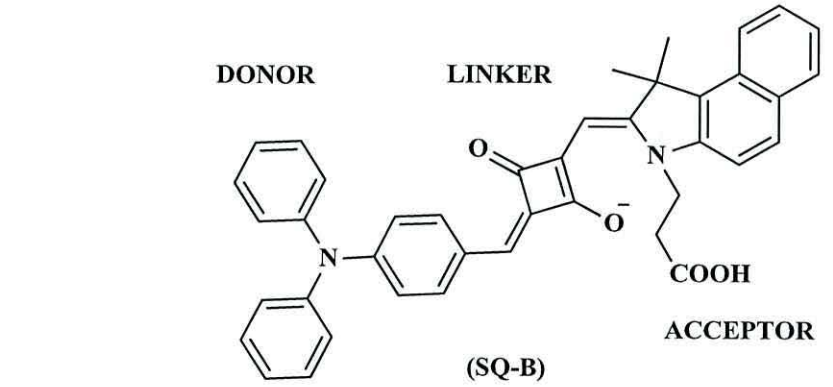

(SQ-B)

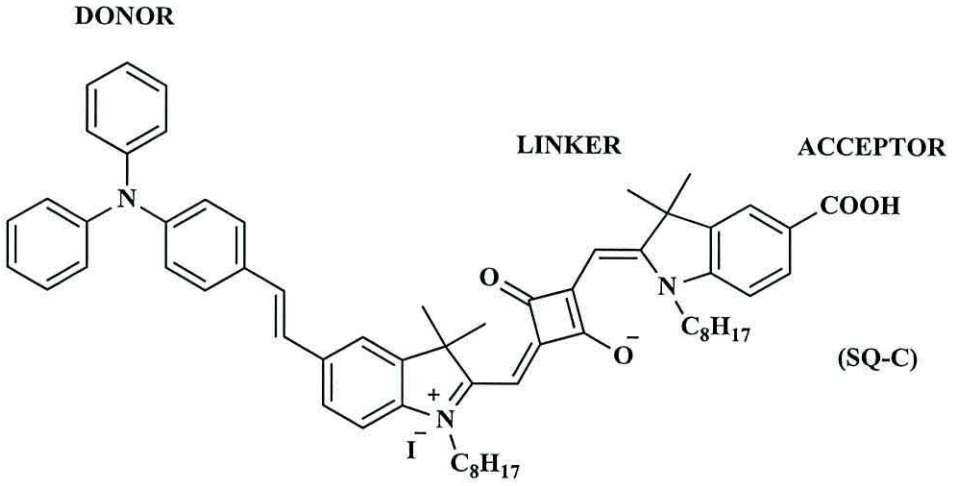

(SQ-C)

Figure 6.3. Molecular structure of different types of (**SQ-A**), (**SQ-B**) and (**SQ-C**).

6.3 References

1. P. J. Holliman, M. Mohsen, A. Connell, M. L. Davies, K. Al-Salihi, M. B. Pitak, G. J. Tizzard, S. J. Coles, R. W. Harrington, W. Clegg, C. Serpa, O. H. Fontes, C. Charbonneau, and M. J. Carnie, *J. Mater. Chem.*, 2012, **22**, 13318–13327.
2. A. Osuka, B. L. Liu, and K. Maruyama, *J. Org. Chem.*, 1993, **58**, 3582–3585.
3. K. Funabiki, H. Mase, Y. Saito, A. Otsuka, A. Hibino, N. Tanaka, H. Miura, Y. Himori, T. Yoshida, Y. Kubota, and M. Matsui, *Org. Lett.*, 2012, **14**, 1246–1249.
4. T. Maeda, S. Mineta, H. Fujiwara, H. Nakao, S. Yagi, and H. Nakazumi, *J. Mater. Chem.*, 2012, **1**, 1303–1309.
5. S. F. Völker, M. Renz, M. Kaupp, and C. Lambert, *Chem. Eur. J.*, 2011, **17**, 14147–14163.